2-D DEPTH AVERAGED MODELLING FOR CURVILINEAR BRAIDED STRETCH OF BRAHMAPUTRA RIVER

A THESIS

Submitted in partial fulfilment of the requirements for the award of the degree of

DOCTOR OF PHILOSOPHY

in

WATER RESOURCES DEVELOPMENT AND MANAGEMENT

by

MD PARWEZ AKHTAR

DEPARTMENT OF WATER RESOURCES DEVELOPMENT & MANAGEMENT
INDIAN INSTITUTE OF TECHNOLOGY ROORKEE
ROORKEE-247 667 (INDIA)

JUNE, 2011

INDIAN INSTITUTE OF TECHNOLOGY ROORKEE
ROORKEE

CANDIDATE'S DECLARATION

I hereby certify that the work which is being presented in the thesis entitled **2-D DEPTH AVERAGED MODELLING FOR CURVILINEAR BRAIDED STRETCH OF BRAHMAPUTRA RIVER** in partial fulfilment of the requirements for the award of the degree of Doctor of Philosophy and submitted in the Department of Water Resources Development & Management of the Indian Institute of Technology Roorkee, Roorkee, is an authentic record of my own work carried out during the period from Jan 2008 to June 2011 under the supervision of Dr. Nayan Sharma, Professor, Dr. R. P. Singh, Professor (Retired), Water Resources Development & Management, and Dr. C.S.P.Ojha, Civil Engineering Department, Indian Institute of Technology Roorkee, Roorkee. The matter presented in this thesis has not been submitted by me for the award of any other degree of this or any other Institute.

(MD PARWEZ AKHTAR)

This is to certify that the above statement made by the candidate is correct to the best of our knowledge.

(C.S.P. OJHA)
Supervisor

(R.P.SINGH)
Supervisor

(NAYAN SHARMA)
Supervisor

Date: June 29th, 2011

The Ph.D. Viva-Voce Examination of **Mr. Md Parwez Akhtar,** Research Scholar, has been held on 21.10.2011

Signature of Supervisors

Signature of External Examiner

ABSTRACT

The Brahmaputra is the largest river in the Indian subcontinent and ranks fifth in the world in terms of discharge. The specific yield from its catchment area is one of the highest in the world due to incidence of very high rainfall on a narrow drainage basin. Significant areas of prime inhabited land are lost every year to river erosion in the Brahmaputra basin. Furthermore, unrelenting bank erosion process has caused channel braiding which created navigation bottle-neck zones in the Brahmaputra due to inadequate draught during non-monsoon. For efficient management of prevailing problem spanning over hundreds of kilometre length along the Brahmaputra, the need has arisen for a convenient scientific methodology which can aid systematic monitoring of braiding behaviour, help prioritization of erosion zones, and maintain navigational all-weather fairway.

River morphological processes are among the most complex and least understood phenomena in nature. Hence for addressing numerous related hydraulic engineering problems, understanding flows through open channels, is of crucial importance. These flows are typically turbulent and highly three- dimensional. Traditional approaches for studying natural river flows and morpho-dynamics study are based on field measurements and laboratory experiments. Owing to site and event specific concerns, field studies of natural open channel flows are very expensive, tedious and time consuming. Similar problems are associated with laboratory physical model studies, which suffer from scale effects owing to non- similarity of one or more dominant non dimensional parameters. To overcome above shortcomings, developments of numerical models that generally do not exhibit aforementioned difficulties are being stressed upon.

The geometric complexities induce very intricate three dimensional turbulent shear flows which are characterized by secondary currents, vortex formation, flow reversal, and anisotropy effects. Majority of existing numerical models have focused primarily on the study of rivers of simplified geometries. The initial attempts in application of mathematical models in conjunction with empirical functions obtained from laboratory

experiments to the investigation of morphological processes can be found in the 1950s. Research in this direction was intensified and broadened in the 1970s and later. However 3-D numerical models are yet to be fully and adequately developed for channel with complex geometry in macro scale river reaches. Solving the equations of motion in these conditions is very difficult and computationally tedious.

In rivers where the width of the flow is large compared to its depth, the vertical acceleration of water is negligible compared to the gravitational acceleration. In this condition, the pressure distribution in depth can be assumed to be hydrostatic. Hence, in order to ease the numerical complexity and without compromising much with the results, the equations of motion can be integrated in depth to derive two-dimensional depth averaged equations. Wherever the channel domain becomes curvilinear in nature, either well defined meanders, braiding, curved bank-lines or 3-D flow structures are bound to develop on account of dominant secondary flows. The secondary flow is transverse circulation induced by centrifugal forces. Incorporating adequately the effect of secondary flow further enhances the two dimensional modelling to assess the realistic flow field. Thus, with less expensive numerical effort, a better and improved flow scenario can be achieved without going into 3-D model development.

Problem identification

The Assam section of the Brahmaputra River is in fact, highly braided and characterized by the presence of numerous lateral as well as mid channel bars and islands (Goswami and Das, 2000). Due to these facts, the research on Brahmaputra River in the past mostly relied on field investigation and physical modelling. Only after 1980s, numerical modelling, especially 1-D modelling has been gradually applied in flow simulation and sediment prediction in Brahmaputra River (Sharma, 2004). Yet successful implementation of 2-D depth averaged modelling in Brahmaputra River reaches in Assam Flood Plains is hardly found in literature due to its highly complex topography and difficulty in reproduction of geometric data mathematically. A number of investigations have been done so far to develop numerical models to represent the processes involved in braided river. Correct process representation of the river

morphology is yet to be achieved by improving fluvial features like impact of secondary flow due to channel bends on the flow field. With this background, development of an enhanced 2-D depth averaged numerical model and its application in identified reach of Brahmaputra River is attempted to critically analyse the effect of flow features for better understanding of braided river behaviour.

Objective of the study

The first objective of proposed research work was set with the application of principles and practices of numerical model development, to derive the appropriate set of mathematical expressions for the secondary flow correction (flow dispersion stress tensor) for depth averaged 2-D model to be used for non-orthogonal curvilinear flow domain. The second objective was to develop numerical algorithm using finite volume method to solve conservative form of governing equations in non-orthogonal grids with incorporated flow dispersion stress terms in momentum equations and compare the results of flow model with and without flow dispersion for general curved channels. The third objective was to apply and verify the proposed numerical model for the Brahmaputra River in selected reach and possible identification of braiding pattern with variability in stage-discharge. The fourth objective was to evolve a simplified braiding indicator to express the measure of braiding intensity for a river reach with incorporated no flow zone within the flow domain.

The study area and data collected

The reach between measured cross sections number-22 (Pandu near Guwahati) to 9 (Jogighopa) released by *Brahmaputra Board, G.O.I.* (spanning over approx. 100 km length in Assam state of Indian Territory) is selected for this study. Fourteen measured river cross-section data (Cross-section no. 22 to Cross section no. 9) for the year 1997 were used. Discharge data of the river Brahmaputra during 1997 was used in the study (*Central Water Commission* and *Brahmaputra Board, G.O.I.*). The digital satellite data comprising scenes of Indian Remote Sensing (IRS) Linear Imaging Self Scanner (LISS-III) sensors for the year 1997 (*Unpublished report of National Disaster Management Authority, Govt. of India*) for the study area, have been used. For model verification and

evaluation, an experimental flume of test section (4.25m×0.15m×0.20m) comprised a contraction in between with 0.002 m^3/s of constant discharge was simulated.

Methodology

The boundary fitted coordinate system has been used to describe a naturally shaped boundary to represent the complex flow domain. The ξ-axis is drawn along the channel for a given channel shape and η- axis is set to intersect the ξ-axis, Then the plane (ξ, η) is divided into the structured cells to form the mesh for computations using Poisson's equation. The governing equations for estimating flow field are transformed from Cartesian co-ordinate system to a Boundary fitted curvilinear co-ordinate system to represent flow domain. Finite Volume Method conserves mass-momentum and can be well applied for highly complex geometry using non-orthogonal grids. The flow field is computed at geometric cell centers using the Finite Volume Method using *SIMPLEC* algorithm. Rhie and Chow's (1983) interpolation technique is used to estimate the velocities at cell faces. The flow field and water depth are computed using the derived transformed governing equations with special attention to boundary implementation. The river braiding is simulated with incorporation of wetting and drying technique into the numerical solver. A *C++* computer code has been developed for numerical model to simulate flow field and mesh generation.

Proposed governing equations

The governing equations for flow simulation are *RANS* (Reynolds Averaged Navier Stokes) equations with depth averaged approximation of continuity and momentum equation in generalized curvilinear coordinate system. Components of dispersion stress terms are included in momentum transport equations as additional source/sink term. The derivation of dispersion stress tensor is done step by step to get revised set of empirical relations to be used in subsequent development of enhanced 2-D numerical flow model. The derived expressions are modifications to earlier relevant investigations (Duan, 2004; Duan and Julien, 2005). The proposed formulations are with simplified mathematical representation and are numerically compatible. These also improved the flow field simulation reasonably.

Validation of the developed 2-D model and salient contribution of the present research work

1-D flow models are insufficient to tackle problems of braided streams due to lack of information with regard to transverse flow field. So, 2-D or 3-D models are used. 3-D models are numerically expensive for macro scale river reaches. Hence, 2-D enhanced model was developed. Most of the 2-D models developed especially for braiding rivers did not account for secondary flow correction probably presuming these corrections to be insignificant for turbulent flows and mild curved bank-lines. But in complex flow situation with considerable braiding, the secondary flow correction is suitably justified to achieve improved flow scenario with nominal additional expense in respect to computational effort with including secondary flow correction using modified terms for dispersion stress tensor in the flow momentum equations.

Developed model was initially verified with flume experiment operating a flow with a contraction, and the validation of the flow simulation was achieved. It is established from the model application in laboratory flume that redistribution of flow concentration in longitudinal and transverse directions are desirably accounted for, using the formulation in curvilinear flow field and are well capable of assessing realistic flow prediction with reasonable approximation.

The model developed in this study has been applied and verified in the selected stretch of Brahmaputra River. It was observed that the effect of dispersion stress tensor in flow field increases with increase in braiding intensity. The model results lend support to this observation. When braiding intensity increases, it evolves multiple channels with meandering configurations within the domain of stream flow. Meandering and bend in evolved multiple channels instigate more discrepancy in the flow-field, if it is approximated with depth averaging. Braiding induces severe bank erosion, due to dominant transverse flow field. So, improved and realistic flow-field estimation will lead to realistic assessment of predictions of bank erosion and river bed evolution for braided alluvial rivers. Better erosion models can be developed with reasonable accuracy using estimated flow field as the prime input.

Based on the obtained results and information from flow simulation for twenty discharge profiles at receding flood of 1997 for Brahmaputra River stretch under this study, an indicator namely *braid power* is proposed based on the model output to express the measure of braiding for a river reach as

$$braid\ powe\ r(\mathrm{N/m^2\text{-}s}) = f_{nf} \cdot \frac{\gamma Q_{inlet} S}{\text{flow Area of Inlet of the Reach}}$$

where, f_{nf} =Ratio of no flow zone area with respect to whole flow domain area, γ=Unit weight of water (N/m^3) and S=Average longitudinal slope of the study reach. Flow area (m^2) is the cross-sectional flow area of the inlet boundary at the given discharge. It was observed that *braid power* increases with decrease in incoming discharge into the reach at a particular instance of time. The rate of decrease or increase of *braid power* depends upon geometric configuration of the reach at the particular instance of time along with other factors

Scope for future work and limitations

The numerical model developed in this research work is limited to flow field simulation in rivers with highly complex geometries and braided configurations. The prime thrust of the present research work is to bring to the fore persistent shortcomings in relation to flow field estimation for rivers with highly braided configuration. The present research work has desirably brought about a significant improvement in dominant transverse flow field estimation in highly braided rivers. The transverse flow field is one of the significant causative factors for stream bank erosion resulting in huge land loss around the vicinity of braided rivers such as Brahmaputra River. However, to model bank erosion and bed evolution with high degree of accuracy, after further research, a robust 2-D sediment transport module with incorporated bank erosion mechanism, clubbed with the present enhanced flow simulation model is required to be developed. To model the moving boundaries, present developed model uses fixed boundary method through implementation of wetting and drying technique including the whole flood plain under the flow domain. However through conducting further research on advanced algorithm using depth adaptive grid generation and temporal deformed mesh technique; a moving

boundary can possibly be implemented to simulate the multiple channels actual flow zones instead of considering the whole flood plain. However, at present numerical implementation of the aforesaid process is quite complex for highly braided rivers with multiple channels like Brahmaputra and possibly be a potential area of research.

****

ACKNOWLEDGEMENT

I wish to record my sincere thanks with profound sense of respect and gratitude for my supervisors **Prof. Nayan Sharma, Prof. R. P. Singh** and **Prof. C.S.P.Ojha**. The words prove to be insufficient to express my deep feelings for their high benevolence and un-hesitated guidance throughout the study period. Without their enthusiasm and determination, the study would not have seen the light of the day.

I am grateful to Prof. D. J. Bergstrom, Department of Mechanical Engineering, U of S, Saskatoon (Canada) for his valuable guidance, help and encouragement during my stay in Saskatoon, to conduct part of my research work in University of Saskatchewan, Saskatoon (Canada) under Graduate Student Exchange Program (GSEP) with I.I.T. Roorkee. I express my heartfelt thanks and gratitude to Prof. D. Kashyap, CED and all the faculty members of WRD&M for their help and encouragement during the course of the study.

I am deeply indebted to the Ministry of Human Resources Development, Government of India, for awarding me MHRD fellowship to complete this Ph.D. work. I do acknowledge National Disaster Management Authority, Government of India for using some specific research related data, during my association with their sponsored project with I.I.T. Roorkee, related to erosion study of Brahmaputra River. I also gratefully acknowledge the various authors and publications from where relevant references have been drawn in this thesis. I express my sincere thanks and compliments to Er. Sanjeev Suman, Er. Mohd. Zafar, Er. Manoj Kumar and Er. Ajay Kumar, Research Scholars, Mr. Pramod Kumar, Lab. Assistant, *CED, IIT* Roorkee and Mr. Neeraj Kumar, WRD&M for their co-operation.

Especially, I acknowledge the utmost co-operation rendered by my parents, father in law Late Qasim Ahmed, brothers Jawed Akhtar, Md. Hashim and my uncle Zakir Hussain during the study. Finally, I heartily acknowledge the utmost co-operation, forbearance and persistent encouragement shown by my wife Rafat and my son Arshaan throughout the study.

29th June, 2011

(MD PARWEZ AKHTAR)

CONTENTS

****

LIST OF FIGURES

****

LIST OF TABLES

****

NOTATIONS

β = width ratio

C_d = frictional stress coefficient

D_{xx}^c, D_{xy}^c and D_{yy}^c

= components of dispersion coefficient tensor in curvilinear coordinates;

D_{xx}, D_{xy} and D_{yy}

= components of dispersion coefficient tensor in Cartesian coordinates.

g = acceleration of gravity;

H = water surface elevation;

h = flow depth;

n = Manning's roughness coefficient;

η_0 = dimensionless zero bed elevation;

ξ = stream-wise direction;

η = transverse direction;

θ_s = angle between the stream-wise and the positive x axis

θ_n = angle between transverse direction towards outer-bank and the positive x axis;

κ = *Von Karman's constant;*

v = kinetic viscosity;

v_t = eddy viscosity;

ρ = density of flow;

r = radius of curvature;

t = time;

τ = time in transformed coordinates

y' = transverse coordinate

$\hat{u}_m$ = depth averaged velocity in curvilinear coordinate system;

U = magnitude of depth averaged velocity;

U^* = shear velocity;

U_x, U_y = depth averaged velocities in Cartesian coordinates;

u_n, U_n = Transverse actual and depth averaged velocities;

u_s, U_s = Stream-wise actual and depth averaged velocities;

x, y = Cartesian coordinate;

z = vertical coordinate;

z_0 = zero velocity level;

B = channel width;

C_D = coefficient of discharge;

H = water surface elevation;

h = flow depth;

I_L = non-dimensionallized values of the longitudinal velocity deviation;

I_L = non-dimensionallized values of the transverse velocity deviation;

J = Jacobian of transformation

k_s = roughness height;

ξ = stream-wise direction;

η = transverse direction;

Γ = diffusitivity;

σ_{IL} = Standard deviation for I_L;

σ_{IT} = Standard deviation for I_T;

f_f = Fraction of flow zone in the domain

f_{nf} = Fraction of no flow zone in the domain

Q = Discharge

λ_w = Wall coefficient

Abbreviations

CFD = Computational Fluid Dynamics

CFL = Courant Fredricks Lewy

CWC = Central Water Commission

FVM = Finite Volume Method

HEC-RAS= Hydrological Engineering Center- River Analysis System

HLPA = Hybrid Linear/Parabolic

IIT = Indian Institute of Technology

IRS = Indian Remote Sensing

LISS = Linear Image Self Scanner

NDMA = National Disaster Management Authority

SIMPLEC= Semi Implicit Pressure Linked Equation Consistent

WAPCOS= Water & Power Consultancy Services

WGS 84 = World Geodetic System 84

****

CHAPTER-1

INTRODUCTION

1.1 GENERAL

Fluvial landforms are produced by the action of flowing water in the terrestrial environment, whereas fluvial geomorphic processes are those natural processes that produce, maintain and change fluvial landforms. The channel pattern or landform of a reach of an alluvial river reflects the hydrodynamics of flow within the channel and the associated processes of sediment transfer and energy dissipation. Channel patterns form a continuum in response to varying energy conditions ranging from straight and meandering to braided forms. Generally, braiding is favoured by high energy fluvial environment with steeper gradients, large and variable discharges, dominant bed load transport and non-cohesive banks lacking stabilization by vegetation (Richards, 1982). The secondary flow component also contributes to the growth of channel deformations (Bathurst *et al.*, 1979).

The Brahmaputra is the largest river in the Indian subcontinent and ranks fifth in the world in terms of discharge. The specific yield from its catchment area is one of the highest in the world due to incidence of very high rainfall on a narrow drainage basin. Relentless stream-bank erosion along with flooding in the densely populated region of the Brahmaputra basin in the Indian province of Assam has become one of the causative factors for impoverishing a large segment of agrarian population every year. Significant areas of prime inhabited land are lost every year to river erosion in the Brahmaputra basin thereby impoverishing the affected people due to sudden loss of home and hearth. Furthermore, unrelenting bank erosion process has caused channel widening which created navigation bottleneck zones in the Brahmaputra due to inadequate draught during non-monsoon. For efficient management of the Brahmaputra, the need has arisen for a convenient scientific methodology to understand its complex channel hydrodynamics, which can aid systematic monitoring of bank-line changes, help prioritization of erosion zones, and facilitate maintenance of navigation for all-weather fairway.

River morphological processes are among the most complex and least understood phenomena in nature. Due to the fact that they intimately affect on our living conditions, scientists and engineers have been looking for better tools to improve our understanding and enhance the quality of our lives ever since the beginning of human civilization. (Wang and Wu, 2004). Understanding flows through open channels, is of crucial importance for addressing numerous hydraulic engineering problems. A prerequisite for arriving at such optimal solutions is that the complex physics of open channel flows can be understood. These flows, however, are typically turbulent, unsteady, and highly three-dimensional; they often take place in stratified environments, and can involve multiple phases. For that reason, their understanding continues to present hydraulic engineers with rather formidable challenge. Traditional approaches for studying natural river flows and morpho-dynamics study are based on field measurements and laboratory experiments. Owing to site and event specific concerns, field studies of natural open channel flows are very expensive, tedious and time consuming. Similar problems, although to a lesser extent, are associated with laboratory physical model studies, which further suffer from scale effects owing to non-similarity of one or more dominant non dimensional parameters. (Sinha *et al.*, 1998). In order to overcome above shortcomings, development of approaches that generally do not exhibit aforementioned difficulties were stressed upon to provide practising engineers with effective tool in the form of numerical models for understanding natural river flows in better way.

Although braiding seems to be best developed in rivers flowing over glacier outwash plains or alluvial fans, perfect braiding is also found to occur in large alluvial rivers having low slope, such as the Brahmaputra in Assam (India) and Bangladesh or the Yellow River in China. The Assam section of the Brahmaputra River is in fact, highly braided and characterized by the presence of numerous lateral as well as mid channel bars and islands (Goswami and Das, 2000). Due to these facts, the research on Brahmaputra River in the past mostly relied on field investigation and physical modelling. Only after 1980s, numerical modelling, especially 1-D modelling has been gradually applied in flow simulation and sediment prediction in Brahmaputra River (Sharma, 2004). Yet success full implementation of 2-D depth averaged modelling in Brahmaputra River reaches in Assam Flood Plains is hardly found in literature due to its highly complex topography

and difficulty in reproduction of geometric data mathematically.

1.2 NEED FOR 2-D OR 3-D MATHEMATICAL MODELLING OF BRAIDED RIVERS

The geometric complexities along with the changing upstream and downstream flow conditions induce very complex three dimensional turbulent shear flows which are characterized by secondary currents, vortex formation, flow reversal, and anisotropy effects. The difficulty in modelling natural river flow is best underscored by the fact that the vast majority of existing numerical models have focused primarily on the study of rivers of simplified geometries. In 1-D mathematical modeling, a number of assumptions are made to achieve feasible solution, yet information with regard to secondary flow field especially transverse flow field is absent. The secondary flow including transverse flow is one of the important causative factors of relentless bank erosion due to severe braiding process in Brahmaputra. Where the flow scenario is within reach flows, and the geometry is complex, at least a 2-D or even a 3-D treatment is required. 1-D modelling can neither generate the bar pool riffle topography commonly found in natural rivers nor adequately simulate the associated local variation in flow and sediment transport conditions. River meanders and plan-form have strong circulation associated with bed topography with water surface gradients and associated pressures. Flow field have both topographic as well as bottom shear stress terms. It implies that application of *CFD* with topographic 1-D modeling fails when there is significant flow variability in either the vertical or the cross stream direction commonly associated with secondary circulation due to flow curvature or turbulence. For predicting the magnitude and timing of an out of bank flow, 1-D models is adequate provided proper attention is given to cross-section spacing and model calibration. However, where the interest lies within reach flow with variability, one need a 2-D, if not a 3-D, treatment. (Bates, *et al.*, 2005)

Several two-dimensional numerical models especially with braided/meandering configuration have been developed to simulate braided rivers (Enggrob and Tjerry, 1999; Lien *et al,,* 1999; Jang and Shimizu, 2007 etc.). However, vast majority of existing numerical flow models have focused primarily on rivers of simplified geometries. More

recently, numerous 2-D and 3-D numerical-empirical models have been developed to simulate morphological changes in channels with mobile bed and bank, both in the laboratory and field. However, these models have some limitations when it comes to treating relatively shallow, wide braided rivers with highly irregular bed profile and complex bank-lines resulting in dominant transverse flow field.

1.3 NEED FOR ASSESSMENT OF SECONDARY FLOW IN BRAIDED BRAHMAPUTRA RIVER

Secondary currents, occur in the plane normal to the axis of the primary flow, they originate from interactions between the primary flow and gross channel features (Prandtl, 1952). Secondary transverse flow results from the imbalance between transverse water surface gradient force and centrifugal forces over the depth due to vertical variation of the primary flow velocity (Lien *et al.*, 1999). In braided rivers, most channel changes are associated with changes in bed morphology, which occur at high discharges, observation is very difficult (Smith, 1970). Any mention of secondary currents in braided systems has been restricted to areas of channel confluence, and the effect of secondary currents in bifurcations and around braid bars has been largely neglected (Sankhua, 2005). A number of attempts have been done to catch the realistic flow field including transverse components in complex geometry like bends, curves (Lien *et al.*, 1999; Odgaard, 1989a; Duan, 2004; Seo *et al.*, 2008). However, assessment of flow-field in braided river with 'secondary flow correction' in complex geometry is hardly found in literature. Estimation of an improved flow field in braided river is expected to lead to realistic assessment of bed changes and bank erosion in braided rivers.

1.4 EARLIER RESEARCH

The difficulty in modelling natural river flow is best underscored by the fact that the vast majority of existing numerical models have focused primarily on the study of rivers of simplified geometries. The initial attempts of significance in application of mathematical models in conjunction with empirical functions obtained from laboratory experiments to the investigation of morphological processes can be found in the 1950s. Later, the

research was intensified and broadened in the 1970s. Since then, a number of 1-D models (*e.g.,* Cunge *et al.*, 1980; Thomas, 1982; Rahuel *et al.*, 1989; Wu and Vieira, 2002) were applied to sedimentation studies in reservoirs and rivers. More recently, numerous 2-D and 3-D numerical-empirical models (e.g., Sheng, 1983; Wang and Adeff, 1986; Spasojevic and Holly, 1993; Jia and Wang, 1999; Wu *et al.*, 2000,) have been developed to simulate sediment transport processes and morphological changes in channels with mobile bed and bank, both in the laboratory and nature. Flow in nature is three dimensional and usually turbulent. 3-D numerical models have been developed (Leschziner and Rodi, 1979; Shimizu *et al.*, 1990; Sinha *et al.*, 1998) to simulate spiral motion/secondary flows. However, 3-D numerical models are yet to be fully and adequately developed for channel with complex bathymetry in long river reaches. In many cases the geometry of the flow boundaries is very complex. Solving the equations of motion in these conditions is very difficult and computationally tedious. In rivers where the width of the flow is large compared to its depth, the vertical acceleration of water is negligible compared to the gravitational acceleration. In this condition, the pressure distribution in depth can be assumed to be hydrostatic and the equations of motion can be integrated in depth to derive two-dimensional depth averaged equations. Irregular boundaries of rivers, however, add to the complexity of these models (Zarrati *et al.*, 2005).

Understanding the processes of morphological behavior in braided rivers is very important for river engineering purposes and prevents disasters from flood, bank erosion and environmental purposes to maintain river ecosystem. The morphological changes of rivers are deeply interrelated to the bed deformation and bank erosion because of the mutual relationship between water flow and sediment transport. In the process of channel development, bars emerge under certain hydraulic conditions as the channel widens from an initially straight channel, with erodible bed and banks (Jang and Shimizu, 2007). Previous investigations examined the mechanical processes of channels with erodible banks theoretically (Ikeda *et al.*, 1981; Parker *et al.*, 1982), and have provided a method to reproduce lateral changes in the channel. In due course, several numerical models have been developed to reproduce braided rivers with fixed banks (Murray and Paola, 1994) and with erodible banks (Sharma, 2004). Numerical models to reproduce the evolution of

meandering channels, taking bank erosion into consideration, have been developed for beds and banks made of uniform sediment (Shimizu *et al.*, 1996; Nagata *et al.*, 2000). Murray and Paola (1994, 1997) reproduced the spatial and temporal features of braided rivers using a relatively simple cellular numerical model in a fixed grid system. Two-dimensional numerical models have been developed to simulate braided rivers (Enggrob and Tjerry, 1999; McArdell and Faeh, 2001; Shimizu *et al.*, 2001). However, these models have some limitations when it comes to treating a relatively shallow, wide channel with moving boundaries due to channel widening, i.e. braided rivers with unconstrained banks. Jang and Shimizu (2005a) proposed a numerical model to simulate braided rivers with erodible banks, and showed the possibility of simulating braided rivers considering bank erosion. Jang and Shimizu (2005a, 2005b and 2007) developed a two dimensional model to simulate the processes of channel evolution from an initially straight channel with relatively high width to depth ratio and erodible banks composed of non-cohesive materials. However, this model had not been verified for a natural braided river with complex bathymetry although model results were compared with laboratory experiments. Jang and Shimizu (2007) found some discrepancies in the model and attributed these discrepancies in computed results to assumed parameters, initial conditions and three dimensional flow features at confluences.

1.5 PROBLEM IDENTIFICATION

As one can observe, a number of investigations have been done so far to develop numerical models to represent the processes involved in wide braided river, correct process representation of the river morpho-dynamics is yet to be achieved by improving features like impact of secondary flow due to channel bends and turbulence on flow field. The intense braided rivers, like the Brahmaputra are hydraulically less efficient, and the formation of braid bars plays an important role in the dissipation of the energy due to friction.

In the above backdrop, the intense variability and complexity of the fluvio-morphological features of the Brahmaputra River is attempted to be captured in sufficient details with development of 2-D depth averaged hydrodynamic numerical model in identified reaches

for Brahmaputra River extracted with remote sensing data analysis to critically analyse the effect of flow features for better understanding of braided river behaviour.

1.6 OBJECTIVE OF THE STUDY

In line with the aforementioned strategy, in the proposed research work, the following objective(s) are set in the mind with the application of updated principles and practices of numerical model development for fluvial morpho-dynamics as well as remote sensing data usage.

i. To derive the appropriate set of mathematical expressions for the secondary flow correction (flow dispersion stress tensor) for depth averaged 2-D model to be used for non-orthogonal curvilinear flow domain.

ii. Development of numerical algorithm using finite volume method to solve conservative form of governing equations in non-orthogonal grids with incorporated flow dispersion stress terms in momentum equations and compare the results of flow model with and without flow dispersion for general curved channels.

iii. Application and verification of the proposed numerical model for the Brahmaputra River in selected reach and possible identification of braiding pattern with variability in stage-discharge.

iv. To evolve a simplified braiding indicator to express the measure of braiding intensity for a river reach with incorporated no flow zone within the flow domain.

1.7 THE STUDY AREA

The reach between measured cross sections number-22 (Pandu near Guwahati) to 9 (Jogighopa) released by *Brahmaputra Board, G.O.I.* (spanning over approx. 100 km length in Assam state of Indian Territory) is selected for flow simulation.

1.8 DATA COLLECTED AND USED

Fourteen measured river cross-section data (Cross-section no. 22 to Cross section no. 9) for the year 1997 were used. Discharge data of the river Brahmaputra during 1997 was used in the study (*Central Water Commission* and *Brahmaputra Board, G.O.I.*). The digital satellite data comprising scenes of Indian Remote Sensing (*IRS*) Linear Imaging Self Scanner (*LISS-III*) sensors for the year 1997 (*Unpublished report of National Disaster Management Authority, Govt. of India*) for the study area, have been used.

For proposed model verification and evaluation, an experimental flume of test section (4.25m×0.15m×0.20m) comprised a contraction in between with 0.002 m^3/s of constant discharge was simulated.

1.9 THE METHODOLOGY

The boundary fitted coordinate system has been used to describe a naturally shaped boundary to represent the complex flow domain. The ξ-axis is drawn along the channel for a given channel shape and η- axis is set to intersect the ξ-axis, Then the plane (ξ, η) is divided into the structured cells to form the mesh for computations using Poisson's equation. The governing equations for estimating flow field, transformed from Cartesian co-ordinate system to a Boundary fitted curvilinear co-ordinate system have been used to represent flow domain. Finite volume method conserves mass-momentum and can be suitably applied for highly complex geometry using non-orthogonal grids. The flow field is computed at geometric cell centers using the Finite Volume Method using *SIMPLEC* algorithm. Rhie and Chow's (1983) interpolation technique is used to estimate the velocities at cell faces. The flow field and water depth are computed using the derived transformed governing equations with special attention to boundary implementation. The river braiding is simulated with incorporation of wetting and drying technique into the numerical solver. A *C++* computer code has been developed for numerical model to simulate flow field and mesh generation.

1.9.1 PROPOSED GOVERNING EQUATIONS

The governing equations for flow simulation are *RANS* (Reynolds Averaged Navier Stokes) equations with depth averaged approximation of continuity and momentum

equation in generalized curvilinear coordinate system. Components of dispersion stress terms are included in momentum transport equations as additional source/sink term. The derivation of dispersion stress tensor is done step by step to get revised set of empirical relations to be used in subsequent development of enhanced 2-D numerical flow model. The derived expressions are modifications to earlier relevant investigations (Duan, 2004; Duan and Julien, 2005). The proposed formulations are with simplified mathematical representation and are numerically compatible. These also improved the flow field simulation reasonably.

1.10 OUTCOME OF THE DEVELOPED 2-D MODEL AND SALIENT CONTRIBUTION OF THE PRESENT RESEARCH WORK

1-D flow models are insufficient to tackle problems of braided streams due to lack of information with regard to transverse flow field. So, 2-D or 3-D models are used. 3-D models are numerically expensive for macro scale river reaches. Hence, 2-D enhanced model was developed. Most of the 2-D models developed especially for braiding rivers did not account for secondary flow correction probably presuming these corrections to be insignificant for turbulent flows and mild curved bank-lines. But in complex flow situation with considerable braiding, the secondary flow correction is suitably justified to achieve improved flow scenario with nominal additional expense in respect to computational effort with including secondary flow correction using modified terms for dispersion stress tensor in the flow momentum equations

Developed model was initially verified with flume experiment operating a flow with a contraction, and the validation of the flow simulation was achieved. It is established from the model application in laboratory flume that redistribution of flow concentration in longitudinal and transverse directions are desirably accounted for, using the formulation in curvilinear flow field and are well capable of assessing realistic flow prediction with reasonable approximation.

The model developed in this study has been applied and verified in the selected stretch of Brahmaputra River. It was observed that the effect of dispersion stress tensor in flow

field increases with increase in braiding intensity. The model results lend support to this observation. When braiding intensity increases, it evolves multiple channels with meandering configurations within the domain of stream flow. Meandering and bend in evolved multiple channels instigate more discrepancy in the flow-field, if it is approximated with depth averaging. Braiding induces severe bank erosion, due to dominant transverse flow field. So, improved and realistic flow-field estimation will lead to realistic assessment of predictions of bank erosion and river bed evolution for braided alluvial rivers. Better erosion models can be developed with reasonable accuracy using estimated flow field as the prime input.

Based on the obtained results and information from flow simulation for twenty discharge profiles at receding flood of 1997 for Brahmaputra River stretch under this study, an indicator namely *braid power* is proposed based on the model output to express the measure of braiding for a river reach as follows.

$$braid\ power(\mathrm{N/m^2 \cdot s}) = f_{nf} \cdot \frac{\gamma Q_{inlet} S}{\text{flow Area of Inlet of the Reach}}$$

Where, f_{nf} =Ratio of no flow zone area with respect to whole flow domain area, γ=Unit weight of water ($\mathrm{N/m^3}$) and S=Average longitudinal slope of the study reach. Flow area ($\mathrm{m^2}$) is the cross-sectional flow area of the inlet boundary at the given discharge. It was observed that *braid power* increases with decrease in incoming discharge into the reach at a particular instance of time. The rate of decrease or increase of *braid power* depends upon geometric configuration of the reach at the particular instance of time along with other factors

1.11 LIMITATIONS AND SCOPE FOR FUTURE WORK

The numerical model developed in this research work is limited to flow field simulation in rivers with highly complex geometries and braided configurations. The prime thrust of the present research work is to bring to the fore persistent shortcomings in relation to flow field estimation for rivers with highly braided configuration. The present research work has desirably brought about a significant improvement in dominant transverse flow field estimation in highly braided rivers. The transverse flow field is one of the

significant causative factors for stream bank erosion resulting in huge land loss around the vicinity of braided rivers such as Brahmaputra River. However, to model bank erosion and bed evolution with high degree of accuracy, after further research, a robust 2-D sediment module with incorporated bank erosion mechanism, clubbed with the present enhanced flow simulation model is required to be developed. To model the moving boundaries, present developed model uses fixed boundary method through implementation of wetting and drying technique including the whole flood plain under the flow domain. However through conducting further research on advanced algorithm using depth adaptive grid generation and temporal deformed mesh technique; moving boundary can possibly be implemented to simulate the multiple channels actual flow zones instead of considering the whole flood plain. However, at present numerical implementation of the aforesaid process is quite complex for highly braided rivers with multiple channels like Brahmaputra and possibly be a potential area of research.

1.12 ORGANISATION OF THESIS

The chapters are organized in the following way

Chapter -1 Description of introductory aspects of the topic studied, underlying objectives and the layout of the thesis.

Chapter-2 Presentation of a relevant comprehensive review of literature and in addition the objective of the present study is also explained.

Chapter-3 Description of the study area

Chapter- 4 Presentation of development of modified dispersion stress tensor in two dimensional curvilinear flow field

Chapter -5 Presentation of formulation of 2-D depth averaged equations for curvilinear domain

Chapter- 6 Presentation of numerical development of mesh generation algorithm for complex physical domain

Chapter-7 Presentation of numerical 2-D hydrodynamic model development for braided river with complex flow domain

Chapter-8 Data acquisition, pre-processing and application

Chapter-9 Presentation of evaluation of the developed numerical model

Chapter-10 Presentation of results and analyses of 2-D flow simulation for Brahmaputra River stretch

Chapter- 11 Presentation of conclusions and scope for future work

Bibliography

Furthermore, at the end of the thesis eight annexure are placed for ready reference.

Appendix I Derivation of Duan (2004)'s dispersion tensor

Appendix II Derivation of stream wise and transverse angles (θs, and θn), trapezoidal rule with non uniform Δy for area computation.

Appendix- III Scanned soft copy of standard Brahmaputra map showing chainage and bearings of pre-defined cross sections

Appendix-IV Graphical data for fourteen field measured predefined cross sections

Appendix-V Graphical processed data for normalized measured cross sections for the image extracted flow domain

Appendix-VI Salient features and computer code modules in *C++* programming language on numerical solution for mesh generation/ flow model.

Appendix –VII Summarized experimental laboratory data for conducted experiment and model results.

Appendix -VIII List of relevant communicated research papers

CHAPTER-2

LITERATURE REVIEW

2.1 INTRODUCTION

The study of alluvial river attempts to explain and describe the typical features of the river. These features appear as a result of complex dynamics of flow over a mobile bed. Channel morphology changes with time and is affected by water and sediment discharge including sediment characteristics, composition of bed and bank materials, and vegetation. The prediction and post-diction of fluvial system behaviour is greatly complicated by the variability of fluvial system morphology and dynamics through time. Moreover, most rivers have been affected by human interventions to one degree or another, so their current condition results from the interplay of the river and social system Within the river system flow regime (Q) and sediment load (Q_s) from the basin are the independent variables that largely determine alluvial channel form as reflected in the adjustments of dependent variables of width, depth, grain size, and pattern (Kondolf *et al.*, 2003). Channels change in different ways through the process of erosion and deposition. Yet considerable uncertainty in its prediction for non-uniform sediments is experienced (Patel *et al.*, 2010). It is often difficult to mathematically represent sediment process into the river modelling. Almost in all cases, river bed profiles are irregular in shape and size. For representing these profiles, mathematical functions are generally used in the conventional methods of idealization. But, the representation becomes difficult when the river geometry exhibits significant variability and complex patterns. The complexity in representing this information is made somewhat easier and quick by application of remote sensing technique clubbing with 2-D hydrodynamic mathematical modeling for better understanding of channel hydrodynamics. A thorough understanding of the morphology of alluvial streams presupposes detailed knowledge of their plan-form characteristics. The plan-form of alluvial streams can be classified into the following three categories:

2.1.1. BRAIDED STREAM

A braided stream can be defined as one which flows in two or more channels around alluvial islands. Leopold and Wolman (1957) stated that braided pattern in alluvial stream develops after local deposition of coarse material, which cannot be transported under local conditions of flow existing within the reach. This coarse material becomes the nucleus for a bar formation, and subsequently grows into an island made up of coarse as well as fine material. The formation of the bar deflects the main stream towards the banks and may cause bank erosion.

2.1.2. MEANDERING STREAMS

A sinuous channel is called meandering stream. It consists of regular or irregular pattern of loops and a distinct sinuous plan-form. A meandering river has a single flow channel, while a braided river has a number of channels (Richards, 1982).

Leopold and Wolman (1957) have defined sinuosity of a stream as the ratio of the thalweg length to the valley length (Figure 2.1). They have arbitrarily classified streams with sinuosity greater than 1.5 as meandering streams. Friend and Sinha (1993) defined the meandering parameter (Sinuosity) as modified sinuosity parameter, and presented as

$$P = L_{cmax} / L_R \tag{2.1}$$

where, P = Modified Sinuosity Parameter, L_{cmax} = mid-channel of the widest channel, where, there is more than one channel and L_R = overall length of the meander belt reach measured along a straight line (Sankhua, 2005).

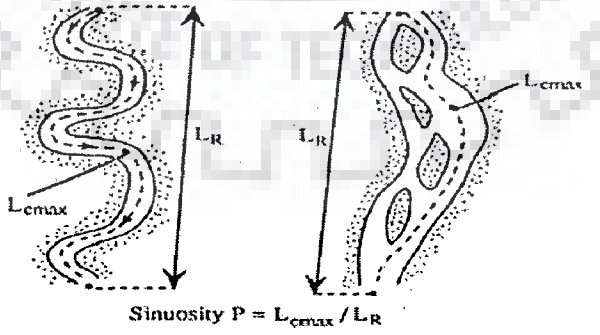

Figure 2.1 Schematic diagram representing the computation of sinuosity for single channel and multi-channel rivers

2.1.3. STRAIGHT STREAMS

A stream in this classification refers to one that does not have a distinct meandering pattern. It is extremely difficult to find straight reach of stream over large lengths. Straight reach implies neither constant depth of the channel nor a straight thalweg. Even though the channel is straight; the line of maximum depth commonly known as thalweg moves from one bank to another bank (Richards, 1982).

2.2 MEASURE OF THE BRAIDING INTENSITY AND EXISTING BRAIDING INDICATORS

Several past studies had presented discrimination between the straight, meandering, and braided streams on the basis of discharge and channel slope. Lane (1957) suggested the following criterion for the occurrence of braiding.

$$S > 0.004 (Q_m)^{-0.25} \quad (2.2)$$

Where, Q_m = mean annual discharge; and S = channel slope.

Using bank full discharge Q_b, Leopold-Wolman in 1957 (Richards, 1982) proposed the relationship for braiding to occur, which also predicts braids at higher slopes and discharges:

$$S > 0.013 Q_b^{-0.44} \quad (2.3)$$

Where, Q_b = bank full discharge.

Antropovskiy (1972) developed the following criterion for the occurrence of braiding

$$S > 1.4 Q_b^{-1} \quad (2.4)$$

Leopold-Wolman (1957) also indicated that braided and meandering streams can be separated by the relationship:

$$S = 0.06 Q^{0.44} \quad (2.5)$$

where, S = channel; and Q = water discharge.

However, these indicators have been criticized by Schumm and Khan (1972) as none of these recognizes the importance of sediment transport. These results imply a higher power expenditure rate in braided streams, a conclusion reinforced by Schumm-Khan's (1972) flume experiments. However, none of these investigators recognizes the control of channel pattern by sedimentology. Since, bed material transport and bar formation are necessary in both meander and braid development processes, the threshold between the patterns should relate to bed load.

Henderson (1961) re-analyzed Leopold-Wolman's data to derive an expression including d_{50}, median grain size (mm):

$$S > 0.002\, d_{50}^{1.15}\, Q_b^{-0.46} \qquad (2.6)$$

Where, d_{50} = median grain size

According to Eq. (2.6), a higher threshold slope is necessary for braiding in coarse bed materials. Bank material resistance affects rate of channel migration and should also influence the threshold, although its effect may be difficult to quantify and also be non-linear since greater stream power is required to erode clays and cobbles than sands.

Parker's stability analysis (1976) indirectly illustrates the effects of bank material resistance by defining the meander - braid threshold as:

$$S/F_r = D/B \qquad (2.7)$$

where, D = mean depth of the flow; B = width of the stream, and Fr = Froude number. However, depth, width and Froude number may be expressed in terms of discharge and bank silt-clay percentage, as suggested by Schumm (Richards, 1982). Meandering occurs when $S/Fr \leq D/B$, braiding occurs when $S/Fr \geq D/B$, and transition occurs in between $S/Fr \sim D/B$.

Ferguson (1981) suggested for braiding to occur, which predicts steeper threshold slopes for braiding in channels with resistant silty banks.

$$S>0.0028(Q_b)^{-0.34}B_c^{0.90} \qquad (2.8)$$

where, B_c = percentage of silty clay content in the bank material.

Measures of the degree of braiding generally fall into two categories:

(i) the mean number of active channels or braid bars per transect across the channel belt and

(ii) the ratio of sum of channel lengths in a reach to a measure of reach- length (total sinuosity). The sinuosity, P is thalweg length / valley length.

Smith (1970) illustrated the measurement of cross-section bed relief, measured by the index.

$$BRI = \frac{2[(T1 + T2 \ldots\ldots..Tn) - (t1 + t2 + t3 + \ldots\ldots.tn)] \pm Te_1, Te_2}{B_L} \quad (2.9)$$

where, T_i = height maxima between hollows, t_i = minima between peaks, B_L= transect length and T_e = end heights.

Sharma (2004) developed Plan Form Index (*PFI*), Flow Geometry Index (*FGI*), and Cross-Slope ratio for identifying the degree of braiding of highly braided river. He mentioned that the braided channels are hydraulically less efficient. Also, the formation of braid bars plays an important role in the modification of the energy losses due to friction. With a view to incorporating the effect of the above hydraulic variables, he proposed new indices namely *PFI, FGI* and *Cross- Slope* formulae have been given below:

$$\text{Plan Form Index} = \frac{\frac{T}{B} \times 100}{N} \quad (2.10)$$

$$\text{Flow Geometry Index} = [\frac{\sum d_i x_i}{W \times D}] \times N \quad (2.11)$$

$$\text{Cross-Slope} = \frac{\frac{B_L}{2}}{(Bank\ level - Av.\ bed\ level)} \quad (2.12)$$

where, T = flow top width (m), B= overall width of the channel (m), B_L= transect length across river width, N= number of braided channel, d_i and x_i are depth and top lateral distance of submerged sub-channel, and D = hydraulic mean depth.

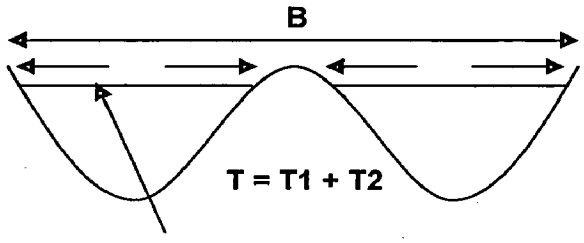

Figure 2.2 Definition sketch for *PFI*

Plan Form Index (*PFI*) in Eq. (2.10) (Definition sketch as shown in Figure 2.2) reflects the fluvial landform disposition with respect to a given water level and its lower value is indicative of higher degree of braiding. It is expressed in percentage, which shows the fluvial landform disposition with respect to a given water level and its lower value indicates higher degree of braiding. For providing a broad range of classification of the braiding phenomenon, the following threshold values for *PFI* are proposed by Sharma (2004).

Highly Braided: $PFI < 4$
Moderately Braided: $19 > PFI > 4$
Low Braided: $PFI > 19$

Braided river reaches and alluvial systems are abundant in many areas. They are characterized by their multi-threaded plan-form, and are agents of substantial sediment transport, erosion and deposition. The high rates of sediment transport, erosion and deposition, and the frequent shifting of river channel positions in braided rivers pose many problems to a whole range of disciplines. Despite this importance, they have been relatively neglected in academic study when compared with the wealth of material on meandering rivers. The majority of studies to-date have been qualitative in nature, with Howard *et al.* (1970) and Murray and Paola (1994) being notable exceptions.

The neglect of braided river study is partly due to the difficulty of undertaking field work and characterizing complex features. Although, advances have been made in the qualitative understanding of flow and sediment processes in braided systems, Bristow and Best (1993) have identified several key issues that remain to be addressed, such as (a) the

mechanisms of braid bar genesis and evolution, (b) flow and sediment dynamics at bifurcations and confluences, (c) the influence of flow stage on plan-form development, (d) the implications of a channel hierarchy system found over a range of channel scales and (e) the influence of secondary currents on the morphological development of braid bars.

Many of the existing braid indicators do not adequately account for the hydraulic parameters and the underwater bars, both of which are seen to have a close relationship with the braiding process. Hence, it can be concluded that there is still a need to formulate new braid indicators by incorporating the above indicators to have a more rational description of the braiding phenomenon. However, newer braiding indicator proposed by Sharma (2004) was used to evaluate the efficacy of its rational use in real physical scenario using temporal as well as spatial remote sensing data analysis of Brahmaputra River (Sharma and Akhtar, 2010).

2.3 NEED FOR 2-D OR 3-D MATHEMATICAL MODELLING OF BRAIDED RIVERS

The geometric complexities along with the changing upstream and downstream flow conditions induce very complex three dimensional turbulent shear flows which are characterized by secondary currents, vortex formation, flow reversal, and anisotropy effects. The difficulty in modelling natural river flow is best underscored by the fact that the vast majority of existing numerical models have focused primarily on the study of rivers of simplified geometries. In 1-D mathematical modelling, a number of assumptions are made to achieve feasible solution, yet information with regard to secondary flow field especially transverse flow field is absent. The secondary flow including transverse flow is one of the important causative factors of relentless bank erosion due to severe braiding process in the Brahmaputra. Where the flow scenario is within reach flows and the geometry is complex, at least 2-D or even a 3-D treatment is required. 1-D modelling can neither generate the bar pool riffle topography commonly found in natural rivers nor adequately simulate the associated local variation in flow and sediment transport conditions. River meanders and plan-form have strong circulation associated with bed

topography with transverse water surface gradients and associated pressures. Resulting flow field has both topographic as well as bottom shear stress terms. It implies that application of *CFD* with topographic 1-D modelling fails when there is significant flow variability in either the vertical or the cross stream direction commonly associated with secondary circulation due to flow curvature or turbulence. For predicting the magnitude and timing of an out of bank flow, 1-D models are adequate (provided proper attention is given to cross-section spacing and model calibration). However, where the interest is within reach flow with variability, one needs a 2-D, if not a 3-D, treatment (Bates, *et al.*, 2005).

Several two-dimensional numerical models have been developed to simulate braided rivers (Enggrob and Tjerry, 1999; Lien *et al.*, 1999 etc.). However, vast majority of existing numerical flow models have focused primarily on rivers of simplified geometries. More recently, numerous 2-D and 3-D numerical-empirical models have been developed to simulate morphological changes in channels with mobile bed and bank, both in the laboratory and field. However, these models have some limitations when it comes to treating relatively shallow, braided rivers with highly irregular bed profile and complex bank-lines resulting in dominant transverse flow field.

2.4 INFLUENCE OF SECONDARY CURRENTS IN BRAIDED CHANNELS

Secondary currents have originally been defined by Prandtl (1952) as currents, which occur in the plane normal to the axis of the primary flow, they originate from interactions between the primary flow and gross channel features. Two types of secondary currents have long been recognized; skew induced and stress induced secondary currents.

There have been few field and laboratory investigations of flow structures in braided rivers and as a consequence their link to braided morphology is little understood. Unlike meandering single-thread rivers, in which observations of key flow processes can be undertaken over a range of flow stages, in braided rivers most channel changes are associated with changes in bed morphology, which occur at high discharges when observation is very difficult (Smith, 1974; Rust, 1978b). Any mention of secondary

currents in braided systems has been restricted to areas of channel confluence, and the effect of secondary currents in bifurcations and around braid bars has been largely neglected(Sankhua, 2005).

Mosley (1976) reported the presence of helical flow at channel confluences in a general flume experiment of confluence behaviour. Using dye injection to visualize flow patterns, he observed that the pattern of secondary flow at channel confluences consisted of a pair of helical cells, converging in the channel centre over the point of maximum scour and diverging at the bed. He concluded that the observed helical flow pattern resulted in steepening of the scour walls beyond their natural angle of repose, giving rise to their characteristic avalanche faces. Mosley further stated that the helical flow structure resulted in most of the sediment transport in the confluence occurring at the channel fringes away from the area of maximum scour. There is also evidence found for smaller cells of reverse rotation further downstream from the channel confluence, resulting in elevated portions of the bed flanking the channel centre line. Mosely (1976) observed that this secondary flow pattern resulted in high rates of sediment transport restricted to the zones between opposing cells.

Best and Roy (1991) proposed that these secondary flow patterns are the result of horizontal separation vortices formed in the toe of the avalanche faces at the entrance to the confluence, particularly when the converging channels are of unequal depth. Another probable cause of the helical circulation is the same mechanism that causes helical flow in meander bends, *i.e.* the relationship between the outwardly directed centrifugal force and the inwardly directed pressure gradient force caused by super-elevation. In the case of channel confluences the centrifugal force would be acting towards the confluence centre and the pressure gradient force would be acting towards the confluence fringes. Mosley (1976) observed a degree of super-elevation in the centre of their model confluences. Ashmore *et al.* (1992) proposed that the flow separation at the confluence entrance probably reinforced, rather than replaced, the circulation due to channel curvature.

Ashmore *et al.* (1992) carried out a field investigation of secondary flow patterns in river confluences on the gravely Sunwapta River, Alberta. They confirmed for the first time in a real river the existence of the secondary flow patterns observed in laboratory experiments by Mosley (1976). Ashmore *et al.*(1992) made measurements in two Y shaped anabranch confluences at relatively high discharge levels and found that the pattern of secondary flow observed in laboratory experiments existed in both of the surveyed cross-sections, although the pattern was much stronger in one of the confluences. In both confluences, the larger of the two helical cells tended to dominate the other in the downstream direction. They conceded that the methods employed to correct velocities in meandering rivers were inappropriate for braided rivers and as a result the flow patterns reported may be susceptible to small errors.

2.5 MODELLING OF BRAIDED RIVER

2.5.1 BACKGROUND OF NUMERICAL MODELLING

Numerical analysis of fluid flow in complex geometrical domains has been the focus of quite a few researchers in the past decade. Such flows typically are representative of those situations occurring in a numerous variety of practical engineering problems. Examples can be found in such diverse areas as aerodynamics, meteorology, nuclear reactor design, compact heat exchangers, turbo-machines, the cooling of electronic packages and river hydrodynamics. The numerical prediction of fluid flow has evolved over the last two decades into an established field known as Computational Fluid Dynamics and often referred to by the acronym *CFD* and within its domain, in case of river hydraulics, it is popularly known as computational river mechanics.

Numerical codes are structured around the numerical algorithms that deal with fluid flow problems. There are four major streams of numerical solution techniques: finite difference, finite volume, finite element, and spectral methods. All numerical methods that form the basis of the solver follow the same steps. These steps are:

2. 5.1.1. Domain discretization

Division of the computational domain into several control volumes, location of nodes at the geometric center of the control volumes, and systematic numbering of nodes constitutes domain discretization. Nodes are the locations (points) where unknowns are calculated.

2.5.1.2 Development of discretization equations

In this step the exact mathematical operations, such as partial derivatives, are converted to approximate algebraic expressions at various nodes.

2.5.2.3 Solution of discretization equations

A set of linear equations, obtained as a result of step mentioned in above section-2.5.1.2, are solved to obtain the values of the variables at various nodes. The manner in which the discretization equations are obtained determines the technique. For example in the finite difference technique the discretization equations are obtained by differentiation. In the finite element technique the discretization equations are obtained by integration. In the finite volume technique the discretization equations are obtained by a combination of differentiation and integration. Finite Volume and finite element are the two methodologies employed most commonly in broader field of Computational Fluid Dynamics (*CFD*). With regard to the task of computing flows in complex geometries, the finite element method appears to be the most natural tool, because of its better geometric flexibility.

2.5.2 REVIEW ON NUMERICAL MODEL DEVELOPMENT IN RIVER MECHANICS

Fluvial geo-morphologists are increasingly using computational fluid dynamics methods to improve understanding of the interactions between channel morphology, discharge, flow structure and sediment transport. If such models can provide an adequate representation of key processes, they have the potential to increase significantly our understanding of river channel dynamics. First, they may increase the spatial density of information beyond what is possible through field measurement. Process investigation in the field is largely based upon point measurement of velocity or sediment transport

processes. A large number of sample sites may be required to obtain sufficient representation of spatio-temporal process characteristics, and this takes time, over which the processes themselves may change (Lane *et al.*, 1999). River morphodynamics is the interaction between hydrodynamics, sediment transport, bank erosion and bed morphology. As a consequence of this interaction, planform migration of the river due to erosion of the banks, widening of the river, degradation and aggradation of the bed, evolution of bedforms and variations in suspended concentrations may result (Abad *et al.*, 2007). To analyse these processes, several approaches have been developed. Theoretical approaches such as Ikeda *et al.* (1981), Johannesson and Parker (1989a), Parker et al. (1982) and Seminara *et al.* (2001) for the case of models in meandering rivers, experimental such as Guy *et al.* (1966), Hooke (1974) and Garcia and Nino (1993) where bed morphology has been studied under fixed-bank meandering channels, or numerical models such as Lyn (1987), Celik and Rodi (1988), Correia *et al.* (1992), Howard (1992), Jin and Steffler (1993), Mosselman (1998), Nagata *et al.* (2000b), Duan *et al.* (2001), Sun *et al.* (2001a), Cao *et al.* (2002), Darby and Delbono (2002), Kassem and Chaudhry (2002), Soulis (2002), Wilson *et al.* (2003), Duc *et al.* (2004) and Vasquez (2006) where applications of models have been presented. The hydrodynamics and morphodynamics of a meandering channel are physically complex, involving diverse phenomena such as secondary flows (also known as helical flow or spiral flow), turbulent flows, sediment transport and bank erosion processes. The Computational Fluid Dynamics (*CFD*) field has been an area of constant improvement, where high-resolution and detailed studies to describe the mean and turbulence structures of laboratory and natural channels have been carried out successfully. For the case of solely meandering configurations, Leschziner and Rodi (1979) conducted 3-D modelling of a single constant-curvature bend (Rozovskii, 1957) under flat conditions, Morvan *et al.*(2002) presented a 3-D hydrodynamic model of a meandering compound channel under flat conditions, Wu *et al.* (2000) presented a 3-D numerical model for hydrodynamic and sediment transport modelling of a single bend (Odgaard and Bergs, 1988), Ferguson and Parsons (2003) reported 3-D numerical modelling of a meander bend with recirculation along the inner bank, and Abad and Garcia (2005) presented a 3-D hydrodynamic numerical simulation of periodic meandering channels at different sinuosities where the importance of

convective accelerations due to bed configurations was described. Even although 3-D numerical simulations are increasingly popular in river studies, its applicability to study morpho-dynamics processes such as erosion/deposition and meander migration is limited since it requires sophisticated implementation of boundary conditions (Ingham and Ma, 2005; Sotiropoulos, 2005) and applications are possible generally for micro or meso scale with small scale time domain cases. Under certain considerations and limitations (Wang and Ribberink, 1986; Lane and Ferguson, 2005), it is possible and even preferred to use 2-D depth-averaged models or even cross-section averaged 1-D models to overcome this problem (Garcia, 2001), in particular for certain engineering applications. The 2-D depth averaged models with secondary flow correction can readily be applied to larger spatial domains with computational ease. Similarly turbulence models such as developed in Erpicum et al. (2008 and 2009) have also been developed for macro rough channel and validated in experimental flumes.

Several 2-D models have been developed to reproduce braided rivers with fixed banks (Murrey and Paula 1994). Dammular *et al.* (1989) presented a 2-D for unsteady flow in curved channel. The results of the numerical model are compared to laboratory test data for the unsteady flow created by an instantaneous dam failure in a test facility (Miller, 1988). Numerical models to reproduce the evaluation of curved channels taking bank erosion into consideration have been developed for bed and banks of non cohesive sediment (Shimizu *et al.*, 1996; Nagata *et al.*, 2000). However these models have some limitations to simulate braided rivers with unconstrained banks. Jang and Shimizu (2005a, 2005b and 2007) proposed a numerical model to simulate braided rivers with erodible banks composed of well sorted material using moving boundary co-ordinate system to naturally shaped boundary and showed possibility of simulating braided river with complex geometries. Jang and Shimizu (2005a, 2005b and 2007) observed that the model somehow reproduces features of braided rivers such as generation of new channels and abandonment of old channel, the bifurcation and confluence as well as channel migration. However this model had not been verified on a natural braided river with complex bathymetry, although model results were compared with laboratory experiments in a controlled environment. Jang and Shimizu (2005a, 2005b and 2007) found some discrepancies in the model and attributed these discrepancies in computed results to

assumed parameters, initial conditions and three dimensional flow features at confluences which indicate that the model itself warrant further improvement in view of real and complex application scenarios.

2.5.3 REVIEW ON 2-D DEPTH AVERAGED MODELLING WITH SECONDARY FLOW CORRECTIONS

The occurrence of the secondary flow is one of the dominant features of flows in bends. Secondary flow results from the imbalance between the transverse water surface gradient force and centrifugal force over the depth due to the vertical variation of the primary flow velocity. In other words, the inward pressure gradient near the bed prevails over the centrifugal force resulting in an inward flow along the bed and an outward flow near the water surface (Lien *et al.*, 1999). This circulatory flow pattern is termed as secondary flow. Measurements by Rozovskii (1961) and de Vriend (1979, 1980 and 1981) have shown that the secondary flow near the water surface moves toward the outer bank, and that near the bed moves toward the inner bank. Consequently, the shear force, which has the same direction as the local flow close to the bed, deviates slightly from the direction of the mean flow (Engelund and Skovgaard 1973).

Pioneering investigations of the flow phenomena in open-channel bends are generally attributed to Thompson (1876) who observed the spiral motion inherent in a channel bend by introducing seeds and dyes into the flow. The 3-D numerical models have been developed (*e.g.* Leschziner and Rodi 1979; Shimizu *et al.* 1990; Sinha *et al.* 1998) to simulate the complicated spiral flow motion in the bend or channel curves. However, 2-D depth-averaged models are often adopted in practice by hydraulic engineers because of their easy implementation and application as mentioned earlier. For 2-D bend-flow modelling, steady-flow models, such as that of Odgaard (1989), have been developed to avoid the possible numerical instability and large amount of computation time. Yen and Ho (1990) developed a numerical model for the simulation of bed evolution in channel bends with fixed walls. They followed Odgaard's concept and adopted several published approximations of the transverse velocity distribution to reduce the depth-averaged water flow equations. An alternative approach for describing bend flow is to use the concept of

moment of momentum (Falcon Ascanio 1979; Jin and Steffler 1993; Yeh and Kennedy 1993). The method couples the depth-averaged continuity and momentum equations with two moment-of-momentum equations derived from the balance among the momentum flux of the convective terms, pressure gradient term, and stress terms for closure purposes. For steady bend-flow models, the determination of flow depth in the flow domain is difficult due to the lack of time derivative of the flow depth in the continuity equation. Among the existing unsteady 2-D bend-flow models, the models developed by Molls and Chaudhry (1995) and Nagata *et al.* (1997) were presented. Molls and Chaudhry's model (1995) simulated the experimental bend-flow data conducted by Rozovskii (1961). They proposed the concept of integrated effective stress, which consists of laminar viscosity stress, turbulence stress, and dispersion stress due to depth averaging. However, they ignored the non-uniform distribution of vertical velocity in the bend-flow simulation. Nagata *et al.*'s model (1997) considers a secondary flow component that was derived by using the vertical distributions of the main and transverse velocities in the same way as Kalkwijk and de Vriend (1980). In their studies, only one of the dispersion stresses acting on the face perpendicular to the streamwise axis and acting in the direction of the transverse axis is used as the secondary flow component. de Vriend (1977) used the perturbation method to derive the velocity distribution over the depth in the shallow curved channel. The vertical velocity distribution of the main flow and secondary flow can be approximated by a logarithmic profile and a nonlinear profile, respectively. Using these velocity distributions, one can obtain the dispersion stresses by numerical integration. Lien *et al.* (1999) proposed an unsteady 2-D depth averaged flow model to capture all the effect of dispersion stresses terms in curved channel flow. This model has been done exclusively for hydrodynamic module without incorporating the sediment module. Hsieh and Yang (2003) has attempted to establish guidelines for users to select more appropriate 2-D models. Lien *et al.* (1999a) calculated the dispersion terms in the momentum equations, which are the integrations of the product of the difference between the depth-averaged and the actual velocity along the verticals. The model (Lien *et al.*, 1999) adopted the curvilinear coordinate and included the dispersion terms deduced from the stream-wise and transverse velocity profiles (de Vriend, 1977). Hydrodynamic modelling of bend flow in the curvilinear coordinate (Kalkwijk and de

Vriend, 1980; Demuren and Rodi, 1986; Odgaard, 1989a; Shimizu and Itakura, 1989; Molls and Chaudhry, 1995; Ye and McCorquodale, 1997; Lien *et al.* 1999; Darby *et al.* 2002; Wu *et al.*, 2004; Hsieh and Yang, 2003) has been effective because the longitudinal and radial coordinates approximately agree with the directions of the main and the transverse flow. In many practical cases, the effect of secondary flow is not significant when the channels are not curved or the curvature effect is small. This study employed the Cartesian coordinate so that the hydrodynamic model can be easily applied to both meandering and non-meandering channels. Instead of including the dispersion terms calculated directly from the stream-wise and transverse velocity profiles, the dispersion terms were converted to those in the Cartesian coordinate. The dispersion terms resulting from the transverse velocity distribution disappeared when the radius of curvature was relatively large or the channel was straight. Additionally, the hydrodynamic model adopted the modified depth-averaged momentum equations, where the density of flow was treated as a variable and changed with the concentration of transported mass enabling the hydrodynamic model to couple with the mass transport model. As for the mass transport model, the depth-averaged convection and diffusion equation, which takes the difference between mass entrainment and deposition from the mobile bed surface as the source/sink term, was solved to obtain the depth-averaged concentration (Duan 2004). Duan (2004) attempted derivation of the dispersion terms (incorporation of secondary flow correction) for the depth-averaged 2-D models using governing equations in Cartesian coordinates. She also compared the results of flow hydrodynamic models with and without the dispersion terms.

The additional dispersion term coming on account of non uniformities in vertical distribution of velocities in the momentum equation in 2-D depth averaged equation has a potential for improvement in its empirical relations with involved flow variables to adequately represent its effect in the morpho-dynamic process in a braided river.

2.5.4 2-D MATHEMATICAL FORMULATIONS PERTAINING TO NATURAL STREAMS

2.5.4.1. Basic governing equations for river flows

The constituent equations for fluid flows are well established and they are basically in the form of a coupled set of partial differential equations, known as the Navier–Stokes equations (Batchelor, 1967). Different ways of numerically solving these equations give rise to different *CFD* techniques in which various forms of these equations may be employed. In the framework of the finite difference/volume technique, the most fundamental solution method is referred to as the Direct Numerical Simulation (*DNS*). In the *DNS* method, the transient form of the Navier–Stokes equations is solved numerically by means of spectral and pseudo-spectral techniques. However, because of the complexity of general industrial, as well as environmental, problems and the limitation in the capabilities of present computer systems, *DNS* is nowadays still primarily limited in its use to the study of some of the very simple but fundamental flow problems, such as simple turbulent channel and pipe flows, flow in plane mixing layers, etc (Bates *et al.*, 2005). It is evident that even when using the Reynolds-averaged Navier–Stokes equations, it is sometimes very difficult to solve large scale, complex unsteady river flows in a fully 3-D model due to the limitations in computer power. This is particularly true when the problem investigated is part of a real river where the flow is turbulent with irregularly shaped banks and beds. Therefore, various simplifications to the governing equations have to be made in order to reduce the dimensions of the problem. Subsequent section presents the Reynolds-averaged Navier–Stokes equations and the 2-D depth-averaged equations which have been commonly employed in *CFD* models of river flow.

It is noted that there have been some attempts to use the Large Eddy Simulation (*LES*) techniques to investigate steady and unsteady flows in river channels (*e.g.* Thomas and Williams, 1995; Bradbrook *et al.*, 2000). Although *LES* itself is a relatively well-established numerical technique, and has been used in numerous engineering and environmental applications, the use of *LES* in river flow modeling is still at an early stage of development.

2.5.4.2 The Reynolds-averaged Navier–Stokes equations

The fundamental parameters required to describe a river flow are the pressure and the velocity of the fluid flow. If the flow is assumed to be incompressible and Newtonian,

then these parameters are solely governed by the constitutional Navier–Stokes equations which are based on the basic physical principles of conservation of mass and momentum. For an incompressible and turbulent fluid flow, the Reynolds-averaged form of the Navier–Stokes equations may be written in a Cartesian coordinate system as follows (Hinze, 1975).

(i) Continuity Equation.

$$\frac{\partial u}{\partial x}+\frac{\partial v}{\partial y}+\frac{\partial w}{\partial z}=0 \tag{2.13}$$

Where u, v and w are instantaneous velocities used in original Navier Stokes Equations. This can further be decomposed as

$u=\bar{u}+u'$

$v=\bar{v}+v'$

$w=\bar{w}+w'$

Where $\bar{u},\bar{v},\bar{w}$ are time averaged velocity components in Cartesian coordinate system, and u',v',w' are fluctuating velocity components in Cartesian coordinates system.

(ii) Momentum Equation

In x direction

$$\rho\frac{Du}{Dt}=f_x-\frac{\partial\bar{p}}{\partial x}+\frac{\partial}{\partial x}\left(\mu\frac{\partial\bar{u}}{\partial x}-\rho\overline{u'^2}\right)+\frac{\partial}{\partial y}\left(\mu\frac{\partial\bar{u}}{\partial y}-\rho\overline{u'v'}\right)+\frac{\partial}{\partial z}\left(\mu\frac{\partial\bar{u}}{\partial z}-\rho\overline{u'w'}\right) \tag{2.14}$$

In y direction

$$\rho\frac{Dv}{Dt}=f_y-\frac{\partial\bar{p}}{\partial y}+\frac{\partial}{\partial x}\left(\mu\frac{\partial\bar{v}}{\partial x}-\rho\overline{u'v'}\right)+\frac{\partial}{\partial y}\left(\mu\frac{\partial\bar{v}}{\partial y}-\rho\overline{v'^2}\right)+\frac{\partial}{\partial z}\left(\mu\frac{\partial\bar{u}}{\partial z}-\rho\overline{v'w'}\right) \tag{2.15}$$

In z direction

$$\rho\frac{Dw}{Dt}=f_z-\frac{\partial\bar{p}}{\partial w}+\frac{\partial}{\partial x}\left(\mu\frac{\partial\bar{w}}{\partial x}-\rho\overline{w'u'}\right)+\frac{\partial}{\partial y}\left(\mu\frac{\partial\bar{w}}{\partial y}-\rho\overline{w'v'}\right)+\frac{\partial}{\partial z}\left(\mu\frac{\partial\bar{w}}{\partial z}-\rho\overline{w'^2}\right) \tag{2.16}$$

where D is total derivative operator (convective acceleration), μ is molecular viscosity, $\bar{p}$ is mean pressure and f_x, f_y and f_z are body forces in x, y and z direction respectively.

The term $-\rho u'^2$ and other similar six terms in above equations are the result of the Reynolds-averaging of the original Navier-Stokes equations known as Reynolds stresses. These terms represent the effect of turbulence on the fluid flow and are not known *a priori*. Thus, we have more unknowns and less number of equations, so above equations are not closed. So, additional closure equations and a set of properly defined boundary conditions for the fluid flow are required. The river flow can be modelled numerically by solving the Reynolds-averaged Navier–Stokes equations in all three directions of the coordinate system.

2.5.4.3 Depth averaged equations

Due to the complexity of solving the full 3-D Navier–Stokes equations, which often place impractical demands on computer resources, there is a practical requirement to reduce the dimension of the governing fluid flow equations and this result in the depth-averaged fluid flow equations.

For a shallow river flow, and in situations where the vertical variations of the fluid flow are less important than the variations of the longitudinal and transverse flows in the river, or the flow is approximately unidirectional, the dimensions of the governing fluid flow equations can be reasonably accurately reduced by integrating the full 3-D equations over the water depth h. This results in the introduction of the depth averaged velocity components of the fluid velocity, $\bar{u}^i$ in the x^i-direction of the horizontal Cartesian coordinate system ($i=1, 2$), as follows:

$$\bar{u}^i = \frac{1}{h}\int_0^h u^i dz \qquad (i = 1, 2) \tag{2.17}$$

where z is the vertical axis of the 3-D Cartesian co-ordinate system. Thus in the depth-averaged approach, the fluid velocities are assumed to be constant throughout the depth and equal to the depth-averaged velocity, $\bar{u}^i$ In addition, from the assumption of the

hydrostatic pressure distributions in the vertical direction, the pressure forces can be evaluated in terms of the depth. However, it should be noted that the assumption of the hydrostatic pressure distribution limits the accuracy of the model in regions of steep slopes and rapid changes in the bed topography. The 2-D depth-averaged Navier–Stokes equations can be expressed in a horizontal. Cartesian coordinate system as follows (Bates *et al.*, 2005)

Continuity Equation

$$\frac{\partial h}{\partial t}+\frac{\partial}{\partial x^i}\left(h\bar{u}^i\right)=0 \tag{2.18}$$

Momentum equation

$$\frac{\partial \bar{u}^i}{\partial t}+\frac{\partial\left(\bar{u}^i\bar{u}^j\right)}{\partial x^j}=-g\frac{\partial h}{\partial x^j}+\frac{1}{\rho}\frac{\partial \tau^{ij}}{\partial x^j}+\frac{\tau_s^i-\tau_b^i}{\rho h}+\frac{1}{\rho h}\frac{\partial}{\partial x^j}\left(\int_0^h \rho\left(u^i-\bar{u}^i\right)\cdot\left(u^j-\bar{u}^j\right)dz\right) \tag{2.19}$$

The turbulence shear stress $\tau_{i,j}$ can be determined using an appropriate turbulence model (*e.g.* Wilson *et al.*, 2003). The depth-averaging also results in the introduction of two other groups of stresses in the equation, i.e. the water surface and bed stresses (τ_s^i and τ_b^i), and the so-called 'dispersion stress terms', namely the last term in above equation, and these terms usually require empirical formulae or models.

2.5.4.4 Bed shear stresses

Water surface shear stresses τ_s^i are usually ignored unless strong winds exist. However, the bed shear stresses τ_b^i are very important and usually have to be obtained experimentally. It is assumed that bed shear stresses can be expressed as a quadratic function of the depth-averaged velocity as follows (Rastogi and Rodi, 1978; Ye and McCorquodale, 1997)

$$\tau_b^i=C_f\rho\bar{u}^i\sqrt{\bar{u}^i\bar{u}^i} \tag{2.20}$$

where C_f is the bed friction coefficient. As the bed shear stresses result primarily from the turbulent flow interactions, there is considerable uncertainty in their evaluation. Typically, they may be determined using various empirical functions (Nezu and Nakagawa, 1993; Lane, 1998). In many applications, the bed friction coefficient is calculated using the Manning's equation as follows:

$$C_f = \frac{gn^2}{h^{\frac{1}{3}}} \tag{2.21}$$

where the parameter n is not a constant but depends on the fluid flow situation under investigation. In an equivalent formulation, the bed shear stresses are evaluated using the nondimensional Chezy coefficient C_s as follows

$$\tau_b^i = \frac{1}{C_s^2}\rho\bar{u}^i\sqrt{\bar{u}^i\bar{u}^i} \tag{2.22}$$

and the Chezy coefficient can be related to the effective bed roughness height K_s is follows

$$C_s = 5.75\log\left(12\frac{h}{K_s}\right) \tag{2.23}$$

It should be noted that there is considerable uncertainty in how to choose the effective roughness, height K_s as well as Manning's n, as it requires information on the grain size. Therefore, both K_s and n are often used as calibration parameters against, for example, measured water surface elevations and fluid velocity. There are also other empirical formulae that may be used to evaluate the bed shear stresses/frictions (Rastogi and Rodi, 1978; Van Rijn, 1987; Nezu and Nakagawa, 1993), and this is clearly an area in which further research is required.

2.5.4.5 Dispersion terms

The dispersion terms, namely the last term in Eq. (5.16), are produced because of the non-uniformities of the fluid flow velocity in the vertical direction during the depth-averaging. The determination of these terms requires knowledge of the information in the secondary flows across the depth which is, however, usually not known *a priori.* Therefore, we usually have to produce a mathematical model for the dispersion terms (*e.g* Lane, 1998; Duan, 2004). However, these terms are frequently found to be negligible in cases such as straight channel flows (Nezu and Nakagawa, 1993). However, the dispersion terms can be very important, particularly when there are strong **secondary flows,** such as fluid flows through a river bend or over channel junctions (Bernard and Schneider, 1992) or in other words river with complex physical domain.

Since there are no additional equations for the dispersion terms arising from the depth-averaging, the treatment of the dispersion terms has been mainly through semi-empirical or empirical models to represent their effects on the transport of momentum. The key element of these models is the representation of the secondary flows resulting from the effects of the lateral curvature of the river and the friction at the bottom of the river. One of the key models for the dispersion terms is that described by Johannesson and Parker (1989), where 2-D forms of the mass and momentum equations are combined with an empirical shape function for the distribution of the primary velocity across the depth. Another approach is that of Bernard (1992) in which the dispersion terms are expressed as a function of the shear stresses associated with the secondary flow, and empirically derived terms are used. However, regardless of the relative importance of the dispersion terms, the present available treatment of these terms is limited in its representation of the vast complexity and variety of secondary flows occurring in natural river flows. This is largely attributed to the lack of understanding of the mechanisms of secondary flow generation in 3-D natural river flows in various bed topographies and channel irregularities. Clearly, more research on the mathematical representation of the dispersion terms is required when modelling complex river flows using the depth averaging approach. However, fluid flow problems with strong secondary flows can be more completely addressed through 3-D simulations (Bates *et al.,* 2005). More recently,

numerous researchers have given formulation to estimate dispersion terms. Some relevant formulations are presented here for illustrations and clarity.

de Vriend (1977) used the perturbation method to derive the velocity distribution over the depth in the shallow curved channel, and the vertical velocity profiles were then verified by the experiments. Later Lien *et al.* (1999a) used in line with adopting the following formulation for dispersion terms into the momentum equation de Vriend(1977) adopted

$$\bar{u} = \bar{\bar{u}}\left[1 + \frac{\sqrt{g}}{\kappa c} + \frac{\sqrt{g}}{\kappa c}\ln\zeta\right] = \bar{\bar{u}} f_m(\zeta) \tag{2.24}$$

$$\bar{v} = \bar{\bar{v}} f_m(\zeta) + \frac{\bar{\bar{u}}\, d}{\kappa^2 r}\left[2F_1(\zeta) + \frac{\sqrt{g}}{\kappa c}F_2(\zeta) - 2\left(1 - \frac{\sqrt{g}}{\kappa c}\right).f_m(\zeta)\right] \tag{2.25}$$

In Eqs. (5.21) and (5.22), $f_m(\zeta) = 1 + \frac{\sqrt{g}}{\kappa c} + \frac{\sqrt{g}}{\kappa c}\ln\zeta$, $F_1(\zeta) = \int_0^1 \frac{\ln\zeta}{\zeta - 1} d\zeta$, $F_2(\zeta) = \int_0^1 \frac{\ln^2\zeta}{\zeta - 1} d\zeta$, $\zeta = (z - z_b)/d$ =dimensionless distance from the bed, r=radius of curvature, $\bar{u}, \bar{v}$ = Depth averaged velocities in stream-wise and transverse directions, $\bar{\bar{u}}, \bar{\bar{v}}$ =time averaged velocities in stream-wise and transverse directions.

Here, the main velocity profile is assumed to have a logarithmic distribution, and the transverse velocity profile is a combination of a logarithmic distribution and a nonlinear distribution of the secondary flow. It is obvious that only the secondary flow due to the curvature of the bend is considered in the formulation of the transverse velocity profile. Such consideration of transverse secondary flow is a main factor to shift the stream wise momentum from the inner region of a bend toward the outer region and to increase the main velocity near the outer bank. In addition, the effect of the secondary flow on the stream wise velocity profile is neglected, and these velocity profiles, used in the model, are inadequate for a reverse secondary eddy that occurred near the surface at the outer bank.

After including the velocity profile, Lien *et al.* (1999a) derived namely *DSXX, DSYY* and *DSXY* as follows to be incorporated as dispersion terms in to the their controlling equation.

$$DSXX = \rho \int_{z_b}^{z_s} (\bar{u} - \overline{\bar{u}})^2 dz = \rho \overline{\bar{u}} d \left(\frac{\sqrt{g}}{\kappa c} \right)^2 \quad (2.26)$$

$$DSYY = \rho \int_{z_b}^{z_s} (\bar{v} - \overline{\bar{v}})^2 dz = \rho \left[\overline{\bar{v}}^2 d \left(\frac{\sqrt{g}}{\kappa c} \right)^2 + \frac{2 \overline{\bar{u}\bar{v}} d^2}{\kappa^2 r} . \frac{\sqrt{g}}{\kappa c} . FF\ 1 + \frac{2 \overline{\bar{u}}^2 d^3}{\kappa^4 r^2} . FF\ 2 \right] \quad (2.27)$$

$$DSXY = \rho \int_{z_b}^{z_s} (\bar{u} - \overline{\bar{u}})(\bar{v} - \overline{\bar{v}}) dz = \rho \left[\overline{\bar{u}\bar{v}} d \left(\frac{\sqrt{g}}{\kappa c} \right)^2 + \frac{\overline{\bar{u}}^2 d^2}{\kappa^2 r} . \frac{\sqrt{g}}{\kappa c} . FF\ 1 \right] \quad (2.28)$$

where

$$FF\ 1 = \int_0^1 (1 + \ln \zeta) \left[2F_1(\zeta) + \frac{\sqrt{g}}{\kappa c} F_2(\xi) - 2 \left(1 - \frac{\sqrt{g}}{\kappa c} \right) f_m(\zeta) \right] d\zeta \quad (2.29)$$

$$FF\ 2 = \int_0^1 (1 + \ln \zeta) \left[2F_1(\zeta) + \frac{\sqrt{g}}{\kappa c} F_2(\xi) - 2 \left(1 - \frac{\sqrt{g}}{\kappa c} \right) f_m(\zeta) \right]^2 d\zeta \quad (2.30)$$

Above equations are integrated using trapezoidal rule. The first term (*DSXX*) indicates that the integration of the products of the discrepancy between the mean and the true velocity distributions in the stream wise direction. The second term (*DSYY*) indicates that the integration of the products of velocity discrepancy in the transverse direction. The third term (*DSXY*) indicates that the integration of the products of velocity discrepancy in the stream wise direction and that in the transverse direction.

Lien *et al.* (1999a) worked on the above formulation in their controlling equations of flow in curvilinear coordinate system to get the solution for their model. They compared the result of their model performance with other investigators and summarized the conclusion as dispersion terms to be important source/sink term in momentum equation and contribute to the transverse convection of the momentum. Their relative contributions in the overall secondary flow effect depend on flows in mild or sharp bends. Lien *et al.* (1999) further concluded that if the dispersion stress terms are neglected, the governing equations reduce to a conventional depth-averaged equation assuming uniform velocity over depth. Hence, the model presented by Lien et al., (1999a) is more applicable for practical application in bend-flow modeling than the conventional depth-averaged models because of its ability to account for the secondary flow effect. In short, the dispersion stresses play an important role in accurately simulating or predicting flow fields in sharp bends as well as in mild bends. Hsieh and Yang (2003) conducted some experimental

analysis to validate the above formulations. Readers are suggested to refer the Hsieh and Yang (2003) for further details. More recently, Duan (2004) derived the mathematical expressions of these terms, assuming that the stream-wise velocity satisfies the logarithmic law written in Eq. (2.31).

$$\frac{u_l}{u_*} = \frac{1}{\kappa} \ln\left(\frac{z}{z_0}\right) \tag{2.31}$$

where, u_l=Velocity in stream-wise direction, z=vertical coordinate, u_*=shear velocity, z_0= calculated according to flow velocity, Integrating the logarithmic velocity profile along the vertical. Eq. (2.31) ends up with

$$\frac{\bar{u}_l}{u_*} = \frac{1}{\kappa}\left[\frac{z_o}{h} - 1 + \ln\left(\frac{h}{z_o}\right)\right] \tag{2.32}$$

where $\bar{u}_l$ = depth-averaged velocity in the stream-wise direction. Combining the above two equations she landed with relation between time averaged and depth averaged velocities. Duan(2004) assumed the transverse profile of the velocity linear and adopted transverse velocity profile proposed by Odgaard (1989a) in the formulation. The dispersion terms at the stream-wise and transverse directions have been derived by Duan (2004) as follows.

$$D_{uu}^{c} = \int_{z_o}^{z_o+h} \rho_m (u_l - \bar{u}_l)^2 dz = \chi^2 \bar{u}_l^2 h\left[-\eta_0 \ln\eta_0 (\ln\eta_0 - 2) + 2\eta_0 (1-\eta_0)(1-\ln\eta_0) - (\eta_0 - 1)^3\right] \tag{2.33}$$

$$D_{uv}^{c} = \int_{z_o}^{z_o+h} \rho_m (u_l - \bar{u}_l)(v_r - \bar{v}_r) dz = 49.0 \bar{u}_l^2 \frac{h^3}{r^2}\left[-\frac{1}{3}\eta_0^3 + \frac{1}{2}\eta_0^2 - \frac{1}{4}\eta_0 + \frac{1}{12}\right] \tag{2.34}$$

$$D_{vv}^{c} = \int_{z_o}^{z_o+h} \rho_m (v_r - \bar{v}_r)^2 dz = 3.5 C \bar{u}_l^2 \frac{h^2}{r}\left[-\eta_0^2 \ln\eta_0 + \eta_0 \ln\eta_0 - \eta_0 + \eta_0^3\right] \tag{2.35}$$

where $\chi = 1/\eta_0 - 1 - \ln\eta_0$, $\eta_0 = z_0/h$ =dimensionless zero-bed elevation, r=radius of curvature, v_r and $\bar{v}_r$ are transverse velocity and depth averaged transverse velocity respectively. The curvilinear dispersion terms transformed to dispersion terms in Cartesian coordinate for incorporation into governing equations through usual transformation procedure. Duan (2004) adopted the efficient element method (Wang and Hu, 1990) as the numerical solver to get the solution. To test the model performance of dispersion terms and verify the developed hydrodynamic model, two sets of experimental data and bend flow conducted by de Vriend (1979) and Rozovski (1961) were adopted. As per Duan (2004)'s conclusion, the verifications by the experiments in mild and sharp curved channel indicated that the effect of dispersion terms on flow hydrodynamic field becomes significant when curvature is increased. However flows in bends are essentially a three dimensional flow feature so 3-D modelling certainly gives better model results. Seo *et al.* (2008) further applied the dispersion coefficient tensor to the mass dispersion and solute transport and used finite element method to validate the results.

2.5.4.6 Turbulent stresses

The stresses which include turbulent effects are determined using the Boussinesq assumption as follows (Wu, 2007)

$$T_{xx} = 2\rho(\nu_t)\frac{\partial U_x}{\partial x} - \frac{2}{3}\rho\kappa \tag{2.36}$$

$$T_{xy} = T_{yx} = \rho(\nu_t)\left(\frac{\partial U_x}{\partial y} + \frac{\partial U_y}{\partial x}\right) \tag{2.37}$$

$$T_{yy} = 2\rho(\nu_t)\frac{\partial U_y}{\partial y} - \frac{2}{3}\rho\kappa \tag{2.38}$$

where ν_t is the eddy viscosity that needs to be determined using a turbulence model. The choices for determining ν_t include the depth-averaged parabolic model, modified mixing

length model, and three depth-averaged linear $k-\varepsilon$ turbulence models. Averaging the parabolic eddy viscosity equation over the flow depth yields

$$\nu_t = \alpha_1 u_* h \tag{2.39}$$

where α_1 is an empirical coefficient. Theoretically α_1 should be equal to $\kappa/6$. However, it has been given various values in practice, because of the anisotropic structures of turbulence in horizontal and vertical directions and the effects of dispersion. According to experiments by Elder (1959), α_1 is about 0.23 for the longitudinal turbulent diffusion in laboratory channels. For transverse turbulent diffusion, Fischer *et al.* (1979) proposed that α_1 is about 0.15 in laboratory channels and 0.6 (0.3-1.0) in irregular waterways with weak meanders.

Equation (2.41) is applicable in the region of main flow. Because the influence of horizontal shear is ignored, significant errors may arise when applied in regions close to rigid sidewalls. Improvement can be achieved through a combination of Eq. (2.41) and Prandtl's mixing length theory mentioned herein as Eq. (2.40).

$$\nu_t = \sqrt{(\alpha_0 u_* h)^2 + (l_h^2 |\bar{s}|)^2} \tag{2.40}$$

where

$$|\bar{s}| = \left[2\left(\frac{\partial U_x}{\partial x}\right)^2 + 2\left(\frac{\partial U_y}{\partial y}\right)^2 + \left(\frac{\partial U_x}{\partial y} + \frac{\partial U_y}{\partial x}\right)^2 \right]^{1/2} \tag{2.41}$$

α_0 is an empirical coefficient similar to α_1 in Eq. (2.39) and has a value of about $\kappa/6$ and l_h is the horizontal mixing length, determined using $l_h = \kappa \min(y', c_m h)$ with y' being the distance to the nearest wall and c_m an empirical coefficient ranging between 0.4 and 1.2 (Wu *et al.*, 2004b).

Rastogi and Rodi (1978) established a depth-averaged k-ε turbulence model through depth-integration of the 3-D standard k-ε model. Readers are suggested to refer to relevant literature for detail information.

2.5.5 FORMULATION OF MASS-MOMENTUM CONTROLLING EQUATIONS IN CURVILINEAR COORDINATE SYSTEM.

2.5.5.1 Governing equations

The governing equations for flow simulation are *RANS* equations with depth averaged approximation of continuity and momentum equations [Eqs.(2.42), (2.43) and (2.44)] in Cartesian coordinate system with secondary flow corrections are (Duan and Julien, 2005).

$$\frac{\partial \rho h}{\partial t}+\frac{\partial}{\partial x}(\rho h U_x)+\frac{\partial}{\partial y}(\rho h U_y)=0 \tag{2.42}$$

$$\frac{\partial}{\partial t}(\rho h U)+\frac{\partial}{\partial x}(\rho h U_x^2)+\frac{\partial D_{xx}}{\partial x}+\frac{\partial}{\partial y}(\rho h U_x U_y)+\frac{\partial D_{xy}}{\partial y}=-\rho g h\frac{\partial H}{\partial x}-C_d \rho U_x\sqrt{U_x^2+U_y^2}+\rho h\nu_t\left(\frac{\partial^2 U_x}{\partial x^2}+\frac{\partial^2 U_x}{\partial y^2}\right) \tag{2.43}$$

$$\frac{\partial}{\partial t}(\rho h U_y)+\frac{\partial}{\partial x}(\rho h U_x U_y)+\frac{\partial D_{xy}}{\partial x}+\frac{\partial}{\partial y}(\rho h U_y^2)+\frac{\partial D_{yy}}{\partial y}=-\rho g h\frac{\partial H}{\partial y}-C_d \rho U_y\sqrt{U_x^2+U_y^2}+h\rho\nu_t\left(\frac{\partial^2 U_y}{\partial x^2}+\frac{\partial^2 U_y}{\partial y^2}\right) \tag{2.44}$$

where U_x and U_y= depth-averaged velocity components in x and y directions, t=time, ρ=density of water (kg/m^3), H=water surface elevation, h=depth of the flow, g=acceleration of gravity, C_d=frictional stress coefficient (for friction shear stress at the bottom in x and y directions); and equals $n^2\rho g / h^{1/3}$ with n=Manning's roughness coefficient; ν_t =eddy viscosity. Homogeneous suspension is presumed. (ρ *is* constant). Wind /rainfall forces are neglected. Coriolis force due to the rotation of the earth is neglected. The equation is valid to homogeneous suspensions to orthogonal system of coordinates in which z- axis is near vertical (small angle). D_{xx}, D_{xy} and D_{yy} are flow dispersion stress components.

Numerous researchers formulated and derived different forms of mass-momentum equations in curvilinear coordinate system based on the above equations in view of

suitability with their adopted discretization schemes during the last decade. Lien *et al.* (1999a) presented an unsteady 2-D depth-averaged flow model with the consideration of dispersion stress terms to simulate the bend-flow field. The model uses an orthogonal curvilinear coordinate system to efficiently and accurately simulate the flow-field with irregular boundaries. Nagata *et al.*, (2000) has adopted generalized non-orthogonal co-ordinate system to formulate the controlling equations with complex flow domain. This is appropriate approach not only on account of its generality, but also due to the fact that it is possible to orient the dependant variable along the grid lines conforming to the shape of the domain and therefore usually along principal streamlines, which will minimize the chance of false diffusion (Patankar, 1980). More recently many researchers for example Duan (2004), Seo *et al.* (2008) developed models with secondary flow corrections and applied and verified in laboratory flume data.

2.6 CONCEPT OF NUMERICAL SOLUTION

River engineering problems are usually governed by nonlinear differential equations in irregular and movable domains, most of which have to be solved using numerical methods. Introduced in this chapter are the discretization methods for 1-D, 2-D and 3-D problems on fixed and moving grids, the solution strategies for the Navier-Stokes equations, and the solution methods of algebraic equations (Wu, 2007). Some of these can be found in Patankar (1980), Hirsch (1988), Fletcher (1991), Ferziger and Peric (1995), Shyy et al. (1996) *etc.*

2.6.1 DISCRETIZATION METHODS

Widely used discretization methods include finite difference method, finite element method, finite volume method, finite analytical method, and efficient element method (Wu, 2007).

The finite difference method discretizes a differential equation by approximating differential operators with difference operators at each point. The finite analytical method discretizes the differential equation using the analytical solution of its locally linearized form, and the efficient element method establishes difference operators using

interpolation schemes in local elements. Because of their similarity, the finite analytical method and efficient element method are herein grouped with the finite difference method (Wu, 2007).

The finite volume method integrates the differential equation over each control volume, holding the conservation laws of mass, momentum, and energy. In the finite element method, the differential equation is multiplied by a weight function and integrated over the entire domain, and then an approximate solution is constructed using shape functions and optimized by requiring the weighted integral to have a minimum residual (Wu, 2007).

The algebraic equations resulting from the finite difference and finite volume methods usually have banded and symmetric coefficient matrices that can be handled efficiently, whereas the algebraic equations from the finite element method often have sparse and asymmetric coefficient matrices that require relatively tedious effort for solution (Wu, 2007). However finite element method handles unstructured meshes, so it can be conveniently applied to complex geometry more efficiently. The choice of numerical method depends on many factors including computation expense, suitability in a particular situation and degree of accuracy required in the final solution etc. In some specific cases like water quality modelling, Lagrangian approach such as Time Driven Method (*TDM*) or Event Driven Method (*EDM*) are more efficient for simulating the chemical transport in a water distribution system than Eulerian approach like finite difference method (*FDM*) (Munavalli and Kumar, 2004) .

Any numerical method may have its advantages and disadvantages, and subjectivity may prevent a modeler from becoming more successful. One has to learn the basic properties such as accuracy, stability, convergence, and efficiency of the used method and know how to take advantage of its strengths and avoid its weaknesses (Wu, 2007)

Finite volume schemes have evolved in recent years into powerful tools for the prediction of shallow water flows (Alcrudo, *et al.* 1992; Jin and Fread, 1997; Sanders and Katopodes, 1999; Tseng and Chu, 2000; Sanders, 2001) as reported by Capart *et al.* (2003). Among other attractive features, these algorithms are noteworthy for their ability

to deal with trans-critical flows and propagating shocks. Favourable comparisons with analytical benchmarks and laboratory measurements have been obtained for complex flows in one and two-dimensional configurations (*e.g.*, Fraccarollo and Toro, 1995; Capart, et al. 1997; Soares *et al.*, 2000; Tseng *et al.*, 2001; Bradford and Sanders 2002). Capart *et al.* (2003) used 1-D flow simulation using *FVM* in more general case of inclined, non prismatic channel characterized by abrupt variation in bathymetry. More recently Kuiry *et al.* (2008) demonstrated numerical simulation using *FVM* for triangular mesh extracted from a triangulated irregular network (*TIN*) form of digital elevation model (*DEM*).

Hence for simulating large rivers, finite volume method (*FVM*) of discretizing conservative form of partially transformed controlling equations in curvilinear coordinate system seems appropriate to use based on the earlier studies. *FVM* solver additionally conserves mass-momentum and can be well applied for highly complex geometry using non-orthogonal grids with reasonable approximation.

2.6.2 DISCRETIZATION BY CO-ORDINATE TRANSFORMATION

The finite volume method offers two methods to discretize equations. One method is to look at physical processes and parameters, and thereby derive the discretized equations. This approach is used by Olsen (1999). The method has the advantage of being easy to understand, facilitating debugging and implementation of new algorithms (Olsen, 2000). However Olsen (2000) mentions difficulty in deriving three groups of terms i.e. the production of turbulence in k-ε model, stress terms in Navier-Stokes equations, non-orthogonal diffusive terms in Navier-Stokes equations. Hence these terms are usually discretized using a method called co-ordinate transformation. The co-ordinate transformation is a transformation between natural Cartesian co-ordinate system and system following the computational domain.

Some finite volume methods used in most of the *CFD* codes are briefly introduced in following sub section.

2.6.2.1 *SIMPLE, SIMPLEC* and *SIMPLER* methods

SIMPLE is an acronym for Semi-Implicit Method for Pressure Linked Equations. The original description was given by Patankar and Spalding (1972). The basic concept of this method as given by Olsen (2000) is to guess a pressure field and calculate the velocities. Then the continuity defect is estimated and it is used to calculate a correction in pressure field. The initially computed variables do not satisfy continuity and are denoted with an index '*'.The correction of the variables is denoted with an index (′). The variables after correction do not have superscript. The process can be written

$$P = P^* + P' \tag{2.45a}$$

$$U = U^* + U' \tag{2.45b}$$

P is the pressure and U is the velocity. Similarly *SIMPLEC* method is the refinement of *SIMPLE* method. In these methods an equation of pressure is not solved directly, instead of that a pressure correction equation is solved. The pressure is obtained by accumulative addition of the pressure correction values. Regarding the difference between the *SIMPLE* and *SIMPLEC* method, the *SIMPLEC* should be more consistent as revised and correct formula is used. The *SIMPLE* method moves slower towards convergence than the *SIMPLEC* method. The *SIMPLER* method is an extension of the *SIMPLE* method. The *SIMPLE/SIMPLEC* method usually gives good velocity corrections, but the correction of pressure is less accurate (Olsen, 2000). It means that a good guess of pressure will give a good velocity correction and overall solution will be of better accuracy and instability. For large rivers with very mild longitudinal slope such as Brahmaputra River where sub-critical flow condition and gradually varied flow persists, a good guess of pressure (water level) can suitably be done. Hence, *SIMPLEC* method is expected to give better results with stability and consistency in specific scenario of flow field simulation for large rivers with mild longitudinal bed slopes.

2.6.2.2 The Rhie and Chow interpolation

The Rhie and Chow interpolation is used to prevent oscillation when using a cell centered discretization scheme. Its derivation is given by Rhie and Chow (1983). The method

introduces additional term when computing the fluxes on the cell faces. The terms can be interpreted as fourth order artificial diffusion. However, method is consistent, as there are no calibration coefficients involved (Olsen, 2000). The motivation for introducing the method originates from the discussion of using staggered and non-staggered variable location in a grid. The staggered grid removes some instability experienced in non-staggered grids. The Rhie and Chow (1983) interpolation is used in connection with estimating the velocities on a grid cell faces when fluxes are calculated. The method uses the pressure gradients from several grid cells to add an extra term to the fluxes. For illustration, Grids for estimation on fluxes on surface e, between cell *P* and *E* will be *W*, *P*, *E* and *EE is* shown in Figure 2.3.

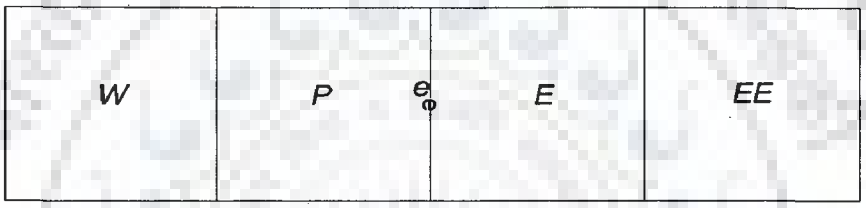

Figure 2.3 Grids for estimating fluxes on surface *e* between cell *P* and *E*

2.6.3 BODY FITTED CO-ORDINATE

The Cartesian co-ordinate system is the most common co-ordinate system used to describe the location of a point in space. It takes advantage of the three base vectors that characterize the system of an ortho-normal system. Computational methods, based on Cartesian or cylindrical coordinate systems, have certain limitations in irregular geometries. When the boundaries of the domain of the physical problem are not aligned along the Cartesian base vector directions, the use of the Cartesian coordinate system is inconvenient and often impractical. A co-ordinate system where principal co-ordinate directions are aligned along the domain boundaries of any physical problem is referred to as a body-fitted coordinate system and is specific to the particular domain of interest. Methods based on the body-fitted grid or non-orthogonal grid system have been developed and used increasingly in the present *CFD* procedure, for details one can refer to Rhie and Chow (1983), Peric (1985), Demirdzic *et al.* (1987), Shyy *et al.* (1988) and Karki and Patankar (1988).

The flexibility offered by body-fitted grid techniques is useful in the modelling of practical problems involving irregular geometries like that of a braided stream. All geometrical details can be accurately incorporated and the grid properties can be controlled to capture useful features in the region of interest. However, the governing equations using the body-fitted coordinate system are much more complex than their Cartesian counterpart. The major differences between the two formulations are based on the grid arrangement and the choice of dependant variables in the momentum equations.

2.6.3.1 General curvilinear coordinate system

The choice of a proper grid arrangement is closely related to that of the dependent variables in the momentum equations. The configuration should be such that it does not admit spurious solutions. The staggered grid arrangement wherein scalar variables are stored at cell nodal centers and velocity components at cell faces, has long been preferred on account of its desirable pressure velocity coupling characteristics as described by Patankar (1980).

When Cartesian velocity components are retained as dependent variables and the coordinates are transformed, such formulation of the governing equations is considered partial co-ordinate transformation. This has been extensively used in the past, primarily on account of its simplicity. The Cartesian velocity components have been widely used as the dependent variables in non-orthogonal coordinate systems (Maliska and Raithby, 1984 and Shyy *et al.*, 1985). The curvilinear components of velocity change their directions and tend to "follow" the grid lines. This feature makes them more attractive for highly non-orthogonal grids and geometries with strong curvature. However, due to the changes in their direction the governing equations are very complicated and involve curvature source terms that account for the fact that momentum is conserved along a straight line.

2.6.3.2 Generalized coordinate transformation

The well-known Cartesian coordinate system is characterized by the three base vectors, which have preferable properties of orthogonality and spatial invariance. However, in the

General Curvilinear Coordinate System, each coordinate needs to be described by two sets of base vectors. Sharatchandara (1995) explained that one of the base vectors will be parallel to the coordinate lines and the second one will be normal to the coordinate surfaces, in order to characterize the system. Figure 2.3 shows the covariant (tangential to a line along which the coordinate ξ varies) base vector ($\boldsymbol{a}_\xi$) in the ξ direction and the contra-variant (normal to the surface S (η,ζ) on which ξ is constant) base vector ($\boldsymbol{a}^\xi$)associated with the ξ coordinate direction. Covariant and contravariant base vectors may be similarly described for the other two coordinate directions (η,ζ).

The coordinate system will be considered as non-orthogonal, if the surfaces of the constant ξ are not normal to the lines along which the coordinate ξ varies, even if the coordinate system is orthogonal at some points of the domain. It has to be noted that if the surface $S(\eta,\xi)$ is perpendicular to the line ξ at point P, then there will be no distinction between the covariant and contra-variant base vectors as can be seen in Figure 2.4.

When the covariant and contra-variant base vectors, at different locations, are oriented in different directions, the body-fitted coordinate system is not spatially invariant. It is more preferable to have a spatially invariant basis for the representation of the base vectors at all points of the domain. The Cartesian coordinate basis, the only such basis in three-dimensional space, is generally used in the representation of the base vectors in a general curvilinear non-orthogonal coordinate system.

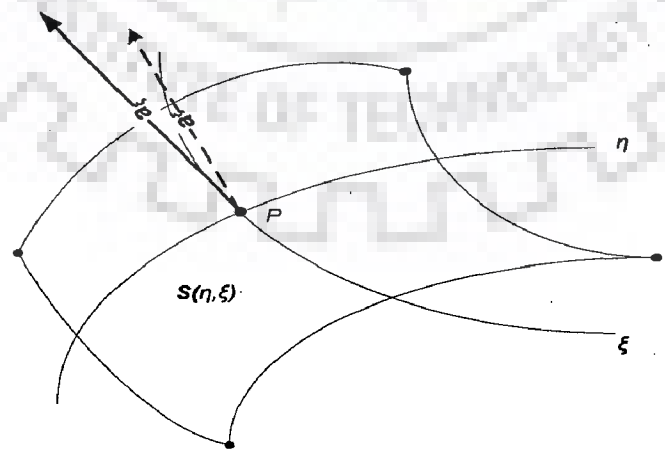

Figure 2.4 Covariant and contra-variant base vectors

When the covariant and contra-variant base vectors, at different locations, are oriented in different directions, the body-fitted coordinate system is not spatially invariant. It is more preferable to have a spatially invariant basis for the representation of the base vectors at all points of the domain. The Cartesian coordinate basis, the only such basis in three-dimensional space, is generally used in the representation of the base vectors in a general curvilinear non-orthogonal coordinate system.

Figure 2.5 shows a non-uniform non-orthogonal physical plane x-y which is to be transformed to a uniform orthogonal computational plane ξ-η. Where ξ and η are known to be as: $\xi = \xi(x, y)$ and $\eta = \eta(x, y)$. It is highly recommended that this transformation be one-to-one and invertible. It is this kind of mapping transformation from the x-y plane to the ξ-η plane where every single-point in the physical domain has its own corresponding point in the computational domain. By following this procedure, we will end up with a number of rows and columns in the computational domain that correspond to rows and columns in the physical domain as mentioned by Sharatchandara (1995).

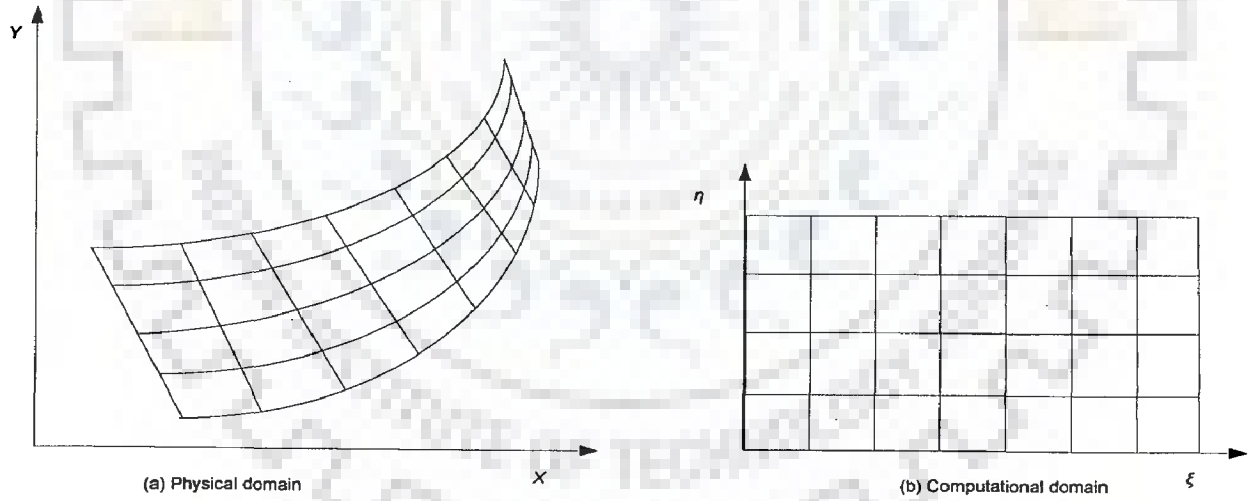

Figure 2.5 Transformation from (a) physical to (b) computational space

2.6.3.3 Grid generation methods

The field of grid generation is very wide and the numbers of studies on this subject are available in literature. Thompson (1982) and Thompson *et al.* (1985) present a comprehensive introduction to the methods of grid generation. Grid generation in one

dimension is straightforward. The two boundaries (*i.e.*, end points) of the physical space must be defined, and the problem reduces to determining the grid spacing in one dimension. One dimensional grid generation is important in itself for the use of one dimensional problem and in two-dimensional grid generation, where the boundaries of two-dimensional space consist of several one-dimensional spaces, and so forth. Grid generation within two- and three-dimensional spaces is considerably more complicated than one-dimensional grid generation (Hoffman, 1992).

Available grid generation techniques can be generally classified into three general categories: (i) Conformal mapping, (ii) Algebraic methods, and (iii) Differential equation methods. Conformal mapping is based on a complex variable theory, which has limitations to two-dimensional problems. Consequently, this method is not as general as the other methods and will not be considered further. Algebraic methods and differential equation methods can be applied to both two and three dimensional spaces. Consequently, they are the methods of choice. A brief overview of both of these will be mentioned in the next section.

2.6.3.3.1 Algebraic methods

The algebraic grid generation technique is based on the specification of algebraic equations for the Cartesian coordinates x, y and z in terms of general curvilinear coordinates ξ, η, and ζ. Karki (1986) summarized the algebraic features of such equations as stretching transformation, shearing transformation, and blending function or isoparametric transformation. For example, the shearing transformation is a linear transformation used to non-dimensionalize the distance between two physical boundaries. The physical domain illustrated in Figure 2.6a can be discretized using the algebraic sheared transformation. The x-coordinate can be transformed by any one dimensional transformation, if needed. It is simply discretized into equally spaced points. The y-coordinate is then discretized into equally spaced points at each x location by the normalizing transformation technique as:

$$y = \left(\frac{\eta - 1}{\eta_{\max} - 1} \right) Y(x) \qquad (1 \le \eta \le \eta_{\max}) \qquad (2.46)$$

where, *Y(x)* is the upper boundary. The results of the complete transformation are illustrated in Figure 2.6b. The reader may refer to Hoffman (1992) for further information.

Transfinite interpolation is considered to be a highly advanced method of algebraic grid generation technique as described by Gordon and Hall (1973). The location of the grid points inside the domain is determined by a series of uniform variation interpolations between the boundaries. The degree of freedom of the blending function can be either linear or higher order which controls the grid spacing and angles at the intersection. The choice of higher order is preferable because it gives more flexibility in controlling the gridline spacing and the angles at which grid lines meet the boundaries. However, this may create an overlapping and crossover of the grid lines. For further information the reader may refer to Thompson *et al.* (1985).

2.6.3.3.2 Differential equation methods

Algebraic grid generation techniques mentioned above have some disadvantages associated with the grid. Discontinuities at the intersection of cell faces, crossover of the gridlines, and undesirable gridline spacing are some of them. A more consistent method

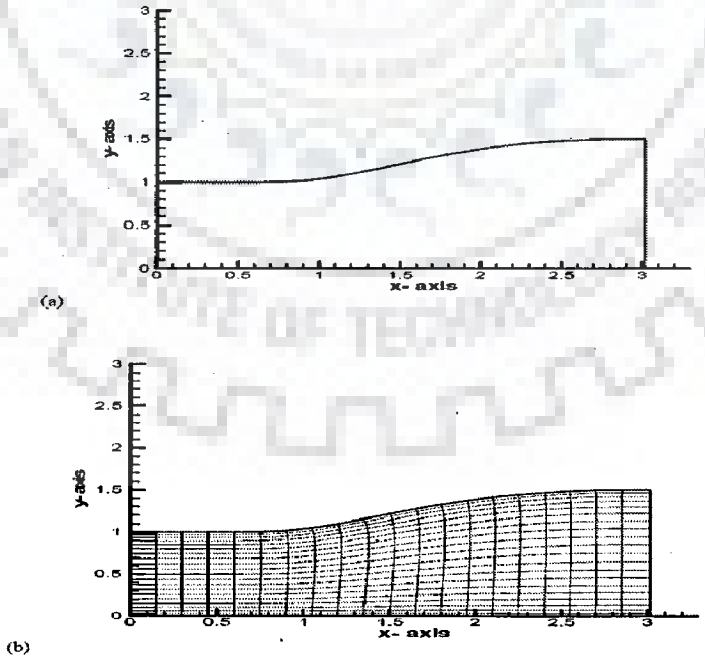

Figure 2.6 Grid generation using normalizing transformation technique (a) physical domain and (b) grid point distribution (Hoffman, 1992).

to overcome these problems is the use of a system of partial differential equations to obtain a higher degree of grid smoothness. Grid generation using partial differential equations involves the following steps: (i) determining the grid point distributions on the boundaries of the physical domain, and (ii) specifying the interior grid points by using partial differential equations that satisfies the grid point distributions on the boundaries.

Any of the three classical types of partial differential equations (*i.e.*, elliptic, parabolic, or hyperbolic) may be used as the governing grid generation equation. The elliptic grid generation technique discussed by Thompson *et al.* (1985) is considered as the well-known method in this field. The most common elliptic partial differential equation is the Poisson equation (in two-dimensional domain):

$$\nabla^2\xi = \xi_{xx} + \xi_{yy} = P(\xi,\eta) \tag{2.47}$$

$$\nabla^2\eta = \eta_{xx} + \eta_{yy} = Q(\xi,\eta) \tag{2.48}$$

Using the inverse transformation and some mathematical manipulations, one can derive the following elliptic partial differential equations for the Cartesian coordinates:

$$\alpha x_{\xi\xi} - 2\beta x_{\xi\eta} + \gamma x_{\eta\eta} = -J^2\left(Px_\xi + Qx_\eta\right) \tag{2.49}$$

$$\alpha y_{\xi\xi} - 2\beta y_{\xi\eta} + \gamma y_{\eta\eta} = -J^2\left(Py_\xi + Qy_\eta\right) \tag{2.50}$$

where

$$\alpha = x_\eta^2 + y_\eta^2 \tag{2.51}$$

$$\beta = x_\xi x_\eta + y_\xi y_\eta \tag{2.52}$$

$$\gamma = x_\xi^2 + y_\xi^2 \tag{2.53}$$

and J is the *Jacobian* of the coordinate transformation defined as:

$$J = x_\xi y_\eta - x_\eta y_\xi \tag{2.54}$$

These sets of equations need to be solved numerically, for x and y with respect to ξ and η with the known prior boundary condition specifications. Parameters or control functions that can control the coordinate line spacing are non-homogeneous terms P and Q.

The three-dimensional grid generation method is a combination of a series of two-dimensional grid slices, as referenced by many researchers. For both internal and external flows, the elliptic grid generation method works fine. However, the hyperbolic grid generation method is preferred for external flow since the hyperbolic equations can be solved by non-iterative marching techniques as proposed by Steger and Sorenson (1980).

2.6.4 NUMERICAL SIMULATION PROCESS AND ACCURACY

The starting point of any numerical simulation process is the physical system which should be described. Figure 2.7 shows schematically the whole procedure that will be performed in a numerical simulation. First, a mathematical formulation for the behavior of the physical system has to be described. This step will yield the first of the three types of systematic errors involved in the simulation procedure as mentioned by Breuer (1998). The *formulation error* describes the difference between the behavior of the physical system and the exact solution of the mathematical formulation. After the mathematical formulation, the basic equations have to be discretized because often no analytical solution exists for a non-linear system of equations. This introduces the second type of error, called *discretization error*, defined as the difference between the exact solution of the mathematical formulation and the exact solution of the discretized equations. In Computational methods, the size of this error can be minimized by choosing the proper discertization method and a sufficiently fine grid. Finally the third type of error, called *convergence error*, is due to the difference between the iterative and the exact solution of the discretized equations. It depends on the solver and the convergence criteria chosen.

These types of errors should be clearly distinguished even though they are in general completely mixed up in the numerical solution of a physical problem. However, one should be aware of these errors that strongly affect the quality of any numerical simulation (Bahaidarah, 2004).

2.6.5 BOUNDARY CONDITIONS

2.6.5.1 Rigid wall boundary conditions

Near a rigid wall, there may be a bank or island as shown in Figure 2.8. The flow is quite complex. A very thin viscous sub-layer exists near a smooth wall, while roughness elements on a rough wall affect the flow significantly. Because the velocity gradient is quite high there, it is of high cost to resolve the flows in the viscous sub-layer and around individual roughness elements. A wall-function approach is often used instead (Wu, 2007).

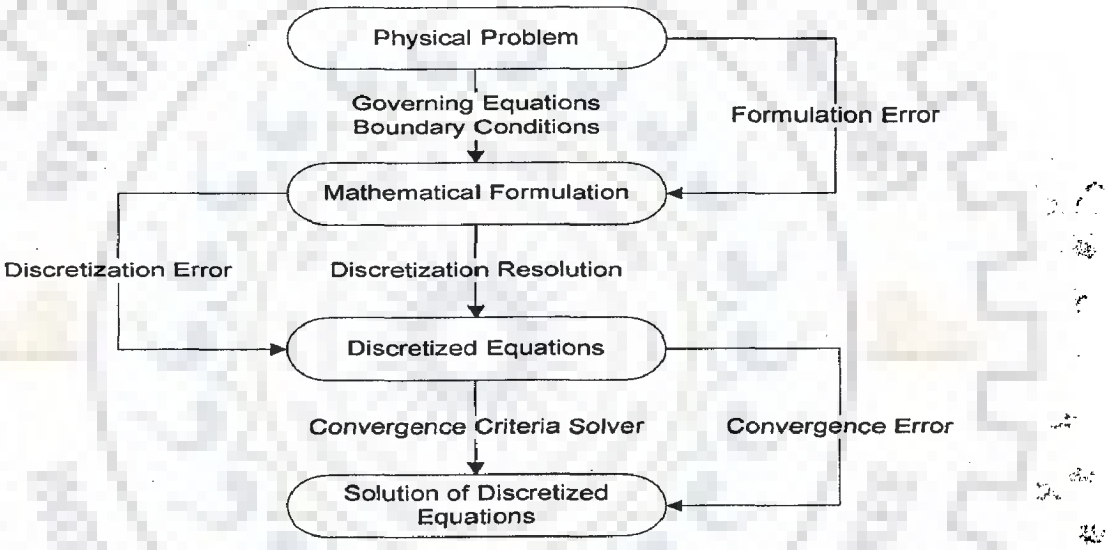

Figure 2.7 Different types of errors involved in a numerical simulation (Bahaidarah, 2004)

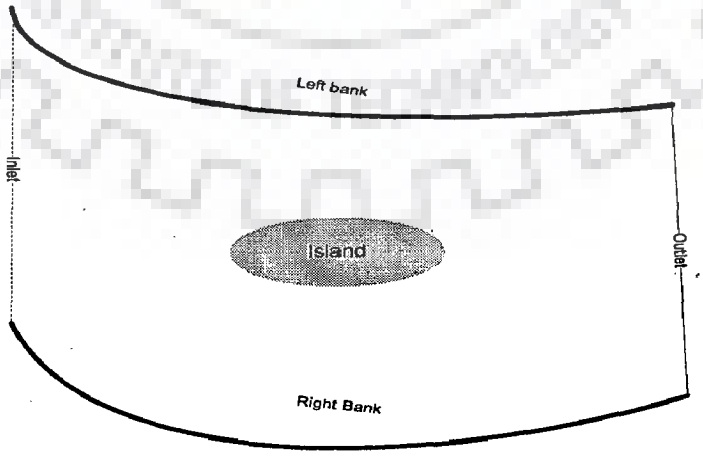

Figure 2.8 A typical horizontal 2-D computational domain (Wu, 2007)

At the sidewall, the logarithmic law is applied to the wall boundary, which is

$$\frac{u}{(u_*)_w} = \frac{1}{\kappa}\ln\left(\frac{y}{y_0}\right) \tag{2.55}$$

where $(u_*)_w$ =depth-averaged shear velocity at the sidewalls, y =distance from the wall and y_0 =location of zero velocity near the wall. Upon obtaining the gradient of velocity, the velocity at the sidewall is calculated based on the velocity at the adjacent internal node (Duan, 2004). Lien *et al.* (1999 a) has used the same logarithmic law of wall in the following way. The law of wall is applied outside the viscous sub-layer and transition layer in the range of $30 < y^+ < 100$, in which $y^+ = u_* y_w / \nu'$ and y_w = distance between the first computational grid point adjacent to the wall and the wall itself. Within the wall region, the universal law of the wall is applied as,

$$u^+ = \frac{1}{\kappa}\ln(Ey^+) \tag{2.56}$$

where $u^+ = u_w / u_*$, u_w =depth-averaged resultant velocity near the wall, and E(roughness parameter)= 9.0. On the basis of law of the wall, a so-called wall function (Rastogi and Rodi, 1978) is formulated, which links the near-wall velocities. Using the logarithmic velocity law; given in Eq. (2.56) and the expression for wall shear stress *i.e.* $\tau_w = \rho u_*^2$ can be expressed as (Biglari and Sturm, 1998)

$$\frac{\tau_w}{\rho} = \frac{\kappa u_* u_*}{\ln(Ey^+)} \tag{2.57}$$

The above wall shear stress relation in Eq. (2.57) is used as the wall boundary condition and is substituted into the momentum equation in the wall region to solve for the velocity component parallel to the wall.

2.6.5.2 Inflow and outflow boundary conditions

For subcritical flow, a boundary condition is needed at each inlet and outlet in order to derive a well-imposed solution while for supercritical flow two boundary conditions

should be specified at each inlet. For the sake of simplicity and cases of macro domain of alluvial rivers, only the subcritical flow case is considered below. The inflow boundary condition is usually a time series of flow discharge. However, a lateral distribution of velocity at the inlet is required in the depth-averaged 2-D model. Duan (2004) has directly used resistance equation for steady flow discharge at inlet. The total discharge is distributed along the cross section according to the local conveyance.

$$q_i = K\frac{h_i^{5/3}}{n} \tag{2.58}$$

where q_i=unit discharge, K=local conveyance coefficient and Manning's roughness coefficient. The current version of her model allows the specifications of roughness coefficient denoted as roughness height or Manning's roughness coefficient for each computational node. However, Duan (2004) has chosen the roughness coefficient as a constant for each case based on the bed roughness conditions described in the original experiments. Because the total discharge can be calculated as the integral of unit discharge across channel width, the following equation was applied.

$$Q = \int q_i ds = K\int \frac{h_i^{5/3}}{n} ds \tag{2.59}$$

where s denotes the direction of channel width and the flow conveyance and K can be obtained as follows:

$$K = \frac{Q}{\int \frac{h_i^{5/3}}{n} ds} \tag{2.60}$$

At the outlet, Duan (2004) has set surface elevation as a constant, which is the observed surface elevation at the experiment. The velocity of the outlet cross section is calculated based on the total discharge and flow depth at the outlet cross section. Wu (2007) mentions that the stream-wise (resultant) velocity U at each computational point of the inlet located in a nearly straight reach may be assumed to be proportional to the local flow depth i.e., $U \propto h^r$ Here, r is an empirical exponent; $r \approx 2/3$ for uniform flow. A

small r value means a fairly uniform distribution of velocity along the inlet cross-section. Therefore, for a given total inflow discharge $Q\left(=\int_0^B Uhdy'\right)$, U is determined by

$$U=\frac{Qh^r}{\int_0^B h^{1+r}dy'} \tag{2.61}$$

where B is the channel width at the water surface, and y' is the transverse coordinate. The inflow velocity direction must also be specified; it essentially determines the two components of velocity in the x and y directions at each point of the inlet. The boundary condition at the outlet may be a time series of the measured water stage, a stage-discharge rating curve measured or generated using the uniform or critical flow condition, or a non-reflective wave condition, depending on the outlet configurations. For tidal flow, the tidal level may also be determined using the major astronomical constituents of tide in the study reach (Wu, 2007). If a k-ε turbulence model is used, boundary conditions should be given for the turbulent energy and its dissipation rate at the inlet and outlet. At the outflow boundary, located in a reach with simple geometry and far from hydraulic structures, the gradients of flow velocity, turbulent energy, and dissipation rate can be given zero (Wu, 2007).

2.6.5.3 Wetting and drying techniques

In the calculation of flows in open channels with sloped banks, sand bars, and islands, the water edges change with time, and some part of the domain might be dry. A number of methods have been reported in the literature to handle this problem. They may be classified into two groups. One group tracks the moving water edges and adjusts the computational mesh to cover the wet domain. This group can use the boundary-fitted grid at each time (iteration) step and achieve better accuracy around the water edges. However, it results in complicated codes and perhaps requires more computational effort. The other group uses the fixed grid that covers the largest wet domain and treats dry nodes as part of the solution domain. The latter group includes the "small imaginary depth," "freezing," "porous medium," and "finite slot" methods (Wu, 2007).

The "small imaginary depth" method uses a threshold flow depth (a low value, such as 0.02m in natural rivers and 0.001m in experimental flumes) to judge drying and wetting at each time step. If the flow depth at a node is larger than the threshold value, this node is considered to be wet, and if the flow depth is lower than the threshold value, this node is dry. The dry nodes are assigned zero velocity. The water edges between the dry and wet areas can be treated as internal boundaries, at which the wall-function approach may be applied. The dry nodes can be excluded from the computation in an explicit algorithm, but must usually be included in an implicit algorithm. In the latter case, the "freezing" method is often adopted (Wu, 2007).

The "freezing" method also adopts a threshold flow depth to judge wetting and drying in the computational domain. At dry nodes, the Manning n is given a very large value, such as 10^{30}; therefore, the calculated velocity is zero and the water level does not change (as it is frozen). The "freezing" method can include dry nodes in an implicit algorithm. However, it should be noted that the water level gradient may induce false flow motions at the dry nodes. To avoid this problem, a horizontal water level profile at the dry nodes may be assumed (Wu, 2007). The "porous medium" method (Ghanem, 1995; Khan, 2000) assumes that the bed at the dry nodes is a porous medium and the flow can extend into the dry bed. Based on a specified minimum depth criterion, either the *St. Venant* or groundwater equations are applied at a particular computational point. The "finite slot" method proposed by Tao (1984) is similar to the "porous medium" method. In the "finite slot" method, a dry node is cut into two slots (with infinitesimal width and infinite depth) parallel to the x and y coordinates, respectively, in which the water is assumed to move. Thus, the water depth is kept positive artificially, even if the bed is dry. Different momentum equations are used at the dry nodes in the "porous medium" and "finite slot" methods, but the continuity equation at the dry nodes in both methods can be written as

$$f\frac{\partial h}{\partial t}+\nabla\cdot\left(h\vec{U}\right)=0 \tag{2.62}$$

where f is the storativity in the "porous medium" method, or the slot width in the "finite slot" method. The slot width is given as

$$f = \begin{cases} \varepsilon_0 + (1-\varepsilon_0)e^{a(z_s - z_b)} & z_s \le z_b \\ \\ 1 & z_s > z_b \end{cases} \tag{2.63}$$

where z_b is the bed elevation; ε_0 is the slot width, with a value between 0.02 and 0.05, when $z_s << z_b$; and a is a coefficient, which is usually larger than 2.0.

2.6.6 GRID ARRANGEMENT AND VELOCITY COMPONENTS

2.6.6.1 Orthogonal coordinate

Orthogonal grid formulation is the most employed scheme for computing fluid flow in complex geometrical domains. This type of grid is popular because either the domain of interest can be mapped onto orthogonal coordinates or nearly orthogonal grids can be generated by using an advanced grid generation technique such as elliptic differential equations. The merit of such a formulation is the simplicity of the governing equations of fluid flow when compared to its non-orthogonal grid counterparts. Additional terms arise because of the non-orthogonality of the coordinate system which would vanish if an orthogonal system were to be employed. The disadvantage of using orthogonal grid generation is the limitation of its applicability. In two-dimensional, the controlling of the gridline spacing is hard even if special techniques were to be used. The generality of the non-orthogonal coordinate formulation makes it more favourable.

2.6.6.2 Staggered and non-staggered grid

It is an issue to select the points in the domains at which the values of the unknown dependent variables are to be computed. The obvious choice is to store all the variables at the same locations and to use the same control volumes to all variables. Such a grid is called "collocated" or non-staggered grid. Since many of the terms in each of the discretized equations are essentially identical, the number of coefficients, that must be computed and stored, are reduced and the programming effort is simplified by this type of grid.

The non-staggered grid arrangement also has significant advantages in complicated solution domains, particularly when the boundaries have slope discontinuities or the boundary condition itself is discontinuous. All flow variables are stored at the cell centers. So solution procedure is simplified using less memory usage with respect to staggered grid arrangement in developed computer programs. A set of control volumes can be intended to fit the boundary including the discontinuity. Other arrangements of the variables lead to some of the variables to be located at the singularities of the grid, which may lead to singularities in the discretized equation as mentioned by Ferziger and Peric (1996). However, a serious drawback of this arrangement is that it may give rise to a checkerboard pressure pattern and a wavy pressure field may be interpreted as uniform by the momentum equations as explained by Patanker (1980) due to weak coupling between velocity and pressure. However, this problem is avoided by adopting Rhie and Chow interpolation technique (1983) into the numerical solver. Rhie and Chow (1983) presented a novel way of treating the convective terms in the momentum equations. They used the pressure difference between adjacent nodes instead of alternate nodes to calculate the cell face velocities. The best advantage of the staggered arrangement is the strong coupling between the velocities and the pressure (Figure 2.9). This will help to avoid some convergence problems and oscillation in the pressure and velocity fields in specific conditions.

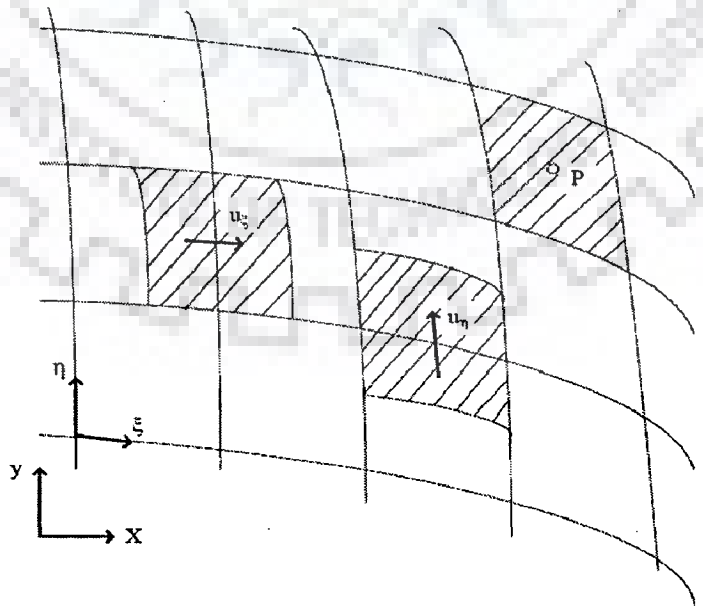

Figure 2.9 Example of staggered grid in two-dimension (Bahaidarah, 2004)

2.7 CHARACTERISTICS AND MODELLING OF BRAHMAPUTRA RIVER

2.7.1 THE BRAHAMPUTRA RIVER SYSTEM

The Brahmaputra River, termed as a moving ocean (WAPCOS, 1993), is an antecedent snow-fed large Trans-Himalayan river which flows across the rising young Himalayan range. Considerable variations in width, gradient, discharge and channel pattern occur throughout its course. Geologically, the Brahmaputra is the youngest of the major rivers of the world and unique in many respects. It happens to be a major river for three countries, *viz.*, China, India and Bangladesh. The river basin of the Brahmaputra is bounded on the north by the Kailas and Nyen- Chen-Tanghla ranges of mountains; on the east by the Salween river basin and the Patkai range running along the Indo-Myanmar border; on the south by the Nepal Himalayas, the Naga and Barail ranges and the Meghalaya Plateau; and on the west by the Ganga river basin (Sarma, 2005).

Throughout its course within India, the Brahmaputra is braided with some well defined nodal points with rock crops where the river width is narrow and restricted within stable banks. All along its course in the valley, abandoned wetlands and back swamps are common. The river carries about 735 million metric tons of suspended sediment loads annually.

The Indian section of the Brahmaputra River receives innumerable tributaries flowing down the northern, north-eastern and southern hill ranges. The mighty Brahmaputra along with the well-knit network of its tributaries controls the geomorphic regime of the entire region, especially the Brahmaputra valley. In the north, the principal tributaries are the Subansiri, the Jia Bhareli, the Dhansiri, the Puthimari, the Pagladiya, the Manas and the Champamati. Amongst these, the Subansiri, the Jia Bhareli and the Manas are the Trans-Himalayan Rivers. The principal south bank tributaries are the Burhi Dehing, the Disang, the Dikhow, the Dhansiri (south), the Kopili and the Krishnai.

It is observed that three Trans-Himalayan tributaries, the Subansiri, the Jia Bhareli and the Manas on the north have a basin more than 10000 km^2, *i.e.*, only two south bank tributaries namely the Dhansiri and the Kopili form a basin area more than 10000 km^2.

The Manas River combined with the Aie and the Beki rivers drains biggest area of 41, 350 km^2. The 442 km long Subansiri River and the 360 km long Burhi Dehing River are considered longest, respectively, among the north-bank and south bank tributaries (Water Year book, CWC, 2002). In terms of the average annual discharge, the Subansiri carries a discharge of 755-771 m^3/sec, which ranks first among all the important tributaries. The Jia Bhareli and the Manas in the north carrying an average annual suspended sediment load of 2013 ha-m and 2166 ha-m, respectively, are the leading rivers in the case of sediment discharge. Of all the north and south bank tributaries, as many as fourteen have sediment yields in excess of 500 tons/ km^2/year, the highest being 4721 tons/km^2 /year (Sankhua,2005).

2.7.2 HYDROLOGIC AND PHYSIOGRAPHIC CHARACTERISTICS OF THE BRAHMAPUTRA RIVER

The statistical details of the river are described below (Sankhua, 2005).

(a) Total basin area from its source to its confluence with Ganga at Goalundo in Bangladesh	580,000 km^2
(i)Basin area within Tibet	293,000 km^2
(ii)Basin area in Bhutan and India	240,000 km^2
(iii) Basin area in Bangladesh	47,000 km^2
(b) Length from its source to outfall in Bay of Bengal	2,880 km
(c) Gradient	
(i) Reach within Tibet	1 in 385
(ii) Reach between Indo-China border and Kobo in India	1 in 515
(iii) Reach between Kobo and Dhubri	1 in 6,990
(iv) Reach within Bangladesh	
First 60 km from Indian Border	1 in 11,340
Next 100 km stretch	1 in 12,360

Next 90 km stretch 1 in 37,700

(d) Observed discharge

(i) Maximum observed discharge at Pandu (on 23.8.1962) 72,727 m^3/sec

(ii) Minimum observed discharge at Pandu (on 20.2.1968) 1,757 m^3/sec

(iii) Average dry season discharge at Pandu 4,420 m^3/sec

(iv) Normal annual rainfall within basin ranges between 2,125 mm in Kamrup District of Assam and 4,142 mm in Tirap district of Arunachal Pradesh.

2.7.3 CHANNEL PROCESS

The Brahmaputra River in India forms a complex river system characterized by the most dynamic and unique water and sediment transport pattern. The Brahmaputra is the fourth largest river in the world (Goswami and Das, 2000). The water yield from per unit basin area is among the highest of the major rivers of the world. The Jia Bhareli, a major tributary, carries a mean annual water discharge of the order of 0.0891 $m^3/sec/km^2$. As estimated by Goswami (1982), the Brahmaputra yields 0.0306 $m^3/sec/km^2$ at Pandu. As regards sediment transport, the river has also set records in carrying large volumes of sediment. The high intensity of monsoon rains, easily erodible rocks, steep slopes, and high seismicity contribute a lot by rendering the river a heavily sediment-laden one. Thus, the Brahmaputra becomes one of the leading sediment carrying rivers of the world. Amongst the large rivers of the world, it is second only to the Yellow river in China in the amount of sediment transport per unit of basin area (Goswami and Das, 2000).

The Brahmaputra is a uniquely braided river of the world. Although braiding seems to be best developed in rivers flowing over glacier outwash plains or alluvial fans, perfect braiding is also found to occur in large alluvial rivers having low slope, such as the Brahmaputra in Assam (India) and Bangladesh or the Yellow River in China. The Assam section of the Brahmaputra River is in fact, highly braided and characterized by the presence of numerous lateral as well as mid channel bars and islands (Goswami and Das, 2000).

The high degree of braiding of the Brahmaputra channel near Dibrugarh and downstream of Guwahati is indicated by the calculated braiding indices of 5.3 and 6.7 respectively for the two reaches, following the method suggested by Brice (1964). A braiding Index of 4.8 for the entire Assam section of the river calculated on the basis of satellite data of 1993 also suggests a high degree of braiding of the Brahmaputra River (Sankhua, 2005). Further, based on remote sensing data study, Sharma and Akhtar (2010) reported a progressive decrease in Plan Form Index (*PFI*) values in different reaches of Brahmaputra River in Assam flood plain during recent years (1990-2007). This is indicative of intensification of braiding process in recent years.

The basin with varied terrain characteristics and being an integral part of the monsoonal regime of south-east Asia shows a marked spatial variation in the distribution of precipitation. The rainfall in the Teesta valley varies from 164 cm in the south to 395 cm in the north. The average annual rainfall in the lower Brahmaputra valley is 213 cm while the same in the north-eastern foothill belt is 414 cm. The basin as a whole has the average annual rainfall of 230 cm with a variability of 15-20%. The Himalayan sector receives 500 cm of rainfall per year, the lower ranges receiving more than the higher areas (Goswami , 1985).

In the sub-Himalayan belt soils with little depth developed over the Tertiary sand stones generally belong to red loam, laterite, and brown hill soil type with admixtures of cobbles and boulders. The greater part of the Brahmaputra valley is made up of new alluvium of recent deposition overlying Tertiary, Mesozoic and Archaean bedrocks. Along the piedmont zone, there occurs some patches of older alluvium extending along the the tributaries flowing from the Himalayan foothills. The soils of the Meghalaya plateau and the Mikir Hills in the south are of laterite and loamy silt and fine silt types.

In general, braiding in the Brahmaputra follows the mechanism of central bar type of braid formation. During high flow, a central bar is deposited in the channel and gradually the bar accretes vertically to the level of the floodplain. It also builds on the downstream end through deposition of bed load material due to the slack water occurring behind the bar. The bar growth causes a decrease in total cross-sectional area leading, thereby, to the

instability of the channel. Lateral erosion then follows on one or both the banks. Through repetition of this process in the divided reach, a well developed braided reach with multiple sandbars and islands is produced (Sankhua, 2005).

In the Assam section of the river, the presence of nodes of stable banks of rock outcrops or stiffed clay formation is found to effect the formation and location of the bars. There are nine nodal reaches of narrow constriction at various locations along the Brahmaputra, which are at Murkongselek (4.8 km), Disangmukh (5.10 km), downstream of Jhanjimukh (3.75), upstream of Dhansiri north (4.0 km), downstream of Dhansirimukh (4.4 km), upstream of Tezpur (3.6 km), Pandu Guwahati (1.2 km), U/s of Sualkuchi (2.4 km) and Pancharatna (2.4 km) (Sankhua, 2005). Since banks are relatively stable in these reaches, the river scours deeper to accommodate the flood discharge. The scoured debris is then deposited in the channel immediately downstream from the narrow section. As a result, the channel becomes wider and bars and islands are produced. Formation of bars causes reduction in cross sectional area and the river, therefore, cuts its banks laterally to accommodate the discharge. Thus, in the downstream of the nodes, intense braiding develops resulting in channel widening through continuous migration of both banks of the Brahmaputra (Sankhua, 2005).

As reported from the studies carried out on braided rivers of the world, the major factors thought to be responsible for braiding and bar formation are steep channel gradient, high erodibility of bank materials, great variability in discharge, overabundance of load, and aggradation of the channel bed. In case of the Brahmaputra River in Assam bar formation and channel division are owing to a combination of factors like high variability in discharge, excessive sediment transport, easily erodible bank materials and aggradation of the channel. Being the fourth largest river in the world with an average discharge of 19,830 m3/sec at its mouth, the Brahmaputra carries 82% of its annual flow at Pandu (Assam) only during the rainy season from May to October (Goswami,1992). The maximum and minimum mean monthly flows in the river during 1990-2002 are 48,160 m^3/sec and 3,072 m^3/sec, respectively. On an average, therefore, the maximum flow is more than fifteen times the minimum (Goswami and Das, 2000).

High variability in discharge of the river is mainly caused by seasonal rhythm of the monsoon and the freeze-thaw cycle of the Himalayan snow. As regards the pattern of sediment transport, the river has the record of carrying excessive sediment load which is believed to be one of the important factors responsible for braiding.

2.7.4 2-D or 3-D mathematical modelling for Brahmaputra River

In view of the extensive review of literature presented in the previous section, it can be summarized that a number of attempts have been done to simulate the realistic flow field including transverse components in complex geometry like bends, curves (Lien *et al.*, 1999; Odgaard, 1989a; Duan, 2004; Seo *et al.*, 2008). However, assessment of flow-field in braided river like that of Brahmaputra with 'secondary flow correction' in complex geometry is hardly found in literature.

Moreover, braiding seems to be best developed in rivers flowing over glacier outwash plains or alluvial fans, perfect braiding is also found to occur in large alluvial rivers having low slope, such as the Brahmaputra in Assam (India) and Bangladesh or the Yellow River in China. The Assam section of the Brahmaputra River is in fact, highly braided and characterized by the presence of numerous lateral as well as mid channel bars and islands (Goswami and Das, 2000). Due to these facts, the research on Brahmaputra River in the past mostly relied on field investigation and physical modelling. Only after 1980s, numerical modelling, especially 1-D modelling has been gradually applied in flow simulation and sediment prediction in Brahmaputra River (Sharma, 2004). Yet successful implementation of 2-D depth averaged modelling in Brahmaputra River Reaches in Assam Flood Plains is hardly found in literature due to its highly complex topography and difficulty in reproduction of geometric data mathematically.

2.8 SUMMARY

In this chapter, a comprehensive review of literature is presented with regard to braided river characteristics, 2-D depth averaged modeling for rivers, secondary flow and its corrections in controlling equations in river flow scenario, discretization methods, coordinate transformation. Investigations in these potential research areas have been

highlighted from earlier works to the developments in more recent years. The gaps in the concurrent research in relation to braided river modelling in particular to Brahmaputra River have also been attempted to be adequately focused.

Based on the comprehensive literature review, following observation can be broadly summarized in relation to mathematical modelling of the braided stream in particular to Brahmaputra River.

1. One dimensional mathematical modelling for flow field simulation in braided river is highly approximated and fallacious on account of numerous assumptions. It considers only unidirectional flow variability. All the model parameters, state variables and forcing functions are approximated through average valued composite representation across the flow in the stream. Naturally, 1-D models are insufficient to deal with secondary currents or helical flow, vortex formation, flow reversal and anisotropy effects.

2. The preferred way to represent the fluvial process in the braided river adequately with inclusion of 3-D flow structures is obviously the development and application of 3-D models. However, there are some practical limitations to apply 3-D models for reach scale modelling. 3-D modelling is to be developed by superimposing numerous fluvial processes especially in braided stream through mathematical functions and has too many imponderables for predicting flow variables. It is computationally tedious and highly expensive in terms of numerical solution algorithm for large flow domain such as where the width of the channel is in the order of 20 km with 100km of reach length.

3. The best alternate way to find the solution is to reduce the dimension of the modelling to ease the computational effort without any significant compromise in the accuracy and objectives. In lieu of that, 2-D model can be applied.

4. In wide braided rivers where water depth is very small in compare to width, the vertical acceleration of flow can be reasonably ignored and pressure is assumed to be

hydrostatic. The velocity is depth averaged to reduce the dimension of the modelling.

5. However, on account of reduction of dimension in 2-D from 3-D , the accounting of secondary flow or helical flow will be reflected in terms of only flow in transverse direction (vertical velocity is ignored as stated earlier)

6. Especially in braided channels where flow domain may have a number of curvilinear multiple channels with considerable skew symmetric flow domain, the accuracy of flow field can possibly be improved with suitable incorporation of realistic secondary flow (effect of vertical acceleration due to skew symmetric domain characteristics) into the governing 2-D flow equations through introducing additional source /sink terms due to flow dispersion tensor (secondary flow corrections). This way an enhanced 2-D depth averaged model can be developed whose result is expected to be close proximity to realistic physical flow scenario.

7. The dispersion stresses due to skew-symmetric flow domain have been estimated empirically by numerous investigators like Lien *et al.* (1999), Hsieh and Wang (1999); Nagata *et al.*(2000); Duan (2004), Duan and Julien (2005), Seo *et al.* 2008 etc. The empirical models given by earlier investigators for estimating flow dispersion stress tensor can possibly be improved further to get better estimation of flow dispersion stresses. Better flow dispersion stress model can bring forth a better 2-D depth averaged enhanced model for realistic prediction of flow field.

8. The skew symmetric flow domain is the essential feature of braided streams. Use of the Cartesian co-ordinate is often inconvenient and impractical representing the skew symmetric irregular geometry when boundaries of the domain are not aligned along the Cartesian base vector directions. Hence body fitted coordinates system is employed whose principal coordinate directions are along the domain boundaries. The flexibility offered by body-fitted grid techniques is useful in the modelling of practical problems involving irregular geometries and like that of a braided stream and capable of capturing useful features in the area of interest.

9. Reviews of earlier works indicated that braided rivers react to changes in flow stage significantly. More quantitative data are needed for research on understanding of the processes involved during the flow stages. The apparent complexity the braided pattern seems to have implications for the nature of the main processes involved in shaping braided morphology, bar genesis and evolution. With significant advances in data acquisition techniques such as remote sensing data usage, use of latest instrument to measure stage discharge at gauge stations and hydro-graphic data collection in close intervals, reliable data become more available on larger rivers, such as the Brahmaputra, the issue of morphological processes and their relationship to channel scale in braided systems can be addressed though multidimensional mathematical modelling with much ease and accuracy.

10. However, a great deal of uncertainty over the true process representation of braided river is yet to be adequately addressed through mathematical modelling of higher dimension. Correct process representation of the distribution of flow concentration at the channel confluences and around the evolved braid-bars, side-bars and islands within the flow domain is yet to be achieved through adequately incorporating its effect through tested mathematical functions into the governing equations of simulating the flow field.

11. The problem of key morphological processes of braided channels has yet to be fully addressed (Bristow and Best, 1993). The apparent similarities of plan-form and cross-sectional characteristics require further investigation ((Bristow and Best, 1993). Similarly it has been demonstrated by many researchers that a proper understanding of the flow and sedimentary processes at channel junctions is fundamental to the braided river morphology (Leopold and Wolman, 1957a; Bridge, 1993; Ashworth, 1996, Sankhua, 2005). The studies to-date that have been carried out to establish models and frameworks for understanding braided river behaviour have been mostly qualitative in nature. The lack of quantitative studies on morphology and evolution braiding pattern with flow stages for braided rivers has impeded the development of the understanding of this complex environment further.

12. From this review of the literature, it is seen that there is a complete lack of quantitative studies on spatio-temporal morphological modelling of the braided rivers due to apparent fallacious estimation of transverse flow concentrations around the braid bars and sidebars which is a one of the prime causative factor for bed evolution, braiding pattern change and influencing the intermittent river bank erosion. Two dimensional enhanced flow models can possibly simulate the braiding process provided adequate distribution of flow concentration including transverse flow field is adequately accounted for into the flow governing equations without going into for numerically and computationally expensive 3-D models for macro scale river simulation. Moreover 3-D models require reliable three dimensional sediment process representations and are highly data intensive. Hence for practical engineering purposes, 2-D enhanced models for braided river can fetch equally significant model results without much improvement apparently with 3-D models which is still at nascent stage of development for macro flow domains with complex bed geometry.

In view of the above, the objective of the present study is framed to develop and test a numerical 2-D enhanced depth averaged model embedded with turbulence and secondary flow attributes along with nonlinear stream boundary in a real braided river like Brahmaputra in Assam flood plain of Indian Territory.

****

CHAPTER-3

DESCRIPTION OF STUDY AREA

3.1 INTRODUCTION

Stretching within the basin periphery of 82°E to 97° 50' E longitudes and 25° 10' to 31° 30' N latitudes the river Brahmaputra envelopes a drainage area of 580000 sq.km and is recognized to be one of the most braided channel river. The hugeness of the river system in terms of the drainage area and the lengths it encompasses may be realised from its aerial extent as under.

Table 3.1 Aerial distribution of the total drainage basin (Bora, 2004)

Country	Basin area (Km^2)	Channel Length (km)
I. Tibet (China)	293000	1,625
2. Bhutan	45000	-
3. India	194413	918
(a) Arunachal Pradesh	81424	278
(b) Assam	70634	640
(c) Nagaland	10803	-
(d) Meghalaya	11667	-
(e) Sikkim	7300	-
(f) West Bengal	12585	-
4. Bangladesh	47000	337

Originating in a great glacier mass at an altitude of 5300 m just south of the lake Konggyu Tso in the Kailas range, about 63 km southeast of Mansarovar lake in southern Tibet at an elevation of 5300m, the Brahmaputra flows through China (Tibet), India and Bangladesh for a total distance of 2880 km, before emptying itself into the Bay of Bengal through a joint channel with the Ganga. It is known as the Tsangpo in Tibet (China), the Siang or Dihang in Arunachal Pradesh (India), the Brahmaputra in Assam (India) and the Jamuna, Padma, and Meghna in Bangladesh.

Before entering India, the river flows in a series of big cascades as it rounds the Namcha-Barwa peak. The river forms almost trough receiving the flows of its tributaries both

from North and South. The river, with its Tibetan name Tsangpo in the uppermost reach, flows through

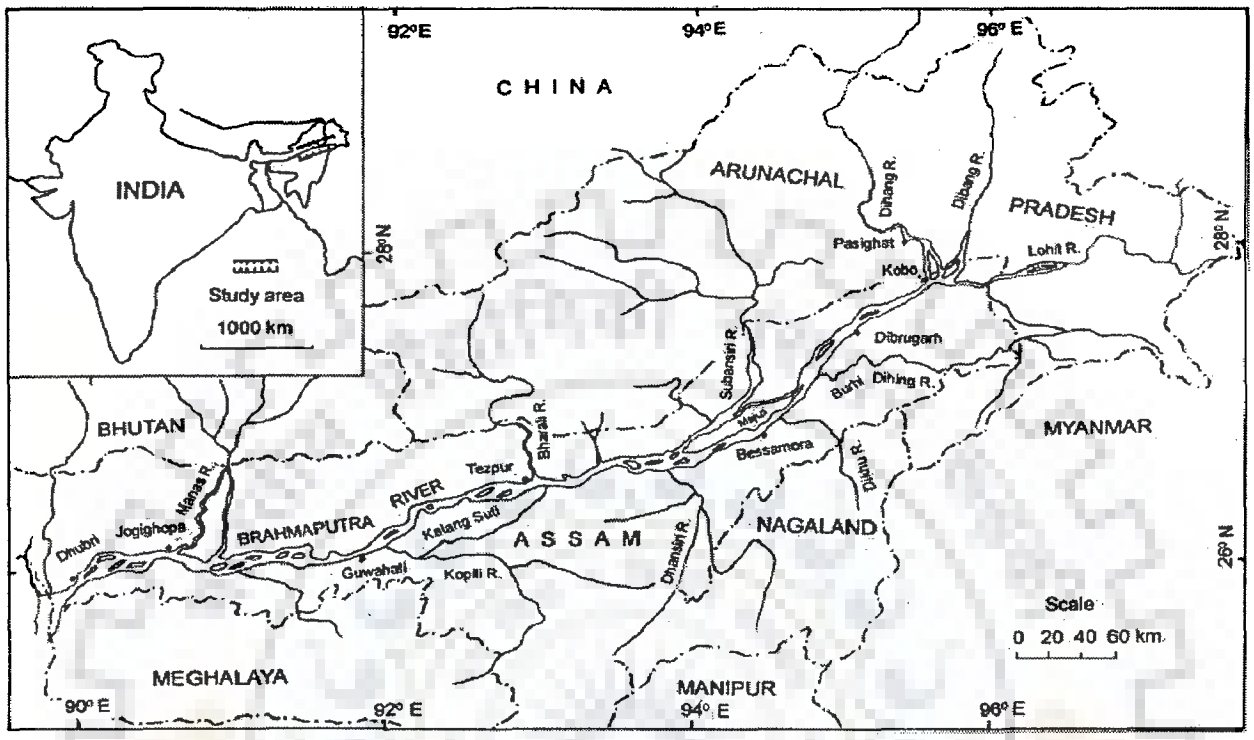

Figure 3.1 Location map of the Brahmaputra River in Assam, India (Sarma, 2005)

southern Tibet for about 1625 km eastward and parallel to tributaries, viz., the Nau Chhu, the Tsa Chhu, the Men Chhu, the Charta Tsangpo, the Raga Tsangpo, the Tong Chhu, the Shang Chhu, the Gya Chhu, the Giamda Chhu, the Po Tsangpo and the Chindru Chhu and the right bank tributaries, viz. the Kubi, the Kyang, the Sakya Trom Chhu, the Rhe Chhu, the Rang Chhu, the Nyang Chhu, the Yarlang Chhu, and the Trulung Chhu join the river along its uppermost reach. At the extreme eastern end of its course in Tibet the Tsangpo suddenly enters a deep narrow gorge at Pe, where in the gorge section the river has a gradient ranging from about 4.3 to 16.8 m/km (Figure 3.2).

The river enters in India near Tuning in Arunachal Pradesh. After travelling for a distance of 278 km up to Kobo, it meets with two rivers the Dibang and the Lohit in Assam near Kobo. Below this confluence point, the river is known by the name of the Brahmaputra. It passes through Assam into Bangladesh and at last it meets with the Ganga near Goalundo in Bangladesh before joining the Bay of Bengal. Its total length is 2880 km comprising 1625 km in Tibet, 918 km in India and 337 km in Bangladesh. It is also one of the most

braided rivers in the world with width variation from 1.2 km at Pandu near Guwahati to about 18.13 km near Gumi few km distances downstream to this point.

Traversing through deep narrow gorges of the Himalayan terrain the Tsangpo takes a southward turn and enters Indian Territory at an elevation of 660 m. The river then enters the State of Assam (India) taking two important tributaries the Dibang and the Lohit. At the exit of the gorge the slope of the river is only 0.27 m/km. At the head of the valley near Dibrugarh the river has a gradient of 0.09-0.17 m/km, which is further reduced to about 0.1 m/km near Pandu (Figure 3.1). The mighty Brahmaputra rolls down the Assam valley from east to west for a distance of 640 km up to Bangladesh border (Table 3.1)(Sarma, 2005).

3.2 LONGITUDINAL SECTION OF THE BRAHMAPUTRA RIVER

The longitudinal section of the Brahmaputra River from its origin to the outfall point is depicted in Figure 3.2. It is observed that Pasighat, stop is quite steep. As one moves from Pasighat to Pandu(Guwahati), bed slope becomes mild indicating that the flow characteristics in downstream reaches is predominantly sub-critical and laden with sediment with wide banklines.

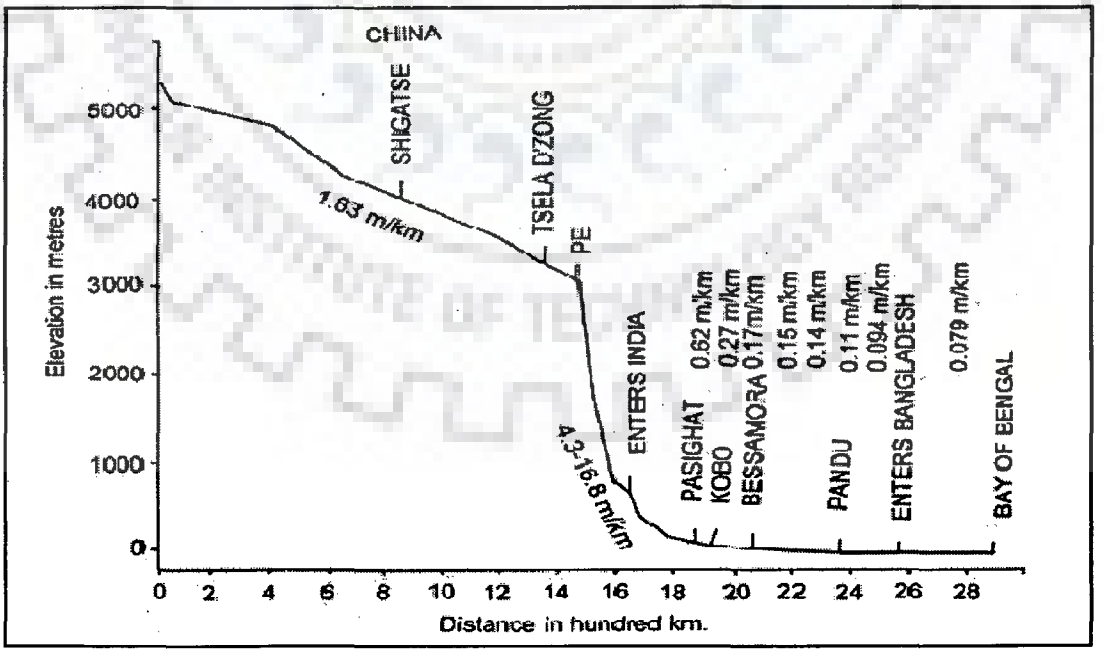

Figure 3.2 Longitudinal profile of the Brahmaputra River (Sarma, 2005)

3.3 STUDY AREA

For the application of developed hydrodynamic model, the reach between measured cross sections number-22 (Pandu near Guwahati) to 9 (Jogighopa) released by *Brahmaputra Board, G.O.I.*(spanning over about 100 km length in Assam state of Indian Territory) has been taken as flow domain and extracted from Satellite image of the year under study. Measured fourteen cross-section data (Cross section 22 to cross section 9) for year 1997 was used (Appendix III). The location of study stretch of Brahmaputra River with respect to whole Brahmaputra River in Assam flood pain in India is shown in Figure 3.3. Flow domain (Primary Flood Plain) of the study stretch is delineated from geo referenced satellite image (IRS-LISS-III satellite imagery) of 1997 was delineated by GIS software tools. The delineated image of the study stretch of Brahmaputra River is shown in Figure 3.4. Figure 3.5 is presented to show the geo-referenced image of the flow domain extracted from the imagery of 1997 for further preprocessing to design the geometric data for 2-D mathematical modelling. Preparation and processing of the geometric data for the study domain is discussed in Chapter 8 of this thesis in detail.

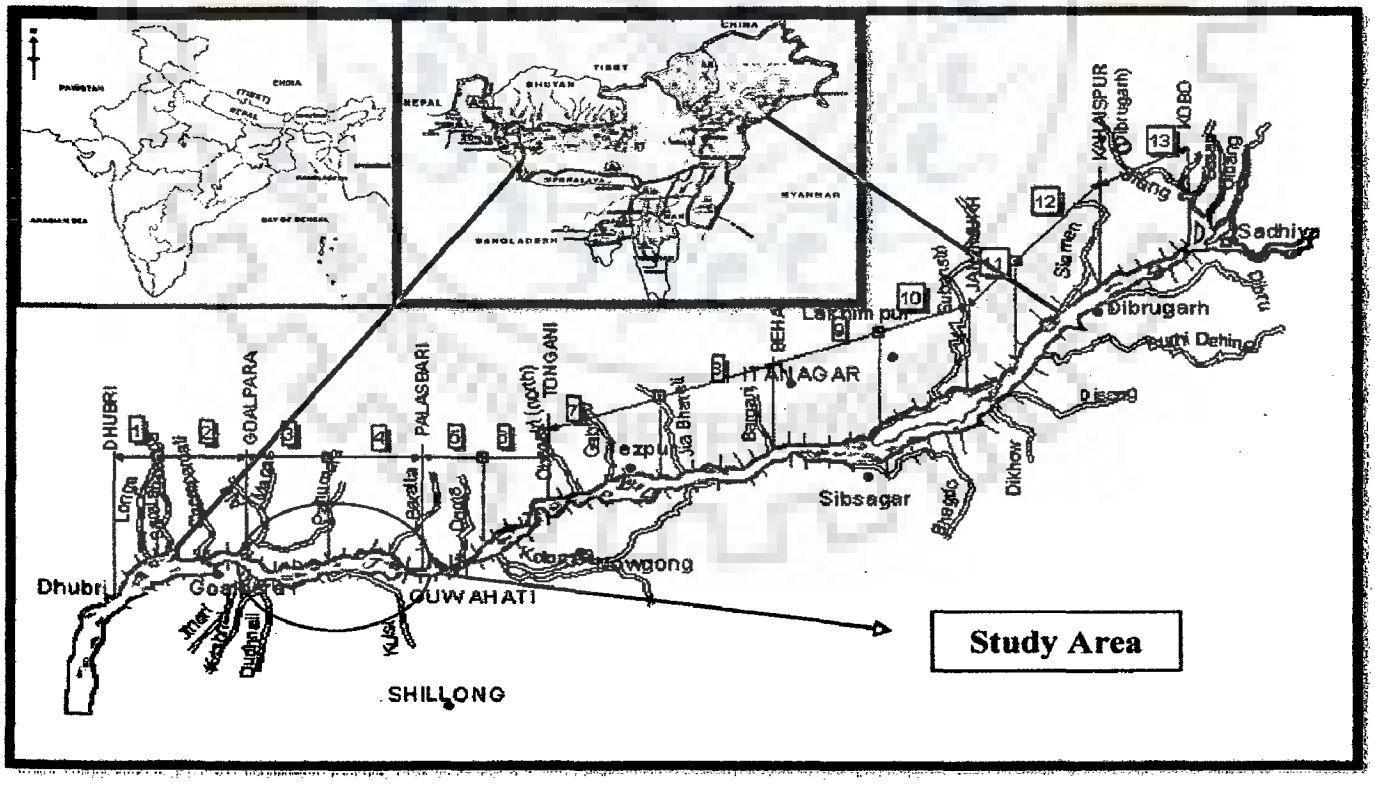

Figure 3.3 Location of study stretch of River Brahmaputra (*NDMA*, 2011)

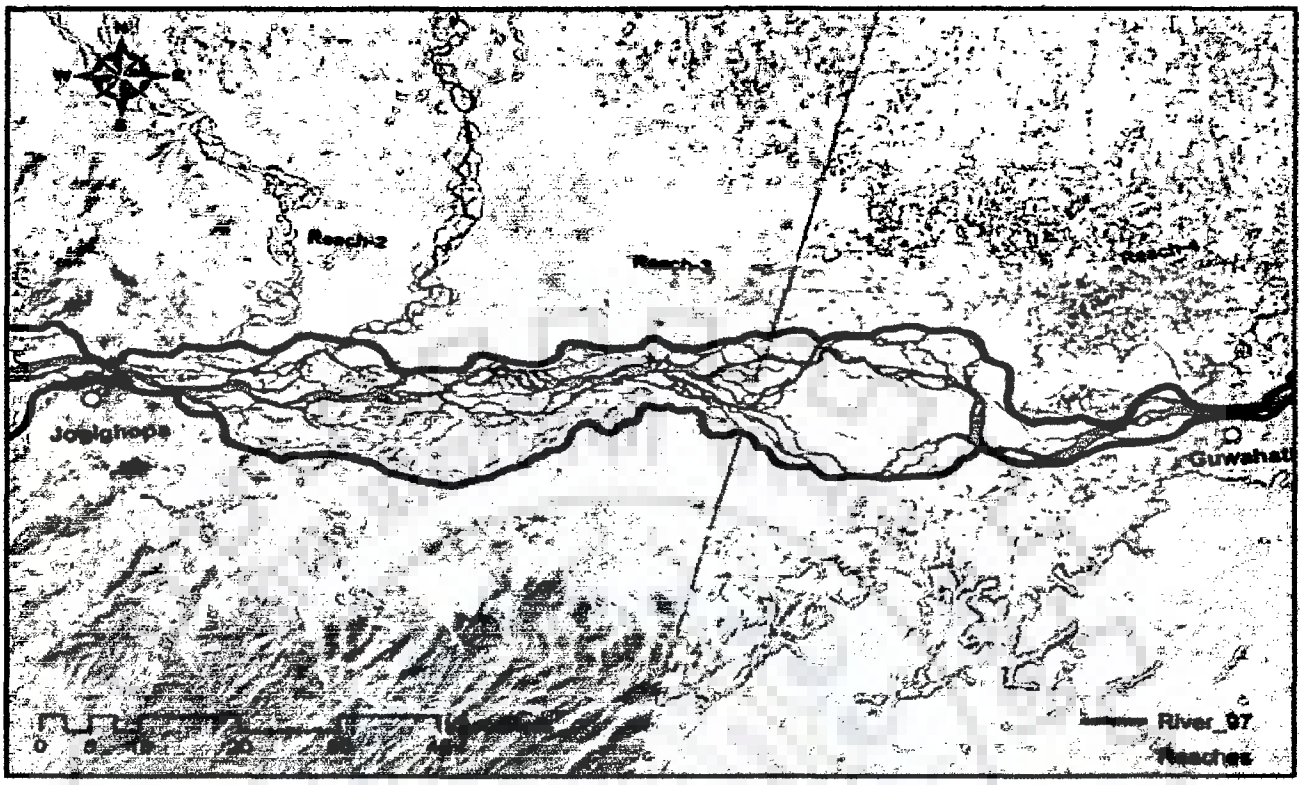

Figure 3.4 Study area delineated from satellite image (*courtesy: NDMA-2011)*

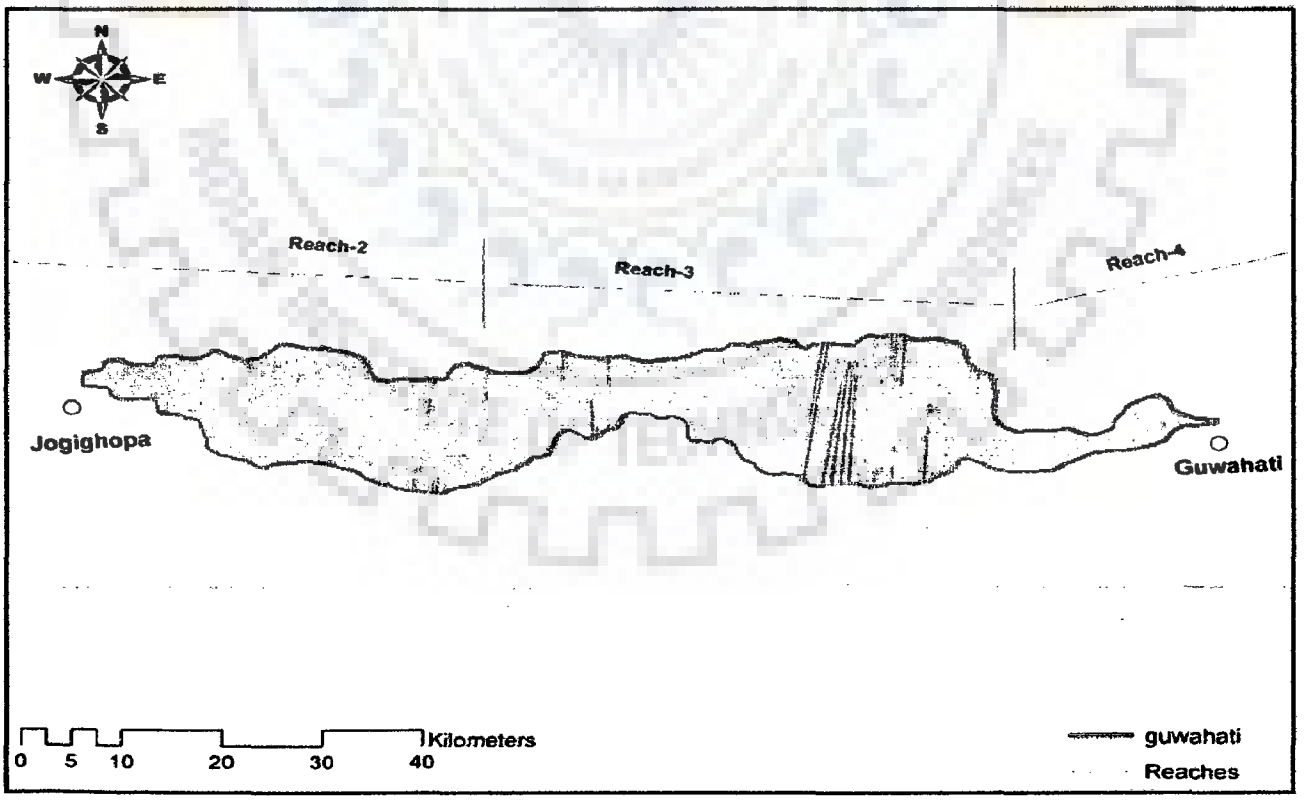

Figure 3.5 River flow domain delineated from satellite image for the year 1997

CHAPTER-4

DEVELOPMENT OF MODIFIED DISPERSION STRESS TENSOR IN TWO DIMENSIONAL CURVILINEAR FLOW FIELD

4.1 INTRODUCTION

The empirical relations for dispersion stress terms in 2-D curvilinear flow field have been given by numerous researchers. Towards this, Engelund and Skovaard (1973) and Shimizu and Itakura (1989) predicted the transverse velocity, however it was valid only near the bed. Lien *et al.* (1999) used orthogonal curvilinear coordinate system and incorporated the dispersion terms derived from stream-wise and transverse velocity profile (de Vriend, 1977). Duan (2004) employed the Cartesian Co-ordinate to facilitate model application in meandering and non meandering channels. Duan (2004) found that in meandering channel, mass diffusion coefficient is much larger than turbulent diffusion coefficient. Mathematical expressions for components of dispersion coefficient tensor have been deduced by integrating the product of discrepancy between the depth averaged and actual velocity. Duan (2004) deduced the dispersion terms with the assumption that the stream-wise velocity satisfies the logarithmic law. It seems that integration by Duan (2004) ignored the role of boundary sub-layer formation at the bed. However, this assumption may not always hold good in many situations. For example, for very mild bed gradient with highly sub-critical flow zones in alluvial river flow case, the boundary sub-layer is rationally assumed to be intact to satisfy logarithmic law of velocity distribution. This chapter attempts to deal with the derivation of flow dispersion tensor in general curved channels which are common features in braided and dynamic alluvial streams. The objective of this chapter is to derive the appropriate set of mathematical expressions for dispersion stress terms for depth averaged 2-D model to be used for complex non-orthogonal curvilinear flow domain with mild bed slope. The numerical model development with finite volume method and the verification of the proposed formulations has been discussed in Chapter 9 of this thesis.

4.2 DISPERSION STRESS TENSOR

Components of dispersion stress terms in Cartesian coordinate which can be included in momentum transport equations are D_{xx}, D_{xy} and D_{yy} . These terms can be expressed as follows (Duan, 2004).

$$D_{xx} = \int_{z_0}^{h+z_0} \rho(u_x - U_x)^2 dz$$
$$D_{xy} = \int_{z_0}^{h+z_0} \rho(u_x - U_x)(u_y - U_y) dz \quad (4.1)$$
$$D_{yy} = \int_{z_0}^{h+z_0} \rho(u_y - U_y)^2 dz$$

where z_0=zero velocity level.

For open channel free surface gravity flow, cohesive terms are non-significant and can be neglected. The depth averaged parabolic eddy viscosity model (zero equation model) is adopted for the turbulence term. The depth averaged eddy viscosity is computed as [Eq.(4.2)] (Kalkwijk and De Vriend, 1980; Zhou, 1995)

$$\nu_t = \frac{1}{6}\kappa U_* h \quad (4.2)$$

Where κ=Von Karman' coefficient and U^*=Shear velocity=$\left[C_d\left(U_x^2 + U_y^2\right)\right]^{1/2}$.

4.2.1 TRANSFORMED GOVERNING EQUATIONS WITH DISPERSION STRESS TENSOR

The transformed depth averaged governing equations in generalized curvilinear coordinate system (ξ, η, τ) for continuity and momentum equation (Eqs.4.3, 4.4 and 4.5) are derived (detail derivation is presented in Chapter 5) as follows.

$$\frac{\partial}{\partial \tau}(\rho h J) + \frac{\partial}{\partial \xi}(\rho h J \hat{u}_\xi) + \frac{\partial}{\partial \eta}(\rho h J \hat{u}_\eta) = 0 \quad (4.3)$$

$$\frac{\partial}{\partial\tau}(\rho hJU_x)+\frac{\partial}{\partial\xi}\left[\rho hJ\hat{u}_\xi U_x\right]+\frac{\partial}{\partial\eta}\left[\rho hJ\hat{u}_\eta U_x\right]-\rho hJ\nu_t\left(\alpha_{11}\frac{\partial^2U_x}{\partial\xi^2}+\alpha_{22}\frac{\partial^2U_x}{\partial\eta^2}\right) \tag{4.4}$$

$$=-\rho ghJ\left(\xi_x\frac{\partial H}{\partial\xi}+\eta_x\frac{\partial H}{\partial\eta}\right)-\rho JC_d(U_x)\sqrt{(U_x)^2+(U_y)^2}+\rho hJ\nu_t\alpha_{12}\frac{\partial^2U_x}{\partial\xi\partial\eta}-\left(\xi_x\frac{\partial D_{xx}}{\partial\xi}+\eta_x\frac{\partial D_{xx}}{\partial\eta}+\xi_y\frac{\partial D_{xy}}{\partial\xi}+\eta_y\frac{\partial D_{xy}}{\partial\eta}\right)$$

$$\frac{\partial}{\partial\tau}(\rho hJU_y)+\frac{\partial}{\partial\xi}\left[\rho hJ\hat{u}_\xi U_y\right]+\frac{\partial}{\partial\eta}\left[\rho hJ\hat{u}_\eta U_y\right]-\rho hJ\nu_t\left(\alpha_{11}\frac{\partial^2U_y}{\partial\xi^2}+\alpha_{22}\frac{\partial^2U_y}{\partial\eta^2}\right)= \tag{4.5}$$

$$-\rho ghJ\left(\xi_y\frac{\partial H}{\partial\xi}+\eta_y\frac{\partial H}{\partial\eta}\right)-C_d\rho J(U_y)\sqrt{(U_x)^2+(U_y)^2}+\rho hJ\nu_t\left(\alpha_{12}\frac{\partial^2U_y}{\partial\xi\partial\eta}\right)-\left(\xi_x\frac{\partial D_{xy}}{\partial\xi}+\eta_x\frac{\partial D_{xy}}{\partial\eta}+\xi_y\frac{\partial D_{yy}}{\partial\xi}+\eta_y\frac{\partial D_{yy}}{\partial\eta}\right)$$

where $\xi_x=\partial\xi/\partial x$, $\eta_x=\partial\eta/\partial x$, $\xi_y=\partial\xi/\partial y$, $\eta_y=\partial\eta/\partial y$, $\alpha_{11}=\xi_x^{\,2}+\xi_y^2$,

$\alpha_{22}=\eta_x^{\,2}+\eta_y^2$, $\alpha_{12}=2(\xi_x\eta_y+\xi_y\eta_x)$, $J=x_\xi y_\eta-x_\eta y_\xi$

In Eqs. (4.3) to (4.5), $\hat{u}_m$ (m=ξ, η) are the velocity components in the curvilinear coordinate (ξ,η,τ) which relate to U_x, U_y as

$$\begin{pmatrix}\hat{u}_\xi\\ \hat{u}_\eta\end{pmatrix}=\begin{pmatrix}\xi_x & \xi_y\\ \eta_x & \eta_y\end{pmatrix}\begin{pmatrix}U_x\\ U_y\end{pmatrix} \tag{4.6}$$

4.2.2 DERIVATION OF DISPERSION STRESS TERMS IN MOMENTUM EQUATIONS

The dispersion terms resulting from the integration of the product of the discrepancy between the *mean* velocity and actual vertical velocity distribution were included in the momentum equations to take into account the effect of secondary current. Free surface flow in natural rivers is generally classified as turbulent-subcritical within the ranges of corresponding values of *Reynolds numbers* and *Froude numbers*. One of the important aspects of the free surface flow is shear velocity parameter which causes variation in velocity in different layers of fluid flow. So from the literature, one can readily assume that the stream wise velocity profile satisfies the logarithmic distribution law, *i. e.*

$$\frac{u_s}{U^*}=\frac{1}{\kappa}\ln\left(\frac{z}{z_o}\right) \tag{4.7}$$

where z=vertical coordinate level (See Figure 4.1), u_s=velocity in stream-wise direction and z_0 is calculated according to flow Reynolds number as follows,

$$z_0 = 0.11\frac{\nu}{U^*} \text{ ..... }, \frac{U^* k_s}{\nu} \le 5;$$

$$z_0 = 0.033\, k_s \text{ ..... }., \frac{U^* k_s}{\nu} \ge 70; \tag{4.8}$$

$$z_0 = 0.11\frac{\nu}{U^*} + 0.033\, k_s .., 5 \ge \frac{U^* k_s}{\nu} \ge 70$$

Where in Eq.(4.8), ν = Kinematic Viscosity; k_s = Roughness height(m) and U^* = Shear Velocity

Ideally, at the bed boundary, u (stream-wise actual velocity) is zero; but for developing numerical scheme, value of base velocity should judiciously be taken non zero value to ensure feasible solutions. Hence, it is well justified to exclude boundary sub-layer thickness (depth up to which boundary sub-layer is formed) and assign non-zero base velocity to achieve numerical solution close to experimental results. In other words, solid physical boundary is replaced with fluvial boundary and corresponding fluvial boundary condition has to be taken into consideration when analyzing the velocity profile vertically (Figure 4.1).

Duan (2004) computed the depth averaged stream-wise velocity

$$U_s = \frac{1}{h}\int_0^h u_s\, dz \tag{4.9}$$

Equation(4.9) implies that the depth in the expression is integrated in denominator, from zero to h, instead of z_0 (*zero bed elevation*) to h. Here, modification can be proposed through computing the depth averaged stream-wise velocity integrated over the depth from zero velocity level (z_0) to water surface elevation (h) as

$$U_s = \int_{z_0}^h u_s\, dz \Big/ \int_{z_0}^h dz \tag{4.10}$$

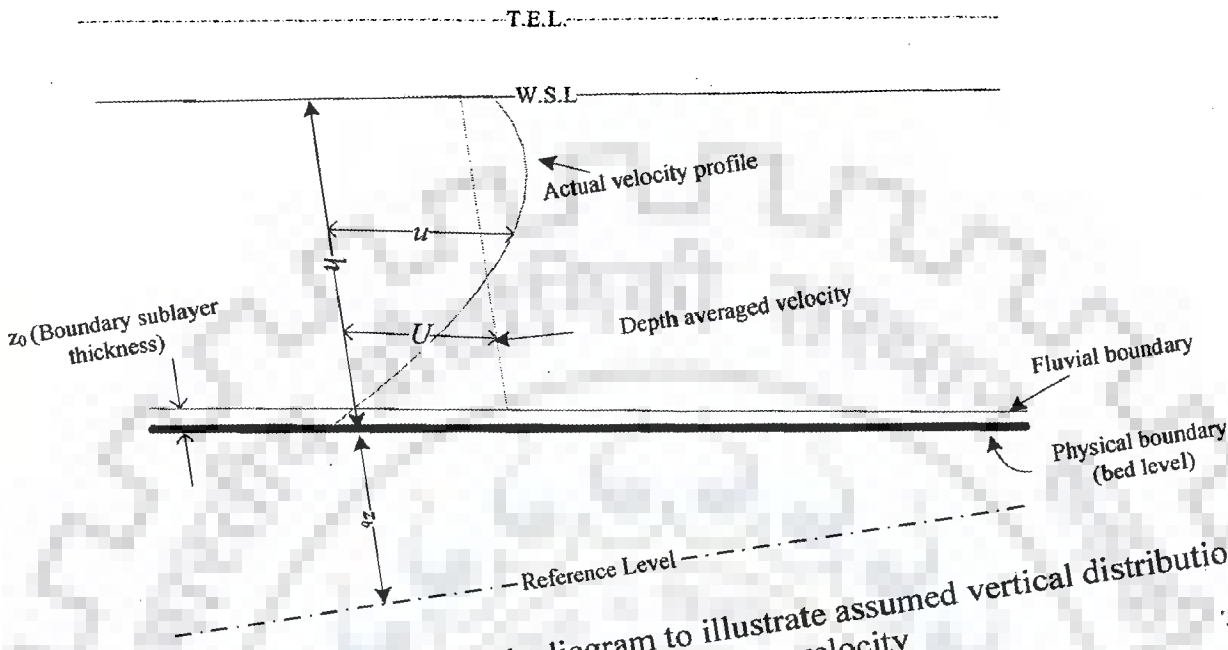

Figure 4.1 Schematic diagram to illustrate assumed vertical distribution of stream-wise velocity

Integrating the logarithmic velocity profile along the depth, from Eq. (4.7), one can finally deduce an expression as follows.

Now

$$U_s = \frac{\int_{z_0}^{h} u_s dz}{(h - z_0)} = \frac{\int_{z_0}^{h} u_s dz}{h\left(1 - \frac{z_0}{h}\right)} \tag{4.11}$$

Let $\eta_0 = {}^{z_0}/_{h}$, Combining Eq. (4.7) and Eq. (4.11), one gets the following expression,

$$\frac{U_s}{U^*} = \frac{1}{\kappa h(1-\eta_0)} \int_{z_0}^{h} \ln\left(\frac{z}{z_0}\right) dz \,, \tag{4.12a}$$

Or,

$$\frac{U_s}{U^*} = \frac{1}{\kappa} \frac{z_0}{h(1-\eta_0)} \left[\frac{z}{z_0} \ln\left(\frac{z}{z_0}\right) - \frac{z}{z_0} \right]_{z_0}^{h}, \tag{4.12b}$$

Or,

$$\frac{U_s}{U^*} = \frac{1}{\kappa} \frac{z_0}{h(1-\eta_0)} \left[\frac{h}{z_0} \ln\left(\frac{h}{z_0}\right) - \frac{h}{z_0} - \frac{z_0}{z_0} \ln\left(\frac{z_0}{z_0}\right) + \frac{z_0}{z_0} \right], \tag{4.12c}$$

Or,

$$\frac{U_s}{U^*} = \frac{1}{\kappa(1-\eta_0)} \left[\ln\left(\frac{h}{z_0}\right) - 1 + \frac{z_0}{h} \right] = \frac{1}{\kappa(1-\zeta_0)} \left[\frac{z_0}{h} - 1 + \ln\left(\frac{h}{z_0}\right) \right], \tag{4.12d}$$

Or,

$$\frac{U_s}{U^*} = \frac{1}{\kappa(1-\eta_0)} \left[-\ln(\eta_0) - 1 + \zeta_0 \right] = \frac{1}{\kappa(1-\eta_0)} \left[\eta_0 - 1 - \ln(\eta_0) \right] \tag{4.12e}$$

Dividing Eq.(4.12e) with Eq.(4.7), one obtains,

$$\frac{u_s}{U_s} = (1-\eta_0) \frac{\ln\left(\frac{z}{z_0}\right)}{\eta_0 - 1 - \ln(\eta_0)} \tag{4.13}$$

Rearranging the above expression, one has

$$\frac{u_s}{U_s} - 1 = \frac{(1-\eta_0)\ln\left(\frac{z}{\eta_0 h}\right) - \eta_0 + 1 + \ln\eta_0}{\eta_0 - 1 - \ln(\eta_0)} \tag{4.14a}$$

Or,

$$\frac{u_s - U_s}{U_s} = \frac{(1-\eta_0)\ln\left(\frac{z}{h}\right) - (1-\eta_0)\ln\eta_0 - \eta_0 + 1 + \ln\eta_0}{\eta_0 - 1 - \ln(\eta_0)} \tag{4.14b}$$

$$u_s - U_s = \frac{U}{\eta_0 - 1 - \ln(\eta_0)} \left((1-\eta_0)\ln\left(\frac{z}{h}\right) - \eta_0 + 1 \right) \tag{4.15a}$$

Or,

$$u_s - U_s = \frac{U_s(1-\eta_0)}{\eta_0 - 1 - \ln(\eta_0)} \left(\ln\left(\frac{z}{h}\right) + 1 \right) \tag{4.15b}$$

The transverse velocity profile is assumed to be linear. As proposed by Odgaard(1989a,b), following relation is adopted for this model.

$$u_n = U_n + 2v_s\left(\frac{z}{h} - \frac{1}{2}\right) \tag{4.16}$$

Where u_n, U_n, and v_s are transverse velocity, depth averaged transverse velocity and the transverse velocity at the water surface. Engelund and Skovgaard (1973) derived the deviation angle of the bottom shear as follows

$$\left(\frac{\tau_n}{\tau_s}\right)_b \approx \left(\frac{u_n}{u_s}\right)_b = 7.0\frac{h}{r}, \tag{4.17}$$

where r=radius of channel curvature and the secondary flow at the surface and the bottom are equal. Therefore Eq. (4.17) is used to express transverse velocity at the surface. Thus,

$$(v_s)_b = 7.0(h/r)(u_s)_b \tag{4.18}$$

Or,

Substituting Eq. (4.18) in Eq. (4.16), one obtains (same as Duan (2004)'s approach),

$$u_n = U_n + 7.0\frac{h}{r}U_s\left(\frac{z}{h} - \frac{1}{2}\right) \tag{4.19}$$

Let us define

$$\frac{(1-\eta_0)}{\eta_0 - 1 - \ln(\eta_0)} \equiv \gamma \tag{4.20}$$

Substituting Eq. (4.20), Eq. (4.15b) and Eq. (4.19) convert to;

$$u_s - U_s = \gamma U_s\left(\ln\left(\frac{z}{h}\right) + 1\right) \tag{4.21a}$$

$$u_n - U_n = 7.0\frac{h}{r}U_s\left(\frac{z}{h} - \frac{1}{2}\right) \tag{4.21b}$$

4.2.2.1 Expressions for dispersion stress tensors

The dispersion stress terms at the stream-wise and transverse directions can be expressed as.

$$D^{c}_{xx} = \int_{z_0}^{h+z_0} \rho (u_s - U_s)^2 \, dz \tag{4.22a}$$

$$D^{c}_{xy} = \int_{z_0}^{h+z_0} \rho (u_s - U_s)(u_n - U_n) dz \tag{4.22b}$$

$$D^{c}_{yy} = \int_{z_0}^{h+z_0} \rho (u_n - U_n)^2 \, dz \tag{4.22c}$$

where D^{c}_{xx} , D^{c}_{xy} and D^{c}_{yy} are dispersion stress terms in curvilinear coordinate system. Substituting Eqs. (4.21a) in Eqs. (4.21b), one can deduce dispersion stress tensor presented in following steps.

(a) The first dispersion term $D_{xx}{}^{c}$

Substituting Eq(4.21a) in Eq(4.22a), one can get,

$$D^{c}_{xx} = \rho \gamma^{2} U_s U_s \int_{z_0}^{h} \left(\ln\left(\frac{z}{h}\right) + 1 \right)^2 dz \tag{4.23}$$

Now consider $z/h=m$, then, $dz=h\ dm$, $m_1=z_0/h=\eta_0$ lower integral bound, $m_2=h/h=1$ upper integral bound. With these substitution Eq.(4.23) becomes

$$D^{c}_{xx} = \rho \gamma^{2} U_s U_s h \left[\int_{\eta_0}^{1} (\ln(m))^2 \, dm + 2m \int_{\eta_0}^{1} \ln(m) dz + (1 - \eta_0) \right], \tag{4.24a}$$

Or,

$$D^{c}_{xx} = \rho \gamma^{2} U_s U_s h \left[\left(m(\ln m)^2 - 2m \ln m + 2m \right)_{\eta_0}^{1} + 2\left(m \ln m - m \right)_{\eta_0}^{1} + (1 - \eta_0) \right], \tag{4.24b}$$

Or,

$$D^{c}_{xx} = \rho \gamma^{2} U_s U_s h \left[2 - \eta_0 (\ln \eta_0)^2 + 2\eta_0 \ln \eta_0 - 2\eta_0 + 2(-1 - \eta_0 \ln \eta_0 + \eta_0) + 1 - \eta_0 \right] \tag{4.24c}$$

One gets the final expression as,

$$D_{xx}^{c} = \rho\gamma^{2}U_{s}U_{s}h\left[-\eta_{0}(\ln\eta_{0})^{2} - \eta_{0} + 1\right] \tag{4.24d}$$

(b) The second dispersion term D_{xy}^{c}

Similar to the above, one can get expression for the Second Dispersion Stress Term

$$D_{xy}^{c} = \rho\int_{z_0}^{h}\gamma U_{s}\left(\ln\left(\frac{z}{h}\right)+1\right)\times 7.0\,\frac{h}{r}U_{s}\left(\frac{z}{h}-\frac{1}{2}\right)dz, \tag{4.25a}$$

Or,

$$D_{xy}^{c} = -7.0\,\rho\gamma\,\frac{h}{r}U_{s}U_{s}\int_{z_0}^{h}\left(\ln\left(\frac{z}{h}\right)+1\right)\left(\frac{1}{2}-\frac{z}{h}\right)dz, \tag{4.25b}$$

Or,

$$D_{xy}^{c} = -7.0\,\rho\gamma\,\frac{h}{r}U_{s}U_{s}\left(\frac{1}{2}\int_{z_0}^{h}\ln\frac{z}{h}dz - \int_{z_0}^{h}\frac{z}{h}\ln\frac{z}{h}dz + \frac{1}{2}\int_{z_0}^{h}dz - \int_{z_0}^{h}\frac{z}{h}dz\right) \tag{4.25c}$$

Again taking $m=z/h$ and integrating and transforming the upper and lower bound as done earlier, and taking h common, one has ,

$$D_{xy}^{c} = -7.0\rho\gamma\frac{h^{2}}{r}U_{s}U_{s}\left(\frac{1}{2}\left[m\ln m-m\right]_{\eta_0}^{1} - \frac{1}{4}\left[2m^{2}\ln m-m^{2}\right]_{\eta_0}^{1} + \frac{1}{2}(1-\eta_0) - \frac{1}{2}\left[m^{2}\right]_{\eta_0}^{1}\right), \tag{4.26a}$$

Or,

$$D_{xy}^{c} = -7.0\rho\gamma\frac{h^{2}}{r}U_{s}U_{s}\frac{1}{4}\left(2\left[-1-\eta_0\ln\eta_0+\eta_0\right]-\left[-1-2\eta_0^{2}\ln\eta_0+\eta_0^{2}\right]+2(1-\eta_0)-2\left[1-\eta_0^{2}\right]\right), \tag{4.26b}$$

Or

$$D_{xy}^{c} = -1.75\,\rho\gamma\,\frac{h^{2}}{r}U_{s}U_{s}\left(\left[-2-2\eta_0\ln\eta_0+2\eta_0+1+2\eta_0^{2}\ln\eta_0-\eta_0^{2}+2-2\eta_0-2+2\eta_0^{2}\right]\right), \tag{4.26c}$$

Or,

$$D_{xy}^{c} = -1.75\,\rho\gamma\,\frac{h^2}{r}U_s U_s\left([-2\eta_0 \ln\eta_0 + 2\eta_0^2 \ln\eta_0 + \eta_0^2 - 1]\right), \tag{4.26d}$$

Or,

$$D_{xy}^{c} = -1.75\,\rho\gamma\,\frac{h^2}{r}U_s U_s\left([-2\eta_0 \ln\eta_0(1-\eta_0) - (1+\eta_0)(1-\eta_0)]\right), \tag{4.26e}$$

Or,

$$D_{xy}^{c} = 1.75\,\rho\gamma\,\frac{h^2}{r}U_s U_s(1-\eta_0)(2\eta_0 \ln\eta_0 + \eta_0 + 1) \tag{4.26f}$$

(c) The third dispersion term D_{yy}^{c}

Using the similar procedure as above, one can obtain the expression for D^{c}_{yy}

$$D_{yy}^{c} = \rho(7)^2\,\frac{h^2}{r^2}U_s U_s\int_{z_0}^{h}\left(\frac{z}{h}-\frac{1}{2}\right)^2 dz, \tag{4.27a}$$

Or,

$$D_{yy}^{c} = 49.0\,\rho\,\frac{h^2}{r^2}U_s U_s\left(\int_{z_0}^{h}\left(\frac{z}{h}\right)^2 dz - \int_{z_0}^{h}\left(\frac{z}{h}\right)dz + \frac{1}{4}\int_{z_0}^{h} dz\right) \tag{4.27b}$$

Again taking $m=z/h$ and integrating and transforming the upper and lower bound as done earlier, one can obtain,

$$D_{yy}^{c} = 49.0\,\rho\,\frac{h^3}{r^2}U_s U_s\left(\left[\frac{m^3}{3}\right]_{\eta_0}^{1} - \left[\frac{m^2}{2}\right]_{\eta_0}^{1} + \frac{1}{4}(1-\eta_0)\right), \tag{4.28a}$$

Or,

$$D_{yy}^{c} = 49.0\,\rho\,\frac{h^3}{r^2}U_s U_s\left(\frac{1}{3} - \frac{\eta_0^3}{3} - \left(\frac{1}{2} - \frac{\eta_0^2}{2}\right) + \frac{1}{4} - \frac{\eta_0}{4}\right), \tag{4.28b}$$

Or,

$$D^c_{yy} = 49.0\rho \frac{h^3}{r^2} U_s U_s \left(\frac{1}{3} - \frac{\eta_0^3}{3} - \frac{1}{2} + \frac{\eta_0^2}{2} + \frac{1}{4} - \frac{\eta_0}{4} \right), \tag{4.28c}$$

Or, finally one may obtain,

$$D^c_{yy} = 49.0\rho \frac{h^3}{r^2} U_s U_s \left(-\frac{\eta_0^3}{3} + \frac{\eta_0^2}{2} - \frac{\eta_0}{4} + \frac{1}{12} \right) \tag{4.28d}$$

The relation between depth averaged velocities in curvilinear coordinates and Cartesian coordinate can be given as (Duan 2004)

$$\begin{aligned} U_x &= U_s \cos\theta_s + U_n \cos\theta_n \\ U_y &= U_s \sin\theta_s + U_n \sin\theta_n \end{aligned} \tag{4.29}$$

where θ_s and θ_n are angles between stream wise, transverse directions pointing outward and positive x-axis respectively. Similarly the dispersion terms in Cartesian coordinates can be related to that in curvilinear coordinates as follows (Duan 2004).

$$\begin{aligned} D_{xx} &= D^c_{xx} \cos^2\theta_s + 2D^c_{xy} \cos\theta_s \cos\theta_n + D^c_{yy} \cos^2\theta_n \\ D_{yy} &= D^c_{xx} \sin^2\theta_s + 2D^c_{xy} \sin\theta_s \sin\theta_n + D^c_{yy} \sin^2\theta_n \\ D_{xy} &= D^c_{xx} \cos\theta_s \sin\theta_s + 2D^c_{xy} (\cos\theta_n \sin\theta_s + \sin\theta_n \cos\theta_s + D^c_{yy} \sin\theta_n \cos\theta_n \end{aligned} \tag{4.30}$$

The dispersion stress terms finally obtained in Eqs. (4.24d, 4.26f and 4.28d) can be transformed by Eqs. (4.29) and Eqs. (4.30) to get modified dispersion stress tensor in Cartesian coordinate system.

4.2.3 COMPARISON OF MODIFIED AND DUAN'S FORMULATIONS

The correlations by Duan(2004) for dispersion stress tensor in curvilinear coordinate system are as follows (Derivation in Annexure-I).

$$D^c_{xx} = \chi^2 U_s U_s h \left[-\eta_0 \ln\eta_0 (\ln\eta_0 - 2) + 2\eta_0 (1-\eta_0)(1-\ln\eta_0) - (\eta_0 - 1)^3 \right] \tag{4.31a}$$

$$D^c_{xy} = 3.5C \frac{h^2}{r} U_s U_s \left(\left[-\eta_0^2 \ln\eta_0 + \eta_0 \ln\eta_0 - \eta_0 + \eta_0^3 \right] \right) \tag{4.31b}$$

$$D^{c}_{xy} = 49\frac{h^3}{r^2}U_s U_s\left(-\frac{\eta_0^3}{3}+\frac{\eta_0^2}{2}-\frac{\eta_0}{4}+\frac{1}{12}\right) \quad (4.31c)$$

For the statistical comparison, theoretical data for a wide rectangular channel is analyzed. A qualitative comparison of variations of dispersion stresses for varying sinuosity with the modified formulation (Eqs.4.24d, 4.26f and 4.28d) and Duan's(2004) formulations (Eqs. 31 a,b and c) have been compared. Four configurations (Curvature 0.34, 0.72, 1.00 and 1.05) were chosen to cover low, moderate, high and very high sinuosity curved channels (Abad and Garcia 2005). The width ratio ($\beta=B/h$, where h=water depth, B=channel width) were chosen as 10, 15 and 20. Longitudinal slope is kept as 0.001 and 0.025 for creating *sub-critical* and *supercritical* condition respectively. Average velocities are estimated using Manning's equation (Manning's n is kept 0.025). z_0 is taken as $D_{50}/30$(Roughness height (k_s) is kept equal to D_{50}=0.44 mm).

It can be seen that expressions of dispersion stress terms as obtained in the present work are not in complete agreement of Duan (2004) formulations as given in Eq. (4.31a). From Eq. (4.31b), it is apparent that for any comparison between the two approaches, the value of *'C'* should have been available. However, in her another paper (Duan and Julien, 2005), there is no C in Eq. (4.31b). Thus, there is lack of enough insight into the adoption of any appropriate value of C. However, in view of Duan and Julien (2005), the value of *'C'* is taken unity for comparative purposes only.

Assuming C as one, an attempt is made to relate Eq.(4.31b) with Eq. (4.26f), developed in the present work. Following empirical relation is obtained.

$D^{c}_{xy}=A_0+A_1\times D^{c}_{xy}$(Duan) (R-Square=0.9854; Adjusted R-Square=0.9847) (4.32)

where A_0=-3.147 and A_1=-103.676

To appreciate the difference between the two expressions for two approaches of dispersion terms (as given in Eqs.4.24d, 4.26f, 4.28d and 4.31), certain computations are done for a variety of conditions (Table 4.1).

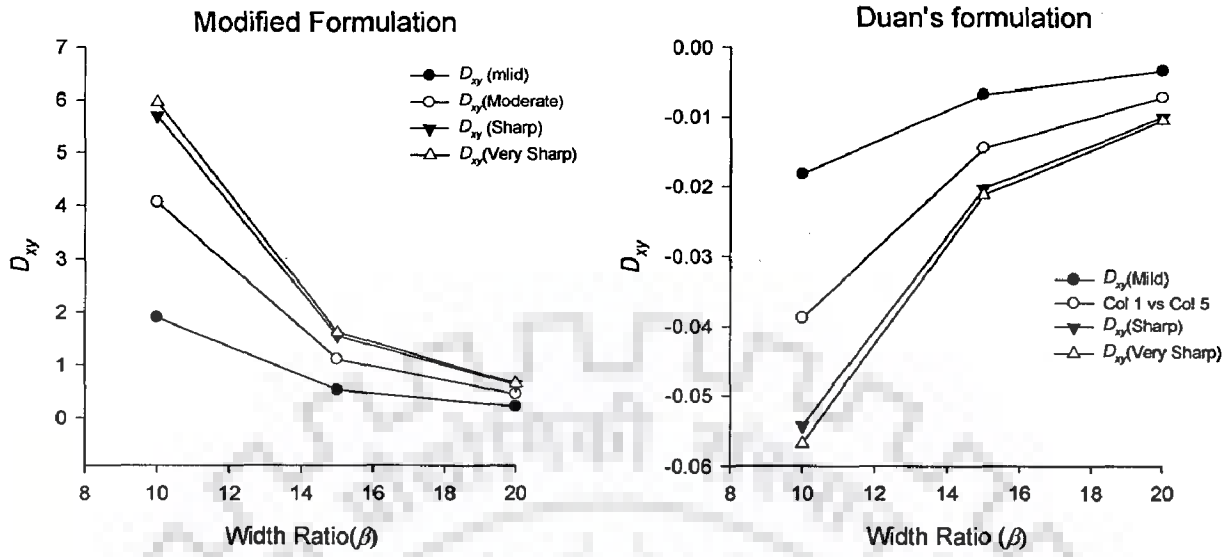

Figure 4.2 Variation of D^c_{xy} (N/m^2) with width ratio (β) for two approaches

The differences do appear in the formulations of the first term (D^c_{xx}) and second terms (D^c_{xy}). The formulation for D^c_{xx} are different for the present approach and Duan's approach yet computed values of this term is similar and close valued, as shown in Table 4.1. However, the modified model (Eq. 4.24d) has much simpler mathematical representation than Duan(2004)'s model (Eq. 4.31a).

The variability of D^c_{xy} for both approaches is shown in Figure 4.2. The trend of the variation is closely related (R-square=0.985), but values of D^c_{xy} differs considerably. Plot of D^c_{xy} against width ratio(β) for both approaches for variety of conditions are shown in Figure 4.2.

The third term D^c_{yy} is identical in both cases as in present formulation and Duan's work. The trend of second terms is statistically similar with very low difference in mean and standard deviation (using statistically determined 'C' value). R-square (0.99 for D^c_{xx} and D^c_{yy}, and 0.98 for D^c_{xy}) and standard error suggests high degree of goodness of fit for both models (For Eqs. 4.26f, and 4.31b). The inconsistency in the values of dispersion stress terms from Duan's model for different hydraulic conditions is evident in the Table 4.1. For example, in modified model's D^c_{xx}, D^c_{xy}, and D^c_{yy} is are varying consistently for different width ratio(β), whereas same terms show inconsistent variations with different β for Duan's Model. These models are developed for sub-critical flow condition; however,

their trends are also analyzed for super-critical flow condition. Plots of variation of different terms with width ratio for sub-critical and super-critical conditions are shown in Figures 4.2 and 4.3.

Table 4.1 Computations of dispersion stress tensor by modified and Duan (2004)'s expressions

S No.	Curve Type	Curvature	Width Ratio (β)	Longitudinal Slope	Velocity (m/s)	Froude Number	Modified Terms (N/m^2)			Duan(2004)-Terms(N/m^2)		
							D^c_{xx}	D^c_{xy}	D^c_{yy}	D^c_{xx}	D^c_{xy}	D^c_{yy}
1		0.34	10	0.001	0.57	0.3304	1.204	1.90	4.00	1.204	-0.0182	4.00
2		0.34	15	0.001	0.43	0.2522	0.512	0.52	0.69	0.512	-0.0068	0.69
3	Mild	0.34	20	0.001	0.36	0.2082	0.280	0.20	0.20	0.280	-0.0034	0.20
4		0.34	10	0.025	2.83	1.6521	30.098	47.56	99.88	30.101	-0.4540	99.88
5		0.34	15	0.025	2.16	1.2608	12.800	12.89	17.23	12.802	-0.1697	17.23
6		0.34	20	0.025	1.79	1.0408	6.994	5.11	4.95	6.996	-0.0844	4.95
7		0.72	10	0.001	0.57	0.3304	1.204	4.06	18.24	1.204	-0.0388	18.24
8		0.72	15	0.001	0.43	0.2522	0.512	1.10	3.15	0.512	-0.0145	3.15
9	Medium	0.72	20	0.001	0.36	0.2082	0.280	0.44	0.90	0.280	-0.0072	0.90
10		0.72	10	0.025	2.83	1.6521	30.098	101.61	455.88	30.101	-0.9699	455.88
11		0.72	15	0.025	2.16	1.2608	12.800	27.54	78.66	12.802	-0.3626	78.66
12		0.72	20	0.025	1.79	1.0408	6.994	10.92	22.61	6.996	-0.1802	22.61
13		1.00	10	0.001	0.57	0.3304	1.204	5.69	35.70	1.204	-0.0543	35.70
14		1.00	15	0.001	0.43	0.2522	0.512	1.54	6.16	0.512	-0.0203	6.16
15	High	1.00	20	0.001	0.36	0.2082	0.280	0.61	1.77	0.280	-0.0101	1.77
16		1.00	10	0.025	2.83	1.6521	30.098	142.16	892.42	30.101	-1.3570	892.42
17		1.00	15	0.025	2.16	1.2608	12.800	38.53	153.98	12.802	-0.5073	153.98
18		1.00	20	0.025	1.79	1.0408	6.994	15.28	44.26	6.996	-0.2522	44.26
19		1.05	10	0.001	0.57	0.3304	1.204	5.95	39.09	1.204	-0.0568	39.09
20		1.05	15	0.001	0.43	0.2522	0.512	1.61	6.74	0.512	-0.0212	6.74
21	very high	1.05	20	0.001	0.36	0.2082	0.280	0.64	1.94	0.280	-0.0106	1.94
22		1.05	10	0.025	2.83	1.6521	30.098	148.76	977.22	30.101	-1.4200	977.22
23		1.05	15	0.025	2.16	1.2608	12.800	40.32	168.62	12.802	-0.5309	168.62
24		1.05	20	0.025	1.79	1.0408	6.994	15.99	48.47	6.996	-0.2639	48.47

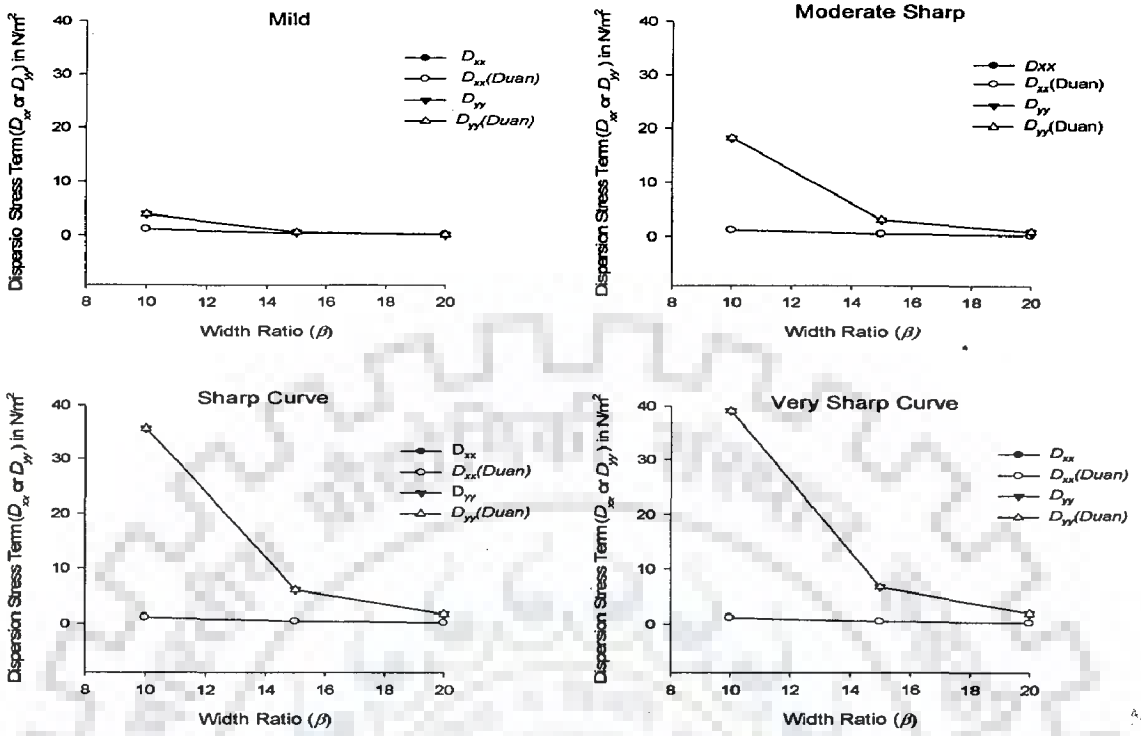

Figure 4.3 Variation of D^c_{xx} and D^c_{yy} with channel width ratio for *sub- critical flow condition*

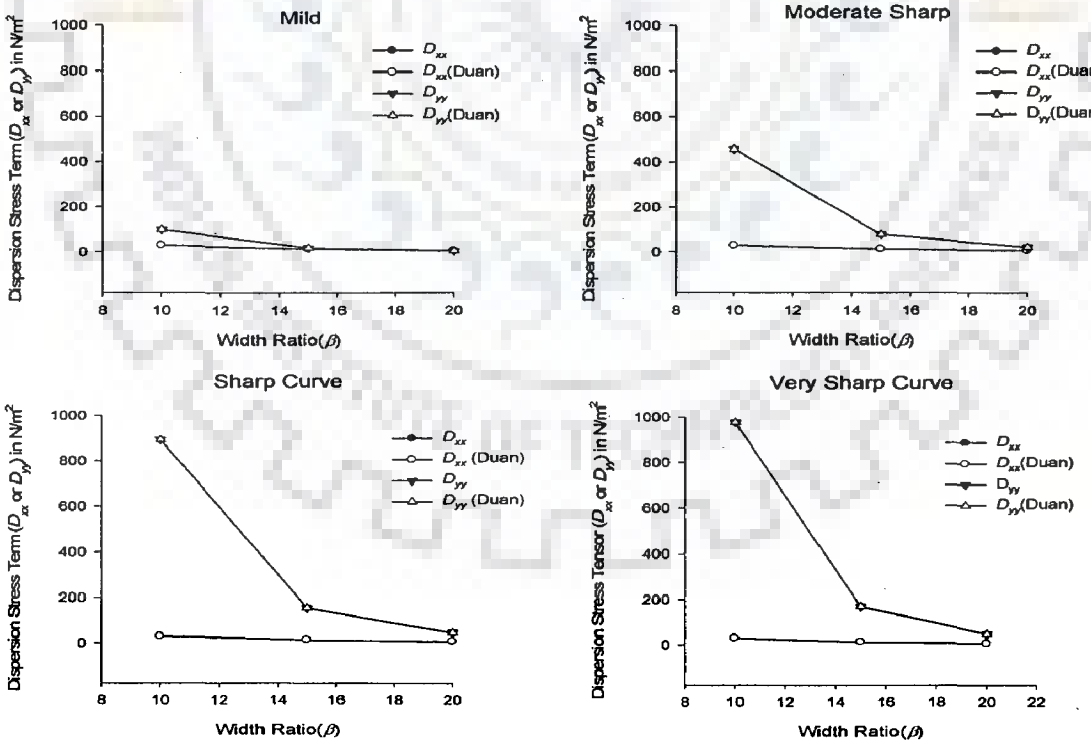

Figure 4.4 Variation of D^c_{xx} and D^c_{yy} with channel width ratio for *super-critical flow condition*

Figure 4.3 shows that D^c_{xx} remains nearly constant with varying sinuosity and β. D^c_{yy} increases sharply with increasing sinuosity and reducing width ratio. For wider channels, variations are low. But for narrow bends transverse deviations in velocity are quite high. The trend remains same in case of supercritical flow condition except higher magnitude of three components of flow dispersion tensor. This is caused due to enhanced transverse mixing of the flow at high turbulence.

4.3 CONCLUDING REMARKS

New expressions for dispersion stress tensor are proposed. A comparison between these terms and one given by Duan (2004), indicates the conditions in which there is a good agreement between the two. An insight is provided to estimate one of the unknown parameters in the Duan (2004)'s dispersion stress tensor. Compared to Duan (2004)'s model, two of the three components of dispersion stress tensor namely D^c_{xx} and D^c_{xy} are considerably simplified in the mathematical representation.

****

CHAPTER-5

FORMULATION OF 2D DEPTH AVERAGED EQUATIONS FOR CURVILINEAR DOMAIN

5.1 GENERAL

The fundamental governing differential equations of fluid flow are the equations of conservation of mass and momentum. Apart from these equations, the fundamental governing differential equation for heat transfer is the equation of conservation of energy. The equation of conservation of mass can be derived from a balance of the mass fluxes across a differential control element and the rate of mass accumulation within the element. The equation of conservation of momentum is derived from a force balance on the control element in conjunction with Newton's second law of motion. The conservation of energy equation is derived from an energy balance on the control element in conjunction with the first law of thermodynamics. Here the focus is on mass and momentum equations.

5.2 GOVERNING EQUATIONS

The differential equations governing the conservation of mass and momentum in depth averaged form in Cartesian coordinate (Duan and Julien, 2005) are,

$$\frac{\partial h}{\partial t}+\frac{\partial hU_x}{\partial x}+\frac{\partial hU_y}{\partial y}=0 \tag{5.1}$$

$$\frac{\partial (hU_x)}{\partial t}+\frac{\partial (hU_x^2)}{\partial x}+\frac{\partial (hU_xU_y)}{\partial y}=-gh\frac{\partial H}{\partial x}-C_dU_x\sqrt{U_x^2+U_y^2}+h\nu_t\left(\frac{\partial^2 U_x}{\partial x^2}+\frac{\partial^2 U_y}{\partial y^2}\right)-\frac{1}{\rho}\left(\frac{\partial D_{xx}}{\partial x}+\frac{\partial D_{xy}}{\partial y}\right) \tag{5.2}$$

$$\frac{\partial (hU_y)}{\partial t}+\frac{\partial (hU_y^2)}{\partial y}+\frac{\partial (hU_xU_y)}{\partial x}=-gh\frac{\partial H}{\partial y}-C_dU_y\sqrt{U_x^2+U_y^2}+h\nu_t\left(\frac{\partial^2 U_y}{\partial x^2}+\frac{\partial^2 U_y}{\partial y^2}\right)-\frac{1}{\rho}\left(\frac{\partial D_{xy}}{\partial x}+\frac{\partial D_{yy}}{\partial y}\right) \tag{5.3}$$

In the Eqs.(5.1 -5.3), H=water surface elevation; h=water depth; U_x, U_y =depth averaged velocities, C_d= bed friction coefficient; ν_t=eddy viscosity; x and y = spatial coordinate

components. D_{xx}, D_{yy} and D_{xy} are dispersion terms explained in Chapter 4 of this thesis. In Cartesian system, consider a non-orthogonal curvilinear plane in (x, y, t), which is to be transformed to a rectangular computational plane (ξ, η, τ) by direct transformation. where, $\xi = \xi\ (x,y,t)$ and $\eta = \eta\ (x,y,t)$ and $\tau = t$

Consider the generic dependent variable $f(x, y, t)$. Applying chain rule of partial derivatives,

$$\frac{\partial f}{\partial x} = \frac{\partial f}{\partial \xi}\frac{\partial \xi}{\partial x} + \frac{\partial f}{\partial \eta}\frac{\partial \eta}{\partial x} + \frac{\partial f}{\partial \tau}\frac{\partial \tau}{\partial x} = \xi_x \frac{\partial f}{\partial \xi} + \eta_x \frac{\partial f}{\partial \eta} \tag{5.4}$$

$$\frac{\partial f}{\partial y} = \frac{\partial f}{\partial \xi}\frac{\partial \xi}{\partial y} + \frac{\partial f}{\partial \eta}\frac{\partial \eta}{\partial y} + \frac{\partial f}{\partial \tau}\frac{\partial \tau}{\partial y} = \xi_y \frac{\partial f}{\partial \xi} + \eta_y \frac{\partial f}{\partial \eta} \tag{5.5}$$

$$\frac{\partial f}{\partial t} = \frac{\partial f}{\partial \xi}\frac{\partial \xi}{\partial t} + \frac{\partial f}{\partial \eta}\frac{\partial \eta}{\partial t} + \frac{\partial f}{\partial \tau}\frac{\partial \tau}{\partial t} = \xi_t \frac{\partial f}{\partial \xi} + \eta_t \frac{\partial f}{\partial \eta} + \frac{\partial f}{\partial \tau} \tag{5.6}$$

$$\tau_x = \tau_y = \tau_z = 0 \ldots and \cdots \tau_t = 1 \tag{5.7}$$

One can express the above Eqs. (5.4) to (5.7) in matrix form as below

$$\begin{pmatrix} \frac{\partial}{\partial x} \\ \frac{\partial}{\partial y} \\ \frac{\partial}{\partial t} \end{pmatrix} = \begin{pmatrix} \xi_x & \eta_x & 0 \\ \xi_y & \eta_y & 0 \\ \xi_t & \eta_t & 1 \end{pmatrix} \begin{pmatrix} \frac{\partial}{\partial \xi} \\ \frac{\partial}{\partial \eta} \\ \frac{\partial}{\partial \tau} \end{pmatrix} \tag{5.8}$$

Similarly, contra-varient velocity component in ξ-direction and η-direction in terms of Cartesian components U_x and U_y can be written easily as taking the advantage of partial derivative rule as,

$$U^{\xi} = \frac{\partial \xi}{\partial x} \cdot U_x + \frac{\partial \xi}{\partial y} \cdot U_y = \xi_x U_x + \xi_y U_y \tag{5.10}$$

$$V^{\eta} = \frac{\partial \eta}{\partial x} \cdot U_x + \frac{\partial \eta}{\partial y} \cdot U_y = \eta_x U_x + \eta_y U_y \tag{5.11}$$

Expressing Eqs.(5.10) and (5.11) in matrix form one has,

$$\begin{pmatrix} U^{\xi} \\ V^{\eta} \end{pmatrix} = \begin{pmatrix} \xi_x & \xi_y \\ \eta_x & \eta_y \end{pmatrix} \begin{pmatrix} U_x \\ U_y \end{pmatrix}$$

Applying the matrix inversion rule, one can get

$$\begin{pmatrix} U_x \\ U_y \end{pmatrix} = \begin{pmatrix} \xi_x & \xi_y \\ \eta_x & \eta_y \end{pmatrix}^{-1} \begin{pmatrix} U^{\xi} \\ V^{\eta} \end{pmatrix};$$

Or,

$$\begin{pmatrix} U_x \\ U_y \end{pmatrix} = \frac{1}{I} \begin{pmatrix} \eta_y & -\xi_y \\ -\eta_x & \xi_x \end{pmatrix} \begin{pmatrix} U^{\xi} \\ V^{\eta} \end{pmatrix}$$

where I =Jacobian, and expressed as, $I = \xi_x \eta_y - \xi_y \eta_x$ or $\frac{1}{I} = J = x_{\xi} y_{\eta} - y_{\xi} x_{\eta}$ (5.12)

U_x and U_y can be expressed in terms of contra-varient velocities U^{ξ}, V^{η} from above expression as,

$$U_x = \frac{1}{I}\left(\eta_y U^{\xi} - \xi_y V^{\eta}\right) = J\left(\eta_y U^{\xi} - \xi_y V^{\eta}\right) \quad (5.13a)$$

$$U_y = \frac{1}{I}\left(-\eta_x U^{\xi} + \xi_x V^{\eta}\right) = J\left(-\eta_x U^{\xi} + \xi_x V^{\eta}\right) \quad (5.13b)$$

5.2.1 TRANSFORMATION OF CONTINUITY EQUATION

Rewriting Eq. (5.1) as below,

$$\frac{\partial h}{\partial t} + \frac{\partial h U_x}{\partial x} + \frac{\partial h U_y}{\partial y} = 0$$

Each term is subjected to transformation through partial differentiation with respect to ξ, η, τ using the *PDE* rule,

For first term of the continuity equation, one can write;

$$\frac{\partial h}{\partial t} = \xi_t \frac{\partial h}{\partial \xi} + \eta_t \frac{\partial h}{\partial \eta} + \frac{\partial h}{\partial \tau} \tag{5.14}$$

For second term of the the continuity equation, one can obtain,

$$\frac{\partial hU_x}{\partial x} = h\frac{\partial U_x}{\partial x} + U_x \frac{\partial h}{\partial x};$$

or,

$$\frac{\partial hU_x}{\partial x} = h\left(\xi_x \frac{\partial U_x}{\partial \xi} + \eta_x \frac{\partial U_x}{\partial \eta}\right) + U_x\left(\xi_x \frac{\partial h}{\partial \xi} + \eta_x \frac{\partial h}{\partial \eta}\right);$$

Putting the expression of U from Eq. (5.13a) into above equation.

$$\frac{\partial hU_x}{\partial x} = hJ\left(\xi_x \frac{\partial(\eta_y U^\xi - \xi_y V^\eta)}{\partial \xi} + \eta_x \frac{\partial(\eta_y U^\xi - \xi_y V^\eta)}{\partial \eta}\right) + J(\eta_y U^\xi - \xi_y V^\eta)\left(\xi_x \frac{\partial h}{\partial \xi} + \eta_x \frac{\partial h}{\partial \eta}\right) \tag{5.15}$$

For third term of the continuity equation, one has,

$$\frac{\partial hU_y}{\partial y} = h\frac{\partial U_y}{\partial y} + U_y \frac{\partial h}{\partial y} \tag{5.15a}$$

$$\frac{\partial hU_y}{\partial y} = h\left(\xi_y \frac{\partial U_y}{\partial \xi} + \eta_y \frac{\partial U_y}{\partial \eta}\right) + U_y\left(\xi_y \frac{\partial h}{\partial \xi} + \eta_y \frac{\partial h}{\partial \eta}\right) \tag{5.15b}$$

Putting the expression of U_y from Eq.(5.13b) into the Eq .(5.15b), one can get,

$$\frac{\partial hU_y}{\partial y} = hJ\left(\xi_y \frac{\partial(-\eta_x U^\xi + \xi_x V^\eta)}{\partial \xi} + \eta_y \frac{\partial(-\eta_x U^\xi + \xi_x V^\eta)}{\partial \eta}\right) + J(-\eta_x U^\xi + \xi_x V^\eta)\left(\xi_y \frac{\partial h}{\partial \xi} + \eta_y \frac{\partial h}{\partial \eta}\right) \tag{5.16}$$

Collecting the terms of derivative operator $\partial/\partial\xi$ in Eqs.(5.15) and Eq.(5.16) and placed together, one obtains,

$$hJ\frac{\partial}{\partial \xi}\left(\overbrace{\xi_x \eta_y U^\xi - \xi_x \xi_y V^\eta} - \eta_x \xi_y \overbrace{U^\xi + \xi_y \xi_x V^\eta}\right) + J\frac{\partial h}{\partial \xi}\left(\xi_x \eta_y U^\xi - \xi_x \xi_y V^\eta - \eta_x \xi_y U^\xi + \xi_x \xi_y V^\eta\right)$$

Cancelling identical terms in above expression,

$$hJ\frac{\partial}{\partial\xi}\left((\xi_x\eta_y-\eta_x\xi_y)U^{\xi}\right)+J\frac{\partial h}{\partial\xi}\left((\xi_x\eta_y-\eta_x\xi_y)U^{\xi}\right)$$

One can recall Eq. (5.12) and substituting the value of J, one gets

$$hJ\frac{\partial}{\partial\xi}\left(\frac{1}{J}\cdot U^{\xi}\right)+J\cdot\frac{\partial h}{\partial\xi}\cdot\left(\frac{1}{J}\cdot U^{\xi}\right);$$

Or,

$$J\cdot\frac{\partial}{\partial\xi}\left(h\cdot\frac{1}{J}\cdot U^{\xi}\right) \tag{5.17}$$

Again, one may collect the terms of derivative operator $\partial/\partial\eta$ in Eq. (5.15) and Eq. (5.16) and placing together, one may get,

$$hJ\frac{\partial}{\partial\eta}\left(\eta_x\eta_yU^{\xi}-\eta_x\xi_yV^{\eta}-\eta_y\eta_xU^{\xi}+\xi_x\eta_yV^{\eta}\right)+\cdot J\frac{\partial h}{\partial\eta}\cdot\left(\eta_y\eta_xU^{\xi}-\eta_x\xi_yV^{\eta}-\eta_x\eta_yU^{\xi}+\xi_x\eta_yV^{\eta}\right) \tag{5.18a}$$

Identical terms may be cancelled in above expression, one obtains,

$$hJ\cdot\frac{\partial}{\partial\eta}\left((\overbrace{-\eta_x\xi_y+\xi_x\eta_y})V^{\eta}\right)+J\cdot\frac{\partial h}{\partial\eta}\cdot\left((\overbrace{-\eta_x\xi_y+\xi_x\eta_y})V^{\eta}\right) \tag{5.18b}$$

Recalling Eq. (5.12) and substituting the value of J, one has

$$hJ\cdot\frac{\partial}{\partial\eta}\left(\frac{1}{J}\cdot V^{\eta}\right)+J\cdot\frac{\partial h}{\partial\eta}\cdot\left(\frac{1}{J}\cdot V^{\eta}\right) \tag{5.18c}$$

Or,

$$J\cdot\frac{\partial}{\partial\eta}\left(h\cdot\frac{1}{J}\cdot V^{\eta}\right) \tag{5.18d}$$

Summing transformed terms in the form of expressions in Eqs. (5.14), (5.17) and (5.18d) and equating to zero to complete the continuity equation, one obtains,

$$\frac{\partial h}{\partial \tau}+\xi_t\frac{\partial h}{\partial \xi}+\eta_t\frac{\partial h}{\partial \eta}+J\frac{\partial}{\partial \xi}(h.\frac{1}{J}.U^{\xi})+J\frac{\partial}{\partial \eta}(h.\frac{1}{J}.V^{\eta})=0 \tag{5.19a}$$

Or,

$$\frac{\partial h}{\partial \tau}+\frac{\partial}{\partial \xi}(\xi_t.h+h.U^{\xi})+\frac{\partial}{\partial \eta}(\eta_t.h+h.V^{\eta})=0 \tag{5.19b}$$

Or,

$$\frac{\partial h}{\partial \tau}+\frac{\partial}{\partial \xi}(\xi_t+U^{\xi}).h+\frac{\partial}{\partial \eta}(\eta_t+V^{\eta}).h=0 \tag{5.19c}$$

For co-ordinate transformation of $\partial(x,y,t)$ using (Hoffman, 1992),

$$\frac{1}{J}=\frac{\partial(\xi,\eta,\tau)}{\partial(x,y,t)} \tag{5.20a}$$

One may have,

$$\frac{\partial}{\partial \tau}(hJ)+\frac{\partial}{\partial \xi}(\xi_t+U^{\xi})hJ+\frac{\partial}{\partial \eta}(\eta_t+V^{\eta})hJ=0 \tag{5.20b}$$

For fixed grid and fixed boundary with time,

$\xi_t=0$; $\eta_t=0$ and $\tau=t$

Equation (5.20b) will be reduced to,

$$\frac{\partial}{\partial t}(hJ)+\frac{\partial}{\partial \xi}(U^{\xi}hJ)+\frac{\partial}{\partial \eta}(V^{\eta}hJ)=0 \tag{5.21a}$$

Or,

$$\frac{\partial}{\partial t}(hJ)+\frac{\partial}{\partial \xi}(\hat{u}_{\xi}hJ)+\frac{\partial}{\partial \eta}(\hat{u}_{\eta}hJ)=0 \tag{5.21b}$$

In Eq. (5.21b), $J = x_\xi y_\eta - x_\eta y_\xi$, $\hat{u}_m (m=\xi, \eta)$ are the velocity components in the curvilinear coordinate (ξ, η, τ) which relate to U_x, U_y as follows

$$\begin{pmatrix} \hat{u}_\xi \\ \hat{u}_\eta \end{pmatrix} = \begin{pmatrix} \xi_x & \xi_y \\ \eta_x & \eta_y \end{pmatrix} \begin{pmatrix} U_x \\ U_y \end{pmatrix} \Leftrightarrow \begin{pmatrix} \alpha_{11} & \alpha_{12} \\ \alpha_{21} & \alpha_{22} \end{pmatrix} \begin{pmatrix} U_x \\ U_y \end{pmatrix} \tag{5.21c}$$

5.2.2. TRANSFORMATION OF MOMENTUM EQUATIONS

5.2.2.1 First momentum equation without diffusive/dispersion terms

Rewriting Eqs. (5.2) and (5.3) without dispersion terms, one has,
In x-direction

$$\frac{\partial (hU_x)}{\partial t} + \frac{\partial (hU_x^2)}{\partial x} + \frac{\partial (hU_x U_y)}{\partial y} = -gh\frac{\partial H}{\partial x} - C_d U_x \sqrt{U_x^2 + U_y^2} + h\nu_t \left(\frac{\partial^2 U_x}{\partial x^2} + \frac{\partial^2 U_x}{\partial y^2} \right) \tag{5.22a}$$

In y-direction

$$\frac{\partial (hU_y)}{\partial t} + \frac{\partial (hU_y^2)}{\partial y} + \frac{\partial (hU_x U_y)}{\partial x} = -gh\frac{\partial H}{\partial y} - C_d U_y \sqrt{U_x^2 + U_y^2} + h\nu_t \left(\frac{\partial^2 U_y}{\partial x^2} + \frac{\partial^2 U_y}{\partial y^2} \right) \tag{5.22b}$$

Terms wise differentiation of left hand side of the first momentum equation in Eq. (5.22a).

(a) *First term, of first momentum equation using the relation Eq.* (5.6).

$$\frac{\partial hU_x}{\partial t} = h\frac{\partial U_x}{\partial t} + U_x \frac{\partial h}{\partial t} \tag{5.23a}$$

One can write, using the relation Eq. (5.6).

$$h\frac{\partial U_x}{\partial t} = h(\xi_t \frac{\partial U_x}{\partial \xi} + \eta_t \frac{\partial U_x}{\partial \eta} + \frac{\partial U_x}{\partial \tau}) \tag{5.23b}$$

Using the expression for U from Eq. (5.13a), one obtains,

$$h\frac{\partial U_x}{\partial t} = hJ(\xi_t \frac{\partial J(\eta_y U^\xi - \xi_y V^\eta)}{\partial \xi} + \eta_t \frac{\partial J(\eta_y U^\xi - \xi_y V^\eta)}{\partial \eta} + \frac{\partial J(\eta_y U^\xi - \xi_y V^\eta)}{\partial \tau}) \tag{5.23c}$$

And,

$$U_x \frac{\partial h}{\partial t} = J\left(\eta_y U^{\xi} - \xi_y V^{\eta}\right)\left(\xi_t \frac{\partial}{\partial \xi} hJ + \eta_t \frac{\partial}{\partial \eta} hJ + \frac{\partial}{\partial \tau} hJ\right) \tag{5.23d}$$

Combining Eqs.(5.23c) and (5.23d), including all terms under derivative operator separately, one can easily write, from differentiation rule (product of two variables).

$$\frac{\partial hU_x}{\partial t} = \frac{\partial}{\partial \xi}\left(h\xi_t\eta_y J^2 U^{\xi} - \frac{h\xi_t\xi_y}{J^2} V^{\eta}\right) + \frac{\partial}{\partial \eta}\left(h\eta_t\eta_y J^2 U^{\xi} - h\eta_t\xi_y J^2 V^{\eta}\right) + \frac{\partial}{\partial \tau}\left(h\eta_y J^2 U^{\xi} - h\xi_y J^2 V^{\eta}\right) \tag{5.24a}$$

Or,

$$\frac{\partial hU_x}{\partial t} = \frac{\partial}{\partial \xi}\left(\left(\xi_t\eta_y U^{\xi} - \xi_t\xi_y V^{\eta}\right)\left(hJ^2\right)\right) + \frac{\partial}{\partial \eta}\left(\left(\eta_t\eta_y U^{\xi} - \eta_t\xi_y V^{\eta}\right)\left(hJ^2\right)\right) + \frac{\partial}{\partial \tau}\left(\left(\eta_y U^{\xi} - \xi_y V^{\eta}\right)\left(hJ^2\right)\right) \tag{5.24b}$$

(b) Second term of first momentum equation

Expanding the second term, one may get,

$$\frac{\partial hU_x^{\,2}}{\partial x} = U_x \frac{\partial hU_x}{\partial x} + hU_x \frac{\partial U_x}{\partial x} \tag{5.25a}$$

Using the relation in Eq. (5.4), one has,

$$U_x \frac{\partial hU_x}{\partial x} = J\left(\eta_y U^{\xi} - \xi_y V^{\eta}\right)\left[\begin{array}{l} hJ^2\left\{\xi_x \frac{\partial}{\partial \xi}\left(\eta_y U^{\xi} - \xi_y V^{\eta}\right) + \eta_x \frac{\partial}{\partial \eta}\left(\eta_y U^{\xi} - \xi_y V^{\eta}\right)\right\} + \\ \left\{J^2\left(\eta_y U^{\xi} - \xi_y V^{\eta}\right)\left(\xi_x \frac{\partial h}{\partial \xi} + \eta_x \frac{\partial h}{\partial \eta}\right)\right\} \end{array}\right] \tag{5.25b}$$

Again same operation can be done for $hU\dfrac{\partial U}{\partial x}$. Combining all terms under derivative operator separately for $\partial/\partial\xi$ and $\partial/\partial\eta$, one can easily write from differentiation rule (product of two variables).

$$\frac{\partial hU_x^{\,2}}{\partial x} = \left[\left\{\frac{\partial}{\partial \xi}\xi_x\left(\eta_y U^{\xi} - \xi_y V^{\eta}\right)^2 hJ^3 + \frac{\partial}{\partial \eta}\eta_x\left(\eta_y U^{\xi} - \xi_y V^{\eta}\right)^2 hJ^3\right\}\right] \tag{5.25c}$$

Expanding the above expression, one obtains,

$$\frac{\partial hU_x^{\,2}}{\partial x} = \left[\left\{\frac{\partial}{\partial \xi_x}\left(\xi_x\eta_y^{\,2}U^{\xi}U^{\xi} + \xi_x\xi_y^{\,2}V^{\eta}V^{\eta} - 2\xi_x\xi_y\eta_y U^{\xi}V^{\eta}\right)hJ^3 + \frac{\partial}{\partial \eta}\eta_x\left(\eta_x\eta_y^{\,2}U^{\xi}U^{\xi} + \eta_x\xi_y^{\,2}V^{\eta}V^{\eta} - 2\eta_x\eta_y\xi_y U^{\xi}V^{\eta}\right)hJ^3\right\}\right] \tag{5.25d}$$

(c) Third term of first momentum equation

Again expanding and resolving the third term of the first equation.

$$\frac{\partial hU_yU_x}{\partial y} = U_yU_x\frac{\partial h}{\partial y} + U_yh\frac{\partial U_x}{\partial y} + U_xh\frac{\partial U_y}{\partial y} \tag{5.26a}$$

Using the relations as in Eqs. (5.13 a, b), one obtains,

$$U_xh\frac{\partial U_y}{\partial y} = J\left(\eta_y U^{\xi} - \xi_y V^{\eta}\right)\cdot hJ\cdot\left(\xi_y\frac{\partial U_y}{\partial \xi} + \eta_y\frac{\partial U_y}{\partial \eta}\right) \tag{5.26b}$$

Or,

$$U_xh\frac{\partial U_y}{\partial y} = hJ^3\left(\eta_y U^{\xi} - \xi_y V^{\eta}\right)\cdot\left(\xi_y\frac{\partial(-\eta_x U^{\xi} + \xi_x V^{\eta})}{\partial \xi} + \eta_y\frac{\partial(-\eta_x U^{\xi} + \xi_x V^{\eta})}{\partial \eta}\right) \tag{5.26c}$$

Shifting all the variables under derivative operators,

$$\frac{\partial hU_xU_y}{\partial y} = \frac{\partial}{\partial \xi}\left[\left(-\eta_x\eta_y\xi_y U^{\xi}U^{\xi} + \xi_x\xi_y\eta_y U^{\xi}V^{\eta} + \eta_x\xi_y^{\,2}U^{\xi}V^{\eta} - \xi_x\xi_y^2V^{\eta}V^{\eta}\right)hJ^3\right] + \frac{\partial}{\partial \eta}\left[\left(-\eta_x\eta_y^2U^{\xi}U^{\xi} + \xi_x\eta_y^2U^{\xi}V^{\eta} + \eta_x\eta_y\xi_yU^{\xi}V^{\eta} - \xi_x\xi_y\eta_yV^{\eta}V^{\eta}\right)hJ^3\right] \tag{5.26d}$$

Combining Eqs. (5.25d) and (5.26d), one can obtain the following expression after collecting terms of identical operator together.

$$\frac{\partial hU_x^{\,2}}{\partial x}+\frac{\partial hU_xU_y}{\partial y}=\frac{\partial}{\partial \xi}\left[U^{\xi}U^{\xi}\eta_y\overbrace{\left(-\eta_x\xi_y+\xi_x\eta_y\right)}+U^{\xi}V^{\eta}\xi_y\overbrace{\left(-\eta_x\xi_y+\xi_x\eta_y\right)}\right]hJ^3$$
$$+\frac{\partial}{\partial \eta}\left[V^{\eta}V^{\eta}\xi_y\overbrace{\left(-\eta_x\xi_y+\xi_x\eta_y\right)}+U^{\xi}V^{\eta}\eta_y\overbrace{\left(-\eta_x\xi_y+\xi_x\eta_y\right)}\right]hJ^3 \tag{5.27a}$$

Or,

$$\frac{\partial hU_x^{\,2}}{\partial x}+\frac{\partial hU_xU_y}{\partial y}=\frac{\partial}{\partial \xi}\left[U^{\xi}(U^{\xi}\eta_y-V^{\eta}\xi_y)\right]hJ^2+\frac{\partial}{\partial \eta}\left[V^{\eta}(-V^{\eta}\xi_y+U^{\xi}\eta_y\right]hJ^2 \tag{5.27b}$$

Combining Eqs. (5.25d), (5.26d) and (5.27d); one has in left hand side of the first momentum equation as

$$\frac{\partial hU_x}{\partial t}+\frac{\partial hU_x^{\,2}}{\partial x}+\frac{\partial hU_xU_y}{\partial y}=\frac{\partial}{\partial \xi}\left[\xi_t(U^{\xi}\eta_y-V^{\eta}\xi_y)+U^{\xi}(U^{\xi}\eta_y-V^{\eta}\xi_y)\right]hJ^2$$
$$+\frac{\partial}{\partial \eta}\left[\eta_t(U^{\xi}\eta_y-V^{\eta}\xi_y)+V^{\eta}(-V^{\eta}\xi_y+U^{\xi}\eta_y\right]hJ^2+\frac{\partial}{\partial \tau}\left(\eta_yU^{\xi}-\xi_yV^{\eta}\right)hJ^2 \tag{5.28a}$$

Or,

$$\frac{\partial hU_x}{\partial t}+\frac{\partial hU_x^2}{\partial x}+\frac{\partial hU_xU_y}{\partial y}=\frac{\partial}{\partial \xi}\left[(\xi_t+U^{\xi})(U^{\xi}\eta_y-V^{\eta}\xi_y)\right]hJ^2+\frac{\partial}{\partial \eta}\left[(\eta_t+V^{\eta})(-V^{\eta}\xi_y+U^{\xi}\eta_y\right]hJ^2$$
$$+\frac{\partial}{\partial \tau}\left(\eta_yU^{\xi}-\xi_yV^{\eta}\right)hJ^2 \tag{5.28b}$$

Expanding the first two terms of right hand side of the first momentum equation in Eq. (5.22a), one has,

$$-gh\frac{\partial H}{\partial x}-C_dU_x\sqrt{U_x^{\,2}+U_y^{\,2}}=-ghJ\left(\xi_x\frac{\partial H}{\partial \xi}+\eta_x\frac{\partial H}{\partial \eta}\right)-C_dJ^3\left(\eta_yU^{\xi}-\xi_yV^{\eta}\right)\sqrt{\left(\eta_yU^{\xi}-\xi_yV^{\eta}\right)^2+\left(-\eta_xU^{\xi}+\xi_xV^{\eta}\right)^2} \tag{5.29a}$$

Equating Eqs. (5.28b) and (5.29a), one gets the transformed first equation of momentum without diffusive terms as

$$\frac{\partial}{\partial \xi}\left[(\xi_t+U^{\xi})(U^{\xi}\eta_y-V^{\eta}\xi_y)\right]hJ^2+\frac{\partial}{\partial \eta}\left[(\eta_t+V^{\eta})(-V^{\eta}\xi_y+U^{\xi}\eta_y\right]hJ^2+\frac{\partial}{\partial \tau}\left(\eta_yU^{\xi}-\xi_yV^{\eta}\right)hJ^2$$
$$=-ghJ\left(\xi_x\frac{\partial H}{\partial \xi}+\eta_x\frac{\partial H}{\partial \eta}\right)-C_dJ^3\left(\eta_yU^{\xi}-\xi_yV^{\eta}\right)\sqrt{\left(\eta_yU^{\xi}-\xi_yV^{\eta}\right)^2+\left(-\eta_xU^{\xi}+\xi_xV^{\eta}\right)^2} \tag{5.29b}$$

Or, using relations given in Eqs.5.13a and 5.13b and for fixed grid and fixed boundary with time, $\xi_t = 0$; $\eta_t = 0$ and $\tau = t$

One may obtain Eq. (5.29b) as,

$$\frac{\partial}{\partial \xi}\left[(U^{\xi})(U_x)\right]hJ + \frac{\partial}{\partial \eta}\left[(V^{\eta})(U_y)\right]hJ + \frac{\partial}{\partial t}U_x hJ = -ghJ\left(\xi_x \frac{\partial H}{\partial \xi} + \eta_x \frac{\partial H}{\partial \eta}\right) - C_d J U_x \sqrt{U_x^{\,2} + U_y^{\,2}} \qquad (5.29c)$$

Or,

$$\frac{\partial}{\partial t}U_x hJ + \frac{\partial}{\partial \xi}\left[U^{\xi}U_x\right]hJ + \frac{\partial}{\partial \eta}\left[V^{\eta}U_y\right]hJ = -ghJ\left(\xi_x \frac{\partial H}{\partial \xi} + \eta_x \frac{\partial H}{\partial \eta}\right) - C_d J U_x \sqrt{U_x^{\,2} + U_y^{\,2}} \qquad (5.29d)$$

5.2.2.2 Second momentum equation without diffusive/dispersion terms

(a) First term of second momentum equation in Eq. (5.22b)

$$\frac{\partial hU_y}{\partial t} = h\frac{\partial U_y}{\partial t} + U_y \frac{\partial h}{\partial t} \qquad (5.30a)$$

Using the chain rule relation given in Eq. (5.6),

$$h\frac{\partial U_y}{\partial t} = h(\xi_t \frac{\partial U_y}{\partial \xi} + \eta_t \frac{\partial U_y}{\partial \eta} + \frac{\partial U_y}{\partial \tau}) \qquad (5.30b)$$

Or,

$$h\frac{\partial U_y}{\partial t} = hJ(\xi_t \frac{\partial J\left(-\eta_x U^{\xi} + \xi_x V^{\eta}\right)}{\partial \xi} + \eta_t \frac{\partial J\left(-\eta_x U^{\xi} + \xi_x V^{\eta}\right)}{\partial \eta} + \frac{\partial J\left(-\eta_x U^{\xi} + \xi_x V^{\eta}\right)}{\partial \tau}) \qquad (5.30c)$$

Similar mathematical operations are done for the first momentum equation adopted here, and one gets,

$$\frac{\partial hU_y}{\partial t} = \frac{\partial}{\partial \xi}\left(-h\xi_t \eta_x J^2 U^{\xi} + h\xi_t \xi_x J^2 V^{\eta}\right) + \frac{\partial}{\partial \eta}\left(-h\eta_t \eta_x J^2 U^{\xi} + \frac{h\eta_t \xi_x}{J^2} V^{\eta}\right) + \frac{\partial}{\partial \tau}\left(-h\eta_x J^2 U^{\xi} + h\xi_x J^2 V^{\eta}\right) \qquad (5.31a)$$

Or,

$$\frac{\partial hU_y}{\partial t} = \frac{\partial}{\partial \xi}\left((-\xi_t \eta_x U^{\xi} + \xi_t \xi_x V^{\eta})(hJ^2)\right) + \frac{\partial}{\partial \eta}\left((-\eta_t \eta_x U^{\xi} + \eta_t \xi_x V^{\eta})(hJ^2)\right) + \frac{\partial}{\partial \tau}\left((-\eta_x U^{\xi} + \xi_x V^{\eta})(hJ^2)\right) \quad (5.31b)$$

(b) Second term of the second momentum equation

$$\frac{\partial hU_y^{\,2}}{\partial y} = U_y \frac{\partial hU_y}{\partial y} + hU_y \frac{\partial U_y}{\partial y} \quad (5.32a)$$

Or,

$$U_y \frac{\partial hU_y}{\partial y} = \left(-\eta_x U^{\xi} + \xi_x V^{\eta}\right)\left[hJ^2\left\{\xi_y \frac{\partial}{\partial \xi}\left(-\eta_x U^{\xi} + \xi_x V^{\eta}\right) + \eta_y \frac{\partial}{\partial \eta}\left(-\eta_x U^{\xi} + \xi_x V^{\eta}\right)\right\} + \left\{J^2\left(-\eta_x U^{\xi} + \xi_x V^{\eta}\right)\left(\xi_y \frac{\partial h}{\partial \xi} + \eta_y \frac{\partial h}{\partial \eta}\right)\right\}\right] \quad (5.32b)$$

Applying the same operation as for the first momentum equation,
one may get,

$$\frac{\partial hU_y^{\,2}}{\partial y} = \left[\left\{\frac{\partial}{\partial \xi}\xi_y\left(-\eta_x U^{\xi} + \xi_x V^{\eta}\right)^2 hJ^3 + \frac{\partial}{\partial \eta}\eta_y\left(-\eta_x U^{\xi} + \xi_x V^{\eta}\right)^2 hJ^3\right\}\right] \quad (5.32c)$$

$$\frac{\partial hU_y^{\,2}}{\partial y} = \left[\left\{\frac{\partial}{\partial \xi}\left(\xi_y \eta_x^{\,2} U^{\xi} U^{\xi} + \xi_y \xi_x^{\,2} V^{\eta} V^{\eta} - 2\xi_y \xi_x \eta_x U^{\xi} V^{\eta}\right)hJ^3 + \frac{\partial}{\partial \eta_y}\left(\eta_y \eta_x^{\,2} U^{\xi} U^{\xi} + \eta_x \xi_x^{\,2} V^{\eta} V^{\eta} - 2\eta_y \eta_x \xi_x U^{\xi} V^{\eta}\right)hJ^3\right\}\right] \quad (5.32d)$$

(c)Third term of the second momentum

$$\frac{\partial hU_y U_x}{\partial x} = U_y U_x \frac{\partial h}{\partial x} + U_y h \frac{\partial U_x}{\partial x} + U_x h \frac{\partial U_y}{\partial x} \quad (5.33a)$$

Expanding and resolving with the same operation done for the first momentum equation,

$$U_y h \frac{\partial U_x}{\partial y} = J\left(-\eta_x U^{\xi} + \xi_x V^{\eta}\right) \cdot hJ \cdot \left(\xi_x \frac{\partial U_x}{\partial \xi} + \eta_x \frac{\partial U_x}{\partial \eta}\right) \quad (5.33b)$$

Or,

$$U_y h \frac{\partial U_x}{\partial y} = hJ^3\left(-\eta_x U^{\xi} + \xi_x V^{\eta}\right) \cdot \left(\xi_x \frac{\partial(\eta_y U^{\xi} - \xi_y V^{\eta})}{\partial \xi} + \eta_x \frac{\partial(\eta_y U^{\xi} - \xi_y V^{\eta})}{\partial \eta}\right) \quad (5.33c)$$

Shifting all the variables under derivative operator,

$$\frac{\partial hU_xU_y}{\partial x}=\frac{\partial}{\partial\xi}\left(-\eta_x\eta_y\xi_xU^\xi U^\xi+\eta_x\xi_x\xi_yU^\xi V^\eta+\xi_x^2\eta_yU^\xi V^\eta-\xi_x^2\xi_yV^\eta V^\eta\right)hJ^3 \\ +\frac{\partial}{\partial\eta}\left(-\eta_x^2\eta_yU^\xi U^\xi+\eta_x^2\xi_yU^\xi V^\eta+\xi_x\eta_x\eta_yU^\xi V^\eta-\xi_x\xi_y\eta_xV^\eta V^\eta\right)hJ^3 \tag{5.33d}$$

Combining Eqs.(5.32) and (5.33), one has,

$$\frac{\partial hU_y^2}{\partial y}+\frac{\partial hU_xU_y}{\partial x}=\frac{\partial}{\partial\xi}\left[U^\xi U^\xi\eta_x\overbrace{\left(\eta_x\xi_y-\xi_x\eta_y\right)}+U^\xi V^\eta\xi_x\overbrace{\left(-\eta_x\xi_y+\xi_x\eta_y\right)}\right]hJ^2 \\ +\frac{\partial}{\partial\eta}\left[V^\eta V^\eta\xi_x\overbrace{\left(-\eta_x\xi_y+\xi_x\eta_y\right)}+U^\xi V^\eta\eta_x\overbrace{\left(\eta_x\xi_y-\xi_x\eta_y\right)}\right]hJ^2 \tag{5.34a}$$

$$\frac{\partial hU_y^{\,2}}{\partial y}+\frac{\partial hU_xU_y}{\partial x}=\frac{\partial}{\partial\xi}\left[U^\xi(-U^\xi\eta_x+V^\eta\xi_x)\right]hJ^2+\frac{\partial}{\partial\eta}\left[V^\eta(V^\eta\xi_x-U^\xi\eta_y\right]hJ^2 \tag{5.34b}$$

Adding Eqs. (5.31) and (5.34),

$$\frac{\partial hU_y}{\partial t}+\frac{\partial hU_y^2}{\partial y}+\frac{\partial hU_xU_y}{\partial x}=\frac{\partial}{\partial\xi}\left[\xi_t(-U^\xi\eta_x+V^\eta\xi_x)+U^\xi(-U^\xi\eta_x+V^\eta\xi_x)\right]hJ^2+\frac{\partial}{\partial\eta}\left[\eta_t(-U^\xi\eta_x+V^\eta\xi_x)+V^\eta(V^\eta\xi_x-U^\xi\eta_x\right]hJ^2 \\ +\frac{\partial}{\partial\tau}\left(-\eta_xU^\xi+\xi_xV^\eta\right)hJ^2 \tag{5.35a}$$

Or,

$$\frac{\partial hU_y}{\partial t}+\frac{\partial hU_y^{\,2}}{\partial y}+\frac{\partial hU_xU_y}{\partial x}=\frac{\partial}{\partial\xi}\left[(\xi_t+U^\xi)(-U^\xi\eta_x+V^\eta\xi_x)\right]hJ^2+\frac{\partial}{\partial\eta}\left[(\eta_t+V^\eta)(V^\eta\xi_x-U^\xi\eta_x\right]hJ^2 \\ +\frac{\partial}{\partial\tau}\left(-\eta_xU^\xi+\xi_xV^\eta\right)hJ^2 \tag{5.35b}$$

Expanding the first two terms of right hand side of the second momentum equation (5.22b), one may obtain,

$$-gh\frac{\partial H}{\partial y}-C_dU_y\sqrt{U_x^{\,2}+U_y^{\,2}}=-ghJ\left(\xi_y\frac{\partial H}{\partial\xi}+\eta_y\frac{\partial H}{\partial\eta}\right) \\ -C_dJ^3\left(-\eta_xU^\xi+\xi_xV^\eta\right)\sqrt{\left(\eta_yU^\xi-\xi_yV^\eta\right)^2+\left(-\eta_xU^\xi+\xi_xV^\eta\right)^2} \tag{5.36}$$

Equating Eqs. (5.35b) and (5.36);

$$\frac{\partial}{\partial\xi}\left[(\xi_t+U^\xi)(-U^\xi\eta_x+V^\eta\xi_x)\right]hJ^2+\frac{\partial}{\partial\eta}\left[(\eta_t+V^\eta)(V^\eta\xi_x-U^\xi\eta_x\right]hJ^2+\frac{\partial}{\partial\tau}\left(-\eta_xU^\xi+\xi_xV^\eta\right)hJ^2$$
$$=-ghJ\left(\xi_y\frac{\partial H}{\partial\xi}+\eta_y\frac{\partial H}{\partial\eta}\right)-C_dJ^3\left(-\eta_xU^\xi+\xi_xV^\eta\right)\sqrt{\left(\eta_yU^\xi-\xi_yV^\eta\right)^2+\left(-\eta_xU^\xi+\xi_xV^\eta\right)^2} \quad (5.37a)$$

Or, using the relation given in Eqs. 5.13a and 5.13b and for fixed grid and fixed boundary with time, $\xi_t=0$; $\eta_t=0$ and $\tau=t$, one may get,

$$\frac{\partial}{\partial\xi}\left[(U^\xi)U_y\right]hJ+\frac{\partial}{\partial\eta}\left[(V^\eta)U_x\right]hJ+\frac{\partial}{\partial t}U_yhJ=-ghJ\left(\xi_y\frac{\partial H}{\partial\xi}+\eta_y\frac{\partial H}{\partial\eta}\right)-C_dJU_y\sqrt{U_x^{\,2}+U_y^{\,2}} \quad (5.37b)$$

Or,

$$\frac{\partial}{\partial t}U_yhJ+\frac{\partial}{\partial\xi}\left[U^\xi U_y\right]hJ+\frac{\partial}{\partial\eta}\left[V^\eta U_x\right]hJ=-ghJ\left(\xi_y\frac{\partial H}{\partial\xi}+\eta_y\frac{\partial H}{\partial\eta}\right)-C_dJU_y\sqrt{U_x^{\,2}+U_y^{\,2}} \quad (5.37c)$$

5.2.3. Diffusive terms

Diffusive terms in Cartesian coordinate are in light of Eqs. (5.22a) and (5.22b,)
In first momentum equation (Eq. 5.22a),

$$h\nu_t\left(\frac{\partial^2U_x}{\partial x^2}+\frac{\partial^2U_x}{\partial y^2}\right) \quad (5.38a)$$

One can expand following terms in view of Eq.(5.4)

$$\frac{\partial U_x}{\partial x}=\xi_x\frac{\partial U_x}{\partial\xi}+\eta_x\frac{\partial U_x}{\partial\eta} \quad (5.38b)$$

$$\frac{\partial^2U_x}{\partial x^2}=\frac{\partial}{\partial x}\left(\xi_x\frac{\partial U_x}{\partial\xi}+\eta_x\frac{\partial U_x}{\partial\eta}\right) \quad (5.38c)$$

Or,

$$\frac{\partial^2 U_x}{\partial x^2} = \xi_x \frac{\partial}{\partial \xi}\left(\xi_x \frac{\partial U_x}{\partial \xi} + \eta_x \frac{\partial U_x}{\partial \eta}\right) + \eta_x \frac{\partial}{\partial \eta}\left(\xi_x \frac{\partial U_x}{\partial \xi} + \eta_x \frac{\partial U_x}{\partial \eta}\right) \tag{5.38d}$$

Or,

$$\frac{\partial^2 U_x}{\partial x^2} = \xi_x{}^2 \frac{\partial^2 U_x}{\partial \xi^2} + 2\xi_x \eta_x \frac{\partial^2 U_x}{\partial \xi \partial \eta} + \eta_x^2 \frac{\partial^2 U_x}{\partial \eta^2} \tag{5.38e}$$

One can write the following term in view of Eq. (5.5)

$$\frac{\partial U_x}{\partial y} = \xi_y \frac{\partial U_x}{\partial \xi} + \eta_y \frac{\partial U_x}{\partial \eta} \tag{5.38f}$$

$$\frac{\partial^2 U_x}{\partial y^2} = \frac{\partial}{\partial y}\left(\xi_y \frac{\partial U_x}{\partial \xi} + \eta_y \frac{\partial U_x}{\partial \eta}\right) \tag{5.38g}$$

Or,

$$\frac{\partial^2 U_x}{\partial y^2} = \xi_y \frac{\partial}{\partial \xi}\left(\xi_y \frac{\partial U_x}{\partial \xi} + \eta_y \frac{\partial U_x}{\partial \eta}\right) + \eta_y \frac{\partial}{\partial \eta}\left(\xi_y \frac{\partial U_x}{\partial \xi} + \eta_y \frac{\partial U_x}{\partial \eta}\right) \tag{5.38h}$$

Or,

$$\frac{\partial^2 U_x}{\partial y^2} = \xi_y{}^2 \frac{\partial^2 U_x}{\partial \xi^2} + 2\xi_y \eta_y \frac{\partial^2 U_x}{\partial \xi \partial \eta} + \eta_y^2 \frac{\partial^2 U_x}{\partial \eta^2} \tag{5.38i}$$

Similarly, the second momentum equation in Eq. (5.3);

$$h\nu_l\left(\frac{\partial^2 U_y}{\partial x^2} + \frac{\partial^2 U_y}{\partial y^2}\right) \tag{5.39a}$$

One can write following term in view of Eq. (5.4)

$$\frac{\partial U_y}{\partial x} = \xi_x \frac{\partial U_y}{\partial \xi} + \eta_x \frac{\partial U_y}{\partial \eta} \tag{5.39b}$$

$$\frac{\partial^2 U_y}{\partial x^2} = \frac{\partial}{\partial x}\left(\xi_x \frac{\partial U_y}{\partial \xi} + \eta_x \frac{\partial U_y}{\partial \eta}\right) \tag{5.39c}$$

Or,

$$\frac{\partial^2 U_y}{\partial x^2} = \xi_x \frac{\partial}{\partial \xi}\left(\xi_x \frac{\partial U_y}{\partial \xi} + \eta_x \frac{\partial U_y}{\partial \eta}\right) + \eta_x \frac{\partial}{\partial \eta}\left(\xi_x \frac{\partial U_y}{\partial \xi} + \eta_x \frac{\partial U_y}{\partial \eta}\right) \tag{5.39d}$$

Or,

$$\frac{\partial^2 U_y}{\partial x^2} = \xi_x{}^2 \frac{\partial^2 U_y}{\partial \xi^2} + 2\xi_x \eta_x \frac{\partial^2 U_y}{\partial \xi \partial \eta} + \eta_x^2 \frac{\partial^2 U_y}{\partial \eta^2} \tag{5.39e}$$

Again, one can write following term in view of Eq.(5.4)

$$\frac{\partial U_y}{\partial y} = \xi_y \frac{\partial U_y}{\partial \xi} + \eta_y \frac{\partial U_y}{\partial \eta} \tag{5.39f}$$

$$\frac{\partial^2 U_y}{\partial y^2} = \frac{\partial}{\partial y}\left(\xi_y \frac{\partial U_y}{\partial \xi} + \eta_y \frac{\partial U_y}{\partial \eta}\right) \tag{5.39g}$$

Or,

$$\frac{\partial^2 U_y}{\partial y^2} = \xi_y \frac{\partial}{\partial \xi}\left(\xi_y \frac{\partial U_y}{\partial \xi} + \eta_y \frac{\partial U_y}{\partial \eta}\right) + \eta_y \frac{\partial}{\partial \eta}\left(\xi_y \frac{\partial U_y}{\partial \xi} + \eta_y \frac{\partial U_y}{\partial \eta}\right) \tag{5.39h}$$

Or,

$$\frac{\partial^2 U_y}{\partial y^2} = \xi_y{}^2 \frac{\partial^2 U_y}{\partial \xi^2} + 2\xi_y \eta_y \frac{\partial^2 U_y}{\partial \xi \partial \eta} + \eta_y^2 \frac{\partial^2 U_y}{\partial \eta^2} \tag{5.39i}$$

5.2.4 Dispersion terms

In Eq. (5.2), one has the dispersion term as,

$$\frac{1}{\rho}\left(\frac{\partial D_{xx}}{\partial x}+\frac{\partial D_{xy}}{\partial y}\right) \tag{5.40a}$$

Using the relation given in Eq.(5.8), one obtains

$$\frac{1}{\rho}\left(\xi_x\frac{\partial D_{xx}}{\partial \xi}+\eta_x\frac{\partial D_{xx}}{\partial \eta}+\xi_y\frac{\partial D_{xy}}{\partial \xi}+\eta_y\frac{\partial D_{xy}}{\partial \eta}\right) \tag{5.40b}$$

Similarly, one has the dispersion term in Eq. (5.3),

$$\frac{1}{\rho}\left(\frac{\partial D_{xy}}{\partial x}+\frac{\partial D_{yy}}{\partial y}\right) \tag{5.40c}$$

Using the relation given in Eq.(5.8), one obtains

$$\frac{1}{\rho}\left(\xi_x\frac{\partial D_{xy}}{\partial \xi}+\eta_x\frac{\partial D_{xy}}{\partial \eta}+\xi_y\frac{\partial D_{yy}}{\partial \xi}+\eta_y\frac{\partial D_{yy}}{\partial \eta}\right) \tag{5.40d}$$

5.2.5 Final transformed momentum equations

Combining Eqs. (5.29d), (5.38e), (5.38i) and (5.40b), and multiplying it by ρ, one gets the complete first transformed momentum equation as;

$$\frac{\partial}{\partial t}(\rho hJU_x)+\frac{\partial}{\partial \xi}\left[\rho hJ\hat{u}_\xi U_x\right]+\frac{\partial}{\partial \eta}\left[\rho hJ\hat{u}_\eta U_x\right]-\rho hJ\nu_t\left(\alpha_{11}\frac{\partial^2 U_x}{\partial \xi^2}+\alpha_{22}\frac{\partial^2 U_x}{\partial \eta^2}\right) \tag{5.41}$$
$$=-\rho ghJ\left(\xi_x\frac{\partial H}{\partial \xi}+\eta_x\frac{\partial H}{\partial \eta}\right)-\rho JC_d(U_x)\sqrt{(U_x)^2+(U_y)^2}+\rho hJ\nu_t\alpha_{12}\frac{\partial^2 U_x}{\partial \xi\partial \eta}-\left(\xi_x\frac{\partial D_{xx}}{\partial \xi}+\eta_x\frac{\partial D_{xx}}{\partial \eta}+\xi_y\frac{\partial D_{xy}}{\partial \xi}+\eta_y\frac{\partial D_{xy}}{\partial \eta}\right)$$

Again, combining Eqs.(5.37d), (5.39e), (5.39i) and (5.40d), and multiplying it by ρ, one gets the second transformed momentum equation as;

$$\frac{\partial}{\partial t}(\rho hJU_y)+\frac{\partial}{\partial \xi}\left[\rho hJ\hat{u}_\xi U_y\right]+\frac{\partial}{\partial \eta}\left[\rho hJ\hat{u}_\eta U_y\right]-\rho hJ\nu_t\left(\alpha_{11}\frac{\partial^2 U_y}{\partial \xi^2}+\alpha_{22}\frac{\partial^2 U_y}{\partial \eta^2}\right)= \tag{5.42}$$
$$-\rho ghJ\left(\xi_y\frac{\partial H}{\partial \xi}+\eta_y\frac{\partial H}{\partial \eta}\right)-C_d\rho J(U_y)\sqrt{(U_x)^2+(U_y)^2}+\rho hJ\nu_t\left(\alpha_{12}\frac{\partial^2 U_y}{\partial \xi\partial \eta}\right)-\left(\xi_x\frac{\partial D_{xy}}{\partial \xi}+\eta_x\frac{\partial D_{xy}}{\partial \eta}+\xi_y\frac{\partial D_{yy}}{\partial \xi}+\eta_y\frac{\partial D_{yy}}{\partial \eta}\right)$$

In Eq. (5.41) and (5.42); $\xi_x = \partial\xi/\partial x$, $\eta_x = \partial\eta/\partial x$, $\xi_y = \partial\xi/\partial y$, $\eta_y = \partial\eta/\partial y$, $\alpha_{11} = \xi_x^2 + \xi_y^2$, $\alpha_{22} = \eta_x^2 + \eta_y^2$, $\alpha_{12} = 2(\xi_x\eta_y + \xi_y\eta_x)$, $J = x_\xi y_\eta - x_\eta y_\xi$, $\hat{u}_m (m=\xi, \eta)$ are the velocity components in the curvilinear coordinate (ξ, η, τ) which relate to U_x, U_y as follows

$$\begin{pmatrix}\hat{u}_\xi \\ \hat{u}_\eta\end{pmatrix} = \begin{pmatrix}\xi_x & \xi_y \\ \eta_x & \eta_y\end{pmatrix}\begin{pmatrix}U_x \\ U_y\end{pmatrix} \Leftrightarrow \begin{pmatrix}\alpha_{11} & \alpha_{12} \\ \alpha_{21} & \alpha_{22}\end{pmatrix}\begin{pmatrix}U_x \\ U_y\end{pmatrix} \tag{5.43}$$

5.3 SUMMARY

In this chapter, step by step mathematical transformation of mass and momentum partial differential equations in Cartesian co-ordinate system (Eqs. 5.1-5.3) to Boundary fitted co-ordinate system (Eqs. 5.21b, 5.41 and 5.42) have been done. In the momentum equations, flow dispersive terms along with diffusive terms have also been included. The transformed flow equations have been further used as governing equations for the solution of flow variables in a complex flow domain in Chapter 7 of this thesis, using control volume approach. The transformation coefficients introduced in Eqs. (5.21b), (5.41) and (5.42) were determined from grid generation algorithm for the flow domain using the numerical scheme described in Chapter 6.

****

CHAPTER-6

NUMERICAL DEVELOPMENT OF GRID GENERATION ALGORITHM

6.1 GENERAL

The governing differential equations for engineering problems are generally derived and expressed in a Cartesian (rectangular) coordinate system. Solving these differential equations in particular require that the continuous physical space be discretized into uniform orthogonal computational space (Hoffman 1992). However, the applications of boundary conditions require that the boundaries of the physical space fall on coordinate lines (surfaces) of the coordinate system. Moreover, accurate resolution of the solution requires that grid points be spread out in regions of small gradients and be clustered in the region of large gradients. Requirement of the grid generation and appropriate co-ordinate transformation has been dealt in detail in chapter 2 of this thesis. The general procedure adopted in this thesis for grid generation is widely referred to (Hoffman, 1992).

6.1.1 GRID GENERATION

In brief, grid generation is the process of determining the coordinate transformation that maps the body fitted non uniform, non orthogonal physical space into transformed uniform orthogonal computational space. For comprehensive detail information, reader may further refer to Thompson (1982) and Thompson *et al.* (1985).

The coordinate transformation must satisfy several requirements. The following list includes the most common requirements (Hoffman, 1992).

(a) The grid in the transformed computational plane must be uniform and orthogonal.

(b) The transformation must be one to one.

(c) The transformation must be nonsingular. That is, the *Jacobian* determinants I and J both must be non-zero.

(d) The transformation must yield a body fitted grid.

(e) The maximum and minimum values of the transformed coordinates must occur on the boundaries of the physical plane (space).

(f) Coordinate lines (surfaces) of the same family must not cross. Reasonable control of the spacing of the points within the physical space must be possible

6.2 2-D GRID GENERATION USING DIFFERENTIAL EQUATIONS

6.2.1 FORMULATION

Grid generation using differential equations involves the generation of a body fitted coordinate transformation using differential equations. In chapter 2 of this thesis, introductory aspect has been discussed.

Grid generation using differential equation involves two steps (Hoffman. 1992).

(i) Grid point distribution on the boundary of the physical plane is determined through algebraic method using polynomial approach.

(ii) Assuming that interior grid point distribution is specified by a differential equation that satisfies the grid point distribution specified on the boundaries and yields an acceptable interior grid point distribution.

The majority of grid generation by differential equations is based on *elliptic PDEs* as generating functions. The most common *elliptic PDE* for grid generation is the Poisson's equation which has been adopted here for this model. Inverse operation of Poisson's equation to get suitable equations for discretization can be found in any standard reference of grid generation (Hoffman, 1992, Thomson *et al.*, 1985)). Details are as follows.

For mapping the body fitted, non-uniform physical plane (x, y, t) into the transformed uniform orthogonal computational plane (ξ, η, t), following elliptic *PDE* (*Poisson's equation.*) used for grid generation.

$$\nabla^2 \xi = P(\xi, \eta) \tag{6.1a}$$

$$\nabla^2 \eta = Q(\xi, \eta) \tag{6.2a}$$

Above equations can be written in expanded form as,

$$\frac{\partial^2 \xi}{\partial x^2} + \frac{\partial^2 \xi}{\partial y^2} = P(\xi, \eta) \tag{6.1b}$$

$$\frac{\partial^2 \eta}{\partial x^2} + \frac{\partial^2 \eta}{\partial y^2} = Q(\xi, \eta) \tag{6.2b}$$

In Eqs. (6.1b) and (6.2b), P and Q are non-homogeneous terms. Coordinates (ξ, η) is known and (x, y) is not known. The objective of the grid generation process is to determine the grid in the x, y space. The inverse transformation will be

$$\left.\begin{aligned} x &= x(\xi, \eta) \\ y &= y(\xi, \eta) \end{aligned}\right\} \tag{6.3}$$

From the chain rule for partial derivative of generic function $f(x, y)$,

$$f_x = f_\xi \xi_x + f_\eta \eta_x \tag{6.4a}$$

$$f_y = f_\xi \xi_y + f_\eta \eta_y \tag{6.4b}$$

In similar manner, second derivatives are given by

$$f_{xx} = (f_x)_x = (f_\xi \xi_x)_x + (f_\eta \eta_x)_x \tag{6.5a}$$

$$f_{xx} = f_\xi \xi_{xx} + \xi_x (f_{\xi\xi} \xi_x + f_{\xi\eta} \eta_x) + f_\eta \eta_{xx} + \eta_x (f_{\eta\xi} \xi_x + f_{\eta\eta} \eta_x) \tag{6.5b}$$

$$f_{yy} = f_\xi \xi_{yy} + \xi_y (f_{\xi\xi} \xi_y + f_{\xi\eta} \eta_y) + f_\eta \eta_{yy} + \eta_y (f_{\eta\xi} \xi_y + f_{\eta\eta} \eta_y) \tag{6.5c}$$

Adding Eqs. (6.5b) and (6.5c). one has,

$$\nabla^2 f = f_{xx} + f_{yy} = (\xi_x^2 + \xi_y^2) f_{\xi\xi} + 2(\xi_x \eta_x + \xi_y \eta_y) f_{\xi\eta} + (\eta_x^2 + \eta_y^2) f_{\eta\eta} + \nabla^2 \xi f_\xi + \nabla^2 \eta f_\eta \tag{6.6a}$$

Let $f = x$ in above equation. Then

$$\nabla^2 x = x_{xx} + x_{yy} = 0 \tag{6.6b}$$

Then Eq(6.6a) becomes,

$$\left(\xi_x^2+\xi_y^2\right)x_{\xi\xi}+2\left(\xi_x\eta_x+\xi_y\eta_y\right)x_{\xi\eta}+\left(\eta_x^2+\eta_y^2\right)x_{\eta\eta}=-\left(Px_\xi+Qx_\eta\right) \tag{6.6c}$$

From direct inverse transformation done in Chapter 5, one may get,

$$\left.\begin{aligned}\xi_x&=Iy_\eta\\ \eta_x&=-Iy_\xi\\ J&=\frac{1}{I}=x_\xi y_\eta-x_\eta y_\xi\end{aligned}\right\}\qquad\left.\begin{aligned}\xi_y&=-Ix_\eta\\ \eta_y&=Ix_\xi\end{aligned}\right\} \tag{6.7}$$

Substituting these results of Eq. (6.7) in Eq. (6.6c) and simplifying gives

$$\left(x_\eta^2+y_\eta^2\right)x_{\xi\xi}-2\left(x_\xi x_\eta+y_\xi y_\eta\right)x_{\xi\eta}+\left(x_\xi^2+y_\xi^2\right)x_{\eta\eta}=-J^2\left(Px_\xi+Qx_\eta\right) \tag{6.8a}$$

Equation can be written in condensed form as

$$\alpha x_{\xi\xi}-2\beta x_{\xi\eta}+\gamma x_{\eta\eta}=-J^2\left(Px_\xi+Qx_\eta\right) \tag{6.8b}$$

Similarly repeating the same step for putting $f=y$ yields

$$\alpha y_{\xi\xi}-2\beta y_{\xi\eta}+\gamma y_{\eta\eta}=-J^2\left(Py_\xi+Qy_\eta\right) \tag{6.9}$$

where

$$\left.\begin{aligned}\alpha&=x_\eta^2+y_\eta^2\\ \beta&=x_\xi x_\eta+y_\xi y_\eta\\ \gamma&=x_\xi^2+y_\xi^2\end{aligned}\right\} \tag{6.10a}$$

Furthermore for orthogonal condition (Zhang and Jia, 2005), one has

$$\beta = x_\xi x_\eta + y_\xi y_\eta = 0 \tag{6.10b}$$

6.2.2 NUMERICAL DISCRETIZATION

The boundary conditions for above equations will be

$$\left.\begin{aligned} x &= F(\xi, \eta) \\ y &= G(\xi, \eta) \end{aligned}\right\} \tag{6.11}$$

These are elliptic *PDEs* with *Dirichlet Boundary Conditions*. Writing equation in finite difference form using second order centered difference approximations of the exact partial derivatives (Figure 6.1)

First equation Eq. (6.8b)

$$\alpha_{i,j}\frac{x_{i+1,j} - 2x_{i,j} + x_{i-1,j}}{\Delta\xi^2} - 2\beta_{i,j}\frac{x_{i+1,j+1} - x_{i-1,j} - x_{i-1,j+1} + x_{i-1,j-1}}{4\Delta\xi\Delta\eta} + \gamma_{i,j}\frac{x_{i,j+1} - 2x_{i,j} + x_{i,j-1}}{\Delta\eta^2} \tag{6.12}$$

$$= -J_{i,j}^2\left(\frac{x_{i+1,j} - x_{i-1,j}}{2\Delta\xi}P_{i,j} + \frac{x_{i,j+1} - x_{i,j-1}}{2\Delta\eta}Q_{i,j}\right)$$

Second Equation Eq. (6.9)

$$\alpha_{i,j}\frac{y_{i+1,j} - 2y_{i,j} + y_{i-1,j}}{\Delta\xi^2} - 2\beta_{i,j}\frac{y_{i+1,j+1} - y_{i-1,j} - y_{i-1,j+1} + y_{i-1,j-1}}{4\Delta\xi\Delta\eta} + \gamma_{i,j}\frac{y_{i,j+1} - 2y_{i,j} + y_{i,j-1}}{\Delta\eta^2} \tag{6.13}$$

$$= -J_{i,j}^2\left(\frac{y_{i+1,j} - y_{i-1,j}}{2\Delta\xi}P_{i,j} + \frac{y_{i,j+1} - y_{i,j-1}}{2\Delta\eta}Q_{i,j}\right)$$

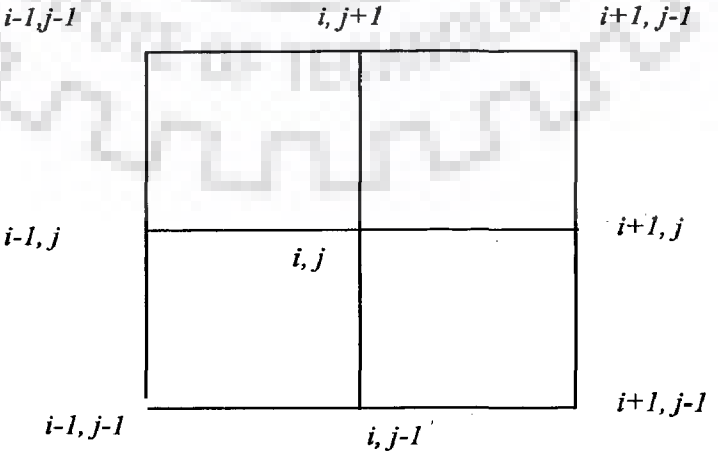

Figure 6.1 Finite difference grid for discretization

where the finite approximation for coefficients are

$$\alpha_{i,j} = x_\eta\big|_{i,j}^2 + y_\eta\big|_{i,j}^2 \tag{6.15}$$

$$\beta_{i,j} = x_\xi\big|_{i,j} x_\eta\big|_{i,j} + y_\xi\big|_{i,j} y_\eta\big|_{i,j} \tag{6.16}$$

$$\gamma_{i,j} = x_\xi\big|_{i,j}^2 + y_\xi\big|_{i,j}^2 \tag{6.17}$$

$$J_{i,j} = x_\xi\big|_{i,j} y_\eta\big|_{i,j} + x_\eta\big|_{i,j} y_\xi\big|_{i,j} \tag{6.18}$$

Similarly the finite difference approximations of x_ξ, x_η, y_ξ and y_η are,

$$\left.\begin{aligned} x_\xi\big|_{i,j} &= \frac{x_{i+1,j} - x_{i-1,j}}{2\,\Delta\,\xi} \\ y_\xi\big|_{i,j} &= \frac{y_{i+1,j} - y_{i-1,j}}{2\,\Delta\,\xi} \\ x_\eta\big|_{i,j} &= \frac{x_{i,j+1} - x_{i,j-1}}{2\,\Delta\,\eta} \\ y_\eta\big|_{i,j} &= \frac{x_{i,j+1} - x_{i,j-1}}{2\,\Delta\,\eta} \end{aligned}\right\} \tag{6.19}$$

Multiplying Eq.(6.12) by $\Delta\xi^2$ and collecting terms yields

$$\begin{aligned} &x_{i-1,j-1}\left(-\frac{\beta_{i,j}}{2}\frac{\Delta\xi}{\Delta\eta}\right)+x_{i-1,j}\left(\alpha_{i,j}-J_{i,j}^2P_{i,j}\frac{\Delta\xi}{2}\right)+x_{i-1,j+1}\left(\frac{\beta_{i,j}}{2}\frac{\Delta\xi}{\Delta\eta}\right)+x_{i,j-1}\left(\gamma_{i,j}\frac{\Delta\xi^2}{\Delta\eta^2}-J_{i,j}^2Q_{i,j}\frac{\Delta\xi^2}{2\Delta\eta}\right) \\ &-2x_{i,j}\left(\alpha_{i,j}+\gamma_{i,j}\frac{\Delta\xi^2}{\Delta\eta^2}\right) \\ &+x_{i,j+1}\left(\gamma_{i,j}\frac{\Delta\xi^2}{\Delta\eta^2}+J_{i,j}^2Q_{i,j}\frac{\Delta\xi^2}{2\Delta\eta}\right)+x_{i+1,j-1}\left(\frac{\beta_{i,j}}{2}\frac{\Delta\xi}{\Delta\eta}\right)+x_{i+1,j}\left(\alpha_{i,j}+J_{i,j}^2P_{i,j}\frac{\Delta\xi}{2}\right)+x_{i+1,j+1}\left(-\frac{\beta_{i,j}}{2}\frac{\Delta\xi}{\Delta\eta}\right)=0 \end{aligned} \tag{6.20a}$$

Similarly, multiplying Eq. (6.13) by $\Delta\xi^2$ and collecting terms yields

$$y_{i-1,j-1}\left(-\frac{\beta_{i,j}}{2}\frac{\Delta\xi}{\Delta\eta}\right)+y_{i-1,j}\left(\alpha_{i,j}-J_{i,j}^2P_{i,j}\frac{\Delta\xi}{2}\right)+y_{i-1,j+1}\left(\frac{\beta_{i,j}}{2}\frac{\Delta\xi}{\Delta\eta}\right)+y_{i,j-1}\left(\gamma_{i,j}\frac{\Delta\xi^2}{\Delta\eta^2}-J_{i,j}^2Q_{i,j}\frac{\Delta\xi^2}{2\Delta\eta}\right)$$

$$-2y_{i,j}\left(\alpha_{i,j}+\gamma_{i,j}\frac{\Delta\xi^2}{\Delta\eta^2}\right) \qquad (6.20b)$$

$$+y_{i,j+1}\left(\gamma_{i,j}\frac{\Delta\xi^2}{\Delta\eta^2}+J_{i,j}^2Q_{i,j}\frac{\Delta\xi^2}{2\Delta\eta}\right)+y_{i+1,j-1}\left(\frac{\beta_{i,j}}{2}\frac{\Delta\xi}{\Delta\eta}\right)+y_{i+1,j}\left(\alpha_{i,j}+J_{i,j}^2P_{i,j}\frac{\Delta\xi}{2}\right)+y_{i+1,j+1}\left(-\frac{\beta_{i,j}}{2}\frac{\Delta\xi}{\Delta\eta}\right)=0$$

In our case $\Delta\xi=\Delta\eta=1$, simplifying, first equation for x variable, one has.

$$x_{i-1,j-1}\left(-\frac{\beta_{i,j}}{2}\right)+x_{i-1,j}\left(\alpha_{i,j}-0.5J_{i,j}^2P_{i,j}\right)+x_{i-1,j+1}\left(\frac{\beta_{i,j}}{2}\right)+x_{i,j-1}\left(\gamma_{i,j}-0.5J_{i,j}^2Q_{i,j}\right)$$

$$-2x_{i,j}\left(\alpha_{i,j}+\gamma_{i,j}\right) \qquad (6.20c)$$

$$+x_{i,j+1}\left(\gamma_{i,j}+0.5J_{i,j}^2Q_{i,j}\right)+x_{i+1,j-1}\left(\frac{\beta_{i,j}}{2}\right)+x_{i+1,j}\left(\alpha_{i,j}+0.5J_{i,j}^2P_{i,j}\right)+x_{i+1,j+1}\left(-\frac{\beta_{i,j}}{2}\right)=0$$

Again the second equation will be for y variable

$$y_{i-1,j-1}\left(-\frac{\beta_{i,j}}{2}\right)+y_{i-1,j}\left(\alpha_{i,j}-0.5J_{i,j}^2P_{i,j}\right)+y_{i-1,j+1}\left(\frac{\beta_{i,j}}{2}\right)+y_{i,j-1}\left(\gamma_{i,j}-0.5J_{i,j}^2Q_{i,j}\right)$$

$$-2y_{i,j}\left(\alpha_{i,j}+\gamma_{i,j}\right) \qquad (6.21)$$

$$+y_{i,j+1}\left(\gamma_{i,j}\frac{\Delta\xi^2}{\Delta\eta^2}+0.5J_{i,j}^2Q_{i,j}\right)+y_{i+1,j-1}\left(\frac{\beta_{i,j}}{2}\right)+y_{i+1,j}\left(\alpha_{i,j}+0.5J_{i,j}^2P_{i,j}\right)+y_{i+1,j+1}\left(-\frac{\beta_{i,j}}{2}\right)=0$$

6.2.3. SOLUTION ALGORITHM

Using *ADI* (*Alternate Direction Implicit Explicit*) Scheme,

For any l^{th} iteration

Step-1

Row wise solutions is obtained

Writing equation Eq.(6.20) in tri-diagonal matrix form for unknowns in a row *i.e* $x_{i-1,j}, x_{i,j}, x_{i+1,j}$ .one has,

$$x_{i-1,j}\left(\alpha_{i,j}-0.5J_{i,j}^2P_{i,j}\right)-2x_{i,j}\left(\alpha_{i,j}+\gamma_{i,j}\right)+x_{i+1,j}\left(\alpha_{i,j}+0.5J_{i,j}^2P_{i,j}\right)=x_{i-1,j-1}\left(\frac{\beta_{i,j}}{2}\right)-x_{i-1,j+1}\left(\frac{\beta_{i,j}}{2}\right)-$$

(6.22a)

$$x_{i,j-1}\left(\gamma_{i,j}-0.5J_{i,j}^2Q_{i,j}\right)-x_{i,j+1}\left(\gamma_{i,j}+0.5J_{i,j}^2Q_{i,j}\right)-x_{i+1,j-1}\left(\frac{\beta_{i,j}}{2}\right)+x_{i+1,j+1}\left(\frac{\beta_{i,j}}{2}\right)=D_i(\text{indicating})$$

Above equation simplified in terms of three consecutive row wise variables at internal nodes,

$$x_{i-1,j}\left(\alpha_{i,j}-0.5J_{i,j}^2P_{i,j}\right)-2x_{i,j}\left(\alpha_{i,j}+\gamma_{i,j}\right)+x_{i+1,j}\left(\alpha_{i,j}+0.5J_{i,j}^2P_{i,j}\right)=D_i \qquad (6.22b)$$

Similarly for y values, Eq. (6.21) is rearranged,

$$y_{i-1,j}\left(\alpha_{i,j}-0.5J_{i,j}^2P_{i,j}\right)-2y_{i,j}\left(\alpha_{i,j}+\gamma_{i,j}\right)+y_{i+1,j}\left(\alpha_{i,j}+0.5J_{i,j}^2P_{i,j}\right)=y_{i-1,j-1}\left(\frac{\beta_{i,j}}{2}\right)-y_{i-1,j+1}\left(\frac{\beta_{i,j}}{2}\right)-$$

(6.22c)

$$y_{i,j-1}\left(\gamma_{i,j}-0.5J_{i,j}^2Q_{i,j}\right)-y_{i,j+1}\left(\gamma_{i,j}+0.5J_{i,j}^2Q_{i,j}\right)-y_{i+1,j-1}\left(\frac{\beta_{i,j}}{2}\right)+y_{i+1,j+1}\left(\frac{\beta_{i,j}}{2}\right)=E_i(\text{indicating})$$

Or,

$$y_{i-1,j}\left(\alpha_{i,j}-0.5J_{i,j}^2P_{i,j}\right)-2y_{i,j}\left(\alpha_{i,j}+\gamma_{i,j}\right)+y_{i+1,j}\left(\alpha_{i,j}+0.5J_{i,j}^2P_{i,j}\right)=E_i \qquad (6.22d)$$

(a)Thomas algorithm for tri-diagonal matrix form for row wise solution

Using appropriate terminologies, Eqs. (6.22b) and (6.22d) can be written in the following form.

At l^{th} iteration

$$A_i\overset{l}{x}_{i-1,j}+B_i\overset{l}{x}_{i,j}+C_i\overset{l}{x}_{i+1,j}=\overset{*}{D}_i \qquad (6.22e)$$

$$A_i\overset{l}{y}_{i-1,j}+B_i\overset{l}{y}_{i,j}+C_i\overset{l}{y}_{i+1,j}=\overset{*}{E}_i \qquad (6.22f)$$

where, $*$ evaluated on the latest best known values of x and y

where,

$$\left.\begin{aligned} A_i &= \alpha_{i,j} - 0.5J_{i,j}^2 P_{i,j} \\ B_i &= -2\left(\alpha_{i,j} + \gamma_{i,j}\right) \\ C_i &= \alpha_{i,j} + 0.5J_{i,j}^2 P_{i,j} \end{aligned}\right\} \qquad (6.23)$$

Stepwise one can compute intermediate variables (*TDMA*) as follows to get the solution,

(i) Generate array of ω and θ,

$$\omega_1 = B_1$$

$$\theta_1 = \frac{C_1}{B_1}$$

$$\omega_i = B_i - A_i \times \theta_i$$

$$\theta_i = \frac{C_i}{\omega_i} \qquad \text{(Array recursively generated)}$$

(ii) Generate another array (ϕ);

$$\phi_1 = \frac{D_1}{\omega_1}$$

$$\phi_i = \frac{D_i - A_i \times \phi_{i-1}}{\omega_i}$$

(iii) Finally, one can generate solution array (in terms of x or y)

$$x_n = \phi_n$$

$$x_i = \phi_i - \theta_i \times x_{i+1}$$

Step-2

Column-wise solutions are obtained.

Writing equation Eq. (6.20) in tridiagonal matrix form for unknowns (column-wise)

$$x_{i,j-1}\left(\gamma_{i,j}-0.5J_{i,j}^2Q_{i,j}\right)-2x_{i,j}\left(\alpha_{i,j}+\gamma_{i,j}\right)+x_{i,j+1}\left(\gamma_{i,j}+0.5J_{i,j}^2Q_{i,j}\right)= \tag{6.24a}$$

$$x_{i-1,j-1}\left(\frac{\beta_{i,j}}{2}\right)-x_{i-1,j}\left(\alpha_{i,j}-0.5J_{i,j}^2P_{i,j}\right)-x_{i-1,j+1}\left(\frac{\beta_{i,j}}{2}\right)-x_{i+1,j-1}\left(\frac{\beta_{i,j}}{2}\right)-x_{i+1,j}\left(\alpha_{i,j}+0.5J_{i,j}^2P_{i,j}\right)+x_{i+1,j+1}\left(-\frac{\beta_{i,j}}{2}\right)=D_j\text{(Indicating)}$$

Or,

$$x_{i,j-1}^{l}\left(\gamma_{i,j}-0.5J_{i,j}^2Q_{i,j}\right)-2x_{i,j}^{l}\left(\alpha_{i,j}+\gamma_{i,j}\right)+x_{i,j+1}^{l}\left(\gamma_{i,j}+0.5J_{i,j}^2Q_{i,j}\right)=D_j^{l-1} \tag{6.24b}$$

Similarly one can rearrange Eq. (6.21) for y,

$$y_{i,j-1}\left(\gamma_{i,j}-0.5J_{i,j}^2Q_{i,j}\right)-2y_{i,j}\left(\alpha_{i,j}+\gamma_{i,j}\right)+y_{i,j+1}\left(\gamma_{i,j}+0.5J_{i,j}^2Q_{i,j}\right)= \tag{6.24c}$$

$$y_{i-1,j-1}\left(\frac{\beta_{i,j}}{2}\right)-y_{i-1,j}\left(\alpha_{i,j}-0.5J_{i,j}^2P_{i,j}\right)-y_{i-1,j+1}\left(\frac{\beta_{i,j}}{2}\right)-y_{i+1,j-1}\left(\frac{\beta_{i,j}}{2}\right)-y_{i+1,j}\left(\alpha_{i,j}+0.5J_{i,j}^2P_{i,j}\right)+y_{i+1,j+1}\left(\frac{\beta_{i,j}}{2}\right)=E_j\text{(Indicating)}$$

Or,

$$y_{i,j-1}^{l}\left(\gamma_{i,j}-0.5J_{i,j}^2Q_{i,j}\right)-2y_{i,j}^{l}\left(\alpha_{i,j}+\gamma_{i,j}\right)+y_{i,j+1}^{l}\left(\gamma_{i,j}+0.5J_{i,j}^2Q_{i,j}\right)=E_j^{l-1} \tag{6.24d}$$

(b)Thomas algorithm for tri-diagonal matrix form for column wise solution

Using appropriate terminologies, Eqs. (6.24b) and (6.24d) can be written in following form

$$A_j x_{i,j-1}^{l}+B_j x_{i,j}^{l}+C_j x_{i,j+1}^{l}=D_j^{l-1} \tag{6.24e}$$

$$A_j y_{i,j-1}^{l}+B_j y_{i,j}^{l}+C_j y_{i,j+1}^{l}=E_j^{l-1} \tag{6.24f}$$

where,

$$\left.\begin{aligned} A_j &= \left(\gamma_{i,j} - 0.5J_{i,j}^2 Q_{i,j}\right) \\ B_j &= -2\left(\alpha_{i,j} + \gamma_{i,j}\right) \\ C_j &= \left(\gamma_{i,j} + 0.5J_{i,j}^2 Q_{i,j}\right) \end{aligned}\right\} \qquad (6.25a)$$

One can stepwise compute intermediate variables (*TDMA*) as follows to get the solution

(i) Generate array of ω and θ

$$\omega_1 = B_1$$

$$\theta_1 = \frac{C_1}{B_1}$$

$$\omega_j = B_i - A_j \times \theta_j$$

$$\theta_j = \frac{C_j}{\omega_j} \qquad \text{(Array recursively generated)}$$

(ii) Generate another array (ϕ).;

$$\phi_1 = \frac{D_1}{\omega_1}$$

$$\phi_j = \frac{D_j - A_j \times \phi_{j-1}}{\omega_j}$$

(iii) Finally, one can generate solution array (in terms of x or y),

$$x_n = \phi_n$$

$$x_j = \phi_j - \theta_j \times x_{j+1}$$

One can update the entire coefficients and go for $(l+1)^{th}$ iteration until solution converges.

(c) Convergence Criteria

Iteration continues until the following condition fulfills,

$$Max.\left|x_{i,j}^{(l)} - x_{i,j}^{(l-1)}\right| \&\& Max.\left|y_{i,j}^{(l)} - y_{i,j}^{(l-1)}\right| \le \varepsilon_1 (say = .0002) \tag{6.25b}$$

where l =number of iteration

6.3. DATA PREPARATION FOR BOUNDARY VALUES

The grid point distribution on the boundaries of the physical space is determined. The boundaries are in one dimensional space. The required grid point distributions can be obtained by Algebraic methods. For the study done in this thesis, Algebraic method using polynomials has been used.

The range of the transformed variable ξ is arbitrary. The most common (used in this calculation) are $0 \le \bar{\xi} \le 1$ and $1 \le \xi \le \xi_{max}$ .Where ξ is an integer. The transformed variables $\bar{\xi}$ and ξ are related as follows.

$$\bar{\xi} = \frac{\xi - 1}{\xi_{max} - 1} \qquad \left(0 \le \bar{\xi} \le 1.,1 \le \xi \le \xi_{max}\right) \tag{6.26}$$

Polynomial expansion can be written as follows,

$$x = a + b\bar{\xi} + c\bar{\xi}^2 + d\bar{\xi}^3 + e\bar{\xi}^4 + f\bar{\xi}^5 ..... \tag{6.27}$$

Differentiating and solving for $\overline{\xi_x}$ yield transformation matrix

$$\overline{\xi_x} = \frac{1}{b + 2c\bar{\xi} + 3d\bar{\xi}^2 + 4e\bar{\xi}^3 + 5f\bar{\xi}^2 .....} \tag{6.28}$$

The coefficients *a, b, c, d, e, f* and so on are determined by applying boundary conditions, constraints and requirements.

$$
\left.
\begin{aligned}
&x = X_1 \rightarrow \bar{\xi} = 0 \rightarrow \xi = 1; \\
&x = X_2 \rightarrow \bar{\xi} = 1 \rightarrow \xi = \xi_{\max} \\
&x = X_i \rightarrow \bar{\xi} = \bar{\xi}_i \rightarrow \xi = \xi_i \\
&x_{\xi i} = X_{\xi i} \rightarrow \bar{\xi} = \left|\bar{\xi}\right|_{\xi i} \rightarrow \xi = \xi_{\xi i}
\end{aligned}
\right\} \qquad (6.28b)
$$

Algorithm steps

(i) Give number of boundaries and constrains

(ii) Select corresponding degree of polynomial

(iii) Generate simultaneous equations of *a, b, c, d, e* and so on by putting in boundary values in polynomial equations.

(iv) Solve simultaneous equations through matrix inverse multiplication for *a, b, c, d*

(v) Using polynomial, determine value of x for corresponding integer values of ξ for the range of $1 \le \xi \le \xi_{\max}$ ($\xi_{\max}$ is fixed by the user appropriately to get desired mesh resolution

(vi) Evaluate corresponding values of y from cubic interpolation from curve data.

(vii) Same procedure is adopted for η if the boundary is aligned by and large along y axis.

6.4. NUMERICAL COMPUTATION OF NON-HOMOGENEOUS TERMS

6.4.1 INTERIOR GRID POINT CONTROL

Poisson's equation used in grid generation Eq. (6.1b) and Eq. (6.2b) essentially contains non homogeneous terms P and Q. The finite difference form also contain the aforementioned terms naturally. Specific functional forms must be chosen for $P(\xi,\eta)$ and

$Q(\xi,\eta)$ to control the interior grid points to desire level of their distribution to optimize orthogonality. If one considers top boundary then the boundary points are fixed. Non-zero values of P tends to move the interior points right or left, thus influencing the angle of intersection of the ξ-line with the boundary. Non-zero values of Q tends to move the interior points up and down, thus influencing the spacing of the η- lines adjacent to the boundary. Similar results can be developed for left, right, and bottom boundaries. Consequently, the angle of intersection of interior grid lines with boundaries and spacing of interior grid lines adjacent to the boundaries can be controlled by the choices for $P(\xi,\eta)$ and $Q(\xi,\eta)$ (Hoffman, 1992).

Numerous numerical approaches have been found in literature to tackle this specific problem.For details reader may refer to Thompson *et al.* (1985), Thomas and Middlecoff (1980), Steger and Sorenson (1979), and Hilgenstock (1988).

The general approach for interior grid point control has two steps.

(i) Specification of $P(\xi,\eta)$ and $Q(\xi,\eta)$ on the boundary to achieve the desired effect at the boundaries.

(ii) Extrapolation of the boundary values of $P(\xi,\eta)$ and $Q(\xi,\eta)$ into the interior of the domain to achieve the desired effect in the interior.

6.4.2 IMPLIMENTATION OF THE TECHNIQUE FOR COMPUTING *'P'* AND *'Q'*

Several techniques for implementing the two steps presented in Secion-6.4.1 are available. Though none of them are foolproof still the technique here, adopted for implementing the interior grid control is implemented by Hilgenstock (1988), which is an iterative approach and quite comfortably implemented to evaluate $P(\xi,\eta)$ and $Q(\xi,\eta)$, widespread in use to effectively solve the problem as presented in Hoffman(1992). After the values of $P(\xi,\eta)$ and $Q(\xi,\eta)$ are determined at the boundaries, interior values are extrapolated exponentially.

Initially $P(\xi,\eta)$ and $Q(\xi,\eta)$ are not known. So the initial values of P and Q is set to zero and Poisson's equation is solved to get interior points and updated recursively while evaluating P and Q for each iteration as follows.

Let us say at n^{th} iteration P and Q are P^n and Q^n

So at $n+1^{th}$ iteration new value of P and Q will be,

$$P^{n+1} = P^n + \Delta P^n \tag{6.29a}$$

$$Q^{n+1} = Q^n + \Delta Q^n \tag{6.29b}$$

n=denotes the iteration level. The initial values of P and Q is set to zero.

Let us define some terminologies,

$\vec{T}_\xi$=Tangent vector to the ξ-line at the boundary. $\vec{T}_\eta$= Tangent vector to the η-line at the boundary. The dot product will give the angle between tangent vectors (see Figure 6.2),

$$\vec{T}_\xi \bullet \vec{T}_\eta = \left|\vec{T}_\xi\right| \cdot \left|\vec{T}_\eta\right| \cos\alpha \tag{6.30a}$$

One has then,

$$\alpha = \cos^{-1}\left(\frac{\vec{T}_\xi \bullet \vec{T}_\eta}{\left|\vec{T}_\xi\right| \cdot \left|\vec{T}_\eta\right|}\right)\alpha \tag{6.30b}$$

Let α^* is the desired angle of intersection. Then, the required correction ΔP^n to P^n is

$$\Delta P^n = +\tan^{-1}\left(\frac{\alpha^n - \alpha^*}{\alpha^*}\right) \tag{6.31}$$

To make the line orthogonal α^* is taken $\frac{\pi}{2}$. The spacing Δs between the boundary point and the first interior point on ξ line is given by

$$\Delta s = \left(\left(x_{i,j-1} - x_{i,j} \right)^2 + \left(y_{i,j-1} - y_{i,j} \right)^2 \right)^{1/2} \tag{6.32}$$

Let's Δs^* be the desired spacing, then the required correction ΔQ^n to Q^n is,

$$\Delta Q^n = + \tan^{-1} \left(\frac{\Delta s^n - \Delta s^*}{\Delta s^*} \right) \tag{6.33}$$

Δs^* may be set as per the domain resolution or conveniently may be taken by user as the smallest permissible spacing of the domain, between the boundary point and the first interior point on ξ -line. Either or both of the correction ΔP^n and ΔQ^n can be over relaxed or under relaxed.

6.4.2.1 Top boundary implementation

For the top boundary, one can calculate $\vec{T}_\xi$ and $\vec{T}_\eta$ as follows,

$$\vec{T}_\xi = \frac{\left(x_{i,j_{max}-1} - x_{i,j_{max}} \right)}{\Delta s_1} \vec{i} + \frac{\left(y_{i,j_{max}-1} - y_{i,j_{max}} \right)}{\Delta s_1} \vec{j} \tag{6.34}$$

$$\Delta s_1 = \left[\left(x_{i,j_{max}-1} - x_{i,j_{max}} \right)^2 + \left(y_{i,j_{max}-1} - y_{i,j_{max}} \right)^2 \right]^{\frac{1}{2}} \tag{6.35}$$

$$\vec{T}_\eta = \frac{dx}{dt} \vec{i} + \frac{dy}{dt} \vec{j} \tag{6.36}$$

where $\vec{i}$ and $\vec{j}$ are unit vectors along x and y axis. $\frac{dx}{dt}$ and $\frac{dy}{dt}$ can be determined as follows,

$$\frac{dx}{dt} = \left(\frac{1}{\Delta t_+ + \Delta t_-} \right) \left[\left(\frac{\Delta t_-}{\Delta t_+} \right) \cdot \left(x_{i+1,j_{max}} - x_{i,j_{max}} \right) + \left(\frac{\Delta t_+}{\Delta t_-} \right) \cdot \left(x_{i,j_{max}} - x_{i-1,j_{max}} \right) \right] \tag{6.37a}$$

$$\frac{dy}{dt} = \left(\frac{1}{\Delta t_+ + \Delta t_-} \right) \left[\left(\frac{\Delta t_-}{\Delta t_+} \right) \cdot \left(y_{i+1,j_{max}} - y_{i,j_{max}} \right) + \left(\frac{\Delta t_+}{\Delta t_-} \right) \cdot \left(y_{i,j_{max}} - y_{i-1,j_{max}} \right) \right] \tag{6.37b}$$

After computing $\vec{T}_\xi$ and $\vec{T}_\xi$, one can compute α from Eq. (6.30b) and ΔP^n from Eq. (6.31). Using value of Δs_1 from Eq. (6.35), ΔQ^n is computed. Then, P and Q for next step are updated.

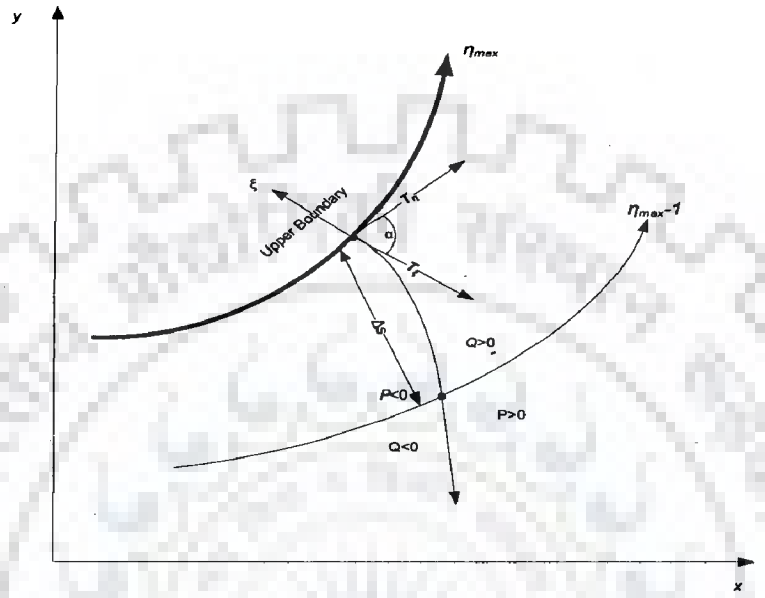

Figure 6.2 Effect of P and Q adjacent to top boundary (Hoffman, 1992)

6.4.2.2 Bottom boundary implementation

For the bottom boundary, one can calculate $\vec{T}_\xi$ and $\vec{T}_\eta$ as follows,

$$\vec{T}_\xi = \frac{(x_{i,1} - x_{i,2})}{\Delta s_2}\vec{i} + \frac{(y_{i,1} - y_{i,2})}{\Delta s_2}\vec{j} \tag{6.38}$$

$$\Delta s_2 = \left[(x_{i,1} - x_{i,2})^2 + (y_{i,1} - y_{i,2})^2\right]^{\frac{1}{2}} \tag{6.39}$$

$$\vec{T}_\eta = \frac{dx}{dt}\vec{i} + \frac{dy}{dt}\vec{j} \tag{6.40}$$

where $\vec{i}$ and $\vec{j}$ are unit vectors along x and y axis. $\frac{dx}{dt}$ and $\frac{dy}{dt}$ can be determined as follows,

$$\frac{dx}{dt}=\left(\frac{1}{\Delta t_{+}+\Delta t_{-}}\right)\left[\left(\frac{\Delta t_{-}}{\Delta t_{+}}\right)\cdot\left(x_{i+1,1}-x_{i,1}\right)+\left(\frac{\Delta t_{+}}{\Delta t_{-}}\right)\cdot\left(x_{i,1}-x_{i-1,1}\right)\right] \tag{6.41a}$$

$$\frac{dy}{dt}=\left(\frac{1}{\Delta t_{+}+\Delta t_{-}}\right)\left[\left(\frac{\Delta t_{-}}{\Delta t_{+}}\right)\cdot\left(y_{i+1,1}-y_{i,1}\right)+\left(\frac{\Delta t_{+}}{\Delta t_{-}}\right)\cdot\left(y_{i,1}-y_{i-1,1}\right)\right] \tag{6.41b}$$

After computing $\vec{T}_{\xi}$ and $\vec{T}_{\xi}$, one can compute α from Eq. (6.30b) and ΔP^{n} from Eq. (6.31). Using value of Δs_1 from Eq. (6.39), ΔQ^{n} is computed. Then, P and Q for next step are for bottom boundary updated.

6.4.2.3 Extrapolation of boundary values to interior points.

Extrapolation of the boundary values of $P(\xi,\eta)$ and $Q(\xi,\eta)$ into interior points of the domain is done to achieve the desired effect in the interior grid points. For this exponential extrapolation is adopted herein (Hoffman 1992).

$$P(\xi,\eta)=P(\xi,1)e^{-\frac{a(\eta-1)}{(\eta_{\max}-1)}}+P(\xi,\eta_{\max})e^{\frac{b(\eta_{\max}-\eta)}{(\eta_{\max}-1)}} \tag{6.42a}$$

$$Q(\xi,\eta)=Q(\xi,1)e^{-\frac{c(\eta-1)}{(\eta_{\max}-1)}}+Q(\xi,\eta_{\max})e^{\frac{d(\eta_{\max}-\eta)}{(\eta_{\max}-1)}} \tag{6.42b}$$

Where first term represents boundary control on the bottom boundary and second term represents the boundary control on the top boundary. Large value of exponential term gives rapid decay and vice versa. Here in the model, the adopted values of coefficients were 9.0. Similarly, for downstream, upstream boundaries P and Q were evaluated and extrapolated. P and Q were averaged to include the effect of all four boundaries of the domain.

6.5 IMPROVED MESH GENERATION SYSTEM

6.5.1 EFFECT CONTROL FOR SMOOTHNESS

A good balance of orthogonality and smoothness without distortion and overlapping, method proposed by Zhang and Jia (2005) is applied by introducing effect control factor on non homogeneous terms P and Q as follows.

For each grid point factor such as (1-r_p) and (1-r_q) were applied to the terms P and Q to get improved P and Q for incorporation of smoothness as

$$P^* = (1 - r_p)P \tag{6.43a}$$

$$Q^* = (1 - r_q)Q \tag{6.43b}$$

In Eqs. (6.43a) and (6.43b),

$$r_p = \frac{|\bar{h}_\xi - h_\xi|}{\bar{h}_\xi} \tag{6.44a}$$

$$r_q = \frac{|\bar{h}_\eta - h_\eta|}{\bar{h}_\eta} \tag{6.44b}$$

P^* and Q^* are improved terms, and $\bar{h}_\xi$ and $\bar{h}_\eta$ are locally averaged scale factor along ξ and η direction.

6.6 MEASURE OF QUALITY OF THE GENERATED GRID.

6.6.1 MEASURE OF MESH QUALITY

Zhang and Jia (2005) mentioned three indices to evaluate the quality of a mesh system i.e. uniformity, orthogonality and adaptivity. Uniformity indicates how uniform the mesh spacing is; Orthogonality is a measure to what extent the mesh lines are perpendicular to each other; and adaptivity indicates the degree of the mesh density distributed in areas where higher resolution and accuracy are desired (Zhang and Jia, 2005). The adaptivity of the mesh is measured by the functional,

$$I_W = \int_D w(x, y) J dA \tag{6.45}$$

Where the Jacobian J, which represents the area of a mesh cell in two dimensions and $w(x,y)$ is the weighing factor. When this integral is minimized, $w(x,y)J$ (with $w(x,y)>0$) should have a uniform distribution, so that where the weighting function is large, the mesh size J should be small.

The weighting function w is often formulated using water depth or bed bathymetry to handle the complex hydrodynamic problems. If the numerical solutions such as the concentration or the velocity gradients are selected, the mesh shall be adaptive dynamically with the numerical solution (Zhang and Jia, 2005). The uniformity of a mesh is measured by the functional

$$I_s = \int_D \left[(\nabla\xi)^2 + (\nabla\eta)^2\right] dA \tag{6.46}$$

The orthogonality which is vital for ease in numerical solution can also be measured as

$$I_o = \int_D (\nabla\xi \cdot \nabla\eta)^2 J^3 dA \tag{6.47}$$

Where the factor J^3 is added to enforce the orthogonality with higher weighting for large cells. If the three indices approach their minimum values, the mesh would have the optimal combination of uniformity, orthogonality and adaptivity. In general, a mesh can be generated by minimizing the sum of the three integrals.

$$I = \lambda_w I_w + \lambda_s I_s + \lambda_o I_o \tag{6.48}$$

Since it is impossible to achieve these three objectives at the same time, for a particular mesh one needs to select the appropriate combination of the coefficients of λ_w, λ_s and λ_o. In our case λ_o is for orthogonality has been stressed upon more than other indices for numerical ease of hydrodynamic solution. It is further to be mentioned here that topographical variations are irregular and large as well as mesh used in this thesis is of fixed domain. So optimizing indices like adaptivity and uniformity may increase complication to get feasible mesh generation with nearly orthogonal grid.

6.6.2 MESH EVALUATION

Zhang and Jia (2005) have suggested a number of indices to evaluate quality of mesh quantitatively by several indicators which have been applied here to check the quality. These are Maximum Deviation Orthogonality (*MDO*), Averaged Deviation from Orthogonality (*ADO*), Maximum Aspect Ratio (*MAR*) and Average grid aspect ratio (*AAR*) (Zhang and Zia, 2005).

$$MDO = \max(\theta_{i,j}) \tag{6.49a}$$

$$ADO = \frac{1}{(ni-2)}\frac{1}{(nj-2)}\sum_{2}^{ni-1}\sum_{2}^{nj-1}\max(\theta_{i,j}) \tag{6.49b}$$

$$MAR = \max(\max(\frac{h_{\xi_{i,j}}}{h_{\eta_{i,j}}}, \frac{h_{\eta_{i,j}}}{h_{\xi_{i,j}}}) \tag{6.49c}$$

where ni and nj are the maximum number of mesh lines in ξ and η directions respectively; and θ is defined as

$$\theta_{i,j} = \arccos\left(\frac{\beta}{h_\xi h_\eta}\right)_{i,j} \tag{6.50a}$$

$$AAR = \frac{1}{(ni-2)}\frac{1}{(nj-2)}\sum_{2}^{ni-1}\sum_{2}^{nj-1}\max(\frac{h_{\xi_{i,j}}}{h_{\eta_{i,j}}}, \frac{h_{\eta_{i,j}}}{h_{\xi_{i,j}}}) \tag{6.50b}$$

For generated mesh to be perfectly orthogonal, *ADO* and *MDO* should be 1.57(π/2). For perfectly smooth mesh, *MAR* and *AAR* should have same for perfect mesh smoothness.

6.7 COMPUTATION OF COEFFICIENT MATRICES FOR THE GRID

Difference formulas for derivatives developed in Hoffman (1992) have been chosen suitably to compute coefficient matrices which are various derivatives or combination of

derivatives between independent variables x and y with ξ and η depending upon the availability of neighborhood nodes.

$$x_\xi = \frac{\partial x}{\partial \xi} = \frac{-11x_{i,j} + 18x_{i+1,j} - 9x_{i+2,j} + 2x_{i+3,j}}{6\Delta\xi}$$

Or,

$$x_\xi = \frac{\partial x}{\partial \xi} = \frac{-2x_{i-1,j} - 3x_{i,j} + 6x_{i+1,j} - x_{i+2,j}}{6\Delta\xi}$$

Or,

$$x_\xi = \frac{\partial x}{\partial \xi} = \frac{x_{i-2,j} - 6x_{i-1,j} - 3x_{i,j} + 2x_{i+1,j}}{6\Delta\xi}$$

Or,

$$x_\xi = \frac{\partial x}{\partial \xi} = \frac{-2x_{i-3,j} + 9x_{i-2,j} - 18x_{i-1,j} + 11x_{i,j}}{6\Delta\xi} \qquad (6.51)$$

$$x_{\xi\xi} = \frac{\partial^2 x}{\partial \xi^2} = \frac{x_{i+1,j} - 2x_{i,j} + x_{i-1,j}}{\Delta\xi^2}$$

Or,

$$x_{\xi\xi} = \frac{\partial^2 x}{\partial \xi^2} = \frac{2x_{i,j} - 5x_{i+1,j} + 4x_{i+2,j} - x_{i+3,j}}{\Delta\xi^2}$$

Or,

$$x_{\xi\xi} = \frac{\partial^2 x}{\partial \xi^2} = \frac{-x_{i-3,j} + 4x_{i-2,j} - 5x_{i-1,j} + x_{i,j}}{\Delta\xi^2} \qquad (6.52)$$

Similarly y_ξ and $y_{\xi\xi}$ can be computed by substituting y in place of x in Eqs. (6.51) and (6.52). Similarly following coefficient matrices can be determined depending upon the availability of neighborhood nodes and suitability.

$$x_\eta = \frac{\partial x}{\partial \eta} = \frac{-11x_{i,j} + 18x_{i,j+1} - 9x_{i.j+2} + 2x_{i,j+3}}{6\Delta\eta}$$

Or,

$$x_\eta = \frac{\partial x}{\partial \eta} = \frac{-2x_{i,j-1} - 3x_{i,j} + 6x_{i,j+1} - x_{i,j+2}}{6\Delta\eta}$$

Or,

$$x_\eta = \frac{\partial x}{\partial \eta} = \frac{x_{i,j-2} - 6x_{i,j-1} - 3x_{i,j} + 2x_{i,j+1}}{6\Delta\eta}$$

Or,

$$x_\eta = \frac{\partial x}{\partial \eta} = \frac{-2x_{i,j-3} + 9x_{i,j-2} - 18x_{i,j-1} + 11x_{i,j}}{6\Delta\eta} \qquad (6.53)$$

$$x_{\eta\eta} = \frac{\partial^2 x}{\partial \eta^2} = \frac{x_{i,j+1} - 2x_{i,j} + x_{i,j-1}}{\Delta\eta^2}$$

Or,

$$x_{\eta\eta} = \frac{\partial^2 x}{\partial \eta^2} = \frac{2x_{i,j} - 5x_{i,j+1} + 4x_{i,j+2} - x_{i,j+3}}{\Delta\eta^2}$$

Or,

$$x_{\eta\eta} = \frac{\partial^2 x}{\partial \eta^2} = \frac{-x_{i,j-3} + 4x_{i,j-2} - 5x_{i,j-1} + x_{i,j}}{\Delta\eta^2} \qquad (6.54)$$

Similarly y_η and $y_{\eta\eta}$ can be computed by substituting y in place of x in Eqs. (6.53) and (6.54). Other coefficients used in the transformed equations are functionally related to above basic derivatives. Functional relations have been derived and presented in Chapter 5 of this thesis in relevant sub-sections. Flow chart of the grid generation algorithm has been presented in Figure 6.3a and continued to Figure 6.3b.

6.8 GRID GENERATED FOR DIFFERENT DOMAINS FROM DEVELOPED CODE

The computer code in *C++* based on the algorithm has been developed to generate efficient meshes starting from simple to curvilinear domain to assess the efficacy of the developed algorithm. The parameters to measure the quality have also been computed to observe the control functions performance while adjusting the internal nodal points to optimize orthogonality and aspect ratio. Some developed meshes in variety of flow domain are presented here illustrate the quality of generated meshes.

Case-I:

In Figure 6.4, a rectangular domain has been discretized with 6 ×41 nodal points. *MDO* and *ADO* is 1.57, indicating the grid to be perfectly orthogonal. Moreover Maximum Aspect Ratio (*MAR*) and Average Aspect Ratio (*AAR*) are also same, indicating the mesh to be perfectly smooth.

Case-II:

In the Figure 6.5, a tapered domain has been taken and the grid quality is assessed. The orthogonality and aspect ratio have been computed with maximum and average values. Generated mesh is orthogonal with slight deviation with perfect orthogonality while computing maximum deviation from perfect orthogonal mesh lines. Still mesh is reasonably perfect orthogonal in character. Aspect ratio deviation from maximum and average is quite high indicating reduced smoothness in comparison to Figure 6.4.

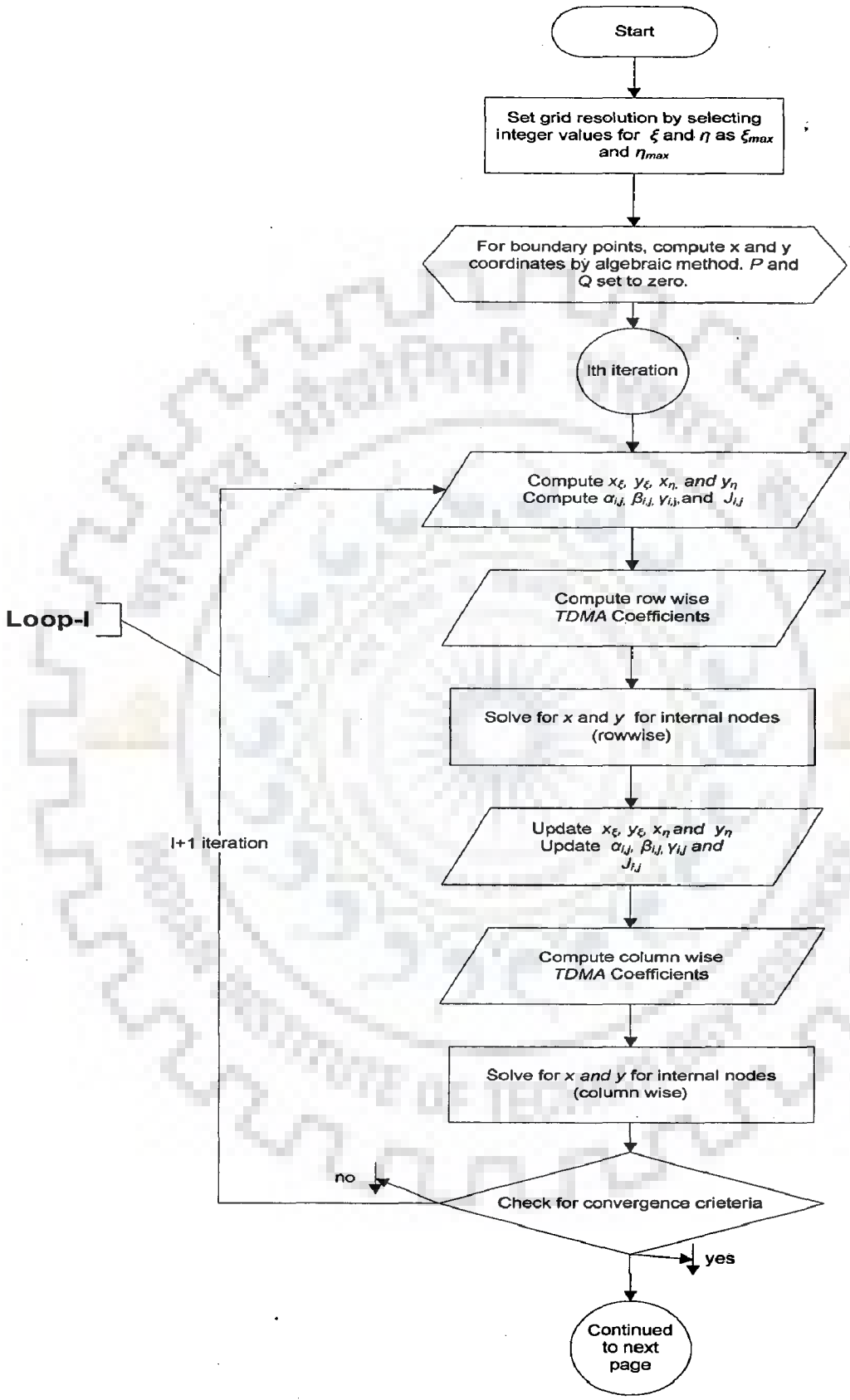

Figure 6.3a Flow chart of grid generation algorithm

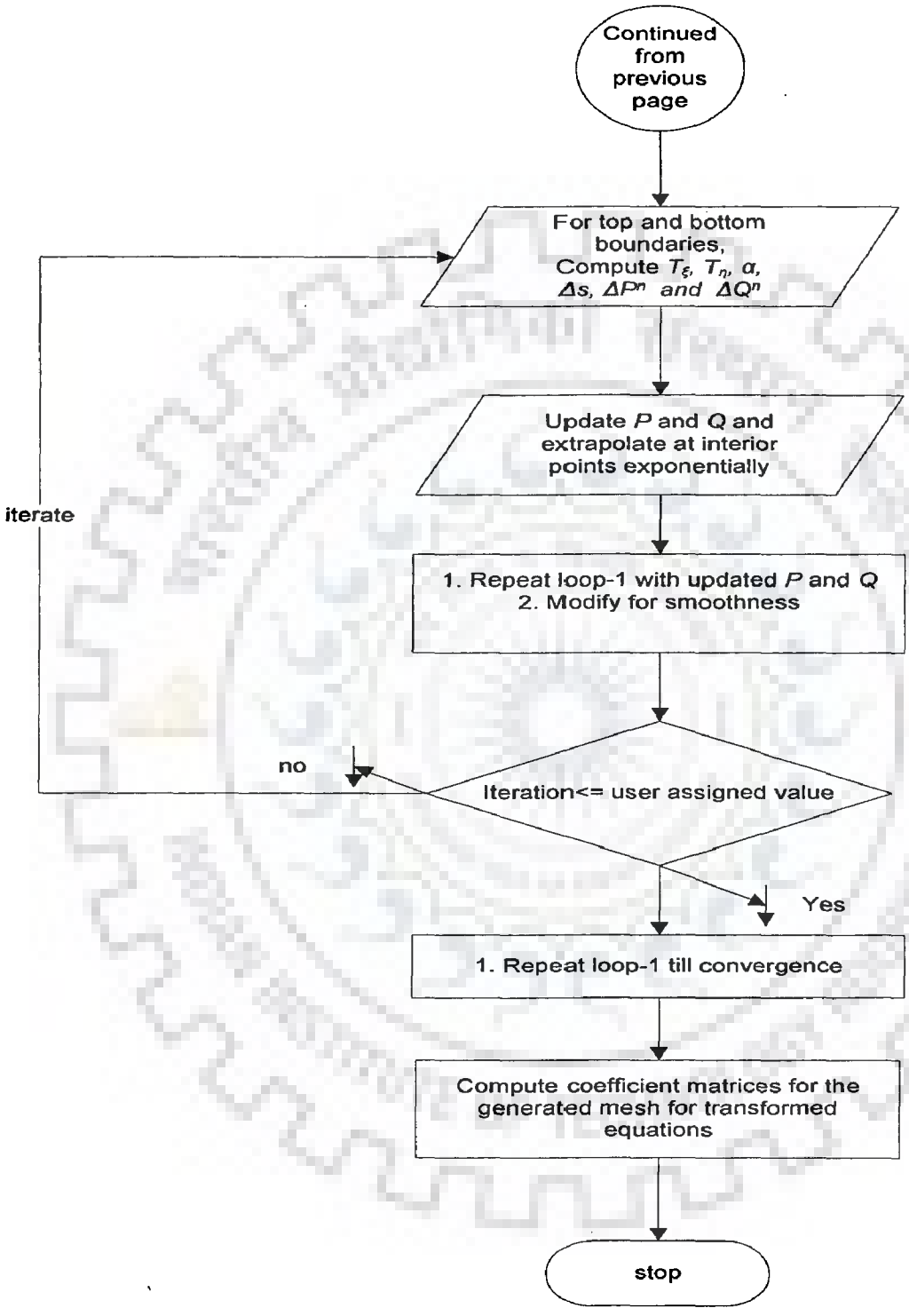

Figure 6.3b Flow chart of grid generation algorithm

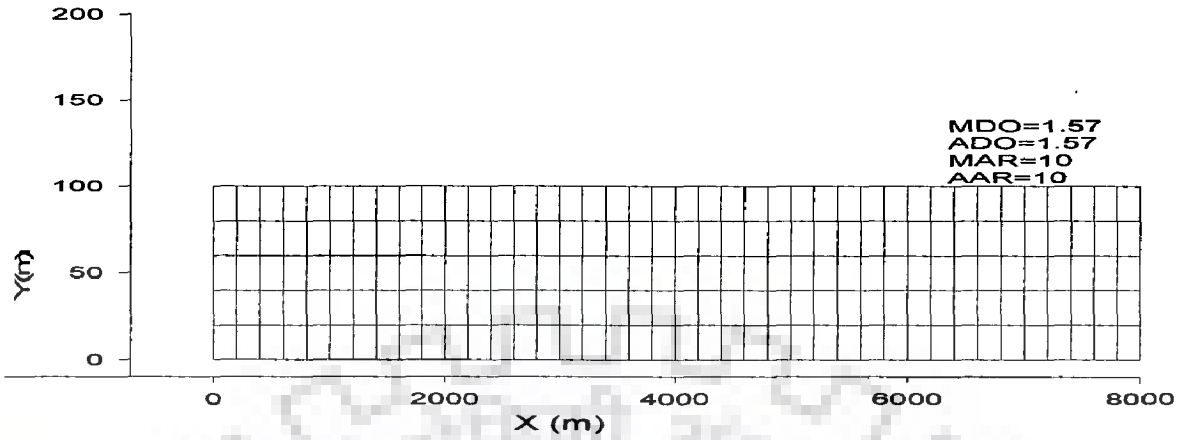

Figure 6.4 A mesh of rectangular domain with 6×41 nodes

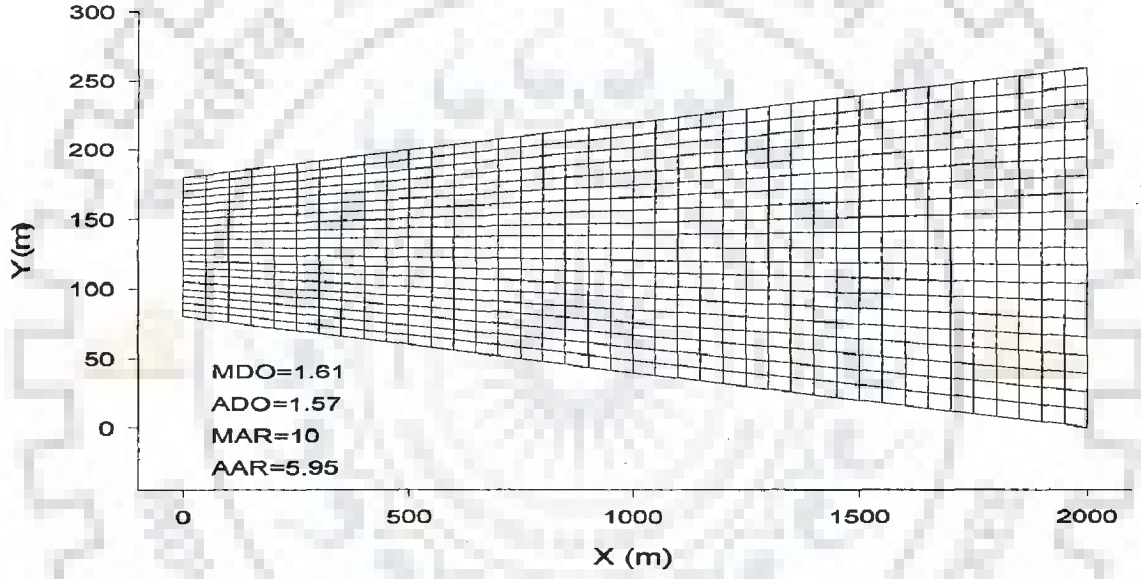

Figure 6.5 A mesh of domain with 21×41 nodes for tapered shape

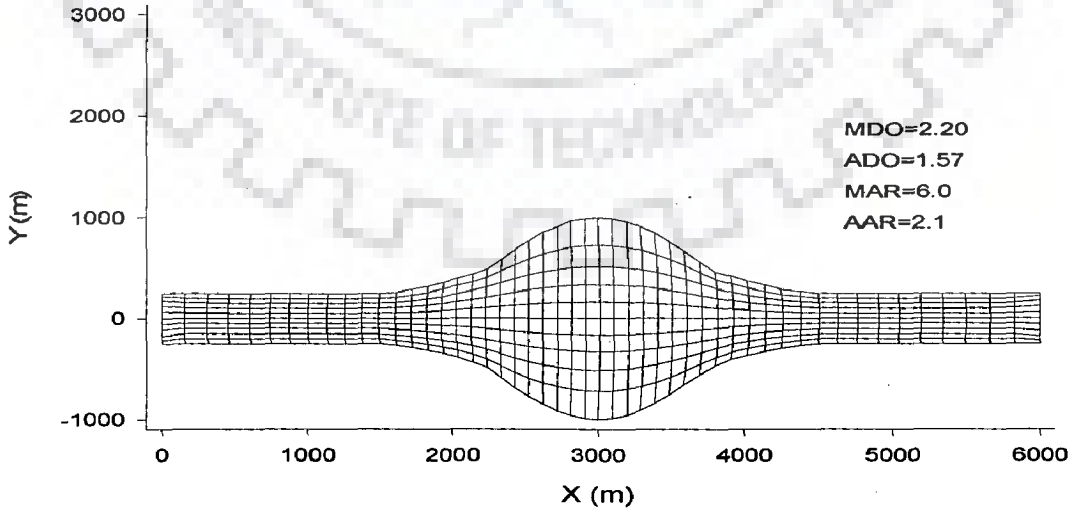

Figure 6.6 A mesh of domain with 11×51 nodes for curved shape

Case-III:

A symmetric curved shape as depicted in Figure 6.6 with 11×51 nodal points has been discretized using orthogonal and smoothness effect control to get the mesh quality for curvilinear symmetric meshes. The computed value of *ADO* suggests mesh to be perfectly orthogonal but *MDO* gives the indication of maximum deviation from orthogonality to be 2.20., which indicates that code has to adjust some nodal points to achieve the general mesh characteristic to be orthogonal. So far *AAR* and *MAR* depend on the number of ξ lines and η lines by user to achieve a close proximity between contra-varient metric scale factors to make the meshes smoother. It should be kept in mind that there should be a reasonable balance between smoothness and orthogonality, as forced smoothness may decrease orthogonality and vice versa (Zhang and Jia, 2005).

6.8.1 COMPARISON OF MESH QUALITY WITH AND WITHOUT SMOOTHNESS CONTROL

Algorithm is modified in view of the effect control procedure described in Section 6.4.3(a) and mesh for an asymmetric curved domain is generated with and without smoothness measure as follows.

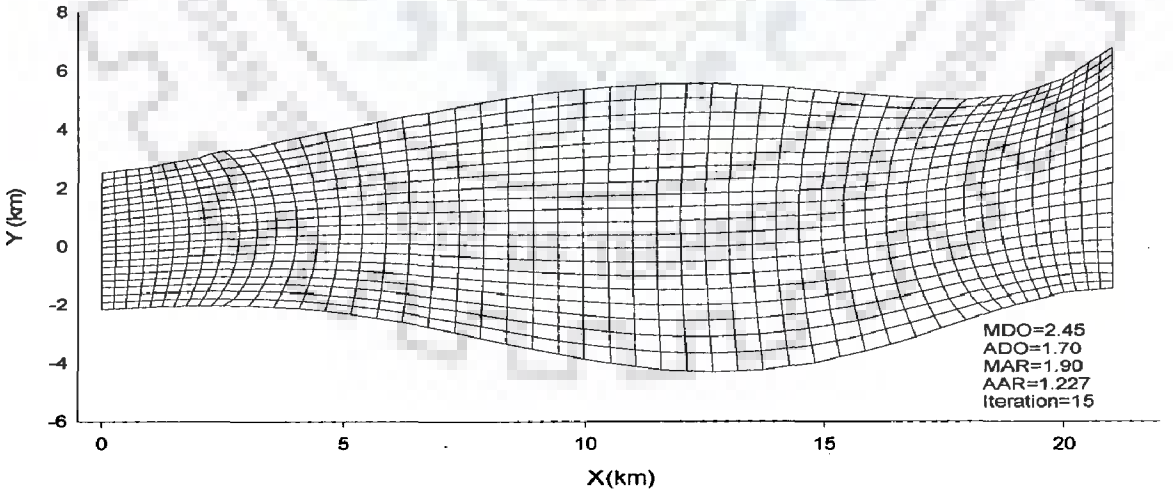

Figure 6.7a A mesh of domain with 21×51 nodes with smoothness control

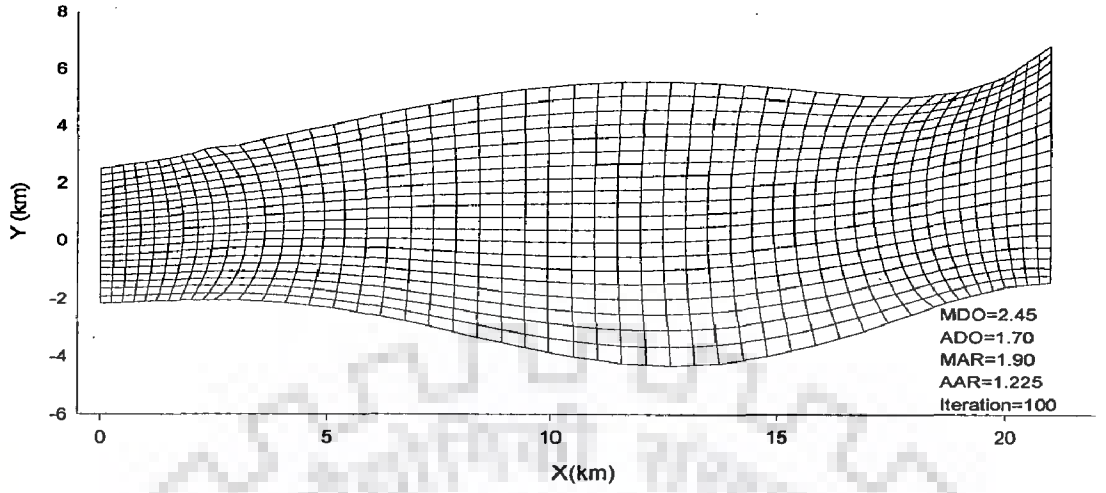

Figure 6.7b A mesh of domain with 21×51 nodes with smoothness control

Figures 6.7a and 6.7b are presented to demonstrate the effect of the smoothness control over the mesh generated. Figure 6.7a depicts the internal control through applying low values non homogeneous terms P and Q through iterating 15 times only to estimate them, whereas Figure 6.7b. the P and Q terms are kept high with 100 iteration, yet on account of smoothness control, grid remains nearly unaltered keeping the orthogonality and smoothness controlled at its optimum values resulting in the grid to be independent of the iteration done to estimate non homogeneous terms P and Q. This gives a perfect balance between orthogonality and smoothness at a time without deciding much for the number of iteration done to evaluate P and Q (as described in section 6.4.2) to get optimum quality of the grid.

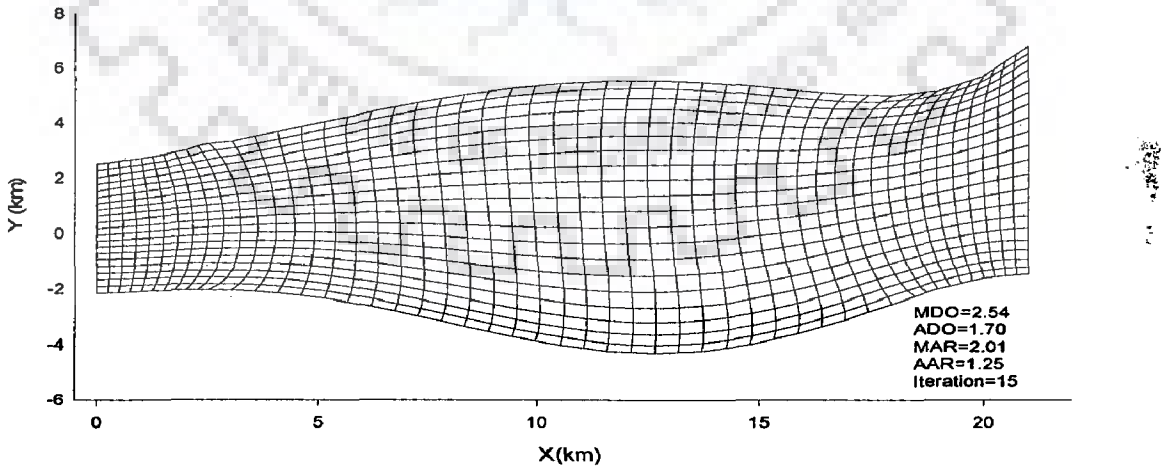

Figure 6.8a A mesh of domain with 21×51 nodes without smoothness control

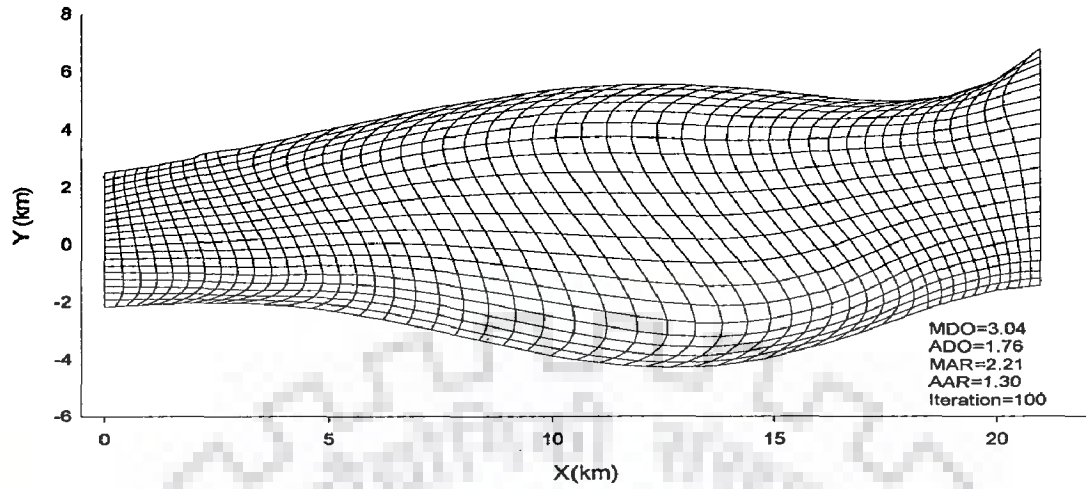

Figure 6.8b A mesh of domain with 21×51 nodes without smoothness control

Figures 6.8a and, 6.8b are presented here to observe the grid quality without smoothness control. When P and Q values are increased, the nodal points adjust to make the grid more skewed thereby changing the average orthogonality considerably at the same time there is no control over aspect ratio also. So, Figure 6.8a is more orthogonal and smooth when compared to Figure 6.8b. Whereas in Figures 6.7a and 6.7b, the orthogonality and smoothness remains unchanged and optimized irrespective of the relative absolute values of the non-homogeneous terms.

6.9 SUMMARY

In this chapter numerical scheme for developing a code for generating grids in the flow domain using Poisson's equation is described in detail. The computer code has been developed in *C++* using finite difference method as stated earlier and clubbed with the flow simulation numerical scheme to facilitate prime input for domain variables and coordinate transformation coefficients to be used in the governing equations for flow simulation boundary fitted flow domain (details in Appendix VI). The evaluation criteria for assessing mesh quality and efficiency have also been described. To make the generated mesh smooth and nearly orthogonal, certain modifications suggested by Zhang and Jia (2005) have also been incorporated in the developed computer code. To illustrate the performance evaluation of the developed computer code, some chosen physical domains with different geometry have also been discretized and quality parameters were evaluated and described further to provide an insight into the mesh evaluation.

CHAPTER-7

NUMERICAL DEVELOPMENT OF 2-D HYDRODYNAMIC MODEL FOR COMPLEX PHYSICAL DOMAIN

7.1 GENERAL

The governing differential equations for mass and momentum in curvilinear coordinate system have been formulated step by step in Chapter 5 of this thesis. As mentioned earlier, finite difference methods for solving these differential equations in particular require that the continuous physical space be discretized into uniform orthogonal computational space (Hoffman 1992). In the process of formulating these controlling equations, coefficients of transformation introduced into the PDEs which have to be evaluated through mesh generation algorithm separately, for a given domain. Moreover, boundary conditions have to be implemented very cautiously to adequately represent and simulate the real physical conditions to solve these equations. In addition, the independent variables x and y change to uniform ξ and η variables. Similarly, dependent variables like Cartesian physical velocities also changes to contra-variant counterparts resulting in requirement of complete transformation of the *PDEs*. Numerical model development for determination of coefficient matrices for transformed controlling equations and appropriate coordinate transformation has been dealt in detail in chapter 6 of this thesis. The complete transformed governing equations in curvilinear coordinate system (Jang and Shimizu, 2007) to be solved in finite difference method is mentioned herein under.

$$\frac{\partial}{\partial \tau}\left(\frac{h}{J}\right)+\frac{\partial}{\partial \xi}\left(U^{\xi}\right)\frac{h}{J}+\frac{\partial}{\partial \eta}\left(V^{\eta}\right)\frac{h}{J}=0 \tag{7.1a}$$

$$\frac{\partial U^{\xi}}{\partial \tau}+\left(U^{\xi}\right)\frac{\partial U^{\xi}}{\partial \xi}+\left(V^{\eta}\right)\frac{\partial U^{\xi}}{\partial \eta}+\alpha_1 U^{\xi}U^{\xi}+\alpha_2 U^{\xi}V^{\eta}+\alpha_3 V^{\eta}V^{\eta}$$

$$=-g\left((\xi_x^2+\xi_y^2)\frac{\partial H}{\partial \xi}+(\eta_x\xi_x+\eta_y\xi_y)\frac{\partial H}{\partial \eta}\right)-\frac{C_d}{hJ}U^{\xi}\sqrt{\left(\eta_y U^{\xi}-\xi_y V^{\eta}\right)^2+\left(-\eta_x U^{\xi}+\xi_x V^{\eta}\right)^2}+D_{\xi} \tag{7.1b}$$

$$\frac{\partial V^{\eta}}{\partial \tau}+\left(U^{\xi}\right)\frac{\partial V^{\eta}}{\partial \xi}+\left(V^{\eta}\right)\frac{\partial V^{\eta}}{\partial \eta}+\alpha_4 U^{\xi}U^{\xi}+\alpha_5 U^{\xi}V^{\eta}+\alpha_6 V^{\eta}V^{\eta}$$

$$=-g\left((\eta_x\xi_x+\eta_y\xi_y)\frac{\partial H}{\partial \xi}+(\eta_x^2+\eta_y^2)\frac{\partial H}{\partial \eta}\right)-\frac{C_d}{hJ}V^{\eta}\sqrt{\left(\eta_y U^{\xi}-\xi_y V^{\eta}\right)^2+\left(-\eta_x U^{\xi}+\xi_x V^{\eta}\right)^2}+D_{\eta} \quad (7.1c)$$

In Eqs. (7.1b) and (7.1c), $\alpha_1=\xi_x\frac{\partial^2 x}{\partial \xi^2}+\xi_y\frac{\partial^2 y}{\partial \xi^2}$, $\alpha_2=2(\xi_x\frac{\partial^2 x}{\partial \xi \partial \eta}+\xi_y\frac{\partial^2 y}{\partial \xi \partial \eta})$, $\alpha_3=\xi_x\frac{\partial^2 x}{\partial \eta^2}+\xi_y\frac{\partial^2 y}{\partial \eta^2})$, $\alpha_4=\eta_x\frac{\partial^2 x}{\partial \xi^2}+\eta_y\frac{\partial^2 y}{\partial \xi^2})$, $\alpha_5=2(\eta_x\frac{\partial^2 x}{\partial \xi \partial \eta}+\eta_y\frac{\partial^2 y}{\partial \xi \partial \eta})$, $\alpha_6=\eta_x\frac{\partial^2 x}{\partial \eta^2}+\eta_y\frac{\partial^2 y}{\partial \eta^2})$, ξ and η = spatial coordinates in the boundary-fitted coordinate system, τ =time coordinate in the coordinate system, x and y=spatial coordinate components in the Cartesian coordinate system, H =water surface elevation($h+z_b$), h=water depth, z_b=bed elevation referred to a horizontal plane, g =gravitational acceleration, C_d=bed friction coefficient, which is written using Manning's roughness coefficient as $gn^2/h^{\frac{1}{3}}$, n=Manning's roughness coefficient, J=Jacobian of the coordinate transformation, U^{ξ} and V^{η} = contra-variant components of flow velocity in the ξ and η directions, U_x and U_y = depth-averaged velocity components in x and y directions, respectively, ν_t = depth-averaged diffusion coefficient ($=\kappa U^* h/6$), κ =Von Karman constant(=0.4), U^*(shear velocity)= $n\left[g\left(U_x{}^2+U_y{}^2\right)\right]^{1/2}/h^{\frac{1}{6}}$.

There are number of nonlinear terms introduced (for example terms with coefficients α_1-α_6) in Eqs. (7.1b and 7.1c) while transforming it from Cartesian coordinate system to Boundary fitted coordinate System. Flow variables such as Cartesian velocities are also transformed to their counterpart such as contra-variant velocities. The introduced additional non-linear source terms are difficult to handle while solving it with numerical procedure. Moreover, solutions are obtained in terms of contra- variant variables which again have to be transformed to get Cartesian physical velocities with mathematical correlations to get as actual set of final results. It introduces additional computations at each computational step. So, models with finite difference solver generally are used for orthogonal grids or nearly orthogonal grids to avoid non-linear curvature source terms,

which in-advertently get introduced in complete coordinate transformation in curvilinear system on account of non-orthogonality which is significant with increasing geometric complexity. This may introduce considerable error propagation when dealing with complex domain with highly non-prismatic channels (*i.e.* Lien *et al.*, 1999; Jang and Shimizu, 2005 and 2007). These models may work efficiently for simple experimental flumes but applied to complex flow geometry like simulating alluvial river. Other investigators (Seo *et al.*, 2008 etc.) applied finite element methods, which is though efficient but requires more computational efforts with enhanced mathematical complexity. Kuiry *et al.* (2008) implemented finite volume method with an implicit solution of the discretized equations. They tested the model theoretically as well as on field problem taken from a tidal reach of River Hoogly in India. For simulating large rivers, finite volume method (*FVM*) of discretizing conservative form of partially transformed controlling equations in curvilinear coordinate system seems most appropriate to use with much computational ease. *FVM* is used because of its simplicity of implementation and good flexibility for space discretization over other methods, as discussed by Tan (1992) and Zhao *et al.* (1996) as reported by Kuiry *et al.* (2008). *FVM* schemes maintain conservation properties in the presence of shocks Hirsch (1988) and their stability is independent of Froude number (Beffa 1994), reported by Kuiry *et al.* (2008). As *FVM* solver additionally conserves mass-momentum, hence it can be suitably applied for highly complex geometry using non-orthogonal grids.

The details with regard to transformed governing equations and secondary flow correction with mathematical derivation are dealt in Chapter 5 of this thesis. Here, development of 2-D numerical model with modified dispersion stress tensor is focused.

7.2 NUMERICAL SOLUTION PROCEDURE

7.2.1 GOVERNING EQUATIONS

The governing equations presented in Chapter 5 (Eqs. 5.21b, 5.41 and 5.42) are discretized using the finite volume method in curvilinear, non-staggered grid. In the curvilinear co-ordinate system, mass and momentum equation can be written in conservative tensor notation form as

Continuity equation

$$\frac{\partial(\rho hJ)}{\partial \tau}+\frac{\partial}{\partial \xi^m}(\rho hJ\hat{u}_m)=0 \tag{7.2}$$

Momentum equations

$$\frac{\partial(\rho hJU_i)}{\partial \tau}+\frac{\partial}{\partial \xi^m}\left(\rho hJ\hat{u}_m U_i-\Gamma hJ\alpha_j^m\alpha_j^m\frac{\partial U_i}{\partial \xi_m}\right)=-\frac{\partial}{\partial \xi_m}\left(\rho ghJ\alpha_j^m H\right)+JS_{u_i} \tag{7.3}$$

In Eq. (7.2) and (7.3), $\hat{u}_m$ (m=1, 2) are the velocity components in the curvilinear coordinate (ξ, η, τ) which relates to U_x, U_y and others as follows, where $\alpha_i^m=\partial\xi_m/\partial x_i$

$$\begin{pmatrix}\hat{u}_\xi\\ \hat{u}_\eta\end{pmatrix}=\begin{pmatrix}\alpha_1^1 & \alpha_2^1\\ \alpha_1^2 & \alpha_2^2\end{pmatrix}\begin{pmatrix}U_x\\ U_y\end{pmatrix}=\begin{pmatrix}\xi_x & \xi_y\\ \eta_x & \eta_y\end{pmatrix}\begin{pmatrix}U_x\\ U_y\end{pmatrix} \tag{7.4}$$

In Eq. (7.3), $\Gamma=\rho\nu_t$ =diffusitiity;

U_i stands for depth averaged velocities (i=x, y), S_{ui} is the corresponding source term in the equation for U_i, J is the *Jacobian* of transformation between Cartesian coordinate system x_i (x_1=x, x_2=y) and the computational curvilinear coordinate system ξ_m (ξ_1=ξ and ξ_2=η)

Source terms includes cross derivative diffusive terms, dispersion stress terms and external forces but excludes the second derivatives of coordinates (curvature terms) that are very sensitive to grid smoothness (Wu, 2007). Expanding Eq. (7.3)

$$\frac{\partial(\rho hJU_i)}{\partial \tau}+\frac{\partial}{\partial \xi}\left(\rho hJ\hat{u}_\xi U_i-\Gamma hJ\alpha_{11}\frac{\partial U_i}{\partial \xi}\right)+\frac{\partial}{\partial \eta}\left(\rho hJ\hat{u}_\eta U_i-\Gamma hJ\alpha_{22}\frac{\partial U_i}{\partial \eta}\right)=-\frac{\partial}{\partial \xi}\left(\rho ghJx_j^1 H\right)-\frac{\partial}{\partial \eta}\left(\rho ghJx_j^2 H\right)+\rho hJS_{u_i} \tag{7.5}$$

where $\alpha_{22}=\eta_x^{\,2}+\eta_y^2=\alpha_1^2\alpha_1^2+\alpha_2^2\alpha_2^2$ and $\alpha_{11}=\xi_x^{\,2}+\xi_y^2=\alpha_1^1\alpha_1^1+\alpha_2^1\alpha_2^1$ (7.6)

Eq. (7.5), can be written for i=x, y

$$\frac{\partial(\rho hJU_x)}{\partial\tau}+\frac{\partial}{\partial\xi}\left(\rho hJ\hat{u}_\xi U_x-\Gamma hJ\alpha_{11}\frac{\partial U_x}{\partial\xi}\right)+\frac{\partial}{\partial\eta}\left(\rho hJ\hat{u}_\eta U_x-\Gamma hJ\alpha_{22}\frac{\partial U_x}{\partial\eta}\right)=-\frac{\partial}{\partial\xi}\left(\rho ghJ\alpha_x^1 H\right)-\frac{\partial}{\partial\eta}\left(\rho ghJ\alpha_x^2 H\right)+\rho hJS_{u_x} \quad (7.7a)$$

$$\frac{\partial(\rho hJU_y)}{\partial\tau}+\frac{\partial}{\partial\xi}\left(\rho hJ\hat{u}_\xi U_y-\Gamma hJ\alpha_{11}\frac{\partial U_y}{\partial\xi}\right)+\frac{\partial}{\partial\eta}\left(\rho hJ\hat{u}_\eta U_y-\Gamma hJ\alpha_{22}\frac{\partial U_y}{\partial\eta}\right)=-\frac{\partial}{\partial\xi}\left(\rho ghJ\alpha_y^1 H\right)-\frac{\partial}{\partial\eta}\left(\rho ghJ\alpha_y^2 H\right)+\rho hJS_{u_y} \quad (7.7b)$$

7.2.2 CONTROL VOLUME SETUP

The computational domain is discretized into finite number of control volumes by a computational body fitted grid. The gridlines are identified as cell faces. The control volume centered at point *P* is embraced by four faces *w*, *s*, *e* and *n* (Figure 7.1). It is connected with four adjacent control volumes centered at points *W*, *E*, *S* and *N*. Here, *W* denotes west (the negative ξ direction), *E* the east (positive ξ direction), *S* the south (negative η direction) and *N* the north (positive η direction). The convection terms in Eq. (7.3) are discretized by Hybrid Linear/Parabolic Approximation (*HLPA*) scheme (Zhu and Rodi, 1991). The *HLPA* scheme is reported to be good at stability and accuracy (Wu, 2007). The diffusion terms are discretized by central difference scheme. The time derivative term is discretized by first order backward scheme.

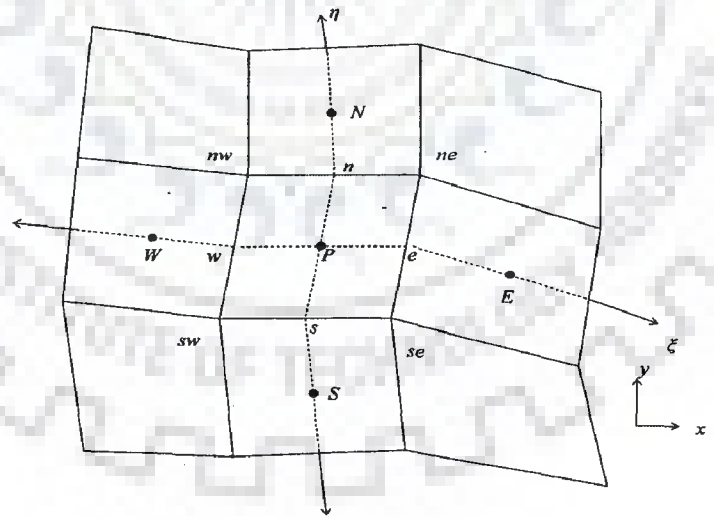

Figure 7.1 Two dimensional control volume

For discretization, non staggered grid is used. It stores all variables on the same set of grid points. Number of coefficients is minimized. It handles more complex geometry

easily. It encounters difficulty in coupling of pressure and velocity (Wu, 2007). It may induce numerical oscillation in pressure field. Rhie and Chow (1983) gave momentum interpolation technique to improve pressure velocity coupling in non staggered grid, which has been adopted to avoid spurious solution.

7.2.3 DISCRETIZATION

Momentum equations in Eqs. (7.7a) and (7.7b) are discretized term wise using *FVM* through integrating over the control volume in Figure 7.1 as follows

i. Transient term

Transient mass of the control volume in Δt

For U_x

$$\left.\frac{\rho_P^{k+1}U_x^{k+1}-\rho_P^{k}U_x^{k}}{\Delta t}\right|_P \cdot (hJ\Delta\xi\Delta\eta)_P \tag{7.8a}$$

For U_y

$$\left.\frac{\rho_P^{k+1}U_y^{k+1}-\rho_P^{k}U_y^{k}}{\Delta t}\right|_P \cdot (hJ\Delta\xi\Delta\eta)_P \tag{7.8b}$$

ii. Convection term

For U_x

$$(\rho hJ\Delta\eta_e\hat{u}_\xi)_e^{k+1}(U_x^{k+1})_e-(\rho hJ\Delta\eta_w\hat{u}_\xi)_w^{k+1}(U_x^{k+1})_w+(\rho hJ\Delta\xi_n\hat{u}_\eta)_n^{k+1}(U_x^{k+1})_n-(\rho hJ\Delta\xi_s\hat{u}_\eta)_s^{k+1}(U_x^{k+1})_s$$

Whichcan be writtenas

$$\dot{m}_e^{k+1}U_{x\ e}^{k+1}-\dot{m}_w^{k+1}U_{x\ w}^{k+1}+\dot{m}_n^{k+1}U_{x\ n}^{k+1}-\dot{m}_s^{k+1}U_{x\ s}^{k+1} \tag{7.9a}$$

For U_y

$$\left(\rho hJ\Delta\eta_e\hat{u}_\xi\right)_e^{k+1}\left(u_y^{k+1}\right)_e-\left(\rho hJ\Delta\eta_w\hat{u}_\xi\right)_w^{k+1}\left(u_y^{k+1}\right)_w+\left(\rho hJ\Delta\xi_n\hat{u}_\eta\right)_n^{k+1}\left(u_y^{k+1}\right)_n-\left(\rho hJ\Delta\xi_s\hat{u}_\eta\right)_s^{k+1}\left(u_y^{k+1}\right)_s$$

Whichcan be writtenas

$$\dot{m}_e^{k+1}U_{y\ e}^{k+1}-\dot{m}_w^{k+1}U_{y\ w}^{k+1}+\dot{m}_n^{k+1}U_{y\ n}^{k+1}-\dot{m}_s^{k+1}U_{y\ s}^{k+1} \tag{7.9b}$$

In Eqs.(7.9a) and (7.9b)

$$\dot{m}_l=\left(\rho hJ\hat{u}_m\Delta m\right)_l \tag{7.10}$$

where $\Delta m=\Delta\xi$ or $\Delta\eta$ and l represent cell faces *w, e, s, n.*

iii. Interpolation of dependent variables at cell faces

Dependent variables are interpolated at cell faces to substitute their values in Eqs. (7.9a) and (7.9b). The interpolation has been done through Linear/Parabolic Hybrid Scheme (*HLPA*) scheme as suggested by Zhu and Rodi (1991) for non-uniform non -orthogonal grids. The implementation of the *HLPA* scheme is as follows. ϕ stands for dependent variables (U_x or U_y).

(a) West face

$\dot{m}_w >= 0$

$$\alpha_w^+=\begin{cases}1 & \left|\phi_P-2\phi_W+\phi_{WW}\right|<\left|\phi_P-\phi_{WW}\right| \\ 0 & \text{otherwise}\end{cases} \tag{7.11a}$$

$\dot{m}_w < 1$

$$\alpha_w^-=\begin{cases}1 & \left|\phi_W-2\phi_P+\phi_E\right|<\left|\phi_W-\phi_E\right| \\ 0 & \text{otherwise}\end{cases} \tag{7.11b}$$

$$\phi_w = U_w^+\phi_W + U_w^-\phi_P + \Delta\varphi_w$$

$$U_w^+ = 0.5\left(1+\frac{|\dot{m}_w|}{\dot{m}_w}\right) \quad U_w^- = \left(1-U_w^+\right) \quad \text{where} \quad \dot{m}_w \neq 0 \tag{7.11c}$$

$$\Delta\phi = \left(\phi_P - \phi_W\right)\left[U_w^+\alpha_w^+\frac{\phi_W-\phi_{WW}}{\phi_P-\phi_{WW}} - U_w^-\alpha_w^-\frac{\phi_P-\phi_E}{\phi_W-\phi_E}\right] \tag{7.11d}$$

$$\phi_w = U_w^+\phi_W + U_w^-\phi_P + \left(\phi_P-\phi_W\right)\left[U_w^+\alpha_w^+\frac{\phi_W-\phi_{WW}}{\phi_P-\phi_{WW}} - U_w^-\alpha_w^-\frac{\phi_P-\phi_E}{\phi_W-\phi_E}\right] \tag{7.11e}$$

(b) East face

$$\dot{m}_e >= 0$$

$$\alpha_e^+ = \begin{cases} 1 & |\phi_E - 2\phi_P + \phi_W| < |\phi_E - \phi_W| \\ 0 & \text{otherwise} \end{cases} \tag{7.11f}$$

$$\dot{m}_e < 1$$

$$\alpha_e^- = \begin{cases} 1 & |\phi_P - 2\phi_E + \phi_{EE}| < |\phi_P - \phi_{EE}| \\ 0 & \text{otherwise} \end{cases} \tag{7.11g}$$

$$\phi_e = U_e^+\phi_P + U_w^-\phi_E + \Delta\varphi_e$$

$$U_e^+ = 0.5\left(1+\frac{|\dot{m}_e|}{\dot{m}_e}\right) \quad U_e^- = \left(1-U_e^+\right) \text{ where } \quad \dot{m}_e \neq 0 \tag{7.11h}$$

$$\Delta\phi_e = \left(\phi_E - \phi_P\right)\left[U_e^+\alpha_e^+\frac{\phi_P-\phi_W}{\phi_E-\phi_W} - U_e^-\alpha_e^-\frac{\phi_E-\phi_{EE}}{\phi_P-\phi_{EE}}\right] \tag{7.11i}$$

$$\phi_e = U_e^+\phi_P + U_w^-\phi_E + \left(\phi_E-\phi_P\right)\left[U_e^+\alpha_e^+\frac{\phi_P-\phi_W}{\phi_E-\phi_W} - U_e^-\alpha_e^-\frac{\phi_E-\phi_{EE}}{\phi_P-\phi_{EE}}\right] \tag{7.11j}$$

(c) South face

$\dot{m}_s >= 0$

$$\alpha_s^+ = \begin{cases} 1 & |\phi_P - 2\phi_S + \phi_{SS}| < |\phi_P - \phi_{SS}| \\ 0 & \text{otherwise} \end{cases} \tag{7.11k}$$

$\dot{m}_s < 1$

$$\alpha_s^- = \begin{cases} 1 & |\phi_S - 2\phi_P + \phi_N| < |\phi_S - \phi_N| \\ 0 & \text{otherwise} \end{cases} \tag{7.11l}$$

$$\phi_s = U_s^+ \phi_S + U_s^- \phi_P + \Delta\varphi_s$$

$$U_s^+ = 0.5\left(1 + \frac{|\dot{m}_s|}{\dot{m}_s}\right) \quad U_s^- = \left(1 - U_s^+\right) \text{ where } \dot{m}_s \neq 0 \tag{7.11m}$$

$$\Delta\phi_s = \left(\phi_P - \phi_S\right)\left[U_s^+ \alpha_s^+ \frac{\phi_S - \phi_{SS}}{\phi_P - \phi_{SS}} - U_s^- \alpha_s^- \frac{\phi_P - \phi_N}{\phi_S - \phi_N}\right] \tag{7.11n}$$

$$\phi_s = U_s^+ \phi_S + U_s^- \phi_P + \left(\phi_P - \phi_S\right)\left[U_s^+ \alpha_s^+ \frac{\phi_S - \phi_{SS}}{\phi_P - \phi_{SS}} - U_s^- \alpha_s^- \frac{\phi_P - \phi_N}{\phi_S - \phi_N}\right] \tag{7.11o}$$

(d) North face

$\dot{m}_n >= 0$

$$\alpha_n^+ = \begin{cases} 1 & |\phi_N - 2\phi_P + \phi_S| < |\phi_N - \phi_S| \\ 0 & \textit{otherwise} \end{cases} \tag{7.11p}$$

$\dot{m}_n < 1$

$$\alpha_n^- = \begin{cases} 1 & |\phi_P - 2\phi_N + \phi_{NN}| < |\phi_P - \phi_{NN}| \\ 0 & \textit{otherwise} \end{cases} \tag{7.11q}$$

$$\phi_n = U_n^+ \phi_P + U_w^- \phi_N + \Delta\varphi_n$$

$$U_n^+ = 0.5\left(1 + \frac{|\dot{m}_n|}{\dot{m}_n}\right) \quad U_n^- = \left(1 - U_n^+\right) \text{ where } \quad \dot{m}_n \neq 0 \tag{7.11r}$$

$$\Delta\phi_n = \left(\phi_N - \phi_P\right)\left[U_n^+ \alpha_n^+ \frac{\phi_P - \phi_S}{\phi_N - \phi_S} - U_n^- \alpha_n^- \frac{\phi_N - \phi_{NN}}{\phi_P - \phi_{NN}}\right] \tag{7.11s}$$

$$\phi_n = U_n^+ \phi_P + U_n^- \phi_N + \left(\phi_N - \phi_P\right)\left[U_n^+ \alpha_n^+ \frac{\phi_P - \phi_S}{\phi_N - \phi_S} - U_n^- \alpha_n^- \frac{\phi_N - \phi_{NN}}{\phi_P - \phi_{NN}}\right] \tag{7.11t}$$

iv. Convection term discretization using *HLPA*

Expressions in Eqs.(7.9a) and (7.9b) can be written using *HLPA* scheme in Eqs.(7.11e),(7.11j), (7.11o) and (7.11t) in terms of variables at cell centers. ϕ stands for dependent variables (U_x or U_y). Then Eqs. (7.9a) and (7.9b) can be expressed as follows.

Using *HLPA* scheme, substituting relations given in Eqs. (7.11e), (7.11j), (7.11o) and (7.11t), one obtains

$$\dot{m}_e\left[U_e^+ \phi_P + U_e^- \phi_E + \hat{\phi}_e\left(\phi_E - \phi_P\right)\right] - \dot{m}_w\left[U_w^+ \phi_W + U_w^- \phi_P + \hat{\phi}_w\left(\phi_P - \phi_W\right)\right] +$$

$$\dot{m}_n\left[U_n^+ \phi_P + U_n^- \phi_N + \hat{\phi}_n\left(\phi_N - \phi_P\right)\right] - \dot{m}_s\left[U_s^+ \phi_S + U_s^- \phi_P + \hat{\phi}_s\left(\phi_P - \phi_S\right)\right] \tag{7.12a}$$

Or,

$$\phi_P\left(\dot{m}_e U_e^+ - \dot{m}_e \hat{\phi}_e - \dot{m}_w U_w^- - \dot{m}_w \hat{\phi}_w + \dot{m}_n U_n^+ - \dot{m}_n \hat{\phi}_n - \dot{m}_s U_s^- - \dot{m}_s \hat{\phi}_s\right)$$

$$+ \phi_W\left(-\dot{m}_w U_w^+ - \dot{m}_w \hat{\phi}_w\right) + \phi_E\left(\dot{m}_e U_e^- + \dot{m}_e \hat{\phi}_e\right) + \phi_S\left(-\dot{m}_s U_s^+ - \dot{m}_s \hat{\phi}_s\right) + \phi_N\left(\dot{m}_n U_n^- + \dot{m}_n \hat{\phi}_n\right) \tag{7.12b}$$

Or,

$$\phi_P\left(\dot{m}_e(U_e^+ - \hat{\phi}_e) - \dot{m}_w(U_w^- + \hat{\phi}_w) + \dot{m}_n(U_n^+ - \hat{\phi}_n) - \dot{m}_s(U_s^- + \hat{\phi}_s)\right)$$

$$-\phi_W \dot{m}_w\left(U_w^+ - \hat{\phi}_w\right) + \phi_E \dot{m}_e\left(U_e^- + \hat{\phi}_e\right) - \phi_S \dot{m}_s\left(U_s^+ - \hat{\phi}_s\right) + \phi_N \dot{m}_n\left(U_n^- + \hat{\phi}_n\right) \tag{7.12c}$$

Thus convection term can be expressed in terms of variables at cell centers i.e. at *W, E, S,* and *N* using the expression obtained in Eq. (7.12c).

v. Diffusive term

In Eqs. (7.7a) and (7.7b), diffusive terms can be discretized using central difference scheme as follows.

$$\left.\begin{aligned}
(\Gamma hJ\alpha_{11})_e \Delta\eta_e \cdot \left.\frac{\partial U_x}{\partial \xi}\right|_e &= (\Gamma hJ\alpha_{11})_e \Delta\eta_e \cdot \frac{(U_x)_E - (U_x)_P}{\Delta\xi_e} \\
(\Gamma hJ\alpha_{11})_w \Delta\eta_w \cdot \left.\frac{\partial U_x}{\partial \xi}\right|_w &= (\Gamma hJ\alpha_{11})_w \Delta\eta_w \cdot \frac{(U_x)_P - (U_x)_W}{\Delta\xi_w} \\
(\Gamma hJ\alpha_{22})_n \Delta\xi_n \cdot \left.\frac{\partial U_x}{\partial \eta}\right|_n &= (\Gamma hJ\alpha_{22})_n \Delta\xi_n \cdot \frac{(U_x)_N - (U_x)_P}{\Delta\eta_n} \\
(\Gamma hJ\alpha_{22})_s \Delta\xi_s \cdot \left.\frac{\partial U_x}{\partial \eta}\right|_s &= (\Gamma hJ\alpha_{22})_s \Delta\xi_s \cdot \frac{(U_x)_P - (U_x)_S}{\Delta\eta_n}
\end{aligned}\right\} \tag{7.13}$$

Segregating expressions of diffusing terms in Eq. (7.13) for Eq. (7.7a)

$$-(\Gamma hJG_{11})_e \Delta\eta_e \cdot \frac{(u_x)_E - (u_x)_P}{\Delta\xi_e} + (\Gamma hJ\alpha_{11})_w \Delta\eta_w \cdot \frac{(U_x)_P - (U_x)_W}{\Delta\xi_w} - (\Gamma hJ\alpha_{22})_n \Delta\xi_n \cdot \frac{(U_x)_N - (U_x)_P}{\Delta\eta_n}$$

$$+(\Gamma hJ\alpha_{22})_s \Delta\xi_s \cdot \frac{(U_x)_P - (U_x)_S}{\Delta\eta_s} \tag{7.14a}$$

Or,

$$-(\Gamma hJ\alpha_{11})_e \frac{\Delta\eta_e}{\Delta\xi_e} \cdot (U_x)_E + (\Gamma hJ\varepsilon_{11})_e \frac{\Delta\eta_e}{\Delta\xi_e}(U_x)_P + (\Gamma hJ\alpha_{11})_w \frac{\Delta\eta_w}{\Delta\xi_w} \cdot (U_x)_P$$

$$-(\Gamma hJ\alpha_{11})_w \frac{\Delta\eta_w}{\Delta\xi_w} \cdot (U_x)_W - (\Gamma hJ\alpha_{22})_n \frac{\Delta\xi_n}{\Delta\eta_n} \cdot (U_x)_N$$

$$+(\Gamma hJ\alpha_{22})_n \frac{\Delta\xi_n}{\Delta\eta_n} \cdot (U_x)_P + (\Gamma hJ\alpha_{22})_s \frac{\Delta\xi_s}{\Delta\eta_s} \cdot (U_x)_P - (\Gamma hJ\alpha_{22})_s \frac{\Delta\xi_s}{\Delta\eta_s} \cdot (U_x)_S \tag{7.14b}$$

Or,

$$-(\Gamma hJ\alpha_{11})_e \frac{\Delta\eta_e}{\Delta\xi_e}\cdot(U_x)_E - (\Gamma hJ\alpha_{11})_w \frac{\Delta\eta_w}{\Delta\xi_w}\cdot(U_x)_W - (\Gamma hJ\alpha_{22})_n \frac{\Delta\xi_n}{\Delta\eta_n}\cdot(U_x)_N$$

$$-(\Gamma hJ\alpha_{22})_s \frac{\Delta\xi_s}{\Delta\eta_s}\cdot(U_x)_S + \left[(\Gamma hJ\alpha_{11})_e \frac{\Delta\eta_e}{\Delta\xi_e} + (\Gamma hJ\alpha_{11})_w \frac{\Delta\eta_w}{\Delta\xi_w} + (\Gamma hJ\alpha_{22})_n \frac{\Delta\xi_n}{\Delta\eta_n} + (\Gamma hJ\alpha_{22})_s \frac{\Delta\xi_s}{\Delta\eta_s}\right]\cdot(U_x)_P \quad (7.14c)$$

Same operations can be done in Eq. (7.7b) for U_y

$$-(\Gamma hJ\alpha_{11})_e \frac{\Delta\eta_e}{\Delta\xi_e}\cdot(U_y)_E - (\Gamma hJ\alpha_{11})_w \frac{\Delta\eta_w}{\Delta\xi_w}\cdot(U_y)_W - (\Gamma hJ\alpha_{22})_n \frac{\Delta\xi_n}{\Delta\eta_n}\cdot(U_y)_N$$

$$-(\Gamma hJ\alpha_{22})_s \frac{\Delta\xi_s}{\Delta\eta_s}\cdot(U_y)_S + \left[(\Gamma hJ\alpha_{11})_e \frac{\Delta\eta_e}{\Delta\xi_e} + (\Gamma hJ\alpha_{11})_w \frac{\Delta\eta_w}{\Delta\xi_w} + (\Gamma hJ\alpha_{22})_n \frac{\Delta\xi_n}{\Delta\eta_n} + (\Gamma hJ\alpha_{22})_s \frac{\Delta\xi_s}{\Delta\eta_s}\right]\cdot(U_y)_P \quad (7.14d)$$

vi. Final discretized equations for momentum equations

Substituting Eq.(7.12c) in (7.9a) and (7.9b) and collecting discretized expressions for transient term, convection term and diffusive term obtained in Eqs.(7.8a), (7.8b), (7.9a) , (7.9b), (7.14c) and (7.14d), one can obtain the following final expression

$$\frac{(\rho U_i)_P^{k+1} - (\rho U_i)_P^k}{\Delta t}(hJ\Delta\xi\Delta\eta)_P = a_W U_{iW} + a_E U_{iE} + a_N U_{iN} - a_P U_{iP} + S(hJ\Delta\xi\Delta\eta)_P \quad (7.15)$$

where,

$$a_{iW} = \dot{m}_w(1-\hat{u}_{wi}) + (\rho\nu_t hJ\alpha_{11})_w \quad (7.16a)$$

$$a_{iE} = -(\dot{m}_e\hat{u}_{ei}) + (\rho\nu_t hJ\alpha_{11})_e \quad (7.16b)$$

$$a_{iS} = \dot{m}_s(1-\hat{u}_{si}) + (\rho\nu_t hJ\alpha_{22})_s \quad (7.16c)$$

$$a_{iN} = -\dot{m}_n\hat{u}_{ni} + (\rho\nu_t hJ\alpha_{22})_n \quad (7.16d)$$

$$a_{iP} = \dot{m}_e(1-\hat{u}_{ei}) - \dot{m}_w\hat{u}_{wi} + \dot{m}_n(1-\hat{u}_{ni}) - \dot{m}_s\hat{u}_{si} + (\rho\nu_t hJ\alpha_{11})_w$$

$$+(\rho\nu_t hJ\alpha_{11})_e + (\rho\nu_t hJ\alpha_{22})_n + (\rho\nu_t hJ\alpha_{22})_s \qquad (7.16e)$$

Source term can be linearised in Eq (7.15) as follows.

$$S\, hJ\Delta\xi\Delta\eta\big|_P = S_{U_i} + S_{iP}U_{iP} \qquad (7.17)$$

In Eq. (7.17) S_{Ui} and S_P are coefficients. S_P must be non positive (Patankar-1980). Eq.(7.15) can be written as

$$a'_P u_{iP} = \sum_{l=N,S,E,W} a_l u_{il} + S'_{ui} \qquad (7.18)$$

In Eq. (7.18), one has

$$a'_P = a_P + \frac{(\rho hJ\Delta\xi\Delta\eta)_P}{\Delta t} - S_p \qquad (7.19a)$$

$$S'_{Ui} = S_{Ui} + \frac{(\rho hJ\Delta\xi\Delta\eta)^o_P}{\Delta t}U^o_{iP} \qquad (7.19b)$$

where subscript k indicates the immediate value at k^{th} *time* step and $k+1^{st}$ subscript is the value after Δt. Pressure value at cell faces can be computed through linear interpolation as,

$$\left.\begin{aligned} H_w &= f_{wP}H_P + (1-f_{wP})H_W \\ H_e &= f_{eP}H_P + (1-f_{eP})H_E \\ H_n &= f_{nP}H_P + (1-f_{nP})H_N \\ H_s &= f_{sP}H_P + (1-f_{sP})H_W \end{aligned}\right\} \qquad (7.20)$$

In Eq. (7.20), $f_{wP} = \dfrac{\Delta L_{wW}}{\Delta L_{Pw} + \Delta L_{wW}}$, $f_{eP} = \dfrac{\Delta L_{eE}}{\Delta L_{Pe} + \Delta L_{eE}}$, $f_{nP} = \dfrac{\Delta L_{nN}}{\Delta L_{Pn} + \Delta L_{nN}}$ and $f_{sP} = \dfrac{\Delta L_{sS}}{\Delta L_{Ps} + \Delta L_{sS}}$

where ΔL gives segment length between given nodes indicated in its subscript in the control volume.

Final discretized equation in Eq. (7.15) can be written using the relations developed in Eqs. (7.18), (7.19a), (7,19b) and (7.20)

$$U_{iP}^{k+1} = \frac{1}{a'_P}\left(\sum_{l=N,S,E,W} a_l U_{il}^{k+1} + S_{Ui}\right) + D_i^1(H_w - H_e) + D_i^2(H_s - H_n) \tag{7.21a}$$

where in Eq. (7.21a) $D_i^1 = \frac{(\rho g h J \alpha_i^1 \Delta\eta)_P}{a'_P}$ and $D_i^2 = \frac{(\rho g h J \alpha_i^2 \Delta\xi)_P}{a'_P}$ (7.21b)

Denoting first term of R.H.S of Eq. (7.21a) as H_{iP}, i.e.

$$U_{iP}^{k+1} = \underbrace{\frac{1}{a'_P}\left(\sum_{l=N,S,E,W} a_l U_{il}^{k+1} + S_{ui}\right)}_{H_{iP}} + D_i^1(H_w - H_e) + D_i^2(H_s - H_n) \tag{7.21c}$$

Under relaxation is introduced to stabilize the iteration solution for Eqs. (7.21c), one can write the Eq. (7.21c) as

$$U_{iP}^{k+1} = \alpha_u\left[H_{iP} + D_i^1\left(H_w^{k+1} - H_e^{k+1}\right) + D_i^2\left(H_s^{k+1} - H_n^{k+1}\right)\right] + (1-\alpha_u)U_{ip}^o \tag{7.22a}$$

where o stands for an old value of variable at $k+1^{th}$ time step and α_u is under relaxation factor (usually taken as 0.8).

One can conveniently write the relation obtained in Eq. (7.22a) for intermediate guessed velocities designated with '*' superscript as

$$U_{iP}^* = \alpha_u\left[H_{iP}^* + D_i^1\left(H_w^* - H_e^*\right) + D_i^2\left(H_s^* - H_n^*\right)\right] + (1-\alpha_u)U_{ip}^o \tag{7.22b}$$

$U_{i,l}^*$, α_u, $U_{i,P}^o$, S_{Ui}^* are guessed velocities, under-relaxation factor (taken as=0.8), old values of velocities and source term respectively. H^*_w, H^*_e, H^*_s and H^*_n are guessed water surface level at cell faces of the control volume centered at P.

Subtracting Eq. (7.22b) from Eq. (7.22a), and neglecting $H_{iP}^{k+1} - H_{iP}^{*}$, one has

$$U_{iP}^{k+1} = U_{iP}^{*} + \alpha_u \left[D_i^1 \left(H'_w - H'_e \right) + D_i^2 \left(H'_s - H'_n \right) \right] \tag{7.23}$$

where in Eq. (7.23), H' with *w, e, n, s* subscripts denote pressure corrections at cell faces. Pressure correction has the following relation,

$$H^{k+1} = H^{*} + H' \tag{7.24}$$

vii. Implementation of momentum interpolation technique proposed by Rhie and Chow (1983).

The scheme uses the non-staggered grid as stated earlier. Velocity and pressure coupling is poor in this case as all dependent variables are stored at the cell centers. It leads to spurious solution. To improve pressure velocity coupling, Rhie and Chow (1983) interpolation technique is implemented. It computes U_i at cell faces as follows.

$$U_{i,w}^{*} = \alpha_u \left[(1 - f_{x,P}) G_{i,PW}^{1*} + f_{x,P} G_{i,P}^{1*} \right] + \alpha_u \left[(1 - f_{x,P}) / a_{PW}^{U} + f_{x,P} / a_P^{U} \right]$$

$$\times \left(\rho g h J \alpha_i^1 \Delta \eta \right)_w \left(H_W^{*} - H_P^{*} \right) + (1 - \alpha_u) \left[(1 - f_{x,P}) U_{i,W}^{o} + f_{x,P} U_{i,P}^{o} \right] \tag{7.25}$$

$$U_{i,e}^{*} = \alpha_u \left[(1 - f_{x,P}) G_{i,PE}^{1*} + f_{x,P} G_{i,P}^{1*} \right] + \alpha_u \left[(1 - f_{x,P}) / a_{PE}^{U} + f_{x,P} / a_P^{U} \right]$$

$$\times \left(\rho g h J \alpha_i^1 \Delta \eta \right)_e \left(H_E^{*} - H_P^{*} \right) + (1 - \alpha_u) \left[(1 - f_{x,P}) U_{i,E}^{o} + f_{x,P} U_{i,p}^{o} \right] \tag{7.26}$$

In Eq. (7.25) and Eq. (7.26), $G_{i,P}^{1*} = H_{i,P}^{*} + D_i^2 \left(H_s^{*} - H_n^{*} \right)$. Where $G_{i,PW}^{1,*}$ and $a_{i,PW}^{U}$ are the values of $G_{i,P}^{1,*}$ and a_P^U for the neighbouring control volume centered at point *W*. $G_{i,PE}^{1,*}$ and $a_{i,PE}^{U}$ are the values of $G_{i,P}^{1,*}$ and a_P^U for the neighbouring control volume centered at point *E*.

Similarly the values of U_i at cell faces *s, n* are calculated as,

$$U^*_{i,s} = \alpha_u\left[(1-f_{y,P})G^{2*}_{i,PS} + f_{y,P}G^{2*}_{i,P}\right] + \alpha_u\left[(1-f_{y,P})/a^U_{PS} + f_{y,P}/a^U_P\right]$$

$$\times\left(\rho g h J \alpha_i^2 \Delta\xi\right)_s\left(H^*_S - H^*_P\right) + (1-\alpha_u)\left[(1-f_{y,P})U^o_{i,S} + f_{x,P}U^o_{i,P}\right] \quad (7.27)$$

$$U^*_{i,n} = \alpha_u\left[(1-f_{y,P})G^{2*}_{i,PN} + f_{y,P}G^{2*}_{i,P}\right] + \alpha_u\left[(1-f_{y,P})/a^U_{PN} + f_{y,P}/a^U_P\right]$$

$$\times\left(\rho g h J \alpha_i^2 \Delta\xi\right)_n\left(H^*_N - H^*_P\right) + (1-\alpha_u)\left[(1-f_{y,P})U^o_{i,N} + f_{x,P}U^o_{i,P}\right] \quad (7.28)$$

In Eqs. (7.27) and (7.28), $G^{2*}_{i,P} = H^*_{i,P} + D^1_i\left(H^*_w - H^*_e\right)$. Where $G^{1,*}_{i,PS}$ and $a^U_{i,PS}$ are the values of $G^{2,*}_{i,P}$ and a^U_P for the neighboring control volume centered at point *S*. $G^{1,*}_{i,PN}$ and $a^U_{i,PN}$ are the values of $G^{2,*}_{i,P}$ and a^U_P for the neighbouring control volume centered at point *N*.

Substracting expressions in Eqs. (7.25), (7.26) and (7.27), (7.28) from same relation [Eqs(7.25-28)] at $k+1^{th}$ time-step, for the interpolated $U^{k+1}_{i,w}$, $U^{k+1}_{i,e}$ and $U^{k+1}_{i,s}$, $U^{k+1}_{i,n}$, one can get following correlations.

$$\left.\begin{aligned} U^{k+1}_{i,w} &= U^*_{i,w} + \alpha_u Q^1_{i,w}\left(H'_W - H'_P\right) \\ U^{k+1}_{i,e} &= U^*_{i,e} + \alpha_u Q^1_{i,e}\left(H'_P - H'_E\right) \\ U^{k+1}_{i,s} &= U^*_{i,s} + \alpha_u Q^2_{i,s}\left(H'_S - H'_P\right) \\ U^{k+1}_{i,n} &= U^*_{i,n} + \alpha_u Q^2_{i,n}\left(H'_P - H'_N\right) \end{aligned}\right\} \quad (7.29)$$

where in Eq. (7.29),

$$\left.\begin{aligned} Q^1_{i,w} &= \left[(1-f_{x,P})/a^U_{PW} + f_{x,P}/a^U_P\right]\left(\rho g h \alpha^1_i \Delta\eta\right)_w \\ Q^1_{i,e} &= \left[(1-f_{x,P})/a^U_{PE} + f_{x,P}/a^U_P\right]\left(\rho g h \alpha^1_i \Delta\eta\right)_e \\ Q^2_{i,s} &= \left[(1-f_{y,P})/a^U_{PS} + f_{y,P}/a^U_P\right]\left(\rho g h \alpha^2_i \Delta\xi\right)_s \\ Q^2_{i,n} &= \left[(1-f_{y,P})/a^U_{PN} + f_{y,P}/a^U_P\right]\left(\rho g h \alpha^2_i \Delta\xi\right)_n \end{aligned}\right\} \quad (7.30)$$

Convection Fluxes (F_w, F_e, F_s *and* F_n) at cell faces w, e, s, and n can be approximated by mid point integral rule as

$$\left.\begin{aligned} F_w &= \rho_w^{k+1}\left(hJ\Delta\eta\right)_w \hat{u}_{\xi,w}^{k+1} \\ F_e &= \rho_e^{k+1}\left(hJ\Delta\eta\right)_e \hat{u}_{\xi,e}^{k+1} \\ F_s &= \rho_s^{k+1}\left(hJ\Delta\xi\right)_s \hat{u}_{\eta,s}^{k+1} \\ F_n &= \rho_n^{k+1}\left(hJ\Delta\xi\right)_n \hat{u}_{\eta,n}^{k+1} \end{aligned}\right\} \qquad (7.31)$$

Equations (7.29) can be written in terms of fluxes at the faces using correlations given in Eqs. (7.4) and (7.31)

$$\left.\begin{aligned} F_w &= F_w^* + a_W^p\left(H'_W - H'_P\right) \\ F_e &= F_e^* + a_E^p\left(H'_P - H'_E\right) \\ F_e &= F_e^* + a_E^p\left(H'_E - H'_P\right) \\ F_n &= F_n^* + a_N^p\left(H'_P - H'_N\right) \end{aligned}\right\} \qquad (7.32a)$$

where in Eqs.(7.32a), one obtains

$$a_W^p = \alpha_u \rho_w^{k+1}\left(hJ\alpha_i^1\Delta\eta\right)_w Q_{i,w}^1 \quad \text{and} \quad a_E^p = \alpha_u \rho_e^{k+1}\left(hJ\alpha_i^1\Delta\eta\right)_e Q_{i,e}^1 \text{ ;}$$

$$a_S^p = \alpha_u \rho_s^{k+1}\left(hJ\alpha_i^1\Delta\xi\right)_s Q_{i,s}^2 \quad \text{and} \quad a_N^p = \alpha_u \rho_n^{k+1}\left(hJ\alpha_i^1\Delta\xi\right)_n Q_{i,n}^2 \text{ ;} \qquad (7.32b)$$

Using relations given in Eq. (7.6), one obtains

$$a_W^p = \alpha_u(\rho h)_w^{k+1}(J\Delta\eta)_w\left(\alpha_{1,w}^1 Q_{1,w}^1 + \alpha_{2,w}^1 Q_{2,w}^1\right) \text{ and } a_E^p = \alpha_u(\rho h)_e^{k+1}(J\Delta\eta)_w\left(\alpha_{1,e}^1 Q_{1,e}^1 + \alpha_{2,e}^1 Q_{2,e}^1\right); \qquad (7.33)$$

$$a_S^p = \alpha_u(\rho h)_s^{k+1}(J\Delta\eta)_s\left(\alpha_{1,s}^2 Q_{1,s}^2 + \alpha_{2,s}^2 Q_{2,s}^2\right) \text{ and } a_N^p = \alpha_u(\rho h)_n^{k+1}(J\Delta\eta)_n\left(\alpha_{1,n}^2 Q_{1,n}^2 + \alpha_{2,n}^2 Q_{2,n}^2\right);$$

Guessed fluxes (F^*) are determined in terms of guessed velocities U^* for using it in Eqs. (7.32a).

viii. Discretization of continuity equation.

Equation (7.2) can be written

$$\frac{\partial}{\partial \tau}(\rho hJ)+\frac{\partial}{\partial \xi}(\rho hJ.\hat{u}_{\xi})+\frac{\partial}{\partial \eta}(\rho hJ.\hat{u}_{\eta})=0 \tag{7.34a}$$

Integrating first order backward difference for Eq.(7.34a)

$$\frac{(\rho h)_P^{k+1}-(\rho h)_P^k}{\Delta t}.(J\Delta\xi\Delta\eta)_P+(\rho hJ\hat{u}_{\xi})_e\Delta\eta_e-(\rho hJ\hat{u}_{\xi})_w\Delta\eta_w+(\rho hJ\hat{u}_{\eta})_n\Delta\xi_n-(\rho hJ\hat{u}_{\eta})_s\Delta\xi_s=0 \tag{7.34b}$$

Substituting correlation given in Eq.(7.31), one has

$$\frac{(\rho h)_P^{k+1}-(\rho h)_P^k}{\Delta t}.\Delta A_P+F_e-F_w+F_n-F_s=0 \tag{7.35a}$$

For incompressible flow and rigid bed condition, above equation can be approximated using relation given in Eq. (7.24)

$$\frac{H'_P+H^*_P-H^k_P}{\Delta t}.\rho_P\Delta A_P+F_e-F_w+F_n-F_s=0 \tag{7.35b}$$

In Eq. (7.34), substituting the values of fluxes from Eqs. (7.32a) and writing it in the following form

$$a^p_P H'_P=a^p_W H'_W+a^p_E H'_E+a^p_S H'_S+a^p_N H'_N+S_P \tag{7.35c}$$

Whereas in Eq. (7.35c)

$$a^p_P=a^p_W+a^p_E+a^p_S+a^p_N+\frac{\rho_P\Delta A_P}{\Delta t} \tag{7.35d}$$

$$S_P = -F_e^* + F_W^* - F_n^* + F_s^* - \frac{(H_P^* - H_P^k)\rho_P \Delta A_P}{\Delta t} \tag{7.35e}$$

Equation (7.35c) can be solved through well known iterative *ADI* scheme explained in Chapter 6.

ix. Implementation of *SIMPLEC* algorithm

SIMPLEC Algorithm mentioned in Wu (2007) and Majumdar *et al.* (1992), adopted in this numerical code in view of the modification in descritized equations, suggested by Van Doormal and Raithby (1984).

Equation (7.23) is modified as,

$$U_{i,P}^{k+1} = U_{i,P}^{*} + \alpha_u \left[\tilde{D}_i^1 (H'_w - H'_e) + \tilde{D}_i^2 (H'_s - H'_n)\right] \tag{7.36a}$$

where $$\tilde{D}_i^m = D_i^m \Big/ \left(1 - \alpha_u \sum_{l=E,W,N,S} a_l^U / a_P^U\right) \tag{7.36b}$$

Using the momentum interpolation technique, the velocity corrections at cell faces in Eqs. (7.29) can be modified as follows

$$\left.\begin{aligned} U_{i,w}^{k+1} &= U_{i,w}^{*} + \alpha_u \tilde{Q}_{i,w}^1 (H'_W - H'_P) \\ U_{i,e}^{k+1} &= U_{i,e}^{*} + \alpha_u \tilde{Q}_{i,e}^1 (H'_P - H'_E) \\ U_{i,s}^{k+1} &= U_{i,s}^{*} + \alpha_u \tilde{Q}_{i,s}^2 (H'_S - H'_P) \\ U_{i,n}^{k+1} &= U_{i,n}^{*} + \alpha_u \tilde{Q}_{i,n}^2 (H'_P - H'_N) \end{aligned}\right\} \tag{7.37}$$

In Eq. (7.37),

$$\left.\begin{aligned} \tilde{Q}_{i,w}^m &= Q_{i,w}^m \Big/ \left(1 - \alpha_u (1 - f_{x,P}) \left(\sum_{l=E,W,N,S} a_l^U / a_P^U\right)_W - \alpha_u f_{x,P} \left(\sum_{l=E,W,N,S} a_l^U / a_P^U\right)_P\right) \\ \tilde{Q}_{i,e}^m &= Q_{i,e}^m \Big/ \left(1 - \alpha_u f_{x,P} \left(\sum_{l=E,W,N,S} a_l^U / a_P^U\right)_P - \alpha_u (1 - f_{x,P}) \left(\sum_{l=E,W,N,S} a_l^U / a_P^U\right)_E\right) \\ \tilde{Q}_{i,s}^m &= Q_{i,s}^m \Big/ \left(1 - \alpha_u (1 - f_{y,P}) \left(\sum_{l=E,W,N,S} a_l^U / a_P^U\right)_S - \alpha_u f_{y,P} \left(\sum_{l=E,W,N,S} a_l^U / a_P^U\right)_P\right) \end{aligned}\right\} \tag{7.38}$$

$$\tilde{Q}^m_{i,n} = Q^m_{i,n} \Big/ \left(1-\alpha_u f_{y,P}\Big(\sum_{l=E,W,N,S} a^U_l / a^U_P\Big)_P - \alpha_u (1-f_{y,P})\Big(\sum_{l=E,W,N,S} a^U_l / a^U_P\Big)_N\right)$$

For depth averaged 2-D *SIMPLEC* algorithm implementation, coefficients a^p_W, a^p_E, a^p_S and a^p_N are determined by Eqs. (7.33) only by replacing $Q^1_{i,w}$, $Q^2_{i,s}$, $Q^1_{i,e}$ and $Q^2_{i,n}$ with modified coefficients such as $\tilde{Q}^1_{i,w}$, $\tilde{Q}^2_{i,s}$, $\tilde{Q}^1_{i,e}$ and $\tilde{Q}^2_{i,n}$ respectively.

x. Cross derivative source term computation

Cross derivative terms are kept as pure source term to avoid instable solution as it is sensitive to grid resolution. Linearising both momentum source terms,

$$\left.\begin{aligned} S_x hJ\Delta\xi\Delta\eta &= S_{Ux} + S_{px}U_{xP} \\ S_y hJ\Delta\xi\Delta\eta &= S_{Uy} + S_{py}U_{xP} \end{aligned}\right\} \quad (7.39)$$

First term of the source term is cross derivative term of the momentum equations to be dealt specially, integrating over the Control Volume. One can get, (7.40a)

$$S_{Ux} = \Gamma hJ\alpha_{12}\iint_{\Delta A}\frac{\partial^2 U_x}{\partial\xi\partial\eta}$$

$$S_{Uy} = \Gamma hJ\alpha_{12}\iint_{\Delta A}\frac{\partial^2 U_y}{\partial\xi\partial\eta} \quad (7.40b)$$

One can represent the Eqs. (7.40a) and (7.40b) as below

$$S_{Ui} = \Gamma hJ\alpha_{12}\iint_{\Delta A}\frac{\partial^2 U_i}{\partial\xi\partial\eta} \quad (7.41)$$

where in Eq. (7.41), i=x or y;

Integrating over the control volume, Eq. (7.41) becomes

$$S_{Ui} = \left((\Gamma hJ\alpha_{12})_e \Delta\eta_e \left.\frac{\partial U_i}{\partial\eta}\right|_e - (\Gamma hJ\alpha_{12})_w \Delta\eta_w \left.\frac{\partial U_i}{\partial\eta}\right|_w\right) \quad (7.42a)$$

Or,

$$S_{Ui} = \left((\Gamma hJ\alpha_{12})_e \Delta\eta_e \frac{(U_i)_{ne} - (U_i)_{se}}{\Delta\eta}\bigg|_e - (\Gamma hJ\alpha_{12})_w \Delta\eta_w \frac{(U_i)_{nw} - (U_i)_{sw}}{\Delta\eta}\bigg|_w \right) \quad (7.42b)$$

Or,

$$S_{Ui} = \left((\Gamma hJ\alpha_{12})\right|_e \left((U_i)_{ne} - (U_i)_{se}\right) - (\Gamma hJ\alpha_{12})_w \left((U_i)_{nw} - (U_i)_{sw}\right)) \quad (7.42c)$$

Equation (7.42c) is used to evaluate cross derivative source terms in terms of velocities at the neighbourhood.

xi. Broad outline steps for *SIMPLEC* algorithm

a) Guess the pressure field H^*;

b) Solve the momentum equations to obtain U_x^* and U_y^* using (7.22b)

c) Calculate H' using *ADI* [Eq. (7.35c)]

d) Calculate H using Eq. (7.24)

e) Calculate U_x^{k+1} and U_y^{k+1} using Eq. (7.36b)

f) Treat the corrected pressure H as new guessed pressure H^*, and repeat the procedure from step b) to f) until converge solution is obtained, and

g) Conduct the calculation of next time step if unsteady flow is to be simulated.

7.2.4 BOUNDARY IMPLIMENTATION

i. Side boundary

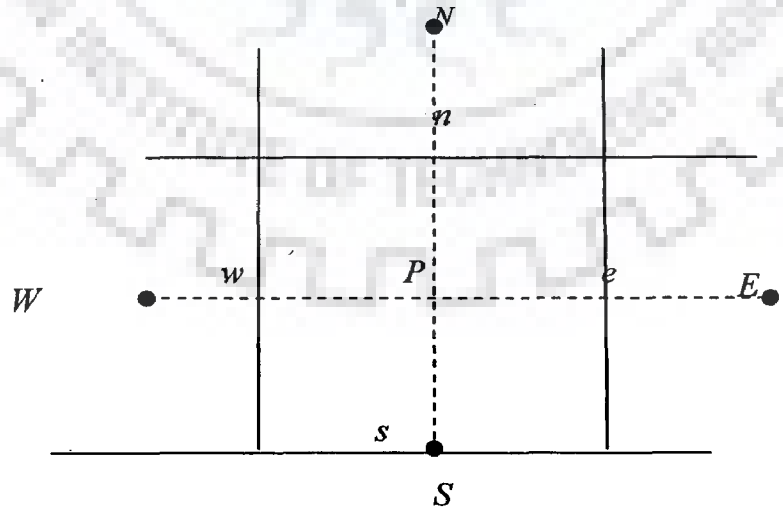

Figure 7.2 Control volume at side boundary

For side boundary implementation, wall function approach given by Wu (2007) is adopted. For south boundary, velocity at wall (point'*s*') is assumed non-slip and assigned zero value. The convection flux is zero when *x*-momentum is integrated over the CV and shear stress is determined as (Figure 7.2),

$$\tau_{xy} = -\lambda_{xy}\,\overrightarrow{Up}\ , \tag{7.43a}$$

where in Eq. (7.43a), *Up* is flow velocity at *P*. λ_{xy} is determined using the relations given in Eqs. (7.43b).

$$\lambda_{xy} = \frac{\rho u_* \kappa}{\ln\left(E y_P^+\right)}$$

$$\text{where}\quad y_P^+ = \frac{u_* y_P}{\nu} \tag{7.43b}$$

where y_P is the distance from the wall to the point *P*, shear velocity is the shear velocity on the wall defined as $u_* = \sqrt{\frac{\tau_{xy}}{\rho}}$. *E* is the roughness parameter given as

$$E = e^{[\kappa(B_0 - \Delta B)]}$$

$$\Delta B = \begin{cases} 0 & k_s^+ < 2.25 \\ \left(B_0 - 8.5 + \frac{1}{\kappa}\ln k_s^+\right)\sin\left[0.4258\left(\ln k_s^+ - 0.811\right)\right] & 2.25 < k_s^+ < 90 \end{cases} \tag{7.43c}$$

$$B_0 - 8.5 + \frac{1}{\kappa}\ln k_s^+ \qquad k_s^+ > 90 \tag{7.43d}$$

In Eq. (7.43d), B_0=additive constant of 5.2 and Roughness Reynolds number $k_s^+ = \frac{u_* k_s}{\nu}$ (Cebeci and Bradshaw, 1977) in zero equation model. This shear stress is moved to source term thus yielding zero coefficients a_S^{Ux} in Eq. (7.22b). Second momentum equation is integrated over CV, the convection flux and normal stress τ_{yy} at face *s* should be zero. Thus a_s^{Uy} will be zero as well in Eq. (7.22b). Flux F_s is zero. So pressure correction at face *s* is not needed. a_S^p in Eq.(7.33) becomes zero. The pressure (water

level) at boundary point S can be extrapolated from values at adjacent internal points. No slip condition (U_x=0, U_y=0) is the appropriate condition at solid walls. Since the wall velocity is known, it is also unnecessary to perform a pressure correction here.

Same analogous boundary condition implemented in north side boundary.

ii. Inlet boundary

- The depth averaged stream-wise velocity at each computational point of the inlet located in a nearly straight reach may be assumed to be proportional to the local flow depth, *i.e.* $U\alpha\ h^r$, where $r\sim 2/3$ for uniform flow (Wu, 2007), given as

$$U=\frac{Qh^r}{\int_0^B h^{1+r}dy'} \tag{7.44a}$$

where, Q=total inflow discharge, B= width of channel at discharge Q and y' = transverse co-ordinate. For assumed uniform flow

$$U_{i,j}=\frac{Q_i h_{i,j}^{\frac{2}{3}}}{\int_0^B h^{\frac{5}{3}}dy'} \tag{7.44b}$$

where denominator in Eq. (7.44b) can be evaluated through trapezoidal rule to evaluate integration along the inflow boundary.

- For a specified discharge Q, formulation will not give directly unique value of inflow flux at each cell if flow depth is unknown. Iteration is needed (Wu, 2007).
- Water level is assumed at face w, and inflow velocity and flux is obtained uniquely using the formula from Eq. (7.44b) (Figure 7.3).
- Flux Correction at face w is zero.

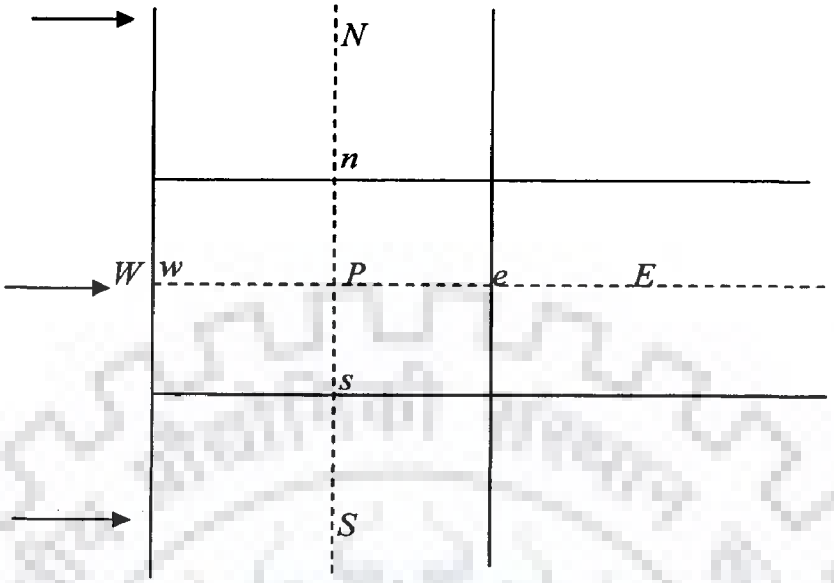

Figure 7.3 Control volume at inlet boundary

- Pressure correction equation becomes.

$$a_P^p H'_P = a_E^p H'_E + a_S^p H'_S + a_N^p H'_N + S_P \tag{7.44c}$$

where, $a_P^p = a_E^p + a_S^p + a_N^p + \frac{\rho_P \Delta A_P}{\Delta t}$ and, (7.44d)

$$S_P = -F_e^* + F_W^* - F_n^* + F_s^* - \frac{(H_P^* - H_P^k)\rho_P \Delta A_P}{\Delta t} \tag{7.44e}$$

- Flow calculation is then carried out over internal points.
- After internal pressure field is obtained, the pressure (water level) at the *w*-face of each inlet can be extrapolated from pressure value at adjacent internal points and new inflow flux can be obtained from usual formula.
- The above procedure is repeated till convergent solution is obtained.
- Source term computations for inlet boundary is done as follows

$$s_{Ux} = (\Gamma h J \alpha_{12})_e [(U_x)_{Ne} - (U_x)_{Pe}] - (\Gamma h J \alpha_{12})_w [(U_x)_{Nw} - (U_x)_{Pw}] \quad (7.44f)$$

$$s_{Uy} = (\Gamma h J \alpha_{12})_e [(U_y)_{Ne} - (U_y)_{Pe}] - (\Gamma h J \alpha_{12})_w [(U_y)_{Nw} - (U_y)_{Pw}] \quad (7.44g)$$

iii. Outlet boundary

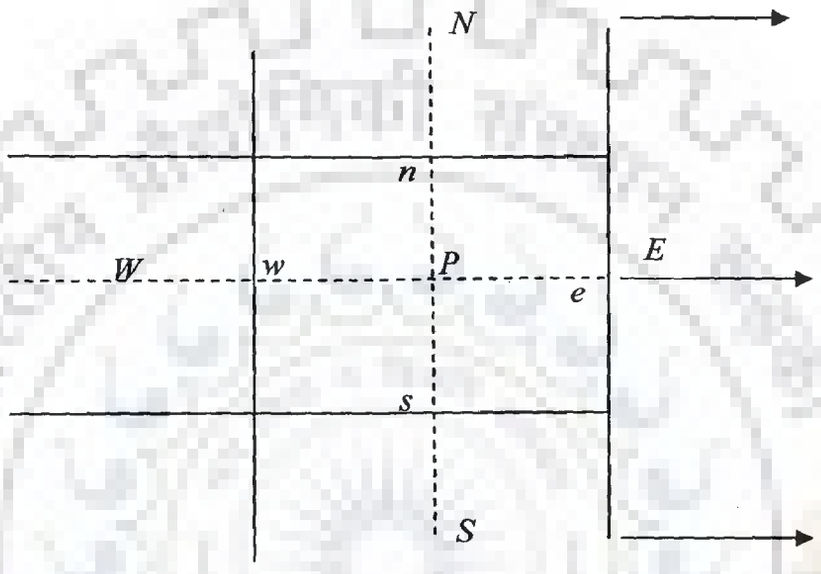

Figure 7.4 Control volume at outlet boundary

- At outlet boundary, pressure (Water Level) is specified for sub-critical flow.
- It is specified at the center of the control volume, *i.e.* at P
- Pressure correction at point P is as earlier stated.

$$a_P^p H'_P = a_W^p H'_W + a_E^p H'_E + a_S^p H'_S + a_N^p H'_N + S_P \quad (7.45)$$

- In this case, pressure correction at point P is zero.
- Flow velocity at the outlet can be extrapolated from the values at adjacent internal points.
- The diffusion flux at the outlet (face e) is zero due to zero gradients (Versteeg and Malalsekera, 1995). Because, the convection terms are usually discretized using an upwind scheme, the coefficient a_E^{ϕ} (where ϕ is U_x or U_y) may actually be zero.

7.2.5 COMPUTATION OF PHYSICAL DOMAIN VARIABLES FOR THE CONTROL VOLUME

In the Figure 7.1, area of Control Volume (ΔA_P) can be given using only the parameter in the Cartesian coordinate system without involving the increment $\Delta\xi$ and $\Delta\eta$ (Peric, 1985; Zhu, 1992a).

$$\Delta A_P = \frac{1}{2}\left|(x_{ne}-x_{sw})(y_{nw}-y_{se})-(x_{nw}-x_{se})(y_{ne}-y_{sw})\right| \tag{7.46}$$

where in Eq. (7.46), Cartesian independent variables (x and y) with subscripts indicate the values at cell vertices located at *North-East* (*ne*), *South-West* (*sw*), *North-West* (*nw*), *South-East* (*se*) and *North-West* (*nw*). For neighborhood nodes *W, E, S, N* and *w, e, s, n* area of control volumes (ΔA_W, ΔA_E, ΔA_S, ΔA_N, ΔA_w, ΔA_e, $_\Delta A_s$ and ΔA_n) are computed using the formula (Eq.7.46) by symmetry, substituting the corresponding x, y values, fluxes can be computed as follows

$$\left.\begin{aligned}
\dot{m}_w &= \rho_w (J\Delta\eta)_w \hat{u}^{k+1}_{\xi,w} = \rho_w \left(b^1_1 u_x + b^1_2 u_y\right)^{k+1}_w \\
\dot{m}_e &= \rho_e (J\Delta\eta)_e \hat{u}^{k+1}_{\xi,e} = \rho_e \left(b^1_1 u_x + b^1_2 u_y\right)^{k+1}_e \\
\dot{m}_s &= \rho_s (J\Delta\xi)_s \hat{u}^{k+1}_{\eta,w} = \rho_s \left(b^2_1 u_x + b^2_2 u_y\right)^{k+1}_s \\
\dot{m}_w &= \rho_n (J\Delta\xi)_n \hat{u}^{k+1}_{\eta,w} = \rho_n \left(b^2_1 u_x + b^2_2 u_y\right)^{k+1}_n
\end{aligned}\right\} \tag{7.47}$$

where in Eqs. (7.47),

$$\left.\begin{aligned}
b^1_1 &= J\alpha^1_1\Delta\eta \approx \left(\frac{\partial y}{\partial \eta}\right)\Delta\eta \qquad b^1_2 = J\alpha^1_2\Delta\eta \approx -\left(\frac{\partial x}{\partial \eta}\right)\Delta\eta \\
b^2_1 &= J\alpha^2_1\Delta\xi \approx -\left(\frac{\partial y}{\partial \xi}\right)\Delta\xi \qquad b^2_2 = J\alpha^2_2\Delta\eta \approx \left(\frac{\partial x}{\partial \eta}\right)\Delta\eta
\end{aligned}\right\} \tag{7.48}$$

The difference equations can be written for cell faces w and s for the Control Volume (Figure 7.1).

$$\left.\begin{array}{lll} b^1_{1P} = y_n - y_s & b^1_{1w} = y_{nw} - y_{sw} & b^1_{1s} = y_P - y_S \\ b^1_{2P} = x_s - x_n & b^1_{2w} = x_{sw} - x_{nw} & b^1_{2s} = x_S - x_P \\ b^2_{1P} = y_w - y_e & b^2_{1w} = y_W - y_P & b^2_{1s} = y_{sw} - y_{se} \\ b^2_{2P} = x_e - x_w & b^2_{2w} = x_P - x_W & b^2_{2s} = x_{se} - x_{sw} \end{array}\right\} \quad (7.49)$$

For cell face n and e, difference equations can be written using formulae given in Eq. (7.49) by symmetry, substituting the corresponding x, y values.

Diffusion parameters can be written at cell faces w and s as

$$\left(\Gamma h J \alpha^1_j \alpha^1_j \Delta\eta\right)_w / \Delta\xi_w = \Gamma_w \frac{\left(b^1_1 b^1_1 + b^1_2 b^1_2\right)_w}{\Delta A_w} \quad (7.50a)$$

$$\left(\Gamma h J \alpha^1_j \alpha^1_j \Delta\xi\right)_s / \Delta\eta_s = \Gamma_s \frac{\left(b^2_1 b^2_1 + b^2_2 b^2_2\right)_s}{\Delta A_s} \quad (7.50b)$$

For cell face n and e, diffusion parameters can be written using formulae given in Eqs.(7.50a) and (7.50b) by symmetry, substituting corresponding b^i_m (i=1 or 2 and m=1 or 2) and ΔA_l (l is n or e).

7.2.6 SOURCE TERM COMPUTATION FOR DISPERSION TERMS OVER THE CONTROL VOLUME

For first momentum equation (Eq. 5.41) and second momentum (Eq. 5.42) explained in Chapter 5, dispersion terms are

$$\frac{\partial D_{xx}}{\partial x}+\frac{\partial D_{xy}}{\partial y}=\xi_x\frac{\partial D_{xx}}{\partial \xi}+\eta_x\frac{\partial D_{xx}}{\partial \eta}+\xi_y\frac{\partial D_{xy}}{\partial \xi}+\eta_y\frac{\partial D_{xy}}{\partial \eta} \tag{7.51a}$$

$$\frac{\partial D_{xy}}{\partial x}+\frac{\partial D_{yy}}{\partial y}=\xi_x\frac{\partial D_{xy}}{\partial \xi}+\eta_x\frac{\partial D_{xy}}{\partial \eta}+\xi_y\frac{\partial D_{yy}}{\partial \xi}+\eta_y\frac{\partial D_{yy}}{\partial \eta} \tag{7.51b}$$

Integrating Eqs. (7.51a) and (7.51b) over the CV shown in Figure 7.1 One has

$$s_{dx}J\Delta\xi\Delta\eta=S_{dx}=\iint_{\Delta A}\alpha_1^1\frac{\partial D_{xx}}{\partial \xi}+\alpha_1^2\frac{\partial D_{xx}}{\partial \eta}+\alpha_2^1\frac{\partial D_{xy}}{\partial \xi}+\alpha_2^2\frac{\partial D_{xy}}{\partial \eta} \tag{7.52b}$$

$$s_{dx}J\Delta\xi\Delta\eta=S_{dy}=\iint_{\Delta A}\alpha_1^1\frac{\partial D_{xy}}{\partial \xi}+\alpha_1^2\frac{\partial D_{xy}}{\partial \eta}+\alpha_2^1\frac{\partial D_{yy}}{\partial \xi}+\alpha_2^2\frac{\partial D_{yy}}{\partial \eta} \tag{7.52b}$$

From Eqs. (7.52a) and (7.52b), one has

$$S_{dx}=\left(J\alpha_1^1.D_{xx}+J\alpha_2^1.D_{xy}\right)_e\Delta\eta_e-\left(J\alpha_1^1.D_{xx}+.J\alpha_2^1.D_{xy}\right)_w\Delta\eta_w$$

$$+\left(J\alpha_1^2.D_{xx}+J\alpha_2^2.D_{xy}\right)_n\Delta\xi_n-\left(J\alpha_1^2.D_{xx}+J\alpha_2^2.D_{xy}\right)_s\Delta\xi_s \tag{7.53a}$$

and

$$S_{dy}=\left(J\alpha_1^1.D_{xy}+J\alpha_2^1.D_{yy}\right)_e\Delta\eta_e-\left(J\alpha_1^1.D_{xy}+J\alpha_2^1.D_{yy}\right)_w\Delta\eta_w$$

$$+\left(J\alpha_1^2.D_{xy}+J\alpha_2^2.D_{yy}\right)_n\Delta\xi_n-\left(J\alpha_1^2.D_{xy}+J\alpha_2^2.D_{yy}\right)_s\Delta\xi_s \tag{7.53b}$$

Using relations in Eqs.(7.48), for Eqs.(7.53a) and (7.53b), one obtains

$$S_{dx}=\left(b_{1e}^1.D_{xx}+b_{2e}^1.D_{xy}\right)_e-\left(b_1^1.D_{xx}+b_2^1.D_{xy}\right)_w+\left(b_1^2.D_{xx}+b_2^2.D_{xy}\right)_n-\left(b_{1s}^2.D_{xx}+b_{2s}^2.D_{xy}\right)_s \tag{7.54a}$$

and

$$S_{dy}=\left(b_{1e}^1.D_{xy}+b_{2e}^1.D_{yy}\right)_e-\left(b_{1w}^1.D_{xy}+\alpha_{2w}^1.D_{yy}\right)_w+\left(b_{1n}^2.D_{xy}+b_{2n}^2.D_{yy}\right)_n-\left(b_{1s}^2.D_{xy}+b_{2s}^2.D_{yy}\right)_s \tag{7.54b}$$

i. Computation of Cartesian dispersion tensor from curvilinear dispersion tensor

Modified empirical expressions were obtained in Chapter 4 for curvilinear dispersion tensor. The curvilinear dispersion components are transformed to Cartesian dispersion terms for using them in Eqs. (7.54a) and (7.54b). Following correlations were used to obtain Cartesian components from curvilinear components of dispersion terms (Duan, 2004)

$$\left.\begin{aligned} D_{xx} &= D^c_{xx}\cos^2\theta_s + 2D^c_{xy}\cos\theta_s\cos\theta_n + D^c_{yy}\cos^2\theta_n \\ D_{yy} &= D^c_{xx}\sin^2\theta_s + 2D^c_{xy}\sin\theta_s\sin\theta_n + D^c_{yy}\sin^2\theta_n \\ D_{xy} &= D^c_{xx}\cos\theta_s\sin\theta_s + 2(D^c_{xy}\sin\theta_s\cos\theta_n + D^c_{xy}\cos\theta_s\sin\theta_n) + D^c_{yy}\sin\theta_n\cos\theta_n \end{aligned}\right\} \quad (7.55)$$

where θ_s and θ_n are angles between stream-wise, transverse directions pointing outward and positive x-axis respectively (Derivation of the formulae for computing θ_s and θ_n is detailed in Appendix-II).

ii. Computation of streamline radius of curvature

Radius of curvature is required to determine the curvilinear dispersion stress tensor explained in Chapter 4. Following correlations used to compute streamline radius of curvature (Jang and Shimizu, 2005; 2007).

$$\frac{1}{r_s} = \frac{1}{U^3}\left[\begin{aligned} &U_x^2\left(\xi_x\frac{\partial U_y}{\partial\xi} + \eta_x\frac{\partial U_y}{\partial\eta}\right) + U_xU_y\left(\xi_x\frac{\partial U_y}{\partial\xi} + \eta_y\frac{\partial U_y}{\partial\eta}\right) \\ &-U_xU_y\left(\xi_x\frac{\partial U_x}{\partial\xi} + \eta_y\frac{\partial U_x}{\partial\eta}\right) - U_y^2\left(\xi_y\frac{\partial u}{\partial\xi} + \eta_y\frac{\partial u}{\partial\eta}\right) \end{aligned}\right] \quad (7.56a)$$

Or,

$$\frac{1}{r_s}=\frac{1}{U^3}\begin{bmatrix} U_x^2\left(\alpha_1^1\frac{\partial U_y}{\partial\xi}+\alpha_1^2\frac{\partial U_y}{\partial\eta}\right)+U_xU_y\left(\alpha_1^1\frac{\partial U_y}{\partial\xi}+\alpha_2^2\frac{\partial U_y}{\partial\eta}\right) \\ -U_xU_y\left(\alpha_1^1\frac{\partial U_x}{\partial\xi}+\alpha_2^2\frac{\partial U_x}{\partial\eta}\right)-U_y^2\left(\alpha_2^1\frac{\partial U_x}{\partial\xi}+\alpha_2^2\frac{\partial U_x}{\partial\eta}\right) \end{bmatrix} \tag{7.56b}$$

In Eq. (7.56b), r_s is radius of curvature, U is stream-wise velocity, others terms are already explained in previous Chapters of this thesis. Multiplying *L.H.S.* and *R.H.S* of Eq. (7.56) with $\Delta A_p = J\Delta\xi\Delta\eta$

$$\frac{\Delta A_P}{r_s}=\frac{1}{U^3}\begin{bmatrix} U_{xP}^2\left((J\alpha_1^1\Delta\eta)_eU_{ye}-(J\alpha_1^1\Delta\eta)_wU_{yw}+(J\alpha_1^2\Delta\xi)_nU_{yn}-(J\alpha_1^2\Delta\xi)_sU_{ys}\right) \\ +U_{xP}U_{yP}\left((J\alpha_1^1\Delta\eta)_eU_{ye}-(J\alpha_1^1\Delta\eta)_wU_{yw}+(J\alpha_2^2\Delta\xi)_nU_{yn}-(J\alpha_2^2\Delta\xi)_nU_{yn}\right) \\ -U_{xP}U_{yP}\left((J\alpha_1^1\Delta\eta)_eU_{xe}-(J\alpha_1^1\Delta\eta)_wU_{xw}+(J\alpha_2^2\Delta\xi)_nU_{xn}-(J\alpha_2^2\Delta\xi)_nU_{xn}\right) \\ -U_{yP}^2\left((J\alpha_2^1\Delta\eta)_eU_{xe}-(J\alpha_2^1\Delta\eta)_wU_{xw}+(J\alpha_2^2\Delta\xi)_nU_{xn}-(J\alpha_2^2\Delta\xi)_sU_{xs}\right) \end{bmatrix} \tag{7.56c}$$

Or,

$$\frac{1}{r_s}=\frac{1}{\Delta A_pU^3}\begin{bmatrix} U_{xP}^2\left((b_1^1)_eU_{ye}-(b_1^1)_wU_{yw}+(b_1^2)_nU_{yn}-(b_1^2)_sU_{ys}\right)+U_{xP}U_{yP}\left((b_1^1)_eU_{ye}-(b_1^1)_wU_{yw}+(b_2^2)_nU_{yn}-(b_2^2)_nU_{yn}\right) \\ -U_{xP}U_{yP}\left((b_1^1)_eU_{xe}-(b_1^1)_wU_{xw}+(b_2^2)_nU_{xn}-(b_2^2)_nU_{xn}\right)-U_{yP}^2\left((b_2^1)_eU_{xe}-(b_2^1)_wU_{xw}+(\alpha_2^2)_nU_{xn}-(\alpha_2^2)_sU_{xs}\right) \end{bmatrix} \tag{7.56d}$$

Equation (7.56d) is used for computing radius of curvature; it is the function of Cartesian velocities at cell vertices and physical domain variables.

7.2.7 COMPUTATION OF BED FRICTION COEFFICIENT

The bottom shear stress appears in momentum equation used explicitly as source term in 2-D modelling, *i.e.*, it affects every cell rather than being a condition that it affect only boundary cells. It is commonly assumed that the shear stress can be expressed as a square law of depth averaged velocity (U) using;

$$\tau_0 = k\rho U^2 \tag{7.57a}$$

The parameter k is then expressed in terms of roughness parameters, such as Chezi's C or Manning's n. For uniform flow it is readily found that equation is equivalent to the Darcy- Weisbach equation with $k=f/8$, Comparing with Manning's equation (Lane and Ferguson, 2005) one has,

$$C_D = k = \frac{g}{C^2} \tag{7.57b}$$

$$C_D = k = \frac{gn^2}{h^{\frac{1}{3}}} \tag{7.57c}$$

Using uncertainty approach it is established that, over a non-uniform river reach U is likely to have far greater spatial variability than n, so will be the dominant control over spatial variation in shear stress as defined in the above equation (Lane and Ferguson, 2005). Physically based alternative to estimate n, is used as mentioned in the following equation (Lane and Ferguson, 2005). The assumption considered is that law of wall holds throughout the full depth to estimate value of C_D at each node.

$$n = \frac{\kappa h^{\frac{1}{6}}}{\sqrt{g}\ln\left(\frac{h}{e \cdot z_0}\right)} \quad \text{(Lane and Ferguson, 2005)} \tag{7.57d}$$

z_0(Roughness height) $= \frac{\kappa_s}{30}$ (Nikuradse, 1930) or more recently $= 0.1D_{84}$, h=flow depth, e=2.71.

7.2.8 MOVING BOUNDARY IMPLIMENTATION (wetting and drying technique)

A number of approaches are available in literature. The methodology, appropriate and extensively used for structured meshes with *FDM* solver is Fixed Grid Method with "discontinuous stair case discretization" (Bates and Horritt, 2005) (Figure 7.5).

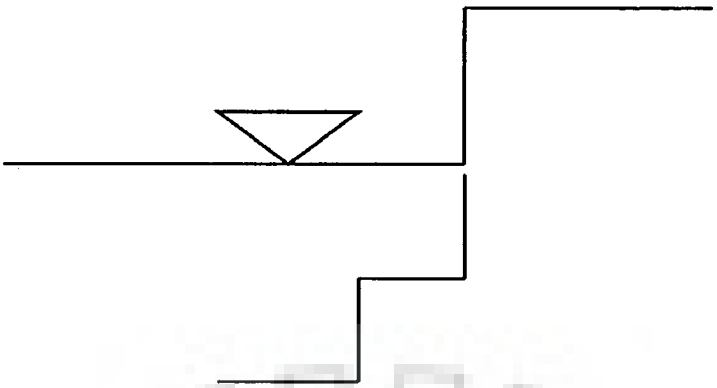

Figure 7.5 Discontinuous staircase discretization at boundary

Such methodology was published in Bradbrook *et al.* (2004). Point wise assumptions and methodology adopted for this model is mention herein.

- ✓ Bed slope at each computational cell is assumed to be zero.
- ✓ Topography is represented as series of planer horizontal element forming discontinuous staircase.
- ✓ Entire element is switched on /off depending upon the computed water level.
- ✓ Assume instantaneous wetting of each element in a manner that conserve mass. However, momentum equations are not still conserved.
- ✓ Boundary should move with the momentum of fluid which generally is small in shallow water flows.
- ✓ Logical 'flag' need to be assigned to each cell to indicate when it becomes wet. So that correction may be applied.
- ✓ Numerical simulation of flow in open channels with slope banks, sand bars and island, the water edges changes with time, with part of nodes being possibly wet or dry.
- ✓ Even for steady flow, the water edges are not known until the computation is finished. So whole domain has to be included initially to solve for momentum equation and water depth is computed for the whole domain implicitly. So

fully implicit solver is used in the model for water depth, all the wet and dry nodes participate in the solution.

- ✓ A threshold flow depth (a small value such as 0.02 m in natural rivers) is used to judge drying and wetting front. If the flow depth is lower than the threshold value, the node is dry. The dry nodes are assigned zero velocity in stream wise and transverse direction.

7.5 OVERALL SOLUTION PROCEDURE AND FLOW CHART

A brief flow chart for the developed numerical scheme is shown in Figures 7.6a as part-A and continued to part-B in Figure 7.6b (computer code details in Appendix-VI and VIB).

The *SIMPLEC* Algorithm being semi implicit scheme, the stability of solution is ensured using the Courant-Fredrich-Lewy(*CFL*) condition (Lien *et al.*, 1999).

$$CFL = \max_{i,j}\left[\left(\frac{|U_{xi,j}|}{\Delta x_i}+\frac{|U_{yi,j}|}{\Delta y_i}\right)\Delta t\right] < 1.0 \qquad (7.58)$$

In the program, the courant number for each computational node is checked at each time step. If, it is greater than one, it is automatically adjusted by reducing the time step. The convergence criteria of this scheme is when difference of calculated velocity and the flow depth at current and previous time step approaches zero which is expressed as

$$\left|\frac{\Psi_{i,j}^{k+1}-\Psi_{i,j}^{k}}{\Psi_{i,j}^{k}}\right| \to 0$$

where, $\Psi = U_x, U_Y$ or h

A small no. is added (1×10^{-6}) before division to avoid zero denominator (7.59)

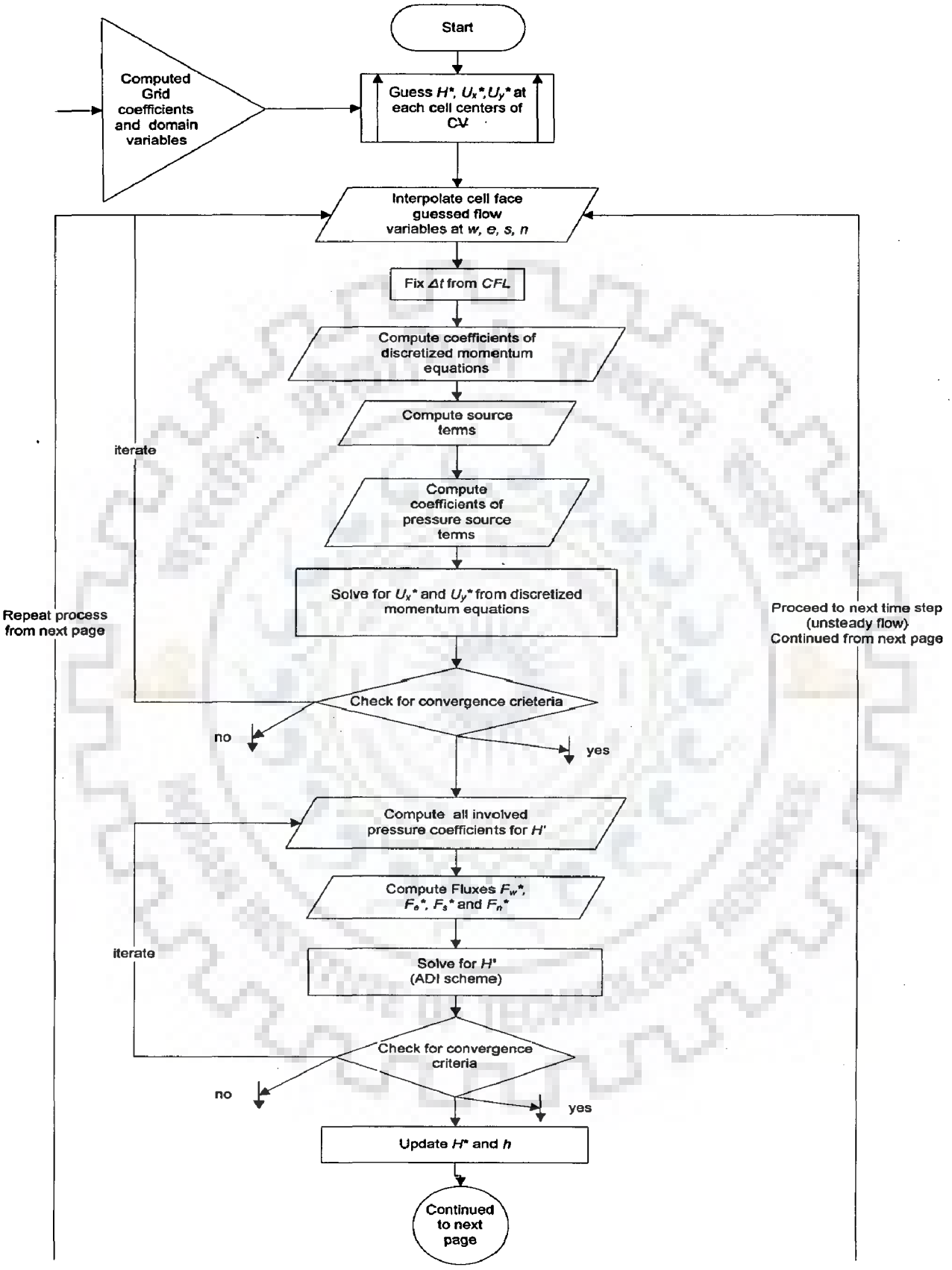

Figure 7.6a Flow chart of numerical scheme (part-A)

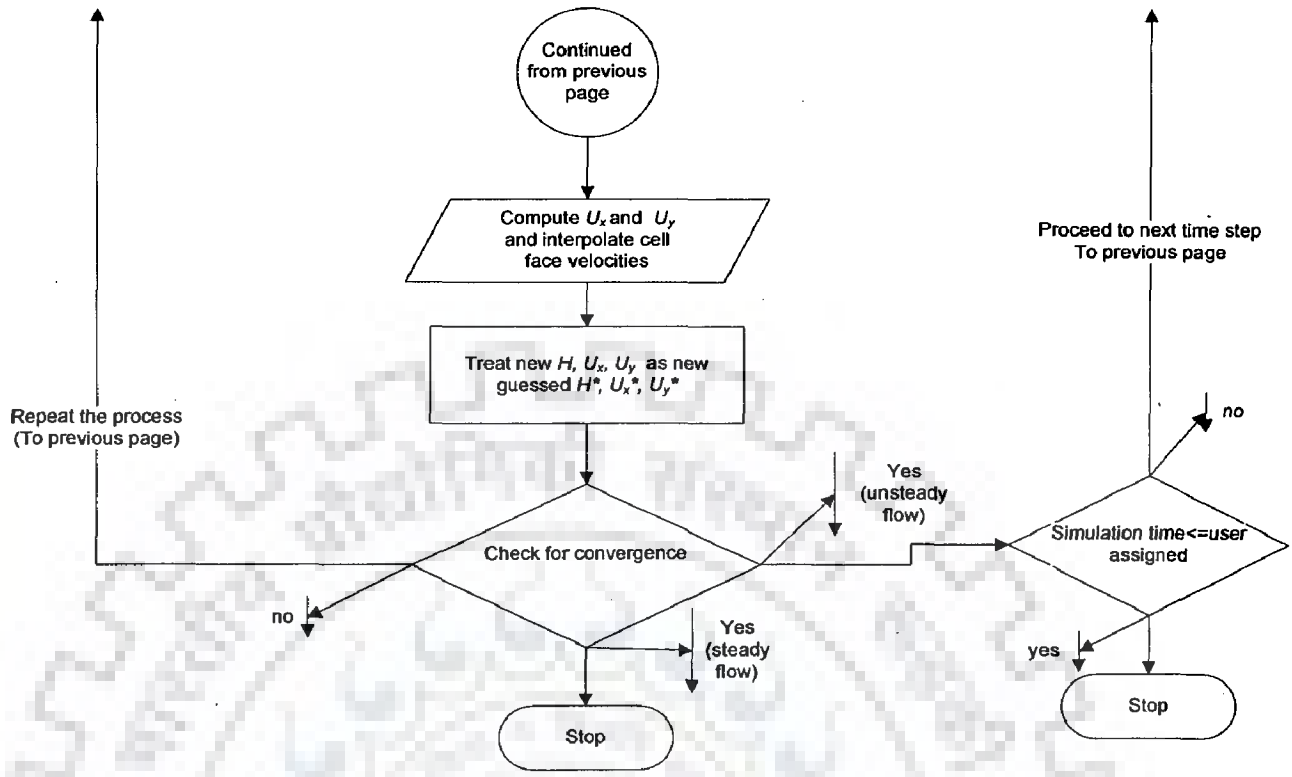

Figure 7.6b Flow chart of numerical scheme (part-B)

7.6 SUMMARY

In this chapter, a detail and comprehensive step wise procedure for solving the governing flow equations in curvilinear co-ordinate system by finite volume method has been given. A *C++* program module (Appendix-VI) has been developed using this numerical code to solve flow equations. For solving governing mass momentum equations derived in Chapter 5, *SIMPLEC* algorithm with incorporated Rhie and Chow's (1983) interpolation technique in non-staggered grid has been adopted. In the solution algorithm moving boundary implementation using wetting and drying technique has been incorporated to simulate moving boundaries, braid bars, islands and no flow zones within the flow domain.

****

DATA ACQUISITION, PRE-PROCESSING AND APPLICATION

8.1 GENERAL

One of the characteristic features of Brahmaputra River is that it has three to four constricted nodal points where the cross-sections remain unaltered and stable with time and space, moreover, around the vicinity within an extent, Brahmaputra follows uniform aligned channel configuration. This gives different segments of Brahmaputra separated with well defined nodal points (with uniform channel width) which is adequately and favourably suited for applying 2-D hydrodynamic mathematical model with relative ease so far as upstream and downstream boundary implementation is concerned. Still, process representation of fully developed braided stream is challenging task on account of the presence numerous 3-D flow structures within the flow domains.

The sediment discharges and flood discharges at certain locations of the river have been continuingly recorded and the river cross sections surveyed periodically. Still, the limitation in the human capacity, instrumentation, the difficulties of the measurement and the risk involved, the actual data acquisition often remain off-set by errors. The importance of the information that could be derived from the analysis of the data is very high in the design, management and future risk and hazard prediction and strategies.

Taking in to account the situation as described above, the present study is a maiden attempt to implement a 2-D hydrodynamic flow simulation model based on the controlling equation and specified boundaries specially keeping in mind the flow behavior of River Brahmaputra in chosen study reach. The algorithms established by the researchers/modelers in the relevant literatures advocate that the success of flow simulation model application depends on the size of the data covering wide patterns of phenomena. More the data sets, better is the result's reliability. The technique is a data driven model requiring gamut of data patterns representing the actual phenomena to accommodate all the possibilities within the patterns of independent and dependent variables.

The study has been carried out on the following data sets and the area of interest.

1. Study domain of the river channel (from Pandu to Jogighopa) -112 km
2. No. of the measured river cross sections (1997)- 14 Numbers
3. Hydrological Data(Jogighopa-Pandu) for the same year(1997)

8.2 DATA SOURCES AND DATA TYPES

8.2.1 HYDROGRAPHIC DATA

Morpho-metric data: the reduced levels of the river cross-sections of post-monsoon period for the year 1997 have been collected in respect of all the 14 pre-defined river cross-sections (Appendix-III) from the *Brahmaputra Board, Government of India.*

8.2.2 DISCHARGE AND STAGE DATA

Discharge and stage data of the river Brahmaputra collected for various cross-sections from *Central Water Commission (CWC), Assam Water Resources Department* and *Brahmaputra Board* have constituted main data resource to the model implementation. The length of data record was for 1997.

8.3 PRE- PROCESSING OF HYDRO GRAPHIC DATA

The Brahmaputra River Basin in terms of its complexity calls for well-defined response models. In the study, the significant steps followed are outlined. The steps are the abstraction of outliers and errors in the data sets. Conceptual or statistical tools as regression and curve fitting were implemented on the variables pertaining to specific river / stream to identify the irrational points; they were either discarded or rectified based on the earlier trends or pattern of the data.

8.4 FRAMING OF THE DATA-SET FOR MODEL APPLICATION

The system contains 2-D hydraulic analysis component for steady flow water surface profile computations. A key element is that component will use geometric data representation and geometric and hydraulic computation routines.

8.4.1 DATA REQUIREMENTS AND INPUT

The basic input data required for 2-D model can be grouped into following categories.

8.4.1.1 Geometric data

(i) Domain discretization

Geometry of the physical system is represented by cross sections, specified by coordinate points (stations and elevations), and the distance between cross sections. The 2-D surface is represented by grid with appropriately chosen nodal point with know x, y and z coordinates. Moreover Hydraulic roughness is computed in case of 2-D by Manning's n values and can vary from node to node depending upon the depth averaged velocity. The river domain boundaries (main channel and largely low flood plain) for the study period is extracted in geographical coordinate system from the remote sensing imagery [Courtesy: *NDMA(2011)*] shown in Figure 8.1a and 8.1b and transformed to Cartesian coordinate system to accurately represent the domain in Cartesian Plane (Figure 8.2a). It is to be understood that the whole cross section includes main channel, low flood plains, and high flood plains. Some reaches within the river study stretch have dykes built for flood protection purposes. These dykes have poor maintenance and are often breached during high flood seasons. The main channel and low flood plains (Primary Flood Plains) are inundated in low and medium flood periods. Keeping in view, care has been taken to extract the flow domain to include primary flood plain and cross sections were fit that must include main channel and low flood plain.

The geo-referenced image covering the river stretch in 1997 was delineated using GIS software tool by the digitizing the bank lines through identifying river sandy bed fringes with vegetative cover along the bank line. The coordinate system of the geo referenced image was *WGS 84*. Thus, x and y of boundary grid points were obtained.

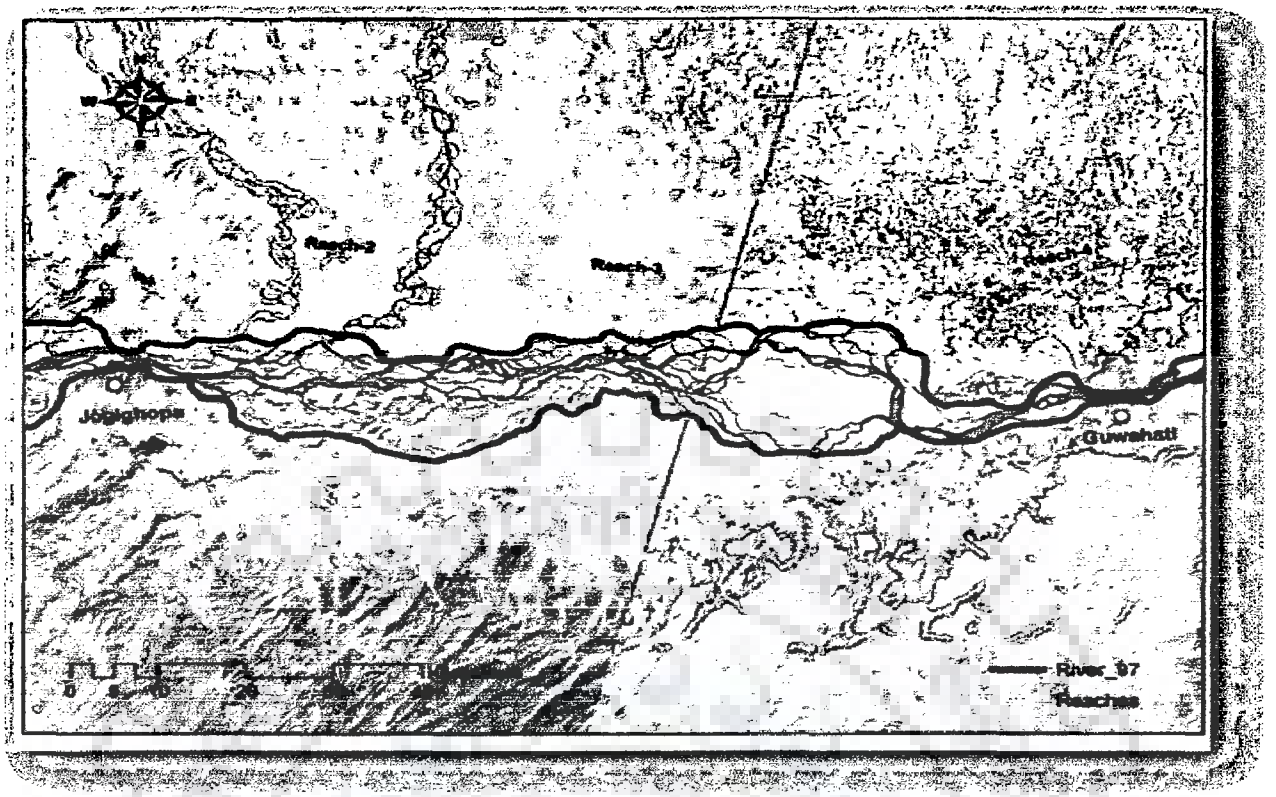

Figure 8.1a Domain delineation through imagery (*IRS LISS III*, Year 1997)

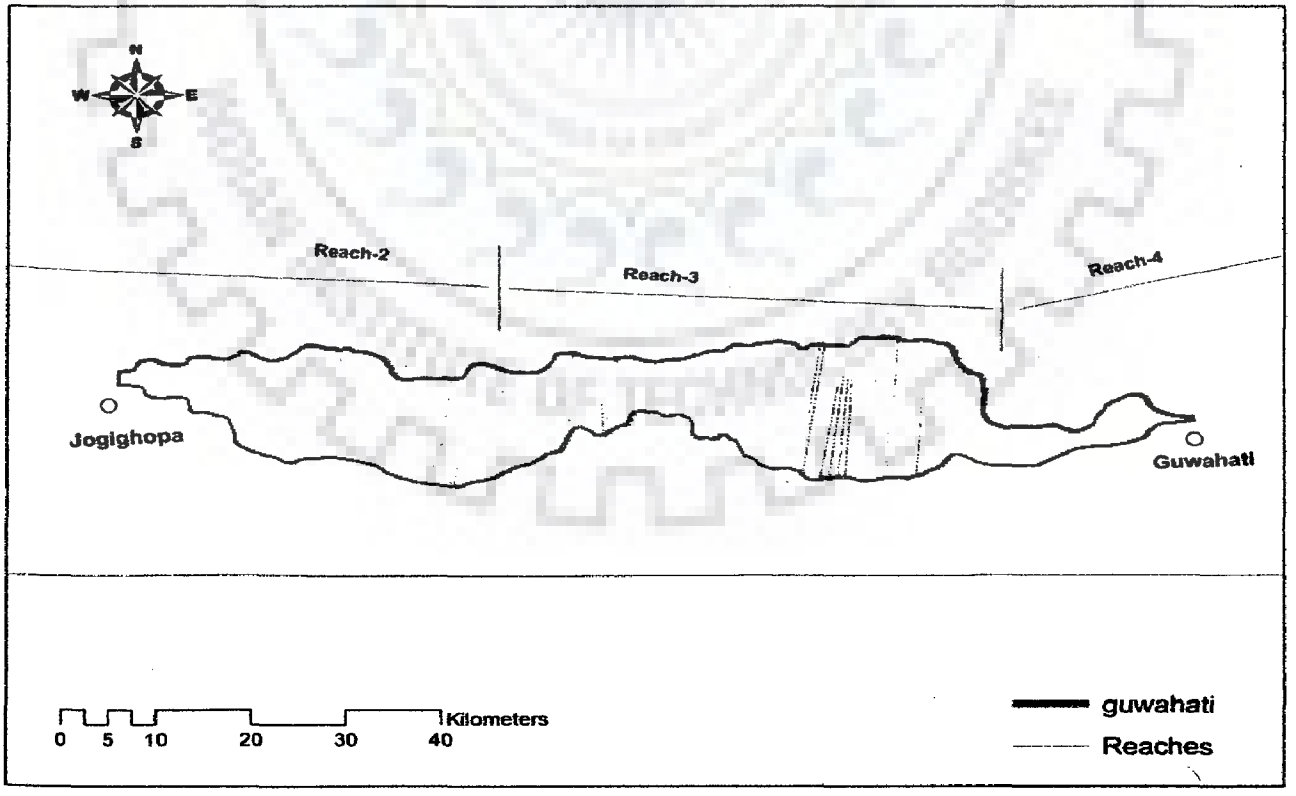

Figure 8.1b Domain delineation through imagery

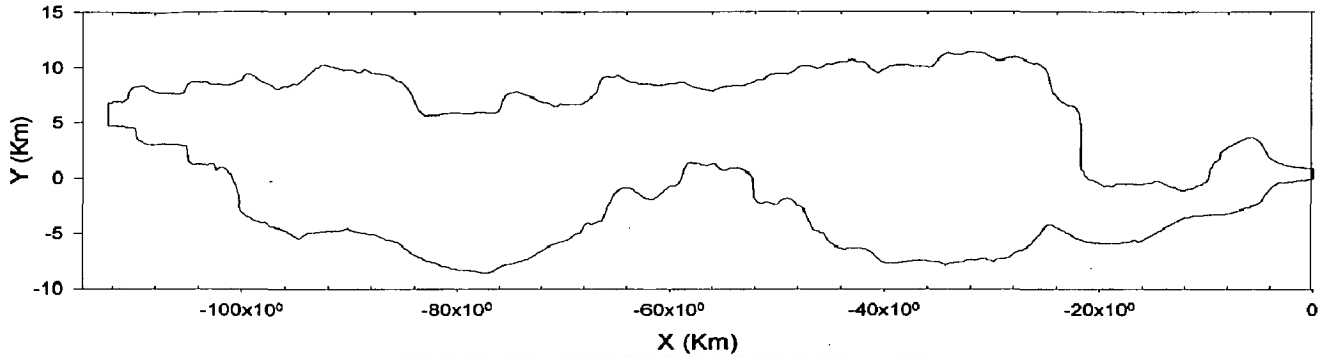

Figure 8.2a Domain in transformed Cartesian coordinate system

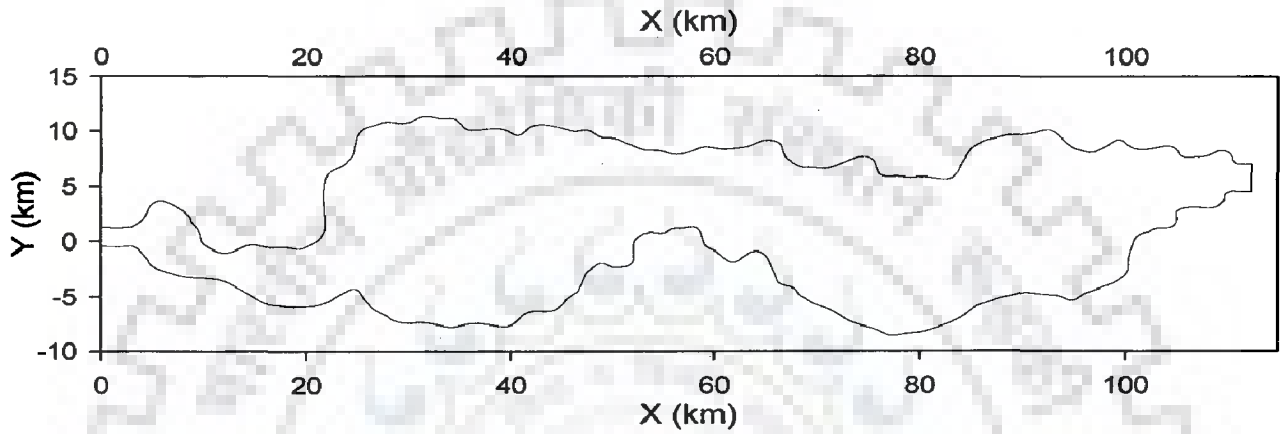

Figure 8.2b Domain in *x-y* Cartesian coordinate

Furthermore, boundary grid points have been refined and evenly redistributed through algebraic method into 451 points along the positive *x*-axis (south and north boundaries) and 51 points along *y*-axis. Domain is re-oriented as, positive *x*-axis aligned with the direction of the flow for convenience in sign convention while applying the controlling transformed partial differential equations for computation of flow field and water depth. Some of the extreme grid points at upstream and downstream of the flow domain is corrected and rectified to fit the measured cross-section in the given orientation which is supposed to be crept in due to manual digitization error while delineating the flood plain from inhabited area in the vicinity of prime inhabited land at Pandu (at upstream location) and Jogighopa (at downstream location). Boundaries are slightly smoothened through three point-Finite Fourier Transform (*FFT*) using a math-processing software to generate an efficient mesh without changing the basic characteristic of the domain (Figure 8.2b).

(ii) Hydrographic data

As discussed in earlier Chapter 3, morpho-metric data in the form of the reduced levels of the river cross-sections of post-monsoon period for the 1997 have been

collected in respect of all the 14 pre-defined river cross-sections from the *Brahmaputra Board, Government of India.*

The data for the cross-section have been normalized and as per their position and orientation (chainage, and bearings), these points are fit accordingly into the domain taken under study. The bearing at cross section-22 is zero and physically identified position on the imagery used to extract the domain, taking reference of C/s -22, cross-sections can be positioned and oriented if chainage and bearing are known (Table-8.1, and standard Brahmaputra map in Appendix- V, *Brahmaputra Board Govt. of India*).

Table 8.1 Study reach of Jogighopa-Pandu(Appendix-V)

S.No.	Name of Site	X-section	chainage (km)	Downstream Reach Length (km)	Bearing of *X*-section
1	Jogighopa	9	82.62	0	0°-30'
2	-	10	92.82	10.2	24 °-40'
3	Dubapara	11	100.98	8.16	16°-00'
4	Dalgoma	12	109.65	8.67	5°-30'
5	Simlitola	13	119.85	10.2	358°-30'
6	Nagarbera	14	128.01	8.16	310°-30'
7	Rangapani	15	137.70	9.69	340°-30'
8	Rangapani	16	146.37	8.67	349°-30'
9	Barakhat	17	156.06	9.69	22°-00'
10	Bitartari	18	167.28	11.22	3°-00'
11	Ganimara	19	175.95	8.67	13°-30'
12	Palasbari	20	182.50	6.55	3°-00'
13	Dharapur	21	189.21	6.71	356°-00'
14	Pandu	22	197.37	8.16	0°-00'

It is further elaborated that boundary geometry for the analysis of flow in natural streams is specified in terms of ground surface profiles (cross sections) and the measured distances between them. Measured cross sections are located at intervals along a stream to characterize the flow carrying capability of the stream and its adjacent floodplain. They extend across the entire floodplain and perpendicular to the anticipated flow lines. Occasionally, it is necessary to layout cross-sections in a curved or dog-leg alignment to meet this requirement (Table 8.1). Every effort has been made to obtain interpolated stream bed data at mesh nodes based on these measured cross-sections so that data will accurately represent the stream and

floodplain geometry. The adopted process of bed interpolation appropriate for the available data set is discussed in subsequent sections. Thus, the river domain is specifically delineated with the flow area with flood plain (outlines the sandy bed of river, see Figure 8.1).

As discussed earlier, cross-sections are fit at the position and bearing as per Table 8.1. The measured cross-sectional data from the left bank of the river is normalized (0-1) and 101 points are extracted through linear interpolation technique to get nodal points for the structured matrix for bed interpolation, discussed in the subsequent section.

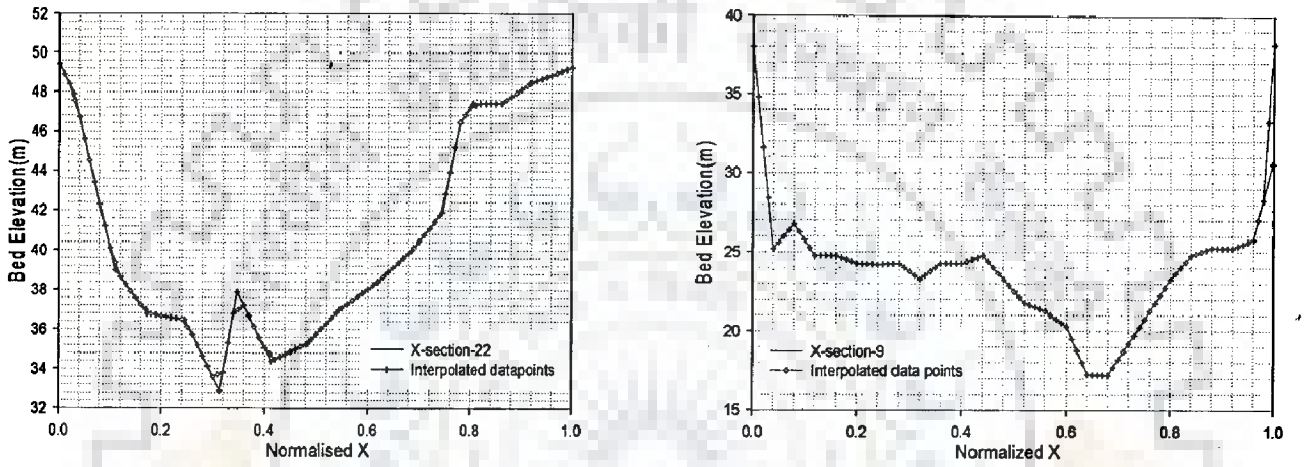

(a) (b)

Figure 8.3 *X*-section data point interpolation (a) cross section -22 (b) cross section-9

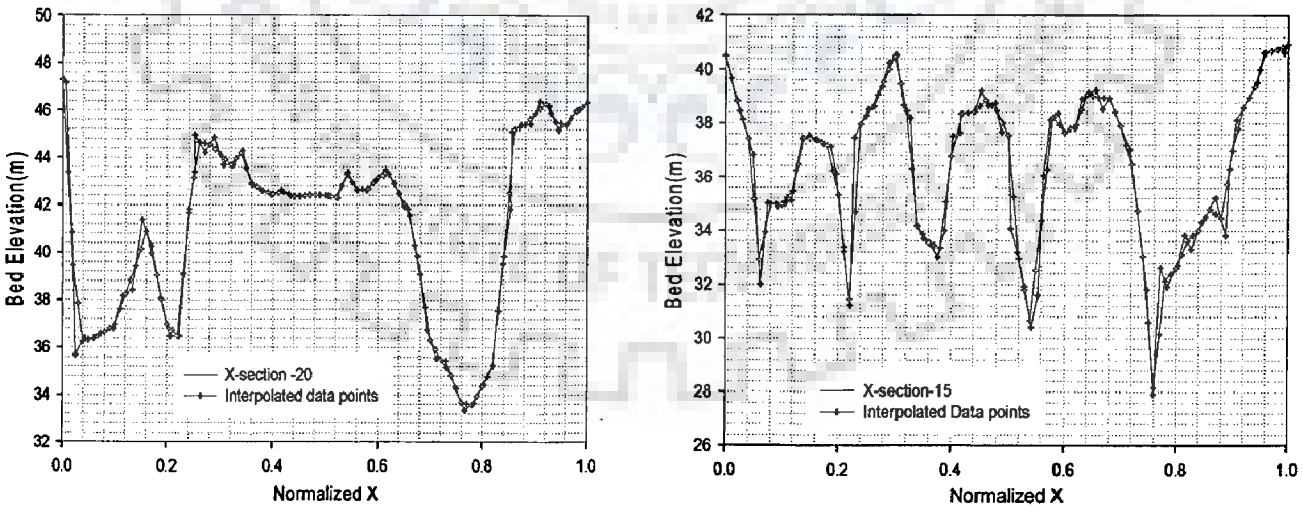

(c) (d)

Figure 8.3 *X*-section data interpolation (c) cross-section-20, (d) cross-section-15

In Figures 8.3a- 8.3d. *X*-sectional data interpolation of 101 points from measured and domain fitted cross-sections numbering 22, 20, 15 and 9 have been depicted for illustration.

(iii) Stream bed interpolation

Stream bed interpolation is a process of interpolating bed elevation from the topology or bathymetrical database onto the mesh nodes. A number of methods and algorithm are available in the literature. For the type of observed data available, Inverse Distance weighing method with structured data base is used which has been also one of the methods as described by Zhang and Jia (2005). Inverse Distance weighing method can be described as follows. Suppose there are known bed level Z_i where $i=1, 2, 3...n$ and Z_b is the bed level at the known grid point (P) which has to be interpolated. The Z_b can be given as

$$Z_b = \frac{\sum_1^n \varepsilon_i . Z_i}{\sum \varepsilon_i} \tag{8.1a}$$

where, ε_i =weighting factor of the respective interpolated point i, weighting factor is taken proportional to inverse of the distance from P to the interpolation points. So finally Z_b can be given as

$$Z_b = \frac{\sum_1^n \frac{Z_i}{d_i} \varepsilon_i .}{\sum \frac{1}{d_i}} \tag{8.1b}$$

where d_i = distance between interpolation point (i) and grid point P (Figure 8.4). As the data base is structured, so structured interpolation of Zhang and Jia, 2005 Algorithm is adopted to interpolate the data at grid points using Eq. (8.1). In the structured interpolation, the cross-sectional measured data set is normalized and refined to improve the accuracy of the interpolation by considering the flow direction. The algorithm is as follows:

1. Refinement is done through normalizing and expanding to desired data points in the transverse direction along each cross section using linear interpolation

2. Each cross section is divided into three parts, left bank, main channel, and right bank appropriately as per the cross section configuration.
3. Equal number of points in these three parts is distributed.
4. Again the database in the longitudinal direction between cross sections is normalized and expanded to desired data points between cross sections, the linear interpolation will be conducted between the corresponding parts of each cross section,

Adopting aforementioned procedure, a structured matrix of data points from measured data points is generated. Now from the quadrilateral formed from these matrix elements, each grid point which has to be interpolated is identified, and using Eq. (8.1b), bed elevation is determined as the x, y co-ordinates of all the neighborhood points and the grid point are already known. This method is stable and reasonable as it interpolates the data along the thalweg if one can appropriately and judicious identify the left over bank, right over bank and main channel for each measured cross sectional data.

As discussed above, X-section is positioned and oriented as per the chainage and bearing given in Table 8.1 numbering X-section-9 (Downstream) to 22 (Upstream) in Figure 8.5. Out of the measured data of each X-section, data are normalized and 101 equally distanced data points are extracted for each X-section (illustrated in Figures 8.3a-8.3d).

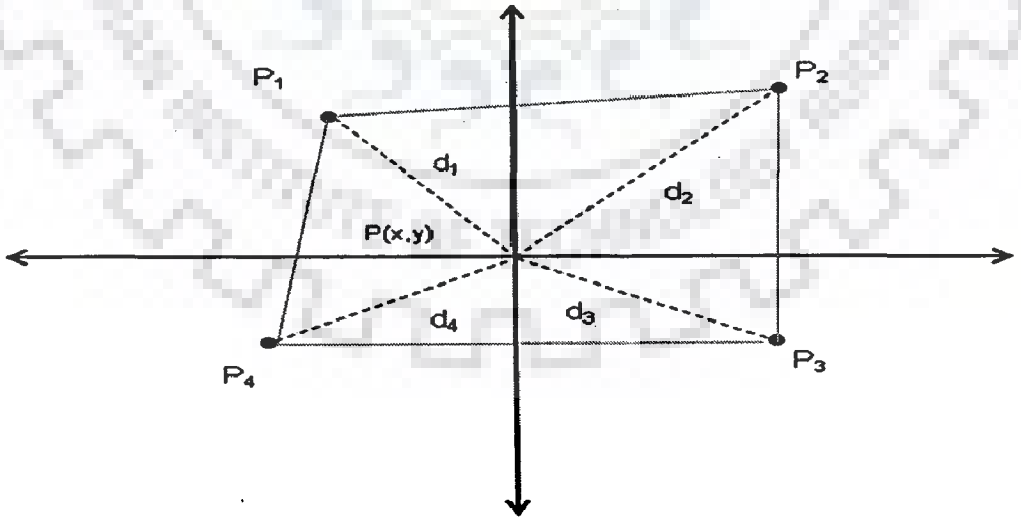

Figure 8.4 Inverse distance weighing method of interpolation

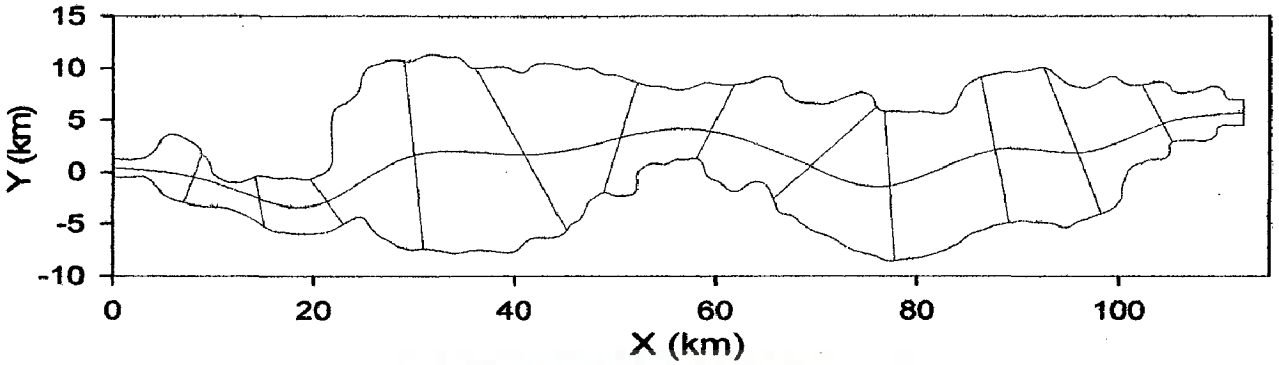

Figure 8.5 Positioning of measured *X*-sections into the domain

Thereafter, from the normalized data point of each *X*-section, 21 data points are linearly interpolated for each set of two adjacent *X*-sections through the *HEC-RAS* geometric interpolation application software (HEC,1997) so as to interpolate the data along the thalweg (deepest bed level), for continuity in the main channel configuration. Thus, a structured matrix of dimension 101×261 for data points is generated, presented in Figure (8.6a) in graphical form and corresponding contour plot of bed elevation is presented in Figure 8.6b and colour map in Figure 8.7a.

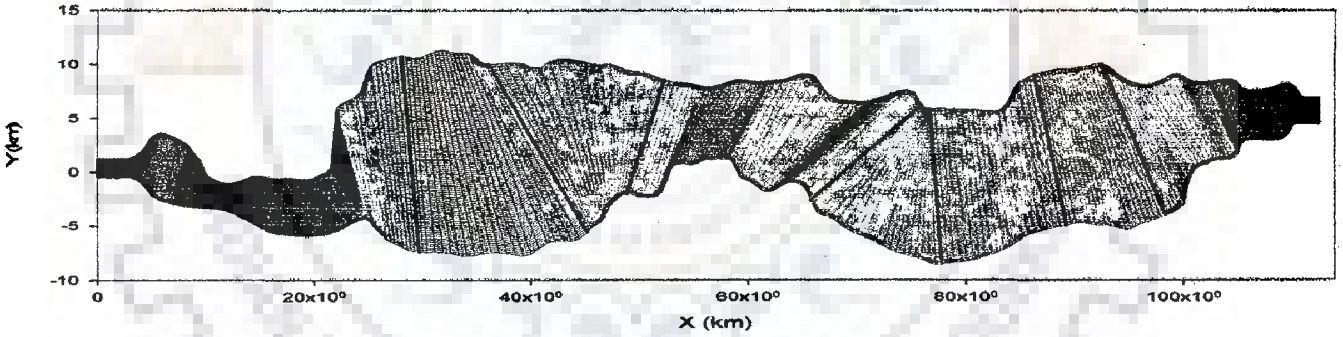

Figure 8.5a Structured matrix for measured data points in the domain

Discretization of the domain is done through the developed computer code (Figure 8.6) and bed level matrix (51×451) is generated by applying the relations mentioned Eq. (8.1), namely *IDW* method.

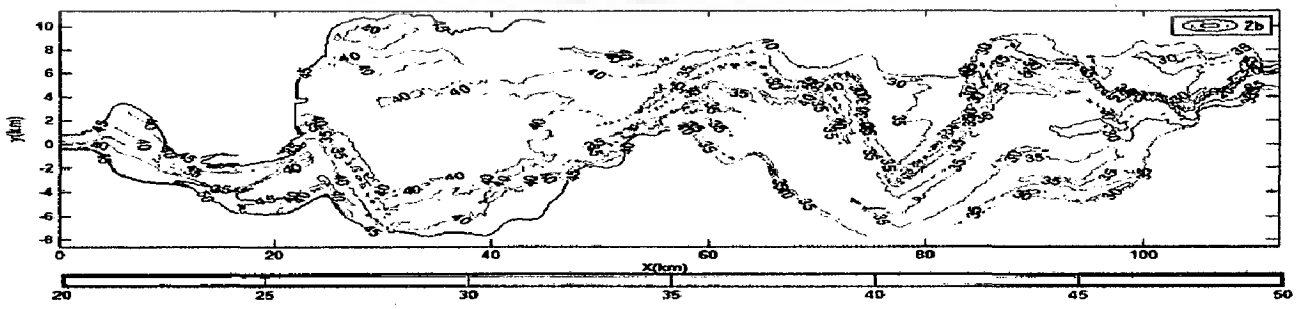

Figure 8.5b Contour plot of structured matrix (z_b in m)

Bed interpolation has also been done by for discretized array[x, y] using Matlab tool using nearest neighborhood technique for comparing and checking the accuracy of the interpolated bed variation from the developed computer code using *IDW* method.

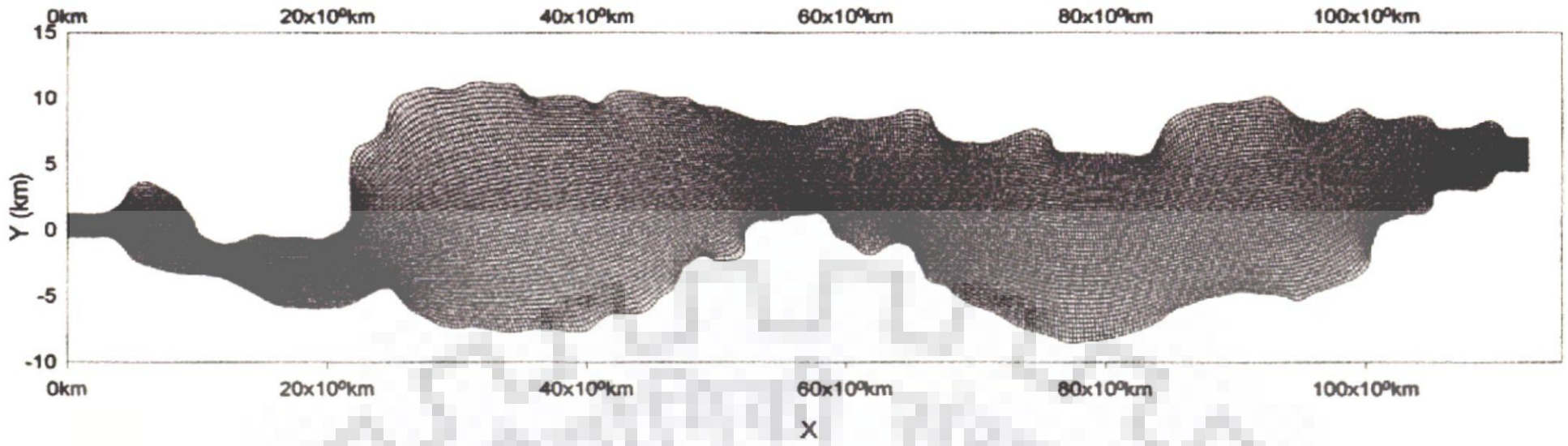

Figure 8.6 Domain discretization in Cartesian co-ordinate system

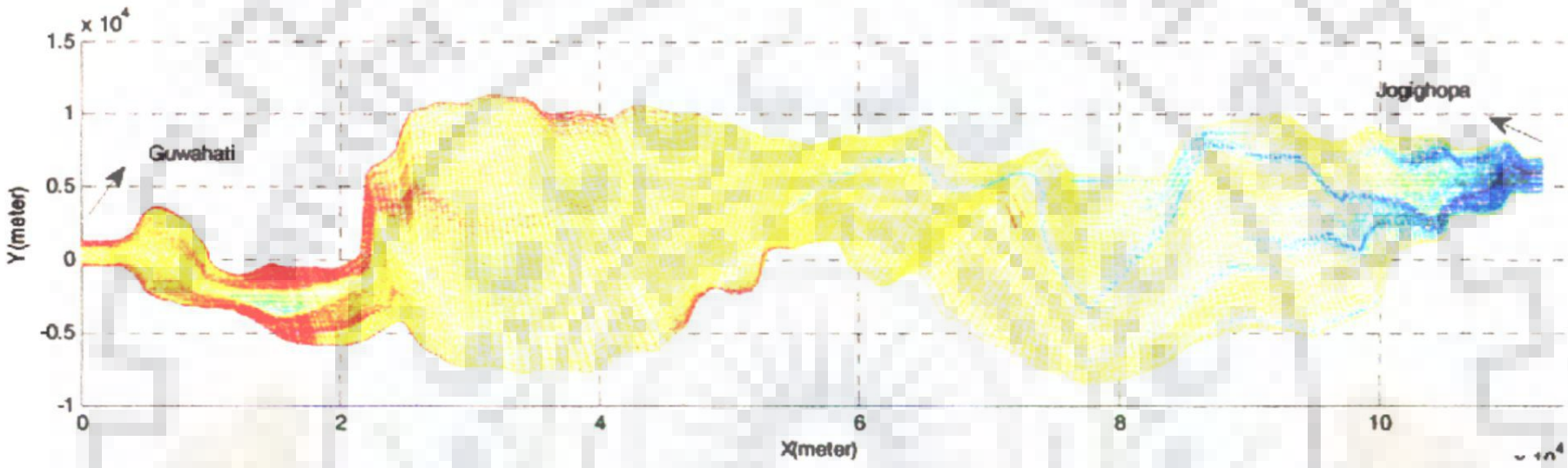

Figure 8.7a Map of structured matrix depicting bed variation from measured data

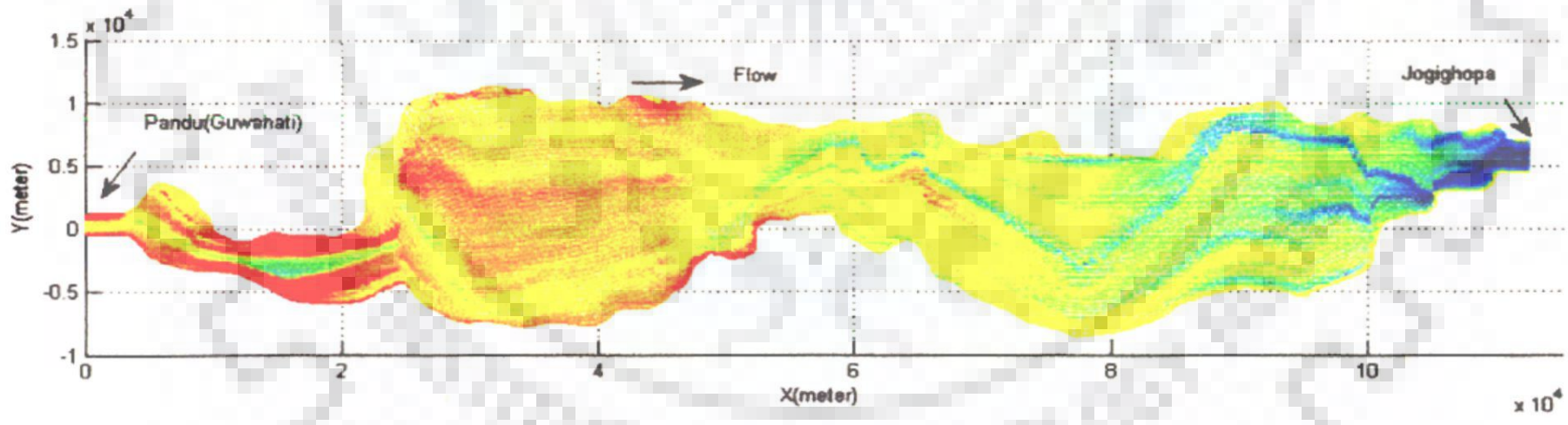

Figure 8.7b Contour map of interpolated bed level using coded *IDW* method

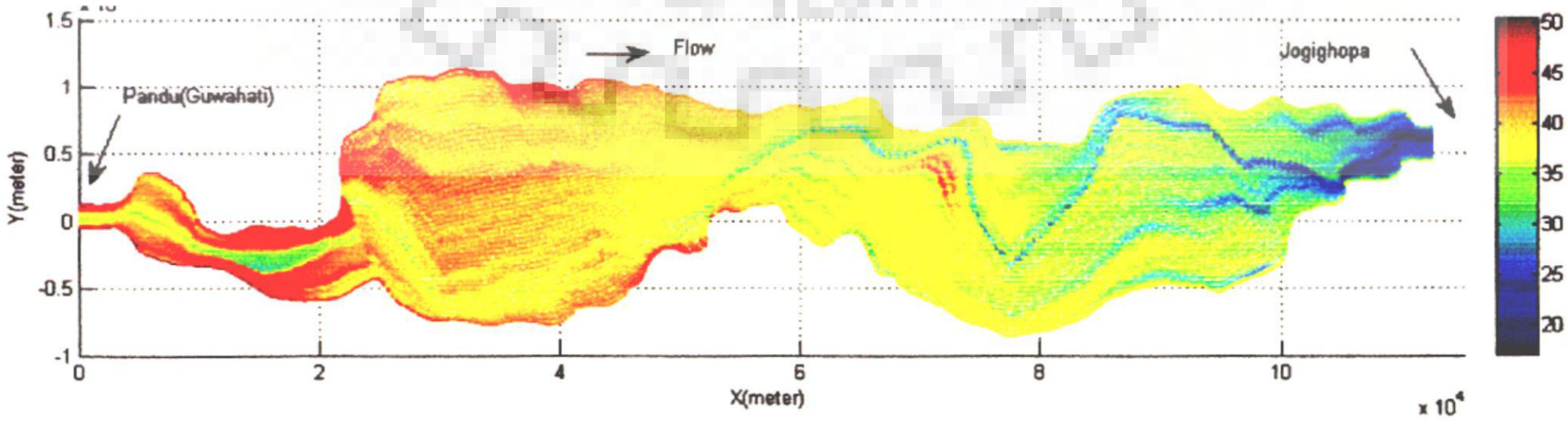

Figure 8.7c Contour map of interpolated bed level using Matlab code

Figure 8.7d 3-D surface plot of generated bed level of the flow domain (bed level in m)

The generated bed data from *IDW* method using the *C++* code and nearest neighborhood method using the Matlab code is presented in Figure 8.7b and 8.7c. Though the pattern of the bed variation in Figs 8.7b and 8.7c is similar to the structures data processed from measured bed variation, yet data generated by *IDW* method do contain some localized discrepancy in comparison to nearest neighborhood method from Matlab code, which is almost identical to Figure 8.7a. Hence, Matlab generated matrix is preferred. Surface Plot is shown in Figure 8.7d.

8.4.1.2 Hydrological data

The hydrologic data consist of water discharges, temperatures and flow durations. The discharge hydrograph is approximated by a sequence of steady inflow discharges each of which occurs for a specified numbers of days or hours depending upon the acquisition of data. Water surface profiles are computed by using the 2-D depth averaged mass momentum equations.

(i) Flow data

The flow in long reaches of river is 3-D dimensional and essentially an unsteady flow. To simulate 2-D flow for such a long reach with width varying from 2km to 22km is heavily data driven. Practically, data required for simulating unsteady flow in 2-D are hard to acquire for such a large alluvial river like the Brahmaputra. Yet for practical engineering purposes, steady flow simulation using 2-D model for large alluvial river provides desirable information and enough insight to approximate realistic flow situation.

Observed flow field data were required in order to perform a steady water surface profile computation and velocity field. Initial steady flow was taken as the peak flow to assure that the whole domain (primary flood plain and full bank flow scenario) is included into the computational domain in 2-D model. The chosen peak steady flow will also provide the initial conditions if the unsteady flow computation is to be performed.

Boundary conditions are necessary to establish the water surface at the ends of the river system (upstream and downstream). In a sub critical flow regime, boundary conditions are necessary at the downstream ends of the river system with hydrograph in the upstream. Figure 8.8 is the rating curve (R-Square=0.95 and Standard Error of

Estimation= 0.229) at extreme downstream node (C/s-9) of the flow domain *i.e* the relation between stage and discharge derived from the data for several years. The trend-line power equation may be fit into downstream C/s in the flow code to compute the corresponding water level for a given flow discharge.

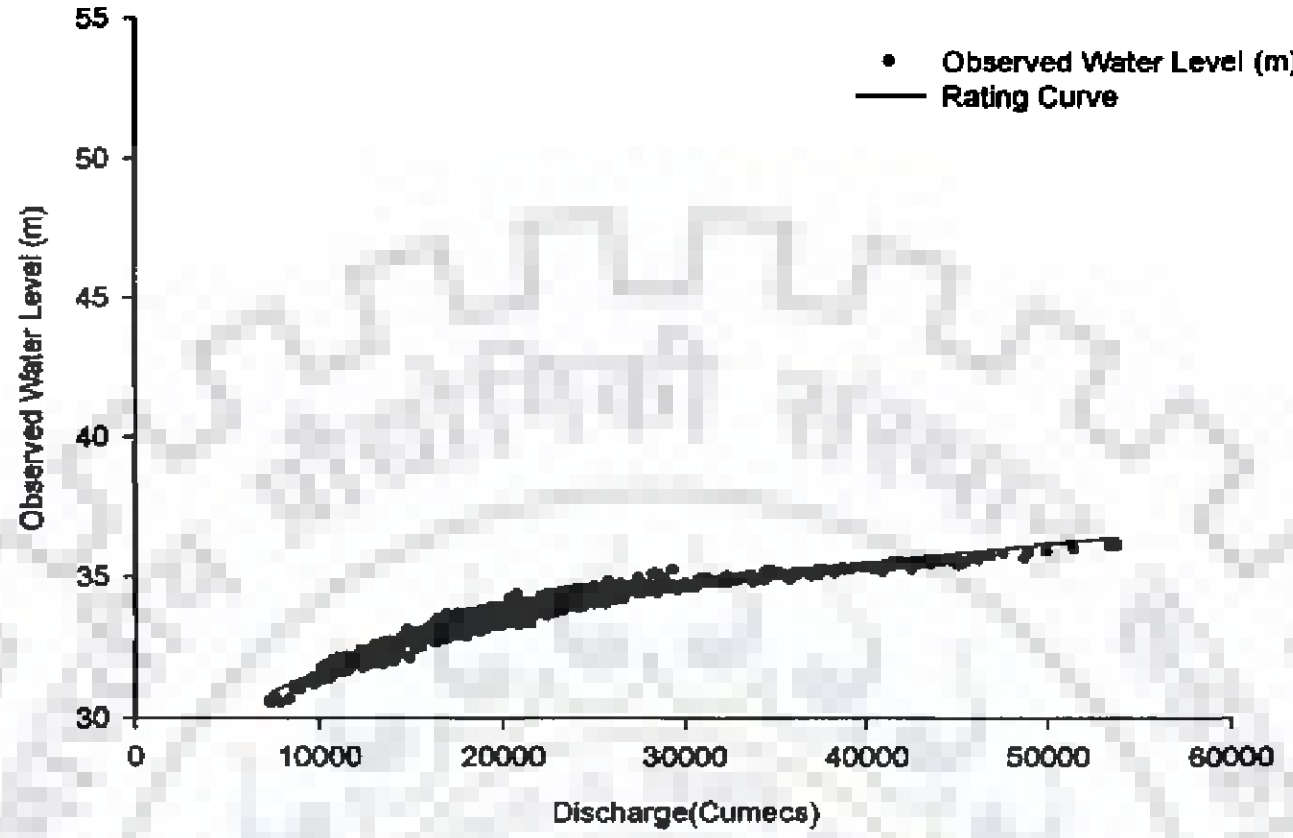

Figure 8.8 Stage-discharge relation at C/s-9 (Jogighopa site)

Similarly, data for measured water level with corresponding discharge have been plotted for last ten years and rating curve (R-square=0.85 and Standard Error of Estimation=0.50) is drawn to establish a mathematical relation of water level with discharge at Pandu. This is to be mentioned here that both the cross sections(9 and 22) are highly stable and configured of rock-outcrops, and straight, considered to be perfect nodal points and quite suitable for boundary implementation for inlet and outlet.

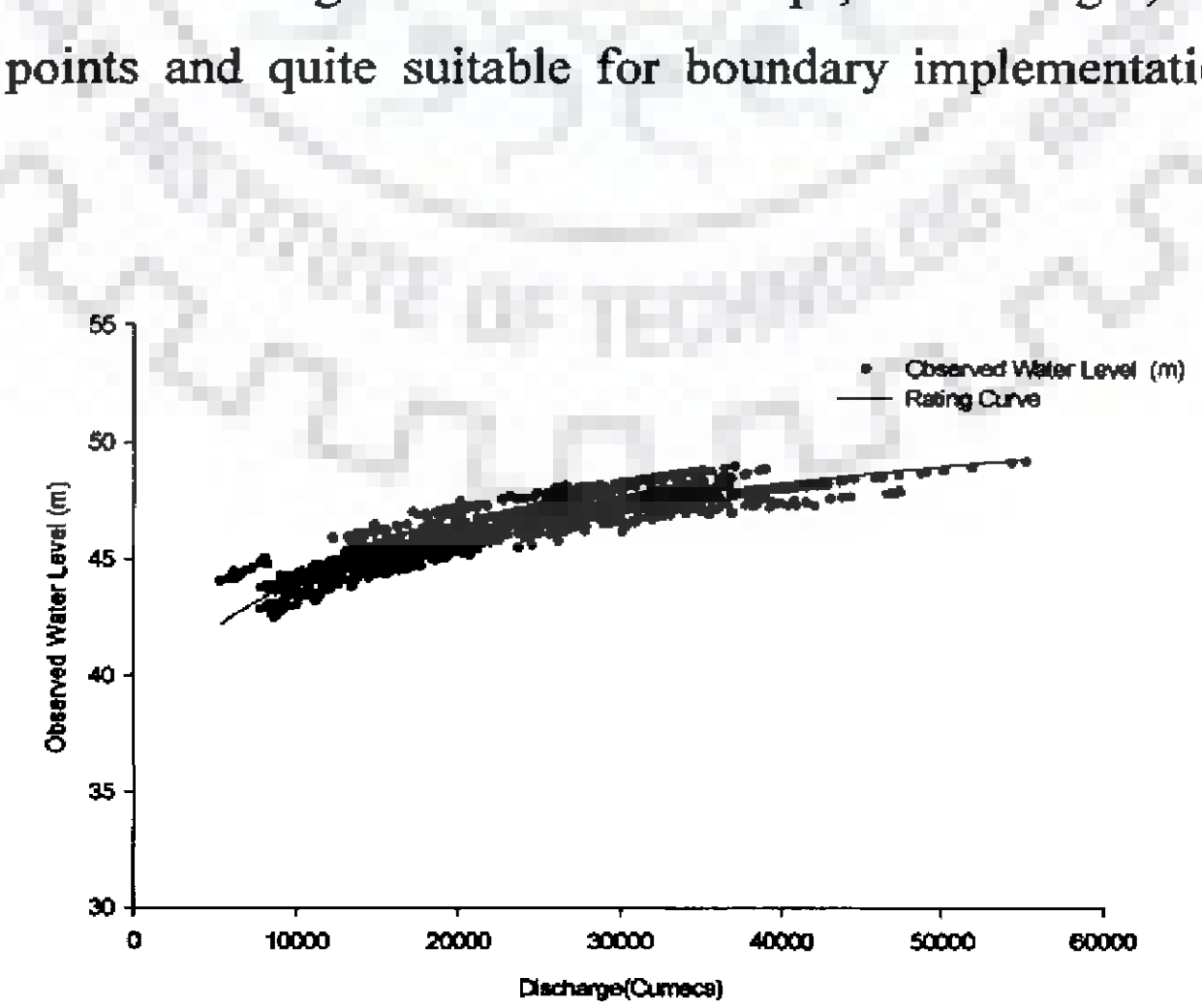

Figure 8.9a Stage-discharge relation at C/s-22 (Pandu site)

Figure 8.9b Stage-time series at C/s-22 (Pandu site) for monsoon period 1997-98

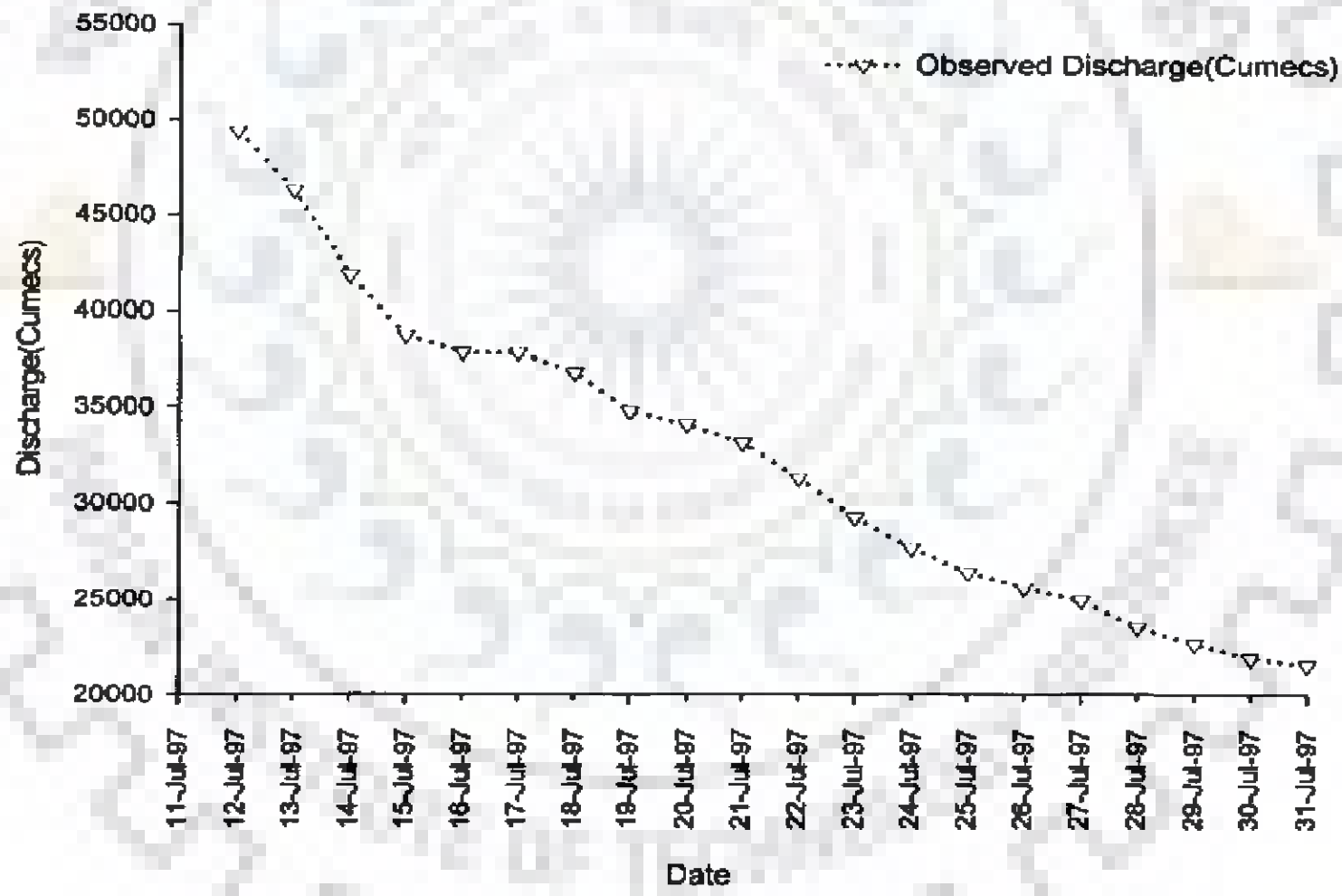

Figure 8.9c Observed discharge at C/s-22 (Pandu site)

Measured daily water level with time is plotted for Monsoon period, 1997-98 in Figure 8.9b. The proposed simulation period is kept from 12th July 1997(00 hrs) to 31st July 1997(2400 hrs) when flood recedes locally to simulate the braiding pattern in the flow domain. The measured discharge data for Pandu (C/s-22) for the specific period is not available from the field. Observed discharge at Pandu is approximated from Figure 8.9a for observed water level since observed water level at Pandu is known from Figure 8.9b for the simulation period. Figure 8.9c depicts plot between

the approximated observed discharge verses observed water level at upstream location at Pandu. Hence, 20 discharge profiles for the receding flood of 1997 (12th July 1997 to 31st July 1997) is available to conduct simulation in developed 2-D flow model.

(ii) Bed Gradation

For computing frictional parameters, gradation of bed material should be known to compute D_{50} or D_{84}. Bed gradation data for each gauge site within the domain predefined *X*-sections could not be procured on account of unavailability. However, character of bed material within the entire study reach can presumed to be similar in nature in downstream reach of Brahmaputra reach. In view of the above, bed material gradation at *X*-section-20 (Palasbari) is taken as representative bed gradation (Figure 8.10) through out the alluvial study reach except where outcrops were present. 2-D flow model was used for 20 discharge profiles for receding flood of 1997 (12th July 1997 to 31st July 1997)

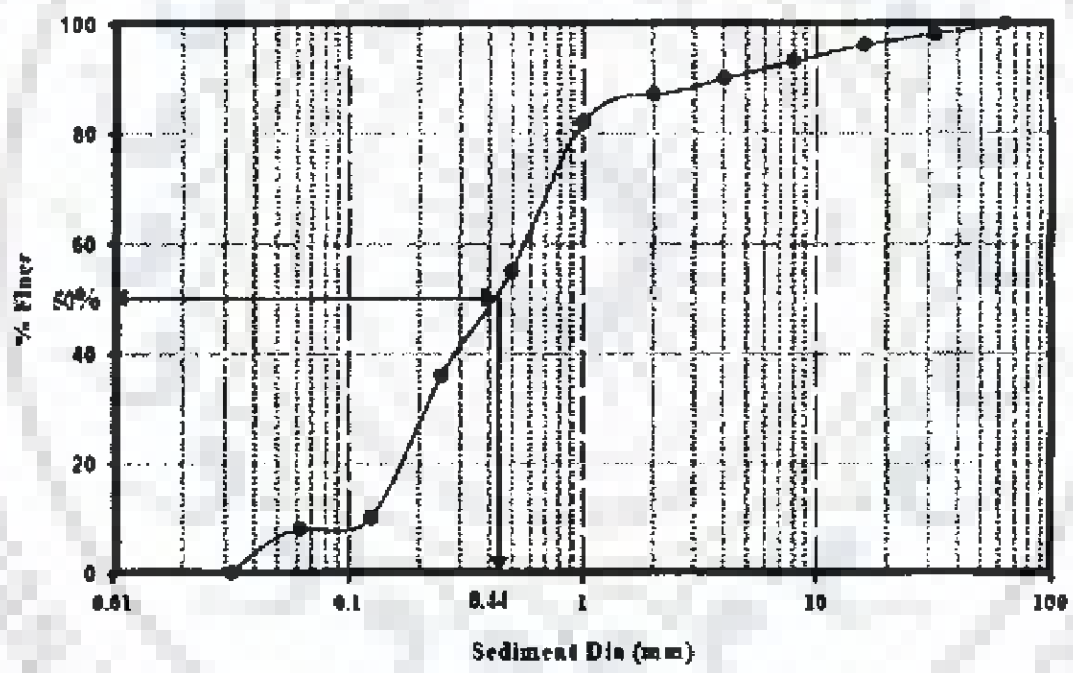

Figure 8.10 Representative bed gradations at Palasbari

8.5 SUMMARY

In this chapter, input data for simulating the flow field in Brahmaputra River braided stretch have been pre-processed and designed suitably to make them mathematically compatible with the developed numerical model. The river geometry of the study stretch is reproduced mathematically using the available observed field cross-sectional data for the year 1997. Bed interpolation has been done mathematically to determine bed elevation at each grid point of the generated mesh for the study flow domain, which is otherwise, impossible to acquire from the field for grid points with such fine grid spacing in both stream-wise and transverse directions.

CHAPTER-9

EVALUATION OF THE DEVELOPED NUMERICAL MODEL

9.1 GENERAL

In this chapter of the thesis, the developed two dimensional enhanced depth averaged model with incorporated modified dispersion stresses tensor as source term in transport equations is used for simulating the flow field in curved flow domain of a laboratory flume. The work utilizes dispersion stress tensor, as developed in Chapter 4 and 5 of this thesis. The proposed model uses boundary fitted non-orthogonal curvilinear coordinate system with irregular boundaries. For numerical solution procedure, the finite volume method with the *SIMPLEC* algorithm and Rhie and Chow's momentum interpolation technique on non-staggered grid is adopted. The details of numerical model development are elaborated in Chapter 6 and 7. The governing equations presented in Chapter 5, are discretized using the finite volume method in curvilinear, non-staggered grid.

For model verification, an experimental flume data with channel contraction was used. The comparison of the simulated velocity field and water surface elevation with new dispersion stress tensor indicated that the incorporation of modified dispersion stress term has the potential for simulating the flow field.

9.2 EXPERIMENT

For validation of the numerical scheme, experimental data were collected in the *Hydraulic Lab.* of *CED, I.I.T. Roorkee* (Figure 9.1a and 9.1b). An experimental rectangular flume of test section 0.15 m and 4.25 meter length and 0.20m deep, was used. The side wall and bottom wall was made of fiber-glass with thin layer of uniform sand sprinkled (D_{50}=0.44mm) at the bed to artificially create roughness. To model the curved bank-lines with opposite sinuosity, a transition of 0.25m was provided at middle with sharp bend for 0.08 meter followed by mild expansion for 0.17m. The schematic line diagram of the experimental setup is shown in Figure 9.2.

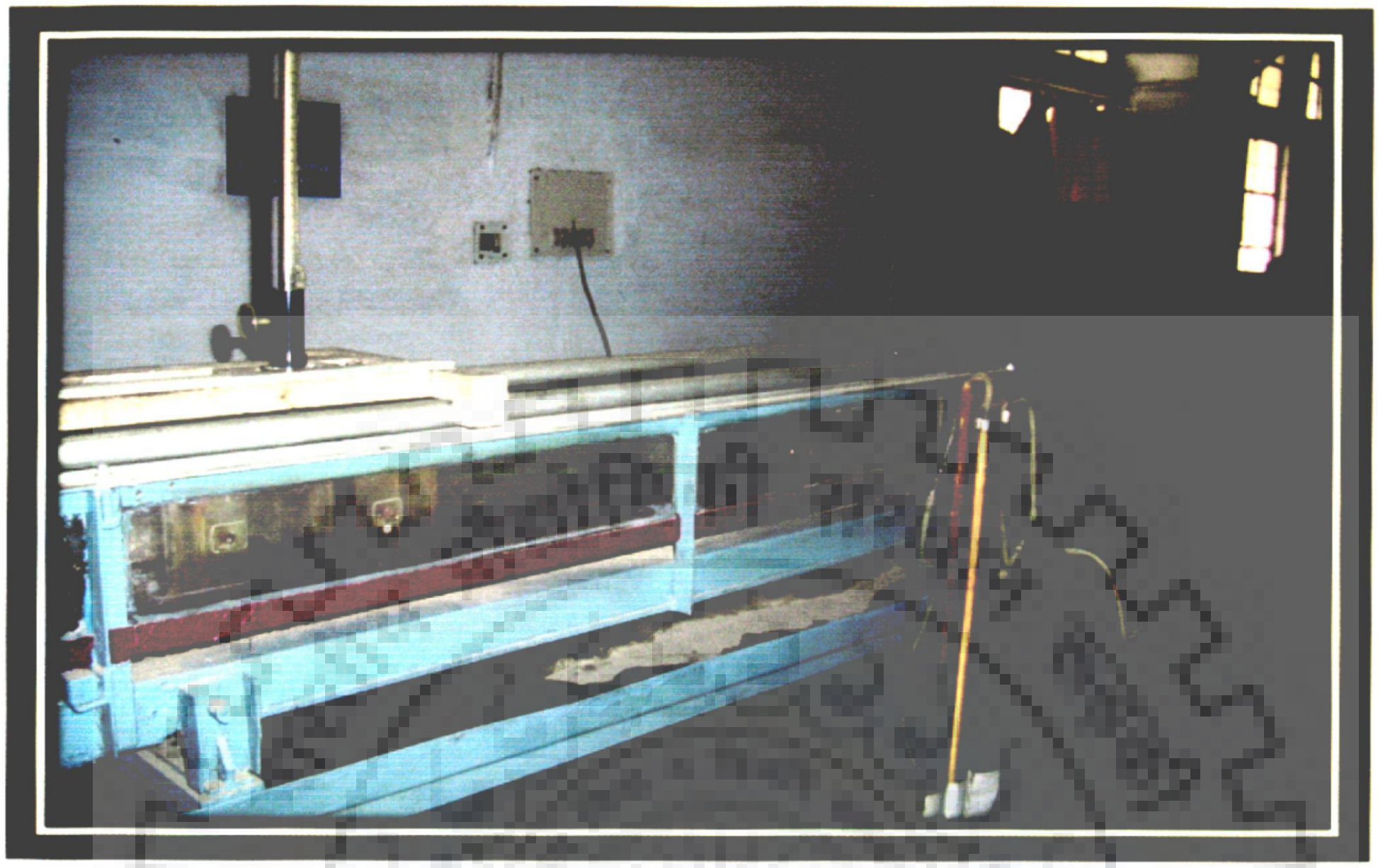

Figure 9.1a Photograph of experimental setup in Hydraulic Lab. *CED* I.I.T. Roorkee

Figure 9.1b Photograph of experimental setup showing flow contraction and inlet

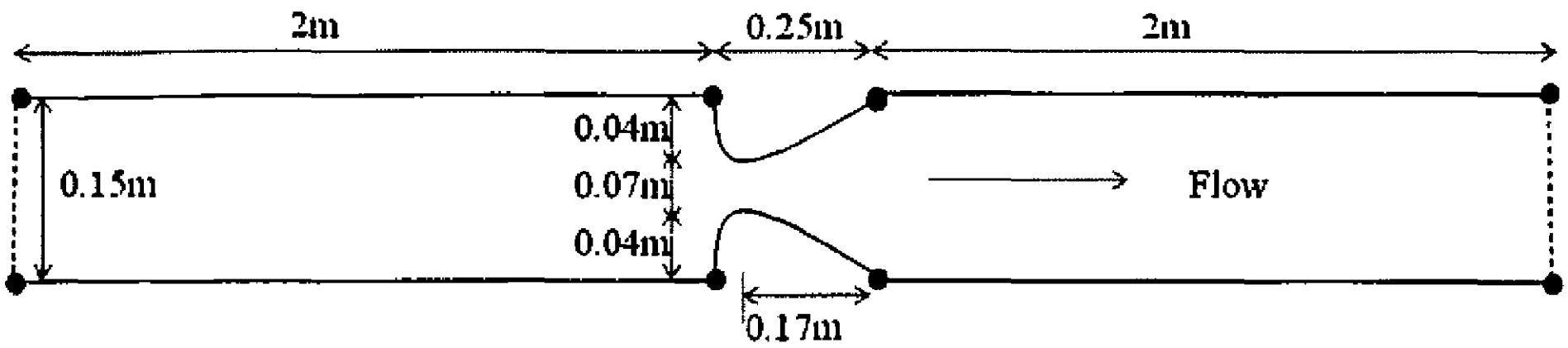

Figure 9.2 Schematic line diagram of experimental setup

Upstream boundary and downstream boundary nodes are kept 2 meters away from the transition boundary to minimize the effect of boundary disturbances on the channel transition part. The bed slope of the channel is kept (1/400). The water is dropped through a galvanized pipe of 102 mm external diameter in the inlet tank. Flow strengtheners in the form of vertical metallic plates of about 6 cm long are placed parallel to channel after the inlet point of channel. A movable carriage with pointer gauge (least count= 1mm) is mounted in the pipe rail. Rail has been fixed at the entire length of channel. A mechanical tailgate is also provided at the end of the channel to control the flow discharge and flow characteristics. Discharge is measured using venturi-meter (Specification: pipe diameter 38 mm, throat diameter 19mm, discharge coefficient(C_D) as 0.98 (pre-calibrated)). Water is released into the channel for sometimes with tailgate partially open (to ensure lowered shear Reynolds Number to avoid incipient motion condition in order to maintain channel bed undisturbed). At the transition, flow changes occur. Tail gate is lowered down gradually to a sufficient level in order to reduce the flow considerably to completely diminish the hydraulic jump formation at the downstream of the transition and thus ensuring full sub-critical (Froude Number(F) <1) flow all along the channel.

9.2.1 RESULTS

The constant discharge is maintained for sometimes to ensure full development of flow with steadiness. Then, the measurements were taken from venturi-meter reading for measuring discharge. Through pointer gauge average water level is measured at regular intervals from upstream nodes to downstream node. The measured discharge computed with venturi-meter formula was 0.001907 cumecs. Measured water levels at the inlet, out let, and at lowest water level were 7.86 cm (water depth=6.79 cm), 6.9

cm(water depth=6.9 cm), 6.69 cm(water depth 6.16cm) keeping the outlet bed level as zero reference (Figure 9.4). (Measured experimental data attached as Appendix-VII)

9.3 MODEL SIMULATION

The flow domain is discretized into structured curvilinear mesh of 16×426 (6816) nodes and 6375 cells (Figure 9.3). Non-staggered grid is used for the finite volume solver. All the state variables (Cartesian velocities, water depths) are computed at the geometric center of each cell control volume. The time step is controlled using *Courant–Friedriche–Lewy (CFL)* condition in order to ensure stability in view of adopted *SIMPLEC* algorithm. While simulating steady flow, calculation is repeated for a number of time steps until solution converges. Convergence criteria adopted was that maximum incremental water depth at the last iteration will be lesser then 0.001 m. Furthermore, mass residual is also computed while solving the momentum equations, iteratively. As the water depth at the inlet is not known priory so initially it is guessed and computation is performed. The water depth is updated at each time step through extrapolating it from internal cell water depth. Computation is iterated until convergence.

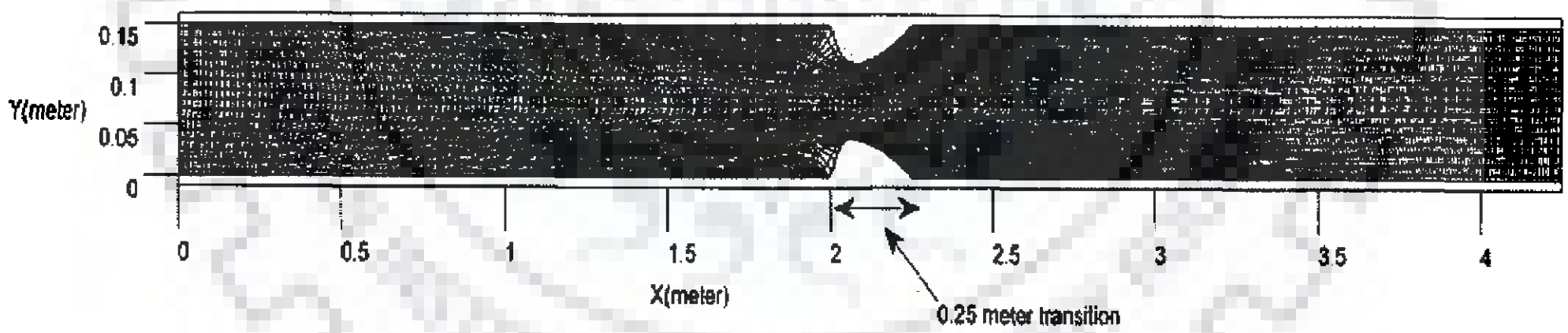

Figure 9.3 Constructed mesh for numerical simulation in the laboratory flume

Flow simulation was conducted for the flume with models without dispersion, with modified dispersion stress terms (derived in Chapter 4 of this thesis) and with dispersion stress terms suggested by Duan (2004) into the momentum transport equations. These flow simulations are designated as ***Case-1*** and ***Case-2*** and ***Case-3*** respectively. In ***Case-3***, value of C in Duan(2004)'s expression (dealt at detail in Chapter 4 of this thesis) for computing D^c_{xy} was kept as unity. Results were analyzed for the whole flow domain with special attention to the transition zone of the flume. The computed discharge after the simulation at the down-stream was 0.001902

(Percentage Error 0.259) and almost same in all *cases*. (Detail model results:Appendix-VII).

9.3.1 COMPARISON OF SIMULATED WITH OBSERVED WATER LEVELS FOR THREE CASES

The comparison of water level with observed water levels is presented in Figures 9.4 and 9.5 and corresponding contour plot of water surface elevations in ***Case-1*** and ***Case-2*** is presented in Figure 9.6. The statistical results for all three *cases* are presented in Table 9.1. Standard error estimators were appropriately chosen to assess the degree of match of computed water levels with observed one. Forty six data points were chosen to show the agreement between simulated and observed values. Statistical parameters demonstrated, suggest that ***Case*-2** has statistically closer and exhibit better accuracy of prediction with observed data than ***Case*-1** and ***Case*-3**.

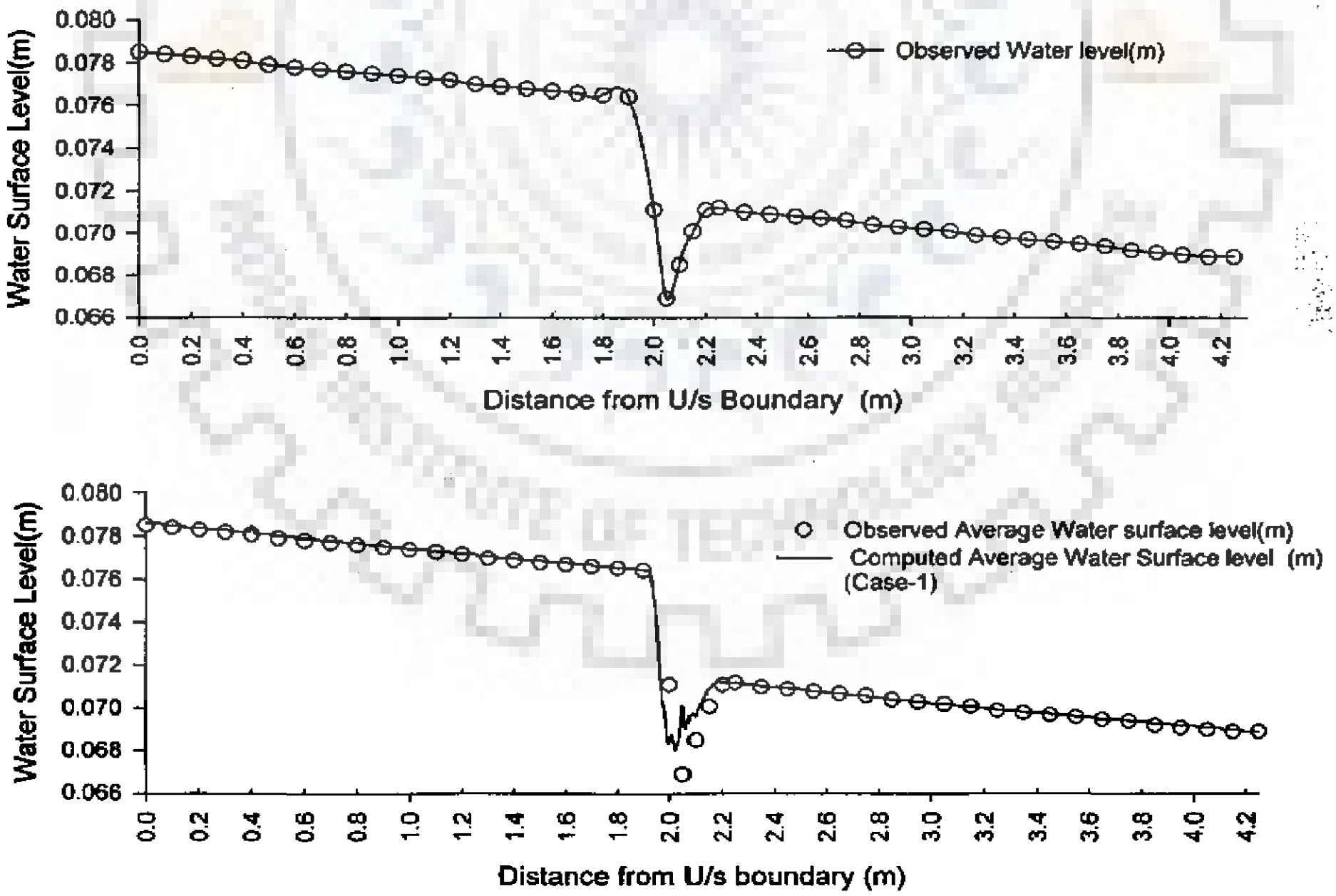

Figure 9.4 Plot of observed *WSL* and comparison plot for computed *WSL* (***Case-1)***

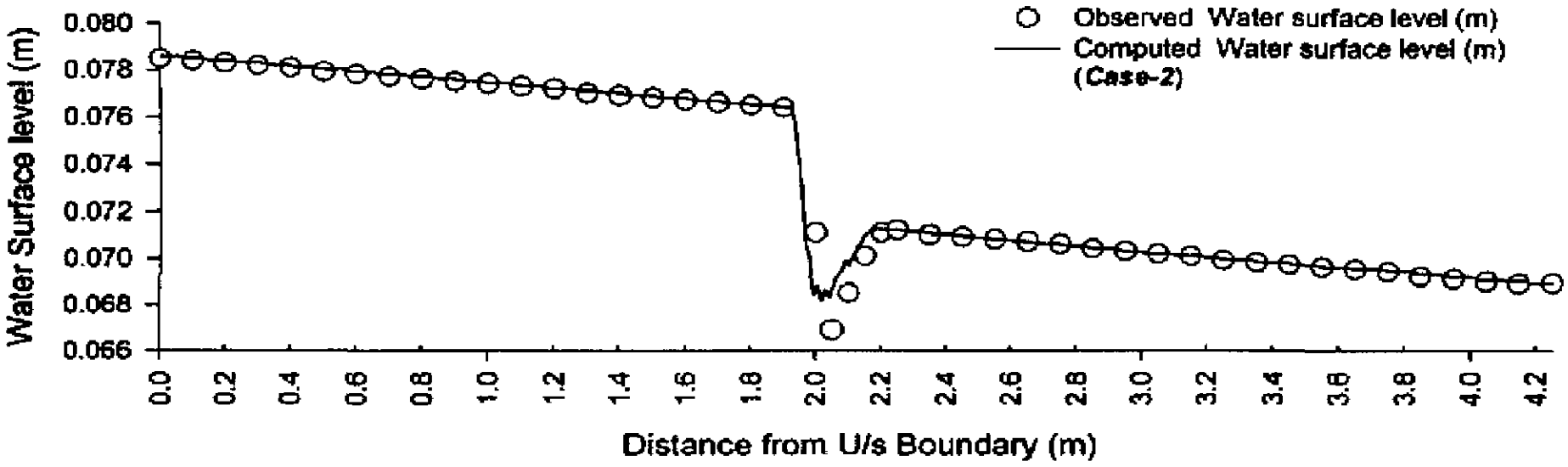

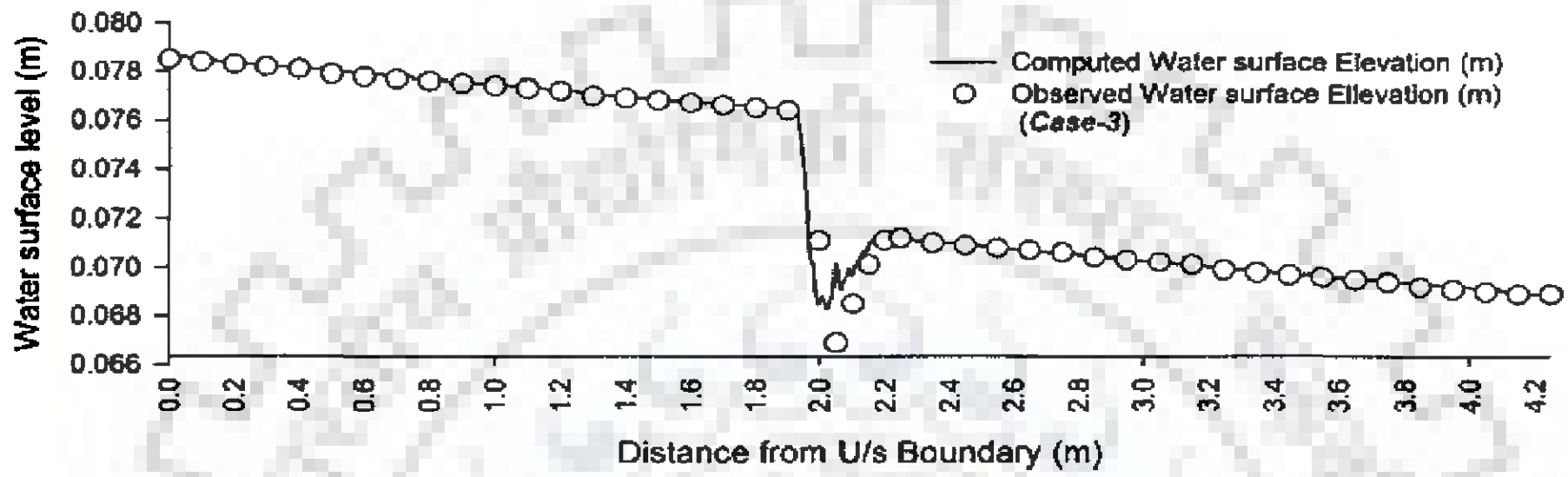

Figure 9.5 Comparison plot for computed *WSL* for ***Case-2*** and ***Case-3***

Table 9.1 Statistical tests for computed and observed data points

S No.	Statistical Parameters Estimation	Computed Vs Observed Water Level			
		Without Dispersion (*Case*-1)	With modified Dispersion (*Case*-2)	With Dispersion (Duan,2004) (*Case*-3)	
1	Correlation Coefficient	0.988	0.991	0.986	No. of data points=46
2	Standard Error	0.00059	0.000520	0.000523	
3	R- Square	0.976	0.999	0.972	
4	F-Test	0.903	0.967	0.928	

The simulated velocity flow field has also been compared statistically to examine to assess the flow field (U_x and U_y) improvement (Table 9.2).

9.3.2 COMPARISON OF FLOW FIELD IN THREE CASES

The correlation and variability of the velocity flow field for ***Case*-2** and ***Case*-3** were computed and with respect to velocity matrices of ***Case*-1** and are shown in Table 9.2.

The vector plot of ***Case-2*** is shown in Figure 9.7. Vector plot for stream-wise velocities and transverse velocities at transition are Figures 9.8a, 9.8b and 9.8c. Correlation coefficient for U_x-matrix is more than U_y-matrix indicating that U_y field has registered a change while including dispersion terms into the governing momentum equations. It is supported by the values of standard error. It also implies that improvement in the flow field is more evident in ***Case*-2** than ***Case*-3**.

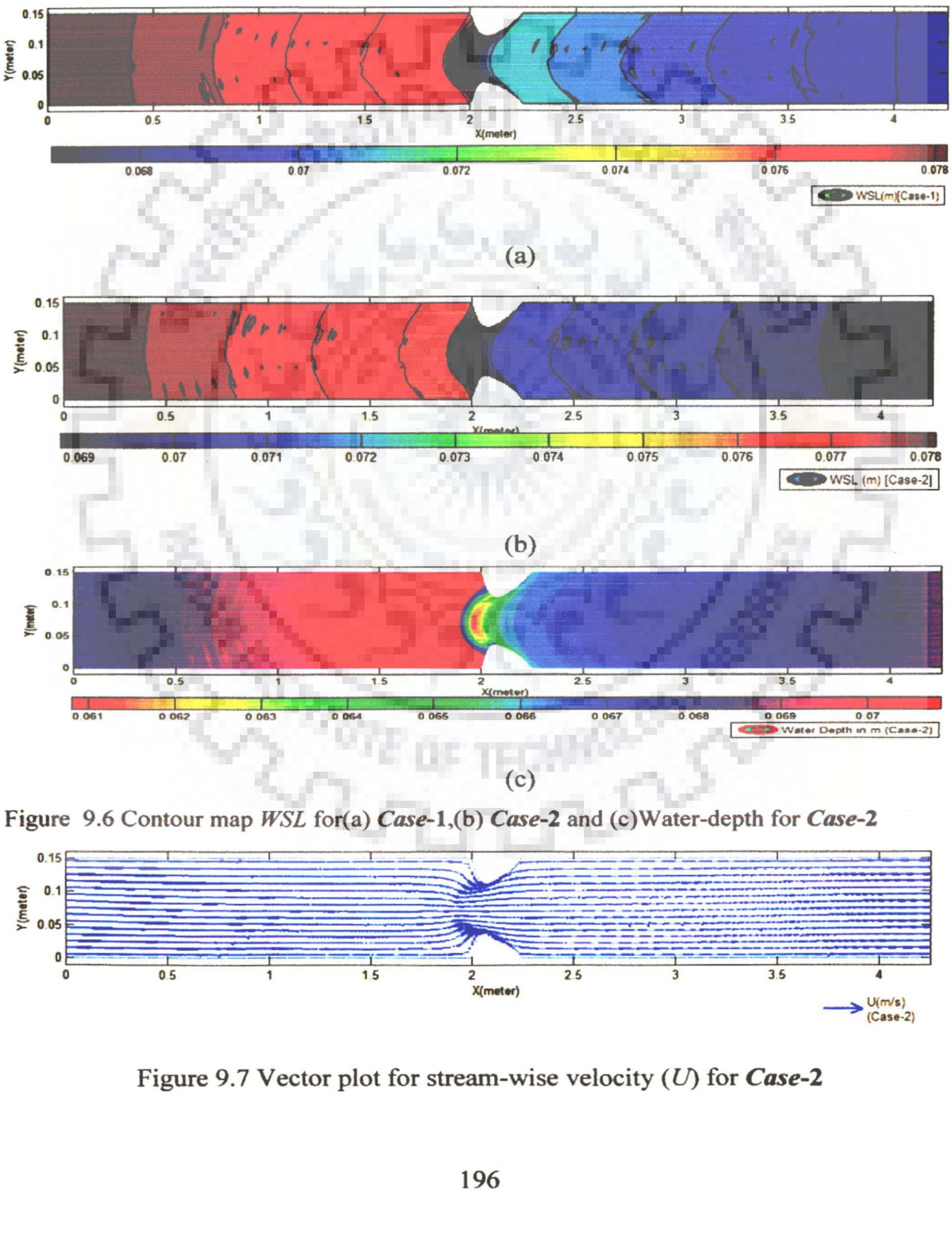

Figure 9.6 Contour map *WSL* for(a) ***Case*-1**,(b) ***Case*-2** and (c)Water-depth for ***Case*-2**

Figure 9.7 Vector plot for stream-wise velocity (U) for ***Case*-2**

Table 9.2 Statistical parameters estimation for velocities for ***Case*-2** and ***Case*-3** with respect to ***Case*-1**

		***Case*-1** vs. ***Case*-2**		***Case*-1** vs. ***Case*-3**		
S. No.	Statistical Parameters	Ux -Matrix	Uy-Matrix	Ux -Matrix	Uy-Matrix	No. of Data points
1	Correlation Coefficient	0.9992	0.9878	0.99946	0.9873	15×425 (6375)
2	Standard Error	0.0016	0.00214	0.0012	0.0023	

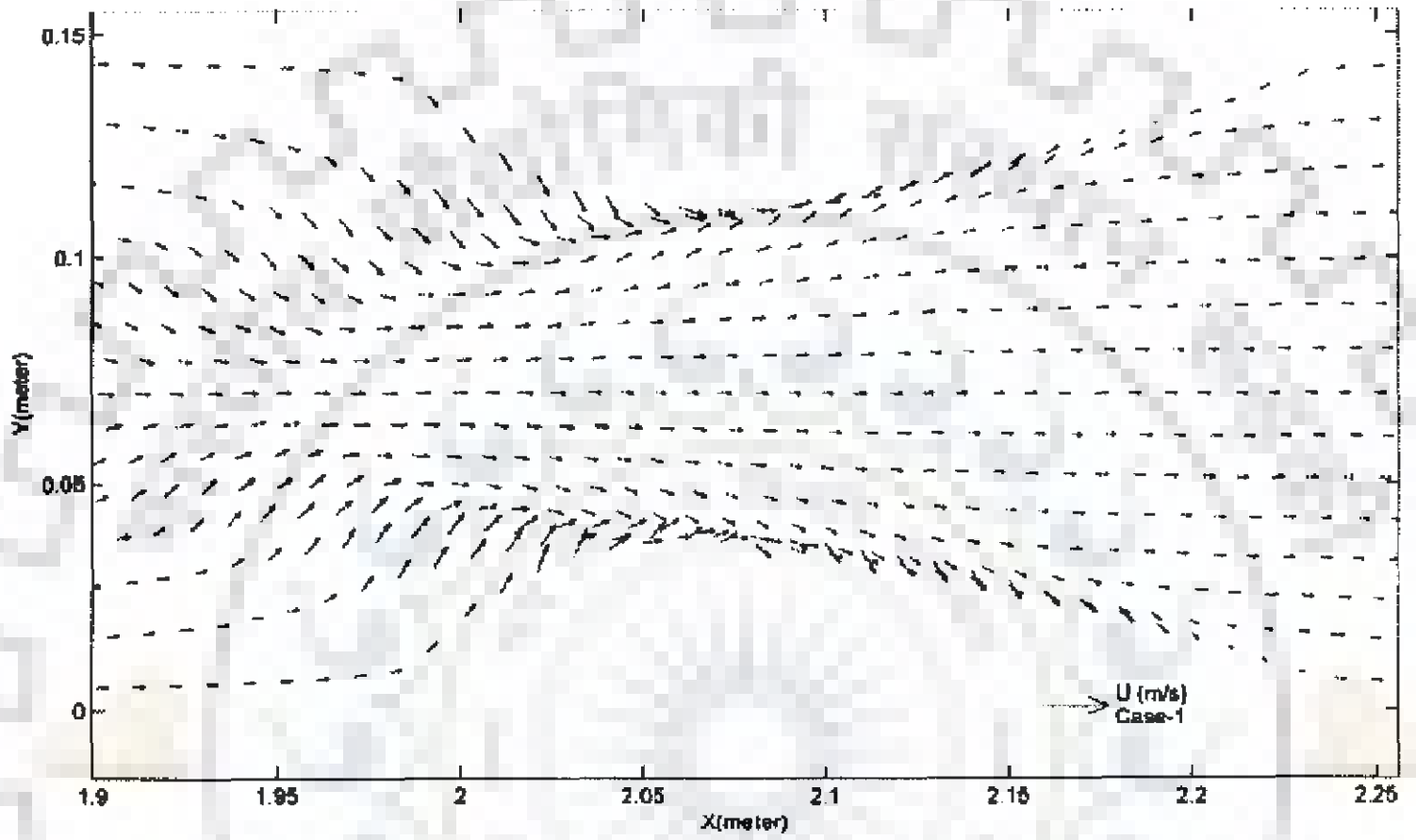

Figure 9.8a Vector plot of stream-wise velocity (U) in transition for ***Case*-1**

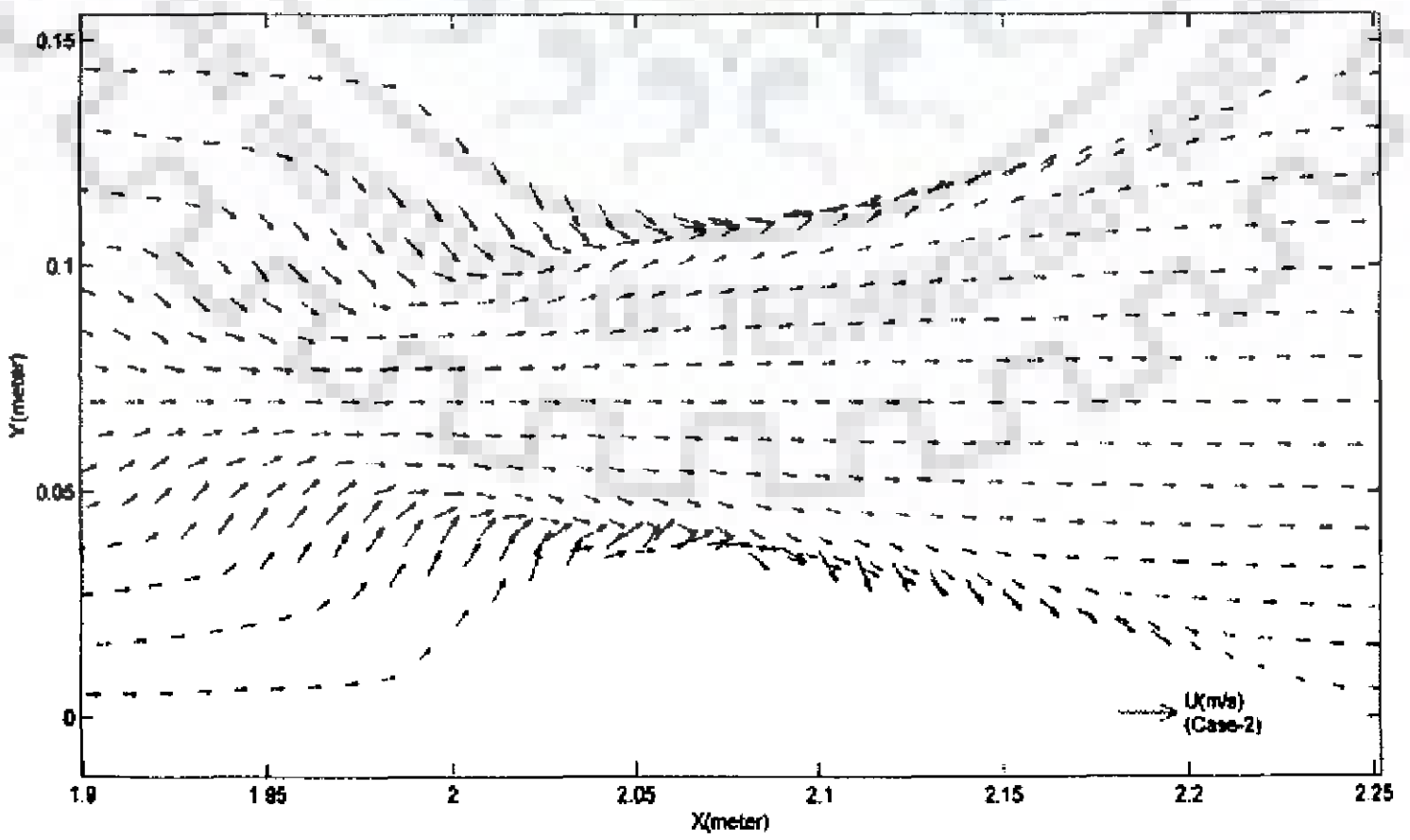

Figure 9.8b Vector plot of stream-wise velocity (U) in transition for ***Case*-2**

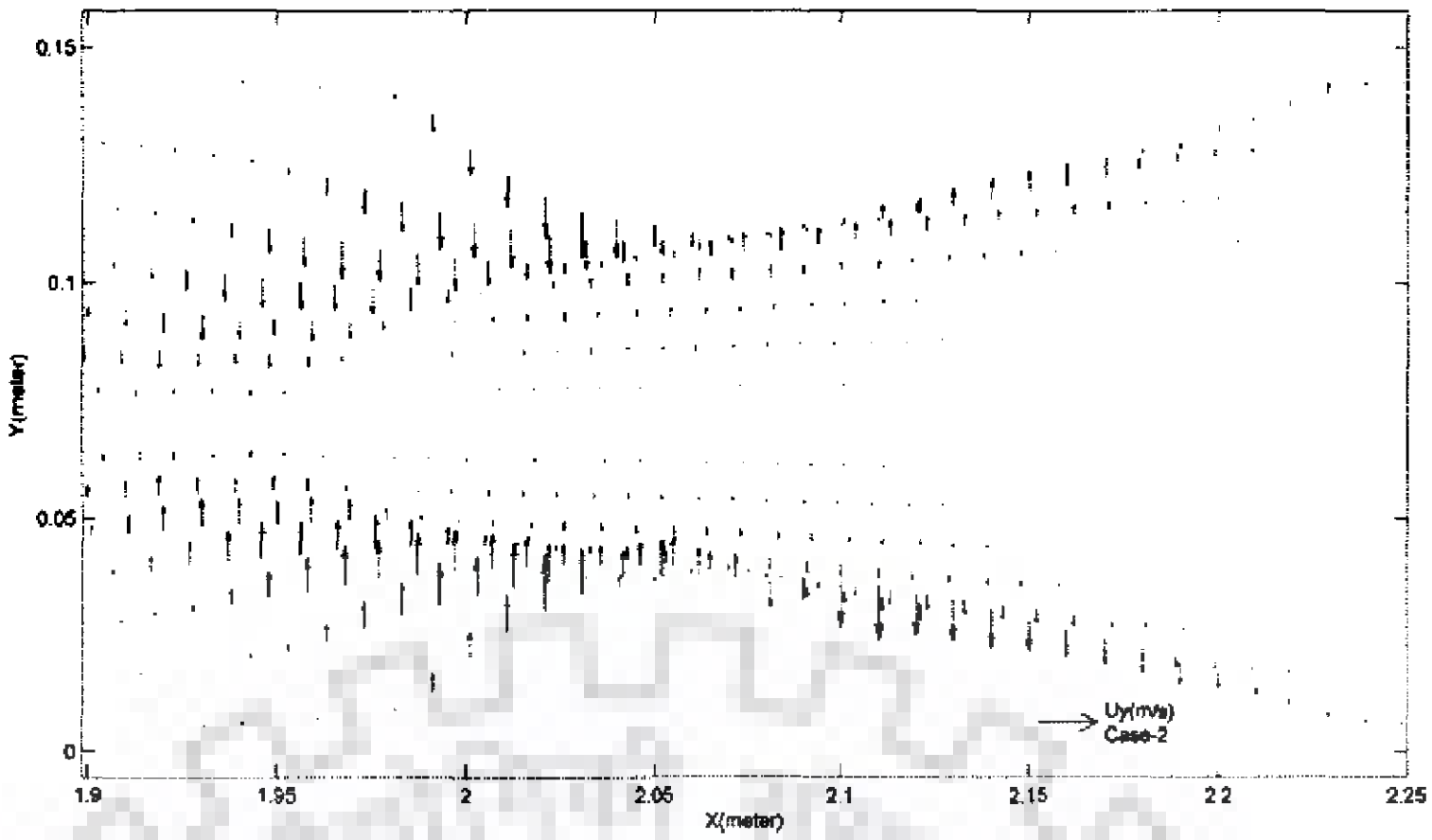

Figure 9.8c Vector plot of transverse velocity (U_y) in transition for ***Case-2***

The computed flow field at computational grid nodes in η-direction (transverse direction) is averaged and *mean* (μ), *standard deviation* (σ) were computed for U_x and U_y for ***Case-1***, ***Case-2*** and ***Case-3*** respectively. It is plotted against longitudinal distance from U/s boundary (Figures 9.9a and 9.9b). The *mean* velocities and its variations, are though close-valued yet if one looks at the corresponding σ-plot (Figure 9.9b), the variation in U_y is quite high in compare to U_x (For U_x, σ ranges 0.0 to 0.04 whereas U_y, σ ranges from 0 to 0.12). *Standard deviation* registered though similar trend, but have lower values in ***Case-2*** and ***Case-3***.

To elaborate the findings, mutual column-wise co-variances of U_x and U_y for ***Case-2*** and ***Case-3*** with ***Case-1*** were computed for computational cell centers transversely (η-direction) and plotted spatially along the channel (Figure 9.11). Spatial changes in co-variances in case of U_y registered a sharp increase in respect to U_x which is marginal. That amply indicates that, when dispersion terms are included in the 2-D flow model, it considerably affects transverse secondary flow pattern which is also quite a good agreement with the expected results with flow dispersion inclusion into the flow simulation.

The contour plot of velocity variation *i.e.* stream-wise velocity U and secondary flow U_y in ***Case-2*** for transition location is presented for illustration (Fig 9.10a and 9.10b). Velocity flow field for the whole domain is shown in Figure 10c.

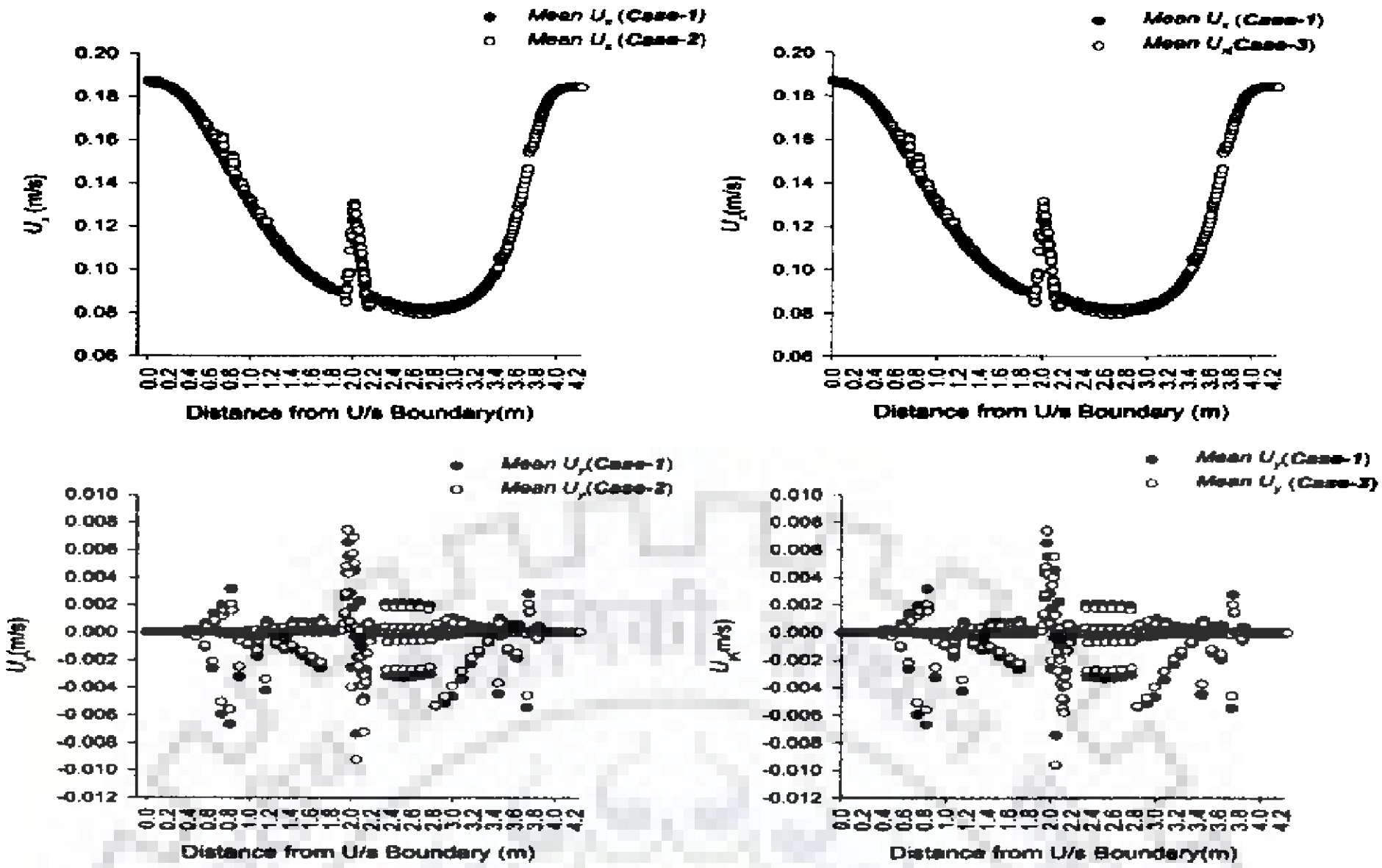

Figure 9.9a Plots for spatial variations of *mean* U_x and U_y for ***Case*-2** and ***Case*-3** with respect to ***Case*-1**

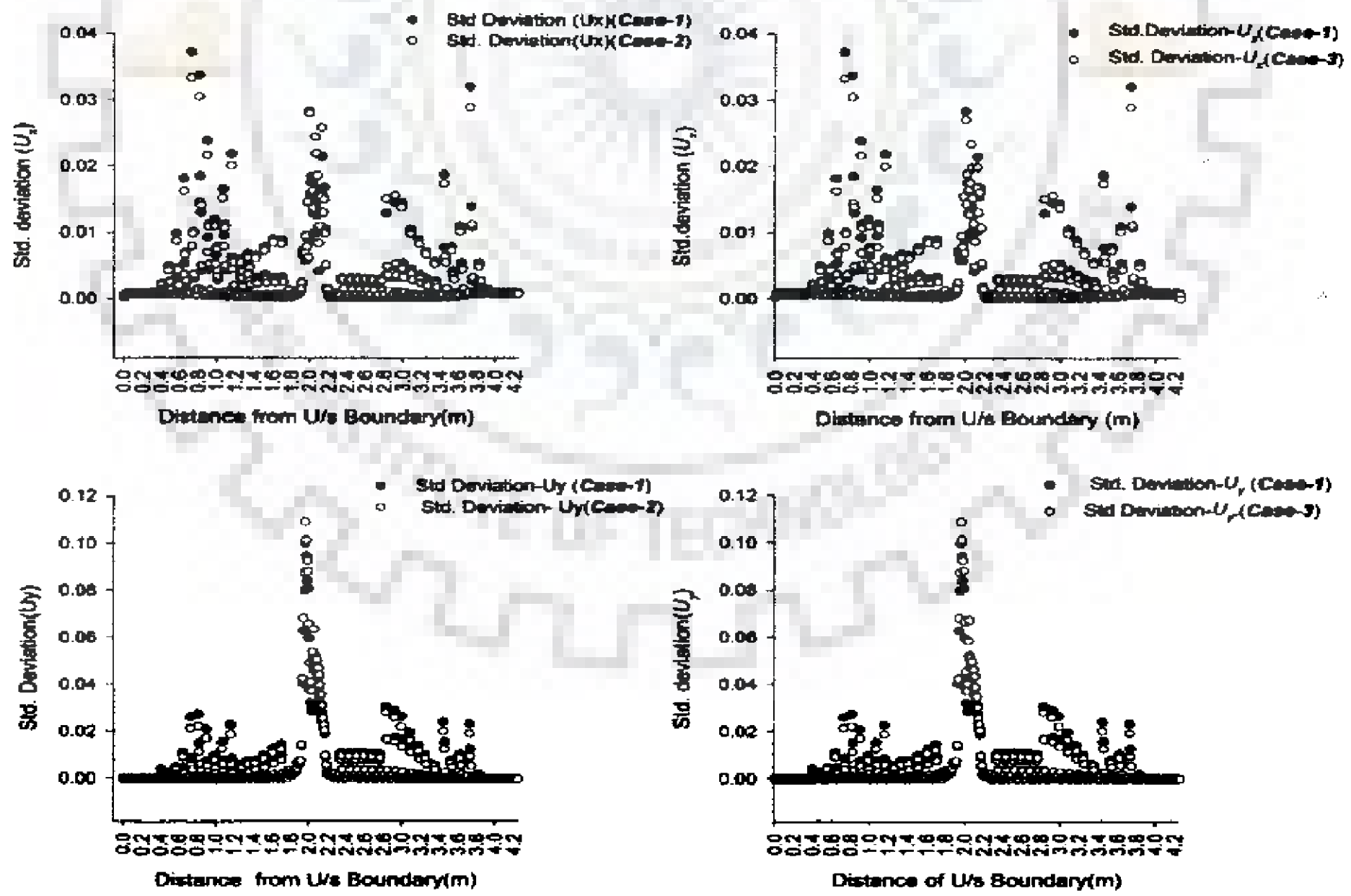

Figure 9.9b Plots for *Standard Deviations* for U_x and U_y for ***Case*-2** and ***Case*-3** with respect to ***Case*-1**

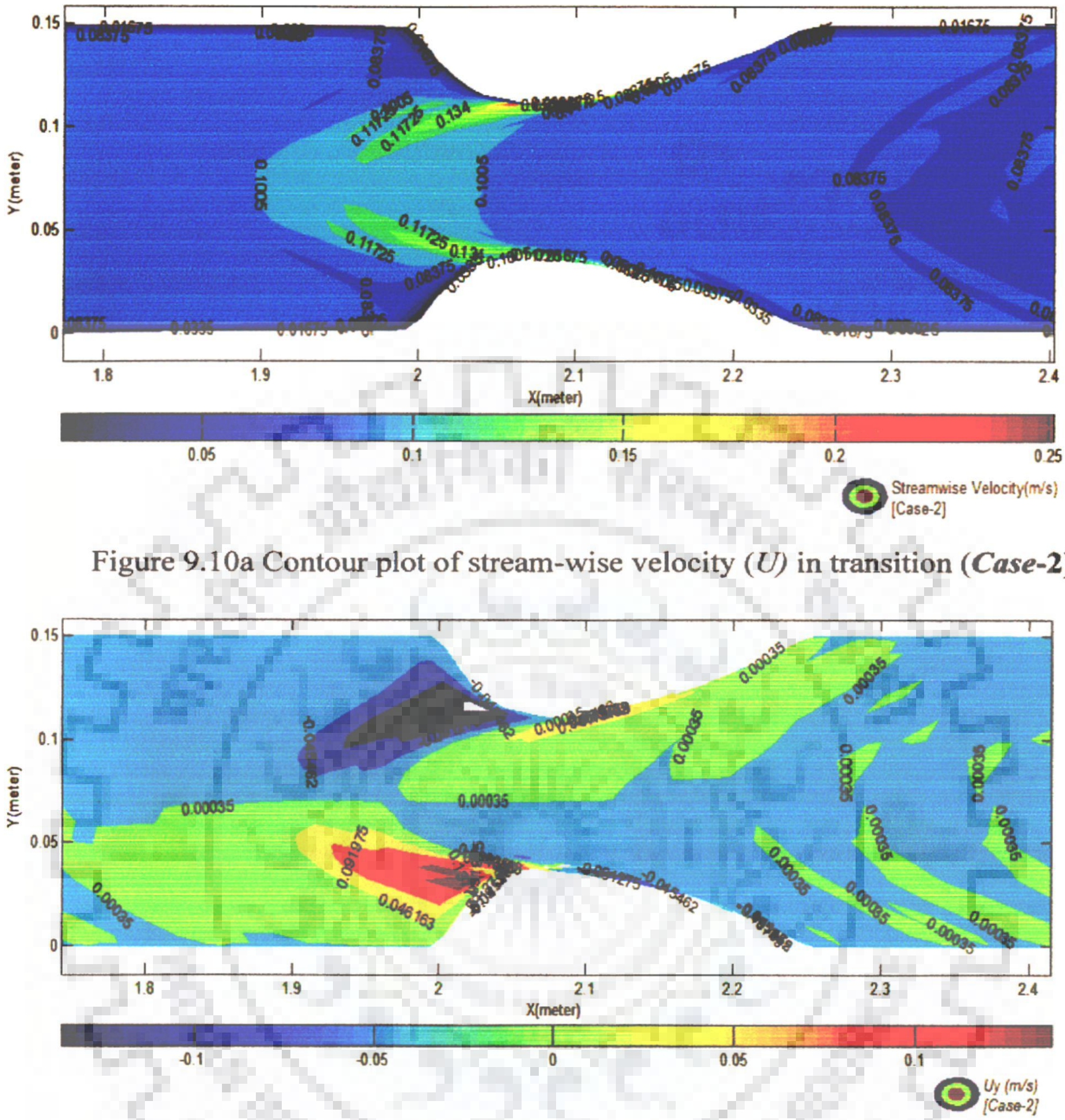

Figure 9.10a Contour plot of stream-wise velocity (*U*) in transition (***Case*-2**)

Figure 9.10b Contour plot of U_y in transition (***Case*-2**)

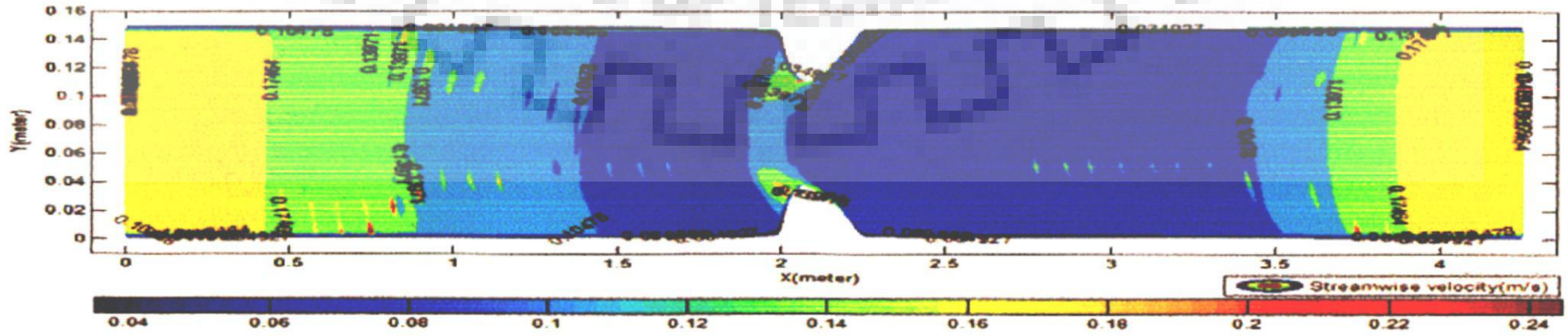

Figure 9.10c Contour plot of *U* for ***Case*-2** for the whole flow domain

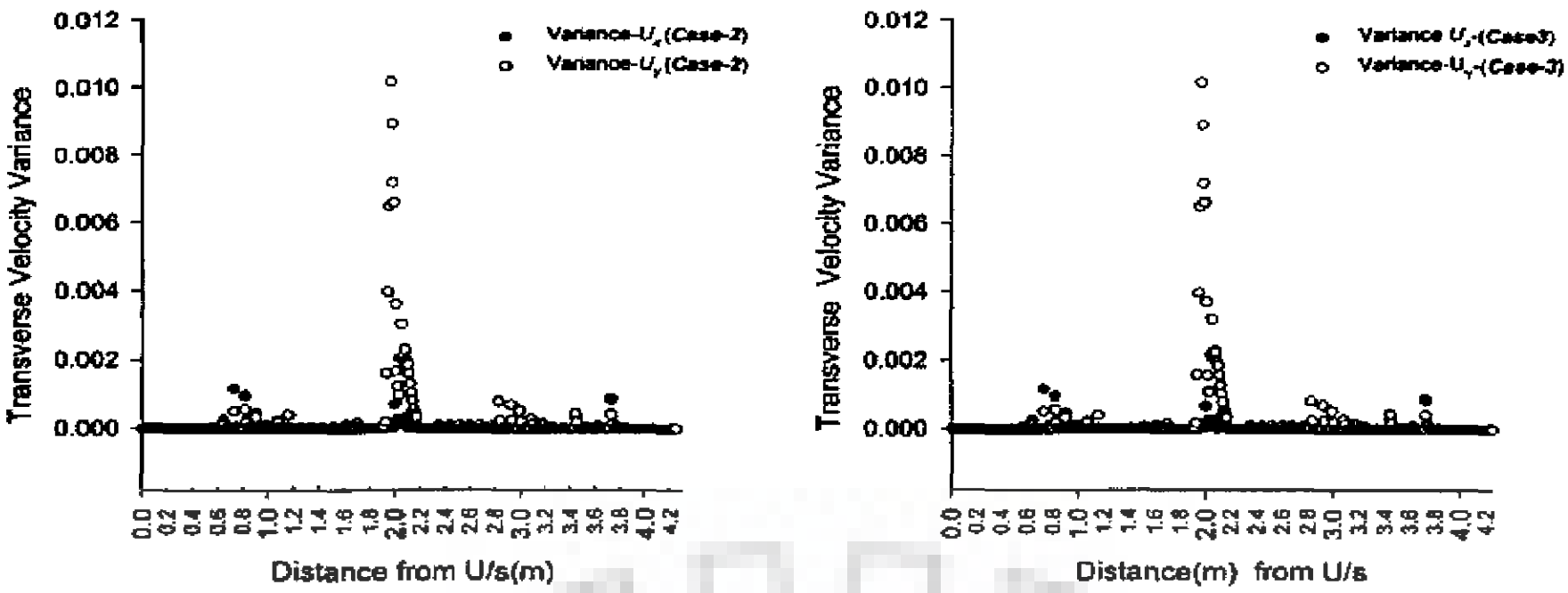

Figure 9.11 Variances of U_x and U_y for ***Case*-2** and ***Case*-3** with ***Case*-1**

9.4 ESTIMATION OF NON-DIMENSIONAL VELOCITY DEVIATION INTENSITIES (I_L and I_T)

To express the shear flow effect by the distribution of the vertical profile, Seo *et al.* (2008) calculated the velocity deviation intensities from their longitudinal and transverse velocity experimental data as follows.

$$I_L = \left(\frac{\frac{1}{h}\int_0^h u_\xi'^2 dz}{U^2} \right) \tag{9.1}$$

$$I_T = \left(\frac{\frac{1}{h}\int_0^h u_\eta'^2 dz}{U^2} \right) \tag{9.2}$$

In Eqs. (9.1) and (9.2), u'_ξ and u'_η =longitudinal and transverse velocity deviations with respect to depth averaged velocities, u_ξ and u_η in ξ and η direction respectively. The values of I_L and I_T were computed for experimental data by Seo *et al.* (2008). In the presented numerical model, the flow dispersion stress terms are adequately accounted for, into the controlling flow equations, hence I_L and I_T can numerically be

computed and analyzed spatially in-depth for possible explanation of associated physical process in the secondary flow scenario in the curvilinear flow domain.

For the whole flow domain, I_L and I_T are computed for ***Case-2*** for all computational cell centers. From the obtained matrices, for each column (transversely in η-direction), *mean* and *standard deviation* of both variables are computed and plotted spatially (Figure 9.12a) along the channel. The corresponding contour plot of transition location is presented in Figure 9.12b. Analyzing the plot of spatial variation of *mean* longitudinal deviation intensities, I_L (Figure 9.12 a), it can be easily inferred that at transition location it dips and again attains to higher values at the end of the transition to its values before the transition. At the same time, *Standard deviation* of I_L (σ_{IL}) increases at the transition. Interestingly, contrary to the trend of I_L, transverse velocity deviation intensities (I_T) plotted (Figure 9.12b). It can be seen that changes occur with considerable increase in I_T in the transition location, associated spatial variations of *Standard deviations* of I_T (σ_{IT}) also increases more than *Standard deviations* of I_L. σ_{IL} at the channel transition ranges from 0 to 0.005 whereas σ_{IT} at the channel transition ranges from 0 to 0.35. The interpretations of these plots strongly and incisively suggest that while in channel transition, on account of secondary flow dominance; the diffusion process becomes predominant, resulting in more turbulence in the flow.

I_T increases with relatively higher magnitude with high σ_{IT} at the transitions and indicates that significantly large variations in true transverse velocity distribution persists in respect to corresponding depth averaged transverse velocity (As transverse true velocity distribution along the depth is assumed to be linear, (See Chapter 4 of this thesis). It is easily inferred that at curvilinear flow domain, owing to persisting centrifugal forces, generation of vertical vortices occurs which instigates redistribution of the flow concentration along the longitudinal and transverse direction with decrease in convective and increase in diffusive process at the channel transitions. The physical interpretations can further be supported with Figures 9.13a, 9.13b, 9.14a and 9.14b. These plots are presented to show distribution of I_L and I_T and the concentration of D_{xx} (Longitudinal Flow Dispersion Stress Term) and D_{yy} (Transverse Dispersion Stress Term) on the flow domain through contour map.

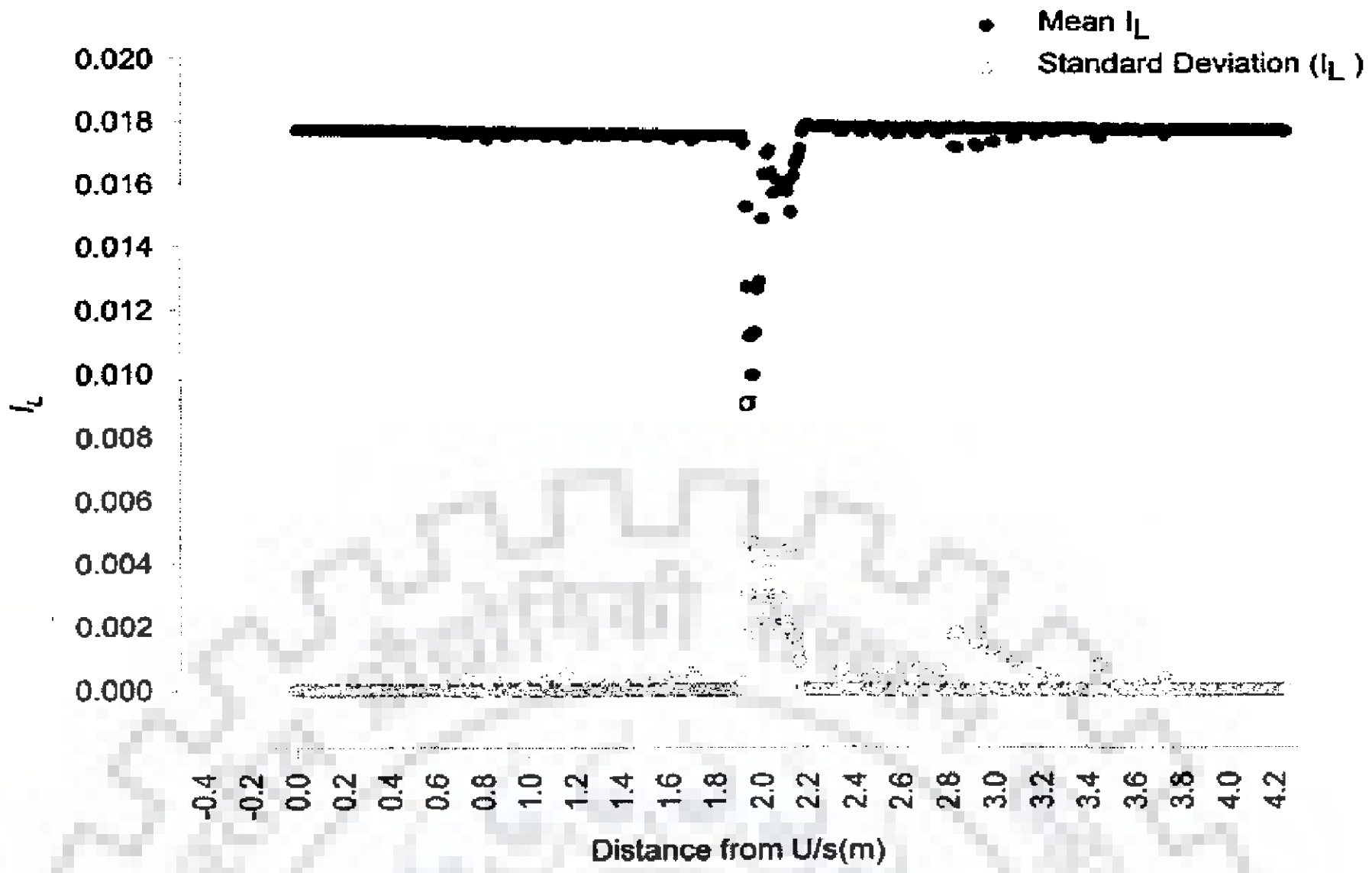

Figure 9.12a Plot of *mean* and *standard deviation* for I_L

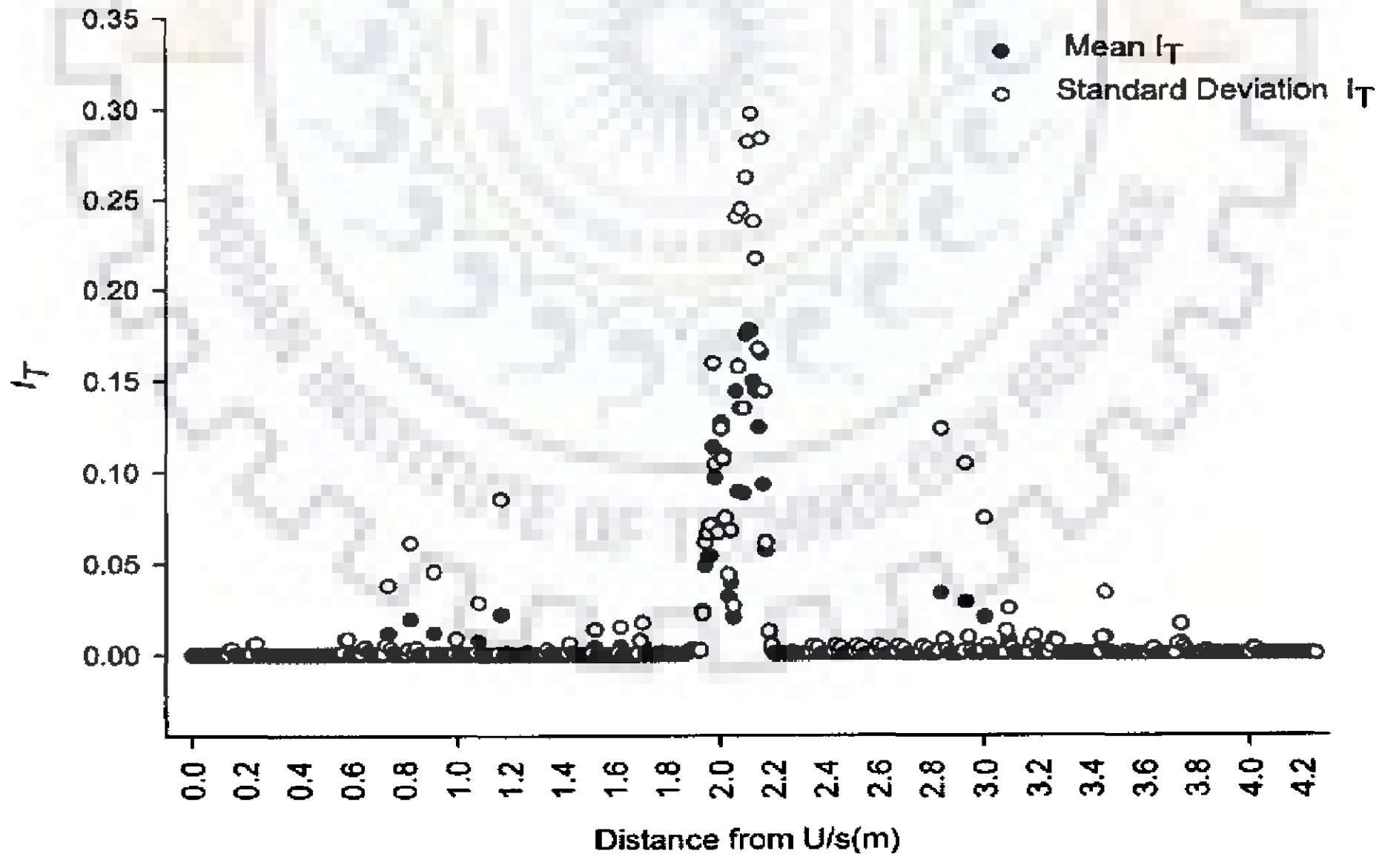

Figure 9.12b Plot of *mean* and *standard deviation* for I_T

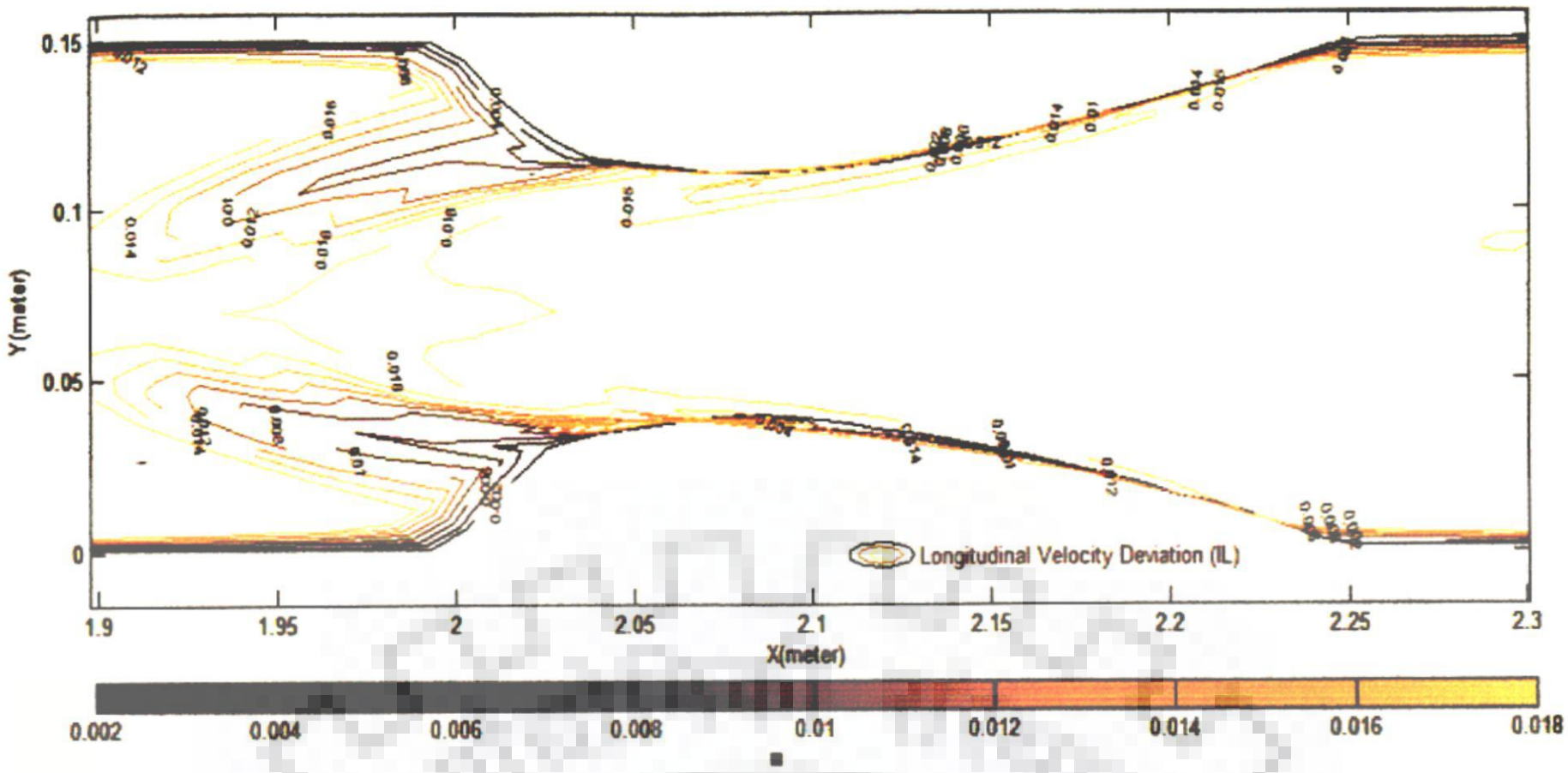

Figure 9.13a Contour plot of I_L at the transition

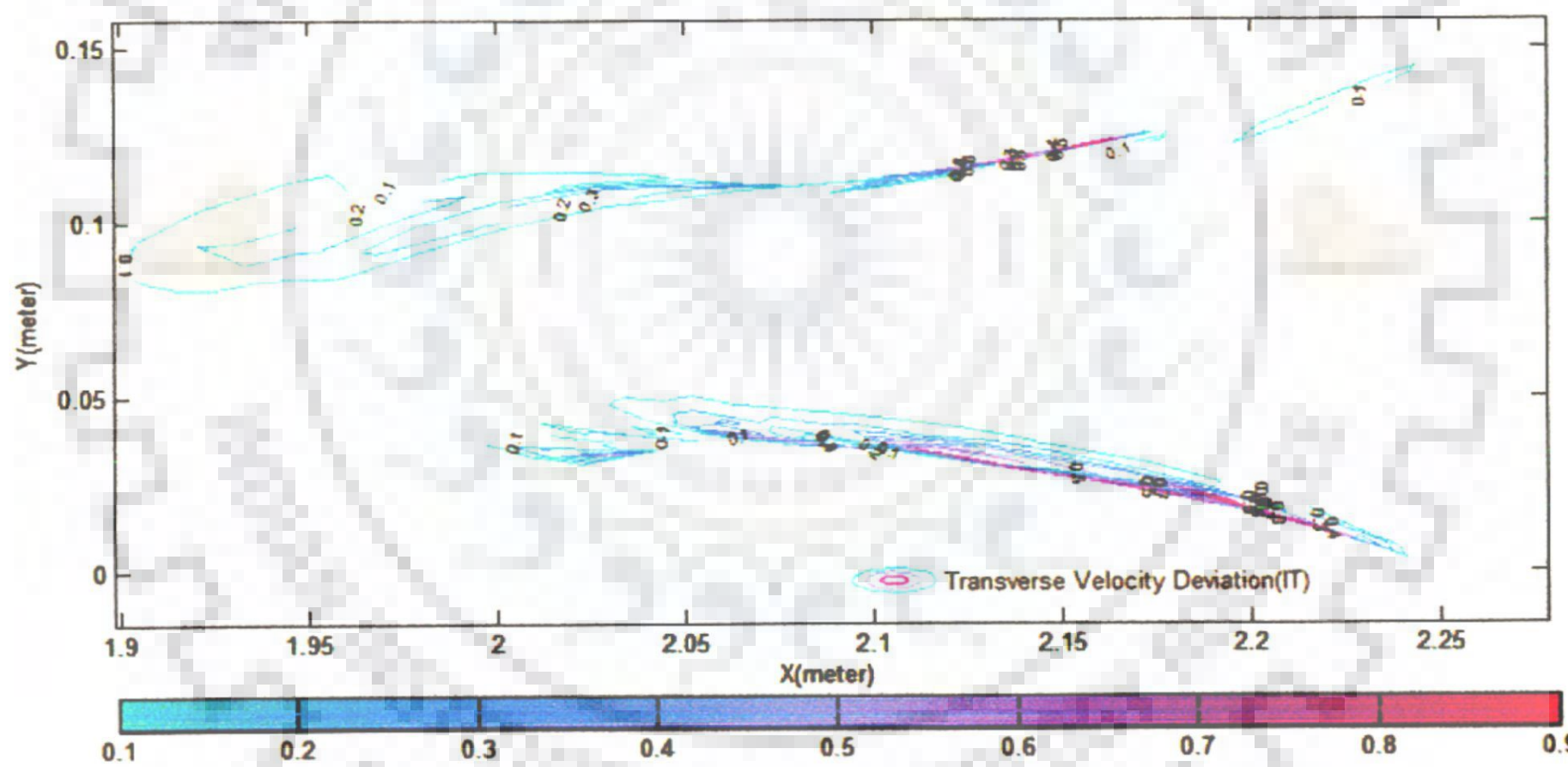

Figure 9.13b Contour plot of I_T at the transition

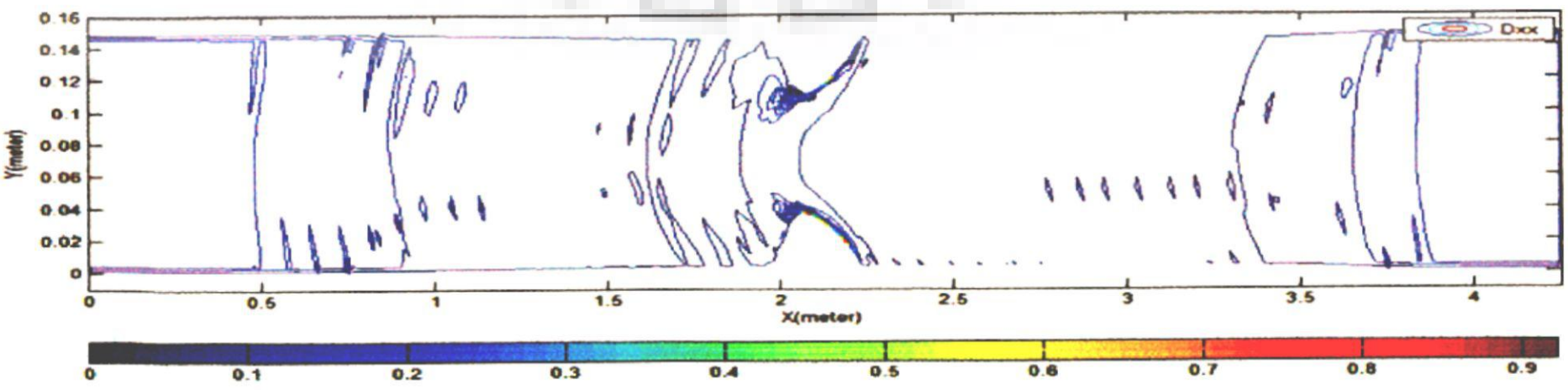

Figure 9.14a Contour plot of D_{xx} (N/m^2) in the whole domain

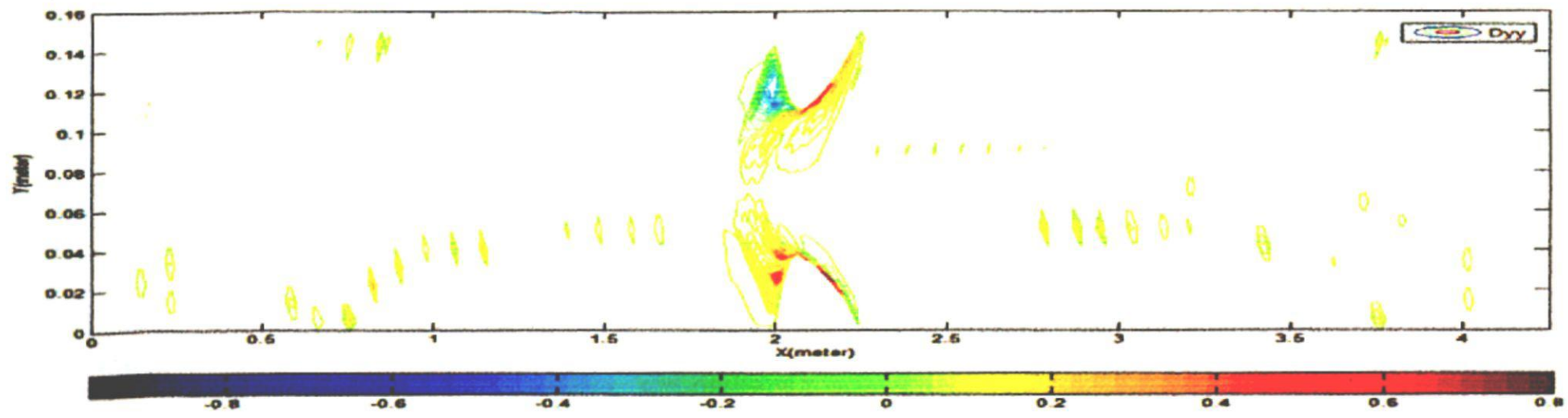

Figure 9.14b Contour plot of D_{yy}(N/m^2) in the whole domain

9.5 CONCLUDING REMARKS

In this chapter, flow simulation was conducted in a laboratory flume with contraction using the developed 2-D flow model. Streamwise and transverse simulated velocities in the flow domain were analyzed along with the simulated water depth at constant discharge of 0.001907 cumecs. The developed 2-D model was verified and evaluated. The flow field using the developed numerical scheme in this thesis indicates that the use of modified dispersion tensor in the governing flow equations leads to better agreement with observed flow variables. Further, it has been observed that flow field simulation using Duan (2004)'s approach is also possible, however the present work indicates the limited potential of the Duan(2004)'s approach in flow field simulation, as compared with the use of the present approach.

****

CHAPTER-10

RESULTS AND ANALYSES OF 2-D FLOW SIMULATION FOR BRAHMAPUTRA RIVER STRETCH

10.1 GENERAL

In this chapter of the thesis, the developed two dimensional enhanced depth averaged model with incorporated modified dispersion stresses tensor as source term in transport equations is used for simulating the flow field in the Brahmaputra River stretch. The work utilizes dispersion stress tensor, as developed in Chapter 4 and 5 of this thesis. The model uses boundary fitted non-orthogonal curvilinear coordinate system with irregular boundaries. The details of numerical model development are discussed in Chapter 6 and 7. The governing equations presented in Chapter 5, are discretized using the finite volume method in curvilinear, non-staggered grid.

As stated earlier in Chapter 8, significant morphological feature of the Brahmaputra River is that it has a number of constricted nodal points where the cross-sections remain unaltered and stable. In addition, the Brahmaputra follows generally uniform aligned channel configuration in the study stretch under consideration. This gives a segment of Brahmaputra separated with well defined nodal points (with stable unbraided channel width) which is adequately suited for applying 2-D developed mathematical model conveniently so far as upstream and downstream boundary implementation is concerned. Still, process representation of fully developed braided stream is challenging due to the presence of numerous 3-D flow structures within the flow domains and difficulty in mathematical reproduction of highly complex river geometry.

Notably, the River Brahmaputra is one of the rivers which are well under the observation of different government agencies. The sediment discharges and flood discharges at certain locations have been continuingly recorded and the river cross sections periodically surveyed. Still, the limitation in the human capacity, instrumentation, the difficulties of the measurement and the risk involved, the actual data acquisition often remain off-set by errors. The importance of the information that

could be derived from the analysis of the data is very high in the design, management and future risk and hazard strategies. Taking in to account the situation as described above, the present study is done to implement a 2-D flow simulation model based on the controlling equations and specified boundaries specially keeping in mind of the flow behavior of River Brahmaputra on chosen study reach. The algorithms established by the researchers /modelers in the literature advocate success of flow simulation model application depends on the size of the data covering diverse patterns of phenomena. More the data sets better is the result's reliability. The study has been carried out for the study domain of the river channel (from Pandu to Jogighopa) - (Approx. 100 km) with 14 numbers of the field measured river cross sections (1997) and hydrological data (Jogighopa-Pandu) for the same year. The details with regard to preprocessing of the data acquired for the model compatible input for the developed model have been described in Chapter 7 of this thesis.

10.2 RESULTS AND DISCUSSIONS

The generated flow domain (primary flood plain with bank full discharge) from satellite imagery and constructed mesh is presented in Figure 10.1. The generated bed elevation with the measured cross-sectional data at predefined locations is shown in Figure 10.2.

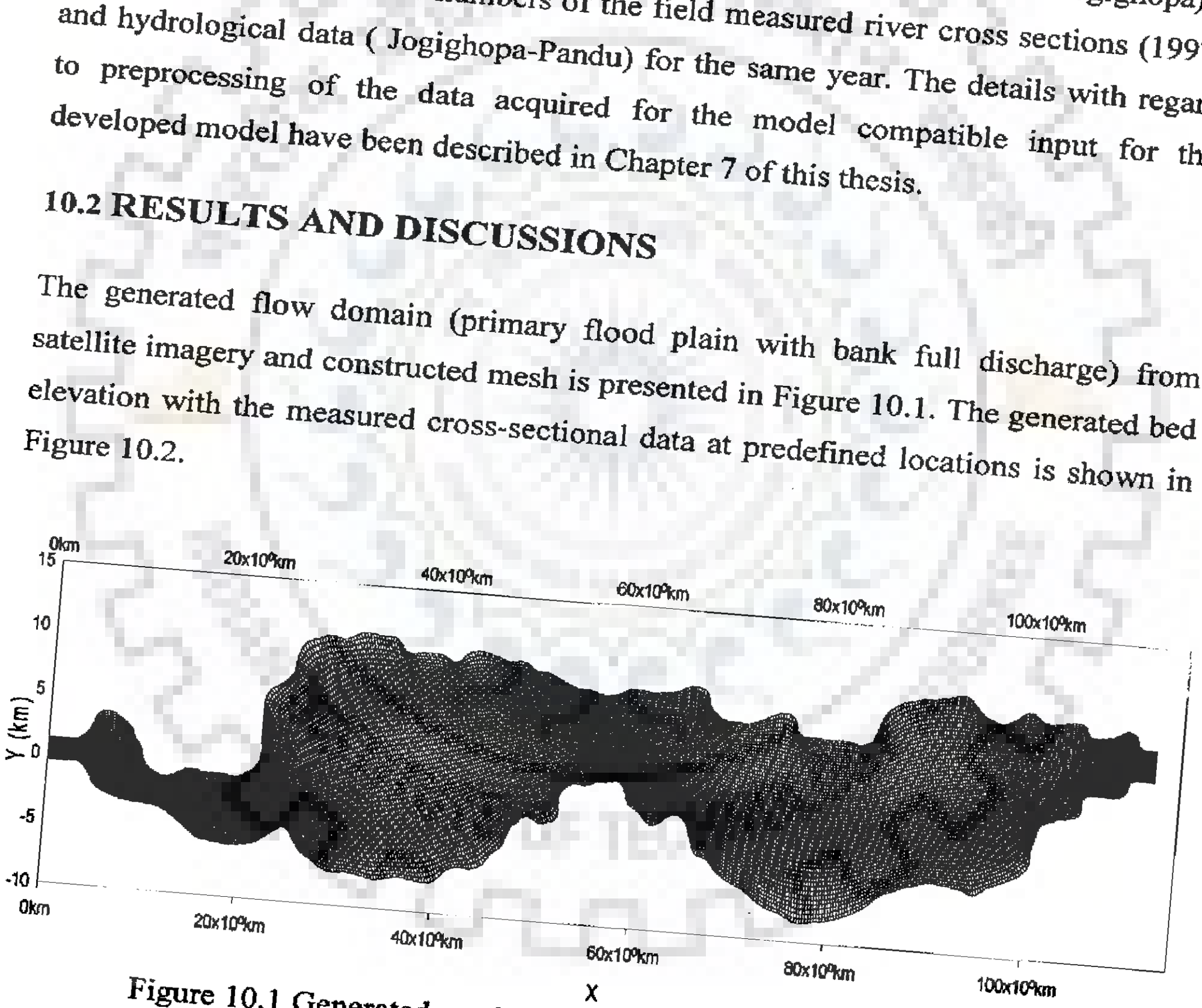

Figure 10.1 Generated mesh for Brahmaputra study river stretch

General outline chart for 2-D model development is presented in Figure 10.3.

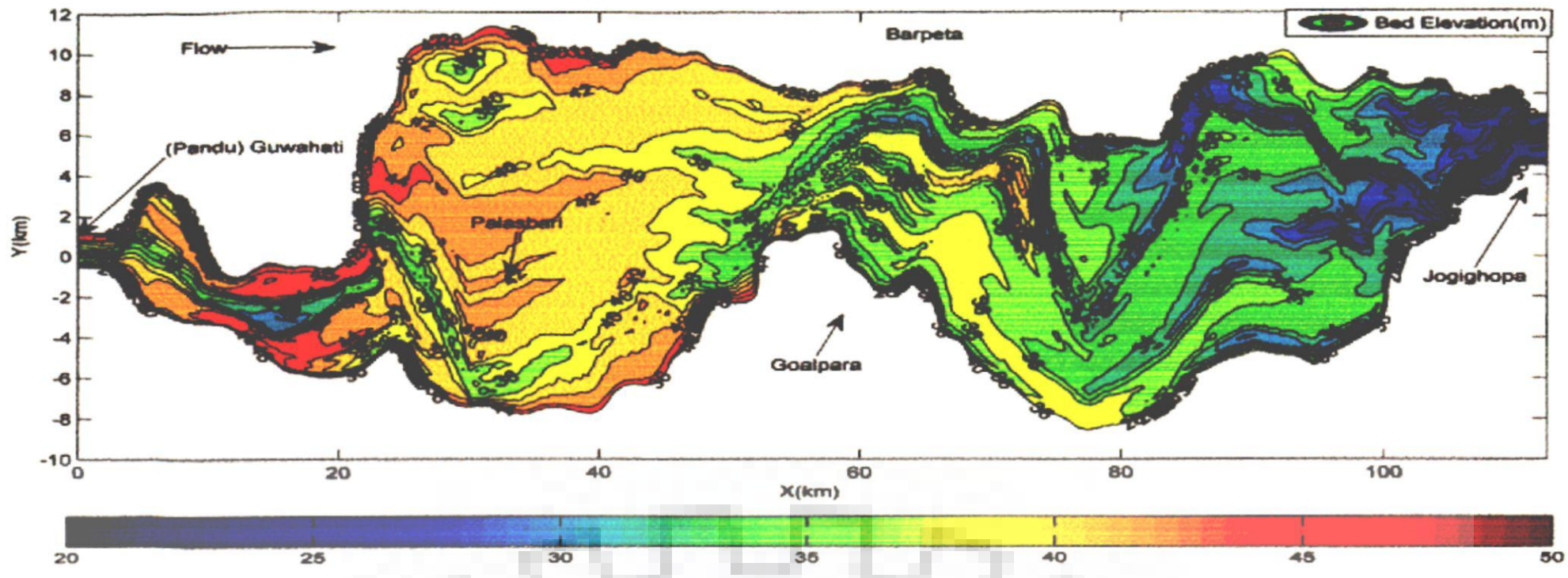

Figure10.2 Generated bed level for Brahmaputra study reach for 1997

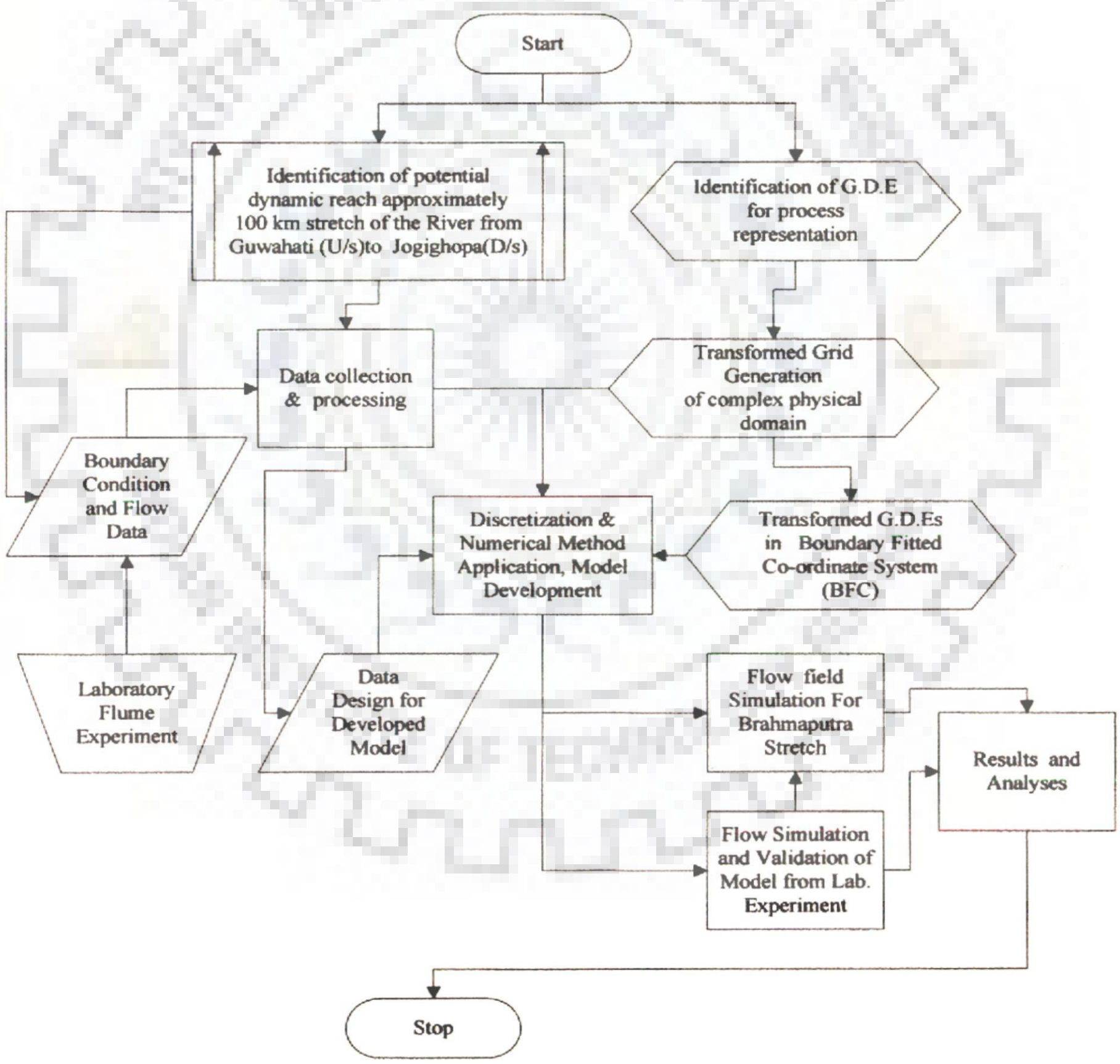

Figure 10.3 General out- line of 2-D flow numerical model development for Brahmaputra study reach

10.2.1 MODEL VALIDATION

Attributes of the study stretch make the Brahmaputra River an ideal example for undertaking the application of the model. At both ends of the reach under study, two important towns are situated namely Guwahati at the upstream end and Goalpara at the downstream end. At these locations, gauge and discharge measurements are made daily by the *Water Resources Department, Govt. of Assam*. The contribution from the tributaries in this stretch forms hardly 0.5 to 1 percent of the main stem peak flow at Pandu (Sharma, 1995). Model verification was done with the help of comparing measured water stages at Pandu site with model simulated water stages. Measured stages at downstream Jogighopa were implemented as downstream boundary condition. Observed discharges were assigned at Pandu as upstream boundary condition and discharge at the downstream boundary were computed from model results as simulated discharges for comparison. 2-D Flow Model was used for 20 discharge *profiles* (designated as *profile*-1 to *profile*-20 respectively) for the flood of 1997 (12th July 1997 to 31st July 1997) and validation results are presented in Figure 10.4 and Table 10.1. It can be seen that the simulated stages are in fair agreement with the measured. Amongst the hydrological data, water level can be considered to be the most reliable primary data with minimum error in comparison to other data. In the above context, the good reproduction of stages is quite encouraging for the enhanced 2-D depth averaged modelling approach considered, for such a highly braided curvilinear stretch of Brahmaputra River.

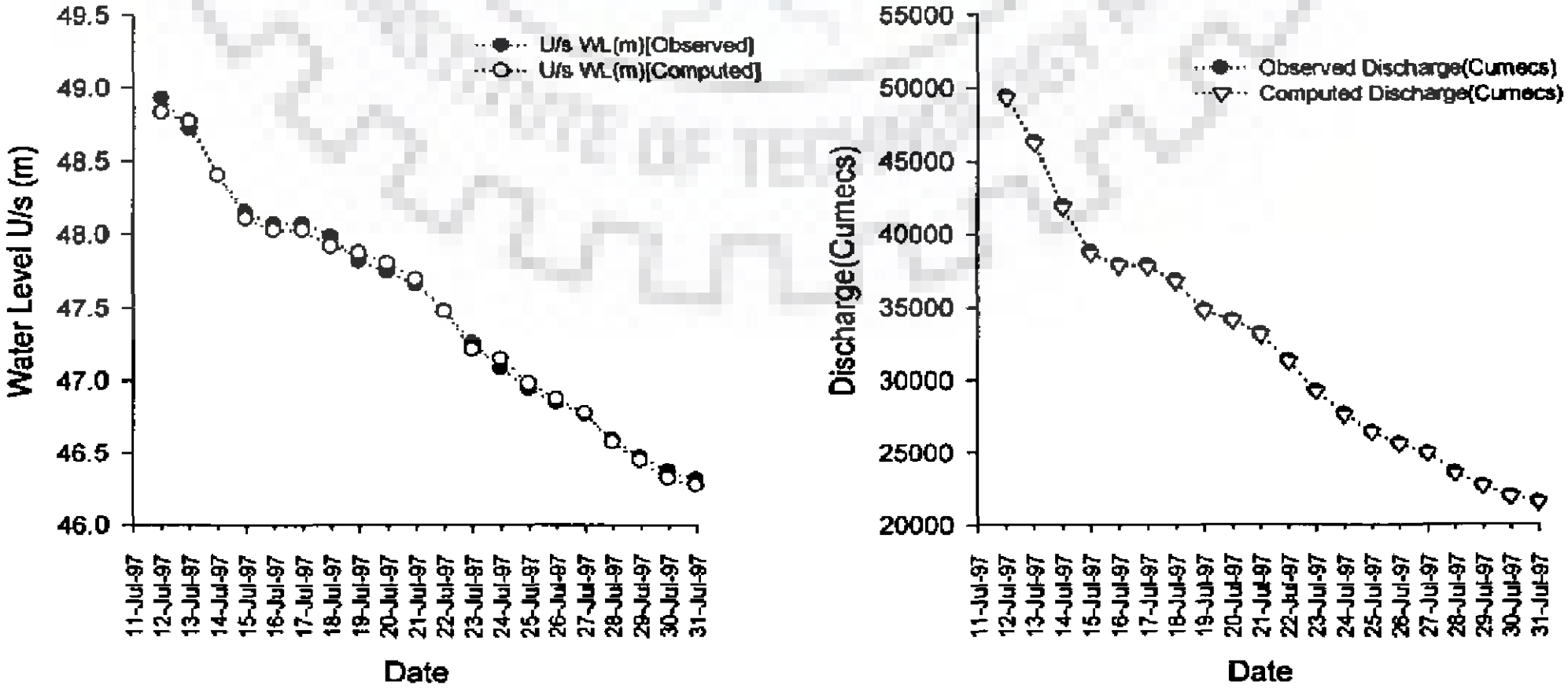

Figure 10.4 Observed verse computed *WSL* plot and discharge for d/s location

Table 10.1 Comparison between measured water stages and discharges upstream and downstream locations respectively for designated *profiles*

profiles	Date	Observed WL(m)	Computed WL(m)	Actual Discharge (Cumecs)	Computed Discharge (Cumecs)	Absolute Error in WL (cm)	Absolute Error in Discharge (Cumecs)
1	12-Jul-1997	48.93	48.83	49389.69	49241.40	10.00	148.29
2	13-Jul-1997	48.72	48.77	46269.77	46141.35	5.00	128.42
3	14-Jul-1997	48.4	48.4	41866.74	41769.65	0.00	97.09
4	15-Jul-1997	48.15	48.1	38725.74	38616.61	5.00	109.13
5	16-Jul-1997	48.07	48.02	37854.29	37753.99	5.00	100.30
6	17-Jul-1997	48.07	48.02	37834.47	37692.20	5.00	142.27
7	18-Jul-1997	47.98	47.91	36788.31	36697.66	7.00	90.65
8	19-Jul-1997	47.81	47.87	34808.59	34691.10	6.00	117.49
9	20-Jul-1997	47.74	47.8	34119.5	34055.45	6.00	64.05
10	21-Jul-1997	47.65	47.69	33153.9	33077.78	4.00	76.12
11	22-Jul-1997	47.48	47.47	31330.32	31240.26	1.00	90.06
12	23-Jul-1997	47.26	47.21	29289.57	29213.12	5.00	76.45
13	24-Jul-1997	47.08	47.15	27649.36	27570.90	7.00	78.46
14	25-Jul-1997	46.94	46.98	26419.21	26357.51	4.00	61.70
15	26-Jul-1997	46.84	46.87	25590.78	25552.40	3.00	38.38
16	27-Jul-1997	46.76	46.77	24936.58	24912.53	1.00	24.05
17	28-Jul-1997	46.59	46.57	23547.83	23530.02	2.00	17.81
18	29-Jul-1997	46.47	46.44	22663.52	22650.32	3.00	13.20
19	30-Jul-1997	46.37	46.32	21920.12	21893.58	5.00	26.54
20	31-Jul-1997	46.32	46.27	21562.88	21541.23	5.00	21.65

10.2.2 VARIATION OF FLOW VARIABLES

10.2.2.1 Variation in water depth and water surface elevation

The contour plot of model simulated water depth for discharge *profiles* 1, 3, 6, 9, 13, 16 and 20 have been shown in Figures 10.5a and 10.5b for the flow domain of the study stretch. One can observe that with decreasing discharges into the flow domain, from *profile*-1 to *profile*-20, flow area shrinks around the deepest bed level with increasing no flow zone or zones with shallow water depths. Highest water depth is around 10-12 m found in the inlet and outlet of the flow domain where the river constricts to narrow with incised configurations. Water depths across the river are as low as 2 m where the river fans out at Palasbari (20 km to 40 km from the inlet at Pandu). Such a large variation of water depth along the thalweg (Deepest bed level) is one of the special features of Brahmaputra River. This special character due to typical bed geometry of

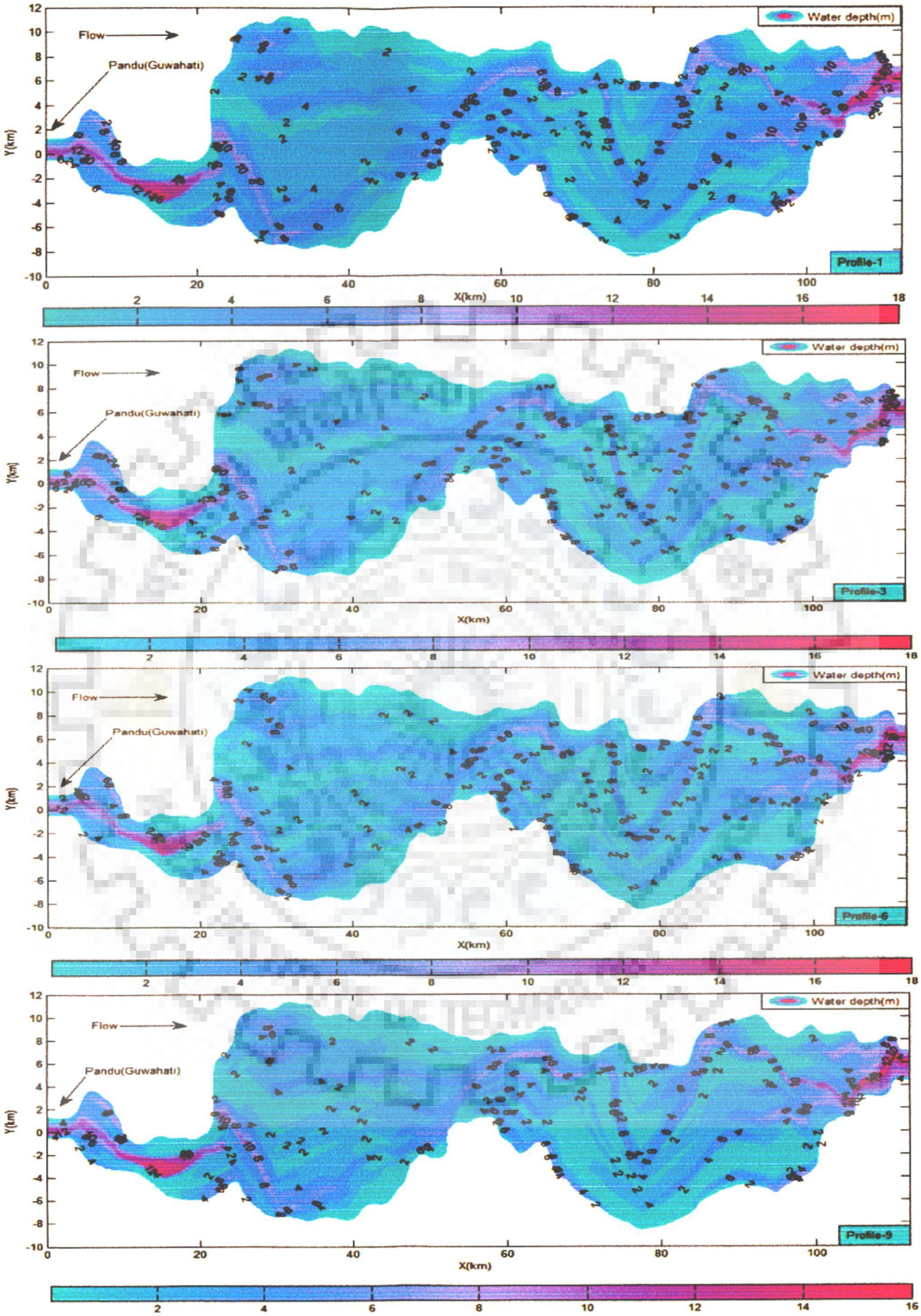

Figure 10.5a Contour-plot for water depth for *profiles* 1, 3, 6 and 9

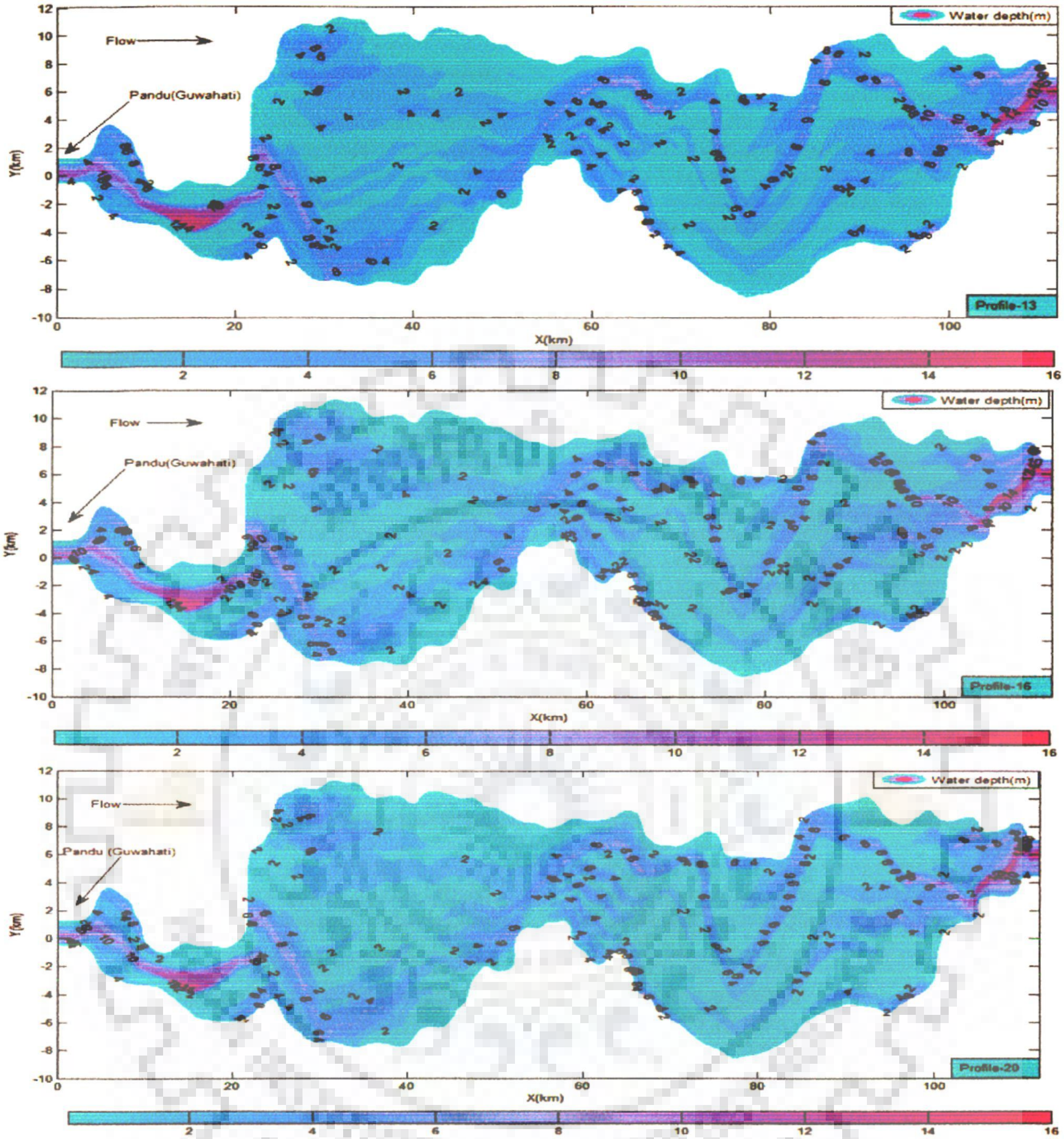

Figure 10.5b Contour-plot for water depth for *profiles* 13, 16 and 20

the river at a particular instance of time induces a very high dissipation of flow energy to the bank-lines through evolution and diminishing of secondary flow field. High dissipation of flow energy makes bank-lines vulnerable to severe river bank erosion. It further increases the sediment load into the river, making the river prone to aggradation in the downstream. When aggradation occurs, it increases the braiding intensity in the downstream. The associated physical process is complex and inter-dependent, making Brahmaputra River prone to relentless bank erosion severed

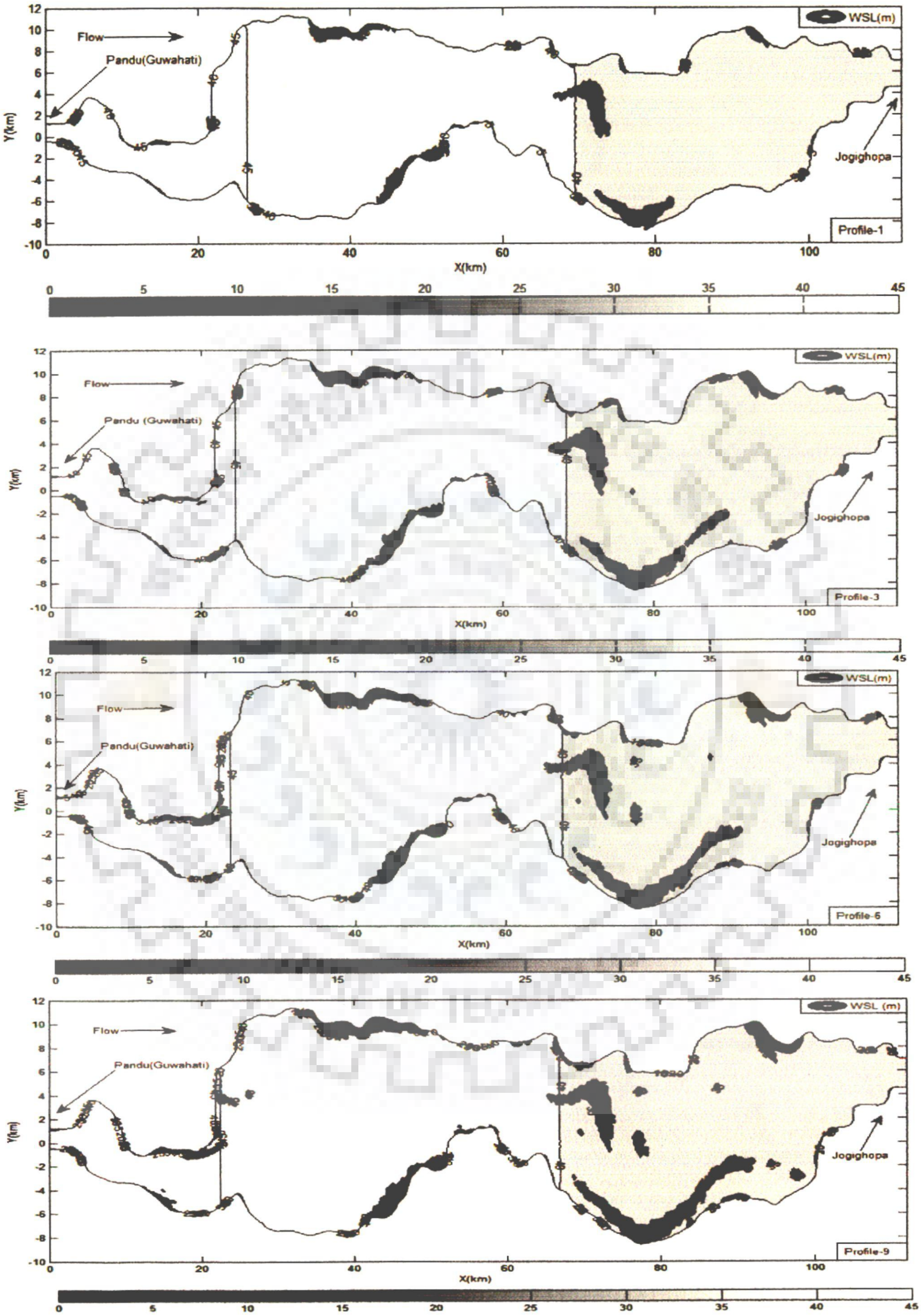

Figure 10.6a Contour-plot for water surface level (WSL) for *profiles* 1, 3, 6 and 9

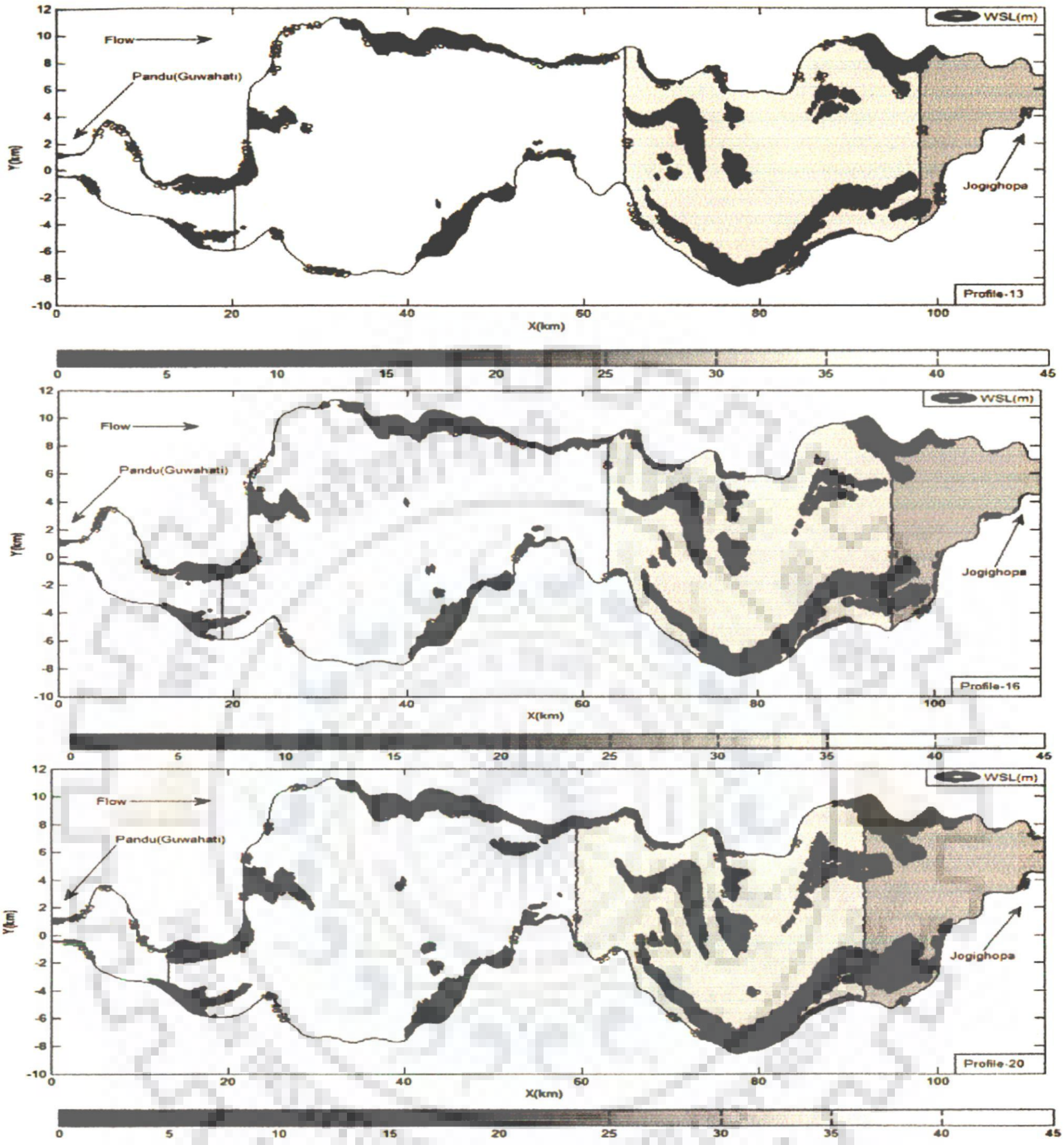

Figure 10.6b Contour-plot for water surface level (*WSL*) for *profiles* 13, 16 and 20

gradually in geological time-scale. Contours for water surface elevation (*WSL*) for the same *profiles* *i.e.* 1, 3, 6, 9, 13, 16 and 20 are presented in Figure 6a and 6b in sequence. Simulated average water surface levels along the river stretch for above mentioned profiles are shown in Figure 10.6c. In Chapter 7, one may recall that the developed 2-D model, wetting and drying technique was incorporated to judge individual grid to be wet or dry by assigning a threshold depth of 0.02m (For natural rivers). In the pressure solver, all wet and dry grids participated in the solution. While computing water surface elevation, those nodes where computed *WSL* was less than

or equal to bed elevation (*i.e.*$H<=z_b$), H value was assigned numerical threshold value of 0.02m for solving momentum equations. In the final results, for practical purposes, H values with 0.02 or lesser were considered as dry nodes with water depth assigned to zero.

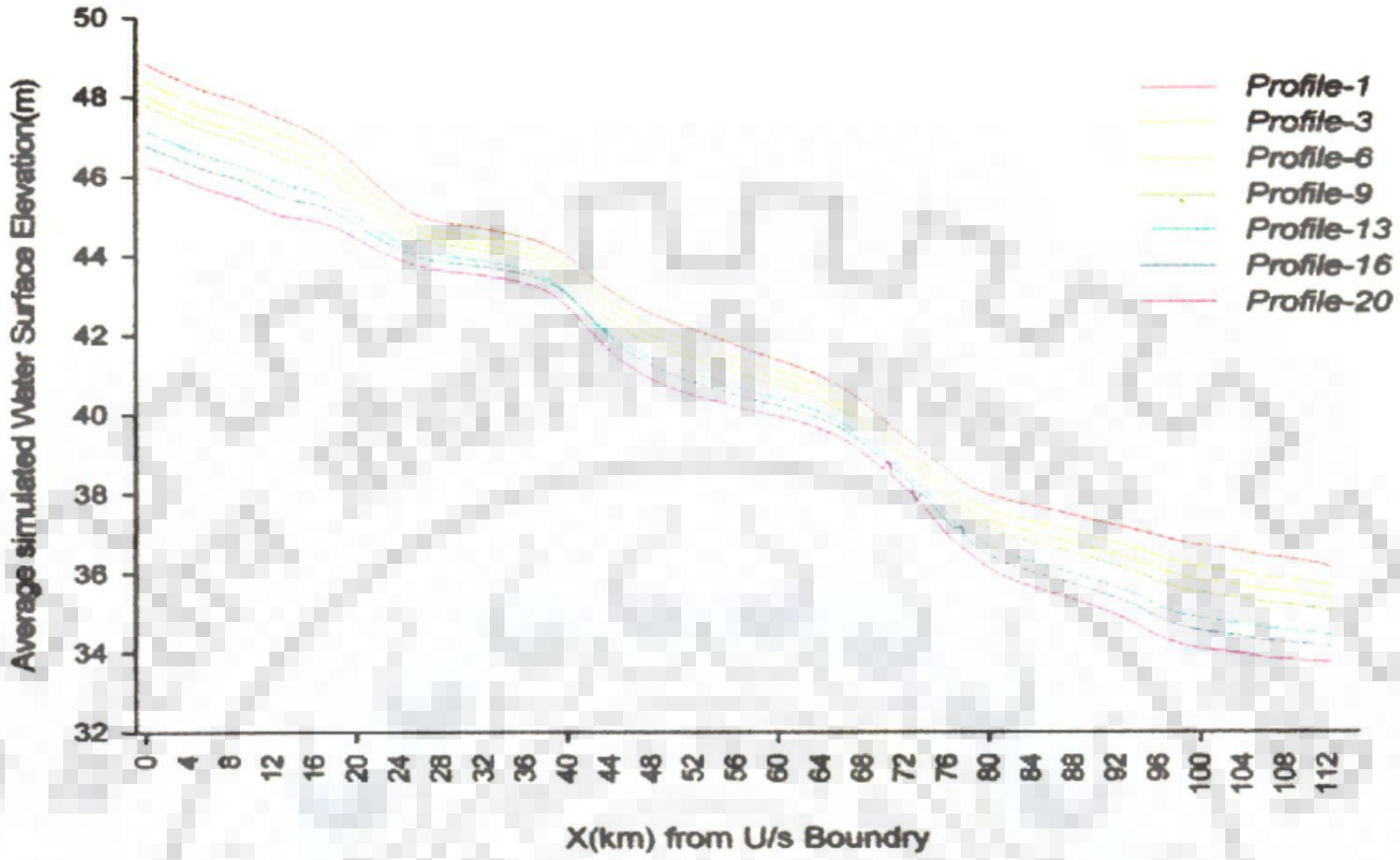

Figure 10.6c Simulated average water surface level (*WSL*) for *profiles* 1, 3, 6, 9 13, 16 and 20

Adopting the methodology mentioned above, the dry zones in the flow domain were simulated for different discharge *profiles*. The dry zones with zero water depth have been shown in black shades in Figures 10.6a and 10.6b for simulated discharge *profiles* namely 1, 3, 6, 9, 13, 16 and 20. At channel bifurcations, although flow-fields are essentially three dimensional, yet braid bars or side bars (simulated dry zones) were approximated with reasonable accuracy using the developed enhanced model through implementing wetting and drying technique without developing numerically more expensive 3-D model for such macro-scale flow field scenario. Looking at the Figures 10.6a and 10.6b, it was observed that braiding intensity was increasing with decreasing discharges, more and more braid bars and side bars were evolved, thereby increasing the proportionate no flow zone in the flow domain.

10.2.2.2 Variation in flow field

Simulated stream-wise velocity vector plots for the study flow domain are presented in Figure 10.7 for discharge *profiles* 13, 16 1nd 20 for illustrating decreasing concentration of flow with decreasing discharges. Figures 10.8a, 10.8b, 10.8c, 10.8d,

10.8e and 10.8f showed here to illustrate the simulated velocities at some important specific locations for *profile*-1. Figures 10.8a and 10.8b are shown to depict the streamwise velocity vector near Goalpara Town (40 to 80 km downstream of Guwahati). Variation of stream-wise velocity along the bank-line of Brahmaputra River in upstream location of Golapara Town is shown in Figure 10.8a and in downstream location of Goalpara Town in Figure 10.8b. The important location chosen was near Guwahati (0 km to 25 km from inlet location at Pandu). At Pandu (Guwahati), river is incised and stable with rock out-crops. Figure 10.8c shows the velocity *profile* from 0 to 10 km from Guwahati where river is narrow and velocity is high. In Figure 10.8d, velocity vector plot is shown for the location 12-25 km from Guwahati, from where river width starts widening almost to 20 km at Palasbari. Similarly, Figures 10.8e and 10.8f are presented to depict the transverse velocity field near Guwahati and Goalpara Town. Figure 10.8f vividly depicts the significant variation of transverse velocities near the bank-lines, which is one of the causative factors for intermittent river bank failure.

The contour plot for the magnitudes of stream-wise velocities for the discharge *profiles* 1, 3, 6 and 6 and *profiles* 9, 13, 16 and 20 are shown in Figures 10.9a and 10.9b respectively. From the figures, it was observed that concentrations of high velocities are confined to certain specific flow regions.

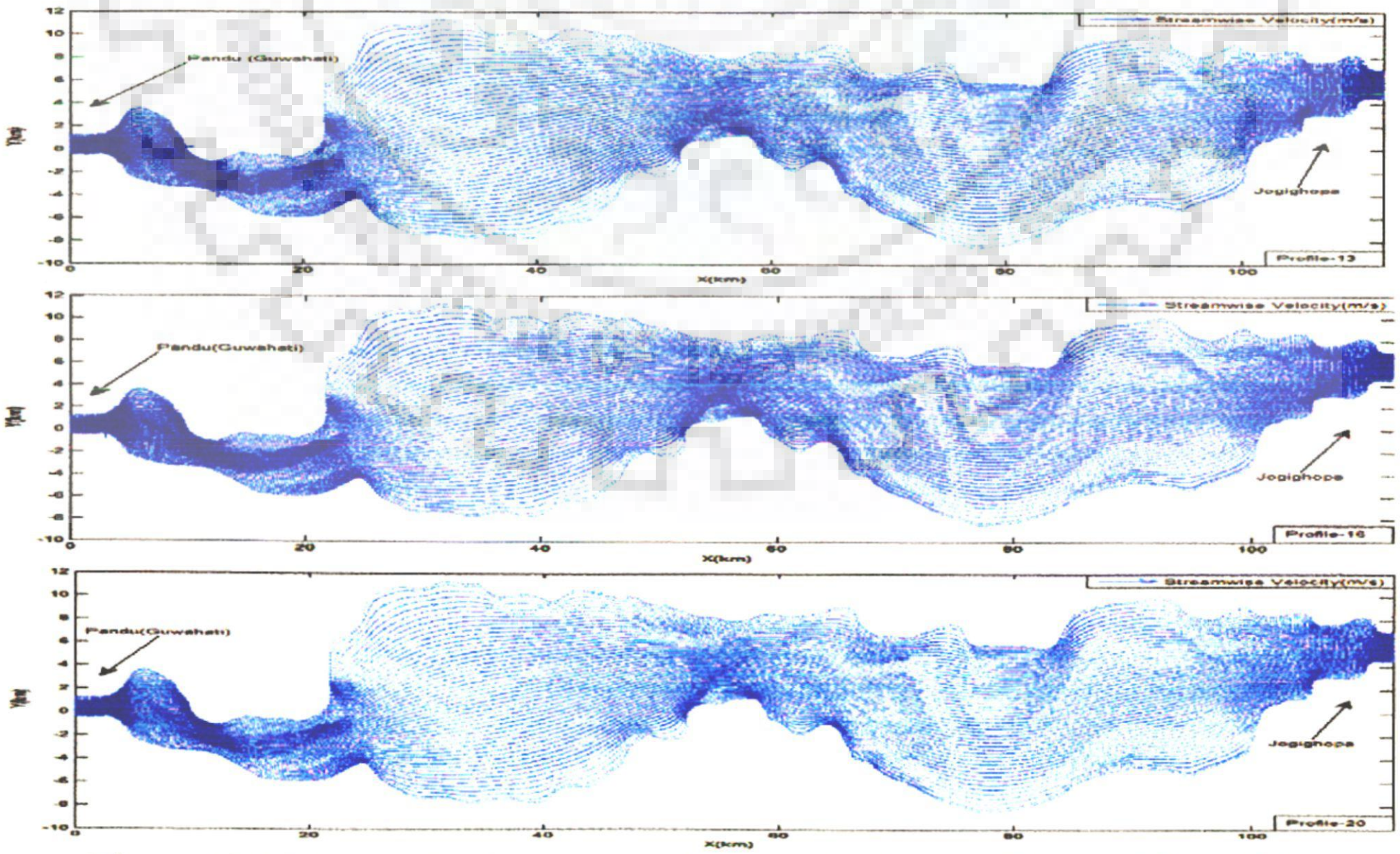

Figure 10.7 Vector-plot for stream-wise velocity for *profiles* 13, 16 and 20

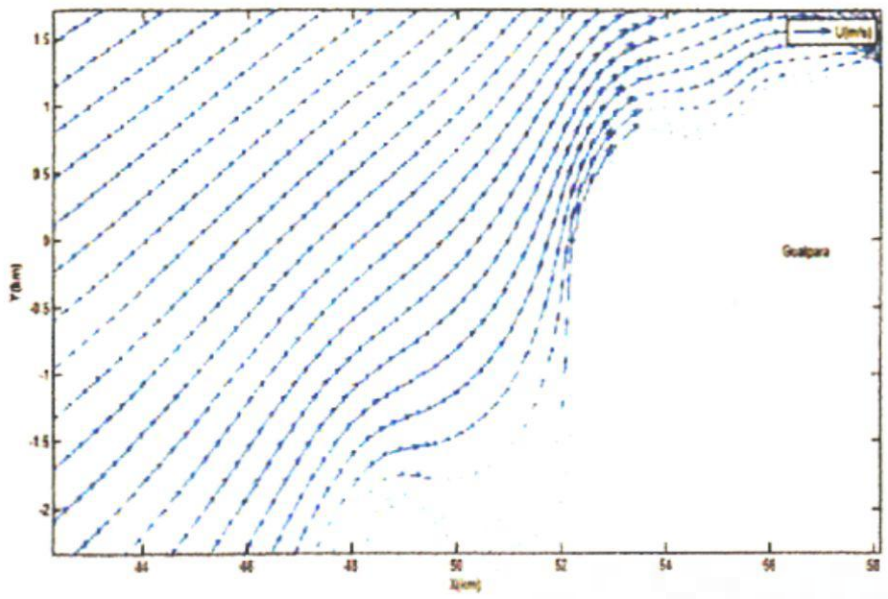

Figure10.8a Vector-plot(U) near Goalpara

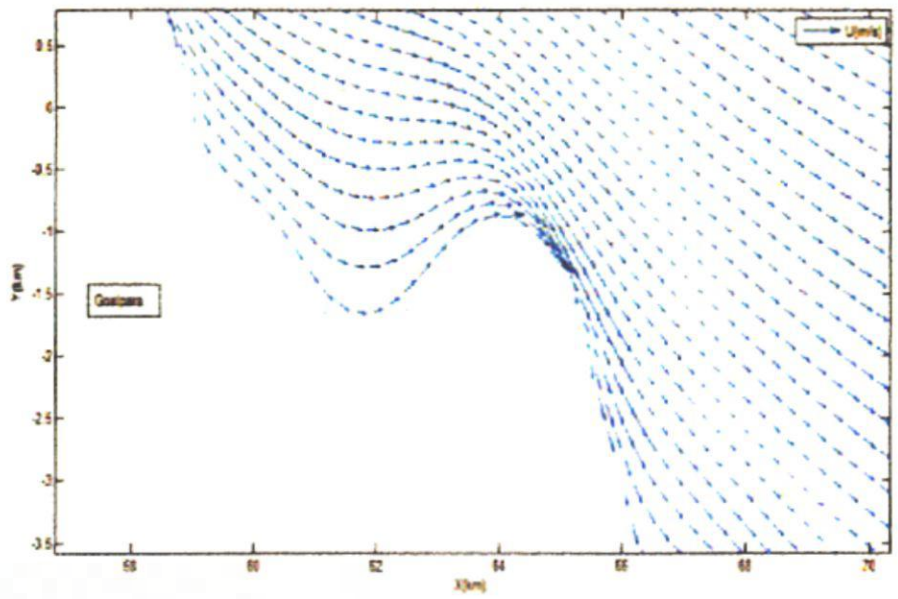

Figure10.8b Vector-plot(U) –Goalpara(w)

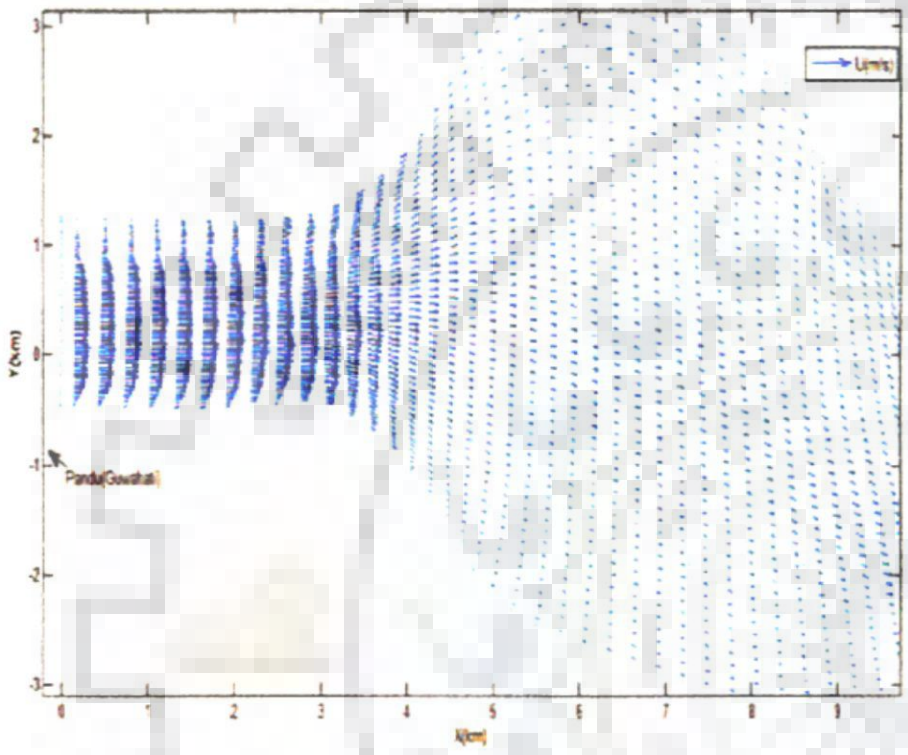

Figure10.8c Vector-plot for U (Guwahati)

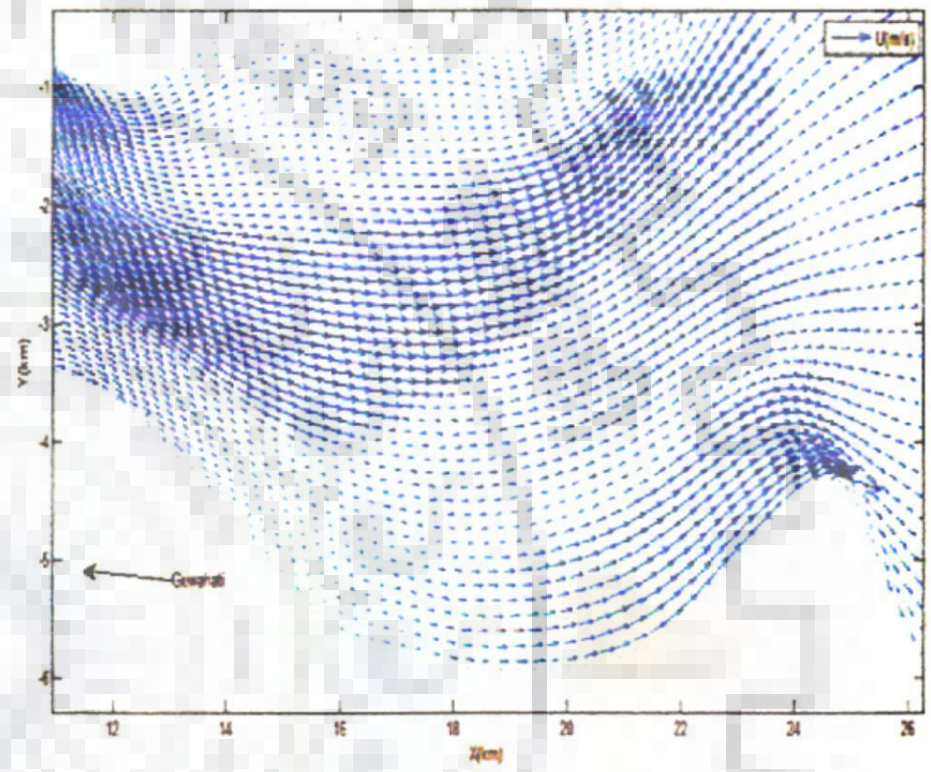

Figure10.8d Vector-plot(U) –Guwahati(w)

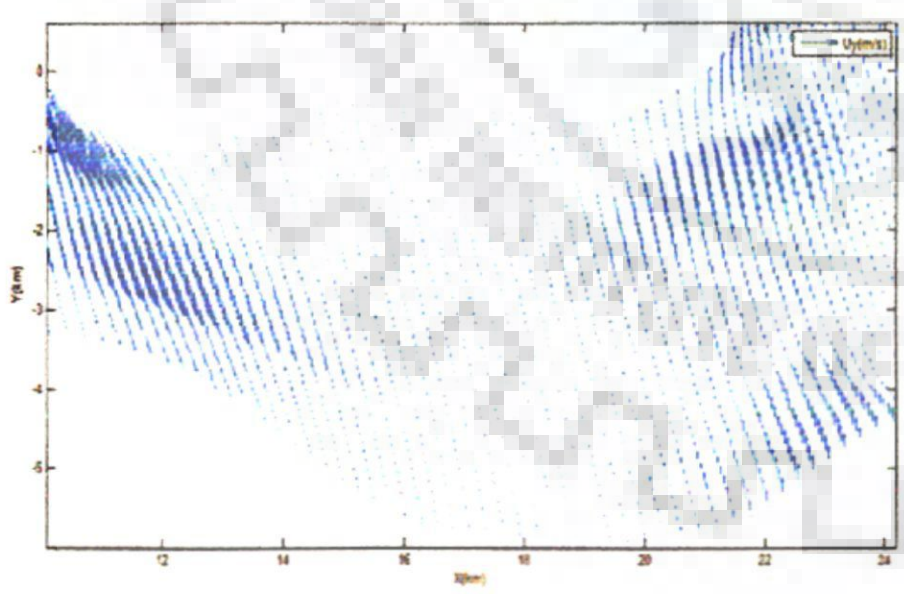

Figure10.8e Vector-plot for U (Guwahati)

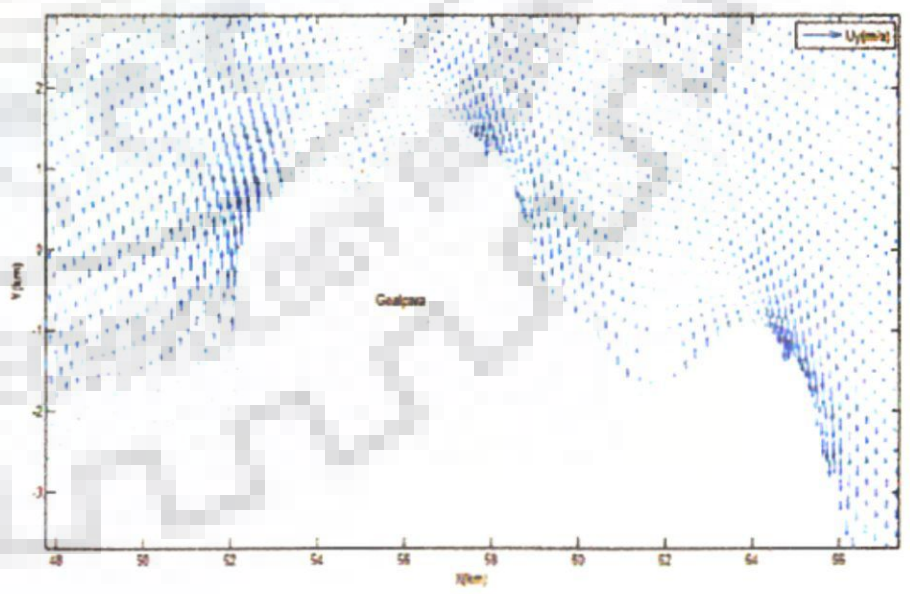

Figure10.8f Vector-plot (U) –Guwahati(w)

These location are at the inlet of the flow domain near Guwahati (streamwise velocity almost 3.5 m/s at discharge *profile*-1, Location- *X*=0-5 km, *Y*=0), at 55km downstream of Guwahati near Goalpara Town (streamwise velocity is 2.5m/s at *profile*-1; Location- *X*= 52-58 km, *Y*=0-4 km), at 65 to 75 km (Location: *X*=65-

75km, Y=8 to -6 km) and at the outlet at Jogighopa (X=112 km, Y=4-7km) .In this simulated flow field these locations did not change due to rigid bed consideration in the developed model. Apart from these locations, magnitude of the velocity in the flow-field is lowered down almost to 0.5 m/s. Moreover, flow field shrinks around the thalweg (deepest bed level) with decreasing discharges.

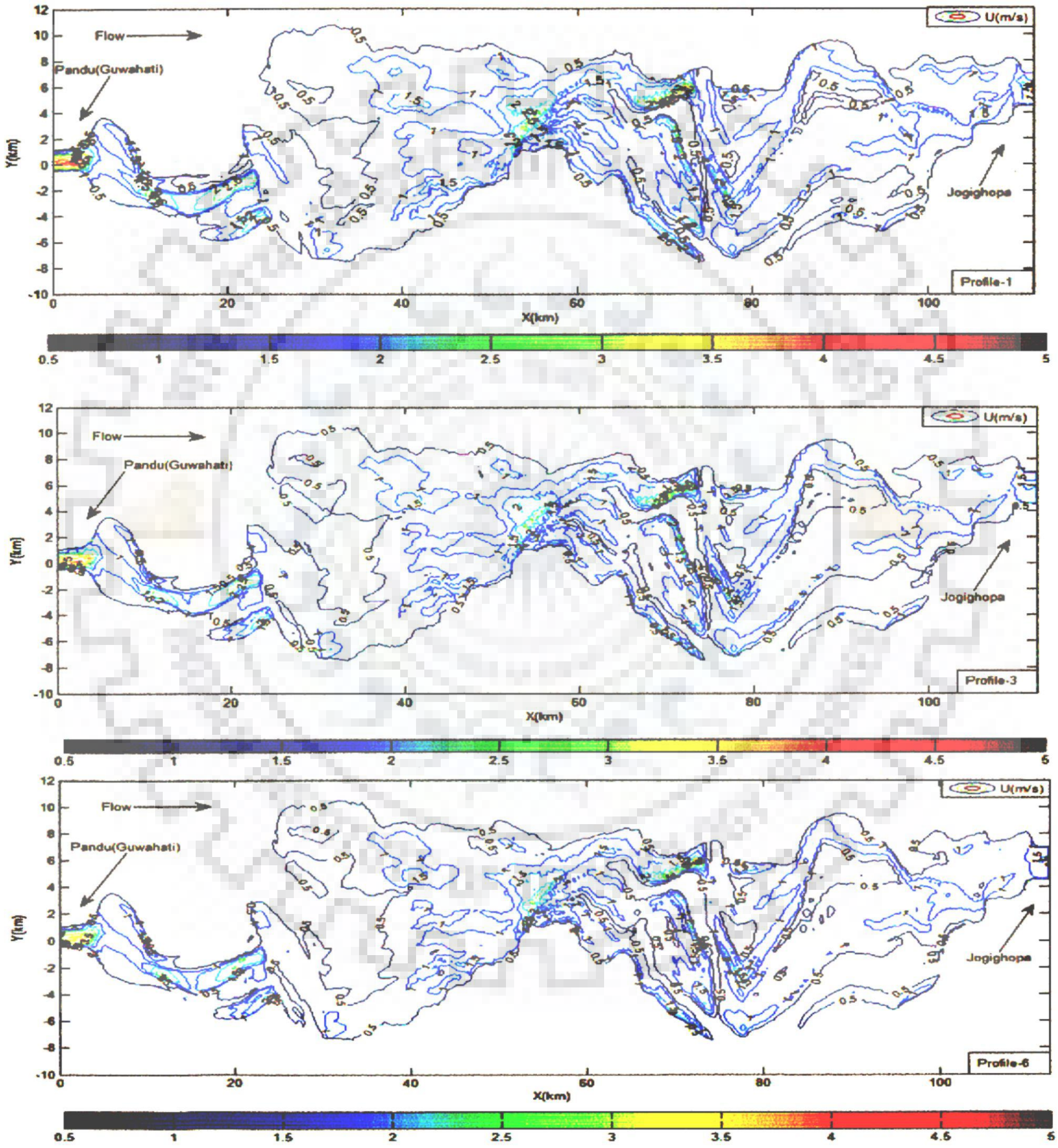

Figure 10.9a Contour-plot for stream-wise velocity for *profiles* 1, 3 and 6

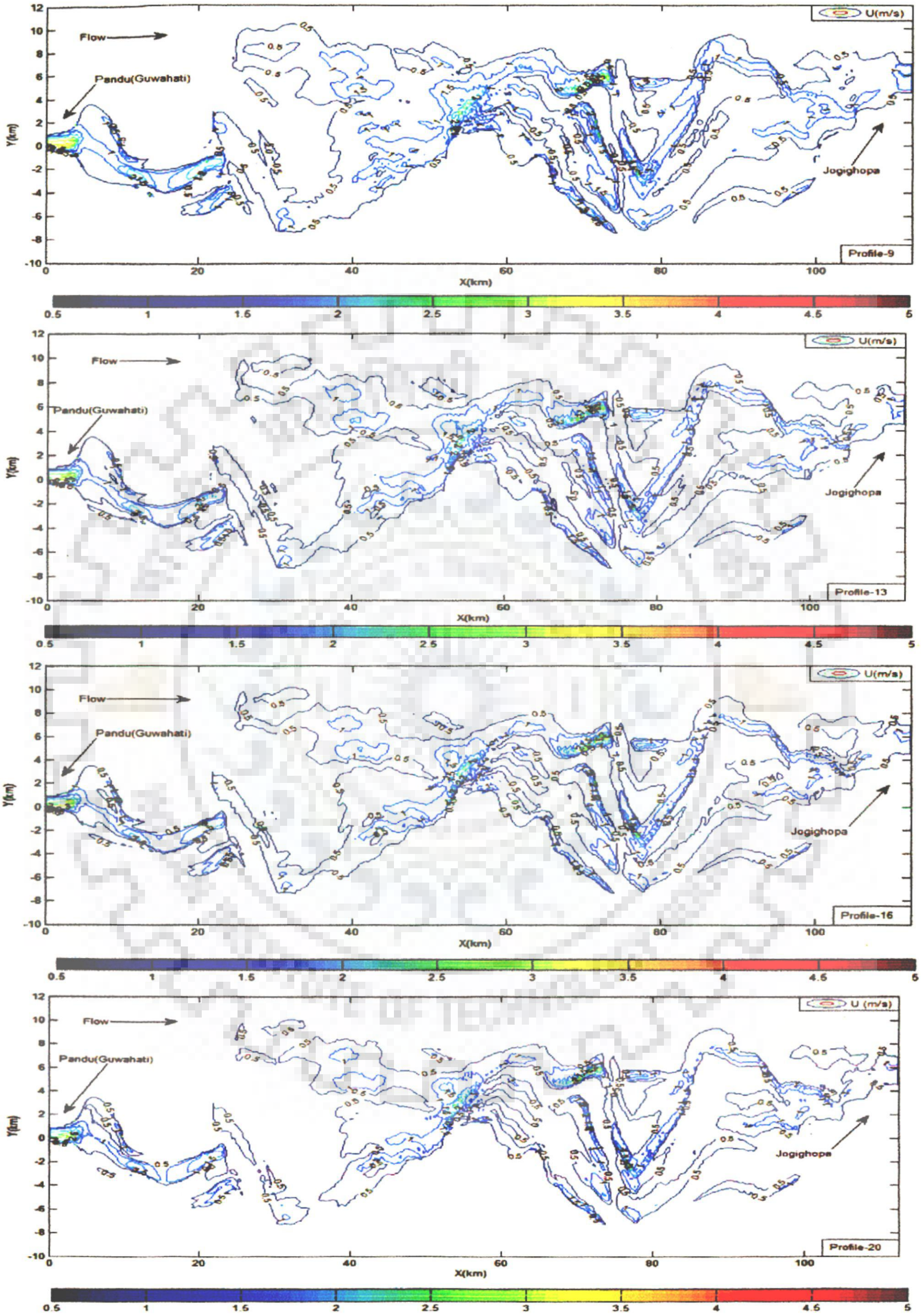

Figure 10.9b Contour-plot for stream-wise velocity for *profiles* 9, 13, 16 and 20

10.2.3 VARIATION OF LONGITUDINAL VELOCITY DEVIATION INTENSITY

Longitudinal velocity deviation intensity (I_L) and transverse velocity deviation intensity (I_T) give the fractional deviations of discrepancy with respect to depth averaged velocity in stream-wise and transverse direction (Seo *et al.*, 2008). I_L and I_T and their variation in curved flow domain have been discussed in detail in Chapter 9 of this thesis. While conducting flow simulation for the Brahmaputra River Stretch, I_L and I_T were computed for all discharge *profiles*. For further analysis, stream-wise deviation I_L was chosen to see its variations along the river stretch under study. *Mean* I_L was obtained through averaging I_L for all cell centers lying at each transverse η-line in the study domain. Thereafter, it was plotted against longitudinal distances from inlet to outlet locations for *profiles* 1, 6, 9, 13, 16 and 20 (Figure 10.10). Spatial variations of I_L helped to identify the meandering behavior of the braided river. It changes rapidly wherever stream has well developed curved flow domain (Figure 10.10). As the discharge decreases (*profile*-1 to 20), *mean* I_L along the reach has more fluctuations with increased numbers of peaks and dips. It indicates that as the discharge decreases, dispersion is more predominant. In other words, when intensity of braiding increases, it evolves multiple channels with meandering configurations. Meandering and bend in evolved multiple channels instigate more discrepancy in the flow-field if it is approximated with depth averaging. So velocity deviations intensities are more prominent fluctuations at low discharges in braided rivers. Hence, at lower discharges with high braiding, dispersion stress terms are well justified to include into the flow model for better assessment of the flow field.

10.2.4 MEASURE OF BRAIDING INTENSITY BY A NEW BRAIDING INDICATOR BASED ON MODEL RESULTS

Contour plots shown in Figures 10.6a and 10.6b were further analyzed. Simulated dry cell nodes (where water depth was zero) for each *profile* were identified and sum of the area of dry cells for each *profile* simulation was evaluated. Thus, area of no flow zone is calculated for each *profile* simulation. Dividing it by total area of flow domain, fractional no flow ratio (f_{nf}) was calculated. No flow area was subtracted from total flow area and fractional flow ratio (f_f) was estimated. Simulated fractional flow ratio and no flow ratio for *profile* 1 to 20 were tabulated in Table 10.2. It was

observed that with decreasing discharges, no flow ratio (f_{nf}) decreases. Simulated no flow ratio verses corresponding observed discharge was plotted and shown in Figure 10.11(a). The rate of decrease of no flow ratio with observed discharge also depends upon the geometric configuration of the flow domain along with other factors.

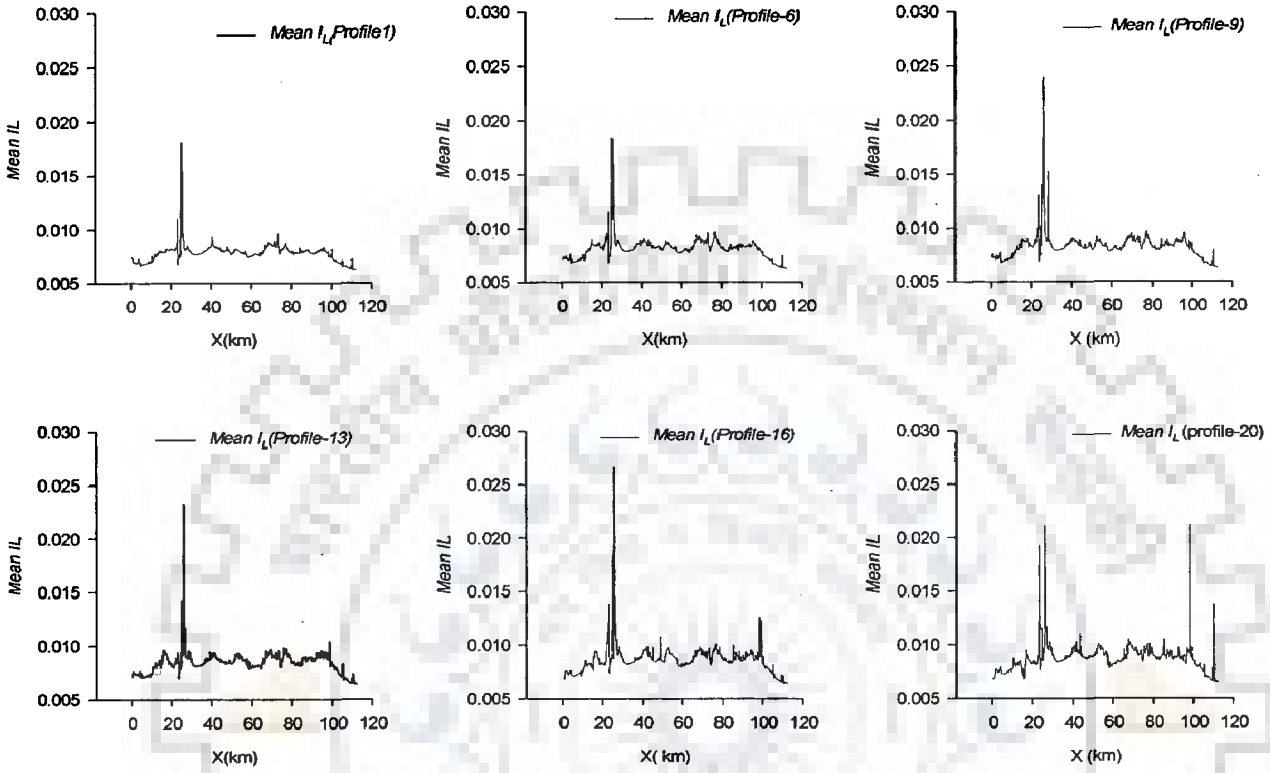

Figure 10.10 *Mean l*ongitudinal velocity deviations (I_L) for *profiles* 1, 6, 9 13 16 and 20

Based on the obtained results and information from flow simulation for twenty discharge *profiles* at receding flood of 1997, an indicator namely *braid power* is proposed based on the model output to express the measure of braiding for a river reach as follows.

$$braid\ power(\mathrm{N/m^2\text{-}s}) = f_{nf} \cdot \frac{\gamma Q_{inlet} S}{\text{flow Area of Inlet of the Reach}} \qquad (10.1)$$

In Eq. (10.1), f_{nf}=Ratio of no flow zone area with respect to whole flow domain area, γ=Unit weight of water (N/m^3) and S=Average longitudinal slope of the study reach. Flow area (m^2) is the cross-sectional flow area of the inlet boundary at the given discharge. The unit of *braid power* is N/m^2-s. If one attempts to fix threshold value of braid power, the following conditions might be the possibility (Table 10.3).

Table 10.2 Model simulated computation of 'No flow Zone' and Estimation of *braid power*

profiles	Date	Fractional Flow Ratio (simulated)	No Flow Ratio (Simulated)	braid-power (N/m^2-s)
1	12-Jul-1997	0.9703	0.0297	0.110
2	13-Jul-1997	0.9684	0.0316	0.111
3	14-Jul-1997	0.9581	0.0419	0.139
4	15-Jul-1997	0.9493	0.0507	0.161
5	16-Jul-1997	0.9462	0.0538	0.168
6	17-Jul-1997	0.9461	0.0539	0.168
7	18-Jul-1997	0.9451	0.0549	0.169
8	19-Jul-1997	0.9384	0.0616	0.180
9	20-Jul-1997	0.9352	0.0648	0.187
10	21-Jul-1997	0.9298	0.0702	0.200
11	22-Jul-1997	0.9173	0.0827	0.228
12	23-Jul-1997	0.9042	0.0958	0.254
13	24-Jul-1997	0.8979	0.1021	0.258
14	25-Jul-1997	0.8867	0.1133	0.278
15	26-Jul-1997	0.8797	0.1203	0.290
16	27-Jul-1997	0.8739	0.1261	0.299
17	28-Jul-1997	0.8606	0.1394	0.320
18	29-Jul-1997	0.8503	0.1497	0.336
19	30-Jul-1997	0.8398	0.1602	0.352
20	31-Jul-1997	0.836	0.164	0.357

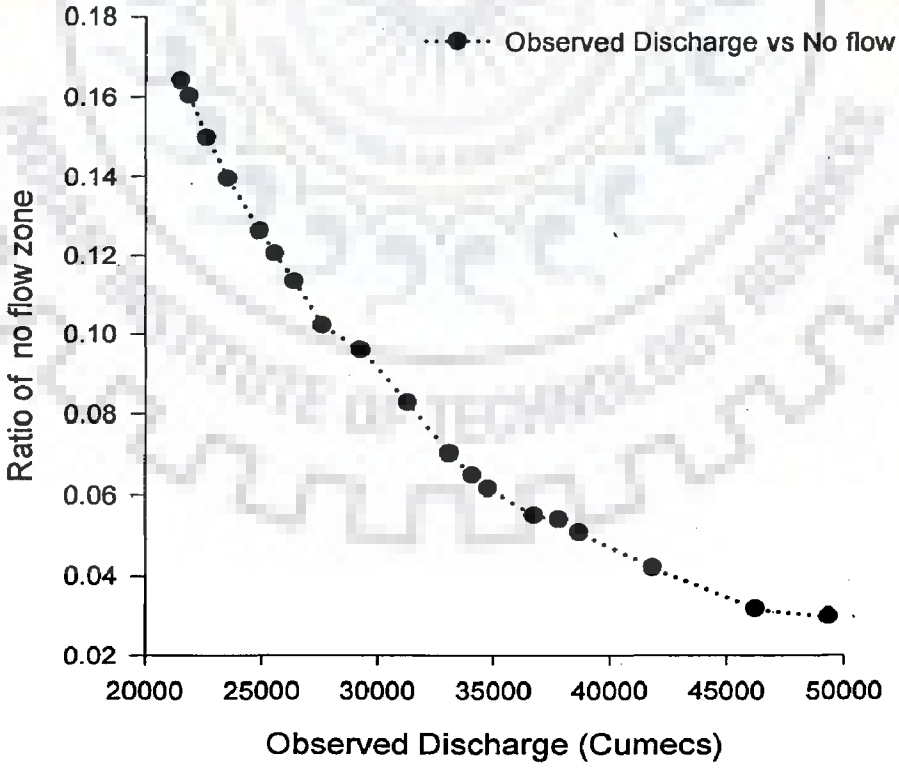

Figure 10.11 (a) Plot for observed discharge vs. no flow ratio (f_{nf}) for the Study Reach

Table 10.3 Threshold values of *braid power* at extreme values of f_{nf}

Conditions	No Flow Ratio (f_{nf})	Flow Ratio (f_f)	Q_{inlet}	Slope (S)	Flow Area (Inlet)	*braid power*
1	1	0	0	-	-	∞
2	0	1	-	-	-	0
3	$0 \le f_{nf} \le 1$	$1 \ge f_f \ge 0$	-	-	-	f_{nf}×(Unit Stream Power per unit depth of the flow at the inlet location of the Reach considered)

Extreme values of f_{nf}, values of *braid power* were assessed. For a given river reach, when f_{nf} approaches 1, Q_{inlet} approaches zero, at the same time flow area at inlet also approaches zero. *Braid power* becomes very large and approaches infinity. Similarly, when f_{nf} approaches zero, *braid power* approaches zero (Eq. 10.1). Within the range of f_{nf} between 0 to 1, *braid power* is nothing but a fraction of unit stream power per unit depth of flow at the inlet location of reach under consideration. The reported average longitudinal slope of the study reach is 0.11 m/km (Figure 3.2 of Chapter 3). Hence, *braid power* was computed for twenty simulated *profiles* and *braid power* verses observed discharge was plotted and presented as Figure 10.13b. It was observed that *braid power* increases with decrease in incoming discharge into the reach at a particular instance of time (Figure 10.11b). The rate of decrease or increase of *braid power* depends upon geometric configuration of the reach at the particular instance of time along with other factors.

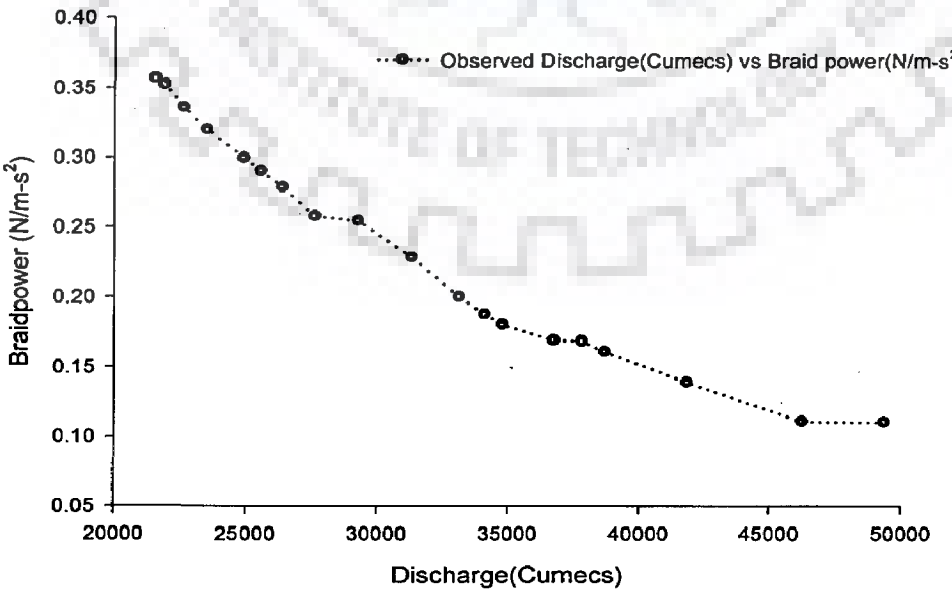

Figure 10.11 (b) Plot for observed discharge vs. *braid power* for the study reach

10.3 CONCLUDING REMARKS

In this study, for the first time, two dimensional enhanced numerical model with boundary fitted coordinate system and secondary flow corrections for the Brahmaputra River stretch with highly braided configuration, has been developed and verified. Braiding induces severe bank erosion, due to dominant transverse flow field. So, improved and realistic flow-field estimation will lead to realistic assessment of predictions of bank erosion and river bed evolution for braided alluvial rivers. Better erosion models can be developed with reasonable accuracy using estimated flow field as the prime input.

****

CONCLUSIONS AND SCOPE FOR FUTURE WORK

11.1 CONCLUSIONS

Conclusions and major contributions of the present research work are summarized as follows.

1. Comprehensive literature review discussed in Chapter 2 succinctly suggests that 1-D flow models are insufficient to tackle problems of braided streams due to lack of information with regard to transverse flow field. In lieu of this, 2-D or 3-D numerical models are to be used. In addition, 3-D models have many imponderables for prediction of flow simulation with braided complexities as well as are computationally tedious for macro scale river reaches. Hence, 2-D enhanced model with secondary flow corrections in governing equations has been developed in this study.

2. Most of the 2-D models developed especially for braiding rivers did not account for secondary flow correction probably presuming these corrections to be insignificant for turbulent flows and mild curved bank-lines.

3. In complex flow situation with considerable braiding, the secondary flow correction is suitably justified to achieve, improved flow scenario by enhancing the model capability through incorporating secondary flow correction using *modified flow dispersion stresses* with nominal additional expense of computational effort.

4. Based on model result, it was observed that redistribution of flow concentration in longitudinal and transverse directions are adequately accounted for, using the formulation in curvilinear flow field and was suitably capable of assessing realistic flow prediction with reasonable approximation.

5. For the first time, two dimensional enhanced numerical model with boundary fitted coordinate system for the Brahmaputra River Stretch with highly braided configuration, has been developed and verified.

6. It has been observed that effect of dispersion stress tensor in flow field increases with increase in braiding intensity. Model results discussed in Chapter 10 adequately supported this statement.

7. When intensity in braiding increases, it evolves multiple channels with meandering configurations. Meandering and bend in evolved multiple channels instigate more discrepancy in the flow-field if it is approximated with depth averaging.

8. Braiding induces severe bank erosion, due to dominant transverse flow field. So, improved and realistic flow-field estimation will facilitate realistic assessment of predictions of bank erosion and river bed evolution for braided alluvial rivers.

9. Based on the obtained results and information from flow simulation for twenty discharge profiles at receding flood of 1997 for Brahmaputra River stretch under this study, an indicator namely *braid power* is proposed in this work based on the model output to express the measure of braiding for a river reach as follows.

$$braid\ power\,(\mathrm{N/m^2\text{-}s}) = f_{nf} \cdot \frac{\gamma Q_{inlet} S}{\text{flow Area of Inlet of the Reach}}$$

where, f_{nf} =ratio of no flow zone area with respect to whole flow domain area, γ=unit weight of water (N/m^3) and S=average longitudinal slope of the study reach. Flow area (m^2) is the cross-sectional flow area of the inlet boundary at the given discharge.

10. It was observed that *braid power* increases with decrease in incoming discharge into the reach at a particular instance of time (Figure 10.13b).

11. The rate of decrease or increase of *braid power* depends upon geometric configuration of the reach at the particular instance of time along with other factors.

11.2 FUTURE SCOPE OF THE STUDY

The prime thrust of the present research work is to bring to the fore persistent shortcomings in relation to flow field estimation for rivers with highly braided configuration. The present research work has desirably brought about a significant improvement in dominant transverse flow field estimation in highly braided rivers. The transverse flow field is one of the significant causative factors for stream bank erosion resulting in huge land loss around the vicinity of braided rivers such as Brahmaputra River. However, to model bank erosion and bed evolution with high degree of accuracy, after further research, a robust 2-D sediment transport module with incorporated bank erosion mechanism, clubbed with the present enhanced flow simulation model is required to be developed. To model the moving boundaries, present developed model uses fixed boundary method through implementation of wetting and drying technique including the whole flood plain under the flow domain. However through conducting further research on advanced algorithm using depth adaptive grid generation and temporal deformed mesh technique; a moving boundary can possibly be implemented to simulate the multiple channels actual flow zones instead of considering the whole flood plain. However, at present numerical implementation of the aforesaid process is quite complex for highly braided rivers with multiple channels like Brahmaputra and possibly be a potential area of research.

****

BIBILOGRAPHY

1. Abad, J.D., Buscaglia Gustavo C., and Garcia Marcelo H. (2007). "2D stream hydrodynamic, sediment transport and bed morphology model for engineering applications." *Hydrol. Process.* (2007) Published online in *Wiley InterScience* DOI: 10.1002/hyp.6697.

2. Abad J.D. and Garcia M. H. (2005). "Hydrodynamics in kinoshita-generated meandering bends: importance for river-planform evolution". *In Proceedings of the 4th IAHR Symposium on River, Coastal and Estuarine Morphodynamics RCEM.* 4–7 October 2005. Parker G, Garcia MH (eds). *Taylor and Francis*: Balkema, Urbana, Il.

3. *Alcrudo, F., Garcia-Navarro, P., [illegible] J. M. (1992). "Flux difference splitting for 1D open-channel flow eq[illegible] *nt. J. Numer. Methods Fluids*, 14: 1009-1018.

4. *Antropovskiy, V.I. (1972). "Critical Relations of Type of Channel Processes", *Soviet Hydrology,* 11: 371-381.

5. Ashmore, P. E., Ferguson, R. I., Prestegaard, K. L., Ashworth, P. J. and Paola, C. (1992). "Secondary flow in anabranch confluences of a braided, gravel-bed stream." *Earth Surface Processes and Landforms,* 17: 299–311. doi: 10.1002/esp.3290170308

6. Batchelor, G.K. (1967). "An introduction to Fluid Dynamics." *Cambridge University Press*.UK

7. Bahaidarah Haitham M. S. (2004). "A numerical study of heat and momentum transfer over a bank of flat tubes". *Ph.D Dissertation*, Dept. of Mechanical Engineering, Texas A&M University

8. Bathurst, J., Thorne, C., and Hey, R. (1977). "Direct measurements of secondary currents in river bends." *Nature (London)*, 269:504–506.

9. Bathurst, J., Hey, R., and Thorne, C. (1979). "Secondary flow and shear stress at river bends." *J. Hydraul. Div., Am. Soc. Civ. Eng.*, 105(10):1277–1295.

10. Bathurst, J., Thorne, C., and Hey, R. (1981). "Closure to 'Secondary flow and shear stress at river bends'." *J. Hydraul. Div., Am. Soc. Civ. Eng.*, 107(5):644-647.

11. Bates P.D., Lane S.N. and Ferguson R.I. (2005). *Computational Fluid Dynamics, Applications in Environmental Hydraulics.* Bates P.D., Lane S.N. and Ferguson R.I. (Eds*), John Wiley and Sons, Ltd.*: United Kingdom.

12. Bates P.D. and Horritt M.S. (2005). "Modelling wetting and drying processes in hydraulic models". *Chapter 6, Computational Fluid Dynamics, Applications in Environmental Hydraulics.* Bates P.D., Lane S.N. and Ferguson R.I. (Eds), *John Wiley and Sons, Ltd.*: United Kingdom.

13. *Beffa, C.(1994)."Practische lösung der tiefengemittelten flachwasser gleichungen." *Communication No. 133, Lab of Hydr.*, ETH Zürich, Zürich.

14. *Bernard, R.S., Schneider, M.L. (1992). "Depth-averaged numerical modeling for curved channels." *Technical Report HL-92-9. Hydraulics Laboratory*, US Army Corps of Engineers.

15. *Bernard R.S.(1993). "Stremr: Numerical model for depth-averaged incompressible flow." *Technical Report REMR-HY-11*, US Army Corps of Engineers.

16. Best, J. L. and Roy, A. G. (1991). "Mixing-Layer Distortion at the Confluence of Channels of Different Depth", *Nature*, 350: 411-413.

17. Biglari, B. and Sturm, T. W. (1998). "Numerical modeling of flow around bridge abutments in compound channel." *J. Hydr. Engrg.*, ASCE, 124(2): 156–164.

18. Bora, A.K. (2004). "Fluvial Geomorphology, Chapter 6" in The Brahmaputra Basin Water Resources, (eds.) Vijay P. Singh, Nayan Sharma and C. Shekhar P. Ojha ©2004 *Dordrecht: Kluwer Academic Publishers.*

19. Bradbrook, K.F., lane S.N., richards, K.S. and Roy A.G.(2000). "Large Eddy

Simulation of periodic flow characteristics at river channel confluences." *Journal of hydraulic research.*, 38(3):207-215.

20. Bradbrook, K.F., Lane, S.N., Waller, S.G. and Bates, P.D. (2004). "Two-dimensional diffusion wave modelling of flood inundation *using* a simplified channel representation." *International Journal of River Basin Management*, 2: 211–223.

21. *Bradford, S. F., and Sanders, B. F. (2002). "Finite-volume model for shallow-water flooding of arbitrary topography". *J. Hydraul. Eng.*, 128(3): 289–298.

22. Brahmaputra Board, Ministry of Water Resources, Govt of India,(1986), Atlas of Brahmaputra Basin, *Volume I.*

23. Brahmaputra Board, Ministry of Water Resources, Govt. of India, (1986), Atlas of Brahmaputra Basin, *Volume II.*

24. *Brice, J.C.(1964)."Channel Patterns and Terraces of the Loup Rivers in Nebraska". *U.S Geological Survey professional paper*, 422-D.

25. *Bridge, J.S, (1993), "The interaction between channel geometry, water flow, sediment transport and deposition in braided rivers", In: Best, J. L, and Bristow, C.S, eds. Braided rivers, *Special Publication no. 75,* Geological Survey of London, pp. 13-63.

26. *Bristow,C.S. and Best, J.L.(1993). "Braided Rivers: Perspectives and Problems." A chapter in 'Braided rivers by Best, J. L. and Bristow, C.S., (Eds. 1993), *Geological Society, London*, Special. Publication, 75: 1-11.

27. *Breuer, M.(1998). "Numerical and modeling influences on large eddy simulation for the flow past a circular cylinder". *Int. J. Heat Fluid Flow* 19: 512-521.

28. Cao Z, Day R, Egashira S. (2002). "Coupled and decoupled numerical modeling of flow and morphological evolution in alluvial rivers". *Journal of Hydraulic Engineering* 128(3):306-321.

29. Capart, H., Eldaho, T. I., Huang, S. Y., Young, D. L. and Zech, Y.(2003). "Treatment of Natural Geometry in Finite Volume River Flow Computations." *Jr. of Hydraul. Engr.* 129(5): 385-393.

30. *Capart, H., Sillen, X., and Zech, Y. (1997). ''Numerical and experimental water transients in sewer pipes.'' *J. Hydraul. Res.*, 35(5): 659–672

31. *Cebeci, T. and Bradshaw, P. (1977). "Momentum Transfer in Boundary Layers." *Hemisphere,* Washington D.C.

32. Celik, I. and Rodi, W. (1988). "Modeling suspended sediment transport in nonequilibrium situations". *Journal of Hydraulic Engineering* 114(10): 1157–1191.

33. Correia, L.R.P., Bommanna, G.K. and Graf, W.H. (1992). "Fully coupled unsteady mobile boundary flow model". *Journal of Hydraulic Engineering* 118(3): 476-494.

34. Cunge, J.A., Holly, F.M. Jr and Verwey A.(1980). "Practical Aspects of Computational River Hydraulics." *London: Pitman.*

35. Darby S.E., Delbono I. (2002). "A model of equilibrium bed topography for meanders." *Earth Surface Processes and Landforms* 27: 1057–1085.

36. Darby, S. E., Alabyan, A. M. and Van De Weil, M. J.(2002). "Numerical simulation of bank erosion and channel migration in meandering rivers". *Water Resour. Res.*, 38(9): 2-1-12.

37. Dammuller D. C., Murty Bhaflamudi S. and Chaudhry Hanif M.(1989). "Modeling of unsteady flow in curved channel." *Journal of Hydraulic Engineering*, 115(11): 1479-1495.

38. de Vriend, H. J. (1977). "A mathematical model of steady flow in curved shallow channel." *J. Hydraul. Res.*, 15(1): 37–54.

39. de Vriend, H. (1979). "Flow measurements in a curved rectangular channel." *Internal Rep. No. 9-97. Tech. Rep.,* Laboratory of Fluid Mechanics, Dept. of Civil Engineering, *Delft Univ. of Technology*, Delft, The Netherlands.

40. *de Vriend, H. (1980). "Velocity redistribution in curved rectangular channels." *J. Fluid Mech.*, 107: 423–439.

41. *de Vriend, H. (1981). "Flow measurements in a curved rectangular channel. Part 2: Rough bottom." *Internal Rep. No. 5-81. Tech. Rep., Laboratory of Fluid Mechanics*, Dept. of Civil Engineering, Delft Univ. of Technology, Delft, The Netherlands.

42. Demirdzic, I., Gosman, A.D., Issa, R.I. and Peric, M.(1987). "A calculation procedure for turbulent flow in complex geometries". *Comput. Fluids* 15(3):251-273.

43. Demuren, A. O., and Rodi, W. (1986). "Calculation of flow and pollutant dispersion in meandering channels". *J. Fluid Mech.*, 172: 63–92.

44. Duan, J.G., Wang, S.Y.and Jia, Y. (2001). "The applications of the enhanced cche2d model to study the alluvial channel migration processes". *Journal of Hydraulic Research* 39(5): 1–12.

45. Duan, Jennifer G. (2004). "Simulation of flow and mass dispersion in meandering channels." *J Hydraul. Eng.*, 130(10):964-976.

46. Duan, J. G. and Pierre Y. Julien, Y. P.(2005). "Numerical simulation of the inception of channel Meandering'." *Earth Surf. Process. Landforms* 30:1093-1110.

47. Duc B.M., Wenka T. and Rodi W.(2004). "Numerical modeling of bed deformation in laboratory channels". *Journal of Hydraulic Engineering.*, 130(9):894–904.

48. Elder, J. W. (1959). "The dispersion of marked fluid in turbulent shear flow." *J. Fluid Mech.*, 5(4): 544–560.

49. Engelund, F., and Skovgaard, O. (1973). "On the origin of meandering and braiding in alluvial streams." *J. Fluid Mech.*, 57:289–302.

50. *Enggrob, H. G.and Tjerry, S.(1999). "Simulation of morphological characteristics of a braided river". *IAHR Symp. on River, Coastal, and Estuarine Morphodynamics*, IAHR, Genova, Italy, 585–594.

51. Erpicum, S., Meile, T., Dewals, B. J., Pirotton, M. and Schleiss, A. J. (2009), 2D numerical flow modeling in a macro-rough channel. *International Journal for Numerical Methods in Fluids*, 61: 1227–1246

52. *Erpicum, S., Meile, T., Dewals, B. J., Schleiss, A. J.and Pirotton, M. (2008)." Comparison of 2D turbulence models for steady flows computation in a macro-rough channel." *2nd International Symposium on Shallow Flows,* The Hong Kong University of Science and Technology., Hongkong, China

53. *Falcon Ascanio, M.(1979). "Analysis of flow in alluvial channel bends". *PhD thesis, Dept. Mech. and Hydr., University of Iowa*, Iowa City, Iowa.

54. Ferguson, R.I. (1981). "Channel form and channel changes.".J. Lewin (Ed), In *British rivers*, pp.90-125.(London: *Allen and Unwin*)

55. Ferguson R.I. and Parsons D.R. (2003). "Flow in meander bends with recirculation at the inner bank". *Water Resources Research,* 39(11): 1322.

56. Ferziger, J.H. and Peric, M. (1995). "Computational Methods for Fluid Dynamics," *Springer- Verlag.*

57. *Fischer, H. B., List, E. J., Koh, R. C. Y., Imberger, J., and Brooks, N. H.(1979). "Mixing in inland and coastal waters," *Academic*, London.

58. Fletcher C.A.J. (1991)."Computational techniques for fluid dynamics." Fundamental and General Techniques *(2nd edn),* vol. II. *Springer*: Berlin, 2: 47-78.

59. *Fraccarollo, L., and Toro, E. F. (1995). "Experimental and numerical assessment of the shallow water model for two-dimensional dambreak type problems." *J. Hydraul. Res.*, 33(6): 843–864.

60. *Friend, P.F. and Sinha, R., (1993), "Braiding and Meandering Parameters", A chapter in 'Braided Rivers' by Best, J. L. and Bristow, C.S., (eds. 1993), *Geological Society*, London, Special Publication. 75:105-111.

61. Garcia M. H.(2001). "Modelling sediment entrainment into suspension, transport and deposition in rivers". Chapter 15, in Model Validation: Perspectives in

Hydrological Science, Anderson M.G. and Bates P. D. (Eds). *John Wiley and Sons, Ltd.:* United Kingdom, 389-412.

62. Garcia M.H. and Nino Y.(1993). "*Dynamics* of sediment bars in straight and meandering channels: experiments on the resonance phenomenon". *Journal of Hydraulic Research* 31(6): 739-761.

63. *Ghanem, A.H. (1995). "Two-dimensional finite element modeling of flow in aquatic habitats." *Ph.D. Thesis, University of Alberta*, Alberta, Canada.

64. *Gordon, W.J., Hall, C.A. (1973). "Construction of curvilinear coordinate systems and applications to mesh generation". *Int. J. Num. Methods in Engineering* 7:461-477.

65. Goswami, D.C. and Das, P.J. (2000), "Report on some characteristics of high flow and low flow in the Brahmaputra river, India", *Guwahati University.*

66. Goswami, D.C. (1985). "Brahmaputra River, Assam, India: Physiography, Basin Denudation, and Channel Aggradation." *Water Resources Research,* 21: 959-978.

67. *Goswami, D.C., (1992), Zonal Planning in Water, In: Planning for Northeastern and Eastern Zone, Adisheshiah, M.S.(ed.), *Lancer Publications*, New Delhi, pp. 9-22.

68. Guy H.P., Simons D.B. and Richardson E. V. (1966). "Summary of alluvial channel data from flume experiments". *Geological Survey Professional Paper*, 462-I.

69. HEC (1997). "HEC-RAS, river analysis system- hydraulic reference manual." *Hydrologic Engineering Center*, Army Corps of Engineers, USA.

70. Henderson, F.M.(1961). "Stability of alluvial channels." *Journal of Hydraulic Division, American Society for Civil Engineering*, 87:109-138.

71. *Hilgenstock, A. (1988). "A fast method for the Elliptoc Generation of Three – Dimensional Grids with Fully Boundary Control." *Proceedings of the Numerical*

Grid Generation in Computational Fluid Dynamics Conference, Edited by S. Sengupta *et al.* pp. 137-146.

72. *Hinze, J. O. (1975). "Turbulence" *McGraw-Hill*, New York.

73. *Hirsch, C. (1988). "Numerical Computation of Internal and External Flows," Vols. 1 & 2, *Wiley.*

74. Hoffman, J.D. (1992). "Numerical Methods for Engineers and Scientists". *McGraw-Hill*, Inc., New York.

75. Hooke R.L. (1974). "Shear-stress and sediment distribution in a meander bend". *Tech. rep.,* UNGI RAPPORT 30. Department of Physical Geography. University of Uppsala.

76. Howard, A.D., Keeth, M.E. and Vincent, L.C. (1970). "Topological and Geometrical Properties of Braided Streams", *Water Resources Research*, 6: 1674-1688.

77. Howard, A. (1984). "Simulation model of meandering." *River meandering,* C. Elliot, ed., ASCE, New York, 952–963.

78. Howard A.D. (1992). "Modeling channel migration and floodplain sedimentation in meandering streams." Lowland Floodplain Rivers Geomorphological Perspectives. *John Wiley and Sons Ltd*: United Kingdom.

79. Hsieh, T. Y., and Yang, J. C. (2003). "Investigation on the suitability of two-dimensional depth-averaged models for bend-flow simulation." *J.Hydraul. Eng.*, 129(8): 597–612.

80. Ikeda, S., Parker, G., Sawai, K. (1981). "Bend theory of river meanders. part 1. linear development". *Journal of Fluid Mechanics* 112: 363–377.

81. Ingham, D.B. and Ma, L. (2005). "Fundamental equations for cfd in river flow simulations". *Chapter 2, Computational Fluid Dynamics, Applications in Environmental Hydraulics.* Bates P.D., Lane S.N., Ferguson R.I. (Eds). *John Wiley and Sons, Ltd.*: United Kingdom, 19–49.

82. Jang, C.L., and Shimizu, Y. (2005a). "Numerical simulation of relatively wide, shallow channels with erodible banks." *J. Hydr. Engrg.* ASCE 131(7):565-575.

83. Jang, C.L. and Shimizu, Y. (2005b). "Numerical experiments of the behavior of alternate bars with different bank strength." *J. Hydr. Res.* IAHR 43(6):596-612.

84. Jang C. L. and Shimizu Y. (2007). "Numerical Analysis of Braided Rivers and Alluvial Fan Deltas." *Engineering Applications of Computational Fluid Mechanics* 1(1):15-24

85. Jia, Y., and Wang, S. Y. (1999). "Numerical model for channel flow and morphological change studies." *J. Hydraul. Eng.,* 125(9):924–933.

86. *Jin, M., and Fread, D. L. (1997). ''Dynamic flood routing with explicit and implicit numerical solution schemes.'' *J. Hydraul. Eng.*, 123:3166–173.

87. Jin, Y. C., and Steffler, P. M.(1993). "Predicting flow in curved open channels by depth-averaged method". *J. Hydr. Engrg.,* ASCE, 119(1):109–124

88. Johannesson, H., and Parker, G. (1989a). "Secondary flow in a mildly sinuous channel." *J. Hydraul. Eng.*, 115(3):289–308.

89. Johannesson, H., and Parker, G. (1989b). "Velocity redistribution in meandering rivers." *J. Hydraul. Eng.*, 115(8):1019–1039.

90. Kalkwijk, J. P. T., and de Vriend, H. J.(1980). "Computation of the flow in shallow river bends". *J. Hydr. Res.*, 18(4):327-342.

91. Karki, K.C., Patankar, S.V.(1988). "Calculation procedure for viscous incompressible flow in complex geometries". *Num. Heat Transfer*, 14:295-307.

92. *Karki, K., (1986). "A calculation procedure for viscous flows at all speeds in complex geometries." *Ph. D. Dissertation*, University of Minnesota.

93. Kassem, A. A. and Chaudhry, M. H. (2002). "Numerical modeling of bed evolution in channel bends". *Journal of Hydraulic Engineering,* 128(5):507–514.

94. Khan, A.A. (2000). "Modeling flow over an initially dry bed. " *J. Hydr. Res.*, IAHR, 38(5): 383–388.

95. Kondolf, Mathias G., Piegey, Herve and Sear David (2003). "Integrating Geomorphological tools in Ecological and management Studies." *Tools in Fluvial Geomorphology.*, 634-642

96. Kuiry, Somendra Nath, Pramanik Kiran and Sen Dhrubajyoti.(2008). "Finite Volume Model for Shallow Water Equations with Improved Treatment of Source Terms." *Jr. of Hydraul. Engr.*, 134(2):231-242.

97. Lane, E.W. (1957). "A study of the shape of channels formed by the natural streams flowing in erodible material". *U.S Army Crops Engg. Div., Missouri River, M.R.D. Sediment.* Ser. No. 9:106.

98. Lane, S.N. (1998). "Hydraulic modelling in hydrology and geomorphology: A review of high resolution approaches." *Hydrological Processes* 12: 1131-1150.

99. Lane, S.N., Bradbrook, K.F., Richards, K.S., Biron, P.A. and Roy, A.G. (1999). "The application of computational fluid dynamics to natural river channels: three-dimensional versus two-dimensional approaches." *Geomorphology* 29: 1-20.

100. Lane S.N. and Ferguson R.I.(2005). "Modelling reach-scale fluvial flows". Chapter 10, Computational Fluid Dynamics, Applications in Environmental Hydraulics. Bates P.D., Lane S.N. and Ferguson R.I. (Eds*), John Wiley and Sons, Ltd.:* United Kingdom, 217–269.

101. *Leopold, L. B. and Wolman, M.G. (1957). "River channel patterns: Braided, meandering and straight". United States, *Geological Survey Professional Paper* 282-B, 35-85.

102. Lien, H. C., Hsieh, T. Y., Yang, J. C., and Yeh, K. C. (1999). "Bend flow simulation using 2D depth-averaged model." *J. Hydraul. Eng.*, 125(10):1097-1108.

103. *Leschziner, M. A. and Rodi, W. (1979). "Calculation of strongly curved open channel flow". *J. Hydr. Div.*, ASCE, 105(10):1297–1314.

104. Lyn, D.A. (1987). "Unsteady sediment-transport model". *Journal of Hydraulic Engineering* 113(1):1-15

105. *Majumdar, S.,Rodi, W. and Zhu, J.(1992). "Three-dimensional finite-volume method for incompressible flows with complex boundaries." *J.Fluids Eng.*, 114: 496-503.

106. *Maliska, C. R. Raithby, G. D., 1984. A method for computing three-dimensional flows using non-orthogonal boundary-fitted coordinates. *Int. J. Num. Methods Fluids*, 4:519-537.

107. McArdell, B. W. and Faeh, R. (2001). "A computational investigation of river braiding." *Gravel-bed rivers* V, M. P. Mosley(ed.) New Zealand Hydrological Society, Wellington, New Zealand, 73-86.

108. *Miller, S. D. (1988). "Investigation of dam-break flows." *Thesis presented to Washington State University,* at Pullman, Wash., in partial fulfillment of the requirements for the degree of Master of Science.

109. Molls, T., and Chaudhry, M. H. (1995). "Depth-averaged open-channel flow model." *J. Hydraul. Eng.*, 121(6): 453–465.

110. Morvan, H., Pender, G., Wright, N.G., Ervine, D.A.(2002). "Three-dimensional hydrodynamics of meandering compound channels". *Journal of Hydraulic Engineering* 128(7): 674–682.

111. Mosely, M. P., (1976). "An experimental study of channel confluences." *Journal of Geology*, 84:535-562.

112. Mosselman E. (1998). "Morphological modeling of rivers with erodible banks." *Hydrological Processes* 12: 1357–1370.

113. Munavalli, G. R., M.S. Mohan Kumar, M. S.(2004). "Modified Lagrangian method for modeling water quality in distribution systems." *Water Research* 38:2973-2988.

114. Murray, A.B. and Paola, C. (1994). "A cellular model of braided rivers." *Nature* 371:54-57.

115. Murray, A. B., and Paola, C. (1997). "Properties of a cellular braided stream model." *Earth Surf. Processes Landforms*, 22, 1001–1025.

116. Nagata, N., Hosoda, T. and Muramoto, Y. (2000). "Numerical analysis of river channel processes with bank erosion". *J. Hydraul. Eng.*, 126(4):243–252.

117. Nagata N, Hosoda T, Muramoto Y.(2000b). "Numerical analysis of river channel processes with bank erosion". *Journal of Hydraulic Engineering* 112(4):243–252.

118. Nagata, T., Hosoda, T., Muramoto, Y., and Rahman, M. M.(1997). "Development of the numerical model to forecast the channel processes with bank erosion". *Proc., 4th Japan-Chinese (Taipei) Joint Seminar on Natural Hazard Mitigation,* 167–176.

119. NDMA (2011). "Study of Brahmaputra river erosion and its control.". Phase-1, *unpublished report* of study conducted by Dept. of Water Resources Development and Management, I.I.T for *National Disaster Management Authority of India, New Delhi.*

120. *Nezu, I. and Nakagawa, H. (1993). "Turbulence in open-channel flows." *Balkema Publishers*, Rotterdam, Netherlands.

121. Odgaard, A. (1989a). "River meander model. I: Development." *J. Hydraul. Eng.*, 115(11):1433–1450.

122. Odgaard, A. (1989b). "River meander model. II: Application." *J. Hydraul. Eng.*, 115(11): 1451–1464.

123. Odgaard, A.J. and Bergs M.A. (1988). "Flow processes in a curved alluvial channel". *Water Resources Research* ,24(1):45–56

124. Olsen, N.R.B. (1999), "Two-dimensional numerical modelling of flushing processes in water reservoirs." *Journal of Hydraulic Research*, 37(1):3-16.

125. Patankar, S.V. (1980). Numerical Heat Transfer and Fluid Flow. *McGraw-Hill*, Inc., New York.

126. Patankar, S.V. and Spalding, D.B. (1972). "A calculation procedure for heat, mass and momentum transfer in three-dimensional parabolic flows", *Int. J. Heat Mass Transfer*, 15:1787-1806.

127. Parker, G., (1976). "On the cause and characteristics scale of meandering and braided in rivers", *Journal of Fluid Mechanics*, 76:459-80.

128. Parker G, Sawai K. and Ikeda S. (1982). "Theory of river meanders. part 2. Nonlinear deformation of finite-amplitude bends." *Journal of Fluid Mechanics* 115:303–314

129. Patel, Prem Lal , Porey, Prakash Devidas and Patel, Shailesh kumar B.(2010). "Computation of critical tractive stress of scaling sizes in non-uniform sediments", *Journal of Hydraulic Research*, 48(4):531 - 537

130. *Peric, M. (1985). "Finite volume method for the prediction of three-dimensional fluid flow in complex duct". *Ph.D. thesis, Imperial College*, London.

131. *Prandtl, L. (1952). "Essentials of fluid dynamics", London, *Blackie and Sons Press Trust of India Report*, (1995), The Sentinel, 7th July, pp. 3.

132. Rahuel, J.L. and Holly, F.M. (1989). "Modeling of riverbed evolution for bed load sediment mixtures" *J. Hydr. Engrg.*, ASCE, 115(11), 1521-1542.

133. *Rastogi, A. K. and Rodi, W. (1978). "Predictions of Heat and Mass Transfer in Open Channels." *Journal of the Hydraulics Division*, 104(3):397-420.

134. Richards, K. (1982). "Rivers: forms and process in alluvial channels." (London: *Methuen & Co. Ltd.*)

135. Rhie, T.M. and Chow, A. (1983). "Numerical study of the turbulent flow past an isolated air foil with trailing-edge separation." *AIAA J.*, 21:1525-1532.

136. Rodi, W. (1984). "Turbulence models and their application in hydraulics—A state of the art review", 2nd Ed., *IAHR*, Delft, The Netherlands.

137. *Rozovskii, I.L. (1957). "Flow of water in bends of open channels." *Academy of Sciences of the Ukrainian SSR*, kiev, U.S.S.R

138. *Rozovskii, I. (1961). "Flow of water in bends of open channels," *Academy of Sciences of Ukrainian S.S.R.*, Translated from Russian, Israel Program for Science Translation, 1-233.

139. Rust, B.R. (1978b). "Depositional Models for Braided Alluvium." In: Miall, A.D., (Ed) *Fluvial Sedimentology,* Canadian Society of Petroleum Geologists Memoirs,. 5: 605-626.

140. *Sanders, B. F., and Katopodes, N. D. (1999). ''Active flood hazard mitigation. I: Bidirectional wave control.'' *J. Hydraul. Eng.*, 125(10):1057–1070.

141. *Sanders, B. F. (2001). "High-resolution and non-oscillatory solution of the St. Venant equations in non-rectangular and non-prismatic channels." *J. Hydraul. Res.*, 39(3): 321–330.

142. Sankhua, R.N. (2005) "ANN based spatio-temporal morphological model of the river Brahmaputra." *Ph.D Thesis, Dept. of WRD&M,* I.I.T. Roorkee

143. Sarma, J.N. (2002). "A Study on pattern of erosion and bankline migration of the River Brahmaputra in Assam using GIS". *Report Disaster Management in North-Eastern region, Dept. of Revenue, Govt. of Assam,* 50-53.

144. Seo, Won., Lee, Myung Eun., and Baek, Kyong Oh (2008). "2D modeling of heterogeneous dispersion in meandering channels." *J. Hydraul. Eng.*, 134(2): 196-204.

145. Seminara G., Zolezzi G., Tubino M. and Zardi D.(2001). "Downstream and upstream influence in river meandering. part 2. planimetric development." *Journal of Fluid Mechanics* 438: 213–230.

146. *Sharatchandra M.C. (1995). "A strongly conservative finite volume formulation for fluidflows in complex geometries using contravariant velocity components".*Ph.D. Dissertation,* Texas A&M University.

147. Sharma, Nayan, (2004). "Mathematical Modelling and Braid Indicators." In The Brahmaputra Basin Water Resources, Vijay P.Singh, Nayan Sharma and C. Shekhar P. Ojha (Ed.), *Dordrecht: Kluwer Academic Publishers,* 47:229-260.

148. Sharma, Nayan and Akhtar, Md Parwez (2010). "A Satellite Data Based Approach to Study Braiding Behaviour for Monitoring and Management of the Brahmaputra River", published in *proceedings of 3rd International Perspective on Current & Future State of Water Resources & the Environment*, January 4-6, 2010

organized by EWRI, American Society of Civil Engineers in IIT Madras, Chennai, India.

149. Sinha S.K., Sotiropoulos F., Odgaard J. (1998). "Three Dimensional Numerical Model for flow through Natural Rivers" *Jr of Hydraulic Engg*, 124(1): 13-53.

150. Sheng, Y.P. (1983). "Mathematical modeling of three-dimensional coastal currents and sediment dispersion: Model development and application", *Technical Report CERC-83*-2, Aeronautical Research Associates of Princeton, Inc., N.J.

151. *Shimizu, Y., Hirano, N., and Watanabe, Y. (1996). "Numerical calculation of bank erosion and free meandering." *Annu. J. Hydr. Engrg.*, JSCE, 40: 921–926 (in Japanese).

152. *Shimizu, Y., Kurabayashi, H., and Fujita, M. (2001). "Numerical calculation of bed deformation in braided stream. " *Annu. J. Hydr. Engrg.*, JSCE, 45, 739–744 (in Japanese).

153. Shimizu, Y., and Itakura, T. (1989). "Calculation of bed variation in alluvial channels." *J. Hydraul. Eng.*, 115(3): 367–384.

154. Shimizu, Y., Yamaguchi, H., and Itakura, T. (1990). "Three-dimensional computation of flow and bed deformation." *J. Hydraul. Eng.*, 116(9): 1090–1108.

155. Schumm, S.A. and Khan, H.R. (1972) "Experimental study of channel patterns," *Bull. of Geological Society of America*, 83:1755-1770.

156. *Shyy, W., Correa, S.M., Braaten, M. E.(1988). "Computation of flow in gas turbine Combustor". *Combust. Sci. Technol.*, 58(1-3): 97-117.

157. *Shyy, W., Udaykumar, H.S., Rao, M.M. and Smith, R.W.(1996). "Computational Fluid Dynamics with Moving Boundaries," *Taylor and Francis.*

158. *Shyy, W., Tong, S.S. and Correa, S. M. (1985). "Numerical recirculating flow calculation sing a body-fitted coordinate system." *Num. Heat Transfer*, Part A, 8: 99-113.

159. Soulis, J.V. (2002). "A fully coupled numerical technique for 2d bed morphology calculations". *International Journal for Numerical Methods in Fluids* 38(1):71–98.

160. Sotiropoulos, F. (2005). "Introduction to statistical turbulence modelling for hydraulic engineering flows". Chapter 5, Computational Fluid Dynamics, Applications in Environmental Hydraulics. Bates P.D., Lane S.N. and Ferguson R.I. (Eds), *John Wiley and Sons, Ltd.*: United Kingdom, 91–120

161. Smith, N.D. (1970), "The Braided Stream Depositional Environment", Comparison of the Platte river with some Silurian Clastic Rocks, *North central Appalacfians, Geological Society of America Bulletin,*.81: 2993-3014.

162. Smith, N.D., (1974), "Sedimentology and Bar Formation in the Upper Kicking Horse River, A Braided Out Wash Stream", *Journal of Geology*, 82: 205-223.

163. *Soares Frazao, S., Morris, M., and Zech, Y. (2000). Concerted Action on Dambreak Modelling: Objectives, Project Report, Test Cases, *Meeting Proceedings. Univ. catholique de Louvain, Civil Engineering Dept., Hydraulics Division, Louvain-la-Neuve, Belgium*, CD-ROM.

164. Steger, J.L. and Sorenson, R.L. (1980). "Use of hyperbolic partial differential equations to generate body-fitted coordinates". *Num. Grid Generation Techniques*, NASA conference publication 2166, Hampton, Va.

165. Spasojevic, M. and Holly, F.M. Jr. (1993). "Three-dimensional numerical simulation of mobilebed hydrodynamics." *Technical Report No. 367, Iowa Institute of Hydraulic Research,* the University of Iowa, USA.

166. Sun T., Meakin P. and Jossang T. (2001a). "Meander migration and the lateral tilting of floodplains". *Water Resources Research*, 37(5): 1485-1502.

167. *Tao, J. (1984). "Numerical modeling of wave run up and break on seashore". *Acta Oceanologica Sinica*, 6(5) (in Chinese).

168. *Tan, W. (1992). "Shallow water hydrodynamics." *Elsevier*, Amsterdam, The Netherlands.

169. Thomas, W.A. (1982). "Chapter 18: Mathematical modeling of sediment movement." Gravel-Bed Rivers, R.D. Hey *et al.*, eds., *John Wiley & Sons, Ltd.*, New York.

170. Thomas P.D. and Middlecoff, J. F. (1980). "Direct Control of the Grid Point Distribution in Meshes Generated by Elliptic Systems, " *Journl. of American Institute of Aeronautics and Astronautics*, 18(6): 652-657

171. Thomas, T.G. and Williams, J.J.R. (1995). "Large eddy simulation of turbulent flow in an asymmetric compound channel." *Journal of Hydraulic Research*, 33:27-41.

172. Thompson, J. (1876). "On the origin and winding of rivers in alluvial plains, with remarks on flow around bends in pipes". *Proc., Royal Soc.*, London, 25: 5.

173. Thompson, J.F. (1982). "Numerical Grid Generation." *North-Holland*, New York.

174. Thompson, J.F., Warsi, Z.U., Mastin, C. W. (1985). "Numerical Grid Generation, Foundation and Applications". *North-Holland*, New York.

175. *Tseng, M. H., and Chu, C. R. (2000). "Two-dimensional shallow water flows simulation using TVD-MacCormack Scheme." *J. Hydraul. Res.*, 38(2): 123–131.

176. *Tseng, M.-H., Hsu, C.-A., and Chu, C. R. (2001). "Channel routing in open-channel flow with surges." *J. Hydraul. Eng.*, 127(2): 115–122.

177. Van Doormal, J.P. and Raithby, G.D. (1984) "Enhancements of the SIMPLE method for predicting incompressible fluid flows." *Num. Heat Transfer*, 7:147-163.

178. *Van Rijn, L.C. (1987). "Mathematical modelling of morphological processes in the case of suspended sediment transport." *Delft Hydraulics Communication No. 382*, The Netherlands.

179. *Vasquez J. (2006). "Two-dimensional finite element river morphology model". *PhD Thesis, Department of Civil Engineering, the University of British Columbia*, Canada.

180. Versteeg, H.K., Malalasekera, W. (1995). "An Introduction to Computational Fluid Dynamics the Finite Volume Method". *Longman Scientific & Technical*, New York.

181. Wang, S. S. Y. and Hu, K. K. (1993). "Improved methodology for formulating finite element hydrodynamic models." *Finite Element in Fluids,* edited by T. J. Chun, Hemisphere publication Cooperation, 8:457-478.

182. *WAPCOS. (1993). "Morphological studies of river Brahmaputra", New Delhi.

183. Wang, Z.B. and Ribberink J.S. (1986). "The validity of a depth integrated model for suspended sediment transport". *Journal of Hydraulic Research* 24(1): 53-67.

184. Wang, S.S.Y. and Wu, W. (2004). "River sedimentation and morphology modeling- the state of the art and future development". *Proceedings of the Ninth International Symposium on River Sedimentation October 18- 21, 2004,* Yichang, China. pp 71-94.

185. *Wilson, C.A.M.E., Stoesser, T., Olsen, N.R.B. and Bates, P.D. (2003). "Application and validation of numerical codes in the prediction of compound channel flows." *Proceedings of the Institution of Civil Engineers-Water and Maritime Engineering*, 156:117-128.

186. Wu Weiming(2007). "Computational River Dynamics." Published by *Taylor & Francis Group,*London,UK., ISBN 978-0-415-44961-8

187. Wu, W., Rodi, W. and Wenka, T. (2000). "3D numerical modeling of low and sediment transport in open channels." *J. Hydraul. Eng.*, 126(1): 4–5.

188. Wu, W. and Vieira, D.A. (2002). "One-dimensional channel network model CCHE1D 3.0 -- Technical manual", *Technical Report No. NCCHE-TR-2002-1*, National Center for Computational Hydroscience and Engineering, The University of Mississippi.

189. *Wu, W., Wang, P. and Chiba, N. (2004b). "Comparison of five depth-averaged 2-D turbulence models for river flows". Archives of *Hydro-Eng. and Environ. Mechanics*, Polish Academy of Science, 51(2): 183-200.

190. Wu, W. (2004). "Depth-averaged 2-D numerical modeling of unsteady flow and non-uniform sediment transport in open channels", *J. Hydraulic Eng.*, ASCE, 135(10), 1013-1024.

191. Ye, J., and McCorquodale, J. A. (1997). "Depth-averaged hydrodynamic model in curvilinear collocated grid." *J. Hydraul. Eng.*, 123(5): 380-388.

192. Yeh, K. C., and Kennedy, J. (1993a). "Moment model of nonuniform channel-bend flow. I: Fixed beds." *J. Hydraul. Eng.*, 119(7): 776-795.

193. Yen, C. L., and Ho, S. Y. (1990). "Bed evolution of channel bends." *J. Hydr. Engrg.*, ASCE, 116(4): 544-562.

194. Zarrati, A.R., Tamai, N., and Jin Y. C. (2005). "Mathematical modeling of meandering channels with a generalized depth averaged model." *J. Hydraul. Eng.* 131(6): 467-474.

195. Zhang Y., Jia, Y. (2005). "CCHE2D Mesh Generator *User's Manual*, National Center for Computational Hydroscience and Engg, US.

196. Zhu, J. and Rodi, W. (1991). "A low dispersion and bounded convection scheme." *Comput. Meths.Appl. Mech. Eng.*, 92: 87-96.

197. Zhou, J. G. (1995). "Velocity-depth coupling in shallow-water flows." *J. Hydraul. Eng.*, 121(10): 717-724.

198. *Zhao, D. H., Shen, H. W., Lai, J. S., and Tabios, G. Q., III. (1996). "Approximate Riemann solvers in FVM for 2D hydraulic shock wave modeling." *J. Hydraul. Eng.*, 122(12): 692-702.

199. *Zhu, J. (1992a) "FAST2D: A computer program for numerical simulation of two-dimensional incompressible flows with complex boundaries." *Institute of Hydromechanics*, Karlsruhe University, Germany.

* *Cross references*

General reference format:

Surname$_1$, A_1.B_1., Surname$_2$, A_2.B_2. and Surname$_3$, A_3.B_3. (year). "Title". *Journal's Name* & Affiliation, Volume No. (Issue No.): paper-pages.

APPENDIX-I

Derivation of Duan (2004)'s Approach

Duan(2004) has suggested the expressions for evaluating dispersion stress terms in curvilinear coordinate system as follows.

$$D_{xx}^{c} = \chi^{2} U_s U_s h\left[-\eta_0 \ln \eta_0 (\ln \eta_0 - 2) + 2\eta_0 (1-\eta_0)(1-\ln \eta_0) - (\eta_0 - 1)^3\right] \quad \text{I (1a)}$$

$$D_{xy}^{c} = 3.5C\chi^{2} \frac{h^2}{r} U_s U_s \left(\left[-\eta_0^2 \ln \eta_0 + \eta_0 \ln \eta_0 - \eta_0 + \eta_0^3\right]\right) \quad \text{I (1b)}$$

$$D_{yy}^{c} = 49 \frac{h^3}{r^2} U_s U_s \left(-\frac{\eta_0^3}{3} + \frac{\eta_0^2}{2} - \frac{\eta_0}{4} + \frac{1}{12}\right) \quad \text{I (1c)}$$

Where $\chi = \dfrac{1}{\eta_0 - 1 - \ln(\eta_0)}$; $\eta_o = \dfrac{z_0}{h}$ = Dimensionless zero bed elevation, U_s =Depth averaged velocity in stream-wise direction. C=constant of integration,

Stepwise derivation of Duan(2004) correlations

Assuming the stream wise velocity profile satisfies the logarithmic distribution law as.

$$\frac{u_s}{U^*} = \frac{1}{\kappa} \ln\left(\frac{z}{z_o}\right) \quad \text{I (2)}$$

Where z = vertical coordinate, z_o = zero bed elevation, u_s= streamwise actual velocity, U^* = Shear velocity, κ = Von kormann's coefficient (0.4 for clear water), z_o = zero bed elevation, can be calculated according to flow Reynold number as follows.

$$z_0 = 0.11\frac{\nu}{U^*} \ldots\ldots\ldots, \frac{U^* k_s}{\nu} \leq 5;$$

$$z_0 = 0.033 k_s \ldots\ldots\ldots, \frac{U^* k_s}{\nu} \geq 70;$$

$$z_0 = 0.11\frac{\nu}{U^*} + 0.033 k_s \ldots, 5 \geq \frac{U^* k_s}{\nu} \geq 70$$

ν = kinematic viscosity; k_s = Roughness height; U^* = Shear Velocity

Stream wise depth averaged velocity (U_s)

$$U_s = \frac{1}{h}\int_0^h u_s dz \quad \rightarrow \quad U_s = \frac{\int_{z_0}^{h} u_s dz}{h} \qquad \text{I (3)}$$

Let, $\eta_o = \frac{z_0}{h} = \text{Dimensionless zero bed elevation}$ I (4)

Putting the value of Eq.I (2) in Eq.I (3), one obtains,

$$\frac{U_s}{U^*} = \frac{1}{\kappa h}\int_{z_0}^{h} \ln\left(\frac{z}{z_0}\right) dz, \qquad \text{I (5a)}$$

Or,

$$\frac{U_s}{U^*} = \frac{1}{\kappa}\frac{z_0}{h}\left[\frac{z}{z_0}\ln\left(\frac{z}{z_0}\right) - \frac{z}{z_0}\right]_{z_0}^{h}, \qquad \text{I (5b)}$$

Or,

$$\frac{U_s}{U^*} = \frac{1}{\kappa}\frac{z_0}{h}\left[\frac{h}{z_0}\ln\left(\frac{h}{z_0}\right) - \frac{h}{z_0} - \frac{z_0}{z_0}\ln\left(\frac{z_0}{z_0}\right) + \frac{z_0}{z_0}\right], \qquad \text{I (5c)}$$

Or,

$$\frac{U_s}{U^*} = \frac{1}{\kappa}\left[\ln\left(\frac{h}{z_0}\right) - 1 + \frac{z_0}{h}\right] = \frac{1}{\kappa}\left[\frac{z_0}{h} - 1 + \ln\left(\frac{h}{z_0}\right)\right], \qquad \text{I (5d)}$$

Or

$$\frac{U_s}{U^*} = \frac{1}{\kappa}\left[-\ln(\eta_0) - 1 + \eta_0\right] = \frac{1}{\kappa}\left[\eta_0 - 1 - \ln(\eta_0)\right] \qquad \text{I (5e)}$$

Dividing Eq.I (1) with Eq.I (5e), one can readily get,

$$\frac{u_s}{U_s} = \frac{\ln\left(\frac{z}{z_0}\right)}{\eta_0 - 1 - \ln(\eta_0)} \qquad \text{I (6a)}$$

Or,

$$\frac{u_s}{U_s} - 1 = \frac{\ln\left(\frac{z}{\eta_0 h}\right) - \eta_0 + 1 + \ln \eta_0}{\eta_0 - 1 - \ln(\eta_0)} \qquad \text{I (6b)}$$

Or,

$$\frac{u_s - U_s}{U_s} = \frac{\ln\left(\frac{z}{h}\right) - \ln \eta_0 - \eta_0 + 1 + \ln \eta_0}{\eta_0 - 1 - \ln(\eta_0)} \qquad \text{I (6c)}$$

Or,

$$u_s - U_s = \frac{U_s}{\eta_0 - 1 - \ln(\eta_0)}\left(\ln\left(\frac{z}{h}\right) - \eta_0 + 1\right) \qquad \text{I (6d)}$$

The transverse velocity profile

The transverse velocity profile of the secondary flow is assumed linear. The profile of the transverse velocity proposed by Odgaard (1989a) is adopted.

$$u_n = U_n + 2v_s\left(\frac{z}{h} - \frac{1}{2}\right) \qquad \text{I (7a)}$$

u_n = actual transverse velocity, U_n = depth averaged transverse velocity and v_s = Transverse velocity at the water surface.

Engelund and Skovgaard *(1973)* derived the deviation angle of the bottom shear and gave that,

$$\left(\frac{\tau_n}{\tau_s}\right)_b \approx \left(\frac{u_n}{u_s}\right)_b = 7.0\frac{h}{r} \qquad \text{I (7b)}$$

r = radius of channel curvature, According to Eq.I (7a), the secondary flow velocities at the surface and the bottom are equal. Therefore, Eq.I (7b) was used as transverse velocity at surface.

So one can write,

$(u_n)_b = 7.0(h/r)(u_s)_b$ I(7c)

At surface, one has from Eq. I (7a)

$$u_n = U_n + 7.0\frac{h}{r}U_s\left(\frac{z}{h} - \frac{1}{2}\right) \qquad \text{I (7d)}$$

Let

$$\chi = \frac{1}{\zeta_0 - 1 - \ln(\zeta_0)} \qquad \text{I (7f)}$$

Thus, in terms of χ, Eq. I (5b) and Eq.I (7d) become,

$$u_s - U_s = \chi U_s\left(\ln\left(\frac{z}{h}\right) - \eta_0 + 1\right) \qquad \text{I (8a)}$$

$$u_n - U_n = 7.0\frac{h}{r}U_s\left(\frac{z}{h} - \frac{1}{2}\right) \qquad \text{I (8b)}$$

Curvilinear dispersion stress terms are as follows

$$D^c{}_{xx} = \int_{z_0}^{h}(u_s - U_s)^2\,dz \qquad \text{I (10)}$$

$$D^c{}_{xy} = \int_{z_0}^{h}(u_s - U_s)(u_n - U_n)dz \qquad \text{I (11)}$$

$$D^c{}_{yy} = \int_{z_0}^{h}(u_n - U_n)^2\,dz \qquad \text{I (12)}$$

The First Term $D_{xx}{}^c$

Subtituting the value of Eq.I (8a) in Eq.I (10), one has,

$$D^c_{xx} = \chi^2 U_s U_s \int_{z_0}^{h}\left(\ln\left(\frac{z}{h}\right) - \eta_0 + 1\right)^2 dz \qquad \text{I (13a)}$$

Or,

$$D^c_{xx} = \chi^2 U_s U_s\left[\int_{z_0}^{h}\left(\ln\left(\frac{z}{h}\right)\right)^2 dz - 2(\eta_0 - 1)\int_{z_0}^{h}\ln\left(\frac{z}{h}\right)dz + (\eta_0 - 1)^2\int_{z_0}^{h}1\,dz\right] \qquad \text{I (13b)}$$

Now consider $z/h=m$, then; $dz=h.dm$, $m1=z_0/h=\eta_0$ lower integral bound, $m2=h/h=1$, upper integral bound.

Transforming Eq.I (13b), one has,

$$D_{xx}^{c} = \chi^2 U_s U_s h\left[\int_{\zeta_0}^{1}(\ln(m))^2\,dm - 2(\eta_0-1)\int_{\zeta_0}^{1}\ln(m)dz + (1-\eta_0)(\eta_0-1)^2\right] \quad \text{I (13c)}$$

Or,

$$D_{xx}^{c} = \chi^2 U_s U_s h\left[\left(m(\ln m)^2 - 2m\ln m + 2m\right)_{\zeta_0}^{1} - 2(\eta_0-1)(m\ln m - m)_{\zeta_0}^{1} - (1-\eta_0)^3\right] \quad \text{I (13d)}$$

Or,

$$D_{xx}^{c} = \chi^2 U_s U_s h\left[2-\eta_0(\ln\eta_0)^2 + 2\eta_0\ln\eta_0 - 2\eta_0 - 2(\eta_0-1)(-1-\eta_0\ln\eta_0+\eta_0) - (1-\eta_0)^3\right] \quad \text{I (13e)}$$

Or,

$$D_{xx}^{c} = \chi^2 U_s U_s h\left[-\eta_0\ln\eta_0(\ln\eta_0 - 2) + 2\eta_0(1-\eta_0)(1-\ln\eta_0) - (\eta_0-1)^3\right] \quad \text{I (13f)}$$

The expression Eq.I (13f) is identical with Duan(2004) as shown as in Eq.I (1a)

The Second Dispersion Term D_{xy}^{c}

Putting the value of from Eqs.A(8) and A(8b), in Eq.A(11); one has,

$$D_{xy}^{c} = \int_{z_0}^{h}\chi U_s\left(\ln\left(\frac{z}{h}\right) - \eta_0 + 1\right)\times 7.0\frac{h}{r}U_s\left(\frac{1}{2} - \frac{z}{h}\right)dz \quad \text{I (14a)}$$

Or,

$$D_{xy}^{c} = -7.0\chi\frac{h}{r}U_s U_s\int_{z_0}^{h}\left(\ln\left(\frac{z}{h}\right) - \eta_0 + 1\right)\left(\frac{1}{2} - \frac{z}{h}\right)dz \quad \text{I (14b)}$$

Or,

$$D_{xy}^{c} = -7.0\chi^2\ln\eta_0\frac{h}{r}U_s U_s\left(\frac{1}{2}\int_{z_0}^{h}\ln\frac{z}{h}dz - \int_{z_0}^{h}\frac{z}{h}\ln\frac{z}{h}dz + \frac{1}{2}(1-\eta_0)\int_{z_0}^{h}dz - (\eta_0-1)\int_{z_0}^{h}\frac{z}{h}dz\right) \quad \text{I (14c)}$$

Again taking $m=z/h$ and integrating and transforming the upper and lower bound as done earlier, taking h common, one obtains,

$$D_{xy}^{c} = 14.0\chi^2 \ln\eta_0 \frac{h^2}{r} U_s U_s \left(\frac{1}{2}[m\ln m - m]_{\eta_0}^{1} - \frac{1}{4}[2m^2 \ln m - m^2]_{\eta_0}^{1} + \frac{1}{2}(1-\eta_0)(1-\eta_0) - \frac{1}{2}(\eta_0 - 1)[m^2]_{\eta_0}^{1} \right) \quad \text{I (14d)}$$

Or,

$$D_{xy}^{c} = -7.0\,\chi \frac{h^2}{r} U_s U_s \frac{1}{4} \begin{pmatrix} 2[-1 - \eta_0 \ln \eta_0 + \eta_0] - [-1 - 2\eta_0^2 \ln \eta_0 + \eta_0^2] + \\ 2(1-\eta_0)(1-\eta_0) + 2(\eta_0 - 1)[1 - \eta_0^2] \end{pmatrix} \quad \text{I (14e)}$$

Or,

$$D_{xy}^{c} = -1.75\,\chi \frac{h^2}{r} U_s U_s \left(\begin{bmatrix} -2 - 2\eta_0 \ln \eta_0 + 2\eta_0 + 1 + 2\eta_0^2 \ln \eta_0 - \eta_0^2 + 2\eta_0 - 2\eta_0^3 - 2 + 2\eta_0^2 \\ +2 - 4\eta_0 + 2\eta_0^2 \end{bmatrix} \right) \quad \text{I (14f)}$$

$$D_{xy}^{c} = 1.75\,\chi \frac{h^2}{r} U_s U_s \left([2\eta_0 \ln \eta_0 - 2\eta_0^2 \ln \eta_0 - 3\eta_0^2 + 2\eta_0^3 + 1] \right) \quad \text{I (14g)}$$

Eq. I (14g) is comparable with Eq.I (2b).

The Third Dispersion Term D_{vv}^{c}

Substituting the values of Eq. I (8b) in Eq.I (12), one can get,

$$D_{yy}^{c} = 49.0 \frac{h^2}{r^2} U_s U_s \int_{z_0}^{h} \left(\frac{z}{h} - \frac{1}{2} \right)^2 dz \quad \text{I (15a)}$$

One can write Eq. I (15a) as

$$D_{yy}^{c} = 49.0 \frac{h^2}{r^2} U_s U_s \int_{z_0}^{h} \left(\frac{z}{h} - \frac{1}{2} \right)^2 dz \quad \text{I (15b)}$$

Or,

$$D_{yy}^{c} = 49.0 \frac{h^2}{r^2} U_s U_s \left(\int_{z_0}^{h} \left(\frac{z}{h} \right)^2 dz - \int_{z_0}^{h} \left(\frac{z}{h} \right) dz + \frac{1}{4} \int_{z_0}^{h} dz \right) \quad \text{I (15c)}$$

Again taking $m=z/h$ and integrating and transforming the upper and lower bound as done earlier, taking h common, one can get,

$$D_{yy}^{c} = 49.0\frac{h^3}{r^2}U_s U_s\left(\left[\frac{m^3}{3}\right]_{\eta_0}^{1} - \left[\frac{m^2}{2}\right]_{\eta_0}^{1} + \frac{1}{4}(1-\eta_0)\right) \qquad \text{I (15d)}$$

Or,

$$D_{yy}^{c} = 49.0\frac{h^3}{r^2}U_s U_s\left(\frac{1}{3} - \frac{\eta_0^3}{3} - \left(\frac{1}{2} - \frac{\eta_0^2}{2}\right) + \frac{1}{4} - \frac{\eta_0}{4}\right) \qquad \text{I (15e)}$$

Or,

$$D_{yy}^{c} = 49.0\frac{h^3}{r^2}U_s U_s\left(\frac{1}{3} - \frac{\eta_0^3}{3} - \frac{1}{2} + \frac{\eta_0^2}{2} + \frac{1}{4} - \frac{\eta_0}{4}\right) \qquad \text{I (15f)}$$

Or,

$$D_{yy}^{c} = 49.0\frac{h^3}{r^2}U_s U_s\left(\frac{1}{3} - \frac{\eta_0^3}{3} - \frac{1}{2} + \frac{\eta_0^2}{2} + \frac{1}{4} - \frac{\eta_0}{4}\right) \qquad \text{I (15g)}$$

Or,

$$D_{yy}^{c} = 49.0\frac{h^3}{r^2}U_s U_s\left(-\frac{\eta_0^3}{3} + \frac{\eta_0^2}{2} - \frac{\eta_0}{4} + \frac{1}{12}\right) \qquad \text{I (15h)}$$

Eq.I (15h) is identical to Eq.I (1c).

APPENDIX-II

(i) Determination of streamline and transverse velocities from cartesian velocities in on orthogonal, non uniform mesh

θ_s=Angle between the streamwise direction and the positive x-axis;

θ_n=Angle between transverse direction pointing towards outer bank and positive x-axis;

$$u_x = u_s \cos\theta_s + u_n \cos\theta_n$$
$$u_y = u_s \sin\theta_s + u_n \sin\theta_n \quad \text{(Duan, 2004)} \qquad \text{II (1)}$$

In Matrix form one can write,

$$\begin{bmatrix} u_x \\ u_y \end{bmatrix} = \begin{bmatrix} \cos\theta_s & \cos\theta_n \\ \sin\theta_s & \sin\theta_n \end{bmatrix} \begin{bmatrix} u_s \\ u_n \end{bmatrix} \qquad \text{II (2)}$$

Matrix inverse operation is done as follows,

$$\begin{bmatrix} u_s \\ u_n \end{bmatrix} = \begin{bmatrix} \cos\theta_s & \cos\theta_n \\ \sin\theta_s & \sin\theta_n \end{bmatrix}^{-1} \begin{bmatrix} u_x \\ u_y \end{bmatrix}, \text{ One obtains,} \qquad \text{II (3)}$$

$$u_s = \frac{1}{|J|}\left(u_x \sin\theta_n - u_y \sin\theta_s\right)$$

$$u_n = \frac{1}{|J|}\left(-u_x \cos\theta_n + u_y \cos\theta_s\right) \qquad \text{II (4)}$$

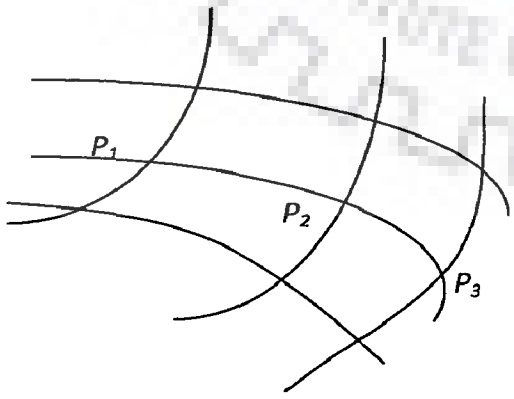

Figure II (1a) Streamwise curve fitting

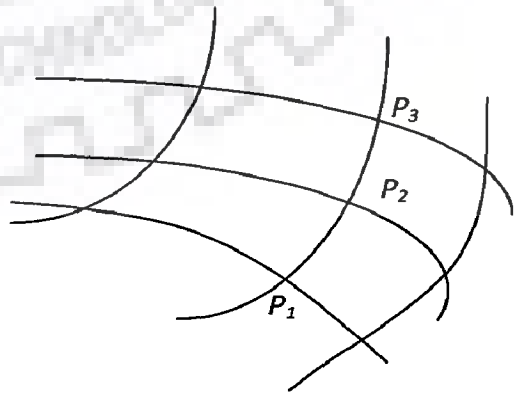

Figure II (1b) Transverse curve fitting

where, $J = \cos\theta_s \sin\theta_n - \sin\theta_s \cos\theta_n$

(ii) Determination of θ_s(Theta s) and θ_nTheta (n)

Polynomial Fitting Curve passing through three points

Consider each set of three consecutive grid points $P_{i,j}$ (x_i,y_i) follow polynomial curve in stream-wise or tranverse direction in 2-D plane (See Figure II(1a) and II(1b) as shown namely $P_1(x_1,y_1)$; $P_2(x_2,y_2$ *and* $P_3(x_3,y_3)$;

Considering simplified approach, the following equation may be adopted for the curve passing through P_1, P_2 and P_3.

$$y = a + bx + cx^2 \qquad \text{II (5)}$$

Tangent to the curve Eq.II (1) can be expressed as,

$$\tan\theta = \left.\frac{dy}{dx}\right|_{P_2} = b + 2cx_2 \qquad \text{II (6)}$$

$$\theta|_{'s'or'n'} = \tan^{-1}(b + 2cx_2) \qquad \text{II (7)}$$

One can evaluate θ_s or θ_n in Eq II(3) if 'b' and 'c' are known.

Computation of coefficients a, b and c

One can write; for point P_1,P_2 and P_3 satisfy Eq. II(5) as below;

$$\begin{aligned} y_1 &= a + bx_1 + cx_1^2 \\ y_2 &= a + bx_2 + cx_2^2 \\ y_3 &= a + bx_3 + cx_3^2 \end{aligned} \qquad \text{II (8a)}$$

Writing in matrix form;

$$\begin{bmatrix} y_1 \\ y_2 \\ y_3 \end{bmatrix} = \begin{bmatrix} a \\ b \\ c \end{bmatrix} \begin{bmatrix} 1 & x_1 & x_1^2 \\ 1 & x_2 & x_2^2 \\ 1 & x_3 & x_3^2 \end{bmatrix} \qquad \text{II (8b)}$$

Matrix inverse application, one gets

$$\begin{bmatrix} a \\ b \\ c \end{bmatrix} = \begin{bmatrix} y_1 \\ y_2 \\ y_3 \end{bmatrix} \begin{bmatrix} 1 & x_1 & x_1^2 \\ 1 & x_2 & x_2^2 \\ 1 & x_3 & x_3^2 \end{bmatrix}^{-1} \qquad \text{II (8c)}$$

Or,

$$\begin{bmatrix} a \\ b \\ c \end{bmatrix} = \frac{1}{|DET|} \begin{bmatrix} y_1 \\ y_2 \\ y_3 \end{bmatrix} \begin{bmatrix} (x_2x_3^2 - x_3x_2^2) & -(x_3^2 - x_2^2) & (x_3 - x_2) \\ -(x_1x_3^2 - x_3x_1^2) & (x_3^2 - x_1^2) & -(x_2 - x_1) \\ (x_1x_2^2 - x_2x_1^2) & -(x_2^2 - x_1^2) & (x_2 - x_1) \end{bmatrix} \qquad \text{II (8d)}$$

where Determinant value is $DET \begin{bmatrix} 1 & x_1 & x_1^2 \\ 1 & x_2 & x_2^2 \\ 1 & x_3 & x_3^2 \end{bmatrix}$ II (8e)

Using Eqs. II (8d) and II (8e), for each set of known grid points one can obtain b and c values. Using II (7), θ_s or θ_n can be determined. Hence, Substituting the values of θ_s and θ_n in Eq. II(4), streamwise and transverse velocity can be evaluated and vice versa from Eq. II(1).

(iii) Trapezoidal rule for area computation for non uniform interval

$$\int_a^b f(x)dx \approx \frac{1}{2}\sum_{k=1}^{N}(x_k - x_{k-1})(f(x_x) - f(x_{k-1}))$$

(Wikipedia references)

APPENDIX-III

Graphical data for fourteen field measured predefined cross sections of the study reach (Pandu-Jogighopa) for the year 1997

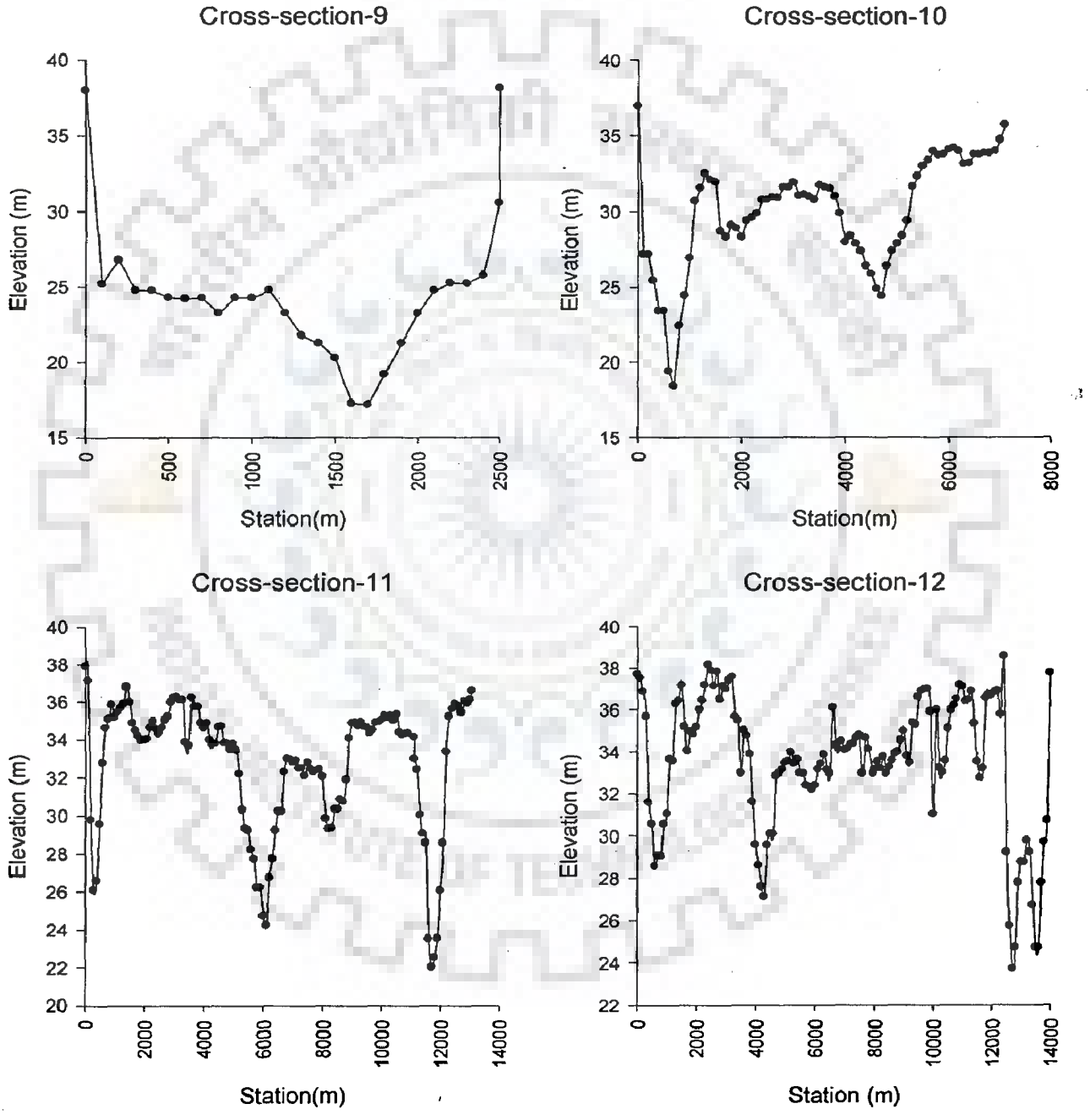

Cross-section -13

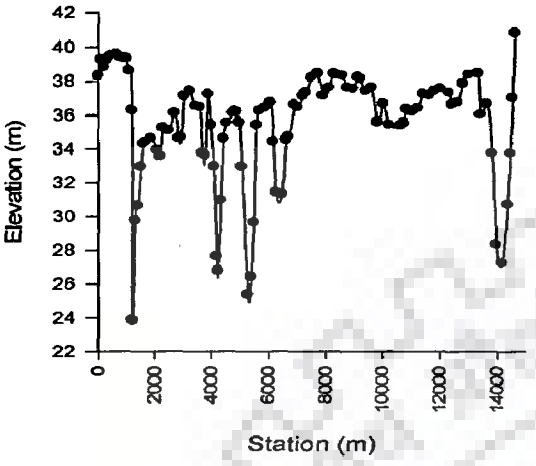

Cross-section -14

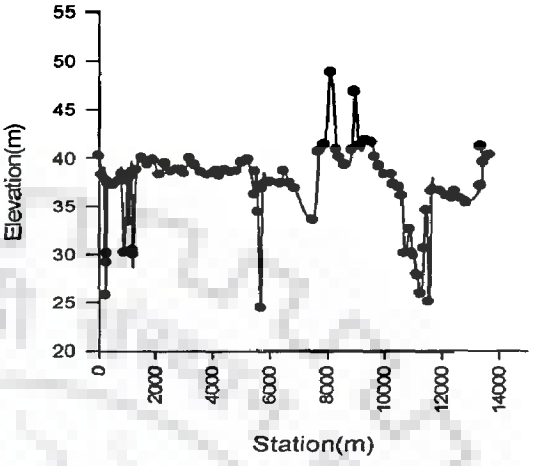

Cross-section-15

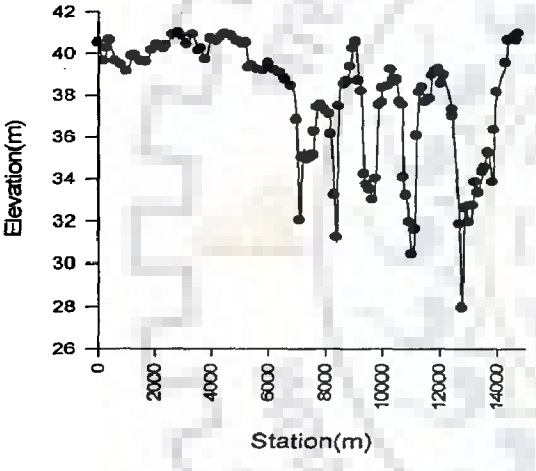

Cross-section 16

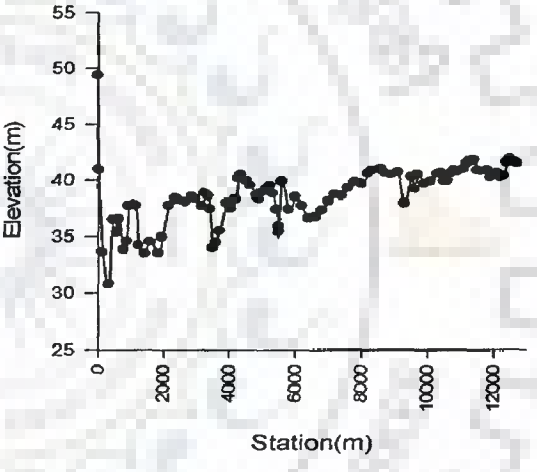

Cross-section-17

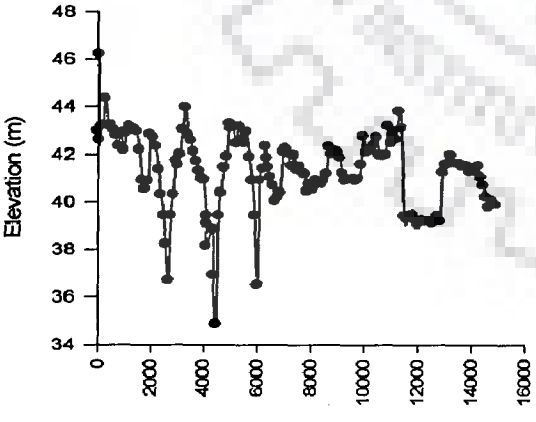

Cross-section-18

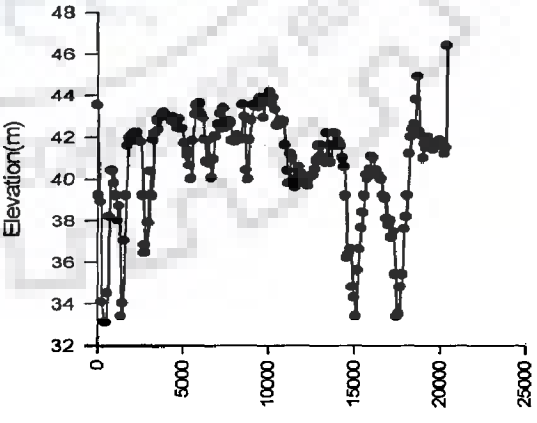

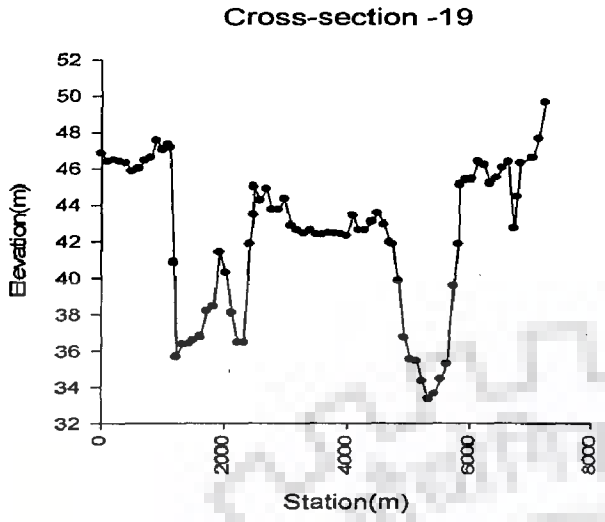
Cross-section -19
Elevation(m)
52
50
48
46
44
42
40
38
36
34
32
0
2000
4000
6000
8000
Station(m)

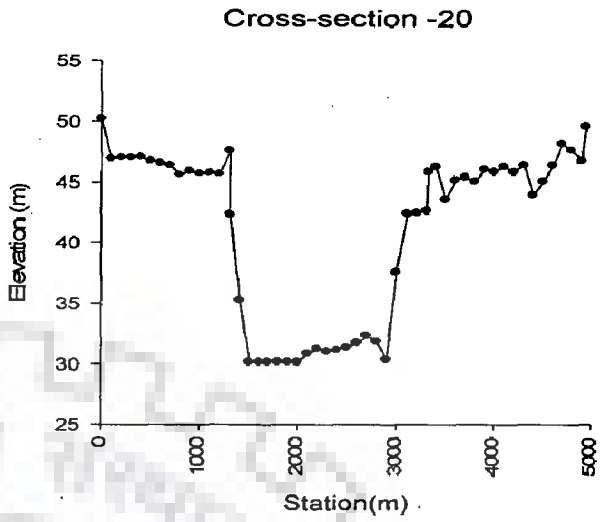
Cross-section -20
Elevation (m)
55
50
45
40
35
30
25
0
1000
2000
3000
4000
5000
Station(m)

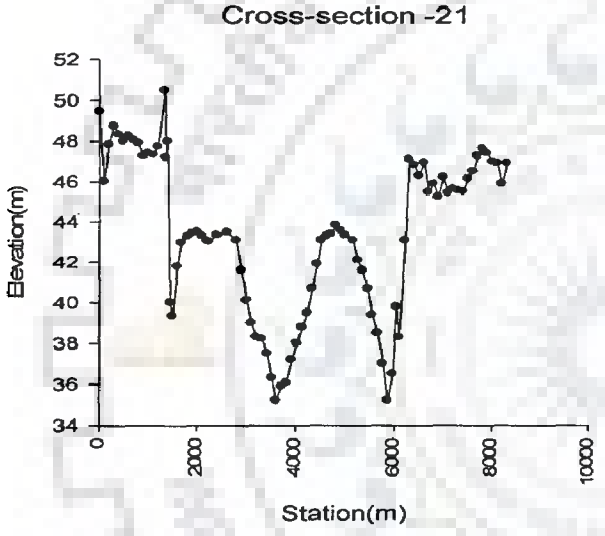
Cross-section -21
Elevation(m)
52
50
48
46
44
42
40
38
36
34
0
2000
4000
6000
8000
10000
Station(m)

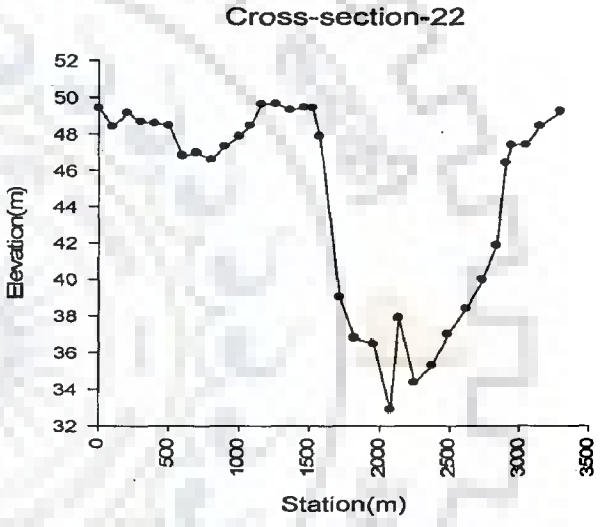
Cross-section-22
Elevation(m)
52
50
48
46
44
42
40
38
36
34
32
0
500
1000
1500
2000
2500
3000
3500
Station(m)

APPENDIX-IV

Preprocessed graphical data of interpolated and measured cross sections data points for the image extracted flow domain of study reach

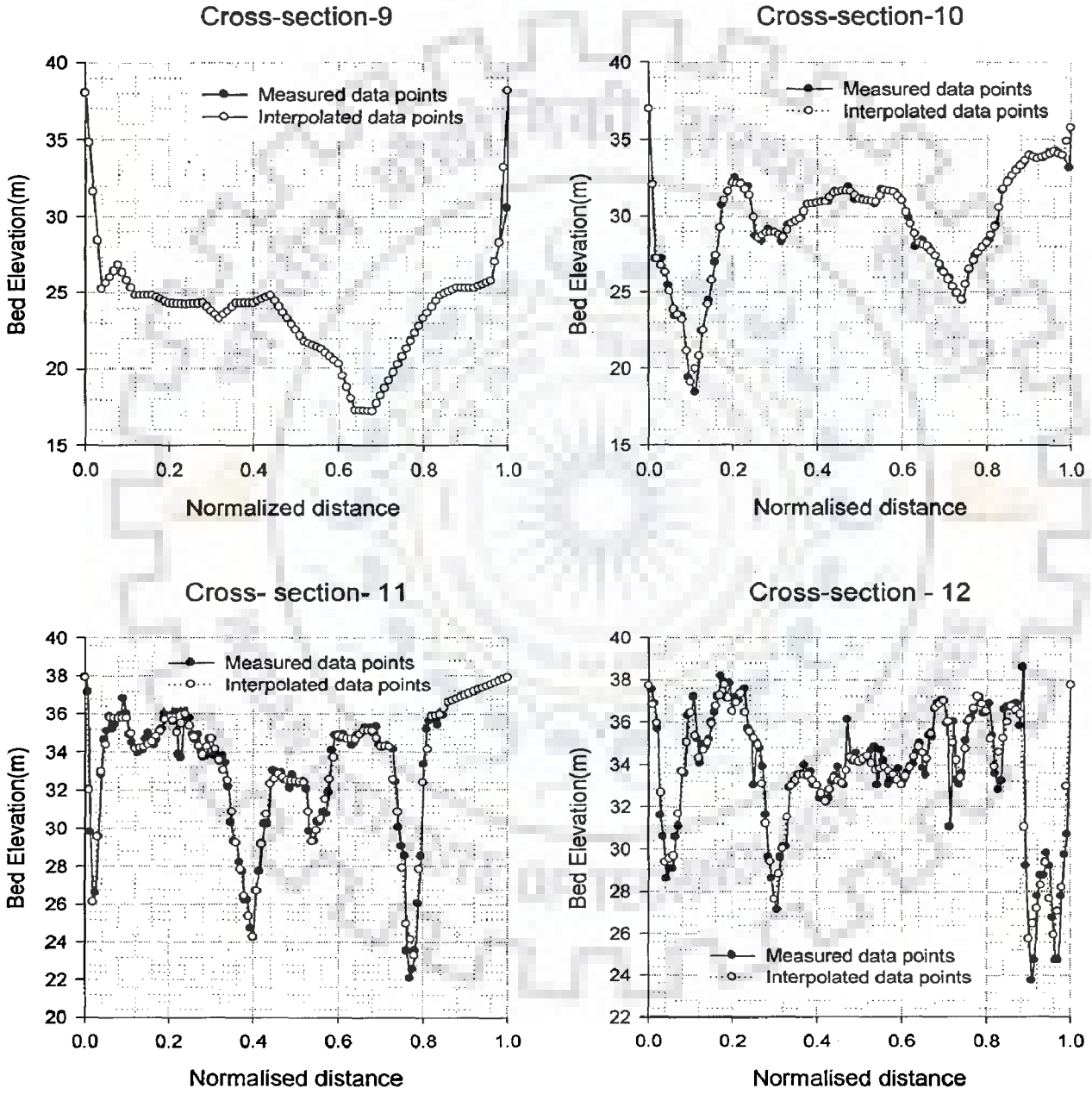

Cross-section- 13

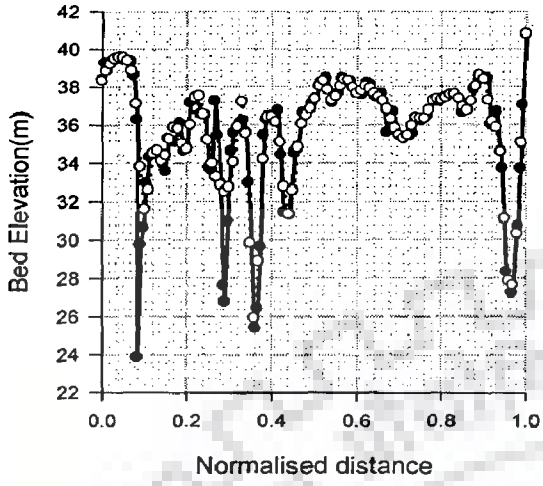

Cross-section-16

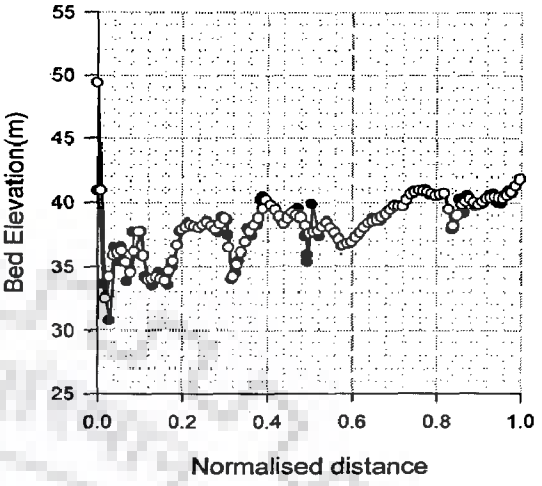

Measured data points
Interpolated data points

Cross-section- 14

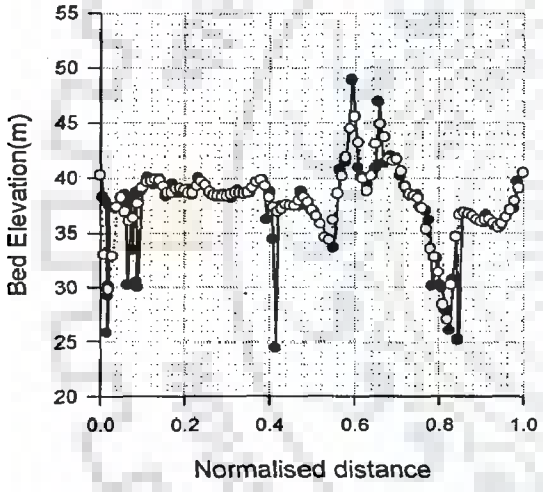

Cross-section-17

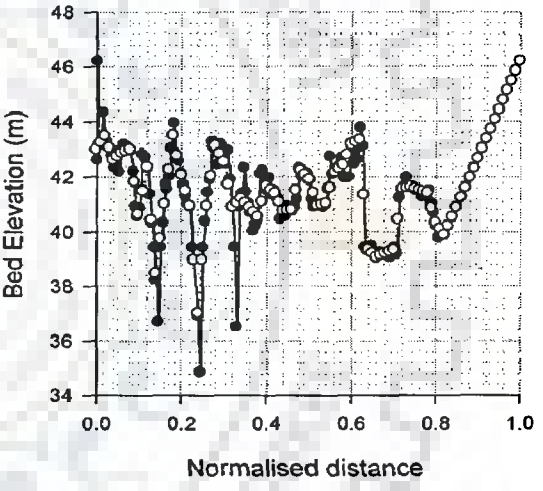

Cross-section-15

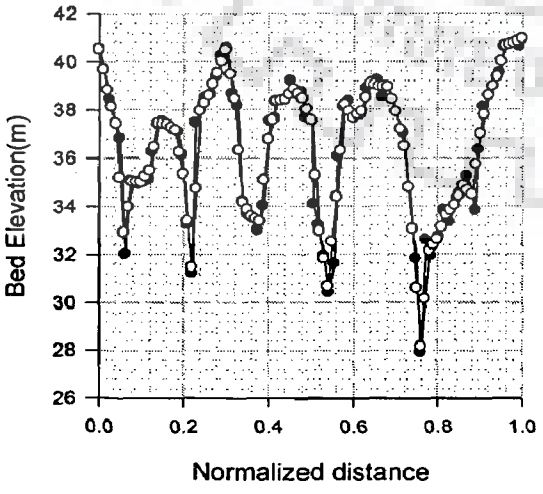

Cross- section-18

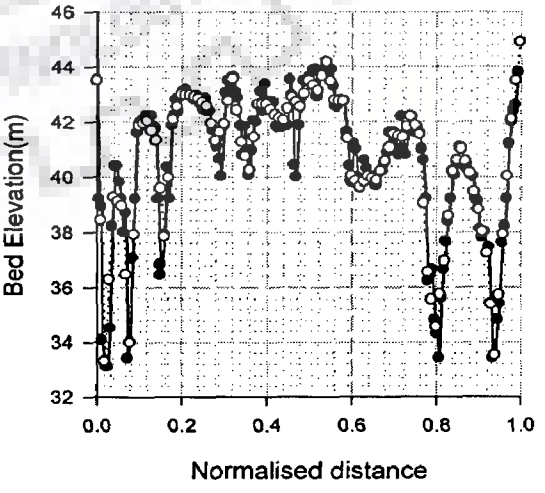

Cross-section-19

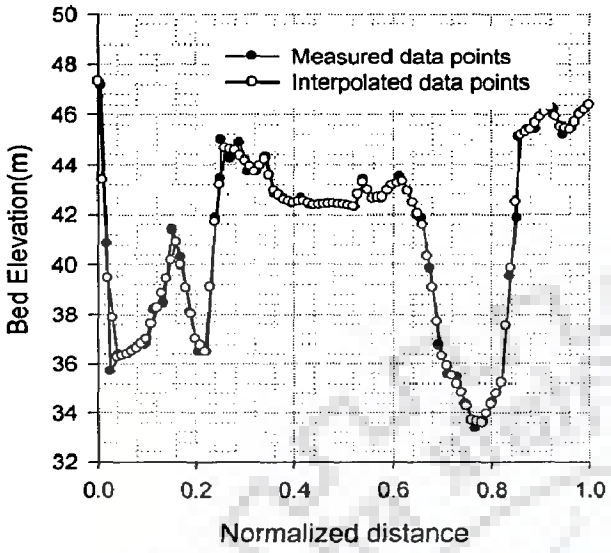

Cross- section-20

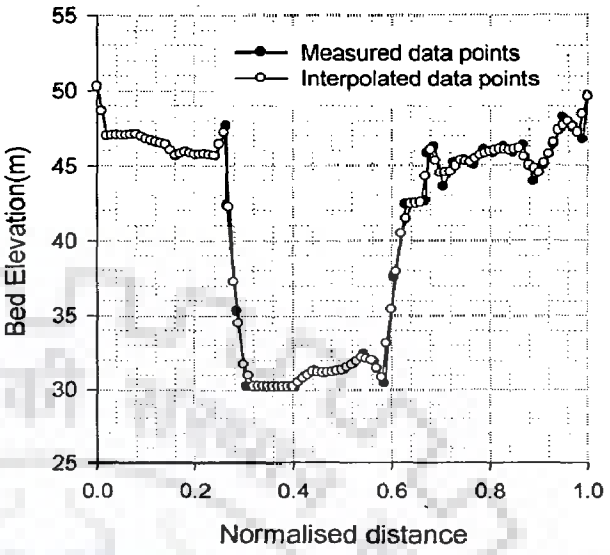

Cross-section-21

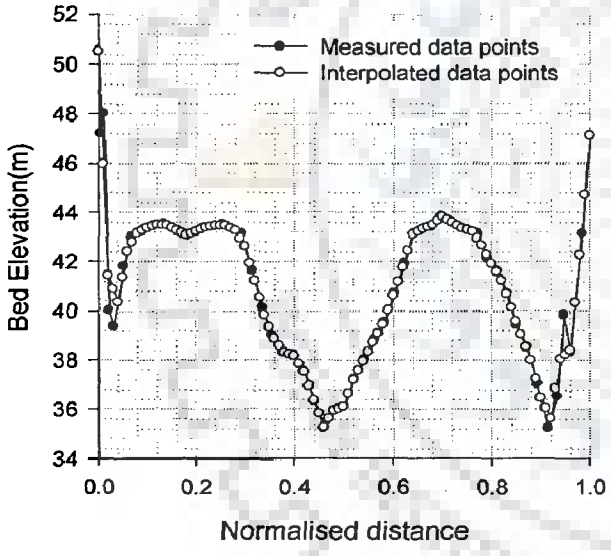

Cross-section-22

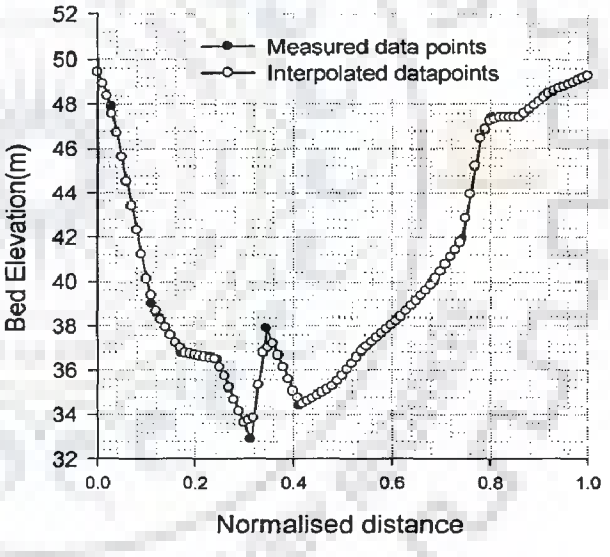

APPENDIX-V

Scanned soft copy of standard Brahmaputra map showing chainage and bearings of pre-defined cross sections (*Brahmaputra Board , GoI*)

(a) Cross-section-2 to Cross-section-43

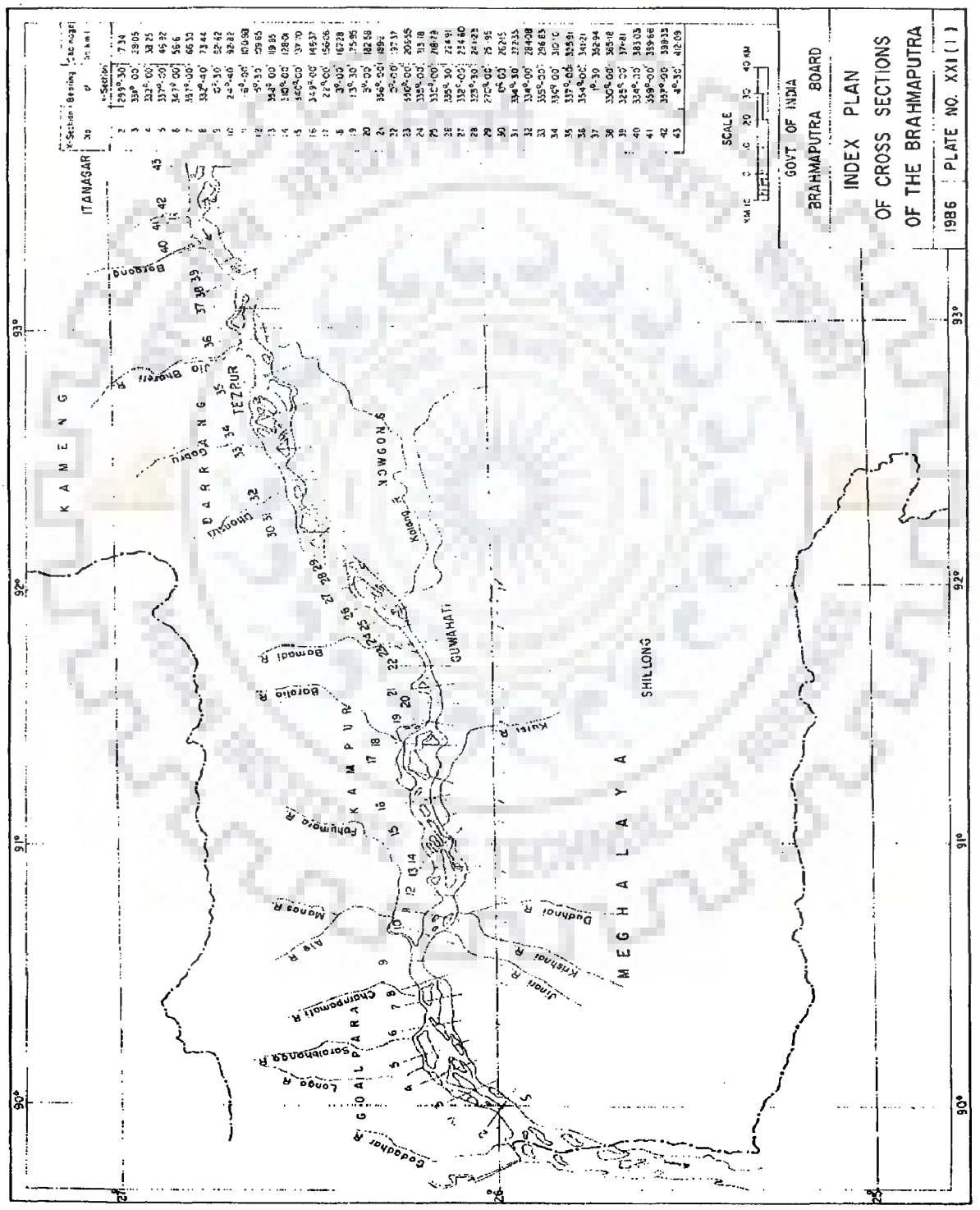

(b) Cross-section-43 to Cross-section-65

APPENDIX-VI

Computer Code modules in *C++* language for numerical coding for mesh generation/ flow model)

1. Salient information about the developed computer program

The complete programming code written in *C++* using Object oriented programming (Oop) is attached as a soft copy in CD-ROM with this thesis as *Appendix-VI B*.

Microsoft Visual Studio.NET 2008 with *C++* console application was used to run the developed program. File system was used to input the extensive data of domain independent boundary variables and bed level data in the form of matrices along with other data like stage discharge relations wherever required. The data was typed in text file (**.txt) and read through programming file system through including header file *fstream* in *C++* plate-form.

Certain input such as name of the input file (**.dat), number of row, number of columns, number of iteration for internal control of grids, discharge and upstream guessed water-level were fed through console application including **.txt. Created **.txt is kept in the same directory to read the file by the code while running the program.

All the given input is written through program file system into created data file (**.dat) to cross check the input data. When the program ends after simulation, the entire user required results is written through file system into the output file (**.OUT file) by calling the appropriate member function of created Class type in the main program. Output file (**.OUT) is created in the same directory in which program file exists. Output may be obtained as per user's choice by writing it in output file through calling class member function by declared object into the main program for writing the data into the output file.

The broad features of Object oriented programming used here are creation of a Class '*mat*' with two types of declared arrays *ar*[N_1][N_2] and *arr* [N_3][N_4] as its private members. Where N_3=1N_1-1 and N_4=2N_2-1. Dynamic programming has been done to optimize the computer memory use. Objects of the class type *mat* are created wherever needed and deleted if the requirement is over. The functional flowchart is given in following figures (in sequence), followed by list of member functions of the class '*mat*'.

** User given file name

2. Functional Flow Chart

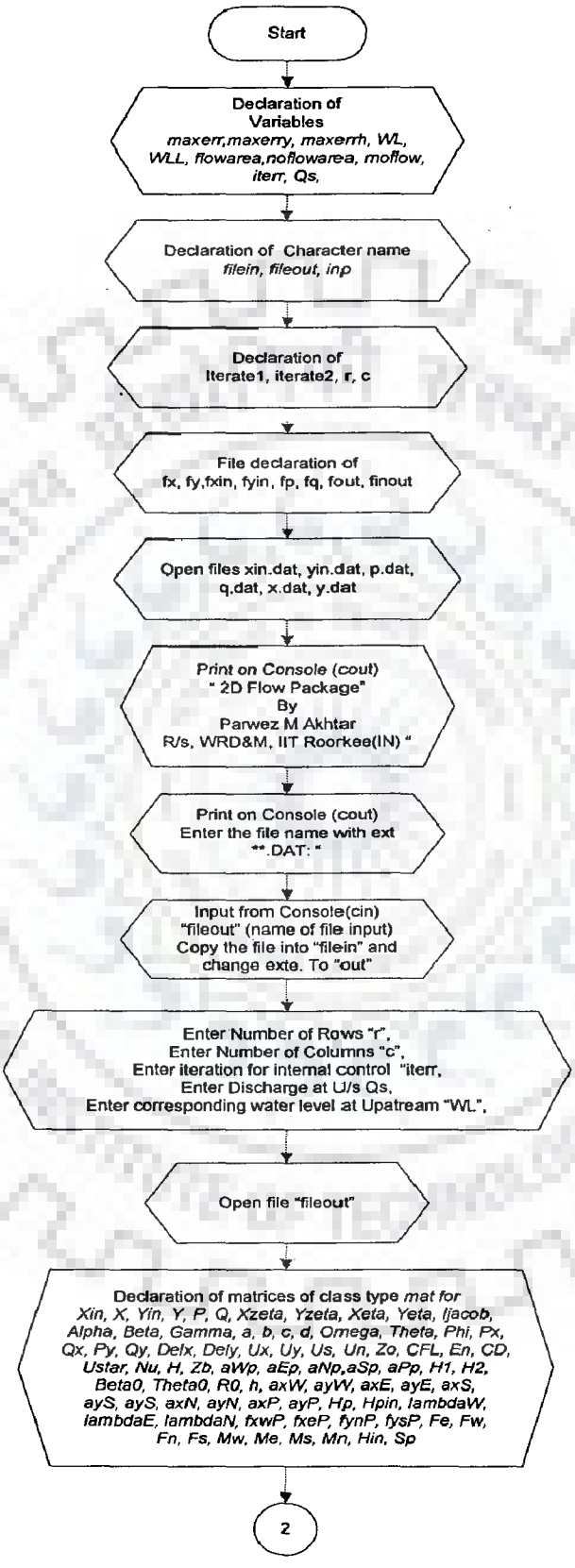

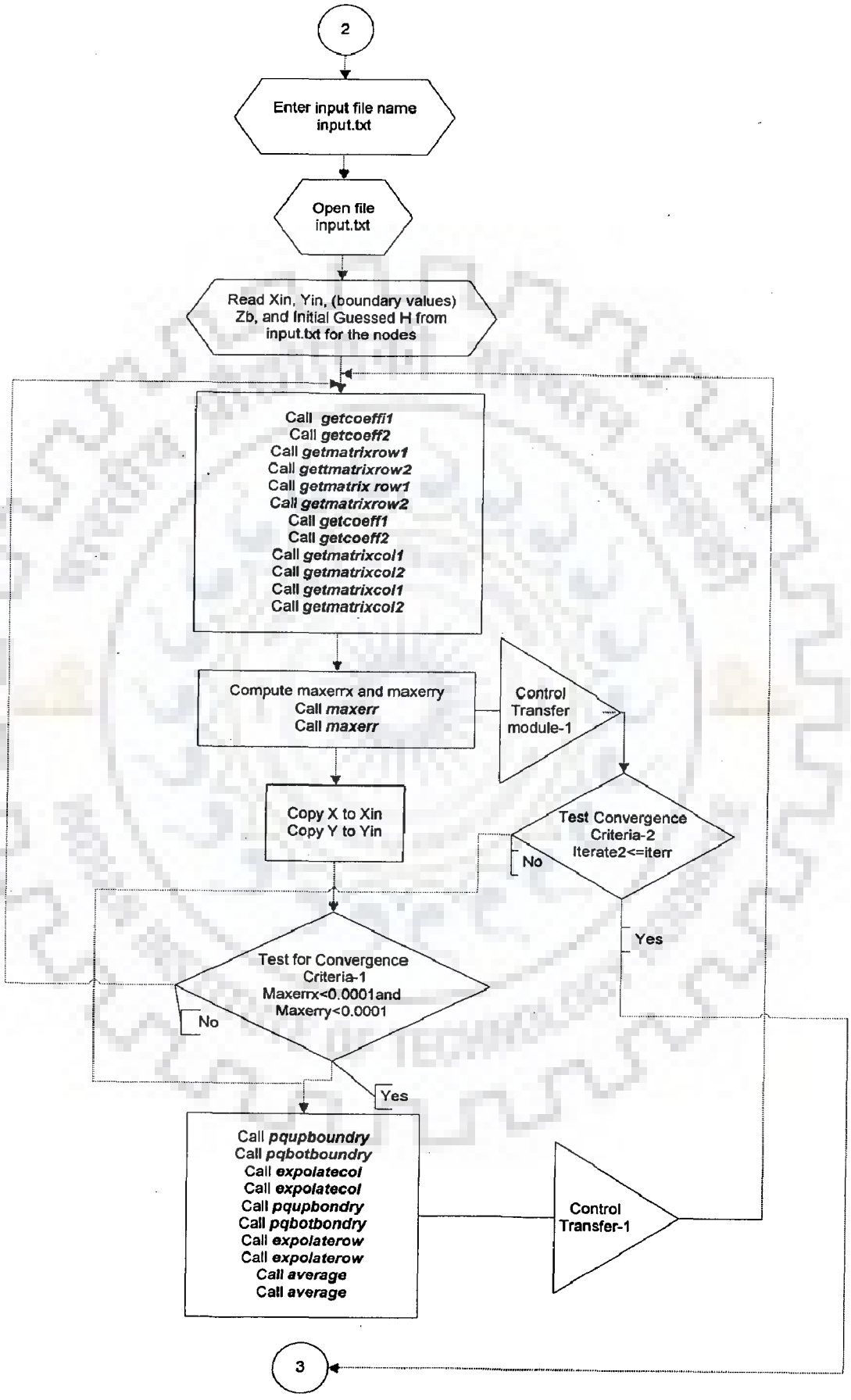
2
Enter input file name
input.txt
Open file
input.txt
Read Xin, Yin, (boundary values)
Zb, and Initial Guessed H from
input.txt for the nodes
Call getcoeffi1
Call getcoeff2
Call getmatrixrow1
Call gettmatrixrow2
Call getmatrix row1
Call getmatrixrow2
Call getcoeff1
Call getcoeff2
Call getmatrixcol1
Call getmatrixcol2
Call getmatrixcol1
Call getmatrixcol2
Compute maxerrx and maxerry
Call maxerr
Call maxerr
Control
Transfer
module-1
Copy X to Xin
Copy Y to Yin
Test Convergence
Criteria-2
Iterate2<=iterr
No
Yes
Test for Convergence
Criteria-1
Maxerrx<0.0001and
Maxerry<0.0001
No
Yes
Call pqupboundry
Call pqbotboundry
Call expolatecol
Call expolatecol
Call pqupbondry
Call pqbotbondry
Call expolaterow
Call expolaterow
Call average
Call average
Control
Transfer-1
3

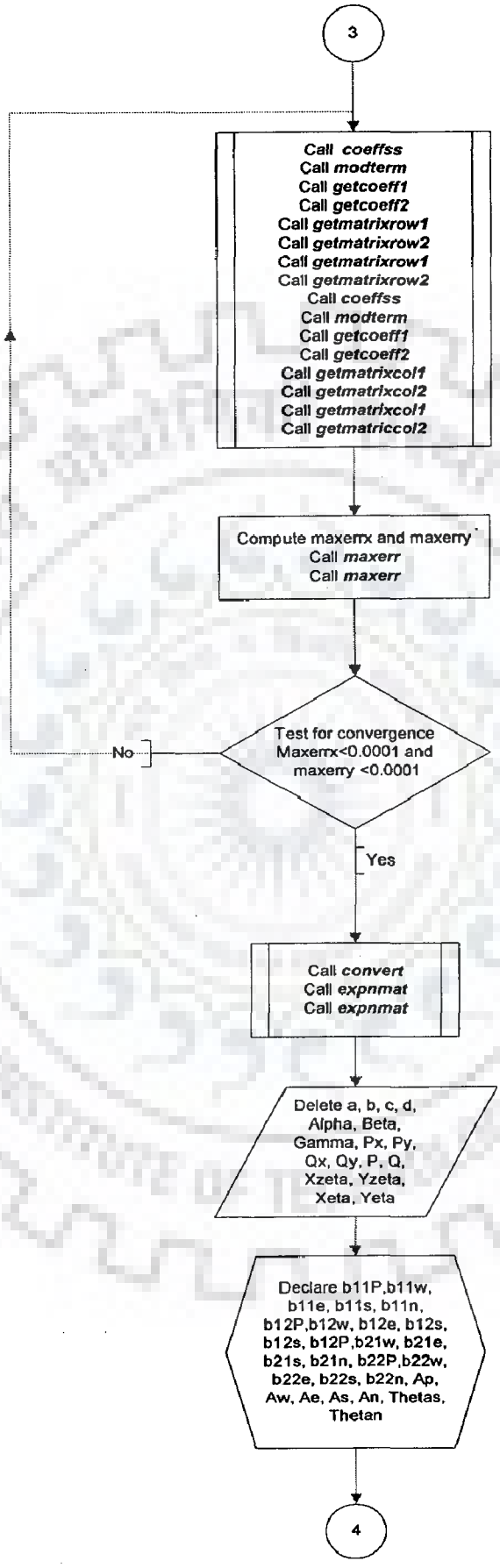
3
Call coeffss
Call modterm
Call getcoeff1
Call getcoeff2
Call getmatrixrow1
Call getmatrixrow2
Call getmatrixrow1
Call getmatrixrow2
Call coeffss
Call modterm
Call getcoeff1
Call getcoeff2
Call getmatrixcol1
Call getmatrixcol2
Call getmatrixcol1
Call getmatriccol2
Compute maxerrx and maxerry
Call maxerr
Call maxerr
Test for convergence
Maxerrx<0.0001 and
maxerry <0.0001
No
Yes
Call convert
Call expnmat
Call expnmat
Delete a, b, c, d,
Alpha, Beta,
Gamma, Px, Py,
Qx, Qy, P, Q,
Xzeta, Yzeta,
Xeta, Yeta
Declare b11P,b11w,
b11e, b11s, b11n,
b12P,b12w, b12e, b12s,
b12s, b12P,b21w, b21e,
b21s, b21n, b22P,b22w,
b22e, b22s, b22n, Ap,
Aw, Ae, As, An, Thetas,
Thetan
4

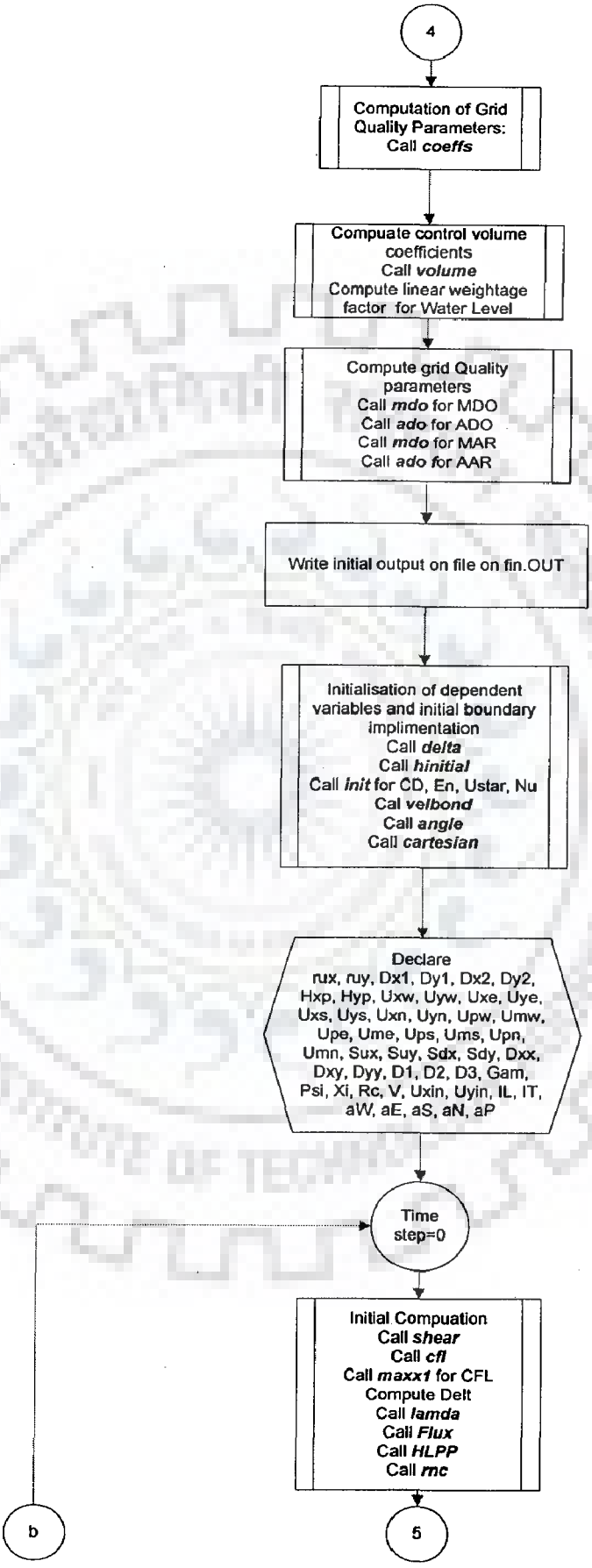
4
Computation of Grid Quality Parameters: Call coeffs
Compuate control volume coefficients Call volume Compute linear weightage factor for Water Level
Compute grid Quality parameters Call mdo for MDO Call ado for ADO Call mdo for MAR Call ado for AAR
Write initial output on file on fin.OUT
Initialisation of dependent variables and initial boundary implimentation Call delta Call hinitial Call init for CD, En, Ustar, Nu Cal velbond Call angle Call cartesian
Declare rux, ruy, Dx1, Dy1, Dx2, Dy2, Hxp, Hyp, Uxw, Uyw, Uxe, Uye, Uxs, Uys, Uxn, Uyn, Upw, Umw, Upe, Ume, Ups, Ums, Upn, Umn, Sux, Suy, Sdx, Sdy, Dxx, Dxy, Dyy, D1, D2, D3, Gam, Psi, Xi, Rc, V, Uxin, Uyin, IL, IT, aW, aE, aS, aN, aP
Time step=0
Initial Compuation Call shear Call cfl Call maxx1 for CFL Compute Delt Call lamda Call Flux Call HLPP Call rnc
b
5

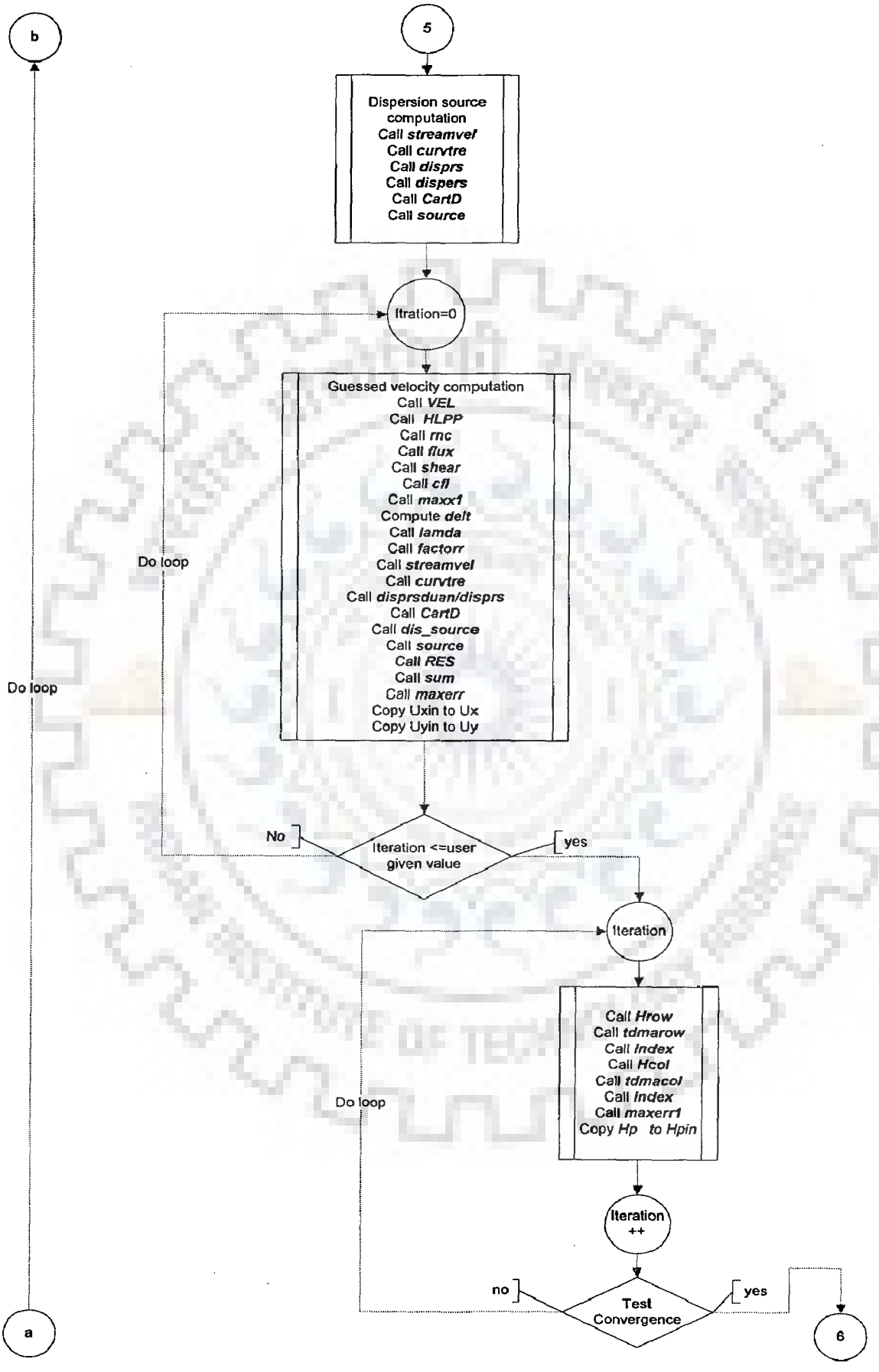
b
5
Dispersion source computation
Call streamvel
Call curvtre
Call disprs
Call dispers
Call CartD
Call source
Itration=0
Guessed velocity computation
Call VEL
Call HLPP
Call rnc
Call flux
Call shear
Call cfl
Call maxx1
Compute delt
Call lamda
Call factorr
Call streamvel
Call curvtre
Call disprsduan/disprs
Call CartD
Call dis_source
Call source
Call RES
Call sum
Call maxerr
Copy Uxin to Ux
Copy Uyin to Uy
Do loop
Do loop
No
Iteration <=user given value
yes
Iteration
Call Hrow
Call tdmarow
Call Index
Call Hcol
Call tdmacol
Call Index
Call maxerr1
Copy Hp to Hpin
Do loop
Iteration ++
no
Test Convergence
yes
a
6

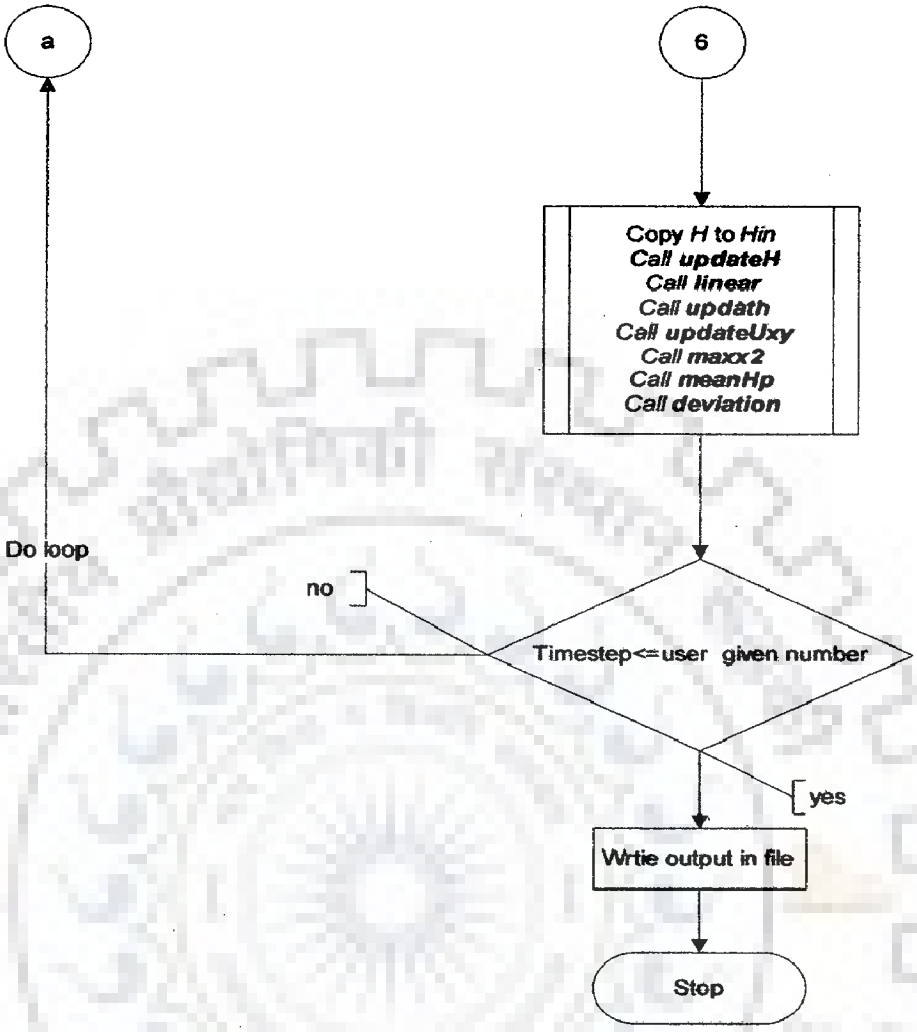

The input through console application for the developed program is shown in Figure VI (1) for illustration.

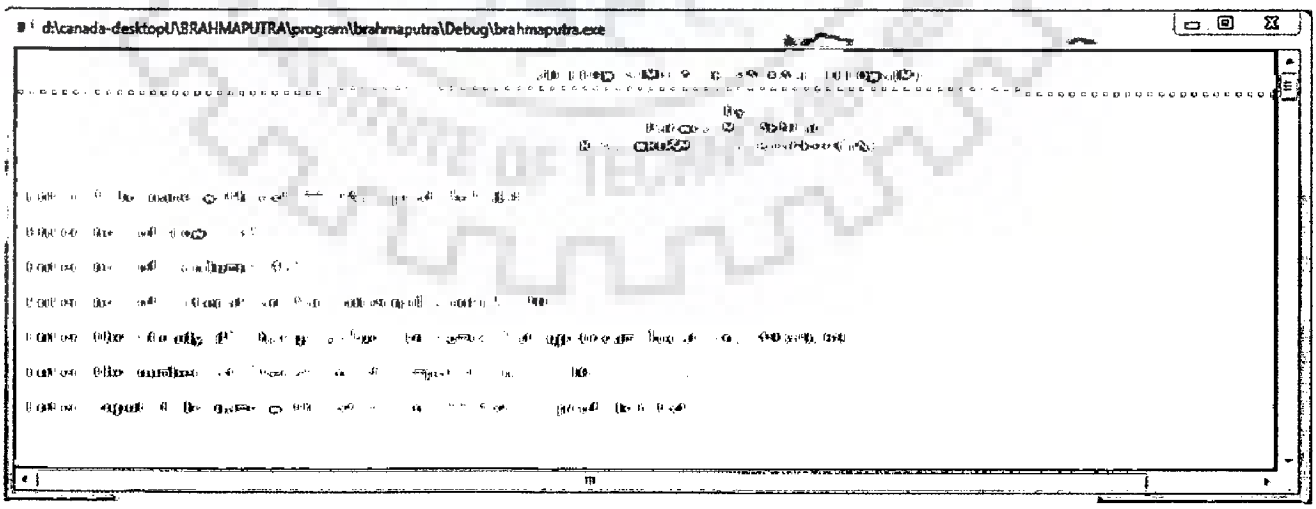

Figure VI (1) Console application window for the developed program

3. Member Functions of Class type '*mat*' (For detail programming code refer the soft copy in CD-ROM)

S N	Name of function	Functional Activity
MF1	rowbond	Reads input boundary coordinates rowwise from note pad(**.txt)
MF2	colbond	Reads input boundary coordinates columnwise from note pad(**.txt)
MF3	getm	Reads array of notepad(**.txt)
MF4	stagein	Reads stage discharge values from notepad(**.txt)
MF5	printm	Print matrix (m×n) into console
MF6	print	Print expanded matrix into console
MF7	expnmat	Expand matrix with dimension (m×n) to (2m-1×
MF8	maxerr	Returns element of maximum value from two matrices (m×n)
MF9	maxerr1	Returns element of maximum valueof errors from two matrices (2m-1×2n-1)
MF10	getcoeff1	Compute derivatives x_ξ, x_η, y_ξ, y_η, and J from x and y matrices
MF11	getcoeff2	Compute tdma coefficients from matrices evaluated from MF10
MF12	getmatrixrow1	Compute rowwise Tridiagonal coefficient matrix from tdma coefficients evaluated from MF11
MF13	getmatrixrow2	Solves for x and y rowwise from Thomas Algorithm from matrices obtained in MF12
MF14	tdmarow	Computes columnwise solution using Thomas algorithm for pressure equation
MF15	getmatrixcol1	Compute columnwise tridiagonal coefficient matrix from tdma coefficients evaluated from MF11
MF16	getmatrixcol2	Solves for x and y columnwise from Thomas Algorithm from matrices obtained in MF15
MF17	tdmacol	Computes columnwise solution using Thomas algorithm for pressure equation
MF18	writearray	Writes array into outputfile (**.dat or **.out)
MF19	writearrayx	Writes expanded matrix into output file(**.dat or **.out)
MF20	pqupbondry	Estimates P and Q for upper boundary of discretized domain
MF21	pqbotbondry	Estimates P and Q for bottom boundary of discritized domain
MF22	pqdnsbondry	Estimates P and Q for downstream boundary
MF23	pqupsbondry	Estimates P and Q for upstream boundary
MF24	expolatecol	Coulmnwise exponential extrapolation of P and Q
MF25	expolaterow	Rowwise exponential extrapolation of P and Q
MF26	average	Computes element wise mean of two matrices (m×n)
MF27	convert	Converts elements of matrix (m×n) from km to meter.
MF28	delta	Computes Δx or Δy for matrix x or y of dimesions(m×n)
MF29	ratingcurve	Computes stage from input discharge for a given functional stage discharge relation for a extreme downstream location
MF30	hinitial	Computes initial guessed value of h and H using linear interpolation of stage at extreme points
MF31	HLPP	Interpolates cell face values of flow variables (U_x and U_y) using HLPA Scheme for nonorthogonal grids
MF32	fxy	Computes linear weighing factors of cell center w.r.t. cell faces for each cell from x and y matrices.
MF33	linear	Compute linear interpolation of variable at cell center from cell faces based on distance.
MF34	flux	Compute fluxes at cell faces and cell centers
MF35	factorr	Compute input coefficients of discretized momentum equations
MF36	source	Compute source terms
MF37	volume	Compute grid coefficients for matrix(m×n)
MF38	VEL	Compute Cartesian velocitities from discretized momentum equations

MF39	RES	Compute residual errors in velocity computation from MF 38
MF40	sum	Computes sum of elements of matix(m×n)
MF41	Hrow	Compute rowwise trigonal coefficient matrix of pressure solver
MF42	Hcol	Compute columnwise trigonal coefficient matrix of pressure solver
MF43	cfl	Compute CFL matrix(m×n) of each cell node
MF44	shear	Compute matrices for Manning's n, C_d, *shear velocity*, *eddy viscosity* and *zero elevation*(z_o)
MF45	lamda	Compute wall function coefficient λ_w(Wu, 2007) for each cell centers
MF46	velbond	Compute initial guessed streamwise velocity at cell centers from discharge (Wu,2007)
MF47	angle	Compute θ_s and θ_n at cell centers
MF48	cartesian	Compute Cartesian volcities from streamwise and transverse velocities
MF49	maxx1	Returns maximum elemental values of marix(m×n)
MF50	maxx2	Returns maximum elemental value from all cell centers
MF51	meanHp	Returns mean elemental value from all cell centers
MF52	coeffs	Returns Grid Quality parameters
MF53	coeffss	Compute x_ξ, x_η, y_ξ, y_η, *and metric coefficients* from final generated grid
MF54	modterm	Modifies non homogeneous terms P and Q using metric coefficients for smoothness of the generated grid
MF55	disprsduan	Computes dispersion stress tensor using Duan's(2004) approach
MF56	curvtre	Computes streamwise radius of curvature and other input parameters for computing dispersion terms
MF57	disprs	Computes dispersion stress tensor using modified approach
MF58	deviation	Computes longitudinal and transverse velocity deviation intensities at cell centers
MF59	streamvel	Computes streamwise velocities from Cartesian velcities
MF60	CartD	Computes Cartesian dispersion tensor from curvilinear dispersion tensor.
MF61	dis_source	Computes sources terms for flow dispersion tensor.
MF62	shrnmat	Shrinks matrix(2m-1×2n-1) to matrix(m×n)
MF63	index	Converts the index of matrix elements.
MF64	updateH	Updates water level with depth increment at each timestep
MF65	updateUxy	Corrects velocity after pressure calculations
MF66	sideH	Updates side boundary waterlevel
MF67	updath	Updates water depth after pressure increnment computations
MF68	ado	Returns average deviation from orthogonality (ADO) for generated mesh
MF69	mdo	Returns maximum deviation from orthogonality(MDO) for generated mesh
MF70	flowarea	Returns flow area of the domain
MF71	noflowarea	Returns noflow area of the domain
MF72	rnc	Interpolates cell variables using Rhie and Chow(1983) approach

APPENDIX-VII

1. Laboratory Experimental details and experimental observed data

Type of Experiment: "Transition in open channel", *Civil Engineering Lab*. I.I.T. Roorkee

Venturimeter Details to measure discharge in the flume:

Pipe Diameter: 38mm, venturi-meter Throat Diameter: 19mm

Cd=0.98,

Discharge through venturimeter= $Q = C_d \cdot \frac{a}{\sqrt{1-\left(\frac{a}{A}\right)^2}} \cdot \sqrt{2g\Delta H}$ VII (1)

a=Area of Throat; A = area of Pipe; Mercury Sp. Gravity=13.6

Manometer reading (after steady condition attained)

h_1=34.20 cm

h_2=17.65 cm

Manometer gauge difference =h_1-h_2=16.55 cm Hg=16.55×13.6=225.08 cm of water

Hence,

ΔH=2.2508 m of water and

a=π× (0.019^2)/4=0.000284 m^2,

A=π× (0.038^2)/4=0.001134 m^2

Substituting the values of A, a, Cd and ΔH in Eq VII (1) the measured discharge computed is 0.001907 cumecs (Through the experimental flume).

The observed water level for the simulated flowfield of discharge 0.001907 cumecs is presented in Table VII (1).

2. Important model results

Table VII (1) Observed data for the conducted experiment

S.N.	Distance from U/s boundary	Gauge reading of bed level	Gauge reading of water level	Ave. water depth	Ave. water level with respect to D/s boundary bed level as zero reference
	cm	cm	cm	cm	cm
1	0	39.92	46.71	6.79	7.85
2	10	39.89	46.70	6.81	7.84
3	20	39.87	46.69	6.82	7.83
4	30	39.85	46.68	6.83	7.82
5	40	39.82	46.67	6.85	7.81
6	50	39.80	46.65	6.85	7.79
7	60	39.77	46.64	6.87	7.78
8	70	39.75	46.63	6.88	7.77
9	80	39.72	46.62	6.9	7.76
10	90	39.7	46.61	6.91	7.75
11	100	39.67	46.60	6.93	7.74
12	110	39.65	46.59	6.94	7.73
13	120	39.62	46.58	6.96	7.72
14	130	39.60	46.56	6.96	7.7
15	140	39.57	46.55	6.98	7.69
16	150	39.55	46.54	6.99	7.68
17	160	39.52	46.53	7.01	7.67
18	170	39.50	46.52	7.02	7.66
19	180	39.47	46.51	7.04	7.65
20	190	39.45	46.5	7.05	7.64
21	200	39.42	45.97	6.55	7.11
22	205	39.41	45.55	6.14	6.69
23	210	39.40	45.71	6.31	6.85
24	215	39.38	45.87	6.49	7.01
25	220	39.37	45.97	6.6	7.11
26	225	39.36	45.98	6.62	7.12
27	235	39.33	45.96	6.63	7.1
28	245	39.31	45.95	6.64	7.09
29	255	39.28	45.94	6.66	7.08
30	265	39.26	45.93	6.67	7.07
31	275	39.23	45.92	6.69	7.06
32	285	39.21	45.9	6.69	7.04
33	295	39.18	45.89	6.71	7.03
34	305	39.16	45.88	6.72	7.02
35	315	39.13	45.87	6.74	7.01
36	325	39.11	45.85	6.74	6.99
37	335	39.08	45.84	6.76	6.98
38	345	39.06	45.83	6.77	6.97
39	355	39.03	45.82	6.79	6.96
40	365	39.01	45.81	6.80	6.95
41	375	38.98	45.80	6.82	6.94
42	385	38.96	45.78	6.82	6.92
43	395	38.93	45.77	6.84	6.91
44	405	38.91	45.76	6.85	6.9
45	415	38.88	45.75	6.87	6.89
46	425	38.86	45.75	6.89	6.89

Table VII (2): Mean and its standard deviation of Cartesian velocities at cell centers of the generated mesh of the flow domain

S. N.	Distance of cell centers from U/s Boundary(m)	Case-1				Case-2				Case-3			
		U_x(m/s)		U_y(m/s)		U_x(m/s)		U_y(m/s)		U_x(m/s)		U_y(m/s)	
		Mean	Std dev. (σ)	Mean	Std dev(σ)	Mean	Std dev(σ)	Mean	Std. dev.(σ)	Mean	Std. dev.(σ)	Mean	Std. dev. (σ)
	1	2	3	4	5	6	7	8	9	10	11	12	13
1	4.88E-03	0.1869	0.000317	0.000000	0.000000	0.1869	0.000211	0.000000	0.000000	0.1869	0.000211	0.000000	0.000000
2	0.0146	0.1866	0.000669	0.000000	0.000000	0.1867	0.000528	0.000000	0.000000	0.1867	0.000528	0.000000	0.000000
3	0.0244	0.1866	0.000769	0.000000	0.000000	0.1866	0.000664	0.000000	0.000000	0.1866	0.000664	0.000000	0.000000
4	0.0342	0.1865	0.000787	0.000000	0.000000	0.1865	0.000686	0.000000	0.000000	0.1865	0.000686	0.000000	0.000000
5	0.0439	0.1864	0.000792	0.000000	0.000000	0.1864	0.000686	0.000000	0.000000	0.1864	0.000686	0.000000	0.000000
6	0.0537	0.1863	0.000792	0.000000	0.000000	0.1863	0.000686	0.000000	0.000000	0.1863	0.000686	0.000000	0.000000
7	0.0634	0.1863	0.000792	0.000000	0.000000	0.1863	0.000686	0.000000	0.000000	0.1863	0.000686	0.000000	0.000000
8	0.0732	0.1863	0.000822	0.000000	0.000000	0.1863	0.000717	0.000000	0.000000	0.1863	0.000717	0.000000	0.000000
9	0.0829	0.1862	0.000790	0.000000	0.000000	0.1862	0.000686	0.000000	0.000000	0.1862	0.000686	0.000000	0.000000
10	0.0927	0.1861	0.000806	0.000000	0.000000	0.1861	0.000686	0.000000	0.000000	0.1861	0.000686	0.000000	0.000000
11	0.1024	0.1860	0.000806	0.000000	0.000000	0.1860	0.000700	0.000000	0.000000	0.1860	0.000700	0.000000	0.000000
12	0.1121	0.1858	0.000792	0.000000	0.000000	0.1858	0.000686	0.000000	0.000000	0.1858	0.000686	0.000000	0.000000
13	0.1219	0.1856	0.000775	0.000000	0.000000	0.1857	0.000700	0.000000	0.000000	0.1857	0.000700	0.000000	0.000000
14	0.1316	0.1855	0.000806	0.000000	0.000000	0.1855	0.000686	0.000000	0.000000	0.1855	0.000686	0.000000	0.000000
15	0.1413	0.1854	0.000809	0.000000	0.000000	0.1854	0.000692	0.000000	0.000000	0.1854	0.000692	0.000000	0.000000
16	0.1511	0.1853	0.000820	0.000000	0.000000	0.1854	0.000730	0.000000	0.000000	0.1854	0.000730	0.000000	0.000000
17	0.1608	0.1851	0.000801	0.000000	0.000000	0.1852	0.000699	0.000000	0.000000	0.1852	0.000699	0.000000	0.000000
18	0.1705	0.1849	0.000781	0.000000	0.000000	0.1850	0.000700	0.000000	0.000000	0.1850	0.000700	0.000000	0.000000
19	0.1802	0.1847	0.000794	0.000000	0.000000	0.1848	0.000693	0.000000	0.000000	0.1848	0.000693	0.000000	0.000000
20	0.1899	0.1845	0.000789	0.000000	0.000000	0.1845	0.000670	0.000000	0.000000	0.1845	0.000670	0.000000	0.000000
21	0.1996	0.1842	0.000775	0.000000	0.000000	0.1843	0.000684	0.000000	0.000000	0.1843	0.000684	0.000000	0.000000

S.N.	1	2	3	4	5	6	7	8	9	10	11	12	13
22	0.2093	0.1840	0.000789	0.000000	0.000000	0.1840	0.000686	0.000000	0.000000	0.1840	0.000686	0.000000	0.000000
23	0.219	0.1837	0.000789	0.000000	0.000000	0.1837	0.000670	0.000000	0.000000	0.1837	0.000670	0.000000	0.000000
24	0.2287	0.1835	0.000814	0.000000	0.000000	0.1834	0.000753	0.000000	0.000000	0.1834	0.000753	0.000000	0.000000
25	0.2383	0.1833	0.000845	0.000000	0.000000	0.1834	0.000777	0.000000	0.000000	0.1834	0.000791	0.000000	0.000000
26	0.248	0.1830	0.000790	0.000000	0.000000	0.1831	0.000700	0.000000	0.000000	0.1831	0.000700	0.000000	0.000000
27	0.2577	0.1827	0.000788	0.000000	0.000000	0.1828	0.000683	0.000000	0.000000	0.1828	0.000683	0.000000	0.000000
28	0.2674	0.1823	0.000776	0.000000	0.000000	0.1824	0.000668	0.000000	0.000000	0.1824	0.000668	0.000000	0.000000
29	0.277	0.1820	0.000771	0.000000	0.000000	0.1820	0.000671	0.000000	0.000000	0.1820	0.000671	0.000000	0.000000
30	0.2867	0.1816	0.000773	0.000000	0.000000	0.1817	0.000653	0.000000	0.000000	0.1817	0.000653	0.000000	0.000000
31	0.2963	0.1812	0.000773	0.000000	0.000000	0.1813	0.000653	0.000000	0.000000	0.1813	0.000653	0.000000	0.000000
32	0.306	0.1808	0.000768	0.000000	0.000000	0.1808	0.000651	0.000000	0.000000	0.1808	0.000651	0.000000	0.000000
33	0.3156	0.1804	0.001005	0.000000	0.000000	0.1804	0.000871	0.000000	0.000000	0.1804	0.000871	0.000000	0.000000
34	0.3253	0.1801	0.000853	0.000000	0.000000	0.1803	0.000712	0.000000	0.000000	0.1803	0.000712	0.000000	0.000000
35	0.3349	0.1796	0.000952	0.000000	0.000000	0.1797	0.000908	0.000000	0.000000	0.1797	0.000908	0.000000	0.000000
36	0.3445	0.1792	0.000792	0.000000	0.000000	0.1793	0.000737	0.000000	0.000000	0.1793	0.000737	0.000000	0.000000
37	0.3542	0.1787	0.000775	0.000000	0.000000	0.1788	0.000657	0.000000	0.000000	0.1788	0.000657	0.000000	0.000000
38	0.3638	0.1782	0.000773	0.000000	0.000000	0.1783	0.000696	0.000000	0.000000	0.1783	0.000696	0.000000	0.000000
39	0.3734	0.1777	0.000811	0.000000	0.000000	0.1778	0.000703	0.000000	0.000000	0.1778	0.000703	0.000000	0.000000
40	0.383	0.1772	0.000847	0.000000	0.000000	0.1773	0.000750	0.000000	0.000000	0.1773	0.000750	0.000000	0.000000
41	0.3926	0.1765	0.000788	-0.000083	0.000320	0.1767	0.000682	0.000000	0.000000	0.1767	0.000682	0.000000	0.000000
42	0.4023	0.1763	0.002309	-0.000175	0.004362	0.1763	0.002014	-0.000093	0.000361	0.1763	0.002031	-0.000093	0.000361
43	0.4119	0.1756	0.001127	0.000209	0.001458	0.1758	0.000860	0.000071	0.000273	0.1758	0.000856	0.000071	0.000273
44	0.4215	0.1750	0.001528	0.000000	0.000000	0.1751	0.001412	0.000000	0.000000	0.1751	0.001412	0.000000	0.000000
45	0.4311	0.1744	0.000959	0.000000	0.000000	0.1746	0.000943	0.000000	0.000000	0.1746	0.000943	0.000000	0.000000
46	0.4407	0.1738	0.000799	0.000000	0.000000	0.1739	0.000711	0.000000	0.000000	0.1739	0.000711	0.000000	0.000000
47	0.4503	0.1732	0.000793	0.000000	0.000000	0.1733	0.000683	0.000000	0.000000	0.1733	0.000683	0.000000	0.000000
48	0.4599	0.1725	0.000782	0.000000	0.000000	0.1726	0.000671	0.000000	0.000000	0.1726	0.000671	0.000000	0.000000

S.N.	1	2	3	4	5	6	7	8	9	10	11	12	13
49	0.4695	0.1719	0.000739	0.000000	0.000000	0.1720	0.000648	0.000000	0.000000	0.1720	0.000648	0.000000	0.000000
50	0.4791	0.1717	0.005008	0.000193	0.002849	0.1720	0.004244	-0.000302	0.001305	0.1720	0.004229	-0.000302	0.001305
51	0.4887	0.1710	0.001981	-0.000205	0.002273	0.1710	0.001122	0.000161	0.000623	0.1710	0.001147	0.000161	0.000623
52	0.4983	0.1699	0.002707	0.000037	0.000528	0.1700	0.002481	0.000111	0.000428	0.1700	0.002507	0.000111	0.000428
53	0.5078	0.1693	0.001230	0.000000	0.000000	0.1694	0.001299	0.000000	0.000000	0.1694	0.001299	0.000000	0.000000
54	0.5174	0.1686	0.000792	0.000000	0.000000	0.1687	0.000727	0.000000	0.000000	0.1687	0.000727	0.000000	0.000000
55	0.527	0.1679	0.000750	0.000000	0.000000	0.1680	0.000660	0.000000	0.000000	0.1680	0.000660	0.000000	0.000000
56	0.5366	0.1671	0.000725	0.000000	0.000000	0.1673	0.000636	0.000000	0.000000	0.1673	0.000636	0.000000	0.000000
57	0.5462	0.1664	0.000754	0.000000	0.000000	0.1665	0.000661	0.000000	0.000000	0.1665	0.000661	0.000000	0.000000
58	0.5557	0.1657	0.000647	0.000000	0.000000	0.1658	0.000568	0.000000	0.000000	0.1658	0.000568	0.000000	0.000000
59	0.5653	0.1668	0.009874	-0.001105	0.004808	0.1666	0.008746	-0.000961	0.003916	0.1666	0.008747	-0.000961	0.003916
60	0.5749	0.1648	0.003163	0.000676	0.002401	0.1651	0.002029	0.000432	0.001718	0.1650	0.002032	0.000432	0.001719
61	0.5845	0.1635	0.004637	0.000421	0.001140	0.1637	0.004370	0.000407	0.001116	0.1637	0.004358	0.000407	0.001116
62	0.5941	0.1628	0.001700	0.000000	0.000000	0.1630	0.002000	0.000000	0.000000	0.1629	0.001982	0.000000	0.000000
63	0.6036	0.1619	0.000762	0.000000	0.000000	0.1621	0.000760	0.000000	0.000000	0.1621	0.000760	0.000000	0.000000
64	0.6132	0.1611	0.000679	0.000000	0.000000	0.1613	0.000608	0.000000	0.000000	0.1613	0.000608	0.000000	0.000000
65	0.6228	0.1603	0.000697	0.000000	0.000000	0.1605	0.000607	0.000000	0.000000	0.1605	0.000607	0.000000	0.000000
66	0.6323	0.1597	0.000604	0.000000	0.000000	0.1598	0.000509	0.000000	0.000000	0.1598	0.000509	0.000000	0.000000
67	0.6419	0.1628	0.018203	-0.002641	0.011288	0.1622	0.016265	-0.002123	0.009276	0.1622	0.016242	-0.002094	0.009297
68	0.6515	0.1598	0.005375	0.001389	0.004697	0.1603	0.003634	0.000725	0.003373	0.1603	0.003619	0.000697	0.003401
69	0.661	0.1577	0.006992	0.000865	0.002085	0.1580	0.006648	0.000894	0.002031	0.1580	0.006646	0.000893	0.002029
70	0.6706	0.1566	0.002270	0.000000	0.000000	0.1569	0.002701	0.000000	0.000000	0.1568	0.002684	0.000000	0.000000
71	0.6802	0.1557	0.000764	0.000000	0.000000	0.1558	0.000802	0.000000	0.000000	0.1558	0.000802	0.000000	0.000000
72	0.6897	0.1549	0.000641	0.000000	0.000000	0.1550	0.000567	0.000000	0.000000	0.1550	0.000567	0.000000	0.000000
73	0.6993	0.1540	0.000637	0.000000	0.000000	0.1542	0.000561	0.000000	0.000000	0.1542	0.000561	0.000000	0.000000
74	0.7088	0.1532	0.000619	0.000000	0.000000	0.1533	0.000556	0.000000	0.000000	0.1533	0.000556	0.000000	0.000000
75	0.7184	0.1527	0.000990	-0.000079	0.001056	0.1528	0.000883	0.000061	0.000822	0.1528	0.000877	0.000061	0.000824

S.N.	1	2	3	4	5	6	7	8	9	10	11	12	13
76	0.7279	0.1610	0.037278	-0.005949	0.026182	0.1601	0.033316	-0.005039	0.021322	0.1599	0.033203	-0.005049	0.021357
77	0.7375	0.1562	0.009950	0.001937	0.008707	0.1568	0.007908	0.001224	0.006028	0.1566	0.007775	0.001241	0.006051
78	0.7471	0.1520	0.010077	0.001394	0.003689	0.1526	0.009822	0.001559	0.003755	0.1525	0.009793	0.001556	0.003748
79	0.7566	0.1497	0.003055	0.000000	0.000000	0.1501	0.003643	0.000000	0.000000	0.1501	0.003626	0.000000	0.000000
80	0.7662	0.1485	0.000810	0.000000	0.000000	0.1486	0.000917	0.000000	0.000000	0.1487	0.000841	0.000000	0.000000
81	0.7757	0.1476	0.000610	0.000000	0.000000	0.1477	0.000534	0.000000	0.000000	0.1477	0.000641	0.000000	0.000000
82	0.7853	0.1468	0.000588	0.000000	0.000000	0.1469	0.000519	0.000000	0.000000	0.1469	0.000519	0.000000	0.000000
83	0.7948	0.1460	0.000605	0.000000	0.000000	0.1461	0.000515	0.000000	0.000000	0.1461	0.000515	0.000000	0.000000
84	0.8044	0.1453	0.001431	-0.000157	0.001176	0.1453	0.001296	-0.000057	0.001036	0.1453	0.001303	-0.000056	0.001039
85	0.814	0.1467	0.033738	-0.006681	0.027441	0.1464	0.030522	-0.005599	0.022202	0.1463	0.030489	-0.005603	0.022236
86	0.8235	0.1520	0.018546	0.003151	0.015311	0.1513	0.014536	0.002007	0.011454	0.1511	0.014273	0.002022	0.011500
87	0.8331	0.1480	0.013024	0.001565	0.006165	0.1489	0.014074	0.001553	0.006250	0.1487	0.013841	0.001545	0.006219
88	0.8426	0.1435	0.004196	0.000037	0.000547	0.1441	0.004989	-0.000048	0.000769	0.1441	0.004936	-0.000046	0.000768
89	0.8522	0.1414	0.000909	0.000000	0.000000	0.1417	0.001124	0.000000	0.000000	0.1417	0.001128	0.000000	0.000000
90	0.8618	0.1405	0.000563	0.000000	0.000000	0.1406	0.000518	0.000000	0.000000	0.1406	0.000512	0.000000	0.000000
91	0.8713	0.1397	0.000540	0.000000	0.000000	0.1398	0.000482	0.000000	0.000000	0.1398	0.000482	0.000000	0.000000
92	0.8808	0.1389	0.000540	0.000000	0.000000	0.1390	0.000482	0.000000	0.000000	0.1390	0.000482	0.000000	0.000000
93	0.8904	0.1382	0.000983	-0.000058	0.000694	0.1383	0.000914	0.000002	0.000648	0.1383	0.000914	0.000003	0.000651
94	0.9	0.1396	0.023901	-0.003223	0.020993	0.1394	0.021670	-0.002495	0.017114	0.1393	0.021627	-0.002498	0.017130
95	0.9095	0.1399	0.009223	-0.000525	0.007702	0.1399	0.006983	-0.000629	0.005294	0.1398	0.006894	-0.000628	0.005320
96	0.9191	0.1390	0.011359	-0.000131	0.002808	0.1391	0.010833	-0.000036	0.002766	0.1391	0.010733	-0.000038	0.002762
97	0.9286	0.1365	0.004442	-0.000187	0.000493	0.1369	0.005222	-0.000174	0.000780	0.1369	0.005168	-0.000173	0.000774
98	0.9382	0.1346	0.000884	0.000000	0.000000	0.1348	0.001146	-0.000078	0.000301	0.1348	0.001129	-0.000077	0.000298
99	0.9477	0.1337	0.000523	0.000000	0.000000	0.1338	0.000456	0.000000	0.000000	0.1338	0.000462	0.000000	0.000000
100	0.9573	0.1329	0.000505	0.000000	0.000000	0.1330	0.000448	0.000000	0.000000	0.1330	0.000448	0.000000	0.000000
101	0.9669	0.1322	0.000508	0.000000	0.000000	0.1322	0.000416	0.000000	0.000000	0.1322	0.000416	0.000000	0.000000
102	0.9765	0.1314	0.000651	0.000068	0.000263	0.1315	0.000608	0.000088	0.000339	0.1315	0.000608	0.000088	0.000342

S.N.	1	2	3	4	5	6	7	8	9	10	11	12	13
103	0.986	0.1305	0.012066	-0.000980	0.009808	0.1306	0.010965	-0.000840	0.008038	0.1305	0.010972	-0.000840	0.008040
104	0.9955	0.1320	0.006585	-0.000521	0.005414	0.1320	0.005186	-0.000329	0.004162	0.1319	0.005094	-0.000330	0.004167
105	1.0051	0.1314	0.007790	-0.000115	0.002013	0.1315	0.007422	-0.000058	0.002040	0.1314	0.007383	-0.000059	0.002040
106	1.0147	0.1294	0.002794	0.000000	0.000000	0.1297	0.003298	-0.000173	0.000458	0.1297	0.003267	-0.000172	0.000455
107	1.0243	0.1280	0.000614	0.000000	0.000000	0.1282	0.000740	0.000000	0.000000	0.1282	0.000743	0.000000	0.000000
108	1.0337	0.1272	0.000456	0.000000	0.000000	0.1273	0.000419	0.000000	0.000000	0.1273	0.000421	0.000000	0.000000
109	1.0434	0.1265	0.000450	0.000000	0.000000	0.1266	0.000414	0.000000	0.000000	0.1266	0.000414	0.000000	0.000000
110	1.0529	0.1258	0.000450	0.000000	0.000000	0.1259	0.000410	0.000000	0.000000	0.1259	0.000410	0.000000	0.000000
111	1.0625	0.1251	0.000705	0.000023	0.000531	0.1252	0.000662	0.000135	0.000522	0.1252	0.000662	0.000136	0.000526
112	1.0721	0.1250	0.016547	-0.001726	0.015547	0.1249	0.015143	-0.001297	0.012766	0.1249	0.015156	-0.001297	0.012771
113	1.0817	0.1268	0.009505	-0.000851	0.007968	0.1267	0.007823	-0.000592	0.006091	0.1267	0.007727	-0.000594	0.006109
114	1.0912	0.1264	0.011306	-0.000384	0.002839	0.1264	0.010667	-0.000277	0.002860	0.1264	0.010580	-0.000278	0.002856
115	1.1008	0.1238	0.004241	-0.000140	0.000638	0.1241	0.004972	-0.000206	0.000872	0.1241	0.004917	-0.000205	0.000866
116	1.1102	0.1221	0.000731	0.000000	0.000000	0.1223	0.000996	-0.000088	0.000340	0.1223	0.000974	-0.000087	0.000336
117	1.1199	0.1213	0.000438	0.000000	0.000000	0.1214	0.000378	0.000000	0.000000	0.1214	0.000378	0.000000	0.000000
118	1.1295	0.1206	0.000414	0.000000	0.000000	0.1207	0.000379	0.000000	0.000000	0.1207	0.000379	0.000000	0.000000
119	1.1389	0.1199	0.000416	0.000000	0.000000	0.1201	0.000380	0.000000	0.000000	0.1201	0.000380	0.000000	0.000000
120	1.1486	0.1194	0.000841	-0.000154	0.000597	0.1194	0.000798	0.000029	0.000603	0.1194	0.000798	0.000029	0.000604
121	1.1582	0.1222	0.021839	-0.004269	0.022910	0.1219	0.020028	-0.003402	0.018728	0.1219	0.019985	-0.003406	0.018743
122	1.1678	0.1189	0.006266	0.000814	0.008632	0.1192	0.004430	0.000461	0.006078	0.1191	0.004468	0.000463	0.006099
123	1.1774	0.1181	0.005703	0.000045	0.002232	0.1183	0.005505	0.000172	0.002245	0.1183	0.005525	0.000174	0.002239
124	1.187	0.1173	0.001602	0.000000	0.000000	0.1174	0.001934	-0.000072	0.000280	0.1174	0.001922	-0.000072	0.000279
125	1.1966	0.1164	0.000448	0.000000	0.000000	0.1165	0.000474	0.000000	0.000000	0.1165	0.000474	0.000000	0.000000
126	1.2062	0.1158	0.000391	0.000000	0.000000	0.1159	0.000362	0.000000	0.000000	0.1159	0.000362	0.000000	0.000000
127	1.2157	0.1152	0.000388	0.000000	0.000000	0.1153	0.000358	0.000000	0.000000	0.1153	0.000358	0.000000	0.000000
128	1.2252	0.1146	0.000360	0.000000	0.000000	0.1147	0.000326	0.000000	0.000000	0.1147	0.000326	0.000000	0.000000
129	1.2348	0.1140	0.000379	0.000000	0.000000	0.1141	0.000346	0.000000	0.000000	0.1141	0.000346	0.000000	0.000000

S.N.	1	2	3	4	5	6	7	8	9	10	11	12	13
130	1.2444	0.1133	0.000487	0.000153	0.000403	0.1133	0.000461	0.000249	0.000519	0.1133	0.000461	0.000249	0.000520
131	1.254	0.1120	0.005926	0.000298	0.005852	0.1120	0.005442	0.000334	0.004959	0.1120	0.005451	0.000334	0.004959
132	1.2636	0.1135	0.003830	-0.000890	0.005600	0.1135	0.003162	-0.000735	0.004685	0.1135	0.003091	-0.000734	0.004683
133	1.2732	0.1130	0.004168	-0.000288	0.001850	0.1131	0.003980	-0.000288	0.001844	0.1131	0.003980	-0.000289	0.001849
134	1.2827	0.1117	0.001500	-0.000068	0.000263	0.1119	0.001729	-0.000091	0.000353	0.1119	0.001729	-0.000091	0.000352
135	1.2924	0.1108	0.000412	0.000000	0.000000	0.1109	0.000425	0.000000	0.000000	0.1109	0.000425	0.000000	0.000000
136	1.3021	0.1102	0.000347	0.000000	0.000000	0.1103	0.000329	0.000000	0.000000	0.1103	0.000329	0.000000	0.000000
137	1.3115	0.1097	0.000360	0.000000	0.000000	0.1097	0.000314	0.000000	0.000000	0.1097	0.000314	0.000000	0.000000
138	1.3212	0.1090	0.000462	0.000257	0.000539	0.1090	0.000475	0.000298	0.000631	0.1090	0.000475	0.000299	0.000632
139	1.3308	0.1078	0.006681	0.000326	0.007505	0.1079	0.006163	0.000384	0.006327	0.1078	0.006183	0.000380	0.006318
140	1.3404	0.1095	0.004344	-0.001274	0.007335	0.1095	0.003646	-0.001074	0.006123	0.1094	0.003578	-0.001065	0.006102
141	1.35	0.1091	0.004907	-0.000455	0.002478	0.1092	0.004663	-0.000447	0.002437	0.1091	0.004656	-0.000444	0.002443
142	1.3596	0.1077	0.001808	-0.000097	0.000374	0.1079	0.002068	-0.000203	0.000553	0.1078	0.002071	-0.000207	0.000566
143	1.3691	0.1067	0.000410	0.000000	0.000000	0.1068	0.000452	0.000000	0.000000	0.1068	0.000450	0.000000	0.000000
144	1.3788	0.1062	0.000304	0.000000	0.000000	0.1062	0.000287	0.000000	0.000000	0.1062	0.000284	0.000000	0.000000
145	1.3884	0.1057	0.000291	0.000000	0.000000	0.1058	0.000288	0.000000	0.000000	0.1058	0.000288	0.000000	0.000000
146	1.398	0.1052	0.000291	0.000000	0.000000	0.1053	0.000288	0.000000	0.000000	0.1053	0.000288	0.000000	0.000000
147	1.4076	0.1047	0.000466	0.000175	0.000465	0.1047	0.000476	0.000195	0.000657	0.1047	0.000476	0.000195	0.000657
148	1.4172	0.1047	0.006544	-0.001233	0.007763	0.1047	0.006083	-0.000981	0.006531	0.1047	0.006085	-0.000981	0.006531
149	1.4268	0.1042	0.003098	0.000780	0.004535	0.1043	0.002503	0.000524	0.003633	0.1043	0.002517	0.000525	0.003636
150	1.4366	0.1035	0.002191	0.000116	0.001100	0.1037	0.002201	0.000112	0.001118	0.1037	0.002205	0.000112	0.001117
151	1.4462	0.1030	0.000512	0.000000	0.000000	0.1031	0.000584	0.000000	0.000000	0.1031	0.000564	0.000000	0.000000
152	1.4557	0.1026	0.000302	0.000000	0.000000	0.1026	0.000280	0.000000	0.000000	0.1026	0.000280	0.000000	0.000000
153	1.4654	0.1021	0.000291	0.000000	0.000000	0.1021	0.000243	0.000000	0.000000	0.1021	0.000243	0.000000	0.000000
154	1.4749	0.1017	0.000290	0.000000	0.000000	0.1017	0.000258	0.000000	0.000000	0.1017	0.000258	0.000000	0.000000
155	1.4846	0.1012	0.000270	0.000000	0.000000	0.1013	0.000267	0.000000	0.000000	0.1013	0.000267	0.000000	0.000000
156	1.4942	0.1008	0.000294	0.000000	0.000000	0.1008	0.000258	0.000000	0.000000	0.1008	0.000258	0.000000	0.000000

S.N.	1	2	3	4	5	6	7	8	9	10	11	12	13
157	1.5038	0.1003	0.000463	0.000195	0.000653	0.1003	0.000481	0.000150	0.000795	0.1003	0.000482	0.000150	0.000795
158	1.5136	0.1006	0.007742	-0.001682	0.010146	0.1005	0.007230	-0.001347	0.008457	0.1005	0.007236	-0.001346	0.008457
159	1.5232	0.0999	0.003605	0.000765	0.005844	0.1000	0.002952	0.000535	0.004627	0.1000	0.002968	0.000535	0.004630
160	1.5329	0.0993	0.002311	0.000108	0.001292	0.0995	0.002323	0.000102	0.001310	0.0995	0.002330	0.000102	0.001309
161	1.5425	0.0989	0.000514	0.000000	0.000000	0.0990	0.000597	0.000000	0.000000	0.0990	0.000598	0.000000	0.000000
162	1.5521	0.0985	0.000271	0.000000	0.000000	0.0985	0.000241	0.000000	0.000000	0.0985	0.000243	0.000000	0.000000
163	1.5619	0.0981	0.000266	0.000000	0.000000	0.0981	0.000233	0.000000	0.000000	0.0981	0.000233	0.000000	0.000000
164	1.5715	0.0977	0.000264	0.000000	0.000000	0.0977	0.000234	0.000000	0.000000	0.0977	0.000234	0.000000	0.000000
165	1.5812	0.0973	0.000263	0.000000	0.000000	0.0973	0.000231	0.000000	0.000000	0.0973	0.000231	0.000000	0.000000
166	1.5908	0.0969	0.000276	0.000000	0.000000	0.0969	0.000252	0.000000	0.000000	0.0969	0.000252	0.000000	0.000000
167	1.6005	0.0964	0.000462	0.000214	0.000717	0.0964	0.000484	0.000165	0.000866	0.0964	0.000486	0.000165	0.000866
168	1.6101	0.0970	0.008965	-0.002203	0.012934	0.0970	0.008431	-0.001796	0.010816	0.0969	0.008436	-0.001796	0.010819
169	1.6197	0.0962	0.003042	0.000707	0.007893	0.0963	0.002423	0.000495	0.006296	0.0963	0.002423	0.000497	0.006301
170	1.6295	0.0957	0.002366	0.000069	0.001696	0.0958	0.002333	0.000227	0.001752	0.0958	0.002340	0.000227	0.001751
171	1.6392	0.0954	0.000555	0.000000	0.000000	0.0954	0.000634	0.000000	0.000000	0.0954	0.000634	0.000000	0.000000
172	1.6489	0.0950	0.000251	0.000000	0.000000	0.0950	0.000228	0.000000	0.000000	0.0950	0.000227	0.000000	0.000000
173	1.6585	0.0946	0.000246	0.000000	0.000000	0.0947	0.000211	0.000000	0.000000	0.0947	0.000211	0.000000	0.000000
174	1.6683	0.0943	0.000247	0.000000	0.000000	0.0943	0.000222	0.000000	0.000000	0.0943	0.000222	0.000000	0.000000
175	1.678	0.0940	0.000258	0.000000	0.000000	0.0940	0.000239	0.000000	0.000000	0.0940	0.000239	0.000000	0.000000
176	1.6877	0.0936	0.000467	-0.000017	0.001094	0.0936	0.000497	-0.000007	0.001180	0.0936	0.000498	-0.000008	0.001181
177	1.6973	0.0944	0.008878	-0.002627	0.014799	0.0943	0.008214	-0.002168	0.012365	0.0943	0.008195	-0.002168	0.012368
178	1.7071	0.0934	0.003289	0.000893	0.009664	0.0936	0.002678	0.000675	0.007878	0.0935	0.002683	0.000676	0.007884
179	1.7168	0.0931	0.002526	0.000033	0.001841	0.0931	0.002491	0.000213	0.001960	0.0931	0.002491	0.000213	0.001959
180	1.7265	0.0928	0.000590	0.000000	0.000000	0.0928	0.000674	0.000000	0.000000	0.0928	0.000672	0.000000	0.000000
181	1.7364	0.0924	0.000236	0.000000	0.000000	0.0925	0.000216	0.000000	0.000000	0.0925	0.000216	0.000000	0.000000
182	1.7461	0.0922	0.000229	0.000000	0.000000	0.0922	0.000191	0.000000	0.000000	0.0922	0.000191	0.000000	0.000000
183	1.7558	0.0919	0.000227	0.000000	0.000000	0.0919	0.000214	0.000000	0.000000	0.0919	0.000214	0.000000	0.000000

S.N..	1	2	3	4	5	6	7	8	9	10	11	12	13
184	1.7655	0.0916	0.000255	0.000000	0.000000	0.0916	0.000252	0.000000	0.000000	0.0916	0.000252	0.000000	0.000000
185	1.7753	0.0913	0.000394	0.000200	0.001318	0.0912	0.000432	0.000212	0.001423	0.0912	0.000435	0.000212	0.001423
186	1.7851	0.0910	0.001208	0.000085	0.003306	0.0910	0.001205	0.000076	0.003422	0.0910	0.001217	0.000076	0.003422
187	1.7948	0.0915	0.000592	0.000071	0.001750	0.0916	0.000514	0.000138	0.001973	0.0916	0.000510	0.000138	0.001974
188	1.8047	0.0910	0.000654	0.000044	0.001352	0.0912	0.000400	0.000144	0.001479	0.0912	0.000400	0.000144	0.001479
189	1.8145	0.0910	0.000411	0.000064	0.001411	0.0909	0.000274	0.000094	0.001387	0.0909	0.000271	0.000094	0.001386
190	1.8242	0.0907	0.000383	-0.000048	0.001578	0.0907	0.000376	0.000019	0.001554	0.0907	0.000383	0.000019	0.001554
191	1.8341	0.0906	0.000469	0.000013	0.001801	0.0905	0.000544	0.000011	0.001791	0.0905	0.000549	0.000011	0.001791
192	1.8439	0.0904	0.000570	0.000022	0.002161	0.0904	0.000515	0.000019	0.002147	0.0904	0.000522	0.000019	0.002147
193	1.8538	0.0903	0.000516	0.000031	0.002558	0.0903	0.000534	0.000032	0.002539	0.0903	0.000545	0.000032	0.002539
194	1.8636	0.0902	0.000607	0.000114	0.003074	0.0902	0.000644	0.000114	0.003059	0.0902	0.000657	0.000114	0.003059
195	1.8735	0.0901	0.000787	0.000194	0.004276	0.0900	0.000866	0.000199	0.004363	0.0900	0.000880	0.000199	0.004363
196	1.8834	0.0898	0.001048	0.000193	0.006781	0.0897	0.001144	0.000204	0.006949	0.0897	0.001173	0.000204	0.006949
197	1.8932	0.0905	0.000738	0.000110	0.005839	0.0905	0.000781	0.000121	0.006012	0.0905	0.000812	0.000121	0.006012
198	1.9031	0.0902	0.000976	0.000114	0.006237	0.0903	0.001024	0.000118	0.006256	0.0902	0.001057	0.000118	0.006257
199	1.9129	0.0899	0.001255	0.000155	0.007618	0.0899	0.001357	0.000159	0.007594	0.0899	0.001389	0.000159	0.007594
200	1.9229	0.0889	0.002134	0.000581	0.013829	0.0886	0.002405	0.000616	0.014515	0.0885	0.002435	0.000615	0.014515
201	1.9329	0.0858	0.006888	0.001289	0.040442	0.0850	0.007225	0.001382	0.042403	0.0849	0.007260	0.001383	0.042404
202	1.9428	0.0915	0.006423	0.002537	0.062864	0.0909	0.006841	0.002791	0.067985	0.0909	0.006902	0.002788	0.067989
203	1.9526	0.0963	0.005744	0.004310	0.079930	0.0957	0.006814	0.004773	0.087417	0.0956	0.006880	0.004772	0.087419
204	1.9625	0.0986	0.007556	0.006535	0.099963	0.0980	0.009433	0.007406	0.109009	0.0979	0.009455	0.007405	0.109010
205	1.9722	0.1090	0.005762	0.005525	0.094561	0.1088	0.007774	0.004267	0.101362	0.1087	0.007729	0.004273	0.101375
206	1.9821	0.1154	0.009374	0.002853	0.084256	0.1171	0.014500	0.000779	0.092406	0.1173	0.015360	0.000893	0.092475
207	1.9918	0.1140	0.008919	0.000543	0.080954	0.1153	0.006202	0.000269	0.087799	0.1152	0.006863	0.000726	0.088142
208	2.0015	0.1226	0.028364	-0.002575	0.059669	0.1265	0.027974	-0.004005	0.065830	0.1261	0.027070	-0.001988	0.066815
209	2.0113	0.1281	0.014841	0.001781	0.037513	0.1304	0.015889	0.005687	0.049239	0.1315	0.014376	0.003504	0.045518
210	2.021	0.1259	0.017567	0.004467	0.032257	0.1292	0.018480	0.006882	0.040810	0.1286	0.018801	0.004098	0.037237

S.N.	1	2	3	4	5	6	7	8	9	10	11	12	13
211	2.0308	0.1218	0.013013	0.004564	0.028859	0.1255	0.016251	0.004977	0.037152	0.1249	0.016443	0.005629	0.040523
212	2.0403	0.1163	0.009786	-0.000336	0.041119	0.1199	0.013646	0.000332	0.053805	0.1186	0.012835	0.001445	0.058871
213	2.0499	0.1150	0.015017	-0.007409	0.052213	0.1175	0.018266	-0.009238	0.063488	0.1168	0.017784	-0.009866	0.067115
214	2.0597	0.1122	0.014208	-0.000026	0.046041	0.1180	0.024457	-0.001840	0.050260	0.1167	0.023163	-0.001553	0.051152
215	2.0692	0.1082	0.012594	0.000344	0.048461	0.1135	0.021915	-0.002452	0.048495	0.1116	0.019835	-0.002506	0.048722
216	2.0788	0.1066	0.013262	0.002234	0.049343	0.1100	0.018603	0.000090	0.050557	0.1075	0.015434	0.000421	0.049911
217	2.0886	0.1038	0.010592	-0.000917	0.046371	0.1074	0.015614	-0.001787	0.045777	0.1043	0.011364	-0.001952	0.045513
218	2.0981	0.0996	0.004097	-0.001113	0.043133	0.1019	0.008317	-0.003886	0.046837	0.0999	0.005538	-0.003520	0.046721
219	2.1076	0.0952	0.010030	-0.003074	0.038960	0.0977	0.010965	-0.004912	0.044144	0.0942	0.010810	-0.005217	0.043221
220	2.1172	0.0927	0.016637	-0.003927	0.035230	0.0954	0.015453	-0.005002	0.039809	0.0926	0.013361	-0.004777	0.039200
221	2.1269	0.0880	0.021437	-0.004821	0.031721	0.0895	0.025766	-0.007262	0.035562	0.0867	0.022913	-0.006358	0.034783
222	2.1366	0.0874	0.012919	-0.002724	0.027951	0.0889	0.010016	-0.003143	0.031084	0.0868	0.012789	-0.003174	0.030419
223	2.1461	0.0849	0.015407	-0.002732	0.023624	0.0859	0.013038	-0.003626	0.025648	0.0841	0.015711	-0.003823	0.025563
224	2.1556	0.0825	0.016845	-0.000606	0.021284	0.0833	0.014957	-0.001569	0.022659	0.0826	0.016005	-0.001305	0.023115
225	2.1652	0.0846	0.010561	0.000700	0.018852	0.0847	0.009816	0.000579	0.020490	0.0841	0.010702	0.000610	0.020606
226	2.1749	0.0844	0.004921	-0.000389	0.009050	0.0841	0.005081	-0.000594	0.009869	0.0838	0.005401	-0.000578	0.009885
227	2.1845	0.0868	0.001388	-0.000516	0.005629	0.0865	0.001575	-0.000657	0.005746	0.0863	0.001735	-0.000677	0.005779
228	2.1942	0.0870	0.001124	-0.000006	0.001579	0.0868	0.001287	-0.000224	0.001732	0.0867	0.001375	-0.000228	0.001734
229	2.2038	0.0878	0.000321	-0.000076	0.002772	0.0878	0.000357	-0.000138	0.002558	0.0878	0.000327	-0.000141	0.002565
230	2.2134	0.0873	0.000127	0.000072	0.002426	0.0874	0.000183	0.000102	0.002255	0.0874	0.000181	0.000101	0.002258
231	2.2232	0.0869	0.000091	0.000023	0.002351	0.0870	0.000129	0.000025	0.002335	0.0870	0.000114	0.000025	0.002335
232	2.2329	0.0866	0.000089	0.000018	0.002081	0.0866	0.000116	0.000087	0.002057	0.0866	0.000113	0.000087	0.002057
233	2.2426	0.0863	0.000101	0.000010	0.001793	0.0863	0.000113	0.000009	0.001805	0.0863	0.000108	0.000009	0.001805
234	2.2524	0.0859	0.000278	0.000033	0.001485	0.0859	0.000274	0.000040	0.001476	0.0859	0.000273	0.000040	0.001476
235	2.262	0.0855	0.000344	0.000136	0.000779	0.0854	0.000397	0.000230	0.000907	0.0854	0.000405	0.000229	0.000906
236	2.2718	0.0853	0.000708	0.000101	0.002050	0.0853	0.000728	0.000054	0.002037	0.0853	0.000744	0.000054	0.002037
237	2.2815	0.0855	0.000449	0.000000	0.000000	0.0856	0.000515	-0.000074	0.000287	0.0855	0.000495	-0.000074	0.000288

S.N.	1	2	3	4	5	6	7	8	9	10	11	12	13
238	2.2913	0.0851	0.000180	0.000151	0.000399	0.0851	0.000233	0.000206	0.000549	0.0851	0.000228	0.000206	0.000549
239	2.3011	0.0847	0.000192	0.000140	0.000371	0.0848	0.000177	0.000070	0.000273	0.0848	0.000176	0.000071	0.000273
240	2.3109	0.0845	0.000178	0.000000	0.000000	0.0845	0.000176	0.000000	0.000000	0.0845	0.000176	0.000000	0.000000
241	2.3206	0.0842	0.000219	0.000000	0.000000	0.0842	0.000229	0.000000	0.000000	0.0842	0.000231	0.000000	0.000000
242	2.3304	0.0838	0.000400	0.000322	0.001337	0.0837	0.000458	0.000371	0.001478	0.0837	0.000464	0.000371	0.001478
243	2.3401	0.0826	0.002945	0.002063	0.009160	0.0826	0.002746	0.001798	0.007965	0.0826	0.002762	0.001799	0.007967
244	2.3499	0.0852	0.002983	-0.003181	0.011178	0.0852	0.002677	-0.002729	0.009464	0.0852	0.002670	-0.002730	0.009470
245	2.3596	0.0847	0.002983	-0.000732	0.003816	0.0848	0.002913	-0.000695	0.003695	0.0848	0.002901	-0.000694	0.003692
246	2.3695	0.0838	0.001260	-0.000059	0.000632	0.0839	0.001389	-0.000152	0.000588	0.0839	0.001386	-0.000152	0.000587
247	2.3793	0.0833	0.000224	0.000000	0.000000	0.0833	0.000243	0.000000	0.000000	0.0833	0.000243	0.000000	0.000000
248	2.3892	0.0831	0.000161	0.000000	0.000000	0.0831	0.000131	0.000000	0.000000	0.0831	0.000152	0.000000	0.000000
249	2.399	0.0829	0.000184	0.000000	0.000000	0.0829	0.000177	0.000000	0.000000	0.0829	0.000182	0.000000	0.000000
250	2.4089	0.0827	0.000213	0.000000	0.000000	0.0827	0.000209	0.000000	0.000000	0.0827	0.000209	0.000000	0.000000
251	2.4187	0.0823	0.000422	0.000348	0.001400	0.0822	0.000481	0.000319	0.001598	0.0822	0.000489	0.000318	0.001598
252	2.4285	0.0811	0.002946	0.002039	0.009074	0.0812	0.002750	0.001772	0.007894	0.0811	0.002766	0.001772	0.007896
253	2.4384	0.0838	0.002986	-0.003228	0.011115	0.0838	0.002632	-0.002687	0.009332	0.0838	0.002625	-0.002689	0.009338
254	2.4483	0.0834	0.003050	-0.000650	0.003785	0.0834	0.002839	-0.000657	0.003664	0.0834	0.002826	-0.000657	0.003664
255	2.458	0.0825	0.001236	-0.000118	0.000457	0.0826	0.001324	-0.000088	0.000730	0.0826	0.001318	-0.000088	0.000730
256	2.4679	0.0820	0.000217	0.000000	0.000000	0.0820	0.000236	0.000000	0.000000	0.0820	0.000237	0.000000	0.000000
257	2.4777	0.0819	0.000171	0.000000	0.000000	0.0819	0.000151	0.000000	0.000000	0.0819	0.000151	0.000000	0.000000
258	2.4877	0.0817	0.000215	0.000000	0.000000	0.0817	0.000218	0.000000	0.000000	0.0817	0.000219	0.000000	0.000000
259	2.4977	0.0813	0.000428	0.000347	0.001430	0.0813	0.000486	0.000319	0.001629	0.0813	0.000493	0.000319	0.001629
260	2.5076	0.0802	0.002935	0.002046	0.009108	0.0802	0.002744	0.001775	0.007922	0.0802	0.002760	0.001776	0.007924
261	2.5175	0.0830	0.002985	-0.003250	0.011184	0.0830	0.002683	-0.002725	0.009460	0.0829	0.002674	-0.002726	0.009465
262	2.5274	0.0825	0.003005	-0.000636	0.003762	0.0825	0.002865	-0.000659	0.003635	0.0825	0.002853	-0.000659	0.003635
263	2.5372	0.0817	0.001203	-0.000117	0.000452	0.0818	0.001309	-0.000147	0.000568	0.0818	0.001306	-0.000146	0.000567
264	2.5471	0.0812	0.000211	0.000000	0.000000	0.0813	0.000226	0.000000	0.000000	0.0813	0.000226	0.000000	0.000000

S.N.	1	2	3	4	5	6	7	8	9	10	11	12	13
265	2.5571	0.0811	0.000170	0.000000	0.000000	0.0811	0.000149	0.000000	0.000000	0.0811	0.000149	0.000000	0.000000
266	2.567	0.0810	0.000214	0.000000	0.000000	0.0810	0.000217	0.000000	0.000000	0.0810	0.000217	0.000000	0.000000
267	2.577	0.0807	0.000431	0.000344	0.001446	0.0806	0.000491	0.000316	0.001647	0.0806	0.000497	0.000316	0.001646
268	2.5869	0.0796	0.002921	0.002043	0.009093	0.0796	0.002732	0.001777	0.007911	0.0796	0.002746	0.001772	0.007912
269	2.5968	0.0824	0.002973	-0.003245	0.011163	0.0823	0.002640	-0.002713	0.009405	0.0823	0.002630	-0.002712	0.009412
270	2.6068	0.0819	0.002950	-0.000615	0.003703	0.0820	0.002864	-0.000655	0.003623	0.0820	0.002861	-0.000651	0.003623
271	2.6168	0.0811	0.001167	-0.000115	0.000444	0.0813	0.001279	-0.000144	0.000559	0.0813	0.001275	-0.000144	0.000558
272	2.6267	0.0808	0.000206	0.000000	0.000000	0.0808	0.000220	0.000000	0.000000	0.0808	0.000219	0.000000	0.000000
273	2.6366	0.0807	0.000167	0.000000	0.000000	0.0807	0.000147	0.000000	0.000000	0.0807	0.000148	0.000000	0.000000
274	2.6465	0.0806	0.000213	0.000000	0.000000	0.0806	0.000215	0.000000	0.000000	0.0806	0.000215	0.000000	0.000000
275	2.6565	0.0803	0.000430	0.000337	0.001448	0.0802	0.000489	0.000308	0.001648	0.0802	0.000497	0.000308	0.001648
276	2.6665	0.0792	0.002902	0.002018	0.008972	0.0793	0.002717	0.001751	0.007804	0.0792	0.002732	0.001752	0.007807
277	2.6765	0.0821	0.002940	-0.003185	0.010971	0.0820	0.002612	-0.002662	0.009246	0.0820	0.002605	-0.002664	0.009251
278	2.6865	0.0816	0.002863	-0.000581	0.003577	0.0817	0.002780	-0.000625	0.003513	0.0817	0.002770	-0.000625	0.003513
279	2.6965	0.0809	0.001111	-0.000110	0.000425	0.0810	0.001228	-0.000139	0.000537	0.0810	0.001224	-0.000138	0.000536
280	2.7065	0.0805	0.000199	0.000000	0.000000	0.0806	0.000211	0.000000	0.000000	0.0806	0.000209	0.000000	0.000000
281	2.7165	0.0805	0.000168	0.000000	0.000000	0.0805	0.000146	0.000000	0.000000	0.0805	0.000148	0.000000	0.000000
282	2.7265	0.0805	0.000165	0.000000	0.000000	0.0805	0.000145	0.000000	0.000000	0.0805	0.000145	0.000000	0.000000
283	2.7365	0.0804	0.000209	0.000000	0.000000	0.0804	0.000208	0.000000	0.000000	0.0804	0.000210	0.000000	0.000000
284	2.7465	0.0802	0.000426	0.000324	0.001435	0.0801	0.000487	0.000292	0.001630	0.0801	0.000493	0.000292	0.001630
285	2.7566	0.0792	0.002877	0.001948	0.008674	0.0792	0.002696	0.001615	0.007548	0.0792	0.002709	0.001616	0.007550
286	2.7667	0.0820	0.002872	-0.003038	0.010510	0.0820	0.002544	-0.002533	0.008856	0.0820	0.002537	-0.002535	0.008862
287	2.7768	0.0816	0.002723	-0.000587	0.003309	0.0816	0.002658	-0.000567	0.003299	0.0816	0.002646	-0.000568	0.003299
288	2.7868	0.0809	0.001022	-0.000101	0.000390	0.0810	0.001131	-0.000128	0.000494	0.0810	0.001127	-0.000127	0.000494
289	2.7969	0.0807	0.000262	0.000000	0.000000	0.0807	0.000193	0.000000	0.000000	0.0807	0.000196	0.000000	0.000000
290	2.807	0.0805	0.000260	0.000000	0.000000	0.0806	0.000224	0.000000	0.000000	0.0806	0.000225	0.000000	0.000000
291	2.8171	0.0805	0.000545	0.000053	0.001750	0.0804	0.000619	0.000014	0.001909	0.0804	0.000630	-0.000001	0.001925

S.N.	1	2	3	4	5	6	7	8	9	10	11	12	13
292	2.8271	0.0820	0.012881	-0.005338	0.030649	0.0827	0.015045	-0.005268	0.028188	0.0827	0.015026	-0.005275	0.028213
293	2.8371	0.0815	0.003670	-0.000102	0.016908	0.0810	0.004932	0.000652	0.016633	0.0809	0.004949	0.000655	0.016646
294	2.8473	0.0814	0.003258	-0.000307	0.003465	0.0812	0.003508	-0.000264	0.003442	0.0812	0.003507	-0.000265	0.003439
295	2.8574	0.0812	0.000972	-0.000092	0.000358	0.0813	0.001076	-0.000116	0.000450	0.0813	0.001074	-0.000116	0.000450
296	2.8676	0.0810	0.000190	0.000000	0.000000	0.0810	0.000192	0.000000	0.000000	0.0810	0.000192	0.000000	0.000000
297	2.8777	0.0810	0.000166	0.000000	0.000000	0.0810	0.000147	0.000000	0.000000	0.0810	0.000147	0.000000	0.000000
298	2.8878	0.0811	0.000165	0.000000	0.000000	0.0811	0.000144	0.000000	0.000000	0.0811	0.000144	0.000000	0.000000
299	2.8979	0.0811	0.000206	0.000000	0.000000	0.0811	0.000204	0.000000	0.000000	0.0811	0.000205	0.000000	0.000000
300	2.9081	0.0811	0.000521	0.000078	0.001610	0.0810	0.000596	0.000045	0.001759	0.0810	0.000602	0.000045	0.001759
301	2.9181	0.0830	0.014433	-0.005131	0.029338	0.0833	0.015583	-0.004713	0.026010	0.0833	0.015563	-0.004714	0.026017
302	2.9283	0.0817	0.004834	0.000720	0.017551	0.0815	0.005277	0.000908	0.015879	0.0815	0.005291	0.000910	0.015892
303	2.9385	0.0820	0.003245	-0.000242	0.002996	0.0819	0.003457	-0.000183	0.003054	0.0819	0.003454	-0.000183	0.003052
304	2.9487	0.0819	0.000850	-0.000078	0.000303	0.0820	0.000935	-0.000109	0.000424	0.0820	0.000931	-0.000109	0.000423
305	2.9589	0.0818	0.000180	0.000000	0.000000	0.0819	0.000174	0.000000	0.000000	0.0819	0.000174	0.000000	0.000000
306	2.9691	0.0819	0.000215	0.000000	0.000000	0.0819	0.000220	0.000000	0.000000	0.0819	0.000219	0.000000	0.000000
307	2.9793	0.0819	0.000504	0.000089	0.001481	0.0818	0.000560	0.000064	0.001614	0.0818	0.000564	0.000064	0.001614
308	2.9894	0.0840	0.014358	-0.004650	0.026462	0.0838	0.013714	-0.003904	0.022060	0.0838	0.013694	-0.003904	0.022066
309	2.9998	0.0824	0.005322	0.001007	0.016751	0.0826	0.004538	0.000702	0.013643	0.0826	0.004549	0.000703	0.013651
310	3.0099	0.0828	0.003199	-0.000163	0.002626	0.0829	0.003180	-0.000090	0.002765	0.0828	0.003179	-0.000091	0.002763
311	3.0201	0.0829	0.000743	0.000000	0.000000	0.0830	0.000829	-0.000093	0.000359	0.0830	0.000827	-0.000093	0.000358
312	3.0304	0.0829	0.000181	0.000000	0.000000	0.0829	0.000175	0.000000	0.000000	0.0829	0.000170	0.000000	0.000000
313	3.0408	0.0831	0.000171	0.000000	0.000000	0.0831	0.000170	0.000000	0.000000	0.0831	0.000105	0.000000	0.000000
314	3.0512	0.0833	0.000168	0.000000	0.000000	0.0833	0.000129	0.000000	0.000000	0.0832	0.000298	0.000000	0.000000
315	3.0614	0.0834	0.000206	0.000000	0.000000	0.0834	0.000197	0.000000	0.000000	0.0834	0.000209	0.000000	0.000000
316	3.0716	0.0835	0.000477	-0.000112	0.001489	0.0834	0.000600	-0.000039	0.001637	0.0835	0.000887	-0.000033	0.001622
317	3.0819	0.0851	0.010491	-0.003408	0.019607	0.0849	0.009780	-0.002828	0.016356	0.0848	0.009767	-0.002790	0.016383
318	3.0922	0.0844	0.004408	0.000854	0.013632	0.0845	0.003819	0.000645	0.011273	0.0845	0.003832	0.000646	0.011282

S.N.	1	2	3	4	5	6	7	8	9	10	11	12	13
319	3.1027	0.0846	0.002770	-0.000016	0.002183	0.0846	0.002788	0.000030	0.002336	0.0846	0.002789	0.000030	0.002336
320	3.1128	0.0848	0.000591	0.000000	0.000000	0.0849	0.000675	-0.000070	0.000270	0.0849	0.000673	-0.000070	0.000270
321	3.1233	0.0849	0.000183	0.000000	0.000000	0.0849	0.000168	0.000000	0.000000	0.0849	0.000170	0.000000	0.000000
322	3.1336	0.0852	0.000153	0.000000	0.000000	0.0852	0.000153	0.000000	0.000000	0.0852	0.000153	0.000000	0.000000
323	3.1439	0.0854	0.000201	0.000000	0.000000	0.0854	0.000155	0.000000	0.000000	0.0854	0.000155	0.000000	0.000000
324	3.1545	0.0857	0.000208	0.000000	0.000000	0.0857	0.000194	0.000000	0.000000	0.0857	0.000194	0.000000	0.000000
325	3.1648	0.0859	0.000442	-0.000038	0.001222	0.0858	0.000499	-0.000035	0.001330	0.0858	0.000502	-0.000035	0.001330
326	3.1752	0.0871	0.008816	-0.002273	0.014239	0.0870	0.008216	-0.001865	0.011925	0.0870	0.008220	-0.001866	0.011927
327	3.1856	0.0871	0.003566	0.000559	0.010003	0.0872	0.003077	0.000384	0.008268	0.0872	0.003081	0.000384	0.008272
328	3.1962	0.0873	0.002319	0.000144	0.001663	0.0873	0.002301	0.000159	0.001810	0.0873	0.002301	0.000158	0.001810
329	3.2069	0.0876	0.000458	0.000000	0.000000	0.0877	0.000511	0.000000	0.000000	0.0877	0.000512	0.000000	0.000000
330	3.2172	0.0879	0.000184	0.000000	0.000000	0.0879	0.000161	0.000000	0.000000	0.0879	0.000163	0.000000	0.000000
331	3.2276	0.0883	0.000221	0.000000	0.000000	0.0883	0.000207	0.000000	0.000000	0.0883	0.000207	0.000000	0.000000
332	3.2382	0.0885	0.000415	0.000069	0.001017	0.0884	0.000468	0.000010	0.001149	0.0884	0.000472	0.000010	0.001149
333	3.2486	0.0896	0.007113	-0.001573	0.010193	0.0895	0.006705	-0.001313	0.008621	0.0895	0.006710	-0.001313	0.008623
334	3.2592	0.0901	0.002989	0.000431	0.007360	0.0901	0.002448	0.000351	0.006107	0.0901	0.002450	0.000351	0.006107
335	3.2698	0.0903	0.001919	0.000038	0.001257	0.0903	0.001918	0.000221	0.001369	0.0903	0.001916	0.000221	0.001369
336	3.2804	0.0907	0.000372	0.000000	0.000000	0.0908	0.000417	0.000000	0.000000	0.0907	0.000417	0.000000	0.000000
337	3.2911	0.0912	0.000207	0.000000	0.000000	0.0911	0.000184	0.000000	0.000000	0.0911	0.000184	0.000000	0.000000
338	3.3018	0.0917	0.000215	0.000000	0.000000	0.0917	0.000188	0.000000	0.000000	0.0917	0.000188	0.000000	0.000000
339	3.3125	0.0923	0.000215	0.000000	0.000000	0.0922	0.000190	0.000000	0.000000	0.0922	0.000190	0.000000	0.000000
340	3.3231	0.0929	0.000226	0.000000	0.000000	0.0928	0.000206	0.000000	0.000000	0.0928	0.000206	0.000000	0.000000
341	3.3337	0.0934	0.000401	0.000048	0.000784	0.0933	0.000443	0.000126	0.000904	0.0933	0.000444	0.000126	0.000904
342	3.3444	0.0943	0.005577	-0.000775	0.005961	0.0942	0.005228	-0.000636	0.005180	0.0942	0.005232	-0.000636	0.005180
343	3.3554	0.0954	0.002589	0.000400	0.004339	0.0954	0.002164	0.000326	0.003663	0.0954	0.002167	0.000325	0.003664
344	3.366	0.0958	0.001561	0.000058	0.000817	0.0958	0.001588	0.000133	0.000880	0.0958	0.001588	0.000133	0.000880
345	3.3769	0.0965	0.000337	0.000000	0.000000	0.0964	0.000354	0.000000	0.000000	0.0964	0.000356	0.000000	0.000000

S.N.	1	2	3	4	5	6	7	8	9	10	11	12	13
346	3.3879	0.0972	0.000240	0.000000	0.000000	0.0972	0.000214	0.000000	0.000000	0.0972	0.000214	0.000000	0.000000
347	3.3985	0.0981	0.000242	0.000000	0.000000	0.0980	0.000211	0.000000	0.000000	0.0980	0.000211	0.000000	0.000000
348	3.4095	0.0989	0.000247	0.000000	0.000000	0.0989	0.000217	0.000000	0.000000	0.0989	0.000217	0.000000	0.000000
349	3.4205	0.0999	0.000261	0.000000	0.000000	0.0998	0.000234	0.000000	0.000000	0.0998	0.000234	0.000000	0.000000
350	3.4314	0.1008	0.000594	-0.000084	0.001456	0.1007	0.000618	-0.000201	0.001488	0.1007	0.000618	-0.000202	0.001490
351	3.4426	0.1052	0.018704	-0.004464	0.024165	0.1048	0.017407	-0.003697	0.020158	0.1048	0.017389	-0.003699	0.020163
352	3.4535	0.1037	0.007663	0.000960	0.015618	0.1038	0.006351	0.000684	0.012569	0.1038	0.006343	0.000689	0.012578
353	3.4646	0.1048	0.005559	-0.000255	0.002525	0.1048	0.005442	-0.000157	0.002645	0.1048	0.005451	-0.000159	0.002649
354	3.4757	0.1056	0.001274	0.000000	0.000000	0.1056	0.001506	-0.000091	0.000353	0.1056	0.001506	-0.000091	0.000353
355	3.4868	0.1067	0.000358	0.000000	0.000000	0.1066	0.000339	0.000000	0.000000	0.1066	0.000339	0.000000	0.000000
356	3.4981	0.1080	0.000315	0.000000	0.000000	0.1079	0.000263	0.000000	0.000000	0.1079	0.000263	0.000000	0.000000
357	3.5092	0.1094	0.000315	0.000000	0.000000	0.1093	0.000281	0.000000	0.000000	0.1093	0.000281	0.000000	0.000000
358	3.5205	0.1108	0.000450	0.000073	0.000281	0.1107	0.000456	0.000012	0.000421	0.1107	0.000456	0.000012	0.000421
359	3.5318	0.1133	0.007786	-0.001384	0.008112	0.1131	0.007230	-0.001187	0.006777	0.1131	0.007230	-0.001187	0.006776
360	3.5432	0.1145	0.004177	0.000521	0.005925	0.1145	0.003480	0.000363	0.004802	0.1145	0.003454	0.000362	0.004802
361	3.5545	0.1160	0.002881	0.000058	0.001235	0.1159	0.002890	0.000135	0.001236	0.1159	0.002890	0.000135	0.001235
362	3.5658	0.1177	0.000679	0.000000	0.000000	0.1176	0.000771	0.000000	0.000000	0.1176	0.000771	0.000000	0.000000
363	3.5773	0.1195	0.000404	0.000000	0.000000	0.1193	0.000378	0.000000	0.000000	0.1193	0.000378	0.000000	0.000000
364	3.5887	0.1214	0.000406	0.000000	0.000000	0.1213	0.000374	0.000000	0.000000	0.1213	0.000374	0.000000	0.000000
365	3.6003	0.1234	0.000443	0.000000	0.000000	0.1232	0.000385	0.000000	0.000000	0.1232	0.000381	0.000000	0.000000
366	3.6117	0.1255	0.000569	0.000000	0.000000	0.1253	0.000553	-0.000074	0.000288	0.1253	0.000553	-0.000074	0.000288
367	3.6233	0.1293	0.010983	-0.001882	0.010605	0.1290	0.010133	-0.001539	0.008751	0.1290	0.010145	-0.001540	0.008753
368	3.6347	0.1306	0.005485	0.000583	0.007126	0.1305	0.004419	0.000311	0.005572	0.1304	0.004416	0.000311	0.005575
369	3.6462	0.1325	0.004516	0.000091	0.001753	0.1324	0.004441	0.000118	0.001785	0.1324	0.004441	0.000117	0.001785
370	3.6578	0.1347	0.001186	0.000000	0.000000	0.1345	0.001389	0.000000	0.000000	0.1345	0.001389	0.000000	0.000000
371	3.6693	0.1369	0.000581	0.000000	0.000000	0.1367	0.000552	0.000000	0.000000	0.1367	0.000552	0.000000	0.000000
372	3.6806	0.1392	0.000585	0.000000	0.000000	0.1390	0.000532	0.000000	0.000000	0.1390	0.000532	0.000000	0.000000

S.N.	1	2	3	4	5	6	7	8	9	10	11	12	13
373	3.6924	0.1416	0.000601	0.000000	0.000000	0.1414	0.000550	0.000000	0.000000	0.1414	0.000550	0.000000	0.000000
374	3.7037	0.1440	0.000633	0.000000	0.000000	0.1439	0.000560	0.000000	0.000000	0.1439	0.000560	0.000000	0.000000
375	3.7151	0.1466	0.000959	-0.000118	0.000902	0.1464	0.000874	-0.000124	0.000721	0.1464	0.000874	-0.000124	0.000721
376	3.7266	0.1546	0.032014	-0.005427	0.023344	0.1536	0.028923	-0.004570	0.019218	0.1536	0.028885	-0.004571	0.019226
377	3.7379	0.1560	0.013895	0.002763	0.012770	0.1558	0.011003	0.002033	0.009537	0.1558	0.010952	0.002037	0.009547
378	3.7492	0.1558	0.010819	0.001463	0.005525	0.1560	0.011189	0.001495	0.005336	0.1560	0.011186	0.001494	0.005332
379	3.7606	0.1563	0.002591	0.000070	0.000270	0.1563	0.003182	0.000086	0.000333	0.1563	0.003173	0.000086	0.000333
380	3.772	0.1582	0.000853	0.000000	0.000000	0.1581	0.000881	0.000000	0.000000	0.1581	0.000881	0.000000	0.000000
381	3.7832	0.1602	0.000792	0.000000	0.000000	0.1601	0.000724	0.000000	0.000000	0.1601	0.000724	0.000000	0.000000
382	3.7943	0.1623	0.000789	0.000000	0.000000	0.1621	0.000720	0.000000	0.000000	0.1621	0.000720	0.000000	0.000000
383	3.8055	0.1642	0.000806	0.000000	0.000000	0.1641	0.000739	0.000000	0.000000	0.1641	0.000739	0.000000	0.000000
384	3.8165	0.1661	0.000824	0.000000	0.000000	0.1659	0.000753	0.000000	0.000000	0.1659	0.000750	0.000000	0.000000
385	3.8276	0.1683	0.005440	-0.000514	0.002001	0.1681	0.004843	-0.000398	0.001656	0.1682	0.004849	-0.000479	0.001665
386	3.8386	0.1698	0.001841	0.000453	0.001214	0.1697	0.001083	0.000339	0.000919	0.1696	0.001122	0.000436	0.000956
387	3.8496	0.1711	0.002715	0.000221	0.000587	0.1710	0.002575	0.000206	0.000553	0.1710	0.002575	0.000206	0.000553
388	3.8606	0.1725	0.001224	0.000000	0.000000	0.1724	0.001303	0.000000	0.000000	0.1724	0.001305	0.000000	0.000000
389	3.8714	0.1738	0.000874	0.000000	0.000000	0.1737	0.000776	0.000000	0.000000	0.1737	0.000776	0.000000	0.000000
390	3.8824	0.1750	0.000890	0.000000	0.000000	0.1749	0.000785	0.000000	0.000000	0.1749	0.000785	0.000000	0.000000
391	3.8931	0.1760	0.000893	0.000000	0.000000	0.1760	0.000785	0.000000	0.000000	0.1760	0.000785	0.000000	0.000000
392	3.9039	0.1771	0.000899	0.000000	0.000000	0.1770	0.000811	0.000000	0.000000	0.1770	0.000811	0.000000	0.000000
393	3.9146	0.1780	0.001384	0.000000	0.000000	0.1779	0.001226	0.000000	0.000000	0.1779	0.001226	0.000000	0.000000
394	3.9252	0.1790	0.001004	0.000000	0.000000	0.1789	0.000856	0.000000	0.000000	0.1789	0.000856	0.000000	0.000000
395	3.9358	0.1796	0.001110	0.000000	0.000000	0.1796	0.000996	0.000000	0.000000	0.1796	0.000996	0.000000	0.000000
396	3.9464	0.1803	0.000952	0.000000	0.000000	0.1803	0.000871	0.000000	0.000000	0.1803	0.000871	0.000000	0.000000
397	3.9571	0.1809	0.000871	0.000000	0.000000	0.1809	0.000770	0.000000	0.000000	0.1809	0.000770	0.000000	0.000000
398	3.9675	0.1814	0.000840	0.000000	0.000000	0.1813	0.000739	0.000000	0.000000	0.1813	0.000739	0.000000	0.000000
399	3.9782	0.1818	0.000844	0.000000	0.000000	0.1818	0.000752	0.000000	0.000000	0.1818	0.000752	0.000000	0.000000

S.N.	1	2	3	4	5	6	7	8	9	10	11	12	13
400	3.9886	0.1822	0.000840	0.000000	0.000000	0.1821	0.000722	0.000000	0.000000	0.1821	0.000722	0.000000	0.000000
401	3.9991	0.1825	0.000844	0.000000	0.000000	0.1825	0.000752	0.000000	0.000000	0.1825	0.000752	0.000000	0.000000
402	4.0094	0.1828	0.000860	0.000000	0.000000	0.1828	0.000799	0.000000	0.000000	0.1828	0.000799	0.000000	0.000000
403	4.0199	0.1832	0.000880	0.000000	0.000000	0.1833	0.000789	0.000000	0.000000	0.1833	0.000789	0.000000	0.000000
404	4.0302	0.1835	0.000857	0.000000	0.000000	0.1835	0.000739	0.000000	0.000000	0.1835	0.000739	0.000000	0.000000
405	4.0406	0.1836	0.000847	0.000000	0.000000	0.1836	0.000743	0.000000	0.000000	0.1836	0.000743	0.000000	0.000000
406	4.0508	0.1838	0.000842	0.000000	0.000000	0.1838	0.000752	0.000000	0.000000	0.1838	0.000752	0.000000	0.000000
407	4.0614	0.1839	0.000844	0.000000	0.000000	0.1839	0.000734	0.000000	0.000000	0.1839	0.000734	0.000000	0.000000
408	4.0715	0.1840	0.000840	0.000000	0.000000	0.1840	0.000734	0.000000	0.000000	0.1840	0.000734	0.000000	0.000000
409	4.0817	0.1841	0.000840	0.000000	0.000000	0.1841	0.000729	0.000000	0.000000	0.1841	0.000729	0.000000	0.000000
410	4.092	0.1841	0.000827	0.000000	0.000000	0.1841	0.000739	0.000000	0.000000	0.1841	0.000739	0.000000	0.000000
411	4.1025	0.1843	0.000842	0.000000	0.000000	0.1843	0.000750	0.000000	0.000000	0.1843	0.000750	0.000000	0.000000
412	4.1128	0.1844	0.000858	0.000000	0.000000	0.1844	0.000750	0.000000	0.000000	0.1844	0.000750	0.000000	0.000000
413	4.1228	0.1844	0.000844	0.000000	0.000000	0.1844	0.000739	0.000000	0.000000	0.1844	0.000739	0.000000	0.000000
414	4.1332	0.1844	0.000827	0.000000	0.000000	0.1844	0.000722	0.000000	0.000000	0.1844	0.000722	0.000000	0.000000
415	4.1432	0.1844	0.000809	0.000000	0.000000	0.1844	0.000704	0.000000	0.000000	0.1844	0.000704	0.000000	0.000000
416	4.1534	0.1844	0.000827	0.000000	0.000000	0.1844	0.000722	0.000000	0.000000	0.1844	0.000722	0.000000	0.000000
417	4.1637	0.1844	0.000840	0.000000	0.000000	0.1844	0.000739	0.000000	0.000000	0.1844	0.000739	0.000000	0.000000
418	4.1738	0.1844	0.000840	0.000000	0.000000	0.1844	0.000734	0.000000	0.000000	0.1844	0.000734	0.000000	0.000000
419	4.1839	0.1844	0.000809	0.000000	0.000000	0.1844	0.000704	0.000000	0.000000	0.1844	0.000704	0.000000	0.000000
420	4.1943	0.1845	0.000840	0.000000	0.000000	0.1845	0.000734	0.000000	0.000000	0.1845	0.000734	0.000000	0.000000
421	4.2044	0.1845	0.000840	0.000000	0.000000	0.1845	0.000734	0.000000	0.000000	0.1845	0.000734	0.000000	0.000000
422	4.2145	0.1844	0.000809	0.000000	0.000000	0.1844	0.000704	0.000000	0.000000	0.1844	0.000704	0.000000	0.000000
423	4.2246	0.1844	0.000840	0.000000	0.000000	0.1844	0.000739	0.000000	0.000000	0.1844	0.000739	0.000000	0.000000
424	4.235	0.1843	0.000809	0.000000	0.000000	0.1843	0.000704	0.000000	0.000000	0.1843	0.000704	0.000000	0.000000
425	4.245	0.1843	0.000840	0.000000	0.000000	0.1843	0.000734	0.000000	0.000000	0.1843	0.000734	0.000000	0.000000

Table VII (3) Observed and computed water level

S.N.	Distance from U/s boundary	Observed Ave. water level	Computed Ave. water level case-I	Computed Ave. water level Case-2	Computed Ave. water level Case-3
	cm	cm	cm	cm	cm
1	0	0.0785	0.0786	0.0786	0.0786
2	10	0.0784	0.0785	0.0785	0.0785
3	20	0.0783	0.0784	0.0784	0.0784
4	30	0.0782	0.0783	0.0783	0.0783
5	40	0.0781	0.07821	0.07821	0.0782
6	50	0.0779	0.07799	0.078	0.0780
7	60	0.0778	0.0779	0.0779	0.0779
8	70	0.0777	0.0778	0.0778	0.0778
9	80	0.0776	0.07769	0.0777	0.0777
10	90	0.0775	0.0777	0.0776	0.0776
11	100	0.0774	0.07751	0.07739	0.0774
12	110	0.0773	0.0774	0.0773	0.0773
13	120	0.0772	0.0772	0.0772	0.0772
14	130	0.077	0.0771	0.0771	0.0771
15	140	0.0769	0.077	0.077	0.0770
16	150	0.0768	0.0769	0.0769	0.0769
17	160	0.0767	0.0768	0.0768	0.0768
18	170	0.0766	0.07671	0.07671	0.0767
19	180	0.0765	0.07656	0.0765	0.0765
20	190	0.0764	0.0764	0.0764	0.0764
21	200	0.0711	0.06913	0.06853	0.0685
22	205	0.0669	0.07	0.06871	0.0701
23	210	0.0685	0.06981	0.06972	0.0697
24	215	0.0701	0.07129	0.07096	0.0708
25	220	0.0711	0.0712	0.07119	0.0712
26	225	0.0712	0.0712	0.0712	0.0712
27	235	0.071	0.0711	0.0711	0.0711
28	245	0.0709	0.07091	0.07089	0.0709
29	255	0.0708	0.07079	0.0708	0.0708
30	265	0.0707	0.0707	0.0707	0.0707
31	275	0.0706	0.0706	0.0706	0.0706
32	285	0.0704	0.07042	0.07039	0.0704
33	295	0.0703	0.0703	0.0703	0.0703
34	305	0.0702	0.0702	0.0702	0.0702
35	315	0.0701	0.0701	0.0701	0.0701
36	325	0.0699	0.07	0.06999	0.0700
37	335	0.0698	0.06985	0.06985	0.0698
38	345	0.0697	0.06977	0.06973	0.0698
39	355	0.0696	0.06959	0.06959	0.0696
40	365	0.0695	0.0695	0.0695	0.0695
41	375	0.0694	0.0695	0.0694	0.0694
42	385	0.0692	0.0693	0.0693	0.0693
43	395	0.0691	0.0692	0.0692	0.0692
44	405	0.069	0.0691	0.0691	0.0691
45	415	0.0689	0.069	0.069	0.0690
46	425	0.0689	0.0689	0.0689	0.0689

Table VII (4) Mean and std dev. of I_L and I_T at cell centers og the generated mesh for ***Case-2***

S.N.	Distance from U/s boundary (m)	I_L		I_T	
		Mean	*Std.dev.(σ)*	*Mean*	*Std. Dev.(σ)*
	1	2	3	4	5
1	0.0049	0.017700	0.000000	0.000000	0.000000
2	0.0146	0.017700	0.000000	0.000000	0.000000
3	0.0244	0.017700	0.000000	0.000000	0.000000
4	0.0342	0.017700	0.000000	0.000000	0.000000
5	0.0439	0.017700	0.000000	0.000000	0.000000
6	0.0537	0.017700	0.000000	0.000000	0.000000
7	0.0634	0.017700	0.000000	0.000000	0.000000
8	0.0732	0.017700	0.000000	0.000000	0.000000
9	0.0829	0.017700	0.000000	0.000000	0.000000
10	0.0927	0.017700	0.000000	0.000000	0.000000
11	0.1024	0.017700	0.000000	0.000000	0.000000
12	0.1121	0.017700	0.000000	0.000000	0.000000
13	0.1219	0.017700	0.000000	0.000000	0.000000
14	0.1316	0.017700	0.000000	0.000000	0.000000
15	0.1413	0.017700	0.000000	0.000759	0.002941
16	0.1511	0.017700	0.000000	0.000776	0.003005
17	0.1608	0.017700	0.000000	0.000000	0.000000
18	0.1705	0.017700	0.000000	0.000000	0.000000
19	0.1802	0.017700	0.000000	0.000000	0.000000
20	0.1899	0.017700	0.000000	0.000000	0.000000
21	0.1996	0.017700	0.000000	0.000000	0.000000
22	0.2093	0.017700	0.000000	0.000000	0.000000
23	0.2190	0.017700	0.000000	0.000000	0.000000
24	0.2287	0.017700	0.000000	0.001874	0.005451
25	0.2383	0.017700	0.000000	0.001927	0.005577
26	0.2480	0.017700	0.000000	0.000000	0.000000
27	0.2577	0.017700	0.000000	0.000000	0.000000
28	0.2674	0.017700	0.000000	0.000000	0.000000
29	0.2770	0.017700	0.000000	0.000000	0.000000
30	0.2867	0.017700	0.000000	0.000000	0.000000
31	0.2963	0.017700	0.000000	0.000000	0.000000
32	0.3060	0.017700	0.000000	0.000000	0.000000
33	0.3156	0.017700	0.000000	0.000000	0.000000
34	0.3253	0.017700	0.000004	0.000072	0.000280
35	0.3349	0.017700	0.000000	0.000000	0.000000
36	0.3445	0.017700	0.000000	0.000000	0.000000
37	0.3542	0.017700	0.000000	0.000000	0.000000
38	0.3638	0.017700	0.000000	0.000000	0.000000
39	0.3734	0.017700	0.000000	0.000000	0.000000
40	0.3830	0.017700	0.000000	0.000000	0.000000
41	0.3926	0.017700	0.000000	0.000000	0.000000
42	0.4023	0.017700	0.000000	0.000000	0.000000
43	0.4119	0.017700	0.000005	0.000000	0.000000
44	0.4215	0.017700	0.000000	0.000000	0.000000
45	0.4311	0.017700	0.000000	0.000000	0.000000
46	0.4407	0.017700	0.000000	0.000000	0.000000
47	0.4503	0.017700	0.000000	0.000000	0.000000
48	0.4599	0.017700	0.000000	0.000000	0.000000
49	0.4695	0.017700	0.000000	0.000000	0.000000
50	0.4791	0.017700	0.000005	0.000000	0.000000
51	0.4887	0.017700	0.000007	0.000000	0.000000
52	0.4983	0.017700	0.000004	0.000000	0.000000
53	0.5078	0.017700	0.000005	0.000000	0.000000
54	0.5174	0.017700	0.000000	0.000000	0.000000
55	0.5270	0.017700	0.000000	0.000000	0.000000
56	0.5366	0.017700	0.000000	0.000000	0.000000
57	0.5462	0.017700	0.000000	0.000000	0.000000
58	0.5557	0.017700	0.000000	0.000000	0.000000
59	0.5653	0.017700	0.000024	0.000212	0.000821

S.N.	1	2	3	4	5
60	0.5749	0.017700	0.000014	0.002265	0.008094
61	0.5845	0.017700	0.000006	0.002322	0.008513
62	0.5941	0.017700	0.000004	0.000000	0.000000
63	0.6036	0.017700	0.000003	0.000000	0.000000
64	0.6132	0.017700	0.000000	0.000000	0.000000
65	0.6228	0.017700	0.000000	0.000000	0.000000
66	0.6323	0.017700	0.000000	0.000000	0.000000
67	0.6419	0.017600	0.000112	0.000937	0.003113
68	0.6515	0.017600	0.000028	0.001349	0.004008
69	0.6610	0.017700	0.000012	0.000398	0.001543
70	0.6706	0.017700	0.000003	0.000094	0.000366
71	0.6802	0.017700	0.000000	0.000000	0.000000
72	0.6897	0.017700	0.000000	0.000000	0.000000
73	0.6993	0.017700	0.000000	0.000000	0.000000
74	0.7088	0.017700	0.000000	0.000000	0.000000
75	0.7184	0.017700	0.000000	0.000000	0.000000
76	0.7279	0.017500	0.000368	0.001625	0.004885
77	0.7375	0.017600	0.000065	0.011300	0.037600
78	0.7471	0.017600	0.000029	0.000843	0.003266
79	0.7566	0.017600	0.000004	0.000393	0.001044
80	0.7662	0.017700	0.000000	0.000000	0.000000
81	0.7757	0.017700	0.000000	0.000000	0.000000
82	0.7853	0.017700	0.000000	0.000000	0.000000
83	0.7948	0.017700	0.000000	0.000000	0.000000
84	0.8044	0.017600	0.000000	0.000000	0.000000
85	0.8140	0.017400	0.000508	0.000749	0.002453
86	0.8235	0.017600	0.000186	0.019100	0.060900
87	0.8331	0.017600	0.000075	0.000290	0.000614
88	0.8426	0.017600	0.000008	0.001036	0.003298
89	0.8522	0.017600	0.000000	0.000000	0.000000
90	0.8618	0.017600	0.000000	0.000000	0.000000
91	0.8713	0.017600	0.000000	0.000000	0.000000
92	0.8808	0.017600	0.000000	0.000000	0.000000
93	0.8904	0.017600	0.000004	0.000000	0.000000
94	0.9000	0.017500	0.000360	0.000102	0.000394
95	0.9095	0.017600	0.000055	0.011700	0.045300
96	0.9191	0.017600	0.000023	0.000103	0.000400
97	0.9286	0.017600	0.000009	0.000180	0.000697
98	0.9382	0.017600	0.000004	0.000000	0.000000
99	0.9477	0.017600	0.000000	0.000000	0.000000
100	0.9573	0.017600	0.000000	0.000000	0.000000
101	0.9669	0.017600	0.000000	0.000000	0.000000
102	0.9765	0.017600	0.000000	0.000000	0.000000
103	0.9860	0.017600	0.000125	0.000000	0.000000
104	0.9955	0.017600	0.000039	0.002221	0.008603
105	1.0051	0.017600	0.000013	0.000000	0.000000
106	1.0147	0.017600	0.000006	0.000095	0.000368
107	1.0243	0.017600	0.000003	0.000000	0.000000
108	1.0337	0.017600	0.000004	0.000000	0.000000
109	1.0434	0.017600	0.000000	0.000000	0.000000
110	1.0529	0.017600	0.000000	0.000000	0.000000
111	1.0625	0.017600	0.000003	0.000000	0.000000
112	1.0721	0.017500	0.000281	0.000152	0.000402
113	1.0817	0.017600	0.000079	0.007398	0.028300
114	1.0912	0.017600	0.000022	0.000094	0.000364
115	1.1008	0.017600	0.000009	0.000265	0.000704
116	1.1102	0.017600	0.000003	0.000000	0.000000
117	1.1199	0.017600	0.000000	0.000000	0.000000
118	1.1295	0.017600	0.000000	0.000000	0.000000
119	1.1389	0.017600	0.000000	0.000000	0.000000
120	1.1486	0.017600	0.000000	0.000000	0.000000
121	1.1582	0.017500	0.000521	0.000239	0.000658
122	1.1678	0.017600	0.000144	0.022000	0.084900
123	1.1774	0.017600	0.000021	0.000000	0.000000
124	1.1870	0.017600	0.000003	0.000190	0.000737
125	1.1966	0.017600	0.000000	0.000000	0.000000
126	1.2062	0.017600	0.000000	0.000000	0.000000
127	1.2157	0.017600	0.000000	0.000000	0.000000

S.N.	1	2	3	4	5
128	1.2252	0.017600	0.000000	0.000000	0.000000
129	1.2348	0.017600	0.000000	0.000000	0.000000
130	1.2444	0.017600	0.000000	0.000000	0.000000
131	1.2540	0.017600	0.000064	0.000115	0.000444
132	1.2636	0.017600	0.000064	0.000695	0.001292
133	1.2732	0.017600	0.000014	0.000165	0.000637
134	1.2827	0.017600	0.000003	0.000098	0.000379
135	1.2924	0.017600	0.000000	0.000000	0.000000
136	1.3021	0.017600	0.000000	0.000000	0.000000
137	1.3115	0.017600	0.000000	0.000000	0.000000
138	1.3212	0.017600	0.000005	0.000000	0.000000
139	1.3308	0.017500	0.000114	0.000139	0.000537
140	1.3404	0.017500	0.000119	0.001187	0.002658
141	1.3500	0.017600	0.000024	0.000180	0.000696
142	1.3596	0.017600	0.000008	0.000270	0.000783
143	1.3691	0.017600	0.000000	0.000000	0.000000
144	1.3788	0.017600	0.000000	0.000000	0.000000
145	1.3884	0.017600	0.000000	0.000000	0.000000
146	1.3980	0.017600	0.000000	0.000000	0.000000
147	1.4076	0.017600	0.000004	0.000000	0.000000
148	1.4172	0.017500	0.000136	0.000167	0.000647
149	1.4268	0.017600	0.000067	0.001904	0.005982
150	1.4366	0.017600	0.000008	0.000306	0.001187
151	1.4462	0.017600	0.000003	0.000000	0.000000
152	1.4557	0.017600	0.000000	0.000000	0.000000
153	1.4654	0.017600	0.000003	0.000000	0.000000
154	1.4749	0.017600	0.000000	0.000000	0.000000
155	1.4846	0.017600	0.000000	0.000000	0.000000
156	1.4942	0.017600	0.000000	0.000000	0.000000
157	1.5038	0.017600	0.000004	0.000000	0.000000
158	1.5136	0.017500	0.000236	0.000268	0.000797
159	1.5232	0.017500	0.000117	0.003615	0.013600
160	1.5329	0.017600	0.000011	0.000000	0.000000
161	1.5425	0.017600	0.000003	0.000087	0.000336
162	1.5521	0.017600	0.000000	0.000000	0.000000
163	1.5619	0.017600	0.000000	0.000000	0.000000
164	1.5715	0.017600	0.000000	0.000000	0.000000
165	1.5812	0.017600	0.000000	0.000000	0.000000
166	1.5908	0.017600	0.000000	0.000000	0.000000
167	1.6005	0.017600	0.000004	0.000000	0.000000
168	1.6101	0.017400	0.000385	0.000381	0.001027
169	1.6197	0.017500	0.000230	0.004145	0.015000
170	1.6295	0.017600	0.000019	0.000000	0.000000
171	1.6392	0.017600	0.000003	0.000169	0.000656
172	1.6489	0.017600	0.000000	0.000000	0.000000
173	1.6585	0.017600	0.000000	0.000000	0.000000
174	1.6683	0.017600	0.000000	0.000000	0.000000
175	1.6780	0.017600	0.000000	0.000000	0.000000
176	1.6877	0.017600	0.000004	0.000000	0.000000
177	1.6973	0.017400	0.000529	0.002204	0.007573
178	1.7071	0.017400	0.000385	0.004883	0.017200
179	1.7168	0.017600	0.000022	0.000000	0.000000
180	1.7265	0.017600	0.000003	0.000273	0.000794
181	1.7364	0.017600	0.000000	0.000000	0.000000
182	1.7461	0.017600	0.000000	0.000000	0.000000
183	1.7558	0.017600	0.000000	0.000000	0.000000
184	1.7655	0.017600	0.000005	0.000000	0.000000
185	1.7753	0.017500	0.000006	0.000171	0.000664
186	1.7851	0.017500	0.000017	0.000450	0.001196
187	1.7948	0.017500	0.000007	0.000742	0.000735
188	1.8047	0.017600	0.000003	0.000069	0.000268
189	1.8145	0.017600	0.000000	0.000000	0.000000
190	1.8242	0.017600	0.000000	0.000000	0.000000
191	1.8341	0.017600	0.000000	0.000000	0.000000
192	1.8439	0.017600	0.000000	0.000000	0.000000
193	1.8538	0.017600	0.000000	0.000000	0.000000
194	1.8636	0.017500	0.000004	0.000000	0.000000
195	1.8735	0.017500	0.000008	0.000352	0.000609

S.N.	1	2	3	4	5
196	1.8834	0.017500	0.000043	0.001432	0.002042
197	1.8932	0.017500	0.000010	0.002777	0.002436
198	1.9031	0.017500	0.000007	0.001861	0.001895
199	1.9129	0.017500	0.000009	0.001412	0.001884
200	1.9229	0.017300	0.000225	0.001432	0.002113
201	1.9329	0.015300	0.001701	0.023800	0.022000
202	1.9428	0.012700	0.003003	0.048200	0.061000
203	1.9526	0.011200	0.003940	0.053500	0.066000
204	1.9625	0.009940	0.004641	0.053600	0.070400
205	1.9722	0.011300	0.004365	0.113100	0.158800
206	1.9821	0.012600	0.004400	0.096300	0.103800
207	1.9918	0.012900	0.004039	0.070800	0.066300
208	2.0015	0.014900	0.002950	0.126600	0.123000
209	2.0113	0.016300	0.002210	0.108000	0.106800
210	2.0210	0.017000	0.002567	0.068000	0.074600
211	2.0308	0.017100	0.002043	0.031600	0.043600
212	2.0403	0.016300	0.003311	0.039200	0.067400
213	2.0499	0.015700	0.004062	0.020100	0.026200
214	2.0597	0.016100	0.002950	0.143500	0.239900
215	2.0692	0.016100	0.002997	0.088900	0.157000
216	2.0788	0.015800	0.002900	0.134200	0.244000
217	2.0886	0.015900	0.002254	0.088000	0.134000
218	2.0981	0.015800	0.002140	0.174700	0.261800
219	2.1076	0.015800	0.002157	0.177100	0.281600
220	2.1172	0.016100	0.001908	0.176800	0.297100
221	2.1269	0.015100	0.004511	0.148900	0.237300
222	2.1366	0.016300	0.001646	0.143900	0.216700
223	2.1461	0.016600	0.001703	0.123800	0.166800
224	2.1556	0.016800	0.001219	0.164300	0.283600
225	2.1652	0.017100	0.000901	0.092500	0.143600
226	2.1749	0.017700	0.000154	0.056300	0.061000
227	2.1845	0.017800	0.000046	0.012000	0.012800
228	2.1942	0.017900	0.000028	0.002931	0.004611
229	2.2038	0.017800	0.000010	0.000196	0.000517
230	2.2134	0.017800	0.000006	0.000596	0.000950
231	2.2232	0.017800	0.000000	0.000072	0.000280
232	2.2329	0.017800	0.000000	0.000152	0.000402
233	2.2426	0.017800	0.000000	0.000000	0.000000
234	2.2524	0.017800	0.000000	0.000000	0.000000
235	2.2620	0.017800	0.000010	0.000000	0.000000
236	2.2718	0.017800	0.000015	0.000286	0.001107
237	2.2815	0.017800	0.000007	0.000107	0.000413
238	2.2913	0.017800	0.000009	0.000000	0.000000
239	2.3011	0.017800	0.000004	0.000000	0.000000
240	2.3109	0.017800	0.000004	0.000000	0.000000
241	2.3206	0.017800	0.000004	0.000000	0.000000
242	2.3304	0.017800	0.000012	0.000101	0.000390
243	2.3401	0.017700	0.000581	0.000304	0.001178
244	2.3499	0.017600	0.000645	0.001967	0.004397
245	2.3596	0.017800	0.000089	0.000362	0.001400
246	2.3695	0.017800	0.000008	0.000865	0.003351
247	2.3793	0.017800	0.000000	0.000000	0.000000
248	2.3892	0.017800	0.000000	0.000000	0.000000
249	2.3990	0.017800	0.000000	0.000000	0.000000
250	2.4089	0.017800	0.000004	0.000000	0.000000
251	2.4187	0.017800	0.000013	0.000142	0.000551
252	2.4285	0.017600	0.000592	0.000305	0.001182
253	2.4384	0.017600	0.000645	0.001987	0.004434
254	2.4483	0.017800	0.000090	0.000352	0.001363
255	2.4580	0.017800	0.000008	0.000904	0.003220
256	2.4679	0.017800	0.000000	0.000000	0.000000
257	2.4777	0.017800	0.000000	0.000000	0.000000
258	2.4877	0.017800	0.000003	0.000000	0.000000
259	2.4977	0.017800	0.000015	0.000164	0.000635
260	2.5076	0.017600	0.000610	0.000317	0.001227
261	2.5175	0.017600	0.000667	0.002053	0.004706
262	2.5274	0.017800	0.000089	0.000354	0.001370
263	2.5372	0.017800	0.000008	0.000845	0.003271

S.N.	1	2	3	4	5
264	2.5471	0.017800	0.000005	0.000000	0.000000
265	2.5571	0.017800	0.000000	0.000000	0.000000
266	2.5670	0.017800	0.000000	0.000000	0.000000
267	2.5770	0.017800	0.000015	0.000174	0.000675
268	2.5869	0.017600	0.000616	0.000333	0.001288
269	2.5968	0.017600	0.000670	0.001952	0.004670
270	2.6068	0.017800	0.000089	0.000658	0.001740
271	2.6168	0.017800	0.000008	0.000867	0.003359
272	2.6267	0.017800	0.000000	0.000000	0.000000
273	2.6366	0.017800	0.000000	0.000000	0.000000
274	2.6465	0.017800	0.000005	0.000000	0.000000
275	2.6565	0.017800	0.000016	0.000178	0.000689
276	2.6665	0.017600	0.000604	0.000336	0.001301
277	2.6765	0.017600	0.000653	0.001919	0.004565
278	2.6865	0.017800	0.000085	0.000642	0.001695
279	2.6965	0.017800	0.000005	0.000783	0.003031
280	2.7065	0.017800	0.000000	0.000000	0.000000
281	2.7165	0.017800	0.000000	0.000000	0.000000
282	2.7265	0.017800	0.000000	0.000000	0.000000
283	2.7365	0.017800	0.000004	0.000000	0.000000
284	2.7465	0.017800	0.000015	0.000176	0.000680
285	2.7566	0.017600	0.000566	0.000326	0.001264
286	2.7667	0.017600	0.000605	0.001898	0.004188
287	2.7768	0.017800	0.000075	0.000272	0.001055
288	2.7868	0.017800	0.000005	0.000698	0.002703
289	2.7969	0.017800	0.000000	0.000000	0.000000
290	2.8070	0.017800	0.000000	0.000000	0.000000
291	2.8171	0.017800	0.000017	0.000166	0.000641
292	2.8271	0.017200	0.001722	0.000781	0.001652
293	2.8371	0.017200	0.001817	0.033600	0.123000
294	2.8473	0.017800	0.000065	0.002281	0.007951
295	2.8574	0.017800	0.000006	0.000747	0.002309
296	2.8676	0.017800	0.000000	0.000000	0.000000
297	2.8777	0.017800	0.000000	0.000000	0.000000
298	2.8878	0.017800	0.000000	0.000000	0.000000
299	2.8979	0.017800	0.000000	0.000000	0.000000
300	2.9081	0.017800	0.000012	0.000153	0.000592
301	2.9181	0.017200	0.001499	0.000459	0.001300
302	2.9283	0.017200	0.001795	0.028400	0.104200
303	2.9385	0.017700	0.000051	0.002530	0.009179
304	2.9487	0.017800	0.000005	0.000551	0.001672
305	2.9589	0.017800	0.000000	0.000000	0.000000
306	2.9691	0.017800	0.000003	0.000000	0.000000
307	2.9793	0.017800	0.000013	0.000135	0.000523
308	2.9894	0.017300	0.001252	0.000706	0.001887
309	2.9998	0.017300	0.001343	0.020400	0.074300
310	3.0099	0.017700	0.000041	0.001378	0.004927
311	3.0201	0.017800	0.000006	0.000437	0.001256
312	3.0304	0.017800	0.000000	0.000000	0.000000
313	3.0408	0.017800	0.000000	0.000000	0.000000
314	3.0512	0.017800	0.000000	0.000000	0.000000
315	3.0614	0.017800	0.000000	0.000000	0.000000
316	3.0716	0.017800	0.000013	0.000091	0.000353
317	3.0819	0.017400	0.000907	0.003637	0.012800
318	3.0922	0.017500	0.000922	0.007368	0.024800
319	3.1027	0.017700	0.000027	0.000909	0.003155
320	3.1128	0.017800	0.000004	0.000292	0.000782
321	3.1233	0.017800	0.000000	0.000000	0.000000
322	3.1336	0.017700	0.000000	0.000000	0.000000
323	3.1439	0.017700	0.000000	0.000000	0.000000
324	3.1545	0.017700	0.000000	0.000000	0.000000
325	3.1648	0.017700	0.000008	0.000000	0.000000
326	3.1752	0.017600	0.000538	0.001854	0.006041
327	3.1856	0.017600	0.000476	0.003746	0.009894
328	3.1962	0.017700	0.000019	0.000815	0.002400
329	3.2069	0.017700	0.000003	0.000170	0.000451
330	3.2172	0.017700	0.000000	0.000000	0.000000
331	3.2276	0.017700	0.000003	0.000000	0.000000

S.N.	1	2	3	4	5
332	3.2382	0.017700	0.000007	0.000000	0.000000
333	3.2486	0.017600	0.000295	0.001255	0.003855
334	3.2592	0.017700	0.000237	0.003041	0.007594
335	3.2698	0.017700	0.000012	0.001789	0.006928
336	3.2804	0.017700	0.000000	0.000000	0.000000
337	3.2911	0.017700	0.000000	0.000000	0.000000
338	3.3018	0.017700	0.000000	0.000000	0.000000
339	3.3125	0.017700	0.000000	0.000000	0.000000
340	3.3231	0.017700	0.000000	0.000000	0.000000
341	3.3337	0.017700	0.000006	0.000000	0.000000
342	3.3444	0.017700	0.000089	0.000372	0.001020
343	3.3554	0.017700	0.000077	0.000208	0.000551
344	3.3660	0.017700	0.000006	0.000000	0.000000
345	3.3769	0.017700	0.000004	0.000000	0.000000
346	3.3879	0.017700	0.000000	0.000000	0.000000
347	3.3985	0.017700	0.000000	0.000000	0.000000
348	3.4095	0.017700	0.000000	0.000000	0.000000
349	3.4205	0.017700	0.000000	0.000000	0.000000
350	3.4314	0.017700	0.000011	0.000000	0.000000
351	3.4426	0.017500	0.000770	0.002964	0.008709
352	3.4535	0.017500	0.000819	0.009290	0.033400
353	3.4646	0.017700	0.000028	0.000354	0.001371
354	3.4757	0.017700	0.000005	0.000209	0.000556
355	3.4868	0.017700	0.000003	0.000000	0.000000
356	3.4981	0.017700	0.000000	0.000000	0.000000
357	3.5092	0.017700	0.000000	0.000000	0.000000
358	3.5205	0.017700	0.000000	0.000000	0.000000
359	3.5318	0.017700	0.000132	0.000227	0.000603
360	3.5432	0.017700	0.000103	0.000356	0.001127
361	3.5545	0.017700	0.000008	0.000000	0.000000
362	3.5658	0.017700	0.000000	0.000000	0.000000
363	3.5773	0.017700	0.000000	0.000000	0.000000
364	3.5887	0.017700	0.000000	0.000000	0.000000
365	3.6003	0.017700	0.000000	0.000000	0.000000
366	3.6117	0.017700	0.000000	0.000000	0.000000
367	3.6233	0.017700	0.000172	0.000638	0.001790
368	3.6347	0.017700	0.000113	0.001151	0.003126
369	3.6462	0.017700	0.000013	0.000000	0.000000
370	3.6578	0.017700	0.000000	0.000000	0.000000
371	3.6693	0.017700	0.000000	0.000000	0.000000
372	3.6806	0.017700	0.000000	0.000000	0.000000
373	3.6924	0.017700	0.000000	0.000000	0.000000
374	3.7037	0.017700	0.000000	0.000000	0.000000
375	3.7151	0.017700	0.000004	0.000000	0.000000
376	3.7266	0.017600	0.000382	0.002578	0.005485
377	3.7379	0.017700	0.000126	0.006551	0.016400
378	3.7492	0.017700	0.000052	0.000999	0.003870
379	3.7606	0.017700	0.000004	0.000642	0.001775
380	3.7720	0.017700	0.000000	0.000000	0.000000
381	3.7832	0.017700	0.000000	0.000000	0.000000
382	3.7943	0.017700	0.000000	0.000000	0.000000
383	3.8055	0.017700	0.000000	0.000000	0.000000
384	3.8165	0.017700	0.000000	0.000000	0.000000
385	3.8276	0.017700	0.000004	0.000375	0.001452
386	3.8386	0.017700	0.000006	0.000396	0.001532
387	3.8496	0.017700	0.000004	0.000000	0.000000
388	3.8606	0.017700	0.000000	0.000000	0.000000
389	3.8714	0.017700	0.000000	0.000000	0.000000
390	3.8824	0.017700	0.000000	0.000000	0.000000
391	3.8931	0.017700	0.000000	0.000000	0.000000
392	3.9039	0.017700	0.000000	0.000000	0.000000
393	3.9146	0.017700	0.000000	0.000000	0.000000
394	3.9252	0.017700	0.000000	0.000000	0.000000
395	3.9358	0.017700	0.000000	0.000000	0.000000
396	3.9464	0.017700	0.000000	0.000000	0.000000
397	3.9571	0.017700	0.000000	0.000000	0.000000
398	3.9675	0.017700	0.000000	0.000000	0.000000
399	3.9782	0.017700	0.000000	0.000000	0.000000

S.N.	1	2	3	4	5
400	3.9886	0.017700	0.000000	0.000000	0.000000
401	3.9991	0.017700	0.000000	0.000000	0.000000
402	4.0094	0.017700	0.000000	0.001085	0.002862
403	4.0199	0.017700	0.000003	0.001121	0.002959
404	4.0302	0.017700	0.000000	0.000000	0.000000
405	4.0406	0.017700	0.000000	0.000000	0.000000
406	4.0508	0.017700	0.000000	0.000000	0.000000
407	4.0614	0.017700	0.000000	0.000000	0.000000
408	4.0715	0.017700	0.000000	0.000000	0.000000
409	4.0817	0.017700	0.000000	0.000000	0.000000
410	4.0920	0.017700	0.000000	0.000000	0.000000
411	4.1025	0.017700	0.000000	0.000000	0.000000
412	4.1128	0.017700	0.000000	0.000000	0.000000
413	4.1228	0.017700	0.000000	0.000000	0.000000
414	4.1332	0.017700	0.000000	0.000000	0.000000
415	4.1432	0.017700	0.000000	0.000000	0.000000
416	4.1534	0.017700	0.000000	0.000000	0.000000
417	4.1637	0.017700	0.000000	0.000000	0.000000
418	4.1738	0.017700	0.000000	0.000000	0.000000
419	4.1839	0.017700	0.000000	0.000000	0.000000
420	4.1943	0.017700	0.000000	0.000000	0.000000
421	4.2044	0.017700	0.000000	0.000000	0.000000
422	4.2145	0.017700	0.000000	0.000000	0.000000
423	4.2246	0.017700	0.000000	0.000000	0.000000
424	4.2350	0.017700	0.000000	0.000000	0.000000
425	4.2450	0.017700	0.000000	0.000000	0.000000

APPENDIX-VIII

List of relevant research papers:

Name of the journal	*Month & year of publication*	*Title of the research paper*	*Single or with Co-author(s)*
1. *Journal of Hydraulic Research* (IAHR)	Under Review	"2-D depth averaged modelling for braided stretch of River Brahmaputra in India"	Akhtar, M.P., Sharma, Nayan and Ojha C.S.P.
2. *Journal of Hydraulic Engineering* (ASCE)	Under Review	"Modified Flow Dispersion Stress Tensor in 2-D Curvilinear Flow Domain Part-A: Model Development"	Akhtar, M.P., Ojha, C.S.P.,Sharma, Nayan and Bergstrom, D. J
3. *Journal of Hydraulic Engineering* (ASCE)	Under Review	"Modified Flow Dispersion Stress Tensor in 2-D Curvilinear Flow Domain Part-B: Flow Field Simulation"	Akhtar, M.P., Ojha, C.S.P.,Sharma, Nayan and Bergstrom, D. J.